THERMAL TRANSMISSION MEASUREMENTS OF INSULATION

R. P. Tye, *editor*

ASTM
STP 660
AMERICAN SOCIETY FOR TESTING AND MATERIALS

THERMAL TRANSMISSION MEASUREMENTS OF INSULATION

A symposium
sponsored by ASTM
Committee C-16 on
Thermal and Cryogenic
Insulating Materials
AMERICAN SOCIETY FOR
TESTING AND MATERIALS
Philadelphia, Pa., 19–20 Sept. 1977

ASTM SPECIAL TECHNICAL PUBLICATION 660
R. P. Tye, Dynatech R/D Company
editor

List price $39.50
04-660000-10

AMERICAN SOCIETY FOR TESTING AND MATERIALS
1916 Race Street, Philadelphia, Pa. 19103

Library of Congress Catalog Card Number: 78-060000

NOTE

The Society is not responsible, as a body,
for the statements and opinions
advanced in this publication.

Printed in Washington, D.C.
December 1978

Foreword

This publication, *Thermal Transmission Measurements of Insulation*, contains papers presented at a symposium on Heat Transmission Measurements held in Philadelphia, Pa., 19–20 Sept. 1977. The symposium was sponsored by Committee C-16 on Thermal and Cryogenic Insulation Materials of the American Society for Testing and Materials. R. P. Tye, Dynatech R/D Company, presided as symposium chairman and editor of this publication.

Related ASTM Publications

Heat Transmission Measurements in Thermal Insulations, STP 544 (1974), $30.75, 04-544000-10

Thermal Insulating Covers for NPS Piping, Vessel Lagging and Dished Head Segments, C 450 Adjunct (1965), $6.25, 12-304500-00

A Note of Appreciation to Reviewers

This publication is made possible by the authors and, also, the unheralded efforts of the reviewers. This body of technical experts whose dedication, sacrifice of time and effort, and collective wisdom in reviewing the papers must be acknowledged. The quality level of ASTM publications is a direct function of their respected opinions. On behalf of ASTM we acknowledge with appreciation their contribution.

ASTM Committee on Publications

Editorial Staff

Jane B. Wheeler, *Managing Editor*
Helen M. Hoersch, *Associate Editor*
Ellen J. McGlinchey, *Senior Assistant Editor*
Helen Mahy, *Assistant Editor*

Contents

PARAMETERS AFFECTING THERMAL PERFORMANCE

HEAT TRANSMISSION MODELS AND MEASUREMENTS

SYSTEMS EVALUATION

OTHER PARAMETERS AND MEASUREMENTS

SUMMARY

Introduction

Some four and a half years have elapsed since the previous C16 symposium on heat transmission in thermal insulations. At that time the implications of the world energy crisis were just making themselves apparent, while now the full consequences are upon us. Energy conservation, particularly within the context of the proper utilization of thermal insulation, is only one of a number of important measures which have to be taken to help alleviate the problem. It is a very critical measure, however, especially in the span of the next five to ten years.

The 1973 meeting proved to be an important milestone, both in the development and subsequent pursuit of knowledge of thermal insulation performance and for the C16 Committee and ASTM. It was a fully international gathering both in terms of the numbers attending and the papers presented. In the latter instance, some 40 percent of the papers were by authors from outside the United States and Canada. The problems which faced us all were not restricted by boundaries, nor were the means of attacking and solving them. There was a realization that we had this common bond and as a result a truly international understanding developed. People inside and outside the United States appreciated better the work of their counterparts, and many new friendships, understandings, and cooperative efforts developed. The subsequent flow of information improved steadily. International membership of C16 increased significantly.

After the meeting, ASTM Committee C16, especially the C16.30 Thermal Measurements Subcommittee, decided that the overall interests of thermal insulation and its applications could be developed at the international level. As a result they were instrumental in proposing that an International Standards Organization (ISO) Committee on Thermal Insulation be established. This was supported enthusiastically by some 17 countries, and ISO Committee 163 was established and its first meeting held in 1976 in Stockholm, the capital of the secretariat country.

At this meeting, it was established that thermal performance and its measurement was the number one priority. Subcommittee 1 on Test Methods was duly established and at its first meeting in Berlin in May, 1977, five working groups were established to develop, as rapidly as possible, international standards for thermal performance of insulation materials and systems. The next meeting for ISO 163 and its subcommittees will be in the United States in October 1978 and several draft documents on thermal performance will be considered for action.

Because of its continuing involvement in the subject and as a focal point for dissemination of technical information on insulation performance, Subcommittee C16.30 decided to hold a further symposium continuing the series. Sufficient work had been carried out in the interim, both in the United States and elsewhere, to warrant a further exchange of ideas. In this way a further improvement in our understanding of the problems would take place. The subcommittee itself had undertaken an extensive philosophical revision of its basic measurement specifications in 1976 based on the position paper presented in 1973. In addition, members of the subcommittee have been involved in developing both a new calibrated hot box and a dynamic probe method test specification for systems and materials, respectively. These are based on subjects discussed in 1973 and are needed in order to anticipate future requirements both in the laboratory and outside.

The subject of thermal performance of thermal insulation, especially under real-life conditions, is a multifaceted and complex subject. A thermal insulation material can no longer be considered in isolation. Its performance must be considered within the context of total performance of the ultimate system, whether this be the building envelope or a complex insulation package for an industrial process.

Reliable laboratory measurements under steady-state conditions are still necessary but are no longer sufficient. Further information is required on actual performance, and the effects of various parameters, including moisture movement, airflow, diurnal and climatic variations, flaws, and other imperfections, quality of installation, etc., all need detailed study. Dynamic and transient analyses and measurements are necessary to supplement the steady-state information. Both laboratory and field measurements are necessary.

The goal of the symposium therefore was to provide the forum for an international exchange of information and ideas in this ever-changing subject and to make everyone aware of the current state of the art. The anticipated result would be to upgrade our overall knowledge, to understand the subject a little better, and in turn to stimulate further research and development.

The truly international group of papers in this publication thus covers the development and improvements which have taken place in the fundamental studies of thermal insulation material and systems performance since 1973. The wide range of subjects covered, including a second C16.30 position paper which extends the 1973 document and outlines future needs in specific areas, should stimulate further work in the whole subject. Such is the present momentum in the field that further conferences and symposia in the series will probably be held more frequently.

In conclusion, I would like to thank all of the contributors for making both the symposium and this publication a success. In addition, I wish

to thank the other members of the Symposium Organizing Committee, Alex Adorjian, Francesco DePonte, and Frank Ruccia, for their valuable assistance. I am confident that our future meetings will prove to be equally as stimulating.

R. P. Tye

Senior scientist, Dynatech R/D Co., Cambridge, Mass. 02139; symposium chairman and editor.

Reference Materials

Reference Materials for Insulation Measurement Comparisons

REFERENCE: ASTM Subcommittee C16.30, "**Reference Materials for Insulation Measurement Comparisons,**" *Thermal Transmission Measurements of Insulation, ASTM STP 660*, R. P. Tye, Ed., American Society for Testing and Materials, 1978, pp. 7–29.

ABSTRACT: This paper addresses the issue: *Adequate standard materials are not available for thermal conductance measurements in the field of thermal insulations.* The need, scope, and benefits of solving this problem are detailed. The National Bureau of Standards (NBS) Special Reference Materials category was adopted as a possible solution to this problem. The materials selection criteria, the NBS certification process, and the applicable measurement methods are described.

A set of materials was identified as potential candidates for insulation measurement comparisons:

1. Air space
2. High-density molded fibrous glass board
3. AA glass fiber blanket insulation
4. Glass fiber appliance insulation blanket
5. Aged polystyrene foam
6. Silicone rubber
7. Borosilicate glass
8. Closed-cell foam glass
9. Silica aerogel composite block
10. Rigidized silica fiber tile
11. Zirconia fiber board
12. Alumina silicate refractory fiber insulation blanket
13. Mineral rock board
14. Calcium silicate
15. Powder or loose fill insulation

This list is intended to be a point of departure and its dissemination may stimulate testing to identify potential reference materials.

KEY WORDS: thermal transmission, thermal insulation, thermal resistance, standard reference materials, research materials, special reference materials, high-density molded fibrous glass board, glass fiber blanket insulation, glass fiber appliance insulation blanket, aged polystyrene foam, silicone rubber, borosilicate glass, closed-cell foam glass, silica aerogel composite block, rigidized silica fiber tile, zirconia fiber board, alumina-silicate refractory fiber insulation blanket, mineral rock board, calcium silicate

This paper is a partial response to a larger charge made by ASTM Committee C16 (Thermal and Cryogenic Insulating Materials) to Subcommittee C16.30 (Thermal Properties) to examine efforts needed to establish a National Voluntary Laboratory Accreditation Program (NVLAP) for thermal testing laboratories. A working group (WG)[1] (subordinate to the NVLAP Task Group) was formed to examine the need for Standard Reference Materials (SRM's) in the context of the technical adequacy of existing standard test methods (STM's). STM's and SRM's would serve together as the basis of specific thermal NVLAP criteria which are to be developed. In addition, the WG was charged to establish priorities based on what can be done best and soonest in the areas of greatest potential impact [*1*].[2] Toward this end, a WG concept evolved that concentrated characterization effort was first needed on materials for use in existing test methods and that these materials should be representative of building and industrial insulations. Thus, this paper deals primarily with materials and materials' properties, not with insulating systems such as walls and panels.

Reasons for the SRM Approach

This materials approach was pursued for several reasons: First, the data base for heat transmission in thermal insulations is not firm and there are large differences in the available data. It is generally thought that the majority of measurements made by the well-known commercial, industrial, and governmental laboratories are of acceptable accuracy; however, the measurements of some laboratories are suspect. The major reason for the observed property differences is associated with the status of the measurement technology. Some organizations have continually obtained wide variations in values on similar materials, even over a limited temperature range, when using modified forms of a basic apparatus. Hence the need for an accreditation program. These differences increase as the temperature conditions become more extreme and heat loss problems increase. Generally the heat-transfer mechanisms are not well-understood and subtle technique differences, such as measurement of temperatures, temperature differences, and emittances, are often not treated in the same manner from one apparatus to another.

These issues were discussed in some detail in an earlier C16.30 position paper [*2*], from which the following paragraph is excerpted:

> These last statements lead to the following key point: there are dangers involved in ascribing the property of thermal conductivity to a material as a result of a single measurement obtained according to a standard test method on a single specimen regardless of how good the test method is. All methods prescribe the measurement of heat fluxes and surface temperature by some means, for some physical configuration of a specimen, from which a resultant thermal conductivity is *calculated*. There is no requirement in these methods, however, that this calculated property must be shown to be independent of area, thickness, and temperature gradient. Therefore, there is no assurance without such a verification that the calculated property is in fact a true thermal conductivity.

Consequently, this WG has adopted the convention of describing the heat-transfer property of insulating reference materials by using thermal resistance per unit thickness, or the thermal resistance from surface to surface, where required. The thermal resistance R of a test specimen is defined by

$$\Delta T = R \cdot q$$

where ΔT is the temperature difference between the surfaces of the specimen (deg) and q is the heat flux per unit area through the specimen (W/m^2). Thus R has the dimensions $m^2 \cdot K/W$ and the thermal resistance per unit thickness has dimensions $m \cdot K/W$. Thermal conductance is defined as the reciprocal of R and apparent thermal conductivity is defined as thermal conductance times the thickness of the specimen. There may also be differences in the performance of materials when evaluated in large- and small-scale tests. One reason for this state is that insulation materials are heterogeneous and this lack of material homogeneity can lead to property variations. If a common set of uniform and reproducible materials (SRM's) were available, then a cooperative measurements program could be launched to improve all measurements as well as to correct unreliable apparatus, inadequate techniques, and to standardize procedures.

The second reason for this materials approach is that, unlike materials of higher density, where heat transport is predominantly by solid conduction mechanisms, both building and industrial insulation heat transfer is by a combination of modes, including solid and gaseous conduction, convection, and radiation. Because each mode is influenced by the specimen environmental and temperature conditions, any realistic NVLAP program must define procedures and materials to deal with this complexity. Selection of a set of characterized SRM's may yield significant advances, but it should be realized that this materials approach is only a partial solution. It is not a panacea, but does add a new dimension needed to obtain improved accuracy and a more complete concept of the properties of insulations.

A third, critical, part of this SRM approach is to select materials whose characteristics match the problem, which includes all possible heat trans-

mission mechanisms, a variety of building and industrial insulations with different thermal resistance per unit thickness, and a variety of measurement techniques. The availability of well-characterized materials which are homogeneous and stable under a variety of measurement conditions is a controlling step in this selection. For insulations in general, one is concerned with thermal resistance per unit thickness of material in the range 2 to 10 m·K/W near room temperature and less than 1 m·K/W near 1000°C, and, almost without exception,[3] a negative temperature coefficient of thermal resistance per unit thickness. In this paper, a number of SRM candidates have been selected that generally meet these criteria. It is anticipated that as test results on these candidates are obtained, the range of applicability of certain candidates, such as the high-temperature ones, will become wider and will lessen the need for overlapping low-temperature candidates, and thus the number of required materials will decrease.

The materials approach of this paper is not new. It has been suggested previously as a means to attack the difficulties associated with measurement of the heat transmission characteristics of insulations [*3,4*]. Some of the history of this subject is traced in the Appendix. Among individuals associated with measurement technology, there is no doubt about the need to attack these difficulties. Their conversations often cite examples of problems which might be resolved by an NVLAP-type program. For example, within the past five years the use of cellulosic insulations has increased dramatically in commercial buildings and houses. The accepted thermal resistance per unit thickness of a typical cellulose insulation is in the the range 24.3 to 25.6 m·K/W [3.5 to 3.7 h·ft² · deg F/(Btu·in.)], yet it is not uncommon to find quoted values that range from 24.3 to 62.4 m·K/W [3.5 to 9 h·ft² · deg F/(Btu·in.)]. The WG believes this is an illustration of poor measurement methodology. From a mechanistic viewpoint a value higher than 38 m·K/W [5.5 h·ft²·deg F/(Btu·in.)] is not possible for a low-density open-cell insulation containing air, since the thermal resistance per unit thickness associated with that value is about 70 percent that of air. Similar examples of erroneous data exist for industrial insulations, particularly at high temperatures, where radiation plays a dominant role. One such case brought to the WG's attention involved a specification for mineral wool insulation in which the specified thermal resistance per unit thickness versus mean temperature data was the average of values reported by several mineral wool manufacturers [*5*]. The resulting average was so high that the specification could not be met. The high average was caused by including data from one company that reported their values as a function of hot-face temperature rather than mean temperature.

[3]Organic foams blown with refrigerant gases do not necessarily have a negative temperature coefficient of thermal resistance per unit thickness near the condensation range of the gas.

Candidate Reference Materials

The following text provides some background information for the selection of candidates tabulated later in this section.

Reference Materials Criteria

Each candidate for insulation reference materials should meet the following criteria [6].

1. The material should be mechanically and chemically stable through the intended test temperature range and possess long-term stability under ambient storage conditions. Ideally the material should be unaffected by heat treatment or at least be in a stabilized condition after a prescribed heat treatment.
2. The material should be capable of being manufactured in sufficiently large and homogeneous lots to permit a practical number of test specimens per calibrated section. Or, alternatively, the manufacturing process should yield test specimens of the required reproducibility and homogeneity to be practical. It is suggested that a practical number of test specimens is such as to meet a demand period of about 10 years.
3. The material should be representative of the thermal transport characteristics of a generic class of commercial insulation material or, alternatively, be a class of material that yields useful diagnostic information about the thermal test conditions.

The initial candidate list was developed with some consideration of representativeness. Additional technical aspects of representativeness and grouping of materials are discussed later.

Description of the SRM Certification Process

In the United States of America the development of SRM's is generally considered to be within the classical functions of the National Bureau of Standards (NBS). The function of the NBS Office of Standard Reference Materials (OSRM) is to coordinate and finance the production and distribution of SRM's. These materials, with specific properties measured and certified by NBS, are an integral part of the national measurement system (they provide traceable data bases). Three categories of reference materials are available in the NBS program [7]:

1. Standard Reference Material (SRM)—detailed characterization with properties measured and certified by NBS.
2. Research Materials (RM)—not certified, but a report of investigation exists for the pertinent properties.

3. Special Reference Materials (GM)—NBS maintains a stockpile as a disinterested third party; general information on properties are available.

With sufficient characterization and testing, a Special Reference Material can be certified as an SRM.

To initiate the production of an SRM, the NBS OSRM must receive a specific proposal from an NBS Technical Division, which may have received requests from an industrial group. The initial information needed includes a proposed SRM title, purpose for the SRM, reasons why the SRM is needed, special characteristics or requirements or both for the material, estimated demand for the SRM, material source other than NBS, and information to aid SRM justification (monetary impact and supporting letters from industry leaders, trade organizations, interested committees) [8]. Special Reference Materials, on the other hand, can be requested directly by any interested group.

Consideration of this procedure and the present status of insulation materials' characteristics and technology led the Working Group to believe that the Special Reference Material Category is the most suitable class of reference materials for present deliberations. This is all that can be expected based on our limited understanding of materials and equipment. The WG believes that additional experience and knowledge of properties will allow their eventual certification as SRM's. This WG listing of candidates may prompt subsequent actions for an entry of an insulation material into this procedure. To date, NBS OSRM has not received any specific proposals for establishing insulation reference materials.

Applicability of Special Reference Materials

The availability of a group of SRM's would provide a source of test specimens for the generic thermal test methods listed in Table 1. This listing is not all-inclusive or restricted to ASTM STM's, but represents a majority of methods currently used to evaluate materials. Table 1 includes steady-state linear and radial heat flow methods and dynamic methods. For each method, subtle operating technique or procedural differences can occur which significantly affect the results obtained. The availability and subsequent use of test specimens would allow method (and procedural) certification.

Measurement Method Considerations and Precautions

Each of the different methods listed in Table 1 may use inherently different techniques to obtain the quantities needed to determine the thermal resistance R of a test specimen as defined by $\Delta T = R \cdot q$. It is not the intent of this report to detail all of the pitfalls[4] which must be avoided to

[4]Typical pitfall problem areas include temperature measurement, power or heat flux measurement, attaining steady-state or equilibrium conditions, misapplication of test method, etc.

TABLE 1—*Thermal test methods that could use Special Reference Materials for measurement comparisons.*

STEADY-STATE LINEAR METHODS:
ASTM Test for Steady-State Thermal Transmission Properties by Means of the Guarded Hot Plate (C 177-76)
ASTM Test for Steady-State Thermal Transmission Properties by Means of the Heat Flow Meter (C 518-76)
ASTM Recommended Practice for Determination of Thermal Resistance of Low-Density Fibrous Loose Fill-Type Building Insulation (C 687-71)
ASTM Test for Thermal Conductance and Transmittance of Built-Up Sections by Means of the Guarded Hot Box (C 236-66)
Calibrated Hot Box[a]
ASTM Test for Thermal Conductivity of Refractories (C 201-68)
ASTM Test for Thermal Conductivity of Insulating Firebrick (C 182-72)
ASTM Test for Heat Flux Through Evacuated Insulations Using a Guarded Flat Plate Boiloff Calorimeter (C 745-73)
STEADY-STATE RADIAL OR SPHERICAL METHODS:
ASTM Test for Thermal Conductivity of Pipe Insulation (C 335-69)
ASTM Test for Thermal Transference of Nonhomogeneous Pipe Insulation at Temperatures Above Ambient (C 691-71)
Various radial heat-flow methods[b,c,d,e]
Various spherical heat-flow methods[f]
DYNAMIC METHODS:
Hot Wire Technique (DIN 51046)
Plane Probe Technique[g,h]
Rate of temperature change[i]

[a]Mumaw, J. R. in *Heat Transmission Measurements in Thermal Insulations, ASTM STP 544*, American Society for Testing and Materials, 1974, pp. 193–211.

[b]Flynn, D. R., *Journal of Research of the National Bureau of Standards*, Vol. 676, 1963, p. 129.

[c]Godbee, H. W. and Ziegler, W. T. in *Proceedings*, Third Conference on Thermal Conductivity, 1963, pp. 557–612.

[d]Godfrey, T. G., Fulkerson, W., Kollie, T. G., Moore, J. P., and McElroy, D. L., ORNL Report No. 3556, Oak Ridge National Laboratory, Oak Ridge, Tenn., 1964.

[e]Kropschot, R. H., Schrodt, J. E., Fulk, M. M., and Hunter, B. J., *Advances in Cryogenic Engineering*, Vol. 5, 1960, p. 189.

[f]Glaser, P. E., Black, I. A., Lindstrom, R. S., Ruccia, F. E., and Wechsler, A. E., NASA Report No. SP-5027, National Air and Space Administration, 1967.

[g]Halteman, E. K. and Gerrish, R. W., Jr., NBS SP-302, National Bureau of Standards, 1968, pp. 507–512.

[h]Jury, S. H. and Godfrey, T. G., ORNL/TM-4956, Oak Ridge National Laboratory, Oak Ridge, Tenn., 1977.

[i]Gibbon, N. C., Matsch, L. C., and Wang, D. I. J. in *Thermal Conductivity Measurements of Insulating Materials at Cryogenic Temperatures, ASTM STP 411*, American Society for Testing and Materials, 1967, p. 61.

obtain satisfactory results by each of the methods. (In large measure this is done by the various ASTM prescriptions.) It is important to note that bad procedures can render good methods useless, and, with the recent upsurge of interest in the use of insulation, there has been a proliferation of laboratories that profess they can conduct measurements of thermal properties of insulation according to the current standards, but in fact,

for reasons mentioned earlier, they do not know the proper way to conduct such measurements [9]. Although the use of the reference materials could alleviate many of these problems, it should be apparent to all that no one method is suitable for all materials and all applications.

Selection Criteria for Insulation Reference Materials

Heat flow through thermal insulations is governed by known physical principles, but its determination from these principles is difficult in practice. For the purpose of assessing thermal measurement capabilities of equipment, a material must be selected which best represents the primary mechanisms of heat flow which occur in the thermal insulations to be evaluated.

Heat flow through thermal insulations is primarily subject to three modes of heat transfer: conduction, radiation and, convection,[5] plus the interactive effects. These enter into the process in varying degrees depending, for example, on the material, the density, and temperature.

Thus, the selection of candidate materials should be based on those materials which will best demonstrate the behavior of these modes within the test equipment. This selection can be made from families of materials falling within the two representative regions shown in Fig. 1.

The upper band of Fig. 1 will best accent the radiative characteristics, while the lower band will accent the conductive mode of heat transfer within the test equipment. The temperature range of the graph should be established for different classes of materials depending on their use temperature and the test equipment capabilities.

Selection of the candidate materials must be based on the following specific considerations as well as on the reference materials criteria detailed earlier:

1. Types of materials being evaluated:
   Their range of usefulness in application.
   Their basic thermal characteristics, which can give an indication of the mechanisms of heat flow involved in the process.
   The expected variability in regard to the measured values.
   Is the problem of variability resulting from the material or from the test methods?
   The materials should be considered on the basis of the variation of thermal properties with temperature.
   The potential candidates should be selected from the family grouping of these insulating materials. The groupings should provide tem-

[5]Convective processes should be the subject of special consideration, since in most applications the characteristics of the insulations tend to minimize if not to eliminate this mode of heat transfer.

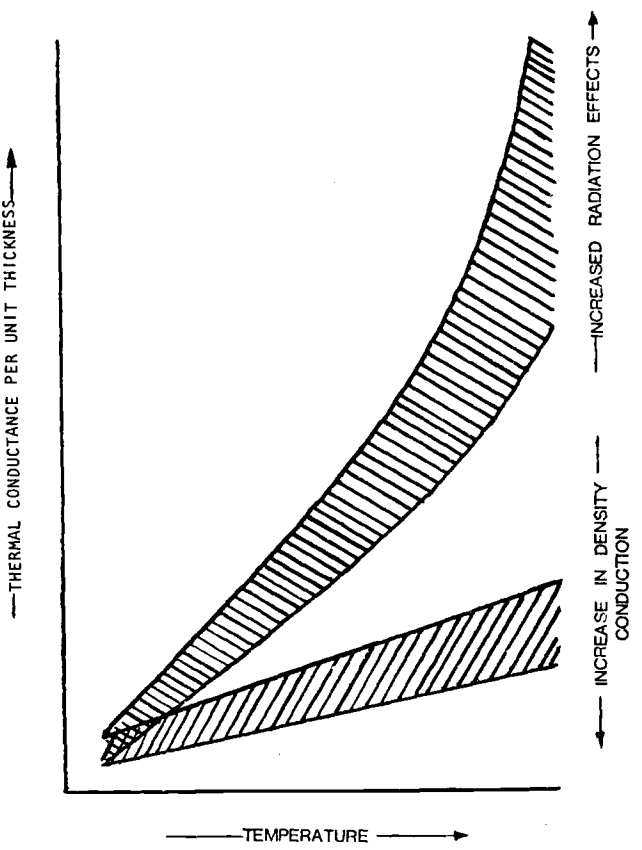

FIG. 1—*Schematic representation of the behavior of the thermal conductance per unit thickness with temperature for density changes in thermal insulations. Lower band represents primary transfer by conduction and upper band represents primary transfer by radiation.*

perature limitations and an indication of the heat flow mechanisms involved.

2. Types of equipment and test methods in use today:
   Temperature limits of the equipment.
   Physical limitation, size, shape of specimen, etc. This would limit the type of reference material to be used.

Reference Material Candidates

The initial set of candidates for reference materials for insulation measurement comparisons recommended by the Working Group is given in Table 2. This initial selection aimed to satisfy the building and industrial insulation interests by being representative of specific products while

TABLE 2—*Recommended candidates for reference materials for insulation measurement comparisons.*

Material	Probable Temperature Range of Applicability, °C	Nominal Bulk Density, kg/m³ (lb/ft³)	Thermal Resistance per Unit Thickness at 25°C, m·K/W [h ft² °F/ (Btu-in.)]	Need or Use
1. Air space	−160 to 200	. . .	. . .	procedural use, test plate emittance, and plate orientation effects
2. High-density molded fibrous glass board	−175 to 150	80 to 160 (5 to 10)	31.5 (4.5)	historical NBS material minimum radiation effect
3. AA glass fiber blanket insulation	−100 to 400	9.6 (0.6)	31.5 to 28.9 (4.5 to 4.2)	radiation effects, temperature coefficient, and geometry (thickness) effects
4. Glass fiber appliance insulation blanket	−100 to 230	11 to 32 (0.7 to 2)	20.4 to 28.9 (2.9 to 4.2)	similar to Item 3
5. Aged polystyrene foam	−180 to 75	48 (3)	21.7 to 22.4 (3.1 to 3.2)	provides useful comparison to 8.9-cm (3½ in.) fiber glass batts; stable after aging
6. Silicone rubber	glass point to 250	1280 to 1600 (80 to 100)	4.08 to 2.77 (0.59 to 0.40)	opaque material, interfacing resistance effects, and thickness edge-loss effects
7. Borosilicate glass	−175 to 800	2000 (125)	0.96 (0.14)	interfacial resistance effects, radiation effects at high temperature, and thickness effects
8. Closed-cell foam glass	−175 to 350	140 to 160 (9 to 10)	16.5 (2.38)	stable with reproducible properties
9. Silica aerogel composite block	−175 to 900	320 (20)	38.5 (5.5)	high thermal resistance per unit thickness tests and steady-state capacity temperature coefficient

10. Rigidized silica fiber tile	−175 to 1000	160 (10)	27.8 (4.00)	radiation effects and known reproducibility
11. Zirconia fiber board	−175 to 2200	480 (30)	11.55 (1.67)	very-high-temperature use, temperature coefficient, and radiation effects
12. Alumina-silicate refractory fiber insulation blanket	−175 to 1250	64 (4)	30.1 (4.34)	radiation and thickness effects, high-temperature geometry effects, and temperature coefficient
13. Mineral rock board	−175 to 650	192 (12)	23.1 (3.3)	radiation effects, temperature coefficient, and geometry effects
14. Calcium silicate	−175 to 700	190 to 220 (12 to 14)	17.3 (2.5)	generic insulation-type radiation and geometry effects and temperature coefficients
15. Powder or loose-fill insulation	. . .	. . .	. . .	specimen preparation techniques, radiation effects, isotropic nature, and temperature coefficient

simultaneously satisfying a generic materials and properties matrix, including ranges of temperature, density, thermal resistance per unit length, and physical size. Commercial availability was a major selection factor. Further research may identify specialty sources of supply for materials not presently commercially available. This list is a point of departure intended to stimulate confirmatory studies that may well identify more suitable materials.

Table 2 lists the estimated allowable temperature range of applicability, the thermal resistance per unit thickness at 25°C, the material density, and the reason for inclusion as a candidate. The following text provides additional information and comments about each entry.

Air Space—This suggested candidate at a nominal 6-mm plate spacing can provide procedural and diagnostic information on the plate emittance and plate orientation effects. Analysis of natural convection across spaces bounded by vertical surfaces agrees with experimental observations [*10*]. Measurements have been completed by the National Research Council of Canada on thin air spaces in guarded hot-plate and heat flow meter apparatuses [*11*].

High-Density Molded Fibrous Glass Board—This candidate has been a successful transfer material for at least 20 years and has proved to be a stable and rugged base within its temperature limitations. This historical NBS-supplied material has a well-known thermal resistance per unit thickness with long-term stability. It would provide a useful tie to the past and to current testing being conducted in Europe on 160-kg/m^3 (10 lb/ft^3) board. This candidate provides a test material with a minimum amount of radiation transmission. The board does contain a binder which probably limits testing to below 150°C [or possibly 176°C (350°F)]. Several companies[6–8] produce this board. NBS has a limited stockpile of this board and their files could provide additional documentation. Owens-Corning Fiberglas Corp. [*12*] experience on three or four production lots shows an average conductance per unit thickness at 25°C mean temperature, for 100 specimens, of 0.0321 W/m·K (0.223 Btu·in./h·ft^2 deg F), and the standard deviation was 0.0027 or 1.2 percent. The actual values ranged from 0.0314 to 0.0330 W/m·K (0.218 to 0.229 Btu·in./h·ft^2· deg F), a total of 5 percent, and the density ranged from 80 to 139 kg/m^3 (5.0 to 8.7 lb/ft^3).

AA Glass Fiber Blanket Insulation—This low-density insulation [9.6 kg/m^3 (0.6 lb/ft^3)] is produced to ASTM Specification for Glass Fiber Blanket Insulation (Aircraft Type) (C 800–75) Type 1, in 1.27-cm-thick (0.5 in.) specimens, by several companies.[9,10] This insulation is bonded

[6]Peabody Noise Control Corporation, 6300 Ireland Place, Dublin, Ohio 43017.
[7]Birma Products Corp., Jernee Mill Road, Sayreville, N.J. 08872.
[8]Vellon, Inc., San Jose, Calif.
[9]Owens-Corning Fiberglas Corporation, Granville, Ohio 43023.
[10]Johns-Manville Co., Denver, Colo. 80217.

with silicone, which extends the useful temperature range to 400°C. It is a very uniform product with a part of its apparent thermal conductivity being due to radiation, which would allow a useful determination of the temperature coefficient of apparent thermal conductivity and be relevant to common building insulations on the market. The availability of 1.27-cm-thick (0.5 in.) specimens would allow testing at several thicknesses (by stacking specimens) and this would provide information about thermal resistance, geometry, and heat loss effects.

Glass Fiber Appliance Insulation Blanket—This product is similar to the previous candidate 3 except that the binder is phenolic resin, which limits its useful temperature to 230°C. This material is available at various densities with appropriate changes in thermal resistance per unit length. Promising results on this candidate have been reported to the Working Group [*13*].

Aged Polystyrene Foam—A variety of different foams is produced, but this particular candidate was produced[11] using methyl chloride as the blowing agent. Depending upon the particular blowing agent, cell size, density, and thickness of the foam, a certain period of aging is required to allow the blowing agent to diffuse out, and oxygen and nitrogen to diffuse into the foam cells. After this has occurred, the cell gas is air and the foam is stable from about −180 to 75°C [*14*]. This candidate provides a semirigid material that would be useful to meet the large section requirements of hot boxes with a thermal resistance per unit thickness near that of 8.9-cm-thick (3½ in.) fiber glass batts.

Silicone Rubber—This candidate is a viable substitute for gum rubber, which is often suggested as an acceptable opaque thermal conductance test material. However, gum rubber has the disadvantages of softening just above room temperature and has a glass transition at a higher temperature than does silicone rubber. Silicone rubber RTV 560 and 5601 are available,[12] with flatter surfaces being produced by room temperature vulcanizing as opposed to high-temperature vulcanizing. The National Research Council of Canada has experience with fabricating and using silicone rubber RTV 560 as an apparatus test material to 250°C [*11*]. Silicone rubber has a high thermal conductivity, which makes it useful for illustrating interfacial resistance effects (temperature sensor placements), and provides a good test on thermal guarding needed to minimize edge-loss errors. Silicone rubber is isotropic, opaque, and available in a range of thicknesses, which would be useful to test some methods. It does possess a glass transition which limits its low-temperature usefulness.

Borosilicate Glass—Pyrex 7740 is available[13] as a typical borosilicate glass. Its high apparent thermal conductivity provides some of the same

[11]Dow Chemical USA, 2020 Dow Center, Midland, Mich. 48640.
[12]General Electric Company, Silicone Division, Schenectady, N.Y.
[13]Corning Glass Company, Corning, N.Y.

advantageous uses as silicone rubber, but it is usable at higher temperatures with a significant radiation contribution. The high apparent thermal conductivity and rigidity provide a means for interfacial resistance tests, and tests for radiation transport. Use of two or more thicknesses would yield information on geometry and radiation interactions.

Closed-Cell Foam Glass—Foamglas is being produced[14] and there has recently been a data release to the American Society of Heating, Refrigeration and Air-Conditioning Engineers on its properties [*15*]. The product has useful load-bearing capacities and is replacing industrial organic insulations. Four laboratories have completed thermal conductivity measurements which show agreements in the ±2 to ±5 percent range [*16*]. This rigid material is stable, apparently has reproducible properties, and has a moderate thermal conductivity over a 500°C temperature span, all of which make it a desirable general material for testing from low to moderate temperatures.

Silica Aerogel Composite Block—Several microporous low-thermal-conductivity insulations are produced (see Footnote 10) to reduce gas conduction effects by limiting the available gas mean free path. MinK 2000 is typical and its high thermal resistance per unit thickness (and low thermal diffusivity) can provide a test of the ability of any system to maintain steady-state conditions. Because of its broad temperature capacity, a good determination of the temperature coefficient would be possible. This material should receive a high-temperature heat treatment prior to any testing. This material, like many of the others, is anisotropic, but this can be a useful advantage in certain tests. Two laboratories have obtained property agreement of better than ±4 percent to 700°C. The apparent thermal conductivity is pressure dependent because of the gas mean free path limitations [*17*].

Rigidized Silica Fiber Tile—This material is produced for use in the Space Shuttle program.[15] Tests at various industrial sites [*16*] have established the variability of this high-temperature insulation. The expected shuttle program duration suggests this product will be available for a prolonged period. This material has uses similar to MinK 2000, except it has a lower thermal resistance per unit thickness, and it would not have to be pretreated prior to a set of measurements, which is a possible requirement for several other suggested materials.

Zirconia Fiber Board—This material is produced[16] customarily as boards, disks, or solid cylinders of various sizes from cubic crystal fibers of zirconia stabilized with yttria. This material may allow testing to very high temperatures, although the quoted 2200°C (maximum service tem-

[14]Pittsburgh Corning Corporation, Pittsburgh, Pa.
[15]Lockheed Missiles and Space Co., Sunnyvale, Calif.
[16]Zircar Products, Inc., 110 North Main St., Florida, N.Y. 10921.

perature) may be too high for use as a reference material. Determination of the thermal resistance per unit thickness and its temperature coefficient over a broad temperature range for this relatively dense material (which should enhance reproducibility) are its main advantages as a candidate.

Alumina-Silicate Refractory Fiber Insulation Blanket—Such materials are produced by several companies [10,17,18] using an Al_2O_3-SiO_2 fiber to yield a good high-temperature furnace insulation. Cerablanket[10] is typical of these products with a modest radiation contribution and relatively high use temperatures. This candidate would allow tests on a relatively new entry in the industrial insulation field, and be useful for showing radiation effects, thickness effects, and for determining the temperature coefficient of thermal resistance per unit thickness.

Mineral Rock Board—This material, as produced,[19] is reputed to be uniform, stable, and low in shot content. It is recommended as a test material that is representative of mineral wool insulations but is without their typical shot content and potential reproducibility problems. The mineral rock board moderate density should provide uniformity, and allow radiation component determinations on a fibrous insulation significantly different from the other listed high-temperature materials. The fairly broad useful temperature span implies useful determinations of temperature coefficient and high-temperature geometry effects.

Calcium Silicate—This material is produced by several major manufacturers [9,10,20] and commands a significant part of industrial insulation usage. The change to asbestos-free calcium silicate insulation has encountered some fragility problems. However, the broad use and potential importance of this material warrants a position among the recommended materials. The conduction factors important to this generic class may be missed by the other suggestions. The material availability alone suggests usage to study geometry effects, as well as to determine radiation and temperature coefficients.

A Powder or a Loose Fill Insulation—The Working Group recognized the need for such an entry. Numerous applications involve use of such insulations, which range from blown and poured building insulations (fiber glass, rock wool, and cellulose) to perlite and vermiculite fills for cryostorage to fills for concrete blocks to powders for nuclear fuel elements. These "powders" are isotropic and general materials in these classes could provide a needed means to compare very different methodologies (linear, radial, and dynamic). Such materials would assist improvements in sampling techniques for measurements. The WG did not consider this

[17]The Babcock & Wilcox Company, Refractories Division, Augusta, Ga. 30903.

[18]The Carborundum Company, High Temperature Insulation Division, P.O. Box 808, Niagara Falls, N.Y. 14302.

[19]Rockwool Aktubolaget Development Corp., S54101 Skovde, Sweden.

[20]Pabco, Insulation Division, 1110 16 Road, Fruita, Colo. 81521.

area in sufficient detail to obtain recommendations; however, Ottawa sand, hollow glass microspheres [*18*], or other available ceramic oxide powders might represent possible choices. The particle size distribution and powder density are important material characterizations which would have to be controlled.

Characterization Properties of Reference Materials

The primary purpose of this paper is to obtain a functioning set of materials with well-characterized thermal resistances per unit thickness. However, this ability to influence heat flow is only one useful property of these materials and, because this property is so often not completely understood, it behooves one to obtain supplementary characteristics of each material. Indeed, this additional information may be as important as the primary purpose in advancing current insulation technology. The evaluation of these candidate materials should have immediate goals such as:

1. Establish the range of properties for each material with respect to dimensional stability, density, and thermal properties.
2. Establish the limits on allowable test temperatures and thermal exposures.
3. Establish the probable reproducibility and accuracy obtainable with general materials and what might be expected for higher-level materials.
4. Establish the general "handleability" of each material since this is an expected use condition.

Satisfying these goals would provide some of the background information needed to move within the NBS-OSRM certification process from a Special Reference Material category to the Standard Research Materials catetory. Information and properties that would be useful in this process are listed in Table 3.

Conclusions

The conclusions of this WG paper are as follows:

1. The Committee C16 (main) charge to C16.30 has identified a significant issue in insulation technology. Briefly stated, the issue is:

> Adequate reference standards are not available for thermal conductance measurements in the field of thermal insulations.

2. The paper identifies two beneficial effects that would result if this problem were solved:

A. The data base for heat transmission in all thermal insulations would eventually be strengthened; currently inexplicable data differences

TABLE 3—*Information that would be useful to know about reference materials.*

GENERAL DESCRIPTIVE INFORMATION

1. Material name; ASTM designation if appropriate
2. Source or sources
3. Production process description, commercial or custom product
4. Material constituents, chemical analysis, fiber characteristics, binders used, special heat treatments
5. Product forms and densities available and prices of products
6. Typical product applications
7. Precautions on product usage

PHYSICAL PROPERTIES AS A FUNCTION OF TEMPERATURE

1. Thermal resistance or thermal resistance per unit thickness or thermal conductivity (where applicable) (method and qualifications)
2. Density
3. Specific heat
4. Thermal diffusivity
5. Thermal shock resistance
6. Thermal expansion coefficient
7. Anisotropy of any physical property
8. Emittance, transmittance, and absorptance

MECHANICAL PROPERTIES AS A FUNCTION OF TEMPERATURE

1. Compressive, tensile, and shear strengths
2. Deflection versus load for different thicknesses, density, and temperatures

OTHER PERTINENT PROPERTIES

1. Combustibility
2. Corrosive effects on materials or by various chemicals
3. Hygroscopic and moisture resistance degradation effects
4. Resistance to airflow
5. Clearly defined maximum-use temperature for various exposure times
6. Linear dimensional changes and other insulation property changes with aging time at temperature
7. Safety (hazard) and health (toxicity) considerations

would be reduced; all thermal measurement techniques would be improved; and the resultant understanding of the mechanisms of heat transport would likely result in the advent of improved insulation materials for building and industrial applications.

B. A realistic NVLAP program to meet the procedural needs of the building and industrial insulation interests would be definable.

While this reference materials approach offers these benefits, it is not a panacea; the technical aspects of the solution will be difficult, expensive, and time-consuming because of the nature of thermal property measurements.

3. The WG's approach to this problem included providing materials selection criteria, a description of the NBS certification process of SRM's and required information, the methods that would use the reference materials, and some method precautions.

4. A recommended set of candidates for reference materials for insulation measurement comparisons was identified as a first suggestion. The intended use of each was briefly described and the additional information needed for each presented.

Recommendations

C16.30 Recommended SRM Program for Thermal Insulations

In an effort to stimulate action on the subject, the C16.30 Working Group is proposing the following plan to raise a limited series of materials to the level of having certified properties. It is hoped that the publication of this first proposed plan as part of the C16.30 activities will stimulate other interested parties to work together more actively in order to initiate action to extend and execute this plan and to develop others.

The recommended approach for obtaining, characterizing, and disseminating reference materials is one that is phased. The approach should attach highest priority to the development of those reference materials that are required most urgently, such as, for example, materials for building insulation applications. In addition, however, there are some which, it is believed, can be characterized faster and at lower cost.

We see that, while the National Bureau of Standards will have a vital role in the overall effort, the ultimate solution can be obtained only through a large, well-planned and well-funded cooperative effort. This will involve not only OSRM, but other Government organizations and agencies, the insulation manufacturers and users, together with independent organizations. In total, the expertise of those having experience and knowledge of materials will have to be combined with that of the measurements experts all working together. Although the roles of the various groups may not be well defined at this time, it is possible to see that within the list of materials recommended for study certain programs or plans can be proposed. ASTM C16 stands ready to provide expertise and to serve in an advisory and coordinating function during any or all of the stages of such plans.

Five phases of such an effort have been identified at this time, and are outlined. The five phases center around the characterization and dissemination of three reference materials: a high-density (80 to 160 kg/m^3) fibrous glass board and a low-density fibrous glass blanket material, both for use at moderate temperatures, and a high-temperature insulation. These phases are designed to run in parallel as shown in Table 4. The identification and screening of new candidate materials for characterization, subsequent to the first three, are included as the last phase. The cooperation and involvement of OSRM were sought and have been promised for the initial two phases. Descriptions of the phases follow.

TABLE 4—*Proposed five-phase SRM program timetable.*

CY	78	79	80	81	82	83

Phase 1: ▼

Existing stock of high-density molded fibrous glass board: (260 to 325 K)

Phase 2: ▽

(*a*) Procure new stock of high-density molded fibrous glass board, characterization in limited range (260 to 325 K)

▽

(*b*) Extend characterization to range 125 to 425 K

Phase 3: ▽

(*a*) Procure stock of glass fiber blanket insulation, characterization in limited range (260 to 325 K)

▽

(*b*) Extend characterization to range 125 to 500 K

Phase 4: ▽

(*a*) Procure stock of silica aerogel composite block, characterization in limited range (260 to 325 K)

▼

(*b*) Extend characterization to range 125 to 1175 K

Phase 5: →

Identify/screen/characterize additional reference material candidates

Phase 1—Systematically examine characterization data for existing NBS stock of high-density fibrous glass board. Use the information to certify the remaining stock of this material as a reference material by NBS-OSRM over the limited temperature range 260 to 325 K (Jan. 1978).

Phase 2—Purchase additional new stock of high-density fibrous glass board, and complete an initial characterization of this material in the limited temperature range 260 to 325 K. Extend the characterization range for this class of material to 125 to 425 K (Oct. 1979).

Phase 3—Purchase a stock of glass fiber appliance insulation blanket for stockpiling by NBS-OSRM. Characterize the properties of this material in two steps, first in the limited temperature range 260 to 325 K (Oct. 1978) and subsequently over the extended temperature range 125 to 500 K (Oct. 1979).

Phase 4—Purchase a stock of silica aerogel composite block for stockpiling by NBS-OSRM. Characterize the properties of this material in two

steps, first in the limited temperature range 260 to 325 K (Oct. 1978) and subsequently over the range 125 to 1175 K (Oct. 1979).

Phase 5—Starting at present, identify new potential materials and, along with the list of candidate materials proposed in this paper, develop a long-range priority order for subsequent reference material characterization. This will most probably involve obtaining small stocks of all candidate materials that pass an initial screening test and accomplishing exploratory characterization of their properties. This is envisioned as a continuing effort of at least five years' duration.

Need for Recommended Program for Thermal Insulations

A wide variety and great quantity of measurements are made to determine various thermal properties of insulating materials of different kinds, under a wide range of conditions. These measurements are made for purposes of quality control, properties certification for materials specifications, advertising data, and other reasons. They are made by materials producers and by private and public independent testing laboratories. The existing data on insulation material thermal properties are sparse and sometimes contradictory. One reason is that accurate performance measurements are complex and difficult.

A primary element in any effort to improve the state-of-the-art knowledge of insulation thermal performance and meaningful data base is a series of well-characterized reference materials which have thermal performance properties that span the range of products in the marketplace. This series of materials would also provide a framework for a reliable data base of insulating materials properties. No reference materials with certified properties are presently available. The main body of this report describes that situation in detail and goes on to identify a number of candidate materials potentially suitable for this purpose, along with a summary of their known properties and ranges of applicability.

A number of identifiable groups have an interest in the development of a series of insulation reference materials. These include testing laboratories, insulation producers, consumers, standards-promulgating bodies, state and Federal agencies that purchase large amounts of insulating materials or that have a regulatory interest, and Federal agencies responsible for energy-related research, development, and demonstration.

As an example of such an interest, there is no quality-assurance procedure to guarantee the reliability and accuracy of the results obtained by measurement laboratories. Standard test methods for measurement of relevent thermal properties, such as those promulgated by ASTM, provide technical tools, but there is no procedure to assure that these methods are correctly applied by individual testing laboratories. The U.S. De-

partment of Commerce is initiating action for development of a National Voluntary Laboratory Accreditation Program for thermal testing laboratories in order to increase the overall confidence level in such performance measurements.

The provision of SRM's having precisely known physical or chemical performance properties falls within the overall scope and objectives of the various national standards laboratories. In the United States there is for this purpose an Office of Standard Reference Materials within the National Bureau of Standards. However, the total scope of the requirements in the thermal insulation field involves more than the provision of a few materials or specimens having known properties at one temperature or condition. The total amount of work required to characterize the numbers of specimens and the temperature ranges and conditions to be covered is well beyond the capabilities of a single organization.

It is felt that the observations made in the foregoing, and the recommendations for action, while obvious, needed to be stated explicitly. The complexity of the interests of the various groups and their potential roles makes this statement necessary, since, in such a situation, some sort of catalyst is necessary to initiate action. It is hoped that this statement will provide that catalyst, and that all interested groups will follow through and initiate and support a successful plan to provide thermal insulation reference materials.

Acknowledgments

The Working Group would like to acknowledge the assistance and advice obtained from a variety of active members of ASTM Committee C16 who recognized the need for a resolution of the reference materials issue. Their constant support encouraged the Working Group deliberations and provides a hopeful basis for initiation of needed laboratory measurements on these materials. The managements of the organizations which employ the Working Group members are gratefully acknowledged for allowing the Working Group members to participate in the various WG meetings at Ft. Lauderdale, St. Louis, Chicago, San Antonio, and Gaithersburg.

APPENDIX

Some of the Relevant History Pertinent to Insulation Measurements

Any account of pertinent history on heat transmission in insulation materials is likely to be incomplete and very dependent on the particular authors. Despite this disclaimer, it seems to this Working Group that a number of noteworthy activities have occurred since 1912, when the first guarded hot plate was built to

provide usable data pertaining to heat transmission in insulation needed for design purposes by the American Society of Refrigeration Engineers. Since that time, several organizations and societies have been particularly active, and at least a limited degree of order has been maintained. However, problems with insulation information are still rampant. Perhaps the appeals of the past 10 years will obtain actions to remove this roadblock. Table 5 outlines several significant acts.

TABLE 5—*Insulation information acts.*

Approximate Year(s)	Description of Act
1900–1910	C. H. Lees (England) work on flat-plate methods
1912	NBS builds first guarded hot-plate (GHP) apparatus
1929–1977	NBS maintenance of GHP to supply calibrations for 300+ laboratories
1939	Formation of ASTM C16 Thermal Insulation Committee
1945	ASTM adopts GHP method as a standard testing method (STM)
1949	ASTM adopts guarded hot box (NBS) as an STM
1951	First ASTM C16 symposium on insulating materials
1951	GHP round-robin on corkboard by Robinson and Watson (NBS)
1952	Vershoor and Greebler (Johns-Manville) paper on gas mean free path effects and theory
1957	Second ASTM C16 symposium on insulations
1959	NBS supplies fiber glass and gum rubber
1961–1977	Annual thermal conductivity conferences held
1962	Shultz shows thickness effect in foams
1964	ASTM adopts heat flow meter as an STM
1966	Third ASTM C16 symposium on insulations
1967	Round-robin on National Physical Laboratory (NPL) (British) fiber glass by International Institute of Refrigeration
1967	Term redefinition by H. E. Robinson (NBS)
1968	Pelanne (Johns-Manville) paper on radiation and interactive effects on insulations
1969	*Thermal Conductivity*, Vols. 1 and 2 (R. P. Tye, Ed.), published. A. W. Pratt lists low conductivity materials for reference purposes
1970–1971	C16 Working Group established on reference materials
1973	Fourth ASTM C16 symposium on insulations; C16.30 measurement philosophy paper; C16.30 proposed materials for reference
1974	C16.30 equipment and standards survey distributed
1975	C16 laboratory accreditation initiated; C16.30 charged; second survey in United States of America and Canada
1976	ORNL/ERDA insulation assessment published and workshop meeting
1977	Fifth ASTM C16 symposium on insulation

References

[1] Carroll, W. L., Minutes, ASTM C16.30 Task Group on Laboratory Accreditation, Ft. Lauderdale, Fla., 10 May 1976 (25 May 1976).

[2] ASTM Subcommittee C16.30, "What Property Do We Measure" *Heat Transmission in Thermal Insulations*, ASTM STP 544, American Society for Testing and Materials, 1974, pp. 5–12.

[3] Pratt, A. W., in *Thermal Conductivity*, Vol. 1, R. P. Tye, Ed., Academic Press, London and New York, 1969, pp. 400–402.

[4] Appendix in *Heat Transmission Measurements in Thermal Insulations, ASTM STP 544*, American Society for Testing and Materials, 1974, pp. 307–309.

[5] RDT Standard M12-6T, Mineral Fiber Thermal Insulation, High Temperature, Rigid, Flexible, and Loose Fill [ASTM Specification for Mineral Fiber Block and Board Thermal Insulation (C 612–70 with Additional Requirements], Division of Reactor Development and Technology, Atomic Energy Commission, March 1973.

[6] Anderson, R. W., Private Communication, Program Outline Recommendation of Reference Materials—Thermal Insulation, 8 Oct. 1976.

[7] Kirby, R. K., in *Workshop on Technical Assessment of Industrial Thermal Insulation Materials—Summary*, ORNL/TM-5515 Oak Ridge National Laboratory, Oak Ridge, Tenn. July 1976, p. 18.

[8] Kirby, R. K., National Bureau of Standards, Private Communication to D. L. McElroy, Oak Ridge National Laboratory, Oak Ridge, Tenn., 1 June 1976.

[9] Govan, F. A., Combustion Equipment Associates, Private Communication to R. K. Kirby, National Bureau of Standards, 2 April 1976.

[10] Raithby, G. D., Hollands, K.G.T., and Unny, T. E., *Transactions, American Society of Mechanical Engineers, Journal of Heat Transfer*, Vol. 99, May 1977, pp. 287–293.

[11] Shirtliffe, C. J., National Research Council of Canada, Private Communication to the Working Group.

[12] Hollingsworth, M., Owens-Corning Fiberglas Corp., Private Communication to R. W. Anderson, Energy Research and Development Administration, 13 Sept. 1976.

[13] Pelanne, C. M., Johns-Manville Co., Private Communication to the Working Group.

[14] Greason, D. M., Dow Chemical USA, Private Communication to D. L. McElroy, Oak Ridge National Laboratory, Oak Ridge, Tenn., 3 June 1977.

[15] Gerrish, R. W., *Advances in Cryogenic Engineering*, Vol. 22, 1974, pp. 242–250.

[16] Tye, R. P., Dynatech Corp., Private Communication to the Working Group.

[17] Tye, R. P., "The Thermal Conductivity of MinK-200 Thermal Insulation in Different Environments to High Temperatures," CONF-691002, 9th Conference on Thermal Conductivity, March 1970, pp. 341–351.

[18] Sparrow, E. M., and Cur, N., *Transactions, American Society of Mechanical Engineers, Journal of Heat Transfer*, May 1977, pp. 232–239.

M. Bertasi,[1] *G. Bigolaro,*[2] *and F. De Ponte*[1]

Fibrous Insulating Materials as Standard Reference Materials at Low Temperatures

REFERENCE: Bertasi, M., Bigolaro, G., and De Ponte, F., "**Fibrous Insulating Materials as Standard Reference Materials at Low Temperatures,**" *Thermal Transmission Measurements of Insulation, ASTM STP 660*, R. P. Tye, Ed., American Society for Testing and Materials, 1978, pp. 30–49.

ABSTRACT: A model is proposed to describe the thermal behavior of relatively high-density fibrous materials. The theoretical approach is compared with experimental results on glass fiber insulating specimens. The results point out the limits of other oversimplified models and the excessive complexity of other models with respect to the precision of results. The agreement between experimental and computed data was considered satisfactory when near to 1 percent.

The theoretical model may be used for computing some limits to obtain reliable standard reference materials with regard to production variations.

The problem of the influence of moisture on measured data is then analyzed, starting from a large set of experimental data obtained on specimens in controlled atmospheres.

KEY WORDS: measuring techniques, thermal conductivity, glass fiber boards, standard reference materials, radiation, humidity, convection, heat-transfer models.

Nomenclature

A	L/D
c	Specific heat at constant pressure, J/kg·K
d	Spacing between two fibers, m
D	Specimen thickness, m
g	Constant of gravity, 9.81 m/s^2
k	λ'/λ_g
K	Airflow permeability, m^2
L	Specimen side, m
n	Number of layers
N	Scattering cross section per unit volume, m^{-1}

[1]Assistant professors, Istituto di Fisica Tecnica, University of Padova, Padova, Italy.

[2]Researcher, Consiglio Nazionale delle Ricerche (CNR), Laboratorio per la Tecnica del Freddo, Padova, Italy.

p	Pressure, Pa
P	Absorption cross section per unit volume, m^{-1}
p_s	Saturation pressure of water, atm
p_v	Partial pressure of water vapor, atm
q_r	Power per unit area exchanged by radiation, W/m^2
Ra	Rayleigh number
s	Mean fiber diameter, m
S	Specimen cross section, m^2
V	Volume flow, m^3/s
T, T_1, T_2	Temperatures, K
α	Glass thickness (parallel path) in a cube of unit side
β	Coefficient of cubic expansion, K^{-1}
γ	Side of a glass square rod in a cube of unit side or s/d
Γ	Glass volume fraction
δ	Glass thickness (series path) in a cube of unit side
Δt	Temperature difference, K
$\epsilon, \epsilon_1, \epsilon_2$	Total hemispherical emissivities
$\lambda_a, \lambda_g, \lambda_m, \lambda_v$	Thermal conductivity of dry air, glass, moist air, and water vapor, W/m·K
λ_r	Radiative heat-transfer coefficient, W/m·K
λ'	Gas thermal conductivity, W/m·K
λ^*	Apparent thermal conductivity of resin-bonded glass fiber boards (RBGFB) without air motion, W/m·K
μ	Dynamic viscosity, kg/m·s
ν	Kinematic viscosity, m^2/s
ξ	$(1/\gamma)k/(1-k)$
ρ, ρ_g	Density, glass density, kg/m^3
ρ_b	RBGFB's bulk density, kg/m^3
σ	Stefan's constant, $5.67 \times 10^{-8} W/m^2 \cdot K^4$
ϕ	Relative humidity

Determination of the thermal conductivity of insulating materials by means of the absolute methods is simple in principle but complex, slow, and costly in practice, and therefore not suitable for quality control for industrial purposes. Therefore, comparative methods were developed; but recalibrations are required and, as a consequence, standard reference materials (SRM's) are required.

The definition of SRM's requires a deep knowledge of the heat-transfer mechanism to state clearly the reliability of the SRM itself.

The purpose of this paper is to study the RBGFB's of relatively high bulk density (80 to 125 kg/m^3) between 100 and 300 K. First of all, heat-transfer mechanisms are summarized; then some analytical models are proposed and predicted values are compared with experimental results on two sets of specimens produced by two different European manufacturers using the TEL[3] process.

[3]TEL is derived from the initials in reverse order of the Laboratoire de' Essais Thermiques, where the process was first developed in 1942.

Heat and Mass Transfer

The heat-transfer mechanism within RBGFB is rather complex and can be due to the conduction in the gas and in the fibers; to the convection in the gas; and to radiative absorption, scattering, and reemission in the whole board. All heat-transfer mechanisms will be reviewed and some empirical formulas recalled.

Conduction

First of all, it is necessary to know the thermal conductivity of the solid matrix and of the gas phase. The first datum should be estimated tentatively, as the chemical composition of glass and of bonding plastic is never specified by the producers of RBGFB.

Among the many types of glass studied by Ratcliffe [1][4], a glass with a density of 2420 kg/m^3 and with the following composition (percent by weight) was selected: SiO_2 : 67.7 percent; K_2O : 1.8 percent; Na_2O : 14.6 percent; B_2O_3 : 4.0 percent; A_2O_3 : 1.8 percent; CaO : 5.4 percent; BaO : 3.3 percent; Fe_2O_3 : 1.3 percent. The best fit of glass thermal conductivity λ_g according to Ratcliffe data at − 150, − 100, − 50, 0 and 50°C is the following polynomial within 0.3 percent

$$\lambda_g = 0.2063 + 4.071 \times 10^{-3}\, T - 4.544 \times 10^{-6}\, T^2, \qquad \text{W/m·K}$$

where T is the mean temperature in deg K.

The thermal conductivity of gas phase is the result of thermal conductivity of dry air and water vapor. Below 250 K, vapor content is so small that the thermal conductivity of dry air differs from that of saturated air by less than 0.1 percent, but at room temperature the presence of water vapor cannot be neglected, as the influence on thermal conductivity may be of the order of 1 percent.

Dry-air thermal conductivity can be computed within the precision of known data with the expression

$$\lambda_a = \frac{0.00264391\, T^{0.5}}{1 + \dfrac{245}{T}\, 10^{-12/T}}, \qquad \text{W/m·K} \qquad (1)$$

The water vapor thermal conductivity λ_v can be evaluated within the precision of known data with the expression

$$\lambda_v = \frac{T^{0.5}}{-138.818 + 480327/T - 4.88631 \times 10^{+7}/T^2}, \qquad \text{W/m·K} \qquad (2)$$

[4]The italic numbers in brackets refer to the list of references appended to this paper.

Up to 310 K, the moist-air thermal conductivity, if the true value of λ_a and λ_v is known, can be evaluated within 0.1 percent with the linear expression

$$\lambda_m = \lambda_v p_v + (1 - p_v)\lambda_a = \lambda_v \phi p_s + (1 - \phi p_s)\lambda_a \tag{3}$$

where

p_v = water vapor pressure, atm,
p_s = saturation pressure, of water at temperature T, atm, and
ϕ = relative humidity.

Water saturation pressure p_s may be evaluated with excellent precision with the formula

$$p_s = e^{[70.4347 - 7362.7/T + 6.95208 \times 10^{-3}T - 9 \ln (T)]}, \quad atm \tag{4}$$

At 310 K, saturated air has a thermal conductivity 2 percent lower than that of dry air and therefore the water vapor properties need not be very precise evaluations, but, at higher temperatures, thermal conductivity of moist air should be evaluated with the formulas of binary mixtures.

Convection

In an RBGFB used as an SRM, natural convection should be negligible to avoid correction factors dependent on specimen thickness, on temperature gradient, and on gradient orientation with respect to the gravity vector. A lot of work was done on the onset of natural convection in porous and fibrous materials—for example, by Fournier and Klarsfeld [2], Bankvall [3,4], and Staicu [5]—and there is general agreement on the fact that natural convection is a function of the modified Rayleigh number Ra defined as

$$Ra = \frac{\beta g c \rho}{\nu} \frac{D\Delta T}{\lambda^*} K \tag{5}$$

where

β = coefficient of cubic expansion,
g = constant of gravity,
ν = kinematic viscosity,
c = specific heat at constant pressure,
ρ = density,
D = specimen thickness,
λ^* = apparent thermal conductivity of the porous medium without air motion,
Δt = temperature difference across specimen, and
K = airflow permeability defined by

$$K = \frac{\dot{V}}{S} \frac{\mu}{\text{grad}\,(p)}$$

where

V = volume flow across section S of specimen,
μ = dynamic viscosity, and
p = pressure.

The group $\beta g c \rho / \nu$ for an assigned gas is a function of temperature only, and for air at atmospheric pressure its value is about 2×10^6 W/m$^4 \cdot$K^2 at 300 K and 10^8 W/m$^4 \cdot$K^2 at 100 K. For horizontal specimens crossed by vertical heat flux, there is no convection if $Ra < 40$; for vertical specimens crossed by horizontal heat flux, there is no convection if $Ra/A < 4$, where A is the ratio between specimen side L and specimen thickness D.

Radiation

Heat transfer by radiation in fibrous materials is rather complex and occurs by absorption and reradiation and by scattering. Scattering is very important, as it takes place each time the refractive index is discontinuous, that is, at each fiber surface, the diameter being of the same order of magnitude as the wavelength of incident radiation. Larkin and Churchill [6] and Linford et al [7] faced the problem by introducing the parameters N and P, defined as the scattering and absorption cross sections per unit volume of insulation respectively. The theoretical and experimental evaluation of these parameters is complex; moreover, very little information is available below room temperature. Above room temperature, N is much larger than P, thus indicating that scattering is far more important than absorption. Assuming $P = 0$, the power q_r transmitted by radiation per unit area is

$$q_r = \frac{(T_1^4 - T_2^4)\,\sigma}{1/\epsilon_1 + 1/\epsilon_2 - 1 + ND}$$

where σ is the Stefan-Boltzman constant and ϵ the total hemispherical emissivity. Indexes 1 and 2 are referred to the opposite surfaces bounding the slab. If $P \neq 0$, the expressions are far more complex. Generally speaking, P and N are not constant but are functions of the temperature and of the mean fiber diameter. Larkin and Churchill observed that the highest value of N will correspond to a mean fiber diameter near to 5μm, while q_r is proportional to the second rather than to the third power of the mean temperature, owing to the dependence of N and P on the temperature.

Defining the coefficient λ_r due to radiation heat transfer, dimensionally equivalent to a thermal conductivity, as

$$\lambda_r = \frac{q_r D}{T_1 - T_2}$$

if $D \gg (1/\epsilon_1 + 1/\epsilon_2 - 1)/N$, then $\lambda_r \simeq \sigma (T_1^2+T_2^2)(T_1+T_2)/N$. If absorption is dominant with respect to scattering

$$\lambda_r \simeq \sigma (T_1^2 + T_2^2)(T_1 + T_2)/P \tag{6}$$

This equation, proposed in a similar form also by Bankvall [8], seems to be suitable for expressing radiation heat transfer at low temperatures, as glass total hemispherical emissivity tends to unity in this range. Only experimental analysis will give a correct answer, but for RBGFB's used as SRM's, as bulk density is relatively high, λ_r is only few percentage points of the total apparent thermal conductivity.

To evaluate the order of magnitude of λ_r, glass fibers were considered oriented along a single direction and in contact with each other to form nontransparent layers whose thickness is the fiber diameter. If Γ is the volume fraction of glass and s is the fiber diameter, the number n of these layers per unit volume is derived as follows

$$n = \frac{4\Gamma}{\pi s}$$

Assuming $\epsilon = 1$ for the glass fibers and for the bounding surfaces of the slab, λ_r is defined as follows

$$\lambda_r = \frac{\sigma (T_1^2 + T_2^2)(T_1 + T_2)}{n + 1} \tag{7}$$

and is the largest possible value if absorption is dominant.

Mass Transfer

Mass transfer phenomena are due to adsorption and desorption of water by the solid matrix of the RBGFB. In thermal conductivity measurements on RBGFB, the gas phase is air taken from the laboratory, and therefore, around room temperature, relative humidity ϕ should be lower than 70 percent (as the dewpoint should be at least 5 K under the cold plate temperature). But the value of ϕ is not far from 70 percent, as the low relative humidity requires cold surfaces much colder than the cold plate, and this means expensive equipment. When relative humidity ranges from 30 to 70 percent, capillary phenomena are prevailing. As clearly pointed out by Marechal [9], vapor pressure in a capillary is defined by the Kelvin law, and therefore content is nearly proportional to relative humidity.

The result is that apparent thermal conductivity is probably affected by the condensation of water when it takes place between the contact surfaces of each fiber, as condensed water reduces contact resistance. It should be pointed out that thermal conductivity of the gas phase decreases with an increase of relative humidity, while the conductivity in the solid matrix increases with relative humidity. Moreover, water adsorption and desorption phenomena are accompanied by latent heat exchanges, which may be very slow, especially below 0°C. These exchanges may create difficulties in establishing steady-state conditions.

Finally, adsorbed water becomes ice below 0°C, thus slightly changing heat-transfer properties in the solid matrix.

An accurate analytical representation of all these phenomena is complex and unnecessary, as water content generally is only a few percentage points by weight, but the operator who uses RBGFB's as SRM's should be aware of these problems in order to avoid unacceptable measurement errors.

Heat-Transfer Models

The purpose of heat-transfer models is that of allowing the prediction of apparent thermal conductivity of RBGFB's from the knowledge of few easily determined parameters. A model may be considered useful when

1. computed and measured values agree,
2. theoretical assumptions describe satisfactorily physical heat-transfer mechanisms,
3. analytical expressions are not too complex, and when
4. parameters required are easily measurable.

A few simple models are now illustrated; in all these models, $k = \lambda'/\lambda_g$, with λ' the thermal conductivity of the gas phase.

Pure Parallel Model

The total heat flux through a cube of unit side is divided into a gas path of cross section $(1 - \Gamma)$ and a glass path of cross section Γ. The apparent thermal conductivity λ^* is

$$\lambda^* = \lambda' [1 - \Gamma (1 - k^{-1})] \tag{8}$$

This considers the glass fibers to be parallel to the heat flux direction.

Pure Series Model

The total heat flux through a cube of unit side crosses first a gas slab of thickness $(1 - \Gamma)$ and then a glass slab of thickness Γ. The apparent thermal conductivity λ^* is

$$\lambda^* = \lambda' \frac{1}{1 - \Gamma(1 - k)} \tag{9}$$

This considers glass fibers to be in layers like those considered in the computation of radiation.

Series and Parallel Model

In the cube of unit side, there is a glass path of cross section α in parallel with a series path where glass thickness is δ. The apparent thermal conductivity λ^* is

$$\lambda^* = \lambda' \left[\frac{\alpha}{k} + \frac{1 - \alpha}{1 - \delta(1 - k)} \right] \tag{10}$$

and hence $\Gamma = \alpha + (1 - \alpha)\,\delta$.

It is like the previous case, but some fibers are parallel to the heat flux.

Inclusions in Square Arrays

Schneider [*10*] gives account of four models of square or circular inclusions in square arrays (see Fig. 1). For square rods of side s and spacing d it is $\gamma = s/d$. Assuming in the usual cube of unit side a slab of gas of thickness $(1 - \gamma)$ in series with a glass element of side and thickness γ and a gas element of side $(1 - \gamma)$ and thickness γ

$$\lambda^* = \lambda' \frac{k - \gamma(1 - k)}{k + \gamma(1 - \gamma)(1 - k)} \tag{11}$$

and hence $\Gamma = \gamma^2$.

Assuming the elements of gas and glass in series, paralleled by a gas path with cross section $(1 - \gamma)$

$$\lambda^* = \lambda' \frac{1 - \gamma(1 - \gamma)(1 - k)}{1 - \gamma(1 - k)} \tag{12}$$

In the hypothesis of heat transfer similar to those used to derive Eq. 11, Schneider [*10*] gives an expression of λ^* for circular rods in square arrays:

$$\lambda^* = \lambda' \left\{ 1 - \gamma \left[1 + \frac{\xi}{(1 - \xi^2)^{1/2}} \ln \left(\frac{1 - (1 - \xi^2)^{1/2}}{\xi} \right) \right] \right\}^{-1}; \quad \xi^2 < 1$$

where

$\gamma = s/d$,
$\xi = (1/\gamma)k/(1-k)$, and
$\Gamma = \pi\gamma^2/4$.

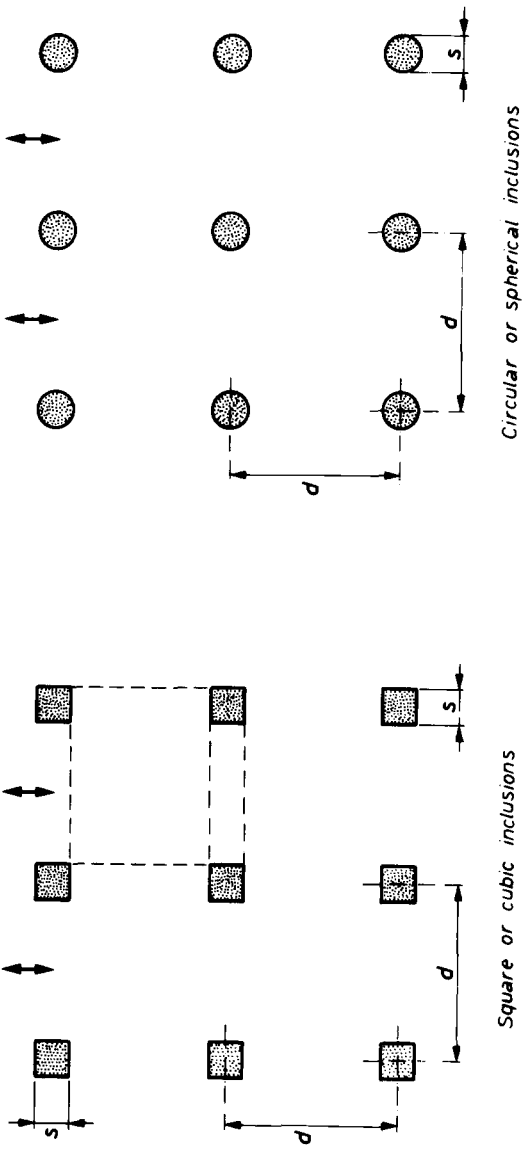

FIG. 1—*Geometrical schematization of RBGFB's to define analytical models. Arrows indicate heat flux directions.*

For the same geometrical configuration, Rayleigh [*11*] derived a series solution in 1892.

These three models are a close geometrical representation of glass fiber boards, though not taking into account random distribution of fibers in parallel planes. The actual distances d are close to the representation of Fig. 1.

A lot of work has been done to predict the thermal conductivity of, generally speaking, heterogeneous materials. Often the approach was that of considering square arrays of inclusions, as in Fig. 1, of cubic, spherical, or more complex shape; in other cases, complex distributions of composite layers were assumed. Some solutions proposed by Schneider [*10*], Gorring and Churchill [*12*], Cheng and Vachon [*13*], Hamilton and Crosser [*14*], Jefferson et al [*15*], and Zanker [*16*] were used in the computations. Expressions are more or less complex, but there is poor geometrical agreement with RBGFB or poor coincidence of computed and measured data; thus no detailed formulas are given here because there is little advantage in their use with respect to the elementary pure parallel, pure series, or series-parallel models.

Experimental Results

Experimental work cited in this paper is part of a joint research program on SRM's supported by the Bureau Communautaire de Reference (BCR), an organization of the European Economic Community; an official document with experimental data from participating laboratories will be released by BCR in 1978. Thermal conductivity data were obtained by the authors on a guarded hot-plate apparatus, while some other data were obtained in other laboratories participating in the joint research program or were released by the manufacturers of the RBGFB's.

Two different producers supplied the RBGFB's, but the manufacturing process was the same and is known as TEL. The characteristics of the two sets of specimens are the following:

	Bulk Density kg/m³	Resin Content, % by weight	Mean Fiber Diameter, μm	Average Fiber Length, m	Air Permeability, m²	Nominal Thickness, mm
Set A	121	15	5	...	...	35
Set B	89	17	4	0.01	$1.4\ 10^{-10}$	35

Apparent Thermal Conductivity

No information is available on glass properties, so that for both sets those cited in the paragraph on conduction were assumed. Thermal conductivity data were measured on horizontal air-cooled double-guarded hot plate apparatus described by De Ponte [*17*]; details on some improvements

of the apparatus are given by Bigolaro [*18*, *19*]. The accuracy of the apparatus, according to computations and interlaboratory comparisons, is 1.5 percent, but reproducibility and stability are generally better than 0.1 percent. Temperature differences across the specimens were 15 K on Set A and 10 K on Set B; in some additional tests, temperature differences were 30 K.

The Rayleigh number, even at temperature differences of 50 K, should be less than 0.015 at 300 K and less than 2.5 at 100 K and therefore well below the limits for the onset of natural convection.

Before comparing experimental data, the contribution of radiation was computed according to Eq 7, assuming the mean fiber diameters just cited: at 310 K, is $\lambda_r = 0.012\,\lambda$ * for Set A, and is $\lambda_r = 0.018\,\lambda$ * for Set B. The analysis of all models gave best results with far smaller values of λ_r in any case, with values no larger than one fourth of the computed values.

At room temperature, relative humidity influences both conduction in the gas phase and moisture adsorption, so that Set A was first tested at relative humidities below 10 percent. The humidity conditions for Set B are not well known but were estimated between 10 and 30 percent. As a consequence, all the models were employed assuming a relative humidity of 10 percent in Eq 3 or in the equivalent expressions for binary mixtures, and λ_r equal to one fourth of the value derived by Eq 7.

For pure series, pure parallel, and series-parallel models, λ_r was first subtracted from each measured value of thermal conductivity, then the values of Γ, α and δ were computed. The averages of these values were then assumed as typical of the model, and the deviations of measured data from computed values through the models are reported in Table 1 for the Set A and in Table 2 for Set B.

In all other models, the value of Γ is defined as $\Gamma = \rho_b/\rho_g$, where ρ_b is the bulk density of the RBGFB and ρ_g the density of glass.

The series model gives good agreement but Γ is overestimated. A change in glass thermal conductivity has little influence, thus pointing out that the geometrical configuration should be refined.

The parallel model is strongly erroneous, as the slopes of computed and measured thermal conductivity are different. This is due to the different dependences of glass and gas thermal conductivities on temperature. Γ is underestimated, therefore the model is in error.

Similar considerations are valid for the series-parallel model. This means that parallel paths are very small in RBGFB's. The square array model described by Eq 11 gives little positive errors. The value of λ_g has little influence: if λ_g is doubled, the increase of computed thermal conductivity is 1 percent; if λ_g is divided by two, the decrease is 2 percent. Therefore the model describes well the heat-transfer mechanism but needs some geometrical refinement. In fact, fibers are circular and not square, and, as glass fibers act like short-circuits in the heat flow paths in the gas, the

TABLE 1—*Percent deviation at indicated temperatures of measured conductivity from computed conductivity on Set A.*

Model	Temperature, K												Remarks
	107	136	165	185	205	226	247	258	269	281	292	312	
Series	0.02	0.67	0.76	0.58	0.32	0.06	−0.15	−0.25	−0.30	−0.61	−0.79	−0.29	$\Gamma = 0.223$
Parallel	−7.29	−3.94	−1.88	−0.97	−0.27	0.34	0.94	1.23	1.55	1.63	1.81	2.86	$\Gamma = 6.4 \times 10^{-3}$
Series and parallel	−6.08	−3.18	−1.44	−0.71	−0.17	0.29	0.76	0.99	1.25	1.26	1.38	2.34	$\alpha = 5.35 \times 10^{-3}$ $\delta = 4.51 \times 10^{-2}$ $\Gamma = 9.67 \times 10^{-3}$
Square array, Eq 11	1.47	2.24	2.45	2.35	2.17	1.97	1.84	1.78	1.76	1.50	1.35	1.9	$\Gamma = 0.0502$ $d = 4.46 \times 10^{-6}$m
Square array, Eq 12	17.0	17.5	17.6	17.4	17.2	16.9	16.8	16.7	16.6	16.3	16.2	16.6	$\Gamma = 0.0502$ $d = 4.46 \times 10^{-6}$m
Circular inclusions	3.09	4.16	4.63	4.68	4.65	4.60	4.60	4.62	4.68	4.51	4.47	5.21	$\Gamma = 0.0502$ $d = 3.96 \times 10^{-6}$m
Spheres	−24.6	−22.7	−21.7	−21.4	−21.2	−21.0	−20.8	−20.6	−20.5	−20.6	−20.6	−19.6	$\Gamma = 0.0502$ $d = 2.18 \times 10^{-6}$m
Square array, Eq 11 modified	−0.52	0.28	0.50	0.40	0.22	0.03	−0.11	−0.17	−0.19	−0.45	−0.60	−0.04	$\Gamma = 0.0502$ $d = 4.46 \times 10^{-6}$m

TABLE 2—*Percent deviation at indicated temperatures of measured conductivity from computed conductivity on Set B.*

Model	Temperature, K										Remarks
	105	134	163	183	203	224	245	267	290	314	
Series	0.10	0.41	0.49	0.34	0.06	−0.31	−0.38	−0.37	−0.80	0.45	$\Gamma = 0.191$
Parallel	−5.81	−3.20	−1.43	−0.66	−0.12	0.25	0.87	1.52	1.71	3.51	$\Gamma = 5.13 \times 10^{-3}$
Series and Parallel	−4.96	−2.68	−1.16	−0.52	−0.10	0.17	0.69	1.25	1.35	3.07	$\alpha = 4.40 \times 10^{-3}$ $\delta = 3.28 \times 10^{-2}$ $\Gamma = 7.54 \times 10^{-3}$
Square array, Eq 11	1.38	1.82	2.02	1.94	1.74	1.44	1.44	1.52	1.17	2.46	$\Gamma = 0.0370$ $d = 5.20 \times 10^{-6}$m
Square array, Eq 12	15.2	15.4	15.4	15.3	15.0	14.7	14.6	14.6	14.2	15.3	$\Gamma = 0.0370$ $d = 5.20 \times 10^{-6}$m
Circular inclusions	3.12	3.83	4.25	4.31	4.24	4.07	4.19	4.39	4.16	5.53	$\Gamma = 0.0370$ $d = 4.61 \times 10^{-6}$m
Spheres	−20.6	−19.3	−18.3	−18.0	−17.8	−17.8	−17.5	−17.0	−17.1	−15.2	$\Gamma = 0.0370$ $d = 2.42 \times 10^{-6}$m
Square array, Eq 11, modified	−0.25	0.20	0.41	0.33	0.13	−0.17	−0.16	−0.08	−0.44	0.89	$\Gamma = 0.0370$ $d = 5.20 \times 10^{-6}$m

side s should be slightly increased. On both sets, best results were obtained multiplying γ by 1.07. Deviations are given in the last rows of the tables.

Circular arrays should reproduce the actual RBGFB's well, but some approximations in deriving the equation give results not fully satisfactory.

Results for a model of spherical inclusions cited by Schneider [*10*] are also given in the tables, but, just as for other similar models tested, the lack of geometrical agreement involves large deviations.

Moisture Gain

Mass gains were measured by the authors in isothermal conditions between 250 and 310 K on a specimen of Set A enclosing an electrical balance loaded with the specimen in a conditioned cabinet. Equilibrium conditions were reached without hysteresis, but at low temperatures many days were required. Mass gains are referred to the standard laboratory atmosphere, as actual dry weight is not known. The plot of results in Fig. 2 points out that temperature has little influence on mass gain and that the latter is roughly proportional to relative humidity when relative humidity ranges from 10 to 80 percent.

The continuous line of Fig. 2 is the result of similar measurements made at a single temperature on a specimen of Set B by a laboratory not directly involved in the joint research program. The mass gain of Set B is similar to that of Set A at low relative humidities but is far larger at high relative humidities. Yet mass gain for both sets in normal operating conditions is always below 1 percent.

Assuming no water adsorption, the RBGFB's thermal conductivity should decrease at high relative humidities (at 310 K, a decrease of 1 percent when relative humidity goes from 0 to 50 percent according to the model), so additional experiments were made with average relative humidities within the specimen around 50 percent on Set A between 250 and 310 K. Thermal conductivity changes were not larger than 0.1 percent; therefore adsorbed water compensated for the presence of vapor in the gas phase. On Set B, which adsorbs more water than Set A, the apparent thermal conductivity increased 0.35 percent at 300 K for an increase of 40 percentage points of relative humidity.

A possible explanation could be that the small amount of water adsorbed by capillarity between the contact points of the fibers greatly decreases contact resistance, thus creating parallel paths quite absent in dry conditions, as pointed out by the models. The presence of water adsorption and desorption may be evident from Figs. 3–5. Figure 3 is a plot of thermal conductivity versus time when changing operating conditions at low temperatures. The specific humidity of the air in the cabinet enclosing the apparatus is negligible in this case, adsorption is extremely slow, and therefore the transient phase of 2 to 3 h is due only to the response time

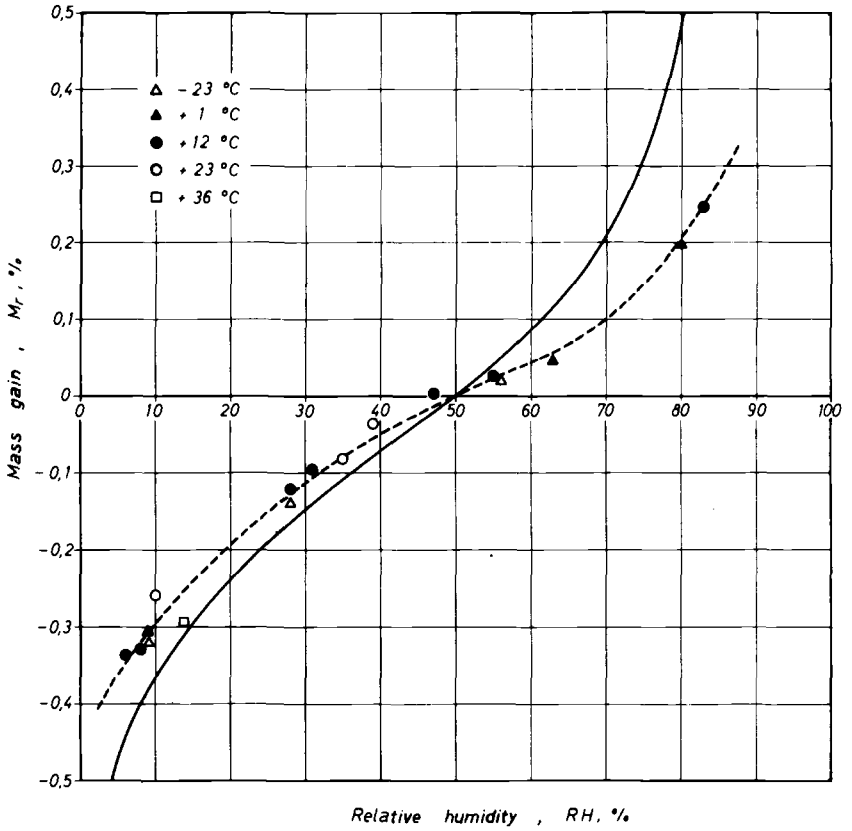

FIG. 2—*Mass gains of two RBGFB's as a function of relative humidity.*

of the apparatus. Figure 4 shows a similar change when the specific humidity is much higher and water adsorption or desorption may require some days to reach steady state. Now the time required to reach equilibrium is far exceeding the response time of the apparatus while the time to reach equilibrium is in good agreement with the transient phases in the experiments on isothermal adsorptions. Adsorption is even more evident in Fig. 5. After a transient phase, the relative humidity is suddenly increased by 10 to 20 percentage points at 7 p.m. on two subsequent days, all other conditions being constant. The apparent thermal conductivity of the RBGFB's at first decreases when relative humidity is increased, then, after many hours, increases again toward its steady-state value.

A strong risk is evident—that of assuming the minima or maxima values in the transient phase of mass transfer as steady-state values, thus making errors on the order of 1 to 2 percent that cannot be accepted in measurements on SRM's.

Also, probably again connected with water adsorption is the relative increase in the conductivity of RBGFB's (always below 1 percent) when moving below 0°C. An explanation could be the ice transition of water.

Conclusions

In all the experimental work made in the joint research program sponsored by BCR, the most stable parameter to define steady-state thermal transmission properties was thermal conductivity, despite differences in thickness and density between the different specimens of the same lot. Data dispersion was slightly larger than 1 percent, so, if this limit of accuracy should be reached, measurements on each couple of specimens are required.

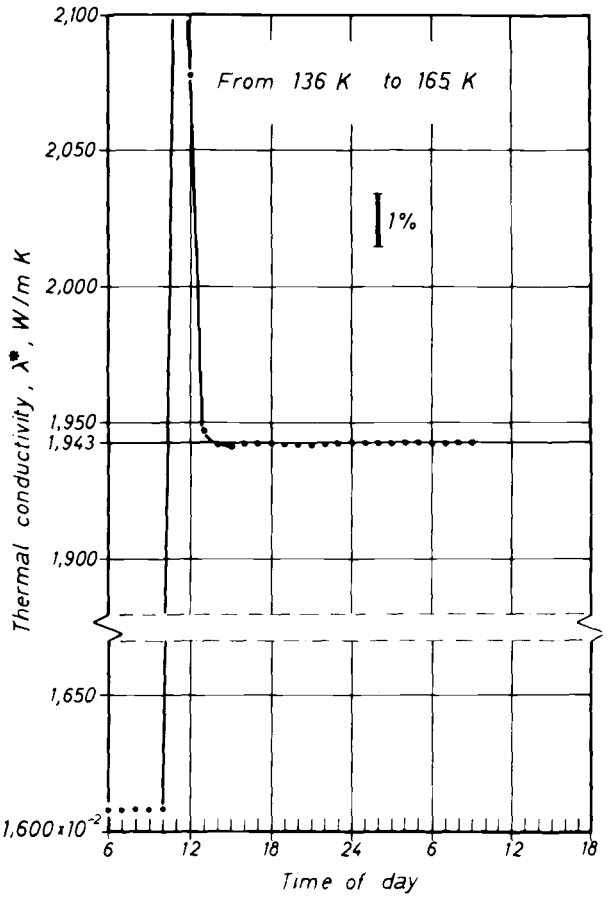

FIG. 3—*Measured thermal conductivity during a transient phase at low temperatures.*

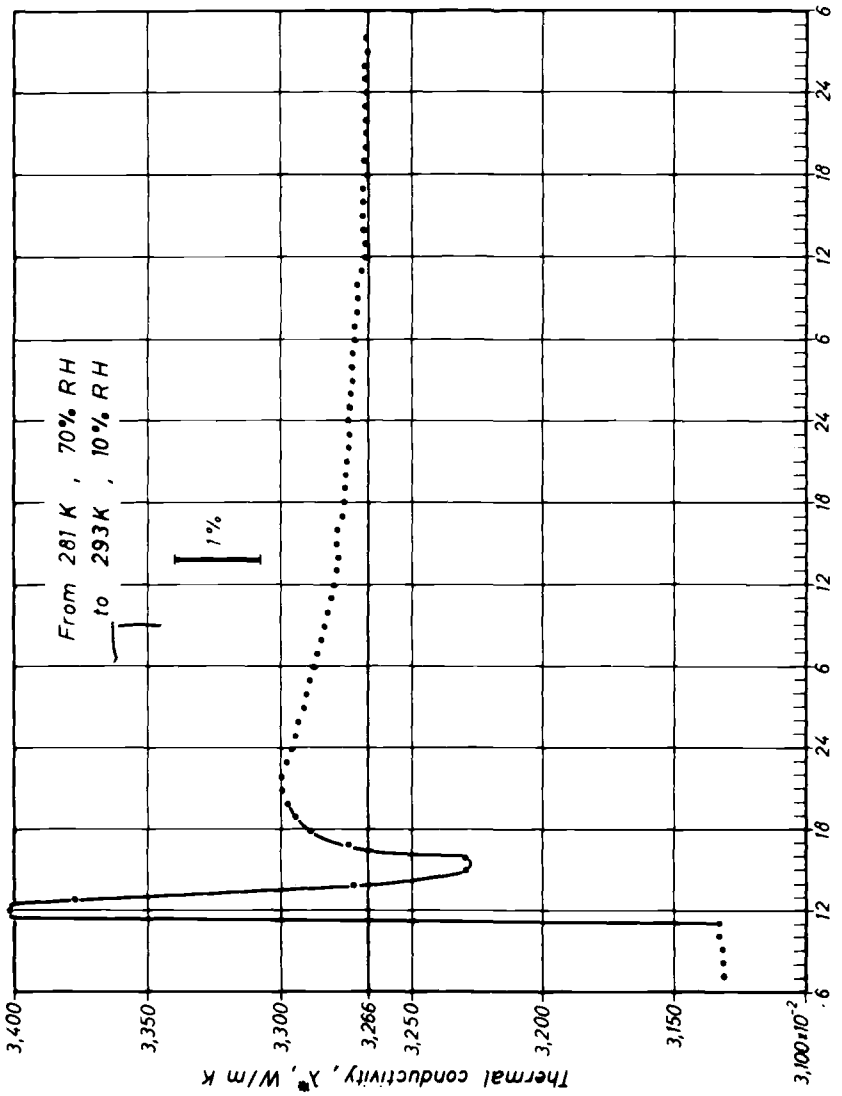

FIG. 4—*Measured thermal conductivity during a transient phase near to room temperature.*

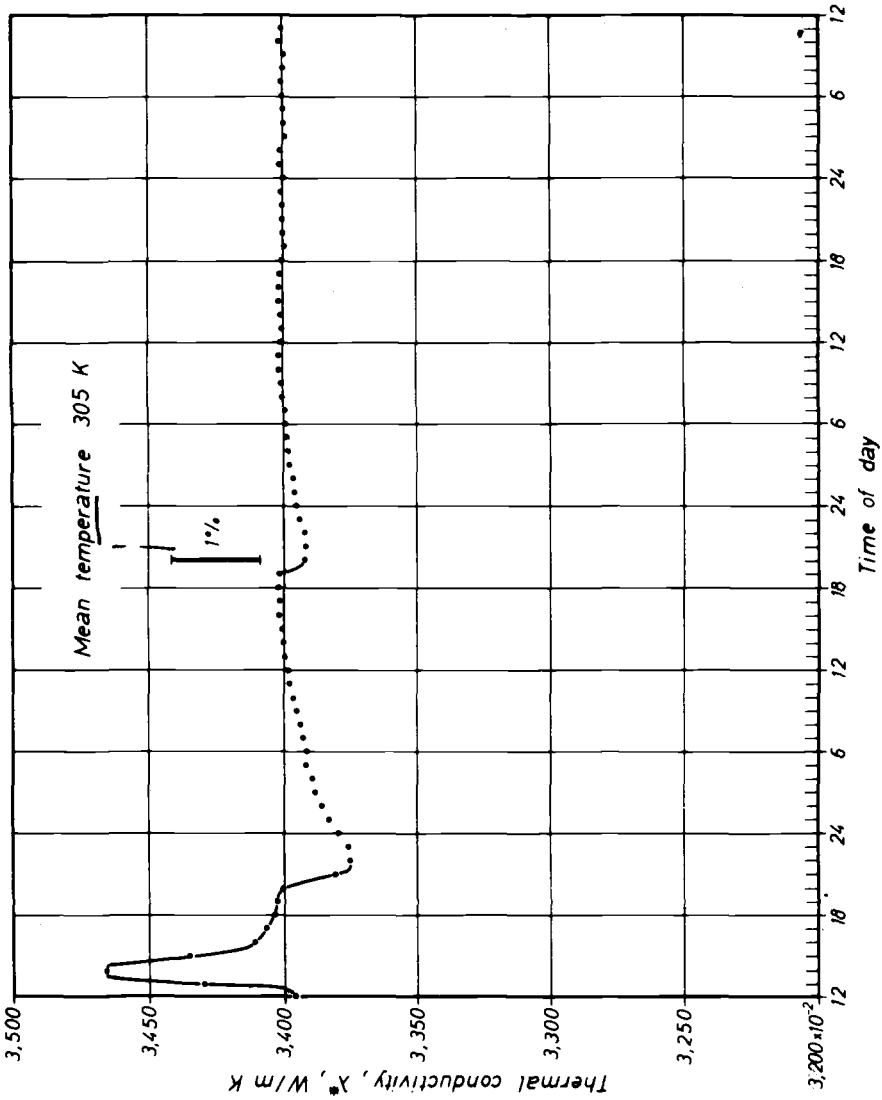

FIG. 5—*Measured thermal conductivity while changing relative humidity.*

The analysis of the model described by Eq 11 in its modified form can help in defining specifications for an RBGFB to be used as an SRM. Both k (and therefore glass thermal conductivity) and γ have little influence on the apparent thermal conductivity; therefore no particular care should be taken to specify solid matrix properties (including aging).

As the conductivity of the gas, on the contrary, directly influences λ^*, in interlaboratory comparisons gas properties should be precisely defined.

The mean fiber diameter influences radiation exchanges, according to the model, and is related to the onset of natural convection, but it was also observed that other RBGFB's with larger mean fiber diameter had larger percentages of fibers not parallel to the isothermal surfaces of the specimen. This results in a lack of geometrical agreement with the proposed model and therefore in larger values of measured thermal conductivity. Fiber orientation should therefore be specified, while an upper limit for the mean fiber diameter defines radiation contribution and the onset of natural convection; the latter property is also directly defined by airflow permeability.

The advantage of the use of high-density RBGFB as SRM's is, besides the little influence of solid matrix properties, the wide independence of thermal conductivity from temperature gradients, as there is no convection and little radiation contribution.

The disadvantages are the effects of humidity; in this respect, Set A is better, as adsorbed water compensates at least quite perfectly for vapor effects. Yet both sets require a long time to reach steady-state conditions and there is the risk of confusing relative minima or maxima as final data. Unfortunately, this problem arises just around room temperature, which is the region of first interest.

A separate analysis of the effect of relative humidity is difficult, as both gas and solid phases are influenced in a similar way; moreover, the order of magnitude of these phenomena is the same for radiation, and all start to be appreciable at the same temperatures. Yet, to correctly specify RBGFB's to be used as SRM's, particular attention should be devoted to the water adsorption characteristics to obtain best results.

References

[1] Ratcliffe, E.H., *Glass Technology*, Vol. 4, No. 4, Aug. 1963, pp. 113–128.

[2] Fournier, D., and Klarsfeld, S., in *Heat Transmission Measurements In Thermal Insulations, ASTM STP 544*, American Society for Testing and Materials, 1974, pp. 223–242.

[3] Bankvall, C.G., *Wärme und Stoffübertragung*, Vol. 7, No. 1, pp. 22–30.

[4] Bankvall, C.G. in *Heat Transmission Measurements in Thermal Insulations, ASTM STP 544*, American Society for Testing and Materials, 1974, pp. 34–48.

[5] Staicu, I.C., *Revue Generale de Thermique*, No. 185, May 1977, pp. 453–459.

[6] Larkin, B.K. and Churchill, S.W., *American Institute of Chemical Engineers Journal*, Vol. 5, No. 4, pp. 467–474.

[7] Linford, R.M.F. et al in *Heat Transmission Measurements in Thermal Insulations, ASTM STP 544*, American Society for Testing and Materials, 1974, pp. 68–84.
[8] Bankvall, C.G., *Journal of Testing and Evaluation*, Vol. 1, No. 3, May 1973, pp. 235–243.
[9] Marechal, C. in *Cahier de la Thermique*, No. 5, *L' isolation Thermique*, Institut Francais des Combustibles et de l' Energie, Vol. 1, Paris, 1975, pp. 242–272.
[10] Schneider, P.J. in *Handbook of Heat Transfer*, McGraw-Hill, 1973, pp. 3-122–3-123.
[11] Rayleigh, L., *Philosophical Magazine*, Vol. 5, No. 34, 1892, p. 481.
[12] Gorring, R.L. and Churchill, S.W., *Chemical Engineering Progress*, Vol. 57, No. 7, July 1961, pp. 53–59.
[13] Cheng, S.C. and Vachon, R.I., *International Journal of Heat Mass Transfer*, Vol. 12, 1969, pp. 249–264.
[14] Hamilton, R.L. and Crosser, O.K., *Industrial & Engineering Chemistry Fundamentals*, Vol. 1, No. 3, Aug. 1962, pp. 187–191.
[15] Jefferson, T.B. et al, *Industrial and Engineering Chemistry*, Vol. 50, No. 10, Oct. 1958, pp. 1589–1592.
[16] Zanker, A, *International Journal of Heat Mass Transfer*, Vol. 13, 1970, pp. 1359–1363.
[17] De Ponte, F. and Di Filippo, P. in *Proceedings*, 13th International Congress on Refrigeration, Washington, D.C., Vol. 1, 1971, pp. 7–14.
[18] Bigolaro, G. et al in *Proceedings*, 14th International Congress on Refrigeration, Moscow, 1975, pp. 433–440.
[19] Bigolaro, G. and De Ponte, F. in *Proceedings*, Meeting Committee B1 of the International Institute of Refrigeration, Washington, D.C., 1976, pp. 35–47.

Marion Hollingsworth, Jr.[1]

An Interlaboratory Comparison of the ASTM C 335 Pipe Insulation Test

REFERENCE: Hollingsworth, Marion, Jr., "**An Interlaboratory Comparison of the ASTM C 335 Pipe Insulation Test,**" *Thermal Transmission Measurements of Insulation, ASTM STP 660*, R. P. Tye, Ed., American Society for Testing and Materials, 1978, pp. 50–59.

ABSTRACT: An interlaboratory round-robin test program has been conducted for comparison of results from the ASTM Test for Thermal Conductivity of Pipe Insulation (C 335-69). Two specimens of glass fiber pipe insulation have been tested over a range of mean temperatures of approximately 50 to 150°C (120 to 300°F). Data from the nine laboratories reporting tests on one specimen show good agreement with an overall expected error of ± 4.2 percent. During the 7½-year test period, the specimen shows some degradation due to handling as is evident from a loss in weight and from a trend toward a slightly higher conductivity in repeat tests conducted by two laboratories. If this specimen change is considered, it is evident that the test error is approximately ± 3 percent.

Tests on the second specimen have been limited to fewer laboratories, but similar results are evident. The general conclusion is that good agreement is obtained for the temperature range investigated. It would be desirable, however, to have a standard specimen which could be used up to the temperature limit of the apparatus and which could stand the repeated handling and temperature exposures without change.

KEY WORDS: insulation, pipe, thermal conductivity, interlaboratory comparison, round-robin, glass fiber, thermal measurements

The measurement of the thermal transmission properties of cylindrical pipe insulations has always occupied a position of secondary importance relative to measurements of flat insulation specimens. A 1973 survey by ASTM Subcommittee C16.30 on Thermal Measurements listed only eight apparatuses in the United States designed for pipe insulations while a total of over 81 were suitable for flat specimens (including both guarded hot plates and heat flow meter apparatuses). The worldwide response (including the U.S. tally) was even more unbalanced—only nine pipe apparatuses and more than 128 for flat specimens. Another indication of the limited interest in pipe insulation testing is the fact that the U.S. National

[1]Scientist, Owens-Corning Fiberglas Corp., Granville, Ohio 43023.

Bureau of Standards does not possess a pipe insulation apparatus and therefore cannot supply measured specimens for calibration or standardization purposes as they do for flat specimens.

These indications of interest probably are in direct proportion to the relative amounts of insulation used. However, the volume of insulation is large and, because of the energy importance of pipe insulations, which often operate with high temperature differences, there remains a strong need for ensuring accurate thermal measurements. In the absence of help from the Bureau of Standards, the next best assessment of test precision is through an interlaboratory comparison program.

The ASTM Test for Thermal Conductivity of Pipe Insulation (C 335-69) was originally issued in 1954. During the intervening 23 years, improvements in equipment and procedures have resulted in several revisions to the method, and indeed a task group under ASTM Subcommittee C16.30 is currently considering further revision. Additionally, a working group of the new International Standards Committee on Thermal Insulation (ISO/TC163/SC1/WG3) has been formed to draft an international standard for the pipe insulation thermal test. In spite of all this activity, there has been no prior interlaboratory comparison program for the test, with the result that estimates of its precision and accuracy have remained untested.

An interlaboratory comparison for a specific test method can serve various purposes. First, it gives information on the precision and repeatability to be expected when several laboratories undertake the test. The results include what may be considered to be the normal range of variation of equipment design and construction and of procedural detail, and thus may provide judgment on the precision to be expected under normal use conditions. In effect, it helps judge whether the test itself is a good or bad method, and when good precision and repeatability are obtained it can aid substantially in promoting wide use of the method in gaining acceptance of test results.

Second, it provides each participating laboratory either with the knowledge that its results are in agreement with the majority of others or, if not, it points the way to needed improvements. This function of providing a check on the performance of an individual laboratory becomes of special importance when, as is the case with pipe insulation, there is no source of calibrated specimens from a recognized standards laboratory.

A third possible benefit, if the published results are identified with the corresponding laboratory names, is to provide a basis for potential users to choose a testing laboratory or to assess data from a particular laboratory. Since the test program reported in this paper was conducted under the auspices of an ASTM committee and since the ASTM policy of not conducting laboratory accreditation programs seems to rule out ASTM-sponsored judgments on individual laboratory performance, the data reported

herein are not identified. However, the general information given should be helpful to those establishing accreditation programs in judging the precision that can readily be achieved.

Finally, a fourth benefit of an interlaboratory comparison program is the information gained on the stability and durability of the specimen material during repeated handling, shipping, and testing.

There are several plans that may be followed in conducting an interlaboratory comparison program. If a suitable reference material is known to be acceptably uniform and stable, then several specimens may be taken from a single sample lot and each participating laboratory given one (or more) for test. Results are then comparable but must be considered in light of the known variability of the material. Another test plan is to use a single specimen that is sequentially tested by the various laboratories. In this case there is no problem with material variability (unless the different laboratories test different areas of the specimen) but results may be affected by handling damage or time-dependent aging. More complicated plans may use several specimens which are sent out following a plan statistically designed to minimize the effects of specimen variability and aging or handling changes.

Actually the tests reported in this paper were not preplanned as a complete program but occurred as the need arose. In the beginning, a specimen, previously measured by Laboratory 1, was sent to Laboratory 2 upon completion of their apparatus. The idea of extending the interchange to other laboratories gradually followed, and the same specimen was sent, in turn, either as new equipment was constructed or as laboratories with existing equipment were contacted. Later a second specimen, consisting of two standard lengths of insulation measured separately by Laboratory 1, was prepared for test on a long calibrated end apparatus, and one of these pieces was subsequently circulated to other laboratories. During the 7½-year period covered by the tests, both specimens have been retested twice by Laboratory 1 and one other retest was conducted by Laboratory 2.

Participating Laboratories

A list of participating laboratories is given in alphabetical order in Table 1. It is believed that this list includes the large majority of pipe apparatuses in North America. Method C 335 does not specify details of construction or dimensions of the apparatus, but fortunately all were of the standard nominal (3 in.) pipe size with diameter of 90 mm (3.5 in.), thus providing the interchangeability necessary for an interlaboratory comparison. Exact details of the participating apparatuses were not included in their reports. It is known that at least five are based upon the double guarded design described in the C 335 Adjunct material available from

TABLE 1—*Participants in the interlaboratory comparison for the ASTM Method C 335 pipe insulation thermal conductivity test.*

Armstrong Cork Co. Research & Development Center Lancaster, Pa. 17604 Attn: Mr. Z. Zabawsky	Jim Walter Research Corp. 10301 Ninth St., North St. Petersburg, Fla. 33702 Attn: Mr. R. G. Miller
Babcock & Wilcox R&D P.O. Box 835 Alliance, Ohio 44601 Attn: Mr. W. H. Wahle	Johns-Manville Research & Engineering Center Box 5108 Denver, Colo. 80217 Attn: Mr. C. M. Pelanne
Department of Public Works Research and Development Laboratories Riverside Drive Ottawa K1A OM2, Ont., Canada Attn: Mr. T. Y. Simizu	Ontario Hydro Research Division 800 Kipling Ave. Toronto, Ont. Canada Attn: Mr. S. J. Oda
Dynatech R/D Co. 99 Erie Street Cambridge, Mass. 02139 Attn: Mr. R. P. Tye	Ownes-Corning Fiberglas Corp. Technical Center P. O. Box 415 Granville, Ohio 43023 Attn: Mr. M. Hollingsworth
Fiberglas Canada Ltd. P.O. Box 3005 Sarnia, Ont., Canada Attn: Mr. G. M. Dalton	Thermal Conductivity Laboratory 1320 West 28th St. Minneapolis, Minn. 55408 Attn: Mr. R. M. Lander

ASTM. Of the remaining, at least three are of a single guarded end design and only one is the calibrated end apparatus also described in the C 335 Adjunct.

Specimens

Specimens used were standard 3-in. pipe insulation size of 90 mm (3.5 in.) inside diameter by 38 mm (1.5 in.) thickness by 914 mm (36 in.) length made of resin-bonded glass fibers molded to an approximate density of 100 Kg/m^3 (6.5 lb/ft^3). Each length was split longitudinally into halves. Since it was not important for the purposes of test comparison, the production history and identifying physical properties for the specimens were not obtained and it is not known whether the material was standard or experimental production. Therefore the test results are useful for comparison purposes only and are not necessarily typical of current commercial glass fiber pipe insulation.

Two specimens were used. Specimen 1 consisted of one length of insulation which was circulated to Laboratories 1 to 9, including retests by Laboratories 1 and 2. Specimen 2 originally comprised two lengths in order to provide the double-length specimen necessary for the calibrated

end apparatus of Laboratory 10. The two lengths were chosen to be nearly equal in weight, and individual tests by Laboratory 1 confirmed that their thermal properties were nearly the same. Subsequent to the tests by Laboratory 10, one length of Specimen 2 was used for other work and the remaining single length was retested twice by Laboratory 1 and then circulated to other laboratories.

Procedure

Specimens were shipped in turn to the various laboratories as arrangements were made. Accompanying instructions specified that the specimen be positioned with the longitudinal joint at the horizontal midplane and secured with three 19-mm-wide (3/4 in.) stainless steel bands. Markings on the specimen designated the top and bottom halves and gave the location of the four surface thermocouples to be held under strips of brown paper secured with masking tape. No additional jackets or covers were used. It is presumed that each laboratory followed the procedures outlined in ASTM C 335-69, which include the following requirements:

1. During each test the air surrounding the apparatus shall be still and shall not change temperature by more than ±1°C (±2°F).
2. For guarded end pipes, the guard to center gap temperature difference during each test shall not exceed 0.5 percent of the temperature drop through the specimen or 0.3°C (0.5°F), whichever is greater.
3. Four successive sets of observations of at least 30-min duration shall give thermal conductivity values differing by no more than 1 percent.
4. Pipe thermal conductivity values shall be calculated by the formula

$$\lambda_p = \frac{q \ln(r_2/r_0)}{L\, 2\pi(t_0 - t_2)} = \frac{q\, r_0 \ln(r_2/r_0)}{A_0\,(t_0 - t_2)}$$

where

λ_p = pipe thermal conductivity, W/m·K (Btu-in./h·ft²·°F),
q = measured heat flow rate, W (Btu/h),
r_0 = outer radius of pipe, m (in.),
r_2 = outer radius of specimen, m (in.),
A_0 = area of center test section—outer pipe surface, m² (ft²),
L = length of test section, m,
t_0 = temperature of pipe surface, °C (°F), and
t_2 = temperature of specimen outer surface, °C (°F).

Summary of Results

The test data reported for both specimens are presented in Fig. 1 and in Table 2. For ease of comparison, Table 3 gives smoothed thermal conductivity values at three mean temperatures. These values were obtained by a least-squares regression based upon the relation (found to fit well for low-density glass fiber insulations) that the logarithm of the thermal conductivity varies linearly with the mean temperature.

Statistical analysis of the data for Specimen 1 indicates that for the temperature range investigated of 50 to 150°C (120 to 300°F) the average

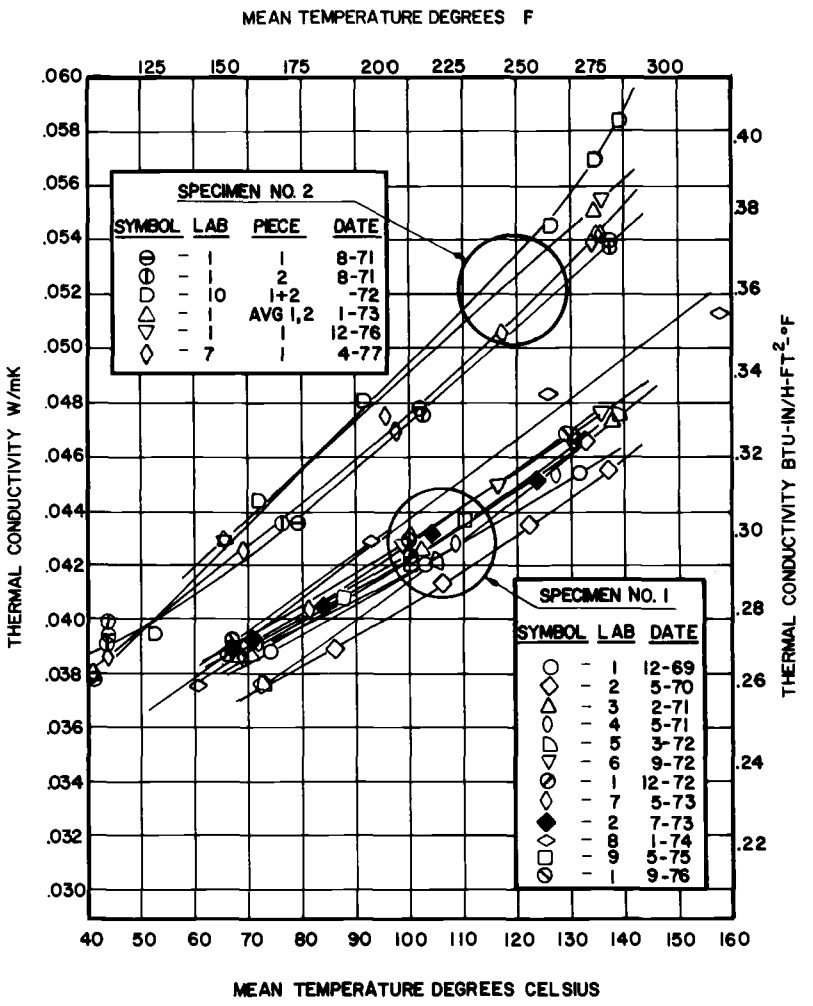

FIG. 1—*Test data for both specimens.*

TABLE 2—*Measured data.*

Piece No.	Laboratory No.	Date	Thermal Conductivity, W/m·K @ Mean Temperature, °C					
			SPECIMEN NO. 1					
...	1	12/69	0.0388 @ 74.2	0.0419 @ 103.3	0.0454 @ 131.7	...	...	...
...	2	5/70	0.0376 @ 72.9	0.0389 @ 86.4	0.0413 @ 106.4	0.0434 @ 122.3	0.0455 @ 137.1	...
...	3	2/71	0.0386 @ 71.1	0.0425 @ 104.4	0.0473 @ 137.8	...	...	...
...	4	5/71	0.0392 @ 72.2	0.0427 @ 108.9	0.0454 @ 127.4	...	...	...
...	5	3/72	0.0376 @ 72.8	0.0421 @ 105.5	0.0474 @ 139.2	...	...	...
...	6	9/72	0.0391 @ 67.4	0.0427 @ 98.7	0.0450 @ 116.7	0.0476 @ 135.8	...	...
...	1	12/72	0.0386 @ 66.9	0.0422 @ 100.1	0.0465 @ 130.9	...	...	...
...	7	5/73	0.0385 @ 69.4	0.0403 @ 81.8	0.0431 @ 100.6	0.0467 @ 131.6	...	...
...	2	7/73	0.0392 @ 71.9	0.0404 @ 84.2	0.0431 @ 104.1	0.0457 @ 123.9	0.0389 @ 69.3	...
...	8	1/74	0.0375 @ 60.9	0.0428 @ 92.7	0.0483 @ 126.1	0.0513 @ 158.0	...	...
...	9	5/75	0.0388 @ 67.7	0.0408 @ 87.7	0.0435 @ 110.3	0.0465 @ 133.2	0.0419 @ 100.7	0.0386 @ 68.0
...	1	9/76	0.0393 @ 67.3	0.0428 @ 100.0	0.0468 @ 129.8	...	...	...
			SPECIMEN NO. 2					
1	1	8/71	0.0378 @ 42.0	0.0435 @ 79.3	0.0477 @ 102.2	0.0540 @ 137.3	0.0393 @ 44.0	...
2	1	8/71	0.0399 @ 44.0	0.0435 @ 76.9	0.0475 @ 102.9	0.0537 @ 137.8	0.0391 @ 43.9	...
1+2	10	1972	0.0480 @ 91.7	0.0584 @ 139.2	0.0545 @ 126.8	0.0568 @ 134.2	0.0568 @ 134.8	0.0444 @ 72.0
		1/73	0.0395 @ 52.6	...	...	...	...	...
Avg. 1,2	1	12/76	0.0429 @ 65.9	0.0551 @ 134.9	...	...	...	...
1	1	4/77	0.0429 @ 65.7	0.0555 @ 136.0	...	...	...	...
1	7		0.0387 @ 44.1	0.0475 @ 95.8	0.0469 @ 97.6	0.0542 @ 135.8	0.0541 @ 134.9	...
			0.0505 @ 117.5	0.0425 @ 69.4	0.0382 @ 42.2	0.0538 @ 134.0	...	...

TABLE 3—*Smoothed thermal conductivity.*

Piece No.	Laboratory No.	Date	Thermal Conductivity, W/m·K @ Mean Temperature 70°C	100°C	130°C	Correlation Coefficient[a]
			SPECIMEN NO. 1			
...	1	12/69	0.0383	0.0416	0.0452	0.999
...	2	5/70	0.0371	0.0406	0.0444	0.998
...	3	2/71	0.0384	0.0421	0.0461	0.999
...	4	5/71	0.0388	0.0420	0.0455	0.991
...	5	3/72	0.0372	0.0413	0.0459	0.999
...	6	9/72	0.0394	0.0429	0.0468	0.999
...	1	12/72	0.0388	0.0424	0.0463	0.998
...	7	5/73	0.0388	0.0426	0.0468	0.992
...	2	7/73	0.0389	0.0425	0.0465	0.998
...	8	1/74	0.0391	0.0433	0.0478	0.976
...	9	5/75	0.0388	0.0422	0.0459	0.995
...	1	9/76	0.0395	0.0430	0.0467	0.998
			SPECIMEN NO. 2			
1	1	8/71	0.0424	0.0472	0.0526	0.993
2	1	8/71	0.0428	0.0473	0.0521	0.995
Avg 1,2	1	8/71	0.0426	0.0472	0.0524	...
1+2	10	1972	0.0432	0.0492	0.0559	0.993
Avg 1,2	1	1/73	0.0435	0.0485	0.0541	1.000
1	1	12/76	0.0436	0.0486	0.0543	1.000
1	7	4/77	0.0425	0.0475	0.0531	0.998

[a]Regression, logarithm of thermal conductivity linear with mean temperature.

maximum error to be expected with 95 percent confidence is 4.2 percent for the tests as conducted. This maximum error is reduced to ± 3.0 percent if calculations are made to eliminate the effect of a slight gradual increase in conductivity caused by weight loss due to repeated handling after the inner layers of binder are burned off at the higher test temperatures. It is felt that this agreement is quite good and should help dispel any fears that the method is not precise.

Discussion

A change in specimen properties was suspected when it was observed that a general upward trend in measured thermal conductivity seemed to follow the chronological order of the tests. To investigate this effect, retests were arranged by two laboratories that had performed earlier tests. The tests by Laboratory 1 show a progressive increase from the first tests in 1969 through the one in 1972 and up to the most recent one in 1976. Since this change in results might be due to changes in apparatus rather than in the specimen, retests were also run on Specimen 2, which had

been stored and remained undisturbed for the period from January 1973 until December 1976. These tests by Laboratory 1 at the beginning and end of this storage period gave almost identical results, thus strongly indicating that changes in Specimen 1 had occurred which are associated with the repeated handling, shipping, and testing. The larger change indicated by the retest on Specimen 1 by Laboratory 2 also indicates an increase in thermal conductivity of the specimen, but this may be due in part to changes in the apparatus, which was rebuilt during the period between tests.

Current recommendations for this type of pipe insulation state that some binder decomposition with resultant strength loss in the inner layers will occur when applied to pipe surfaces of 180°C (350°F) but that satisfactory performance at considerably higher temperatures is readily achieved with suitable precautions. During the testing program, the pipe temperature ranged upward to above 260°C (500°F) and the resultant binder loss in the inner surface layers became evident. Also during the program, the specimens were observed to have lost from 4 to 5 percent weight. Since the weight loss is considerably higher than can be explained by binder loss in the inner layers, it is evident that some fiber loss occurred due to the repeated installation and handling of the specimens and this loss caused the increase in thermal conductivity observed as the test program proceeded.

A statistical analysis was run on the data from Specimen 1 to obtain an estimate of the error to be expected for the test, both with and without the specimen change effect. Tests for homogeneity of variance showed that there was no statistically significant variation of error with temperature and that, at the 95 percent confidence level, the maximum error including the specimen change effect was estimated to range from ±4.6 percent at the lower temperatures to ±3.8 percent at the higher temperatures, with an average of ±4.2 percent. The effect of the specimen change was treated by adjusting the data to a common time, using the assumption that thermal conductivity increased linearly with time. Then an analysis of covariance again showed no statistically significant temperature effect and, at the 95 percent confidence level, the maximum error, if the specimen had not changed, was estimated to be ±3.2 percent at the lower temperature, ±2.7 percent at the higher temperatures, with an average of ±3.0 percent.

Conclusions and Recommendations

The results of this interlaboratory comparison program, conducted over a 7½-year period and involving 10 laboratories, indicate that the ASTM Method C 335 pipe insulation test can give results within an average

maximum expected error of about ±3 percent when used in the temperature range from 50 to 150°C (120 to 300°F).

Two recommendations are evident. One is that any future programs should be better designed to handle the specimen change effect either by search for a material more able to resist degradation due to repeated handling or by a test plan statistically designed to minimize the effect. The other recommendation is to try to find suitable specimen materials that will allow the tests to be extended to higher temperatures where heat losses are greater and guarding and other test errors more likely.

C. M. Pelanne[1]

Does the Insulation Have a Thermal Conductivity? The Revised ASTM Test Standards Require an Answer

REFERENCE: Pelanne, C. M., **"Does the Insulation Have a Thermal Conductivity? The Revised ASTM Test Standards Require an Answer,"** *Thermal Transmission Measurements of Insulation, ASTM STP 660*, R. P. Tye, Ed., American Society for Testing and Materials, 1978, pp. 60–70.

ABSTRACT: An improved understanding of the heat flow processes in thermal insulations has mandated a conceptual revision of the basic ASTM test methods [ASTM Standard Test Method for Steady-State Thermal Transmission Properties by Means of the Guarded Hot Plate (C 177-76), *ASTM Book of Standards*, Part 18, and ASTM Standard Test Method for Steady-State Thermal Transmission Properties by Means of the Heat Flow Meter (C 518-76), *ASTM Book of Standards*, Part 18] applicable to heat transmission through thermal insulations. The test methods as previously written allowed almost exclusively the measurement of thermal conductivity, a property which thermal insulations, for the most part, do not have. The author discusses the factors which have prompted the change.

KEYWORDS: test data, thermal conductivity, thermal performance, insulations, thermal, infrared radiation, thickness effects, temperature effects, heat flow mechanisms

In 1976, major conceptual revisions were introduced in the two major ASTM test methods [ASTM Standard Test Method for Steady-State Thermal Transmission Properties by Means of the Guarded Hot Plate (C 177-76), *ASTM Book of Standards*, Part 18, and ASTM Standard Test Method for Steady-State Thermal Transmission Properties by Means of the Heat Flow Meter (C 518-76), *ASTM Book of Standards*, Part 18] applicable to the measurement of the insulating property of thermal insulations. The change in philosophy which prompted these revisions was heralded in an ASTM C16.30 subcommittee position paper published in *ASTM STP 544* [1].[2] These changes will have a great impact on the insulating industry

[1]Senior research specialist, Johns-Manville Research and Development Center, P. O. Box 5108, Denver, Colo. 80217.

[2]The italic numbers in brackets refer to the list of references appended to this paper.

since they question the validity of the thermal conductivity concept when describing the principal property of insulations. In the past, the two methods of measurement allowed, almost exclusively, the measurement of thermal conductivity, a property which thermal insulations, for the most part, do not have. The revised methods are in fact more applicable to the measurement of insulations than they were in the past.

Advances in thermal insulation technology, both in the measurement techniques and improved understanding of the principles of heat flow prevailing in the insulating materials, have prompted these changes.

The recognition of the presence of these effects will require the revision of a number of material specifications.

Discussion

We all know of the general confusion resulting from differences in reported results of measurements. Much of this problem has been attributed to experimental error. It should be attributed, for the most part, to a lack of knowledge of the conditions applied to the test. In materials such as insulations, which permit the flow of heat by various modes, the influence of radiation is such that the boundaries have an influence on the results. The distance between the plates, their emittance, and their temperatures will all affect the measured value. The fact is that, if the conditions under which the test was performed are not properly stated, we cannot predict the performance in actual practical applications.

The changes in the test methods will not allow us to measure the resistive property—not necessarily the thermal conductivity—of the insulations under specified conditions, thus providing the user with data which will permit him to draw more valid conclusions on how the material will perform in actual practice.

To illustrate the reasons for this change in philosophy, let us see what the insulation is doing in the process of retarding the flow of heat. Figure 1 represents the following:

1. The radiative heat transfer between two 0.093-m^2 (1 ft^2) radiantly black infinite surfaces, one at 38°C (100°F) and the other at the temperature indicated on the graph. This does not include the convective and conductive heat flow components of heat transfer, both of which are small in comparison.

2. The heat transfer resulting from the placement of a 2.54-cm (1 in.) thickness of insulation [approximately 160 kg/m^3 (10 lb/ft^3) refractory fiber] between these two plates.

There is quite a difference. For instance, consider an 1100°C (2000°F) hot-face temperature; the radiant heat flow in this situation is over 189000

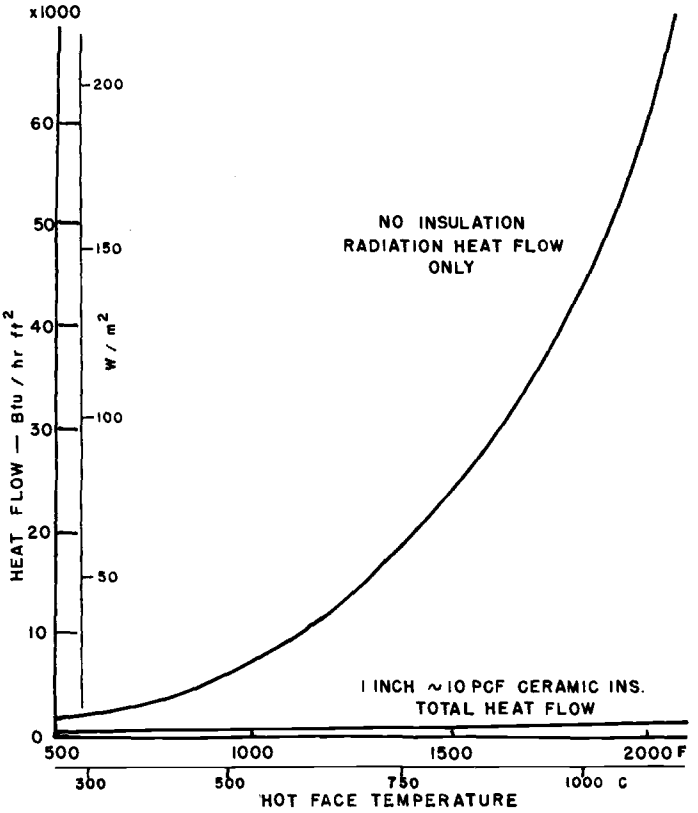

FIG. 1—*Heat flow versus hot-face temperature—cold face held at 38°C (100°F)* [*1 pcf* (*lb/ft³*)=*16.02 kg/m³*].

W/m² (60000 Btu/h/ft²) with no insulation. With insulation, the total heat flow through the insulation is only about 4700 W/m² (1500 Btu/h/ft²). Over 184 000 W/m² (58000 Btu/h/ft²) have been conserved. This is a ratio of 40 to 1.

The emphasis on radiation is strong because it is of most importance in the insulation process. Of the modes of heat transfer—electromagnetic radiation (infrared radiation), atomic or molecular motion (conduction), and mass motion (convection)—only the conductive elements, solid or gaseous, can be assessed in terms of thermal conductivity.

Radiation is the primary mode of heat transfer. The other two modes, conduction and convection, come into play only as they interfere with the primary mode. If the molecules did not absorb the radiant energy, they would not heat up to develop a difference in temperature to promote molecular and mass motion. The function of the insulation in relation to

these modes is primarily to minimize radiation transfer and minimize or eliminate convective transfer while introducing a minimum of solid conduction. Most insulations have a negligible effect on gas conduction. To obstruct the radiative transfer, we place as many radiation absorbers as possible between the temperature boundaries, without increasing the solid conduction. Since a gas is often present, we create as many small cells as possible to inhibit convection. We have only limited control over gas conduction. Thus, we have an insulating material.

Mechanisms of Heat Transfer

To examine the mechanisms of heat transfer within the insulation, we shall use the familiar term "thermal conductivity," or k, which is the simplified expression describing the combined "conductive" effects within a very complex system [2–3].

Basic Equation: Apparent Thermal Conductivity

$$k_{\text{app.}} = k_g + k_{cv} + k_s + k_{rc} + k_{rt} + k_i$$

where

$k_g = k$ of air or other gas, $\times$ $(1 - F)$, where F is the volume fraction of the solid portion of the system,
$k_{cv} = k$ of convection under specific conditions,
$k_s = k$ of solid particle-to-particle conduction,
$k_{rc} = k$ of radiation conduction (interparticle radiation),
$k_{rt} = k$ of radiation transmission (influenced by bounding surfaces), and
$k_i = k$ attributable to interaction with gas.

The "apparent thermal conductivity" of mass insulations is the sum of all (or portions) of the following mechanisms of heat transfer: thermal conductivity of air, thermal conductivity of the solid components of the insulating structure, the conductive heat transfer within the pore structure, the radiation heat transfer within the structure, and the interactions of these mechanisms.

Let us consider the relative level of these terms and how they contribute to the thermal conductivity value as you see it in the insulation data. Figure 2 shows the breakdown of these mechanisms under very specific conditions for typical glass fiber insulations [3]. This diagram demonstrates the importance of radiation in the insulating process of insulation.

In Table 1, we show how each of these mechanisms is modified by the presence of insulation or modification of the boundaries. This table gives us an opportunity to consider the influence of the emittance of the boundaries on the apparent k. Variations in apparatus plate emittances have

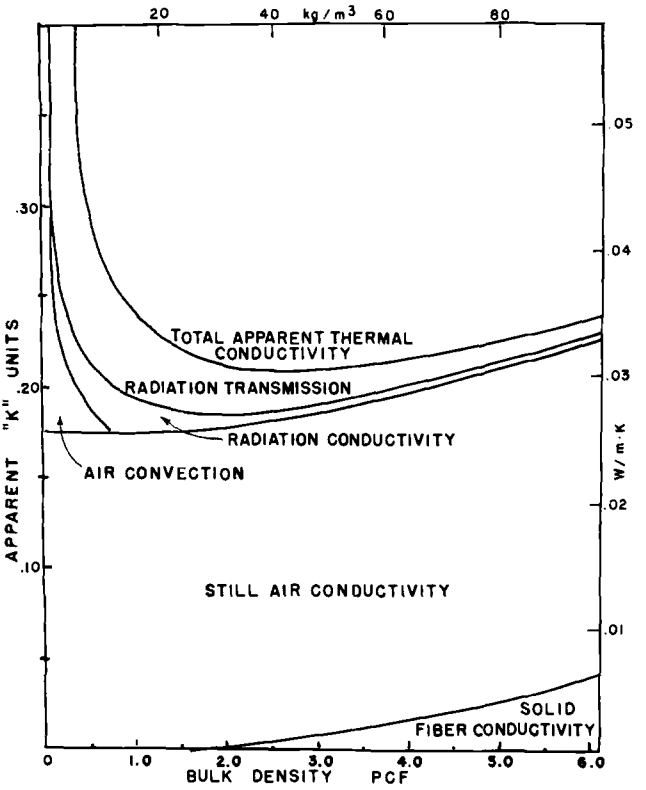

FIG. 2—*Breakdown of 'thermal conductivity" components versus density for a typical glass fiber insulation [38°C (100°F) hot face, 10°C(50°F) cold face, 25.4 mm (1.0 in.) thickness, black boundaries].*

TABLE 1—*Work of glass fiber insulation (conditions of test: upward heat flow—hot face 38°C, cold face 10°C).*

SOURCE OF HEAT FLOW	BOUNDARY EMITTANCE: BLACK SURFACE ε=0.95 — W/m·K (Btu in/hr ft² F) — NO INSULATION	BLACK SURFACE ε=0.95 — GLASS FIBER	GOLD SURFACE ε=0.08 — NO INSULATION	GOLD SURFACE ε=0.08 — GLASS FIBER
RADIATION	.152 (1.054)	.011 (.077)	.007(.046)	.004(.030)
CONDUCTION AIR	.026(.178)	.026(.177)	.026(.178)	.026 (.177)
CONDUCTION SOLID	0	.002(.016)	0	.002(.016)
CONVECTION	.063 (.435)	0	.063(.435)	0
INTERACTION		.002(.014)		.007 (.047)
TOTAL "λ "	.240 (1.667)	.041(.284)	.095(.659)	.039(.270)

been observed frequently to cause significant differences in the test results. It is mandatory that the emittance be included in the apparatus performance check.

An analysis of the modes of heat transfer through fibrous insulations at higher temperatures shows a similarity. The graphs in Fig. 3 [3] compare the corresponding functions at 260°C (500°F), 538°C (1000°F), and 816°C (1500°F). Air conduction increases from approximately 0.04 W/m·K to approximately 0.07 W/m·K, but radiation increases at a tremendously greater rate. This is because the air conduction is approximately proportional to the square root of the absolute temperature while the radiation function is proportional to T^4. Thus, in fibrous insulation as the temperature increases, radiation remains as the most important component of heat transfer. Radiation is the controlling factor in the shape of the k curve.

Temperature Difference

Now, remembering that radiation is, in insulating, our prime objective and that it is the controlling factor affecting the shape of the k curve, let us consider two specific test conditions:

1. A hot surface of 204°C (400°F) and a cold surface of 93°C (200°F). The Δt is 111°C (200°F) and the mean 148.5°C (300°F).

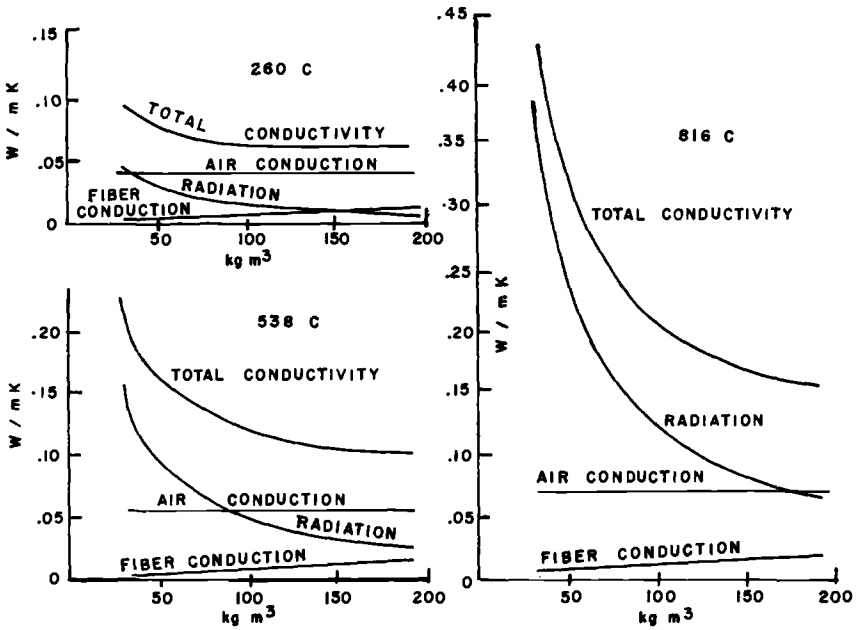

FIG. 3—*Contribution of each mode of heat transfer.*

2. A hot surface of 287°C (550°F) and a cold surface of 10°C (50°F). The Δt is 260°C (500°F) and the mean 148.5°C (300°F).

These are typical test conditions. The first is obtained with a circular guarded hot plate, the second with a square guarded hot plate with cold water cold surface plates. Both give us results at 148.5°C (300°F) mean temperature.

The radiative flux generated between the bounding surfaces is, in the first case, about 1900 W/m² (600 Btu/ft²/h), and, in the second, it is 5240 W/m² (1660 Btu/ft²h). This can result in great differences in the reported results.

It may be said that radiation is not always the controlling factor in the shape of the curve. Conduction often is. This was very true in the past when insulations were dense but today it is not economical to design a dense insulation. A comprehensive picture of the relationship between thermal conductivity and density is presented in Fig. 4.

The influence of radiation on the k versus mean temperature curve is generally reflected in a sharp upward inflection in the curve as shown in

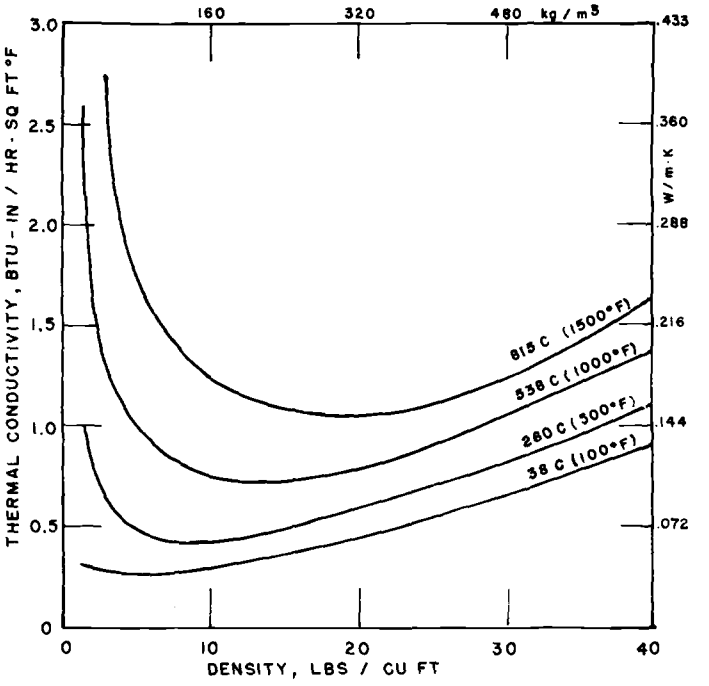

FIG. 4—*Thermal conductivity versus density.*

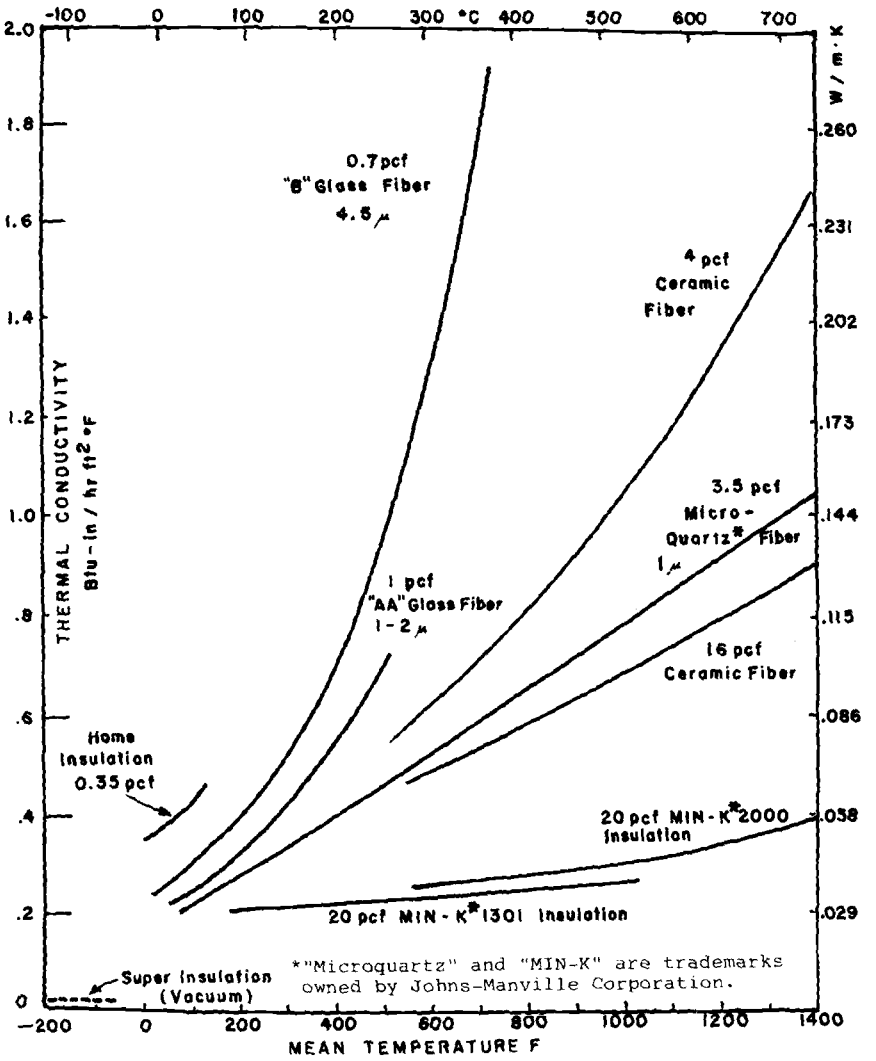

FIG. 5—Thermal conductivity relationship of various insulations over a wide temperature range [1 pcf (lb/ft³) = 16.02 kg/m³].

Fig. 5. This figure shows the relationship between various insulations over a wide temperature range. The insulations having the flattest k_a versus-temperature curve most probably have a thermal conductivity; the ones which rise sharply with increasing temperatures must be questioned. Fortunately, dense insulations, which probably have a thermal conductivity, are most frequently used for high-temperature applications.

Effect of Thickness

Since radiation is so important and the transfer of energy by radiation, between parallel plates, is basically independent of distance, it becomes apparent that the distance between the measurement plates introduces a new variable. This phenomenon, known as the "effect of thickness," has had a significant impact on the measurement of relatively low-density materials used at ambient temperatures. The phenomenon, illustrated schematically in Fig. 6, has been extensively described by Jones in 1968 [*4*], Kostyler and Komanovkaya in 1972 [*5*], Cammerer in 1973 [*6*], and more recently by Lao and Skochdopole in 1976 [*7*].

Insulations are most frequently used at thicknesses other than those at which the heat flow has been measured. When reported in terms of thermal conductivity, unless this intrinsic property can be shown to exist, the results cannot be applied directly to determine the heat loss in the application.

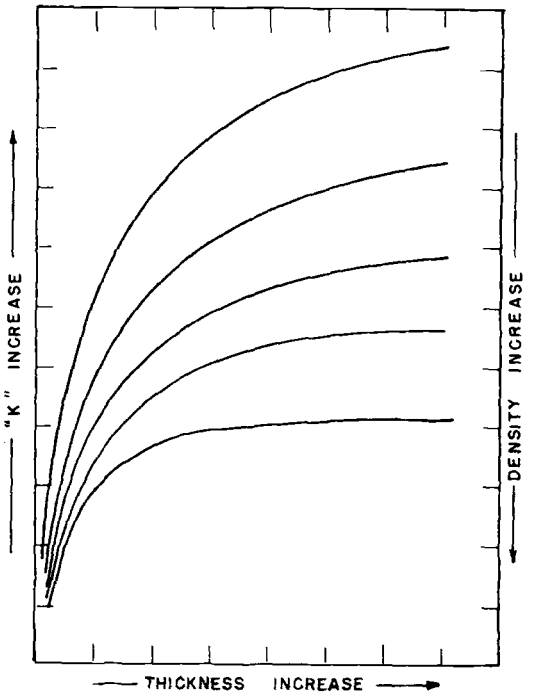

FIG. 6—*Schematic diagram of the effect of thickness.*

Conclusions and Impact

Recognition of the presence of these effects will result ultimately in the revision of a number of material specifications, which refer to these two primary test methods, when they require a thermal conductivity value to describe the insulating property of the thermal insulations, an intrinsic property which may not exist in the subject materials.

The revisions in the materials specifications and standards are mandatory, since the approach used to contend with the heat flow within a specific material is characteristic of the materials. The test specifications, ASTM C 177 and C 518, can specify only how to deal with the problem in a general way. The liberal use of the term "thermal conductivity" or k was convenient and simple; since it no longer may apply or its use is at the least questioned, in regard to insulation, it behooves the materials specification and standard writer to consider the problem with great care.

In all instances, it is most important that the way we represent insulation performance with numbers be translatable and useful in engineering design.

Earlier, in discussing the heat transfer through thermal insulations, it was mentioned that thermal conductivity, k, when describing a property of insulations, is open to theoretical questioning. We recognize that the numbers expressing heat flow resistive properties should be used with caution. The methods of measurement may not exactly represent the condition of heat flow involved in applications. The test methods are designed to represent practical average conditions. It is therefore recommended that the data and their source be understood and cautiously interpreted. This does not minimize their usefulness.

It is the recognition of these facts, through a better understanding of the heat-transfer process through insulations and the advances in the design of more efficient insulation systems, that has promoted the changes in the test methods. We are advancing the art of heat flow measurement into more of a science.

The changes in the test methods demand that one consider the property being measured with more care. In a number of instances, this will lead us to new test equipment, equipment more representative of application conditions. In the meantime, the requirement will be that test conditions be more clearly defined and reported with the results, and that an intrinsic thermal conductivity be reported only if it truly applies.

In any case, it should result in a better-informed user of the data and, hopefully, in much more reliability when data are compared: thus we can separate the poor from the good test data.

The insulation performance has not and will not change, but the goals of the user will have a better chance of being met.

References

[1] ASTM Subcommittee C16.30 in *ASTM STP 544 Heat Transmission Measurements in Thermal Insulations*, American Society for Testing and Materials, 1974.

[2] Pelanne, C. M., "Experiments on the Separation of Heat Transfer Mechanisms in Low-Density Fibrous Insulation," 8th Thermal Conductivity Conference, Purdue University, Lafayette, Ind., 7–10, Oct. 1969.

[3] Pelanne, C. M., *Journal of Thermal Insulation*, Vol. 1, July 1977, pp. 48–80.

[4] Jones, T. T., "The Effect of Thickness and Temperature on Heat Transfer Through Foamed Polymers," Seventh Conference on Thermal Conductivity, National Bureau of Standards, Washington, D.C., Sept. 1968.

[5] Kostylev, V. M. and Komarovskaya, N. V., *Inzhenerno-Fizicheskii Zhurnal*, Vol. 22, No. 5, May 1972.

[6] Cammerer, W. F., "Thermal Conductivity as a Function of the Thickness of Insulating Materials," Institut International du Froid (International Institute of Refrigeration), IIF-IIR Commission BI, Zurich, 1973–1974, pp. 189–200.

[7] Lao, B. Y. and Skochdopole, R. E., "Radiant Heat Transfer in Plastic Foams," Society of the Plastics Industry, 4th International Cellular Plastic Conference, Montreal, Canada, 15–19 Nov. 1976.

Materials and Structures

C. G. Bankvall[1]

Natural Convective Heat Transfer in Permeable Insulation

REFERENCE: Bankvall, C. G., **"Natural Convective Heat Transfer in Permeable Insulation,"** *Thermal Transmission Measurements of Insulation, ASTM STP 660*, R. P. Tye, Ed., American Society for Testing and Materials, 1978, pp. 73–81.

ABSTRACT: This paper describes the natural convective heat transfer in permeable insulation. Equations and results are given to calculate the influence from natural convection upon the heat transfer in insulated structures.

KEY WORDS: heat transfer, thermal insulation, permeability, natural convection, thermal conductivity

Most highly insulating materials are porous; that is, they usually contain large amounts of air or other gas. The pore system can be closed, as in many cellular plastics, or open, as in mineral wool. The mechanisms of heat transfer in a porous material are: conduction in solid phase constituting the insulation, radiation within the material, and conduction due to the gas confined in the insulation.[2] In an open-pore material like mineral wool, the transport of heat can be further increased by natural or free convection. In this paper it is assumed that there is no influence from forced convection and that the whole space is filled with insulation. The problems of forced convection and gaps and air spaces around the insulation are dealt with in a subsequent study.[3]

Permeability

Natural or free convection can be considered as the heat transfer by flow of fluid due to the interaction between the field of gravity and tem-

[1]Doctor of engineering, Docent, Statens Provningsanstalt, Swedish National Testing Institute, S-501 15 Borås, Sweden.

[2]Bankvall, C. G., "Heat Transfer in Fibrous Materials," *Journal of Testing and Evaluation*, American Society for Testing and Materials, May 1973, p. 235.

[3]Bankvall, C. G., this publication, pp. 409–425.

perature-induced density variations in the fluid. In a space insulated with porous material, the resistance to airflow will increase as compared with the air space. The deformation of the temperature field due to gas flow will consequently be less pronounced.

The mechanisms of flow processes through porous media are complicated. Equations used are therefore generally semi-empirical. The basic equation is that of Darcy. In cases of viscous streamline or laminar flow, and if compressibility can be ignored, this equation can be written in the following form

$$u = \frac{Q}{A} = -\frac{B_o}{\eta} \cdot \frac{\partial p}{\partial x} \tag{1}$$

where

u = apparent linear flow rate, m/s,
Q = volume flow (m^3/s) across the cross-sectional area A, m^2,
η = dynamic viscosity, Ns/m^2,
B_0 = specific permeability coefficient, m^2, and
$\partial p/\partial x$ = pressure gradient governing the flow, Pa/m.

The specific permeability can be regarded as the fluid conductivity of the porous material, and the value of B_0 is determined by the structure of the material. From the defining equation it is seen that B_0 has dimensions of length squared (m^2) and it is roughly a measure of the mean square pore diameter of the material. In a unisotropic porous material the permeability will have different values in different directions. In the mineral-wool insulation, the fibers are generally oriented randomly in parallel fiber planes. The permeability coefficient in two directions can therefore be assumed to be the same and the principal directions of interest are $B_\perp$ and $B_\parallel$ as is shown in Fig. 1.[4]

Vertical Space

The natural convection in the vertical insulated space can be solved theoretically for stationary flow in two dimensions.[5] The situation is defined in Fig 2. The solution will have the general form

$$Nu = f\,[Ra_0,\ h/d,\ \text{BOUND}] \tag{2}$$

[4]Bankvall, C. G. "Natural Convective Heat Transfer in Insulated Structures," Lund Institute of Technology, Report 38, 1972.

[5]Bankvall, C. G. "Natural Convection in Vertical Permeable Space," *Wärme- und Stoffübertragung*, Vol. 7, 1974.

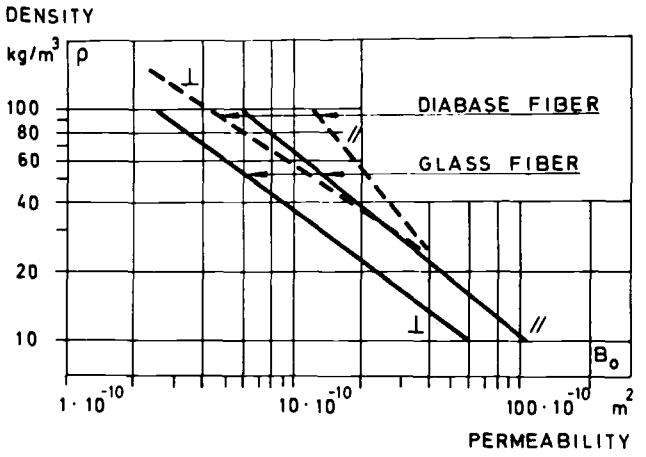

FIG. 1—*Experimental specific permeability values for different mineral-wool densities.*

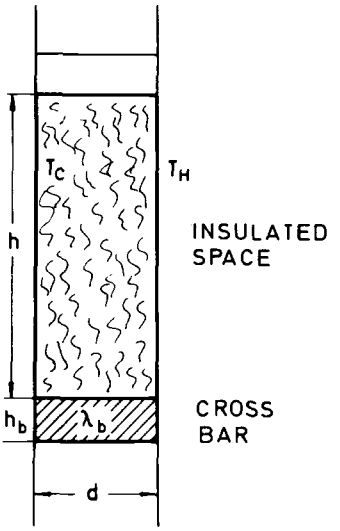

FIG. 2—*Vertical permeable space.*

where
Nu is the Nusselt number and is defined by

$$Nu = \frac{\lambda_{cv}}{\lambda_o} \tag{3}$$

where
λ_o (W/m · K) is the thermal conductivity of the material when no convection

is present. λ_{cr} denotes the effective thermal conductivity of the material with convective flow.

The modified Rayleigh number is defined by

$$Ra_0 = \frac{g \times \Delta T \times d \times B_0 \times (\rho C_p)_f}{\nu \times \lambda_0 \times T_m} \tag{4}$$

where

g = gravitational acceleration,
$\Delta T, T_m$ = temperature difference and mean temperature, respectively, K,
$(\rho C_p)_f$ = heat capacity of the fluid, and
ν = kinematic viscosity, m^2s.

This can also be written

$$Ra_0 = C_{air,0} \frac{d \times \Delta T \times B_0}{\lambda_0} \tag{5}$$

where

$$C_{air,0} = \frac{g \times \rho C_p}{\nu \times T_m} \tag{6}$$

The coefficient $C_{air,0}$ depends solely upon the air, and varies with the mean temperature, as is shown in Fig. 3.

Referring to Eq 2, *h/d* and BOUND indicate that the aspect ratio and the relevant boundary conditions will be the other influencing factors.

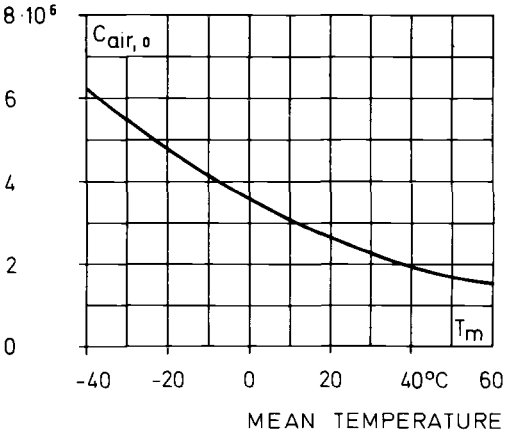

FIG. 3—*Coefficient for calculation of* Ra_0*-value for permeable space.*

The influence of the aspect ratio *h/d* and the modified Rayleigh number on the convective heat transfer in the space is calculated in Fig. 4 for insulated horizontal boundaries. As could be expected, it is found that the heat transfer decreases as the aspect ratio increases. This phenomenon is explained by the convective flow from one vertical side to the other at the top and at the bottom of the space. In a space with large height, this end-region flow will influence a comparatively small part of the total space.

If the aspect ratio, on the other hand, decreases below about 1, the convective flow will be restricted and the convective heat transfer will diminish again (footnote 5). Theoretically the aspect ratio is the height-thickness ratio of the space. The actual convective flow path in a permeable insulation may, however, give another aspect ratio. In order to calculate the convective heat transfer, the actual aspect ratio must, of course, be used.

Previously, the horizontal boundaries have been considered as perfectly insulating. This has been done because this is the situation where the convective flow most influences the heat transfer. As the conductivity of the horizontal boundaries increases, the temperature field at the boundaries will restrict the deformation of the temperature field in the insulated space and reduce the convective flow. This is illustrated in Fig. 5, where the *Nu*-value is shown for a given Ra_0-value as a function of the ratio between the thermal conductivity in the insulation and the horizontal crossbars. The size of the insulated space and the crossbars is specified in the figure.

The vertical boundaries have thus far been considered as having constant temperature. In many practical cases, this is not the situation. In Figs. 6 and 7 the Nusselt number is shown when the vertical temperatures

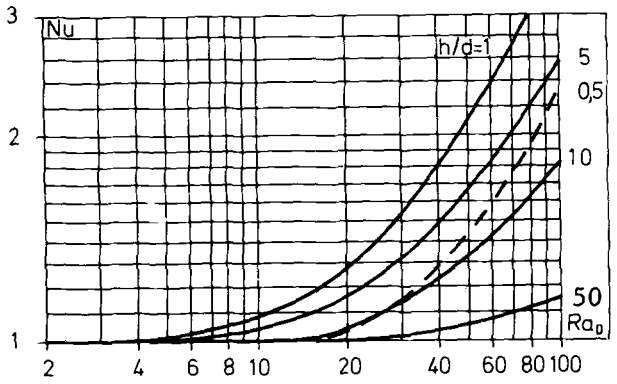

FIG. 4—*Natural convective heat transfer in permeable space with isothermal vertical and insulated horizontal boundaries.*

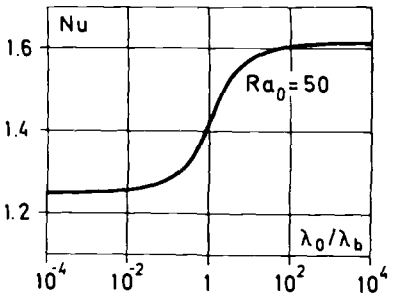

FIG. 5—*Influence of thermal conductivity ratio upon the convective heat transfer in a vertical structure (0.5 by 0.10 m insulated space and 0.05 by 0.10 m crossbar).*

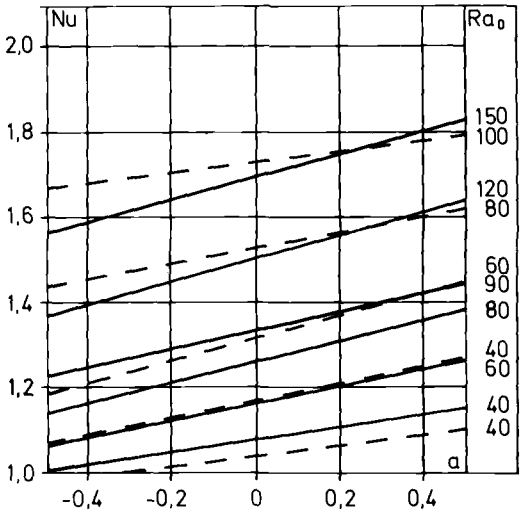

FIG. 6—Nu-*values at vertical temperatures* T(Y) = T + a × ΔT (y/h − *0.5) and for different* Ra_0 *and* h/d *values. Conductive horizontal boundaries:*--- h/d = *5;* ——— h/d = *10.*

vary linearly over the height of the space. The temperatures at the height y are

$$T_H(Y) = T_H + a \times \Delta T \times \left(\frac{y}{h} - \frac{1}{2}\right)$$

$$T_C(Y) = T_C + a \times \Delta T \times \left(\frac{y}{h} - \frac{1}{2}\right)$$

where a is given in the figures.

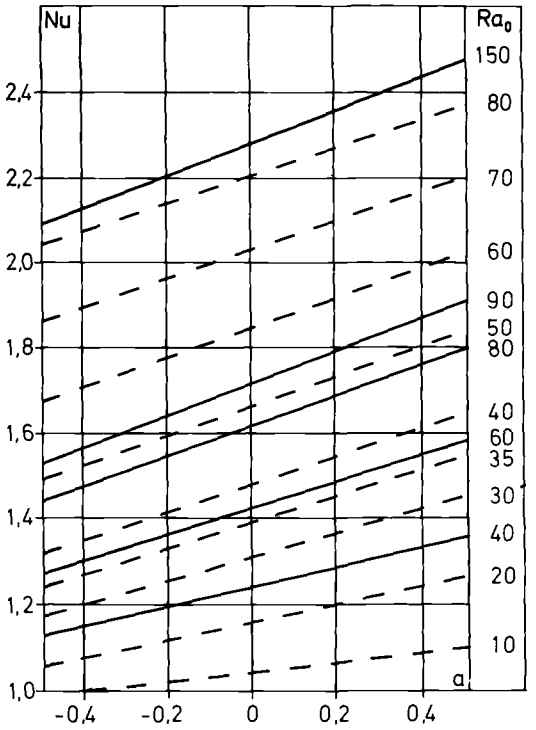

FIG. 7—Nu-*values at vertical temperatures* T(Y) = T + a × ΔT (y/h − *0.5) and for different* Ra_0 *and* h/d *values. Insulated horizontal boundaries:*--- h/d = *5;* ——— h/d = *10.*

Figure 6 shows the situation with conductive horizontal boundaries and Fig. 7 with insulated horizontal boundaries. The variation in the Nusselt number due to variation in vertical boundary temperature can be approximated as a straight line for the investigated Ra_0 and h/d values.

From the foregoing, it can generally be stated that the temperature boundary conditions will increase or decrease the convective flow and heat transfer in the space, depending upon whether they restrict the convective flow deformation of the temperature field or not. This is actually self-evident.

Horizontal Space

In the previous section the natural convection in the vertical insulated space was treated in some detail. It is quite possible to calculate the convective heat transfer in the horizontal permeable space in the same way, and analytical and numerical calculations are available in the liter-

ature. The conditions of convection are also well established experimentally. This situation is illustrated in Fig. 8 (footnote 4).

It has been found that there exists a critical modified Rayleigh number value above which natural convection will be present. The criterion for natural convection in horizontal insulated space is

$$Ra_0 = C_{\text{air},o} \frac{h \times \Delta T \times B_0}{\lambda_0} > 4\pi^2 \tag{9}$$

The coefficient $C_{\text{air},o}$ is given in Fig. 3 for different mean temperatures.

The convective flow in the horizontal permeable space is phenomenologically slightly different from that in the vertical space. The important influencing factors in the horizontal case are included in the Ra_0-value.

Summary

The natural convective heat transfer in a fully insulated space is governed by the modified Rayleigh number, Ra_0, the aspect ratio, h/d, and the boundary conditions. The Ra_0-value can be calculated from the equations given earlier. The influence of boundary conditions and aspect ratio can be estimated from the presented results.

In the case of the horizontal space, a critical Ra_0-value $= 4\pi^2$ exists. If only normal-building physical applications are considered, the temperature on the warm side can be assumed to be 20°C and on the cold side it is seldom below −20°C. In Fig. 9 the minimal specific permeability values necessary to exceed the critical Ra_0-value at $\Delta T = 40$°C and T_m

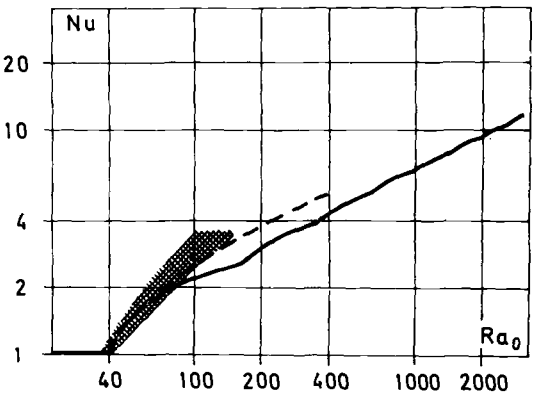

FIG. 8—*Convective heat transfer in horizontal permeable space. Comparison between analytical results* (——), *numerical calculation* (- -), *and experimental results* (*marked area*).

= 0°C are given as a solid line for different λ_0-values and $h = 0.30$ m. This figure gives an indication of what the conditions have to be to induce natural convective heat transfer in the horizontal space.

In the vertical permeable space, the situation is slightly more complicated, since both aspect ratio and boundary conditions often influence the amount of natural convective heat transfer in the space. In order to investigate the implications of this under normal applications, assumptions are made similar to those in Fig. 9: $\Delta T = 40$°C, $T_m = 0$°C, and $d = 0.20$ m.

Unlike the horizontal case, no critical Ra_0-value exists in the vertical case. The condition for 5 percent natural convective heat transfer is therefore illustrated in Fig. 10 for different specific permeabilities, B_0, and thermal conductivities, λ_0. The Ra_0-value when calculating this figure was taken from Fig. 4 and is valid for those boundary conditions. The aspect ratio was chosen as 1, since this represents a situation with approximately maximal convective heat transfer.

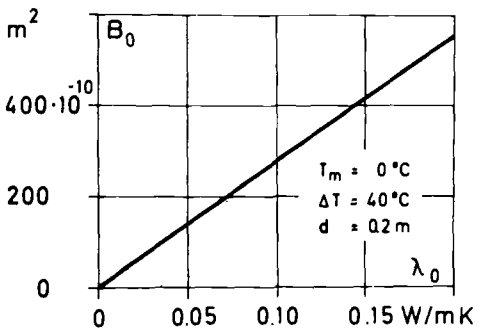

FIG. 9—*Minimal specific permeability for natural convective heat flow in horizontal insulation of different thermal conductivity.*

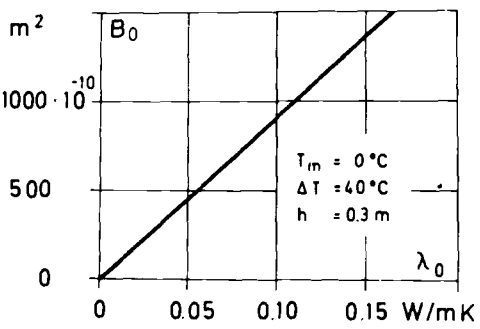

FIG. 10—*Minimal specific permeability for 5 percent natural convective heat flow in vertical insulations of different thermal conductivity* (h/d = 1).

M. Bomberg[1] *and C. J. Shirtliffe*[1]

Blown Cellulose Fiber Thermal Insulations: Part 1—Density of Cellulose Fiber Thermal Insulation in Horizontal Applications

REFERENCE: Bomberg, M. and Shirtliffe, C. J., **"Blown Cellulose Fiber Thermal Insulations: Part 1—Density of Cellulose Fiber Thermal Insulation in Horizontal Applications,"** *Thermal Transmission Measurements of Insulation, ASTM STP 660*, R. P. Tye, Ed., American Society for Testing and Materials, 1978, pp. 82–103.

ABSTRACT: This paper presents results of a study with the following objectives:

1. Determine the effects of transport and placement conditions on the initial density of the insulation.
2. Establish a standardized method for producing specimens of blown cellulose fiber insulations.
3. Investigate the factors that cause the material to settle after placement.
4. Establish a standardized method to produce settlement in the specimens comparable with those found in field studies.

A method recommended for producing settlement in the specimens consists of two procedures, one simulating settlement by impact produced on the standardized containers, and the other causing settlement under climatic cycling of the material.

KEY WORDS: cellulose fiber, thermal insulation, density, settlement, settled density, residual density, moisture effects, blown insulation, blowing, pneumatic transport of insulation, thermal conductivity

Cellulose fiber insulation consists of small tufts of fiber and minute pieces of paper mixed with fine particles of chemical additives. The thermal performance of the cellulose fiber insulation depends not only on the composition and structure of the material as produced during the milling operation, but also on the way the material is fluffed and configured while being blown into place. The blowing process produces a structural network of fibers. Both the density and the stability of the structure depend on the conditions of blowing.

[1]Research officers, National Research Council of Canada, Division of Building Research, Ottawa, Ont., Canada.

All blown fibrous insulations can be assumed to settle after being applied. The density may gradually increase until some equilibrium is reached. The density changes may be too small to be measured over the span of several months. Regardless of what actually occurs, the density at this stage is often called "settled density."

The settled density can be determined only by making measurements in the field. Results of field measurements, however, have shown a considerable scatter which can be explained only by studying the factors that have a significant effect on the density during blowing and on the subsequent settlement. Both sets of factors and the scope of the study on the relative significance of the factors are given in Tables 1 and 2.

The objective of this study was to find a method to produce specimens for testing that are representative of the material as it exists in the attics of buildings. Such a method must consist of two parts:

1. The technique for blowing specimens.
2. The method of obtaining settled density.

TABLE 1—*Variables affecting density of blown cellulose fiber insulations.*

Factors			Scope of
Element	Variable	Effect	study in the research
The material	degree of milling chemical content moisture content	- density variations: batch to batch, and bag to bag	bag to bag variability
The machine	design blower design air setting	- feeding to the blower - flow path changes - material to air ratio	3 machines with 3 blower designs studied
The hose	size, design and length	- fluffing during transport	one size and design used air pressure in the hose studied - recycling of material performed
The nozzle	geometry	- changes in air pressure and the flow of material	no nozzle used for horizontal applications
Position of the nozzle	relative to the machine relative to the specimen	- density changes due to vertical transport - impact on the material already blown	0 and 91 cm height examined 8-30 cm and 91 cm examined
The size of the container	shape and area depth	- flow pattern - impact of material on walls and material already in the container	2 shapes and 4 sizes examined 3 depths examined

TABLE 2—*Variables affecting settlement of blown cellulose fiber insulations.*

Factor	Cause	Effect	Study	Conclusion of the study
variations in air pressure	barometric pressure temperature	non-reversible deformation	air pressure variation	not significant
variation in temperature	climate	reversible thermal movements non-reversible deformation	thermal cycling	little significance
humidity variation	climate moisture accumulation in attics	adsorption, absorption and desorption, interparticle capillary forces causing movements	humidity cycling	significant
gravity	gravity field	time dependent displacement	observation in laboratory	little significance
impact	environment	particle displacement	impact (drop test)	significant

Scope of the Research

Machines Used in the Tests

A number of different designs of blowing machines are available. Most of them break the compressed material from the bags into small lumps which pass through the blower, thus producing fine particles carried by the airstream.

Three blowing machines were used during the study.

Machine 1—A Shelter Shield blowing machine produced by Diversified Insulations Inc., Hamel, Minn. It was equipped with two 10-fingered agitators in the hopper. The air setting was continuously variable and the indicator was marked at 1/8-in. (3 mm) intervals from 0 to 2 in. (5.08 cm). A 1-hp (0.75 kW) Tornado blower (Model 8805) was used on the machine.

Machine 2—An Incel Corporation blowing machine produced by the Incel Corp., Bluffton, Ind., with one agitator in a hopper. The agitator had relatively long "fingers" which forced an ample supply of insulation into the blower. This machine used a 1.5-hp (1.1 kW) blower, Model RMI 8950, produced by Robbins and Myers, Springfield, Ohio. The air setting was continuously variable but was not graduated.

Machine 3—A Thermtron blowing machine produced by Thermtron Inc., Fort Wayne, Ind. Its three agitators, each having a different rate of rotation, provided a more than adequate supply of material to the blower. The unit had twin blowers, one 0.8 hp (0.6 kW) and one 1 hp (0.75 kW). In almost all applications the 0.8-hp (0.6 kW) blower (Model HP33WS),

produced by Clement's Manufacturing Company, Chicago, Ill., was used. Unlike Machines 1 and 2, the air setting of Machine 3 was in discrete steps. There were five holes with diameters of about 1/8, 1/4, 1/2, 1, and 1¼ in. (3, 6, 13, 25, and 32 mm). Adjustment of the air setting is shown in Fig. 1. The same value of air setting, that is, 3/8 in. (9.5 mm), does not represent the same rate of airflow in each of the three machines tested.

All three machines were supplied with standard 5-cm-inside diameter corrugated plastic hose. In the preliminary series, lengths of 15 and 23 m were used; in the main testing series, a 30-m length was used. The hose was used without a nozzle for blowing into horizontal space. (For simplicity, the end of the hose is termed the nozzle in this paper.)

Materials Used in the Tests

All the 35 materials used for the tests were obtained from the regular production of manufacturers in the United States and in Canada. The fire retardant used was either aluminum sulphate or a combination of two or three of the following chemicals: aluminum sulphate, borax, boric acid,

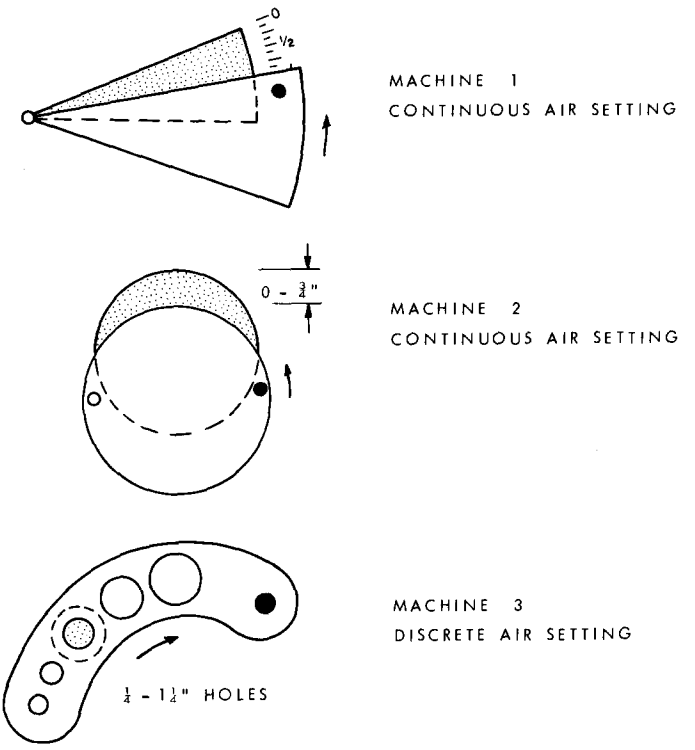

FIG. 1—*Adjustment of air setting in the three tested machines (1 in. = 25.4 mm).*

ammonium sulphate, and calcium sulphate. The formula and quantity of fire retardant are not known exactly, but in general the amount varied from 16 to over 30 percent by weight. The source of the cellulose was newsprint except in one case. The moisture content of the paper varied due to the wetness of the cellulose stock and the variable hygroscopic properties of the fire retardants. The moisture content of the products varied between 5 and 10 percent by weight.

The materials were numbered randomly from 1 to 35.

Effect of Transport and Placement Conditions on the Applied Density

Effect of Nozzle Height and Hose Length

Changes in density caused by hose length and the height of the end of the hose above the machine were checked by blowing the same material in two different ways. In the first, the hose end was 3.3 m above the machine. In the second, the end of the hose was only 91 cm above the base of the machine. In each case a 10-mm (3/8 in.) air opening was used; the end of the hose was directed horizontally. Three containers, 91 by 35 by 15 cm, were filled. The densities obtained in these two tests were 31.6 and 31.7 kg/m^3. It was judged that the height of the nozzle above the machine did not have a significant effect on the density of the material transported to the nozzle.

The effect of the hose length was checked by blowing the same material twice, that is, by recycling it. Several materials were recycled and the final density compared with the density after the first blowing. The densities of the specimens produced from the recycled materials were almost identical to the original densities. The variations were less than 1.5 percent or 0.5 kg/m^3. In each case this is well within the standard deviation of 0.64 to 1.8 kg/m^3. (It should be noted that standard deviations refer to a small specimen size.)

Effect of Specimen Size and Shape of the Container

The effect of shape and size of the container was studied to establish a controlled method for producing specimens of blown cellulose fiber insulations. Four different-size containers were used in a series of tests. Two, three, four, or six containers of each size were filled with each material tested. The material blown into the small (43 by 43 by 7.5 cm or 43 by 43 by 15 cm) containers showed greater variations in density than that blown into the larger (91 by 35 by 10 cm or 91 by 35 by 15 cm) containers. The variations were probably caused by the impact of the material on the walls of the container.

The importance of size and depth of the container is shown in Fig. 2.

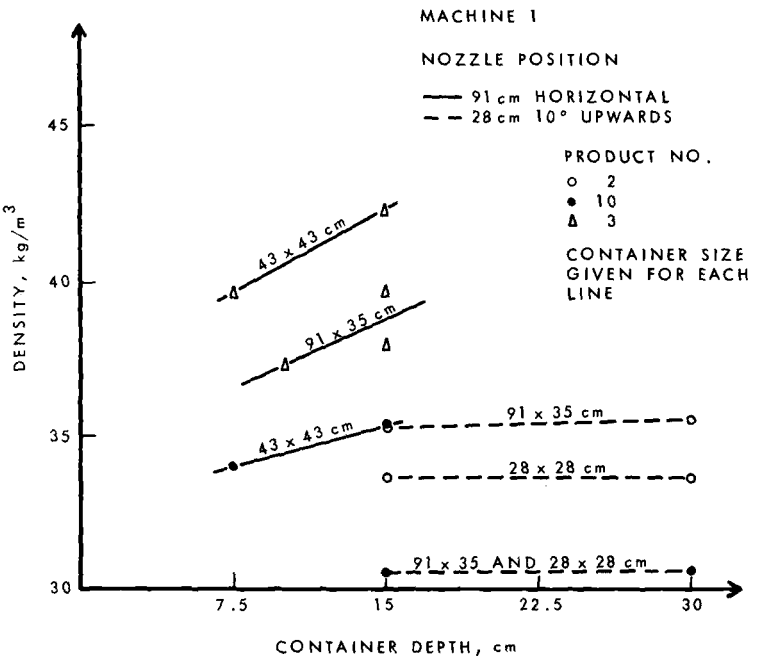

FIG. 2—*Density as affected by the thickness of the blown layer and container dimensions.*

Two different techniques of placing the insulation were used: horizontal blowing from a height of 91 cm, and 10 deg upward blowing from a height of 28 cm.

The effect of container size and depth depends on the blowing technique and structure of the tested material. For the same material when blown with the nozzle 28 cm above the bottom of the container and pointed 10 deg upward, the effect of depth became negligible. For the same material and the aforementioned blowing technique, the effect of container size was less than 5 percent.

Effect of Air Setting

Products 10, 19, and 23 were blown using Machine 2 with the nozzle pointed horizontally at a height of 91 cm and various air settings. The results are plotted in Fig. 3.

Changes in the air setting significantly affect the density of the cellulose fiber insulations. With Machine 2, the minimum density was obtained at the 38 and 51 mm (1½ and 2 in.) air settings. The density of Product 23 varied about 20 percent with air setting. The density of Product 10 varied about 15 percent but that of Product 19 varied only about 10 percent.

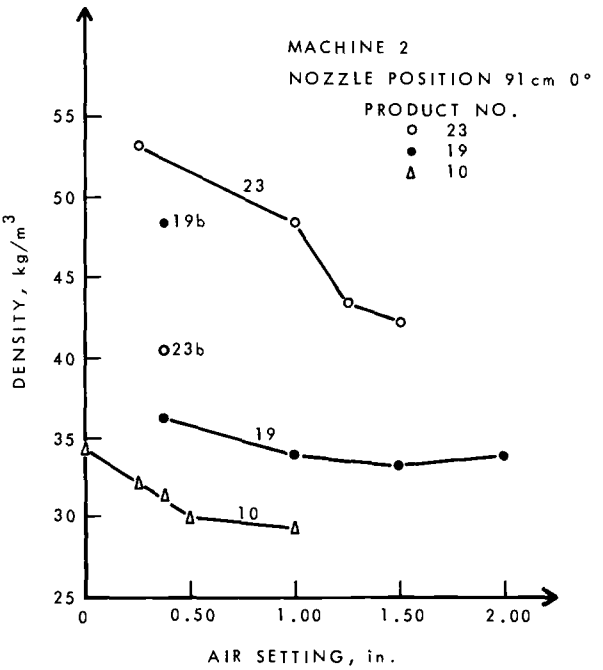

FIG. 3—*Effect of air setting on the density of specimens produced with Machine 2 blowing horizontally from a 91-cm height.*

It appears that a method specifying a selected air setting, position, and height of the nozzle will not produce minimum density for various cellulose fiber insulation products.

Combined Effect of Hose Position and Air Setting

Figure 4 illustrates the different positions of the nozzle used in a series of tests. In each case the air settings were varied. The results of the tests can be obtained from the Division of Building Research/National Research Council of Canada (DBR/NRC).

The variation in density caused by changes in the air settings when blowing downward from a height of 15 cm is shown in Fig. 5. Products 3 and 12, when blown with Machine 1, gave a minimum density at the air setting between 6 and 3 mm (¼ and ⅛ in.). The minimum density was obtained with the same machine at an air setting between 38 and 51 mm (1½ and 2 in.) when the material was blown from a height of 91 cm. The air setting cannot be considered as an independent variable. The mass of material per volume of air or the rate of mass flow of the material and the

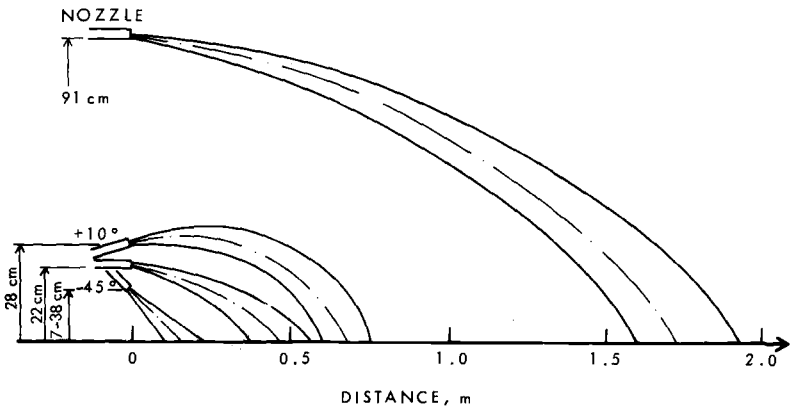

FIG. 4—*Positions of the nozzle and path of material.*

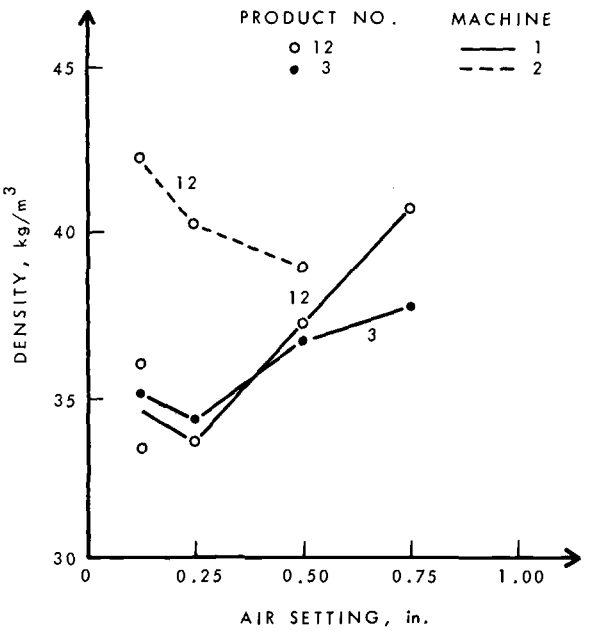

FIG. 5—*Density versus air setting when blowing downward from a 15-cm height using Machines 1 and 2.*

air velocity at the nozzle might be better indicators than the air setting, but these were not measured in the tests.

The effect of the air setting on the density can vary with the design of the machine. This is shown in Fig. 5, where it can be seen that Product

12 when blown with Machines 1 and 2 gave densities differing by several percentage points. There was a higher air velocity at the nozzle for the same air setting with Machine 2 than with Machine 1. Variations from bag to bag of the products were eliminated from most of the tested materials by recycling them two to four times. This produced a material that was more uniformly fluffed and allowed a better comparison of the machines.

The three techniques for blowing cellulose fiber, each using a range of air settings, were compared to see if the same density could be obtained on different machines. Figure 6 shows the density of three products as determined on three blowing machines and different blowing techniques. Differences of up to 20 percent occurred for the same material using different blowing machines. These differences can be significantly reduced if the optimum air setting is selected for the given machine. By a series of preliminary blowings, one can find the air setting that will give the minimum density and use it for the actual test. There are limitations to this approach, since the flow becomes nonuniform if the air setting is too low, and excessive dusting occurs if the air setting is too high. The air

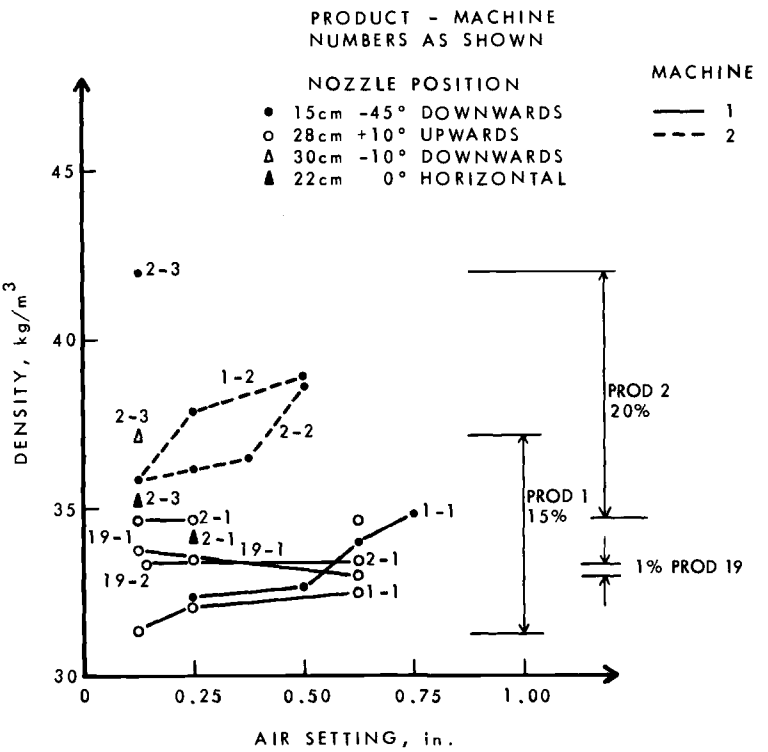

FIG. 6—*Density of Products 1, 2, and 19 determined with Machines 1, 2, and 3.*

velocity at the nozzles could not be standardized because of the limited range of adjustment on the machines. The sensitivity of the density to this velocity made it impossible to standardize the blowing technique with the nozzle pointed downward. Figure 6 shows that the density was not seriously affected by this velocity when the hose was pointed 10 deg upward.

Recommended Method for Producing Specimens of Blown Cellulose Fiber Insulations

The hose should be pointed 10 deg upward and the end of the hose kept 28 cm above the surface when blowing. This method is sufficiently reproducible to be accepted as the standard blowing technique. The air setting can be selected by conducting a series of tests with the given machine; a minimum of four settings should be used. Widely different air settings should be used first. The lowest setting should be that which will give a uniform flow of material and the highest that which will not produce excessive dust. Two intermediate air settings should then be used. The air setting which produces the minimum or near minimum density should then be chosen for the actual test. A minimum of four containers, 91 by 35 by 15 cm, should be used for the actual test.

Two products were blown with this technique, but applying three machines (the results are shown in Fig. 7). For Product 25 the greatest

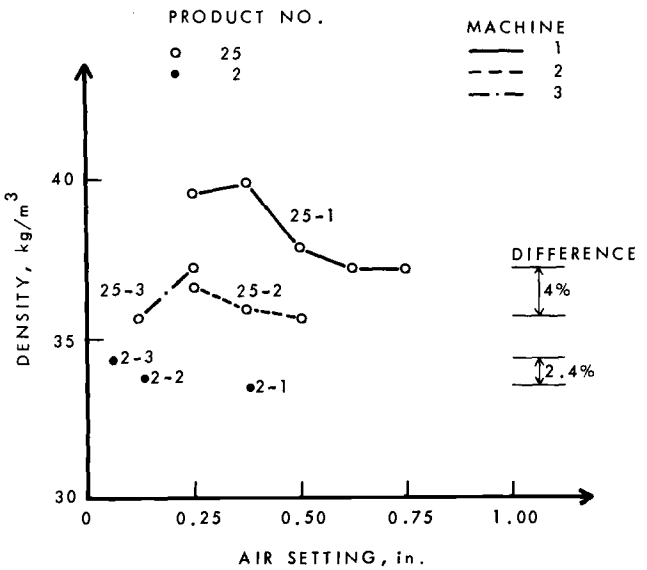

FIG. 7—*Density of Products 25 and 2 determined with recommended blowing technique on Machines 1, 2, and 3.*

variation in density using the three machines was 4 percent, for Product 2 it was only 2.4 percent. This is much less than the 20 percent difference found for the same product using any of the other blowing techniques. The standard deviation was less than 0.64 kg/m^3. This method appears to be simple and effective even though it is not the usual method of installing insulation in attics by blowing.

Reproducibility of Density Determinations

It is recommended that the proposed blowing technique have a reproducibility not worse than horizontal blowing at the 91-cm level. (Results of tests by blowing horizontal at this level are given in Table 3.) All products were manufactured from newsprint except Product 23, which was manufactured from cardboard. The standard deviation of the tests on Product 23 was about twice that determined when testing newsprint-based cellulose fiber insulations. The average standard deviation was 1.07 kg/m^3. When testing six specimens, requesting a confidence level of 95 percent, and assuming a t-distribution function, the density should fall within the confidence interval: $2 \times t \times s/\sqrt{n} = 2 \times 2.571 \times 1.07/\sqrt{6} =$ 2.24 kg/m^3. The densities of the tested materials were between 22.4 and 41.6 kg/m^3 with an average value of about 33.6 kg/m^3. These figures show that the density determined using six specimens should, with a 95 percent confidence level, fall within 6.7 percent of a true average for 33.6-kg/m^3 specimens.

An estimate of the accuracy of the proposed blowing technique (28 cm, 10 deg upward) can be made using the mean standard deviation determined from tests performed according to the proposed method. The mean standard deviation for four density measurements in containers 91 by 35 by 15 cm was 0.75 kg/m^3. Using $t = 3.182$ for four specimens, the 95 percent confidence interval becomes 2.40 kg/m^3. That is, the density determination with four specimens tested according to the new method will be practically as accurate as the determination with six specimens and horizontal blowing from a height of 91 cm. These figures reflect, primarily, only the variability of the product from bag to bag, since two to three bags of material are used for density determinations. They do not show the differences that occur between batches from different production lots. Several production lots would have to be tested to examine the product variability, but this is beyond the scope of this research.

Field Measurements on Cellulose Fiber Insulations

During March 1977 the density of Products 3, 10, and 12 was measured *in situ* after being exposed in Ottawa for two winters. The materials in two 2-story and three 1-story houses were tested. Insulation was added

TABLE 3—*Density of horizontal layer, in kilograms per cubic metre, determined for several products by horizontal blowing on 91-cm level into containers mainly 91 by 35 by 10 cm or sometimes 91 by 35 by 15 cm. Tests carried out in 1975 and 1976 at DBR/NRC.*

Product	Machine	Density in containers, kg/m^3							
		1	2	3	4	5	6	Mean	Standard Deviation
1	2	38.9	38.9	37.3	36.0	35.7	36.7	37.3	1.28
1	2	36.4	36.7	37.5	35.6	34.1	33.2	35.6	1.60
2	2	29.2	29.3	29.3	30.0	28.7	28.8	29.0	0.32
2	3	28.2	25.5	28.5	29.3	29.2	28.8	28.2	1.44
3	2	37.2	38.9	36.7	35.4	38.6	38.4	37.5	1.44
4	2	28.2	28.2	27.1	27.1	27.4	27.6	27.7	0.48
5	2	35.7	37.2	37.5	33.3	33.8	34.4	35.4	1.76
6	2	33.3	34.1	33.3	33.5	34.0	33.8	33.6	0.32
6	2	33.5	34.0	33.6	34.3	33.8	34.6	34.0	0.48
7	2	33.6	33.2	32.5	31.7	33.3	35.2	33.3	1.12
8	2	31.2	34.3	34.4	33.3	36.5	36.7	34.4	2.08
9	2	22.3	22.6	21.9	21.9	21.6	22.6	22.1	0.32
10	2	31.4	32.5	34.0	33.6	33.8	35.4	33.5	1.44
11	4	31.1	32.2	33.0	32.2	31.6	31.4	31.9	0.64
12	2	39.7	40.7	38.6	41.5	38.0	36.7	39.2	1.76
17	2	30.8	33.8	35.4	35.2	31.9	35.1	33.6	1.92
19	1	33.8	33.6	33.0	33.0	--	--	33.3	0.48
20	1	38.9	39.9	40.5	40.0	38.3	37.0	39.1	1.28
21	1	34.3	34.9	34.8	34.4	34.6	33.8	34.4	0.32
22	1	29.8	30.6	31.7	30.8	30.9	32.4	31.1	0.96
23	1	35.1	42.1	43.4	43.4	41.2	38.4	40.7	3.20
24	1	30.3	30.4	31.1	30.8	32.5	32.4	31.2	0.96

to existing glass fiber batts or loose-fill material fibers in the fall of 1975. The thickness of the layer of cellulose fiber insulation varied between 10 and 25 cm.

The density of the material was determined *in situ* in the following way:

1. After removing an adjacent section of cellulose, a metal sheet was slowly inserted horizontally under the cellulose insulation.
2. A 25 by 25 cm area of material on the metal sheet was selected and five thickness measurements were made.
3. A 25 by 25 cm box with sides 25 cm high and open top and bottom was pushed through the insulation to the metal sheet.
4. The insulation within the metal box was removed and weighed. It was then dried in a 50°C oven and reweighed.

The results of these tests are given in Table 4.

Product 10 from House 1 was packed into plastic bags and taken to the laboratory. After selecting a proper air setting, five 91 by 35 by 25 cm containers were filled, and the density measured. The mean density was 30.9 kg/m^3 and 31.1 kg/m^3 for the 15- and 25-cm-deep containers, respectively. The density of 31.1 kg/m^3 as blown in the laboratory and the density determined *in situ*, 46.9 kg/m^3, can be compared directly because

TABLE 4—*Density determined in attics of five houses in Ottawa during March 1977.*

Property Tested	House 1 product 10	House 2 product 10	House 3 product 3	House 4 product 12	House 5 product 12
mean layer thickness, cm	22.9	10.7	10.2	10.2	12.5
mean moisture content, % weight	7.0	9.9	10.2	9.8	9.3
density, kg/m^3 wet material	49.5	45.3	35.1	42.1	40.5
	47.9	40.2	35.2	38.4	45.3
	45.8	43.7	36.2	41.0	45.5
	45.8	42.0	34.8	40.8	42.8
	48.5	42.3	38.6		42.9
	46.0	43.6	40.8		51.6
	44.9	42.0	34.3		
	47.6	39.1			
mean wet density, kg/m^3	46.9	42.3	36.4	40.5	44.9
mean density of a dry material, kg/m^3	45.2	38.4	33.0	37.0	42.4
layer below the blown material	glass fiber batt	glass fiber batt	blown glass fiber	glass fiber batt	blown rockwool

1. the moisture content of material in the attics was almost the same as that of the material conditioned in the laboratory, and
2. it has been demonstrated that recycling has little effect on density.

The 51 percent apparent increase in density may not all be due to settlement, since the density at which the material was actually applied cannot be determined. Laboratory tests on the material removed from the attic showed a variation in density of 3 percent. The hose position would not cause a variation greater than 8 percent. It seems reasonable to assume that there was a settlement in the material of about 40 percent. In other houses the settlement seemed to be much lower. In House 2, Product 10 had an apparent increase in density of 36 percent. Probable settlement in House 2 was between 25 and 30 percent. The difference between the density determined in the house and the blown density obtained from the method used at DBR/NRC indicates a maximum possible settlement of the material. Settlement in the house will probably be smaller because the density at which the material was actually applied is likely to be higher than that obtained by the DBR method. In House 4 and 5, where Product 12 was used, probable settlements are in the range of 15 to 30 percent. In House 3, where Product 3 was used, there was no significant settlement. The variability in these estimations of settlement suggests a need for a study of the factors influencing the settlement of cellulose fiber insulations.

Laboratory Measurements of Moisture Content in Horizontal Layers

The ability of the material to absorb moisture was studied under laboratory conditions. The material was placed in containers located between two steady environments, one at 24°C and 50 percent relative humidity and the other at a temperature below the dew point so that internal condensation would occur close to the bottom of the container. The bottom surface of the containers was drilled with a few hundred small holes, allowing excessive moisture to pass to an underlying porous fiberboard layer.

Three series of tests were conducted with different temperature gradients. The gradients were chosen so that the zone of condensation varied in thickness. The resulting moisture contents in the condensation zones are given in Table 5.

Moisture content in the condensation zone appears to be in the range 150 to 200 percent by weight except for Product 23, which was made of cardboard. This specimen absorbed less moisture.

Water accumulated only in a very narrow layer adjacent to the lower surface of the material; the bulk of the material remained relatively dry. Moisture contents between 8 and 11 percent at the upper surface (Table 5) lie in the same range as average values determined *in situ*.

Effect of Impact and Oscillation of the Climatic Conditions on the Settlement of the Material

From January 1974 to March 1977 the thermal resistance of cellulose fiber insulations tested at DBR were determined using a 45-cm vertical guarded hot plate (GHP) apparatus. Two matched specimens, 45 cm square and either 7.5 or 15 cm thick, were placed in polyethylene-covered frames and held in a vertical position on either side of the heater plate. Settlements occurred during the testing period, which usually lasted 2 to 5 days. The amount of settlement in this period is given in Table 6. Settlement occurred in every case even though it was different for the two thicknesses. The extent of the settlement was dependent on the amount of support from the surrounding surfaces. It was approximately 4 percent for 7.5-cm specimens and 10 percent for 15-cm specimens.

TABLE 5—*Moisture contents, weight percent, in the layers adjacent to the upper and lower surfaces of the cellulose insulation exposed to the vapor condensation test.*

Prod. No.	Series 1		Prod. No.	Series 2		Series 3
	Upper	Lower		Upper	Lower	Lower
10	9.0	44.0	1	9.5	181	224
12	10.1	47.7	2	10.6	208	-
19	9.4	52.1	3	11.0	185	214
21	8.2	53.4	22	10.6	151	209
25	8.3	48.7	23	6.4	56	149

TABLE 6—*Density changes during thermal resistance testing in 45-cm GHP apparatus at DBR/NRC.*

Test Number	Product Number	Density as blown kg/m^3	Using 7.5 cm frames for R-value test			Using 15 cm frames for R-value test		
			before	after	% change	before	after	% change
1	3	37.6	39.7	42.0	5.6	42.6	48.7	14.3
2	4	26.6	27.4	28.5	4.1	29.5	32.7	10.9
3	5	35.2	38.4	39.7	3.3	36.7	42.3	15.3
4	6	34.0	34.6	36.2	4.6	36.0	41.6	15.6
5	7	33.3	33.4	36.2	6.8	39.4	42.3	7.3
6	8	34.4	33.8	36.0	6.6	35.0	40.7	16.0
7	9	22.1	23.4	23.9	2.1	24.0	24.7	2.7
8	10	33.5	34.9	35.6	1.8	34.4	38.0	10.2
					mean 4.4%			mean 9.8%

Settlement During Air Pressure Changes

A cylindrical container with a diameter of 15 cm and a height of 30 cm was filled to the depth of 18.8 cm with a part of Product 10 that was taken from House 1. The density of the material in the container was 38.4 kg/m^3.

A top was placed on the container and the pressure of the air in the cylinder was raised to about 200 Pa above atmospheric pressure. It was slowly lowered to about 200 Pa below atmospheric pressure. The pressure cycle lasted about 15 min. The cycling was continued for 2 days, then the container was opened.

The final thickness was 18.8 cm. No measurable settlement had occurred. The cycling of the air pressure is not a significant factor.

Settlement Due to Humidity Changes

Product 10 was blown into two open containers, 43 by 43 by 18 cm, at densities of 34.1 and 34.3 kg/m^3. The containers were exposed alternately to 21°C and 50 percent relative humidity and 21°C and 98 percent relative humidity in 3- or 4-day intervals for a total of two weeks. Two cycles were completed. The final densities were 39.6 and 40.2 kg/m^3—16 to 17 percent higher than at the beginning.

Product 3 was tested in the same way. The settlement was found to be 9.5 percent.

Product 2 was also blown into two frames 28 by 28 by 15 cm and two frames 28 by 28 by 30 cm. The frames were placed in a climatic chamber with a temperature of 4°C and 98 percent relative humidity. After two days the thickness was measured. The settlements were found to be 5.2 and 6.2 percent for the 15-cm-thick specimens and 7.4 and 8.6 percent for those 30 cm thick.

Humidity changes play a significant role in the settlement of the material. The thickness of the specimen appears to influence this effect. Tests should be performed on two sets of the specimens with different thicknesses.

Settlement Due to Temperature Changes

Specimens of Products 3 and 10 were placed in a set of open containers, 12 and 30 cm deep. The containers were placed in a climatic chamber where the temperature was cycled, within a 24-h period, between 4 and 21°C. The relative humidity of the air was maintained at approximately 98 percent.

The thickness of the material was measured after 5 and 8 days of exposure (Table 7). The settlement for the 12-cm-thick specimens was not measurable; for the 30-cm thickness it was 6 to 8 percent. These data are insufficient to draw conclusions. It appears, however, that temperature

variations when applied together with changes in relative humidity and the elapse of time may contribute to settlement.

Settlement Due to Impact

Two containers, 91 by 35 by 15 cm deep and each weighing about 4 kg, were filled with Product 1 and then dropped three times from a height of 15 cm onto a concrete floor. The density was measured before and after dropping. This process was continued for a total of 42 drops; the density versus the number of drops was plotted (Fig. 8) for four tests performed on the same material. The scatter in the results becomes larger with increasing number of drops. The effect of each additional drop decreases continually, as would be expected.

The densities of a number of specimens of different products were measured after three, six, and twelve drops from a 15-cm height. Figure 9 shows on a semilogarithmic plot the dependence of the average of specimen densities on the number of drops. There is no visible limit of density increase during this test.

Figure 10 shows the effect of the initial density on the dependence of density on the number of impacts. The increase in density in the drop test does not appear to depend on the initial density. A product of light density does not settle more than denser, more compacted materials. Further testing has shown that the increase of density with impact (Fig. 9) appears to be representative of all the cellulose fiber insulations blown with this type of equipment.

Material taken from House 1 and reblown in the laboratory had a mean density before settlement of 30.9 kg/m^3. When dropped 18 times from a 15-cm height, the density reached 36.8 kg/m^3. This density was still far less than the in-place density of 46.9 kg/m^3. It appears that it is not practical to require the drop test alone to produce as much settlement as is found *in situ*.

TABLE 7—*Effect of temperature cycling between 4 and 21°C with constant relative humidity at 98 percent relative humidity on settlement of cellulose fiber blown insulation.*

Container depth, cm	Product	% change after 5 days	% change after 8 days
10	3	0	0
	10	0	0
20	3	0	1
	10	1	4
30	3	5	6
	10	6	8

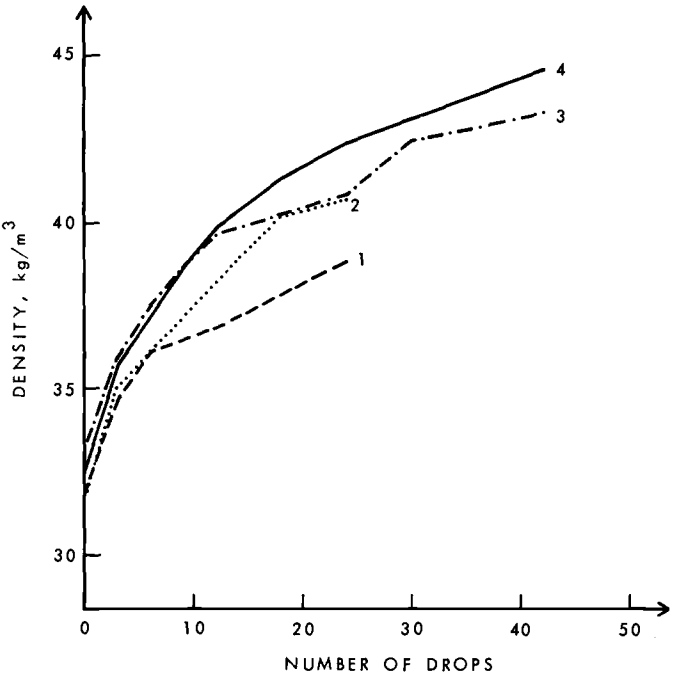

FIG. 8—*Density of Product 1 versus number of drops; four containers of material tested.*

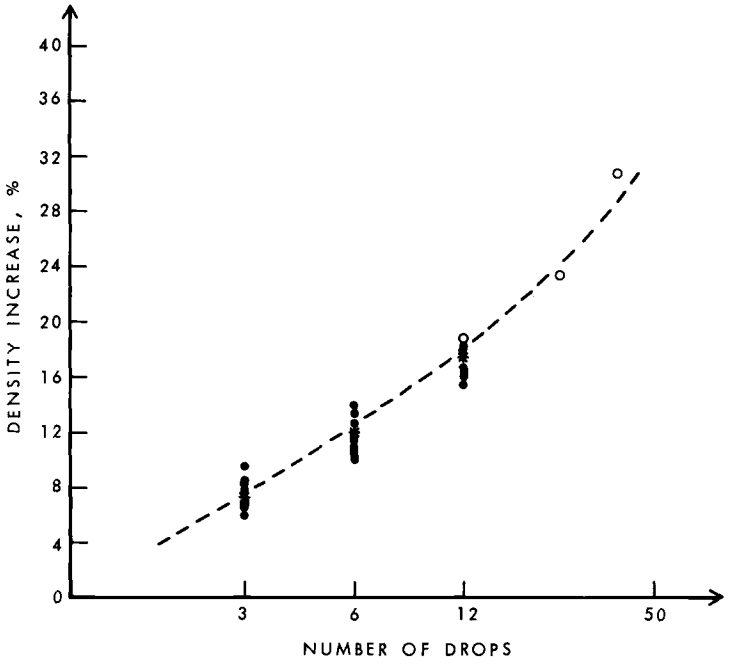

FIG. 9—*Increase in density due to drop test.*

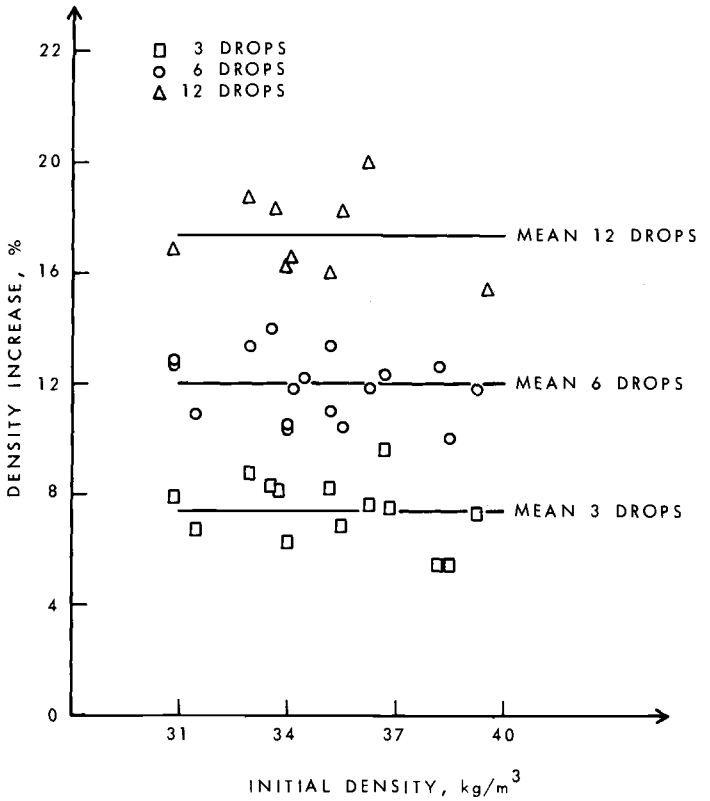

FIG. 10—*Effect of initial density on settlement due to drop test.*

Recommended Method for Producing Settlement in the Specimens

Both temperature and humidity vary considerably in attics. These fluctuations can be assumed to play an important role in the settlement of the insulation material.

The following procedure is recommended for producing a settled density:

1. Blow the material into 90 by 35 by 15-cm and 45 by 35 by 30-cm containers and determine density as blown using the procedure already described.
2. Blow the material into two containers 28 by 28 by 15 cm and two containers 28 by 28 by 30 cm using the same blowing techniques.
3. Drop three 90 by 35 by 15-cm and three 45 by 35 by 30-cm containers six times from a 15-cm height onto a concrete floor.

4. Measure the thickness and calculate the average percent decrease in thickness during the drop test on six containers (designated as S_d).

5. Place two 28 by 28 by 15-cm and two 28 by 28 by 30-cm containers in a climatic chamber at 4 ± 1°C and 98 ± 1 percent relative humidity for four days.

6. Remove the containers from the chamber and place in a conditioned room with climate 23 ± 2°C and 50 ± 5 percent relative humidity for at least three days.

7. Repeat steps (5) and (6) until four exposures in the 4°C-chamber have been completed.

8. Measure the thickness and calculate the average percent decrease for four containers (designated S_c).

9. The settled density is determined by multiplying the density as blown into the 90 by 35 by 15-cm and 45 by 35 by 30-cm containers by the factor $s = 100/(100 - S_d - S_c)$.

Table 8 gives density as blown, percentage decreases during the drop test, and climatic cycling and settled density for several tested materials. The settlement percentages in cycling 15- and 30-cm-thick specimens do not show a significant difference. In a few cases, figures 2 to 3 percent higher are generated for the thick specimens. On average, however, the results are the same for both thicknesses tested. The dropping tests, reported in Table 8, were performed only on 15-cm-thick specimens. The scatter in the settlement determined on various containers is larger than the scatter in the climatic cycling.

To increase the reproducibility of the test and to account for the dependence of the settled density on the specimen thickness, an average of eight containers is recommended in the final version of the proposed method. The containers have the same volume but two thicknesses: 15 and 30 cm. Table 9 gives percentage of settlement during the drop test on containers 15 and 30 cm deep. The difference between 15- and 30-cm-thick specimens is too small to analyze the effect of thickness on the settled density of cellulose fiber insulations. It justifies, however, testing both thicknesses and averaging the results.

Comments on Settled Density Determination

The goal of the proposed method of density determination is to ensure product quality assurance for the purpose of standardization, that is, to achieve an average material coverage and thickness for predicting the thermal resistance in material specifications. There is a wide variability in the settled density of cellulose fiber insulations. In about 40 products tested at NRC (until March 1978), settled densities varied between 35 and 58 kg/m^3, with 50 percent of the materials falling in the range of settled

TABLE 8—*Density changes during settlement testing.*

Product Number	Density as blown kg/m^3	Settlement in Percent								Settled Density kg/m^3
		Dropping				Cycling of Samples 15 cm		30 cm		
26	41.3	9.4	9.7	9.3	11.5	7.9	9.0	8.3	9.5	49.0
25	37.3	10.4	9.3	13.3	11.5	11.4	11.1	11.9	10.4	41.8
27	45.8	10.7	12.0	11.8	10.3	10.0	10.8	10.5	11.0	55.7
10*	30.9	14.6	9.8	12.7	--	20.9	20.1	21.8	20.0	41.2
28	34.6	9.4	9.7	8.4	9.7	13.5	12.5	12.8	13.1	42.3
29	30.6	10.5	7.7	10.0	9.7	10.4	10.6	13.0	13.4	37.2
30	35.7	11.6	7.0	9.3	9.1	10.0	6.0	9.2	8.6	42.1
31	37.5	11.7	10.7	9.9	8.6	6.9	8.0	9.2	7.9	44.4
32	38.1	9.0	9.2	8.7	9.9	6.8	7.1	9.7	9.9	44.9
6	33.2	8.6	9.0	9.3	9.4	7.9	8.8	8.5	9.6	39.1
33	47.1	13.5	11.1	11.4	9.6	13.0	10.9	11.3	10.7	57.8
5	34.3	9.8	10.5	12.1	9.3	11.0	9.3	11.7	10.8	41.4
34	30.8	9.6	9.8	10.9	10.3	14.3	15.5	14.0	15.0	38.4
35	30.1	10.3	9.2	9.7	10.0	10.3	10.6	13.8	12.8	36.7

* Material removed from the house

TABLE 9—*Percent settlement during drop test.*

Material Code	container number							
	15 cm deep				30 cm deep			
	1	2	3	4	5	6	7	8
333-163	10.5	10.7	12.4	10.5	12.3	12.4	12.4	11.6
335-190	10.3	8.6	11.4	9.4	11.5	11.7	13.4	10.4
334-180	11.8	11.6	11.8	12.0	13.4	13.7	13.7	13.6
339-37	9.9	9.3	11.8	11.4	14.9	14.6	14.8	15.5

densities between 40 and 45 kg/m^3. It is therefore important for manufacturers to examine the several factors that influence the settled density, for example, size and length of fibers in the finished product, amount and type of added chemicals, their mixing, and sieve size. These factors were not studied in the reported work. Another aspect of settled density testing is product quality control, as the density of the finished product varies depending on the raw materials used in the actual production batch.

There is therefore a need for another, quicker method for settled density determinations. Comparison with one such method will be discussed in another paper.

Acknowledgment

This research was performed in the Thermal Properties Laboratory of the Energy and Services Section, Division of Building Research, National Research Council of Canada. The authors wish to express their gratitude to Gerry Theriault for his contribution to the development of the testing methods, to Roger Marchand for building the special instrumentation, and Nicole Normandin and Gareth Keatley for making many of the measurements.

This paper is a contribution from the Division of Building Research, National Research Council of Canada and is published with the approval of the director of the Division.

C. J. Shirtliffe[1] *and M. Bomberg*[1]

Blown Cellulose Fiber Thermal Insulations: Part 2—Thermal Resistance

REFERENCE: Shirtliffe, C. J. and Bomberg, M., "**Blown Cellulose Fiber Thermal Insulations: Part 2—Thermal Resistance**," *Thermal Transmission Measurements of Insulation, ASTM STP 660*, R. P. Tye, Ed., American Society for Testing and Materials, 1978, pp. 104–129.

ABSTRACT: The thermal resistance of a number of commercial blown loose-fill cellulose fiber thermal insulations has been measured using the guarded hot plate and heat flowmeter methods. An equation describing the variation of thermal resistance with temperature, temperature difference, density, and thickness has been derived from these measurements and, with lesser precision, from the data provided by other investigators. The equation does not include the effects of chemical content, moisture content, chemical composition, or structure of the paper particles. The thermal resistance of a layer of insulation was found not to be directly proportional to thickness. The equation for thermal resistance fits the National Research Council of Canada (NRC) data with a standard deviation of less than 3.5 percent for thickness of 50 to 305 mm.

KEY WORDS: cellulose fiber, cellulose fiber thermal insulation, blown insulation, cellulosic fiber insulation, thermal resistance, thermal conductivity, newsprint, paper, thermal properties, thickness effect

Cellulose (or cellulosic) fiber thermal insulation (CFI) is made primarily from ground newsprint. The ground newsprint is blended with finely powdered chemicals which impart a measure of resistance to fire, fungus, and vermin.

Commercial cellulose fiber insulations may contain between 1 and 38 percent of chemicals by weight. Most of those meeting the standards contain between 18 and 25 percent. The additives are usually a blend of borax, boric acid, and aluminum sulphate. Aluminum sulphate alone has been used in insulations that are not intended to meet rigorous standards on corrosion and fungus growth. Other chemicals, such as soda ash,

[1]Research officers, National Research Council of Canada, Division of Building Research, Ottawa, Ont., Canada.

ammonium sulphate, oxides, phosphates, silicates, clay, portland cement, and garden fertilizer, have been used but have not been satisfactory.

After being blown into attics or walls, the material has a final density of about 40 to 50 and 60 to 100 kg/m^3 (2.6 to 3.5 and 4.0 to 7.5 lb/ft^3), respectively. The material provides more thermal resistance per unit thickness at a competitive price than low-density mineral fiber insulation. As its manufacture entails a recycling of a material that is normally wasted, the material may play a major part in the retrofitting of residential buildings.

The first large-scale commercial production of cellulose fiber insulations in North America began between 1925 and 1935. Reports of research studies on this material are scarce. The earliest documented work known to the authors was that carried out at the University of Saskatchewan in the early 1950's and for the National Cellulose Manufacturers Association by Dynatech Inc. in the 1960's. Little information was published, however, until after 1970. Since then, a few technical and semitechnical papers have appeared and there are now four materials standards for the material—three in the United States:

1. ASTM Standard Specification for Cellulosic Fiber (Wood-Base) Loose-Fill Thermal Insulation (C 739-73);
2. General Services Administration Specification for "Thermal Insulation Blanket; and Insulation Thermal (Loose Fill for Pneumatic or Poured Application): Cellulose Vegetable and Wood Fiber (GSA HH-I-515c);"
3. National Cellulose Insulation Manufacturer's Association Standard Specification for "Cellulosic Fiber (Wood Base) Loose-Fill Thermal Insulation (NCIMA N101-73);" and one in Canada:

Canadian Government Specifications Board Provisional Standard for "Thermal Insulation, Cellulose Fiber, Loose Fill (CGSB 51-GP-60P)."

The adoption of these standards has reduced the variability of the composition of cellulose fiber insulation and enabled the properties to be predicted with more accuracy than formerly.

This paper presents the results of measurements of the thermal resistance of a layer of cellulose fiber insulation. An equation was developed that approximates the results for thicknesses between 50 and 305 mm and densities between 30 and 100 kg/m^3. The reason for restricting the range of the study is evident from the simplicity of the dependence of thermal resistance on density and thickness shown in Fig. 1. Most of the cellulose fiber insulations used in practice have properties that fall in this region.

A complete equation would include the effects of thickness of the layer, density, mean temperature, temperature difference, moisture content, degree of milling, amount and formulation of the chemical treatment, and the integrity of the cellulose fibers in the basic newsprint or paper stock. The last three factors have the least effect on thermal resistance. Few manufacturers control any of the variables except the chemical formulation

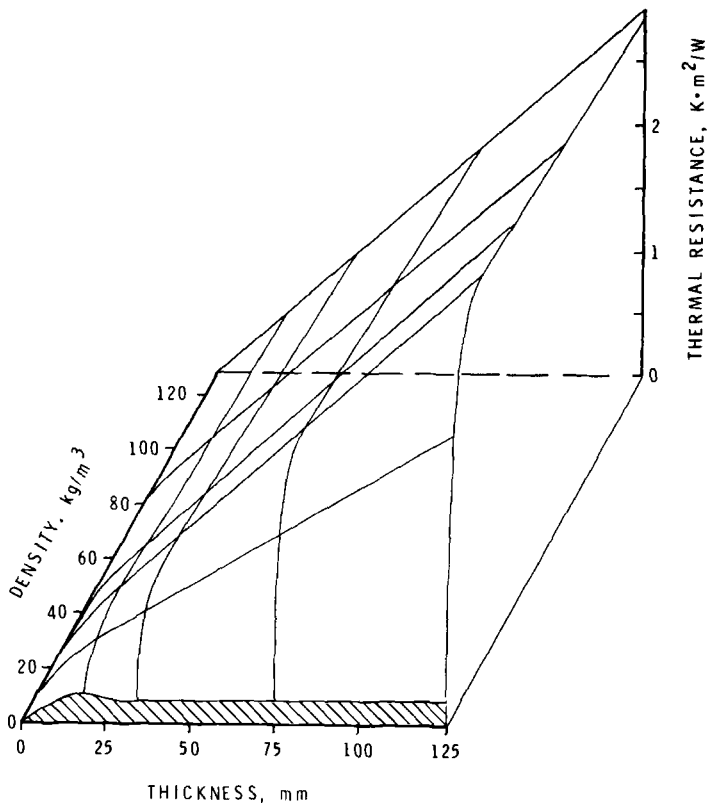

FIG. 1—*Approximate relationship between thermal resistance of cellulose fiber insulation and density and thickness of layer showing complexity at thickness below 50 mm and densities below 40 kg/m³.*

and quantity of the chemical in the product. Results of another study have shown these to be of little significance. Any deviation of individual measurements from the average curve reflects the consequences of ignoring these and other variables.

The moisture content of the material affects its density. At standard conditions the moisture content will depend on the paper stock, chemical formulation, and the amount of chemical used. As the variation of thermal resistance with density is included in the equation, the effect of the chemical formulation on the thermal resistance is at least partially included.

Moisture distribution in the material will be nonuniform due to the temperature gradient imposed across the material during the test. The degree of dependence of the measured thermal resistance on this temperature gradient indicates the importance of the moisture distribution.

The equation that has been derived for thermal resistance does not

describe the performance of any specific material for a given application; it represents a good estimate of the expected performance for current commercial materials. During the initial study, over 75 measurements were made on 30 commercial materials. Results of 39 measurements on 20 materials made by Tye [*1*][2] as well as 14 on three materials made by Anderson and Wilkes [*2*] and for the Public Service Co. of Colorado were also analyzed. Additional tests on 29 materials measured at 76-mm thickness, three high-density specimens, and 12 measurements on two materials differing only in chemical content, communicated to the authors by Anderson [*3*], are included as a secondary check on the analysis.

Previous Measurements

Tye [*1*] showed that the apparent thermal conductivity, and therefore the thermal resistance, of 25- and 35-mm layers of cellulose insulation is dependent on the density, the mean temperature, and the moisture content. Tye's measurements, on 29 materials, covered a temperature range of −20 to +40°C, a density range of 24 to 123 kg/m^3, moisture contents of 0 to 12.5 percent, and thicknesses from 6 to 52 mm. A special procedure was used by Tye to produce the specimens.

The 14 measurements collected from other sources such as Anderson and Wilkes [*2*] and a private communication from the Public Service Co. of Colorado included those on materials with thicknesses from 127 to 203 mm and densities from 29 to 64 kg/m^3. Large commercial blowers were used to produce the specimens and it was reported that there were problems with fire-retardant separation during specimen preparation. The specimens may also have contained some high-density clumps due to the characteristics of the large blowers. Some settlement could also have occurred during the initial stages of the measurements. These data are listed in Table 1*b*.

The measurements in all the studies were made by experienced laboratory personnel using either ASTM Tests for Steady-State Thermal Transmission Properties by Means of the Guarded Hot Plate (C 177-76) or Steady-State Thermal Transmission Properties by Means of the Heat Flow Meter (C 518-76). The test conditions were essentially identical in all three studies.

Preparation of Specimens in Current Study

The materials used in the present study were obtained directly from manufacturers in standard commercial packages and stored in an air-con-

[2]The italic numbers in brackets refer to the list of references appended to this paper.

ditioned space with humidity ranging from 30 to 60 percent until the specimens were prepared.

The materials were blown through a small commercial cellulose fiber blower into frames of appropriate thickness, using, in most cases, a machine made by Diversified Insulation, Inc. of Minneapolis, Minn. A 0.75-kW (1 hp) Model 8806 Toronado blower on the machine fluffed the material, then the air and material were transported through a hose 15 m long and 5 cm in diameter. The end of the hose was held either horizontally, 91 cm above the bottom of the specimen frames, or at a 10-deg upward slope, 28 cm above the bottom of the frames [*4*]. The specimens of the same material blown by the two methods appeared to have a consistent texture and structure and on average had the same thermal resistance.

Before testing, the specimens were conditioned for 1 to 4 weeks in a room at 22°C and 50 percent relative humidity. Moisture content of the conditioned specimens varied between 8 and 12 percent by weight.

The frames that contained the material during the measurement of the thermal resistance were made of Plexiglas, plywood, or extruded polystyrene foam and were covered on one or both sides before testing with 0.05 to 0.10 mm clear or black polyethylene.

Equipment used in the testing was either a 30- or 40-cm-square horizontal heat flowmeter apparatus of the Armstrong Cork design which conforms to ASTM C 518-76 or a vertical guarded hot-plate apparatus, 46 or 60 cm square, conforming to ASTM C 177-76. Earlier calibration had shown that the apparatus would give results agreeing to within approximately $\pm\frac{1}{2}$ percent. Table 1*a* lists the test conditions, apparatus, and specimen size.

Tests were performed generally in accordance with the requirements of the test methods. The amount of edge insulation required by the test methods for conditions where the ambient did not equal the mean temperature of the specimens could not always be achieved because of space limitations. The effects of edge losses were calculated and the results corrected.

Precision of Measurements

The electronic measuring equipment used to measure the heat flux, temperature differences, and heat meter thermopile outputs contributed errors of less than 0.1 percent to the results. The principal errors were those due to edge losses and uncertainties in the calibration of the heat flowmeters. From a number of checks, the errors in the calibration of the heat flowmeters were found to be less than 1 percent; errors due to edge losses were more difficult to estimate.

Estimation of Edge Losses

A two-dimensional finite-element computer program was used to solve the steady-state temperature field at the center of the edge of each apparatus for various thicknesses of specimens, temperature differences, ambient temperatures, and amounts of edge insulation. The calculated temperatures were compared with edge temperatures, measured with thermocouples. Additional measurements were made with ambient temperatures other than the mean of the hot and cold surfaces to introduce known additional errors. The calculations agreed well with the measurements. It is considered that edge losses were estimated with sufficient accuracy to allow their use for making corrections where necessary.

In a few cases the ambient temperature was 4°C below the mean temperature. The edge-loss corrections for this condition for the 229- and 305-mm-thick specimens in the heat flowmeter apparatus with 2.7 $K \cdot m^2/W$ edge insulation ranged from 8 to 22 percent. After the uniformity of the ambient temperature was improved and the level was brought to the mean temperature of the specimens, estimates showed this loss to be less than 1 percent. This is less than the uncertainty in the calculation, and so corrections were not made on tests performed with these conditions.

In testing thinner specimens, edge losses introduced errors of less than 1 percent.

Results

General

The experimental results are given in Table 1a and illustrated in Figs. 2–7.

Specimens for testing were generally taken from different samples of material. Variability between samples was not known but observations in another study [*4*] showed that the density variations from batch to batch of the same material could be considerable. Measurements on specimens of the same material from three samples with the same density gave identical thermal resistances.

All calculations were made in the imperial system of units and then converted to the SI system.

Fitting Curves to Data

The National Research Council of Canada (NRC) data and that obtained from Tye were divided into sets according to the thickness of the specimens. Sets of data for thicknesses of approximately 25, 35, 76, 150, and

TABLE 1a—*NRC data on cellulose fiber insulation.*

Test No.	Product No.	Apparatus[a]	Thickness, mm	Density, kg/m³	Moisture Content, % weight	Thermal Resistance, R, K·m²/W
1	10	2	50.8	56.2	8.8	1.28
2	10	1	50.8	48.1	6.0	1.30
3	10	2	50.8	48.1	1.7	1.32
4	15	1	50.8	48.1	7.5	1.28
5	14	1	76.2	32.2	8.7	1.87
6	16	2	25.4	74.3	3.9	0.64
7	13	1	63.5	73.4	11.4	1.46
12	11	1	76.4	35.6	7.0	2.06
14	10	1	76.4	36.4	15.3	2.06
16	9	1	76.5	23.4	8.8	1.94
18	8	1	76.4	35.6	8.1	2.02
20	7	1	76.7	36.2	10.2	2.00
22	6	1	76.7	36.3	7.2	2.04
24	3	1	76.7	42.0	9.2	2.04
26	3	1	63.8	44.7	...	1.68
27	3	1	89.2	79.5	...	2.19
30	3	3	305.7	47.8	...	7.48
31	3	3	305.7	47.8	...	7.20
32	4	1	76.8	28.5	8.4	2.00
34	5	1	76.8	39.7	10.1	2.03
36	1	1	76.7	44.7	5.4	2.00
37	18	1	76.8	55.0	8.6	1.96
38	17	1	76.8	40.7	12.1	1.94
39	2	1	76.1	34.0	5.0	2.04
40	19	1	76.8	54.8	5.1	1.99
42	20	1	76.6	43.1	5.8	1.97
43	21	1	76.9	36.5	7.2	2.00
44	22	1	76.8	34.8	5.5	2.03
45	16	1	76.9	45.2	8.0	1.94
46	23	1	76.7	48.1	5.9	1.90
47	28	1	76.7	43.4	...	1.96
48	32	4	75.4	47.6	...	1.99
49	30	1	76.7	44.9	...	2.00
50	31	1	76.7	48.2	...	1.94
51	31	1	76.7	48.2	...	1.94
52	31	1	76.7	48.2	...	1.94
53	26	1	76.9	48.1	...	1.98
54	35	1	76.7	37.8	...	2.04
55	36	1	76.9	37.3	...	2.09
56	34	1	76.9	38.6	...	2.02
57	33	1	76.9	68.6	...	1.98
81	3	1	76.0	40.7	8.5	1.99
82	3	1	228.2	40.5	8.5	5.69
83	3	3	230.0	49.0	9.2	5.53
84	3	2	12.8	40.7	8.5	0.37
85	3	2	39.4	39.7	8.5	1.12
86	3	2	65.9	40.5	8.5	1.88

[a] Apparatus:
1: 45-cm guarded hot plate.
2: 30-cm guarded hot plate.
3: 60-cm guarded hot plate.
4: 45-cm heat flowmeter.

TABLE 1a—*Continued.*

Test No.	Product No.	Apparatus[a]	Thickness, mm	Density, kg/m³	Moisture content, % weight	Thermal Resistance, R, K·m²/W
87	32	1	75.4	47.8	...	1.99
88	32	1	299.8	47.8	...	7.25
89	28	1	76.7	43.2	...	1.96
90	28	1	299.7	41.8	...	7.40
91	3	3	305.5	53.0	14.8	7.48
92	37	1	76.6	42.0	...	1.97
93	37	1	152.6	39.4	...	3.72
94	30	1	76.7	44.9	...	2.00
96	25	1	76.9	46.0	...	1.97
97	25	1	299.9	46.0	...	7.52
98	25	1	299.9	46.0	...	7.26
99	37	1	76.0	78.8	...	1.83
33	4	1	152.7	32.7	8.4	3.68[b]
35	5	1	152.4	42.3	10.1	3.92[b]
13	11	1	152.4	38.0	7.0	3.99[b]
15	10	1	152.2	37.8	15.3	3.83[b]
17	9	1	152.4	24.8	8.8	3.71[b]
19	8	1	152.2	40.7	8.1	3.84[b]
21	7	1	152.8	42.3	10.2	3.79[b]
23	6	1	152.7	41.7	7.2	3.85[b]
25	3	1	152.8	48.7	9.2	3.69[b]
28	3	1	152.3	80.1	...	3.51[b]
33	4	1	152.7	32.7	8.4	3.67[b]
35	5	1	152.4	42.3	10.1	3.92[b]

[a]Apparatus:
1: 45-cm guarded hot plate
2: 30-cm guarded hot plate
3: 60-cm guarded hot plate.
4: 45-cm heat flowmeter.
[b]Values of thermal resistance corrected with regard to side heat losses.

TABLE 1b—*Thermal resistance tests on cellulose fiber insulation: data from Public Service Co. of Colorado (measurements according to ASTM C 518-76).*

Product No.	Thickness, mm	Density, kg/m³	Thermal Resistance, R, K·m²/W
40	152.4	43.5	3.77
40	139.7	47.7	3.47
40	127.0	52.3	3.16
12	203.2	39.7	5.14
12	190.5	42.3	4.94
12	177.8	45.4	4.62
12	165.7	48.9	4.28
12	152.4	52.9	3.86
12	139.7	57.7	3.58
12	127.0	63.6	3.22
12	152.4	38.5	4.10
12	139.7	42.0	3.66
12	127.0	46.3	3.27
12	76.0	78.8	1.82

TABLE 1c—*Thermal resistance tests on cellulose fiber insulation: data from Anderson* [3] (*Product 30b has a 4 percent higher chemical addition than Product 30a; moisture contents are approximately 10 percent.*)

Product No.	Thickness, mm	Density, kg/m³	Thermal Resistance, R, K·m²/W
30a	101.6	24.1	2.58
30a	101.6	32.1	2.61
30a	101.6	40.1	2.69
30a	101.6	48.1	2.59
30a	101.6	56.1	2.54
30a	101.6	64.2	2.44
30b	101.6	24.1	2.61
30b	101.6	32.1	2.63
30b	101.6	40.1	2.70
30b	101.6	48.1	2.61
30b	101.6	56.1	2.60
30b	101.6	64.2	2.45
30b	25.4	43.3	0.66
30b	50.8	43.3	1.29
30b	101.6	43.3	2.53
30b	152.4	43.3	3.81
30b	203.2	43.3	5.03
30b	25.4	64.2	0.61
30b	50.8	64.2	1.22
30b	101.6	64.2	2.39
30b	152.4	64.2	3.56
30b	203.2	64.2	4.76

TABLE 1d—*NRC data on cellulose fiber insulation obtained after analysis of data in Table 1.*

Test No.	Product No.	Apparatus	Thickness, mm	Density, kg/m³	Moisture Content, % Weight	Thermal Resistance, R, K·m²/W
100	41	4	75.1	38.3	...	1.946
101	42	4	74.9	51.9	...	1.923
102	43	4	74.9	54.3	...	1.912
103	44	4	75.1	42.7	...	1.925
104	45	4	74.9	39.9	...	1.945
105	46a	4	75.2	38.3	...	2.015
106	46b	4	75.2	37.3	...	...
107	47	4	74.8	42.5	...	1.954
108	48	4	75.0	36.0	...	1.931
109	49	4	74.9	41.2	...	1.963
110	50	4	75.4	44.8	...	1.994
111	51	4	76.7	44.3	...	1.937
112	52	4	76.9	45.2	...	1.973
113	53	4	75.0	42.1	...	...
114	54	4	75.0	37.6	...	...
115	55	4	75.0	37.8	...	2.018
116	56	4	76.7	36.9	...	1.983

TABLE 1*d*—*Continued*

Test No.	Product No.	Apparatus	Thickness, mm	Density, kg/m³	Moisture Content, % Weight	Thermal Resistance, R, K·m²/W
117	57	4	75.0	41.5	...	...
118	58	4	76.7	36.6	...	2.045
119	59	4	76.9	48.7	...	1.982
120	60	4	76.0	57.9	...	...
121	61	4	76.6	39.5	...	1.972
122	62	4	76.9	38.5	...	2.021
123	63	4	76.9	55.6	...	1.912
124	64	4	75.1	48.8	...	1.959
125	65	4	76.7	42.3	...	1.959
126	66	4	76.9	32.2	...	2.091
127	67	4	75.0	32.7	...	...
128	68	4	75.2	42.0	...	1.943
129	69	4	75.1	42.7	...	1.983
130	70	4	75.0	36.1	...	1.979
131	71	4	75.0	45.9	...	1.916
132	72	4	75.0	36.6	...	1.959
133	73	4	75.2	34.8	...	1.943
134	74	4	76.8	49.1	...	1.967
135	75	4	75.1	46.3	...	1.946
136	3	4	153.1	114.4	...	3.416
137	3	1	153.1	64.1	...	3.792

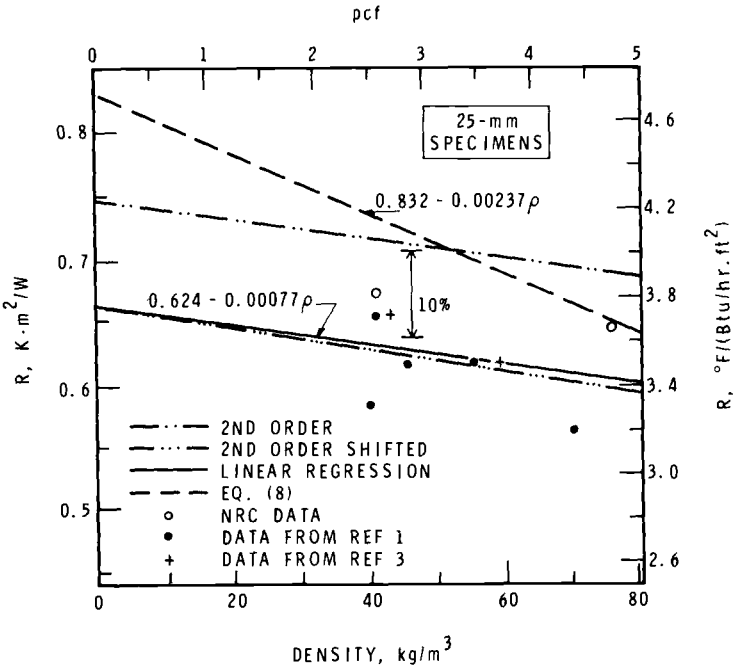

FIG. 2—*Thermal resistance versus density for 25-mm thickness of cellulose fiber insulation.*

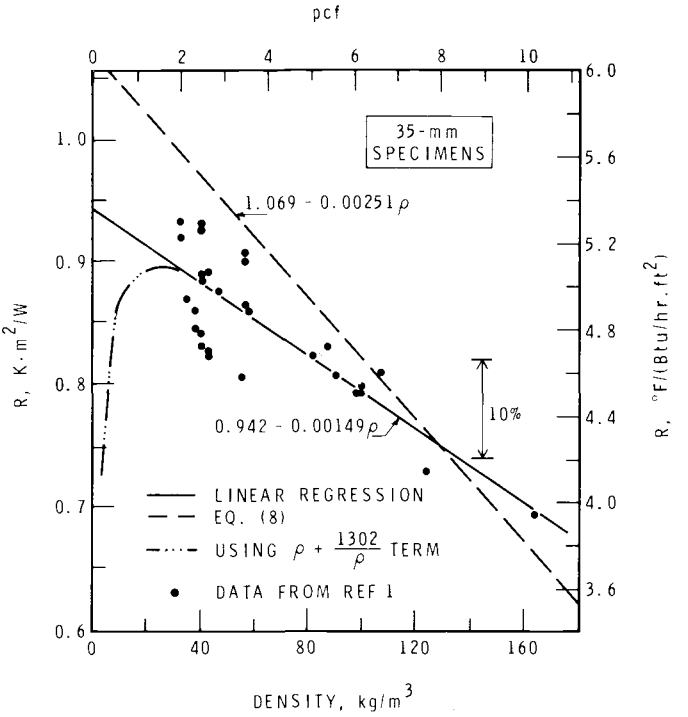

FIG. 3—*Thermal resistance versus density for 35-mm thickness of cellulose fiber insulation.*

305 mm (1, 1.37, 3, 6, and 12 in.) were selected. A variation up to 10 percent in thickness was allowed in any set.

The dependence of thermal resistance (R) on the density was examined first. Equations of the form $R = A + B\rho$ were fitted to the data by linear regression, where R is thermal resistance ($K \cdot m^2/W$) and ρ the density (kg/m^3). Coefficients A and B were assumed to have the form $A = C + DL$ and $B = E + FL$, where L is the specimen thickness (mm); coefficients C, D, E, and F were determined by linear regression. The equations for A and B were substituted back into the equation for R, giving an equation of the form $R = (C + DL) + (E + FL)\rho$.

The equation was then used to adjust the measured R so as to eliminate the variation due to thickness within the sets. The corrected data sets are shown in Figs. 2–5 and 7; the scatter within each corrected set was still too large to justify using higher-order equations in the fitting of the curves to the data.

Coefficients A and B were recalculated from the corrected data by linear regression (Figs. 8 and 9). Values of A and B and the correlation coeffi-

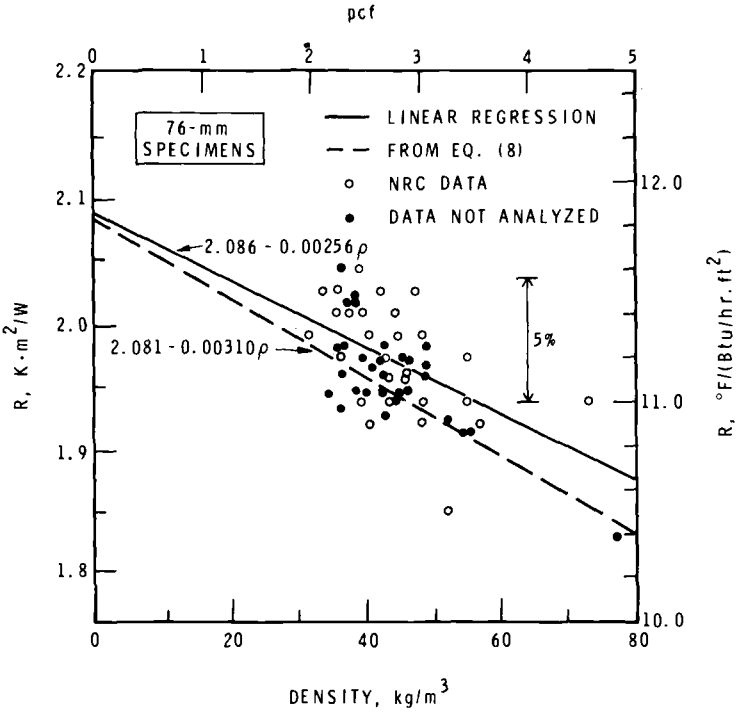

FIG. 4—*Thermal resistance versus density for 76-mm thickness of cellulose fiber insulation.*

cients are listed in Table 2*a*. Equations were again fitted to the A and B coefficients using linear regression (Table 2*b*). The correlation coefficients indicate that the fit of the data for the four greatest thicknesses is adequate to describe the relationship and does not mask any special effects near zero thickness. Equations were also fitted through all points; the equations, correlation coefficients, and standard deviation are listed in Table 2*b*. The data for the 102-mm specimens provided by Anderson [*3*] and the 30 extra measurements are plotted in the same figures to indicate the type of agreement obtained.

Substituting the third set of coefficients into $A + B\rho$ gives the following equation, which describes the dependence of thermal resistance on density and thickness

$$R = (0.205 + 0.0247L) - (0.00201 + 0.0000143L)\rho \quad (1)$$

or, in imperial units, °F/(Btu/h·ft²), in., and lb/ft³

$$R = (1.165 + 3.56L) - (0.183 + 0.0331L)\rho \quad (2)$$

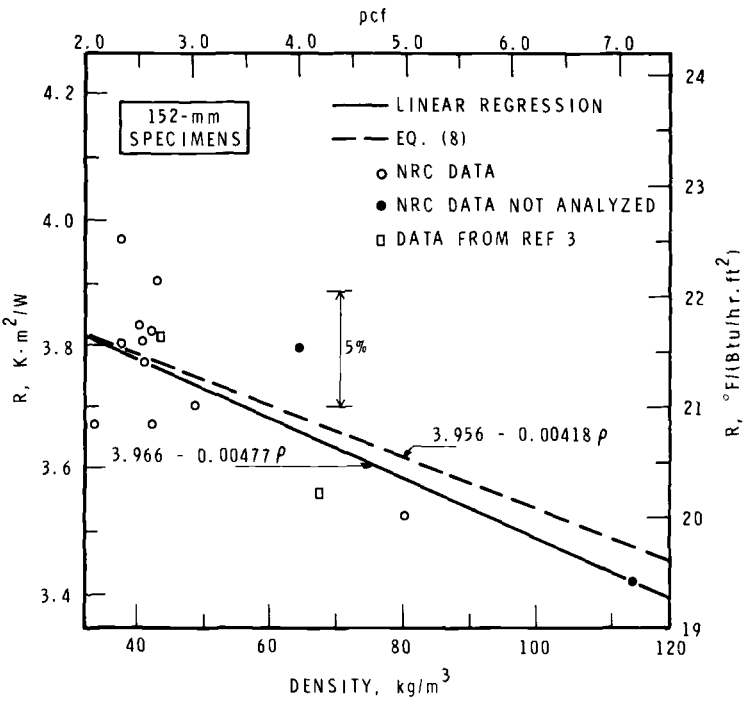

FIG. 5—*Thermal resistance versus density for 152-mm thickness of cellulose fiber insulation.*

Table 3 gives a comparison of the equations obtained by evaluating Eq 1 at given thicknesses with the equations obtained by linear regression, that is, the least-squares fit to the data of R versus ρ at these thicknesses. The agreement is reasonable for thicknesses over 50 mm.

Equation 1 does not give a zero resistance at zero thickness. Higher-order equations for the coefficients A and B would be required to describe the thermal resistance of thin layers of materials. A second-order fit for A and B is included in Table 2*b* for comparison. The thermal resistance for specimens with thicknesses over 50 mm can be represented adequately by the linear equation. Again the equations for Anderson's data and the 30 additional measurements are included as a check.

Equation 1 was evaluated at each thickness and for a number of densities. The resulting curves are plotted in Figs. 2–7 for comparison with the data and curves found by linear regression. The density term in Eq 1 is related to the conduction through the cellulose fiber.

Equation 1 should also contain a term containing the variable 1/density to describe the reduction of the radiation component of heat transfer in the material with increasing density. This would justify a variable in the

equation of the form $\rho + C\rho^{-1}$, where C is a constant that can be determined from the density at which the maximum resistance occurs. The results of both Tye [*1*] and Anderson [*3*] can be used to show that at densities below about 24 kg/m^3 (1.5 lb/ft^3) the radiation component must increase at a rapid rate with density [*5*]. The result of such a fit to Tye's data for 35-mm specimens and Anderson's results for 102-mm specimens is shown in Figs. 3 and 10, respectively. Above 40 kg/m^3 with the 35-mm specimens, the curve falls about 0.5 percent higher than the line shown, within about the width of the line. This more complex form of the equation was not used since there were insufficient data to establish the curve below densities of 32 kg/m^3 and it did not affect the results for density greater than 40 kg/m^3. In Fig. 10, the linear equation and the equation using the $\rho + 1302\rho^{-1}$ term do not agree. Further data would be necessary to distinguish which equation is more representative at higher densities or if the Anderson data contained errors.

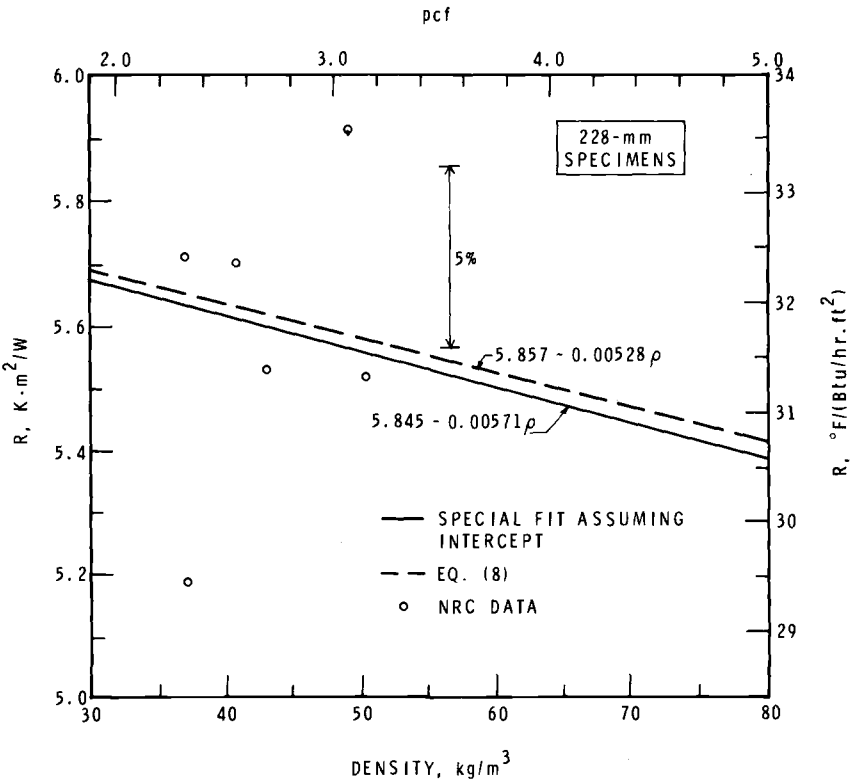

FIG. 6—*Thermal resistance versus density for 229-mm thickness of cellulose fiber insulation.*

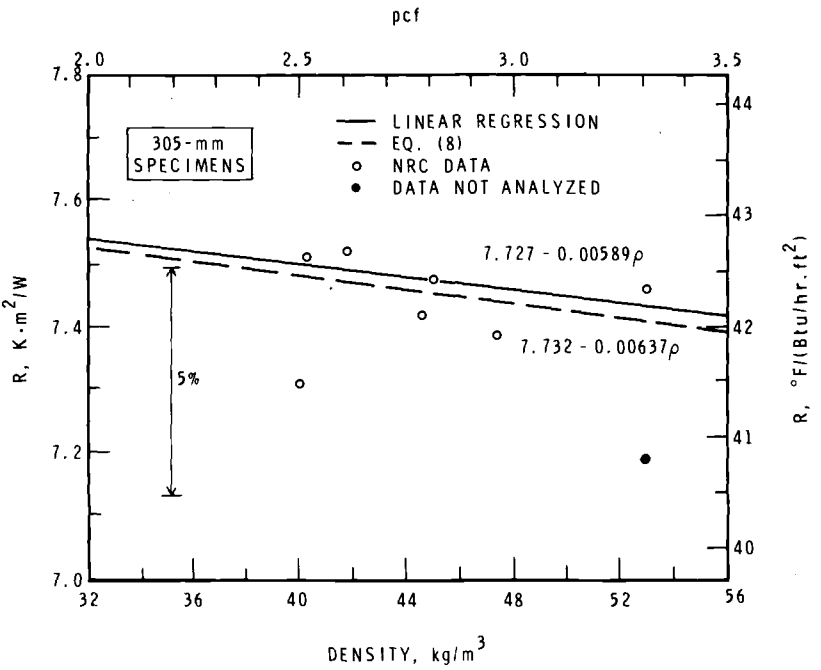

FIG. 7—*Thermal resistance versus density for 305-mm thickness of cellulose fiber insulation.*

The equation for R in terms of ρ and L was checked against the remainder of the data, including that by Tye, at thicknesses of 13, 25, 39, 51, 64, 89, and 228 mm (0.5, 1.0, 1.55, 2.0, 2.5, 3.5, and 9 in.). The results are shown in Fig. 6 and in Table 4. The agreement is good, except at the 13- and 25-mm thicknesses, but this region was of little interest.

Thermal Resistance Versus Thickness

A check of the relationship between thermal resistance and thickness was made by using a carefully selected set of data in which the thickness varied from 13 to 305 mm and the density between 40 and 48 kg/m³. Adjustments to the thermal resistance were made to correct the data to a density of 40.4 kg/m³. One curve of the form $R = G + HL$ was fitted to the corrected data for the 50-mm thickness and above using linear regression. Other equations were obtained by including the data for thicknesses below 50 mm. The resulting equations are listed in Table 5. The linear equations obtained using 15 and 13 points, respectively, are

$$R = 0.143 + 0.0240L \tag{3}$$

$$R = 0.192 + 0.0238L \tag{3a}$$

Equation 1 at the same density gives

$$R = 0.124 + 0.0241L \tag{4}$$

Equations 3 and 4 are plotted with the data in Fig. 11. The two techniques for curve fitting yield approximately the same equation at this density; thus the form of Eq 1 and the value of the constants in it appear to be adequate to describe the dependence of thermal resistance in the range of variables considered. Anderson's data agree well with both curves.

Anderson's data and Eq 1 evaluated at a density of 64.2 kg/m^3 are plotted in Fig. 12. The agreement is somewhat poorer than at the lower density; this may be due to error in the data caused by transient heat flows.

Thickness and Density Changes

A further check of the adequacy of the form of the equation was made by comparing Eq 1 for resistance in terms of density and thickness with

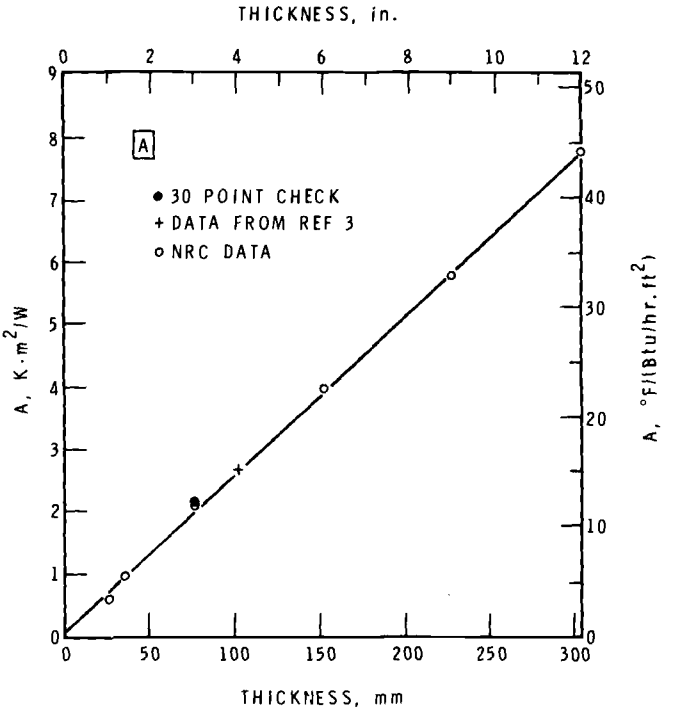

FIG. 8—*Three-point linear fit for coefficient* A *in the equation* R = A + Bρ *(Table* 2a).

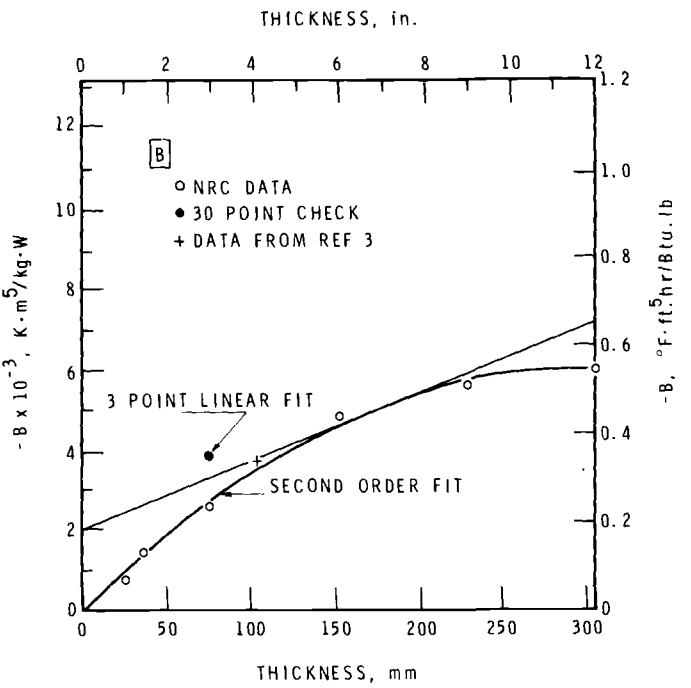

FIG. 9—*Three-point linear and second-order fit for coefficient* B *in equation* R = A + Bρ (Table 2a).

TABLE 2a—*Values of coefficients* A *and* B *in the equation* R = A + Bρ.

Thickness, mm	*A*, K·m²/W	*B*, K·m⁵/W·kg × 10^{-3}	Correlation Coefficient
25	0.642	−0.772	−0.285
35	0.942	−1.487	−0.846
75	2.132	−3.913	−0.563
76	2.086	−2.565	−0.501
102	2.744	−3.606	−0.654
152	3.966	−4.776	−0.520
228	5.845*	−5.710[b]	...
305	7.726	−5.896	−0.427

[a]Interpolated
[b]Using value of *A* and data in Fig. 6.

TABLE 2*b*—*Equations in coefficients* A *and* B *in terms of the thickness*, L, *mm, of the layer.*

Number of Points	Coefficients	Correlation Coefficient	Standard Deviation of $A + B\rho$: 83 Points	
			%	Value
5	$A = 0.0731 + 0.02561L$	$r = 0.99971$	3.7	0.109
6	$-B = 0.957 \times 10^{-3} + 1.881 \times 10^{-5}L$	$r = -0.954$		
4	$A = 0.1310 + 0.02498L$	$r = 0.99987$	3.7	0.110
5	$-B = 1.383 \times 10^{-3} + 1.696 \times 10^{-5}L$	$r = -0.949$		
3	[a] $A = 0.2052 + 0.02468L$	$r = 1.0000$	3.3	0.099
4	[b] $-B = 2.015 \times 10^{-3} + 1.430 \times 10^{-5}L$	$r = -0.923$		
6	$A = -0.007934 + 0.02704L - 5.663 \times 10^{-6}L^2$	$r = 0.99990$	5.1	0.135
6	$-B = -1.652 \times 10^{-4} + 4.382 \times 10^{-5}L + 7.856 \times 10^{-8}L^2$	$r = -0.998$		
6	As above with $A' = A + 0.9294$	---	2.8	0.075
6	$B' = B$	---		

[a]These coefficients were used in deriving Eq. 8.

TABLE 3—*Comparison of Eq 1 with least-squares fit of thermal resistance versus density*, ρ *kg/m*^{3}.

Thickness, mm	Identification	Equation for Thermal Resistance, K·m²/W	Correlation Coefficient
25	least squares	$0.624 - 0.00077\rho$	−0.285
	Eq 1	$0.822 - 0.00237\rho$	
35	least squares	$0.942 - 0.00149\rho$	−0.846
	Eq 1	$1.069 - 0.00251\rho$	
75[a]	least squares	$2.132 - 0.00391\rho$	−0.563
	Eq 1	$2.058 - 0.00308\rho$	
76	least squares	$2.086 - 0.00256\rho$	−0.501
	Eq 1	$2.081 - 0.00310\rho$	
102[b]	least squares	$2.744 - 0.00355\rho$	−0.638
	Eq 1	$2.724 - 0.00347\rho$	
152	least squares	$3.966 - 0.00477\rho$	−0.520
	Eq 1	$3.956 - 0.00418\rho$	
305	least squares	$7.727 - 0.00589\rho$	−0.427
	Eq 1	$7.732 - 0.00637\rho$	

[a]Additional 30 data points.
[b]Data by Anderson [*3*].

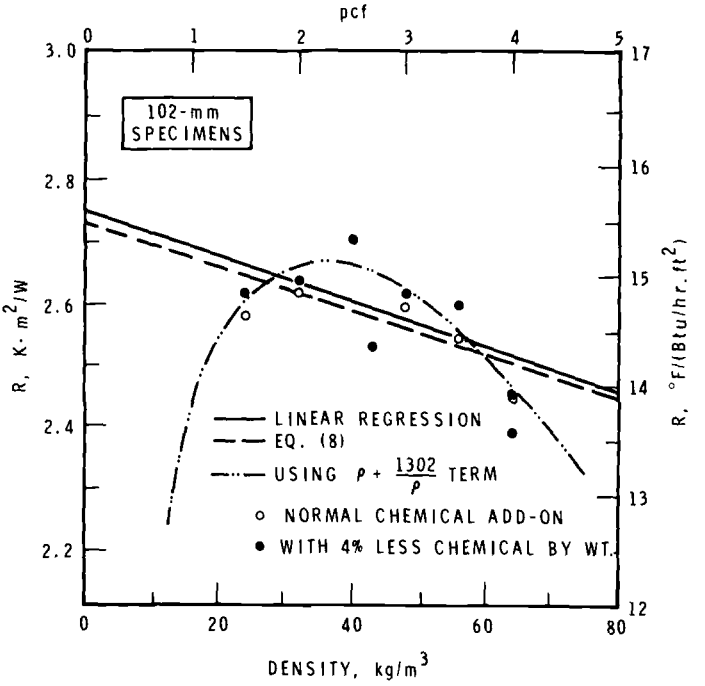

FIG. 10—*Thermal resistance versus density for 102-mm-thickness cellulose fiber insulation (data from Anderson* [3]).

TABLE 4—*Difference between eq 8 for calculated thermal resistance*, Rc, *and the measured thermal resistance*, Rm.

Thickness, mm	No. of Points	Rc–Rm, K·m²/W	% Difference	
			Average	Max
13	...	0.06	16	16
25	7	0.09	14	27
35	31	0.06	7	16
39	...	0.05	4	4
51	...	0.02	1	2
64	2	−0.03	−2	2
75	30	+0.02	−2	4
76	33	−0.01	−0.6	6
89	...	−0.04	−2	2
150	12	0.04	1.2	4
228	4	+0.05	+1	9
305	8	+0.03	+0.4	3
Average 50 to 305	...	0.01	−0.4	4

TABLE 5—*Equations derived from data on selected materials with varying thicknesses and a corrected density of 40.4 kg/m³. Density range: 40.4 to 47.6 kg/m³; thicknesses measured: 13, 25, 40, 75, 152, 228, and 305 mm.*

Range of Thickness, mm	No. of Measurements Used	Equation for R, K·m²/W	Correlation Coefficient
(1) 40 to 305	13	$0.192 + 0.0238L$	0.9991
(2) 25 to 305	14	$0.162 + 0.239L$	0.9991
(3) 13 to 305	15	$0.143 + 0.240L$	0.9992
(4) 13 to 305	15	$0.092 + 0.0250L - 2.98 \times 10^{-6}L^2$	0.9992

Notes:

1. Differences in R given by (1), (2), and (3) at 76 = 1.7 percent and at 305 mm = 0.2 percent.
2. Equation 1, when evaluated at 40.4 kg/m³, gives $R = 0.124 + 0.0241L$.
3. Differences between all four equations at both 76 and 305 mm thickness were less than 2.5 percent.

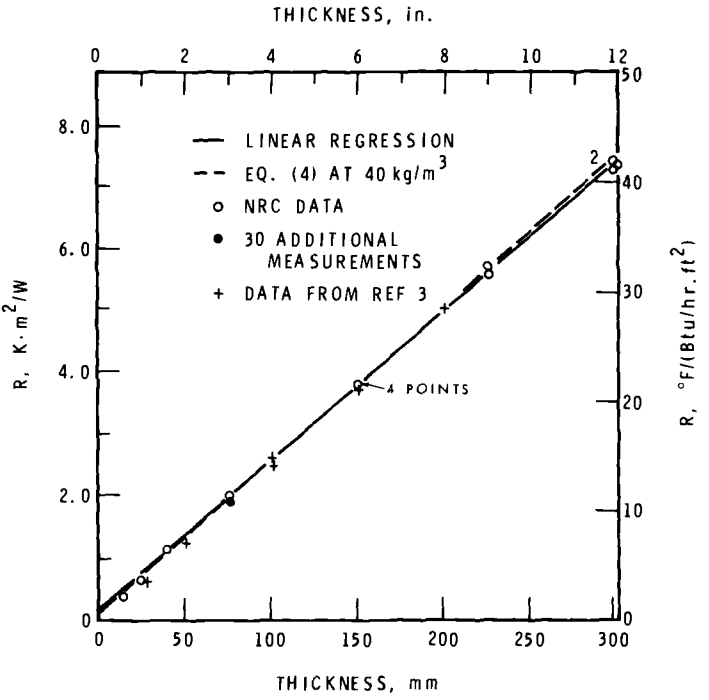

FIG. 11—*Thermal resistance versus thickness for cellulose fiber thermal insulation, density 40 kg/m³ (2.52 lb/ft³).*

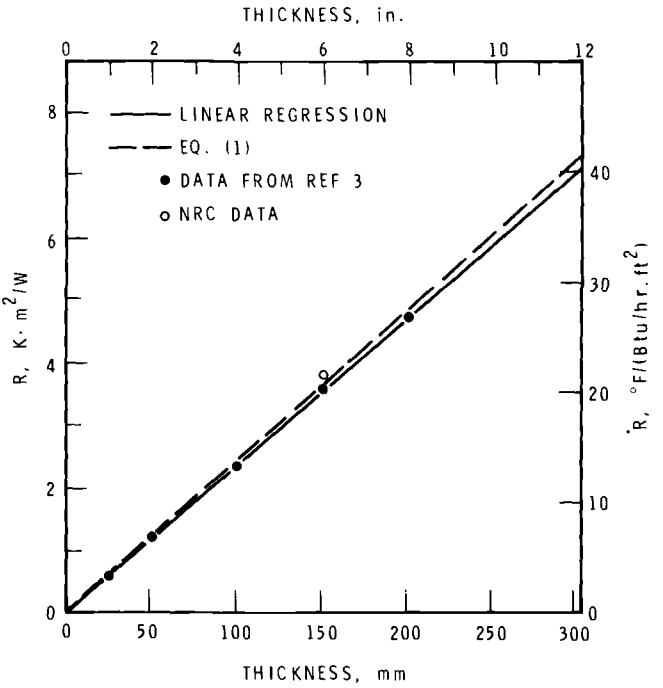

FIG. 12—*Thermal resistance versus thickness for cellulose fiber thermal insulation, density 64.2 kg/m³ (4 lb/ft³).*

data on three materials obtained from The Public Service Co. of Colorado. In these measurements the thermal resistance of a given specimen was measured first at full thickness, then at a number of progressively reduced thicknesses. Five measurements were made on one specimen; three measurements were made on each of the other two (Fig. 13). Equation 1, which has the same slope as the data in every case, accounts for simultaneous density and thickness changes.

The thermal resistances of the specimens used in these tests were higher than those predicted by Eq 1. This may be partly due to the degree of milling of the paper in the materials and differences in chemical formulation. This behavior was similar to that observed in NRCC measurements on the same materials.

Effect of Temperature Difference

Measurements were made at 25, 76, and 305 mm with temperature differences of 11 and 44°C rather than the usual 22°C. The percentage variation in R was found to be 0, +0.0013, and +0.12 percent/deg C, respectively.

An average value of 0.04 percent/deg C could have been used. Because the measurements at 305 mm are least reliable, a value of 0 percent/deg C is recommended until further information becomes available.

Effect of Mean Temperature on Thermal Resistance

Cellulose fiber insulation is an air-filled material operating well above the region where the mean free path length of air molecules approaches that of the spacing between fibers and controls the thermal conductance. It was assumed that variation of conductance, C, with mean temperature, T, is given by

$$C = C_o [1 + H(T - 24)] \tag{5}$$

where C_o is the thermal conductance at 24°C and H is a constant. The dependence of thermal resistance on temperature will therefore be

$$R = R_0/ [1 + H(T - 24)] \tag{6}$$

The term $\{1/[1 + H(T - 24)]\}$ cannot be readily inverted to give a convergent series, so this form must be retained.

The data obtained by Tye [*1*] were used to establish the value of H. His data covered a range of −18 to +50°C. The final value as determined by least squares in SI units was

$$R = R_0/[1 + 0.00289 (T - 24)] \tag{7}$$

Equation for Thermal Resistance

The equation for thermal resistance becomes

$$R = \frac{(0.205 + 0.0247L) - (0.00201 + 0.0000143L)\rho}{[1 + 0.00289 (T - 24)]} \tag{8}$$

The equation fits the NRC data with a standard deviation of less than 3 percent (approximately 0.1). Almost all the observations fall within 10 percent of Eq 8; most of the data fall within 4 percent of the equation. The remaining difference between the observations and the equation are more likely due to the form of the paper particles and to chemical composition than to errors in the measurements.

Adjusting the Constant Term in Eq 8

Equation 8 describes the dependence of thermal resistance on density and with thickness of the specimen, for thicknesses greater than 50 mm. The equation appears to have the correct form to fit the data. There does appear to be a problem, however, in determining the correct constant or

zero-thickness intercept. A check was made to see if the constant in Eq 8 could be adjusted to yield better results. The difference between the thermal resistance calculated from Eq 8, Rc, and the measured thermal resistance, Rm, is summarized in Table 4 as $Rc - Rm$. The increase of the 0.01 units to the constant in Eq 8 indicated by the average from 50 to 305 mm is hardly justified by precision in the measurements.

Adding Higher-Order Terms in Thickness and Adjustment of Slope

The fit of Eq 8 to the observations is shown in Figs. 2–7 and 13. Figure 2, for the 25-mm thickness, shows a large discrepancy between the curve from Eq 8 and that from the linear regression. This discrepancy indicates that either A or both A and B in the equation $R = A + B\rho$ should have higher-order terms in L. The equation for R obtained from a second-order fit to both A and B gives better agreement. The standard deviation from the data, however, is large and, to improve the agreement, the equation must be shifted as indicated by the last set of coefficients in Table 2*b*.

As already mentioned, most cellulose fiber insulation is generally applied at densities over 30 kg/m^3 and at thicknesses greater than 50 mm. There

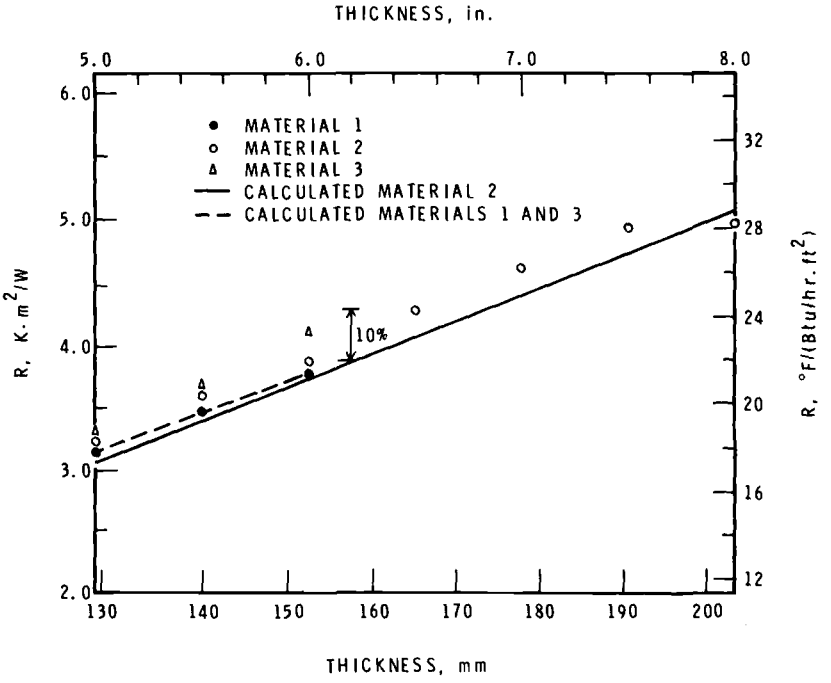

FIG. 13—*Comparison of Eq 8 with data from Table 1b when thickness decreases and density increases.*

appears to be little reason to complicate the equations with terms that become negligible in the normal range of use. The uncorrected linear equation is sufficiently accurate for material in thicknesses greater than 50 mm.

Discussion

Thickness Effects

The thermal resistance of low-density insulation materials is not necessarily directly proportional to thickness. A theoretical model was proposed by Poltz [*6*] in 1962 to explain this phenomenon in cellular plastics. His equations can be rearranged to produce an equation in the form

$$R(L) = R(0) + r(\infty)\, L \tag{9}$$

The thermal resistance at thickness L is equal to an apparent thermal resistance for zero thicknesses of material $R(0)$ plus the thermal resistance per unit thickness of material measured at large thicknesses, $r(\infty)$, multiplied by the thickness of the specimen. The equation will hold only at thicknesses greater than the mean free path length [*7*] for radiation in the insulation. The equation for the thermal resistance of the layer of material can be interpreted as the sum of the thermal resistances of two layers for which there are widely different heat-transfer mechanisms. The same form of equation can be deduced by examining the radiation heat transfer through absorbing or scattering gases.

Examples of such dependence were given by Shirtliffe [*8*], Cammerer [*9*], and more recently by Lao and Skochdopole [*7*]. At least two manufacturers of mineral fiber insulation investigated this dependence and have been using similar equations in the design of such insulations since the mid-1960's. The existence of a thickness dependence for cellulose fiber insulation was measured in the early 1970's at the Division of Building Research. The effect in this material may be due to radiation as in plastic foams and also to moisture gradients.

It is not simple to measure the thickness effect. Marechal [*10*], in a discussion of Cammerer's paper, attempted to show that there was no such effect. He claimed it was due to errors in measurement of surface temperatures in the test apparatus. Edge losses can also vary with the thickness of the specimen and can either mask the thickness effect or make it appear more pronounced. This is especially true if a small amount of edge insulation is used on the apparatus. When the ambient temperature is lower than the mean temperature of the specimen, the error will produce results that indicate a thickness effect greater than actually exists. Other errors in measurement may also tend to have the same effect. The con-

tribution of such errors is recognized in ASTM Specifications C 177-76 and C 518-76.

The thickness effect measured in this study is not due to surface contact or errors in surface temperature measurements. The errors in such measurements are at least two orders of magnitude smaller than the measured thickness effect. The computer calculations of edge-loss errors, although not exact, showed that the edge losses were too small to cause the observed thickness effect. Unless some as yet unexplained or unrecognized effect is found, the thickness effect determined in these measurements must be assumed to be real.

Second Analysis of the Data

The observations were analyzed to see if the resulting equation was highly dependent on the data selected. Additional data were used, equal weight was placed on the data, and less precise corrections were made to individual measurements.

The equation in SI units obtained was

$$R = \frac{(0.253 + 0.0241L) - (0.00178 + 0.0000075L)\rho}{[1 + 0.00289\,(T - 24)]} \tag{10}$$

The standard deviation on 77 measurements made at NRCC was about 3 percent (approximately 0.1).

Equation 10 gives values for a 40-kg/m^3 material very close to those given by Eq 8. The difference in R at 50 mm was +0.032 (1.6 percent) and at 305 mm +0.043 (0.6 percent). These are small differences. The slopes between 76 and 305 mm differ by 1.3 percent.

Conclusions

The equation for thermal resistance (in SI units) (Eq 8)

$$R = \frac{(0.205 + 0.0247L) - (0.00201 + 0.0000143L)\rho}{[1 + 0.00289\,(T - 24)]}$$

will, on average, describe the thermal resistance of layers of newsprint-based cellulose fiber insulation with thicknesses between 50 mm and 305 mm, with densities of 32 to about 100 kg/m^3, for applied temperature differences of 5 to 45°C, and for mean temperature from −20 to +50°C. The thermal resistance of individual materials may differ from the value obtained by the equation by as much as 10 percent. This difference is probably due to the shape of the particles of paper and the formulation and amount of powdered fire retardant in the product. The standard deviation of the fit was about 3 percent (approximately 0.1) for the NRC

data and 6 percent (approximately 0.2) when data from the other sources were included. Anderson's data and 30 additional data points agree well with the equations, and inclusion of this in the analysis would improve the equations slightly.

Terms were suggested that would extend the equation to densities between 15 and 32 kg/m^3 and thicknesses of 10 to 50 mm. Additional observations would be required, however, to establish these terms with certainty.

The equation developed in this study contains terms to account for the so-called "thickness effect" on thermal resistance for low-density insulations over 50 mm thick.

Acknowledgments

The authors would like to acknowledge the excellent cooperation received from R.P. Tye, A. Déjarlais, R.W. Anderson, The Public Service Co. of Colorado, and a number of members of ASTM Committee C-16 in the gathering of data and discussion of the results. We would like also to acknowledge the many suggestions for improving the specimen preparation made by J.G. Theriault and C. St. Jacques and the meticulous work of J.G. Theriault, R. Marchand, G. Keatley and N. Normandin in the specimen preparation and measurements. This paper is a contribution from the Division of Building Research, National Research Council of Canada, and is published with the approval of the director of the Division.

References

[1] Tye, R.P., *Journal of Testing and Evaluation*, Vol. 2, No. 3, May 1974, pp. 176–179.
[2] Anderson, R.W. and Wilkes, P., "Survey of Cellulosic Insulation Materials," ERDA 77-23, UC-95d, Energy Research and Development Administration, Jan. 1977.
[3] Anderson, R.W., private communication.
[4] Bomberg, M. and Shirtliffe, C.J. this publication, pp. 82–103.
[5] Pelanne, C.M. in *Proceedings*, Eighth Conference on Thermal Conductivity, Plenum Press, New York, 1969, pp. 897–911.
[6] Poltz, H. *Allgemeine Wärmetechnik*, Vol. 4, 1962, pp. 64–71.
[7] Lao, B.Y. and Skochdopole, R.E. in *Proceedings*, Society of the Plastics Industry, International Cellular Plastics Meeting, Montreal, Canada, Nov. 1976, pp. 175–182.
[8] Shirtliffe, C.J. *Canadian Building Digest*, National Research Council of Canada, Division of Building Research, No. 149, Ottawa, Ont., Canada, 1972.
[9] Cammerer, W.F. in *Proceedings*, International Institute of Refrigeration (IIR) Commission B, Zurich, 1973–1974, pp. 189–195.
[10] Marechal, D., Discussion of Ref 9, pp. 196–200.

M. Degenne,[1] *S. Klarsfeld,*[1] *and M-P. Barthe*[1]

Measurement of the Thermal Resistance of Thick Low-Density Mineral Fiber Insulation

REFERENCE: Degenne, M., Klarsfeld, S., and Barthe, M-P., "**Measurement of the Thermal Resistance of Thick Low-Density Mineral Fiber Insulation,**" *Thermal Transmission Measurements of Insulation, ASTM STP 660*, R. P. Tye, Ed., American Society for Testing and Materials, 1978, pp. 130–144.

ABSTRACT: The use of light and thick insulating materials (fibrous and cellular) is becoming more and more frequent. This led us to the building of a thermal resistance measuring apparatus equipped with large-size heat flowmeters. The construction and performance of such an instrument, which allows thermal measurements on light insulating materials of thickness up to 120 mm, are described.

The apparatus, using one single specimen, is equipped with a bi-guarded hot plate and a heat flowmeter. This gives the possibility of performing both relative (with the heat flowmeter) and absolute measurements and of cross-checking the results.

Such flexibility allows the study of some anomalies concerning the calibration constant of the relative measurement apparatus, which is being employed more and more in industrial quality control.

KEY WORDS: mineral fiber, building insulation, thermal insulation, heat transfer, guarded hot plate, heat flowmeter, thermal resistance, thermal conductivity, reference materials

During previous studies concerning the correlation between apparent thermal conductivity and structural parameters of fibrous insulating materials, the importance of taking into account a large number of measurements to characterize such materials and the advantage of using a heat flowmeter method were explained [1–4].[2] As a matter of fact, such instruments allow measurements in a short time (15 to 40 min per measurement) and offer fast collection of results. Specimens are then measured

[1]Engineering supervisor, Heat Transfer Laboratory manager, and Research Center manager, respectively, Saint Gobain Industries, Centre de Recherches Industrielles, B. P. 19 - 60290 Rantigny, France.

[2]The italic numbers in brackets refer to the list of references appended to this paper.

at temperatures close to the ambient; the side dimensions of the specimens vary between 200 and 400 mm, with thicknesses between 30 and 60 mm.

In recent years, due to energy saving considerations, insulation thicknesses have increased considerably, sometimes reaching 300 mm. Moreover, fibrous materials used in building insulation have become thicker and are of a low density. Under such conditions, the question arises whether it is practical to continue performing apparent thermal conductivity measurements on these products with the same instrument as in the past, or is it necessary to build instruments equipped with larger-size plates?

Taking into account the plate sizes, some standards for instance, ASTM Recommended Practice for Determination of the Thermal Resistance of Low-Density Mineral Fiber Blanket-Type Building Insulation (C 653-70), suggest that specimens be split when their thicknesses exceed the acceptable maximum thickness [ASTM Test for Thermal Conductivity of Materials by Means of the Guarded Hot Plate (C 177-71) and Ref *5*]. With that as a starting point, the following two questions were studied:

1. Is the thermal conductivity of a split specimen representative of an unsplit specimen, that is, at full thickness?
2. Is the calibration constant of heat flowmeter instruments still applicable when measuring the thermal conductivity or the thermal resistance of light products, when determined from heavy-density standards?

To answer both questions, a new heat flowmeter instrument was developed. With a hot plate of the bi-guarded type [*6*], it is possible to associate each result obtained by the relative method with the corresponding absolute measurement of the thermal flux. This instrument and the first collected results are described herein. Such results give useful indications not only with regard to quality and production control, but also with regard to certification requirements. In addition, they have been very interesting from a more basic point of view, relative to understanding the heat-transfer mechanism in fibrous insulating materials and especially the role played by radiation.

Instrument Description

Since it does not deal with technology, this paper does not describe the details of construction of the instrument, but only explains its operating principle; however, some features of its technical characteristics and performance are described and emphasized. The important findings obtained during recent years in the field of thermal conductivity measurements of insulating materials have been taken into account. For more details, see Refs *6* and *7* and the ASTM Test for Steady-State Thermal Transmission Properties by Means of the Heat Flow Meter (C 518-76).

Operating Principle

The new instrument is of the asymmetrical type, using one specimen with heat flowing from bottom to top. The plates dimensions are 500 by 500 mm and the heat flow density is measured within a central area of 250 by 250 mm.

The originality of this instrument stems from the fact that it offers to the operator the possibility of performing both relative and absolute measurements on specimens whose thickness can reach 120 mm. Such measurements can be made simultaneously if required.

Relative measurements are made possible by a heat flowmeter located in contact with the cold plate. One face of the flowmeter makes up the isothermal cold surface. In the case of such a relative measurement, a calibration constant is associated with the instrument, the value of which is determined with the help of a standard specimen.

Absolute measurements are performed using a bi-guarded hot plate which allows measurement of dissipated power, and a face of which makes up the isothermal hot surface.

The instrument operates in either of two ways:

1. At "imposed" hot and cold temperatures, in which case one measures the heat flow density. This is the relative method, using a heat flowmeter.
2. At a given heat flow density (electrical power), in which case one measures the resulting hot and cold temperatures. This is the absolute method.

In the second case, the ease of measuring the hot and cold temperatures, and the power adjustment flexibility, makes it possible to perform absolute measurements under the same conditions as relative measurements; cold and hot faces can be set at the same temperatures by adjusting properly the heat supplied in the metering area.

The steady-state heat flux through the specimen and the heat flowmeter is calculated as follows

$$\phi = \lambda \frac{\Delta T}{D} = SV \tag{1}$$

where

ϕ = heat flow density or heat flux, W/m^2,
$\Delta T = T_2 - T_1$ = temperature difference between hot (T_2) and cold (T_1) faces, K,
D = specimen thickness, m,
λ = thermal conductivity, W/m·K
S = sensitivity of the heat flowmeter, W/m^2·V, and
V = voltage at the flowmeter connections, V.

It is assumed that the heat flow density is the same through the specimen center and the heat flowmeter, that the heat transfer is solely by conduction, and that the contact resistances are negligible between the specimen faces and the plates surfaces.

Under these assumptions, the first equation (Fourier law) allows λ to be determined by the absolute method, and the second equation allows the same by the relative method. The possibility of associating, each time, the heat flow density value ϕ with the heat flowmeter indication V permits the establishment of stability or the variation of S for the different types of insulating materials to be checked.

Hot Plate

The hot plate used is of the bi-guarded type with a unidirectional heat flow as already described in Ref *6* and as presently used in the reference instrument. Its construction is detailed in Fig. 1. Side and lower heat losses are limited by a guard ring-shaped section and by a lower guard plate, each one being monitored by a zero-balance controller of which the sensors are a thermopile and a heat flowmeter, respectively. The only principle modifications to this hot plate since its construction in 1969 concern the power supply [*6*]. The stabilized d-c power supply of the heating resistance is monitored by an electric temperature controller, the sensor of which is located in the center of the hot plate as close as possible to the heating resistance. The voltage applied to the resistance connections is made of a succession of non-periodic square waves. A counting device allows the ratio between the heating time and the total measurement time to be calculated; from this, it is possible to deduce the efficient power dissipated by the metering area

$$P = UI \frac{t_C}{t_T} \tag{2}$$

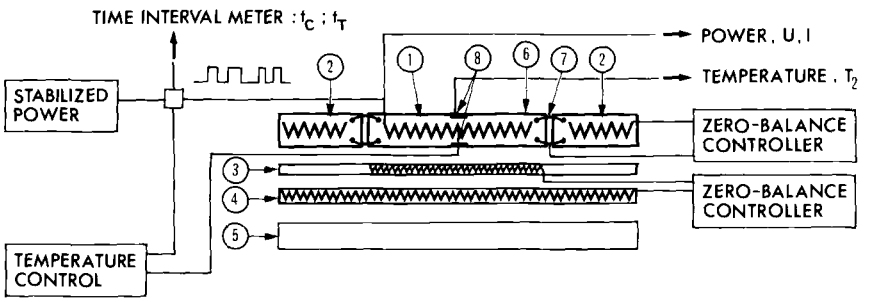

FIG. 1—*Bi-guarded hot plate. Key:* 1. *Guarded hot plate, central section*: 2. *guarded hot plate, guard section*; 3. *heat flowmeter (zero-balance controller)*; 4. *lower guard plate*; 5. *support plate (insulation)*; 6. *hot face*, T_2; 7. *thermopile*; 8. *platinum resistance temperature detector*.

where

P = dissipated power, W,
U = voltage at the heating resistance connections during heating time, V,
I = intensity, A,
t_C = heating time, s, and
t_T = measurement time, s.

The measurement should be performed for one hour if a 1 percent accuracy on the power measurement is desired. This new power supply method reduces the time needed to reach a steady-state condition after starting the instrument or when changing the mean measurement temperature, and it allows the hot plate to be maintained at a present temperature whatever the measured specimen.

Cold Plate; Heat Flowmeter

The cold plate, as the hot plate, has a composite structure encompassing (Fig. 2)

1. a cold plate in which flows a liquid supplied by a Freon compressor,
2. an auxiliary hot plate,
3. a damping layer, and
4. a heat flowmeter.

The free face of the heat flowmeter makes up the cold face of the instrument; it is in contact with the specimen to be measured. The other face of the heat flowmeter is in contact with a layer of insulating material which separates it from the auxiliary hot plate, but ensures a uniform contact on the whole surface and the damping of the temperature oscillations generated by the control.

The role of the auxiliary hot plate, the heating of which is monitored by a temperature controller, is to adjust with a very good stability the

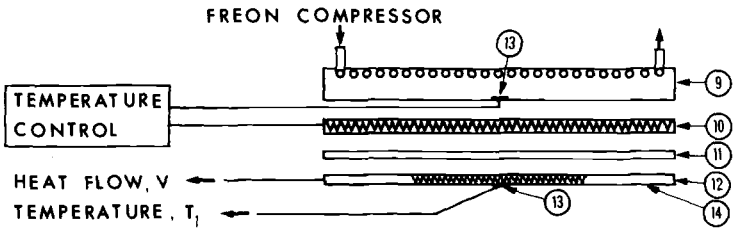

FIG 2—*Cold plate. Key*: 9. *refrigerated heat sink*; 10. *auxiliary hot place*; 11. *damping insulating layer*; 12. *heat flowmeter (250 by 250 mm)*; 13. *platinum resistance temperature detector (100 Ω)*; 14. *cold face*. T_1.

temperature of the heat flowmeter face in contact with the specimen. The set point is adjustable to get the desired cold temperature T_1.

Both measurement and control heat flowmeters are built according to new techniques that wholly eliminate the use of thermocouple wires and welds. Cold and hot junctions are made with the help of metallization and photoetching (see Fig. 3). These techniques made possible the construction of heat flowmeters of large dimensions (250 by 250 mm), which, however, are not yet commercially available. The sensibility of these flowmeters is high due to the considerable increase in the number of junctions per unit area. The aforementioned techniques allow the heat flowmeter to be produced with a high degree of uniformity and repeatability. The surfaces of the flowmeter are painted black.

Assembling and Positioning of Plates; Ambiance

Both the hot and cold plates of the instrument are horizontal; the lower, or hot, plate is fixed, and the upper, or cold, plate is movable. The cold

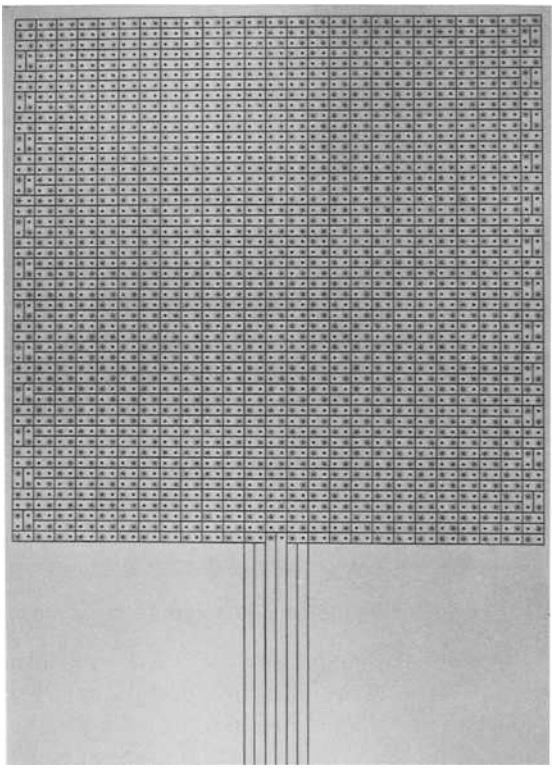

FIG. 3—*Heat flowmeter.*

plate can be lowered or raised from outside the instrument with the help of a mechanism which permits a vertical continuous displacement, along with a good parallelism of both isothermal flat surfaces. This displacement mechanism is well adapted to measurements on resilient materials such as the ones studied herein.

The thickness determination is made through a calibrated rectilinear potentiometer.

The assembly plates' specimen is put inside a parallelepipedal volume, the cross section of which is close to the area of the measurement plates, and which is limited by insulated walls.

The instrument is not conditioned in temperature and humidity, but it is located in an air-conditioned room (24°C mean temperature and relative humidity around 45 percent), ensuring very stable operating conditions.

Measurements

The instrument operating conditions are determined as follows: The cold and hot face temperatures are preset on the controllers, and the measurement thickness is set digitally after introducing the specimen.

Relative Measurements—The voltage V at the heat flowmeter connections (digital voltmeter) is determined; the thickness (digital voltmeter) is checked; the temperatures T_1 and T_2 (digital resistance thermometer) are checked; and ΔT is computed.

Absolute Measurements—The voltage U and the intensity I at the heating resistance connections during heating periods (digital voltmeter) are determined; the heating time (electronic stopwatch) is measured; the ratio t_C/t_T is calculated; the thickness (digital voltmeter) is checked; the temperatures T_1 and T_2 (digital resistance thermometer) are checked; and ΔT is computed.

In both the relative and absolute cases, one checks the uniformity of temperatures T_2 and T_1 of the hot and cold plate faces using the control thermocouples (digital voltmeter).

Table 1 gives the technical characteristics and performances of the apparatus.

Comparison with Previous Results and Foreign Laboratories' Results

For reasons of continuity in the analysis of the performances of the instrument discussed herein, the comparison data between laboratories and instruments already published in Ref *6* are addressed again. We add to these the results of measurements made on reference fiber glass slabs recently supplied to specialized laboratories by the Bureau National de Métrologie (BNM) [*8*]. Figure 4 shows the following:

1. On the one hand, thermal conductivities as a function of temperature, determined by the National Bureau of Standards (NBS) on a fiber glass specimen (density, 162 kg/m^3), which are considered as reference values.

2. On the other hand, present results obtained on the same specimen with the bi-guarded hot plate (400 by 400 mm) instrument [6] (our metrological reference), and the new instrument operating at $\bar{T} = 24°C$ in the absolute-measurement version.

Figure 5 takes up again:

1. On the one hand, the results collected with the 400 by 400 mm instrument on fiber glass slabs (density, 88 kg/m^3) appertained to a lot

TABLE 1—*Thermal resistance measurement apparatus: technical characteristics and performances.*

Specimen:	
surface	500 by 500 mm
thickness	20 to 120 mm
metering area	250 by 250 mm
Isothermal surfaces:	
temperatures of the metering faces:	
range of possible temperatures	$0 < T_1 < 30°C$ $20 < T_2 < 50°C$
temperature heterogeneity	$< 0.2°C$
temperature stability	$< \pm 0.02°C$
parallelism	± 0.1 mm
Heat flowmeter:	
number of junctions	1250
metering area	250 mm × 250 mm
thickness	6 mm
sensitivity	10^4 W/m^{2}V
heat flux stability (between 400 and 1500 μV)	4 μV, that is, 0.3 to 1%
Ambiance (measurement room):	
mean temperature stability	$\pm 0.5°C$
relative humidity	$45 \pm 5\%$
Measurement devices:	
digital voltmeter (control thermocouples, power, heat flowmeter)	20 000 digits resolution: 1 μV
digital thermometer (resistance sensor) (hot and cold faces)	20 000 digits resolution 0.01°C
thickness	
displacement sensor	
linearity	0.5%
accuracy	0.1 mm
digital voltmeter	2000 digits
stopwatch:	resolution 0.1 mm
resolution	10^{-2}s
Reproductibility:	$\pm 1\%$
Accuracy:	see Figs. 4 and 5

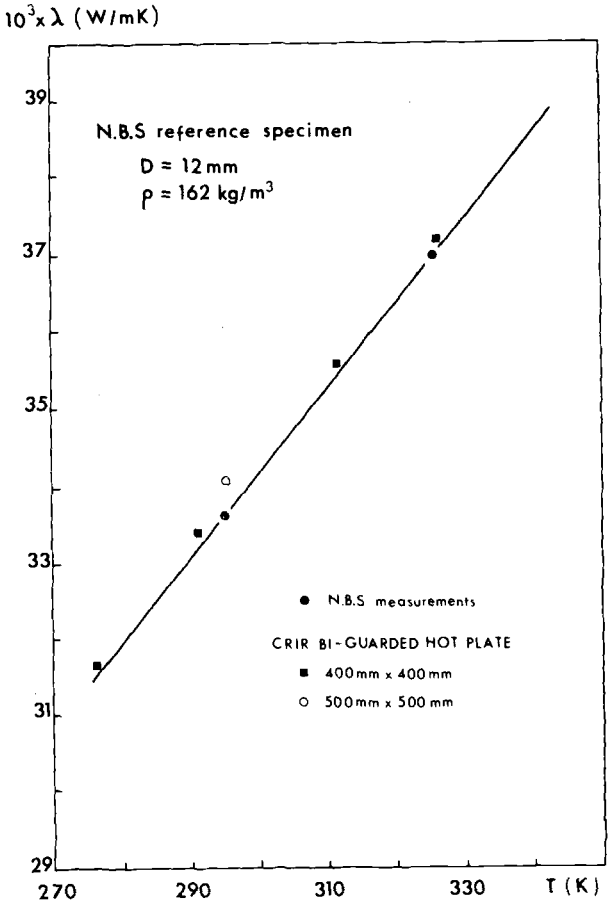

FIG. 4—*Thermal conductivity λ versus mean temperature measured for NBS reference specimen.*

which was used for round-robin comparative tests, between different laboratories, organized by the Institut International du Froid (IIF) [9]. The reference data which characterize these materials were obtained by the National Physical Laboratory,Teddington, England.

2. On the other hand, the data on the reference slabs from BNM obtained with both of our instruments. Their physical characteristics (density, fiber diameter, percentage of binder, thermal conductivity) are very close to those of the reference lot from IIF [*10*].

In examining all these data, one can observe a good correspondence between the results obtained with the previous metrological 400 by 400 mm reference instrument and the new 500 by 500 mm instrument as well as the satisfactory concurrence between the results reported here and

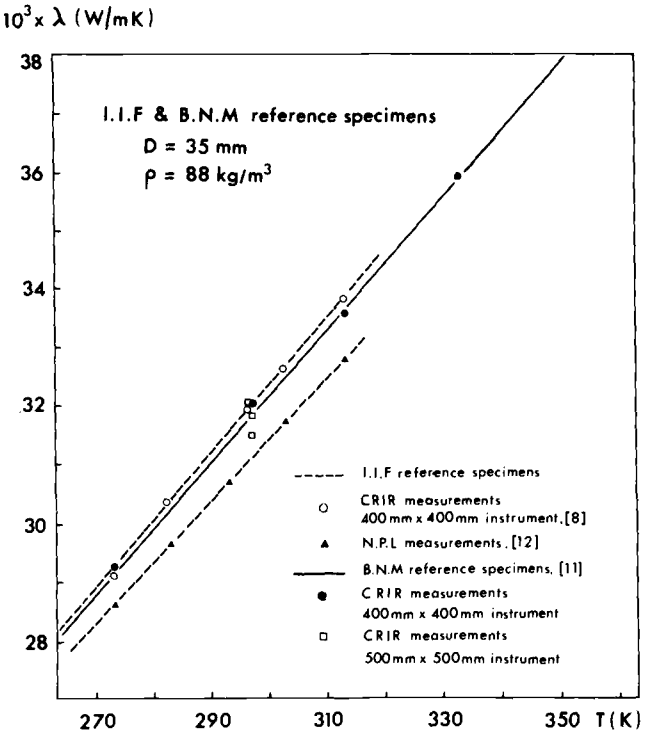

FIG. 5—*Thermal conductivity λ versus mean temperature for IIF and BNM reference specimens.*

those collected on identical or similar reference products by both NBS and NPL laboratories. In all cases, differences between results at $\bar{T}$ = 24°C remain less than 2 percent.

Results

Dispersion Due to Measurement Equipment

Most of the specifications concerning thermal conductivity measurements do not prescribe plate dimensions, though some indicate a relationship to be satisfied between the area of the specimens (which is equal to the instrument plate area) and their maximum acceptable thickness (ASTM Method C177-71[3] and Ref *5*). Consequently, it becomes mandatory

[3]The standard ASTM Test Methods C 177-76 and C 518-76 give, in their most recent issue, more detailed explanations of errors due to thermal losses that depend on several parameters related to instrument technology. The authors did not have access to these new issues in time to take them into account in this paper.

to use relatively thin products or to split thick products when measuring with an instrument having small plates (ASTM Method C 653-70).

In the case of light-density fibrous insulating materials, which are usually thick, splitting of the specimens increases considerably the heterogeneity of the fiber distribution when comparing any one of the split specimens with the original unsplit one.

One may observe in Fig. 6 the dispersion of results as a function of increasing plate area. As a matter of fact, the total dispersion of the thermal conductivity measurements as a function of density $\lambda(\rho)$ decreases notably when the plate area of the instrument goes from 200 by 200 mm to 400 by 400 mm, and then to 500 by 500 mm.[4] The standard deviations σ_λ in these three cases are 4.9, 1.6, and 1.4, respectively.

It follows that the measuring instrument must be properly chosen according to the nature of the product to be evaluated and that splitting of light-density thick products such as the one studied here is not the best procedure for the future.

Calibration Curve

According to the operating principle explained earlier, the instrument described herein allows one to determine the calibration curve of its heat flowmeter and to calculate the values of their associated calibration constants.

Figure 7 represents the correlation between heat flow densities that cross six fiber glass specimens of different thermal conductance ($0.23 < \Gamma < 2.9$ W/m$^2\cdot$K) or thermal resistance ($0.3 < R < 4.3$ m$^2\cdot$K/W) and the voltage supplied by the instrument heat flowmeter. The six fiber glass specimens represent low- and high-density insulants; the white and black points on Fig. 7, respectively. We can define light and heavy fibrous materials with regard to the minimum value of the function $\lambda = f(\rho)$ (Fig. 8). At left of this minimum are the "low-density" products. In this range of densities we have coupled heat transfer: radiation and conduction. At right of the minimum, the conduction heat transfer is largely predominant, the radiation heat transfer being negligible.

At the figure scale the function $\varphi = f(V)$ is practically a straight line, the slope of which represents the sensitivity, S, of the flowmeter. The linearity is better than 1 percent (except the first point). According to these results, it seems that the calibration constant is independent of the conductance of the reference slab and of the fact that the heat transfer is purely conductive or coupled with radiation.

[4]The 500 by 500 mm instrument used for these measurements was old and without any capability for absolute measurements, or, consequently, for correcting its own calibration constant.

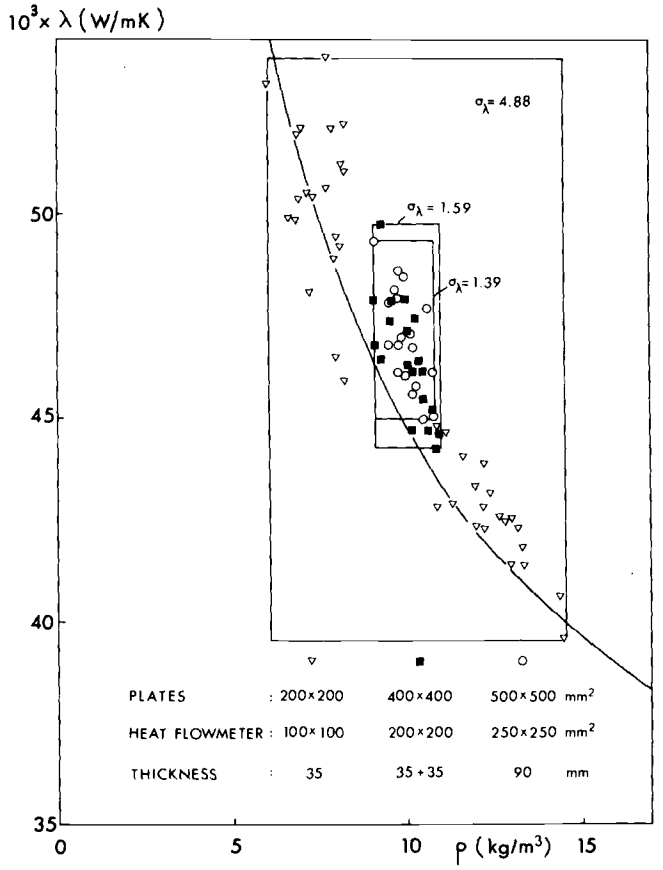

FIG. 6—*Thermal conductivity λ versus mass/volume measured for low-density fibrous insulating materials. Mean temperature: 297 K.*

Influence of Thickness

Four families of products having densities between 10 and 20 kg/m³ and thickness increasing progressively (25, 45, 95, and 115 mm) were measured. We observed a systematic increase of the thermal conductivities as the specimens get thicker.

This thickness influence will not be noted with homogeneous materials which are opaque to radiation; it can only be explained—errors due to thermal losses being put aside—by the "semitransparency" of certain types of insulating materials. This phenomenon has already been reported by several authors, but in most cases for cellular plastic insulants. It is all the more pronounced as the density decreases and the mean temperature increases. Such an effect is theoretically predictable owing to the

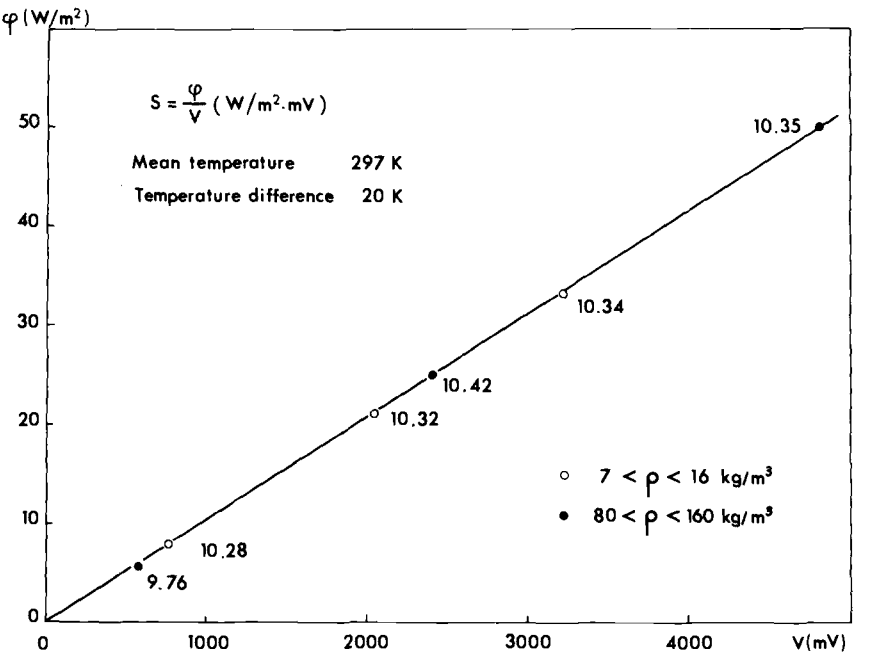

FIG. 7—*Calibration curve.*

Hamaker model, describing the total heat transfer through a porous medium as a coupling of heat transfer by conduction and by radiation [*11–14*].

One conclusion is obvious: The thermal conductivity associated with a fibrous or cellular light insulating material is not an intrinsic property of the product, since it depends on the particular conditions under which it has been determined (thickness in the present case, but also measurement plates' emissivities and temperatures T_1 and T_2). This is one of the reasons why this "conventional" value of λ associated with the product is called by some authors "apparent," "effective," or "equivalent" thermal conductivity.[5]

Practically, for the user, it seems more convenient and more cautious, as far as risks of errors are concerned, to get rid of the ambiguous term "apparent thermal conductivity" and to express the thermal conductance, Γ, or its reciprocal, the thermal resistance $R = I/\Gamma$, using ϕ, ΔT, and D. These symbols define the material as it is produced (taking into consideration its nominal production thickness). In addition, they are defined under standardized measurement conditions as close as possible to the actual use conditions.

[5]In this paper, all mentioned thermal conductivities are apparent.

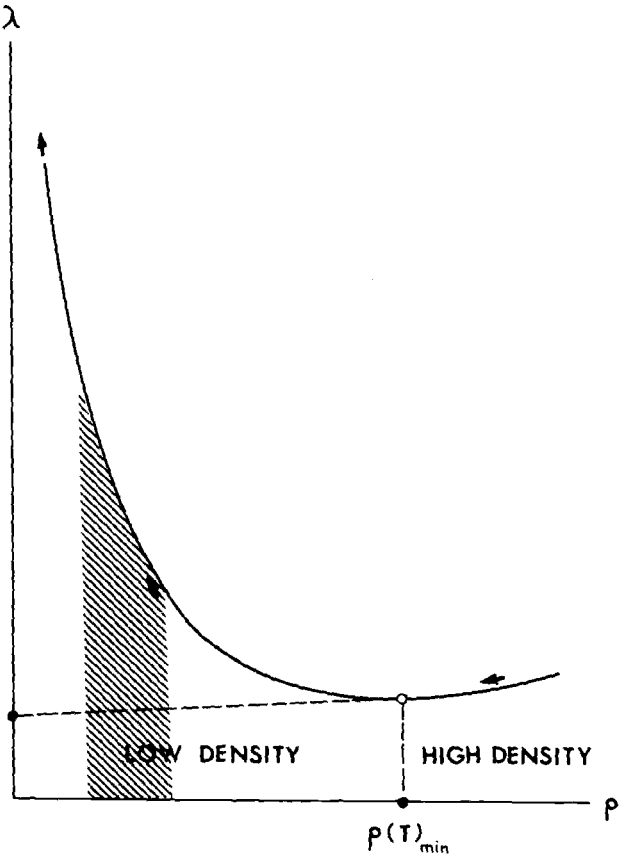

FIG. 8—*Thermal conductivity λ versus mass/volume for a fibrous insulating material (qualitative correlation).*

Conclusions

The results obtained here with the new instrument required additional corroboration and more precise evaluations of sources of errors (especially those due to thermal losses). On the other hand, the influence of the measurement thickness on the apparent thermal conductivity, according to the structural factors of the fibrous insulants, will have to be determined. Still, the whole of the collected results give interesting and practical information, particularly with regard to the production control of light-density fibrous insulating materials. In summary, the following can be stated:

1. It is preferable not to perform heat-transfer measurements on split specimens, because of their structure and the influence of thickness on measurement results.

2. The calibration constant of instruments using a heat flowmeter does

not seem to vary appreciably with the range of measured conductance and the type of the fibrous material. It is recommended, however, that until this result is corroborated, the reference slabs be of the same type as the material to be measured.

Acknowledgments

The authors wish to thank M. Levecque, president of Certain Teed Corp., who drew their attention to the importance of metrological problems raised by the light insulation products, and M. Sauvage, technical director of the Insulation Department of Saint-Gobain Industries for his interest and his encouragement. They wish also to acknowledge the help of J. Boulant, who participated very actively in the development of the new instrument, J-L. Jaouen, who performed most of the measurements, and M. Hyrien, who took part in the discussion and interpretation of the results.

References

[1] Fournier, D., Andre, G., and Klarsfeld, S., *Supplément au Bulletin de l'Institut International du Froid*, Annexe 1966–2, Commission 2, Trondheim, Norway, 1966.

[2] Fournier, D., Andre, G., and Klarsfeld, S., in *Proceedings*, 12th International Congress of Refrigeration, Madrid, Vol. 2, 1967, pp. 117–127.

[3] Fournier, D. and Klarsfeld, S. in *Heat Transmission Measurements in Thermal Insulations, ASTM STP 544*, American Society for Testing and Materials, 1974, pp. 223–242.

[4] Klarsfeld, S., La Conductivité Thermique des Isolants Fibreux en Relation Avec Leur Structure," Comptes-rendus Scientifiques, Groupement Universitaire de Thermique, Paris, 1976.

[5] "Détermination de la Conductivité Thermique apparente au Moyen d'un Fluxmètre Thermique," International Standard ISO 2581, 1975(E).

[6] Fournier, D. and Klarsfeld, S., *Supplément au Bulletin de l'Institut International du Froid*, Annexe 1969–7, Commission 2 et 6, Liège, Belgium, 1969 pp. 321–331.

[7] Bankvall, C.G., "Guarded Hot Plate Apparatus for the Investigations of Thermal Insulation," National Swedish Institute for Building Research, Stockholm D5, 1972.

[8] Catalogue des Matériaux de Référence Français, Bureau National de Métrologie, Service des Matériaux de Référence, Feb. 1977.

[9] "Mesures Comparatives Internationales de Conductivité Thermique," *Bulletin de l'Institut International du Froid*, Annexe 1–1968, pp. 30–59.

[10] "Panneaux de Référence en Fibre de Verre Pour Mesures Comparatives de Caractéristiques Thermiques," Saint-Gobain Industries, Centre de Recherches Industrielles de Rantigny (CRIR), Rapport Interne No. 132/71, 1971.

[11] Larkin, B.K., "A Study of the Rate of Thermal Radiation Through Porous Insulating Materials, Ph.D thesis, University of Michigan, Ann Arbor, Mich., 1957.

[12] Linford, R.M.F. et al in *Heat Transmission Measurements in Thermal Insulations, ASTM STP 544*, American Society for Testing and Materials, 1974, pp. 68–84.

[13] Pelanne, C.M., "Experiments on the Separation of Heat Transfer Mechanisms in Low-Density Fibrous Insulation," *Proceedings*, Eighth Conference on Thermal Conductivity, Purdue University, West Lafayette, Ind., Oct. 7–10, 1968, Plenum Press, N.Y., 1969, pp. 897–911.

[14] Epherre, J.F., Combarnous, M.A., and Klarsfeld, S., *Supplement au Bulletin de l'Institut International du Froid*, Annexe 1977–2, Commission B 1, Washington, D.C., 1976, pp. 55–62.

Line Source Methods for Insulations

H. A. Fine[1]

Analysis of the Applicability of the Hot-Wire Technique for Determination of the Thermal Conductivity of Diathermanous Materials

REFERENCE: Fine, H. A., "**Analysis of the Applicability of the Hot-Wire Technique for Determination of the Thermal Conductivity of Diathermanous Materials,**" *Thermal Transmission Measurements of Insulation, ASTM STP 660*, R. P. Tye, Ed., American Society for Testing and Materials, 1978, pp. 147–153.

ABSTRACT: The hot-wire technique has been used to measure the thermal conductivity of many electrically and thermally insulating materials and the effective thermal conductivity of some diathermanous materials. An analysis of the heat transfer in diathermanous materials is presented which indicates that the method will not give a correct value of the effective thermal conductivity when radiation conduction is of importance. Until an exact solution to this heat-transfer problem is found, an ASTM standard for hot-wire type measurements on diathermanous materials is not recommended.

KEY WORDS: thermal conductivity, hot-wire technique, diathermanous materials

Nomenclature

b	Radial position equal to wire radius and inner surface of specimen
C_p	Specific heat
C_{p_w}	Specific heat of wire
$e_{b\lambda}(\lambda, T)$	Monochromatic black-body emissive power
H	"Outer conductivity" at the surface $r = b$, that is, the reciprocal of the contact resistance
I	Current
$i'_\lambda(\lambda, W)$	Directional monochromatic intensity
k_c	Thermal conductivity
k_{eff}	Effective thermal conductivity
k_r	Radiation conductivity
M_w	Mass of wire per unit length
N	Dimensionless parameter, $k_c\alpha/4\sigma T^3$

[1]Assistant professor, Department of Metallurgical Engineering and Materials Science, University of Kentucky, Lexington, Ky. 40506.

n Refractive index
Q Rate of heat generation per unit length of wire, I^2R
q''' Rate of heat generation per unit volume within a material
q_c Heat flux due to conduction
q_r Heat flux due to radiation
q_T Total heat flux
R Resistance per unit length of wire
r Radial position coordinate
T Temperature
$T_s(b,t)$ Specimen temperature at position b and time t
$T_w(t)$ Wire temperature at time t
t Time
W Hemispherical angular position
x Position coordinate in planar specimen
x_0 Thickness of planar specimen
α Absorption coefficient
α_λ Monochromatic absorption coefficient
θ Dimensionless temperature
λ Wavelength
π Density
σ Stephan-Boltzman constant
τ Dimensionless position, αx
τ_0 Optical thickness, αx_0

The hot-wire or probe technique has been used by many investigators to determine the thermal conductivity of many different types of materials. The procedure and the analysis of results have been given in *Thermal Conductivity* [*1*][2]. It has also been shown that for materials within which conduction heat-transfer predominates, the agreement between results obtained using the hot-wire and other techniques is excellent [*2*]. However, when heat transfer occurs by combined radiation and conduction, such as within a diathermanous material, the results obtained from the hot-wire technique may be in serious error.

Analysis of the Hot-Wire Technique

Opaque Materials

The thermal conductivity of an opaque material is calculated from the results of a hot-wire experiment and the solution of Fourier's Second Law for unidirectional radial heat flow in a cylindrical specimen, subject to a uniform constant temperature initial condition, a constant temperature at infinite-radius boundary condition, and a second boundary condition resulting from constant heat generation by a cylindrical perfect conductor at the axis of the specimen, that is, the hot-wire with resistance R per unit length and carrying current I. For a wire of unit length and radius b, the latter boundary condition is [*3*]

[2]The italic numbers in brackets refer to the list of references appended to this paper.

$$M_w C_{p_w} \frac{\partial T_w(t)}{\partial t} = Q - H\,(2\pi b)\,[T_w(t) - T_s\,(b,t)] \tag{1}$$

At the inside surface $r = b$ of an opaque specimen with thermal conductivity k_c

$$H\,(2\pi b)\,[T_w(t) - T_s\,(b,t)] = -k_c\,(2\pi b)\,\frac{\partial T_s\,(b,t)}{\partial r} \tag{2}$$

or combining Eqs 1 and 2

$$M_w C_{p_w} \frac{\partial T_w(t)}{\partial t} = Q - k_c\,(2\pi b)\left[-\frac{\partial T_s\,(b,t)}{\partial r}\right] \tag{3}$$

Diathermanous Materials

For diathermanous materials, that is, materials which are semitransparent to thermal radiation, the general equation for heat transmission by conduction and radiation within a stagnant body is [4]

$$\rho C_p \frac{\partial T}{\partial t} + \nabla \cdot (q_c + q_r) = q^m \tag{4}$$

where

$$\nabla \cdot q_c = \nabla\,(k_c \nabla T) \tag{5}$$

and

$$\nabla \cdot q_r = \int_{\lambda=0}^{\infty} \alpha_\lambda \left[4e_{b\lambda}\,(\lambda,T) - \int_{w=0}^{4\pi} i'_\lambda\,(\lambda,W)\,dW\right] d\lambda \tag{6}$$

At steady state and without heat generation *within* the material, Eq 4 becomes

$$\nabla \cdot (q_c + q_r) = 0 \tag{7}$$

However, Eq 7 still yields a nonlinear integrodifferential equation when combined with Eqs 5 and 6, for which few exact solutions have been determined.

For a large body of diathermanous material, the radiation heat transfer *within* the material can be approximated by a diffusion-like mechanism [*4–6*]. Using this approximation, which is called the diffusion or Rosseland approximation, Eq 6 becomes

$$\nabla q_r = \nabla\,(k_r \nabla T) \tag{8}$$

where k_r is the "radiation conductivity" and, for a material with refractive index n and absorption coefficient α, equals [*4–6*]

$$k_r = \frac{16n^2\sigma T^3}{3\alpha} \tag{9}$$

Combination of Eqs 5, 7, and 8 yields

$$\nabla (k_c \nabla T + k_r \nabla T) = \nabla (k_{\text{eff}} \nabla T) = 0 \tag{10}$$

where k_{eff} is the "effective thermal conductivity" of the material and equals

$$k_{\text{eff}} = k_c + k_r \tag{11}$$

Finally, integration of Eq 10 yields the total heat flux per unit area and per unit time, q_T, due to combined conduction and radiation

$$q_T = -k_{\text{eff}} \nabla T \tag{12}$$

Because of the similarity between Eq 12 and Fourier's First Law for conduction heat transfer, it has been proposed that the hot-wire technique can also be used to measure the effective thermal conductivity of a diathermanous material [*7,8*].

Discussion

The diffusion approximation for combined radiation and conduction heat transfer is not valid at the boundaries [*9*], and simple substitution of k_{eff} for k_c in Eqs 2 and 3 and $k_{\text{eff}}/\rho C_p$ for the thermal diffusivity in Fourier's Second Law should not allow k_{eff} to be found by the hot-wire technique. As mentioned previously, few exact solutions have been determined for combined radiation and conduction heat transfer. It should therefore not be surprising that exact solutions are not available for transient radiation and conduction heat transfer or for the steady state case in cylindrical coordinates. Exact solutions have been calculated for unidirectional heat transfer by combined radiation and conduction between two infinite, black, isothermal, parallel plates [*9*] and two infinite, nonblack, isothermal, parallel plates [*10*]. These results can be used to illustrate the error which occurs when analyzing the results of hot-wire experiments.

For planar geometry, the total heat flux within an object must be constant at steady state. However, a hot surface adjacent to a diathermanous substance cannot produce the same radiant heat flux as a layer of the diathermanous material at the same temperature [*9*]. Thus, more heat must be transferred by thermal conduction near the hot boundary of a diathermanous material in order for the total flux, that is, the radiant heat flux plus the conduction heat flux, to be constant. This higher-conduction heat flux can be obtained only by a higher temperature gradient at the hot boundary, as shown in Fig. 1. Except for the region adjacent to the hotter surface, the exact and approximate solutions for combined heat transfer

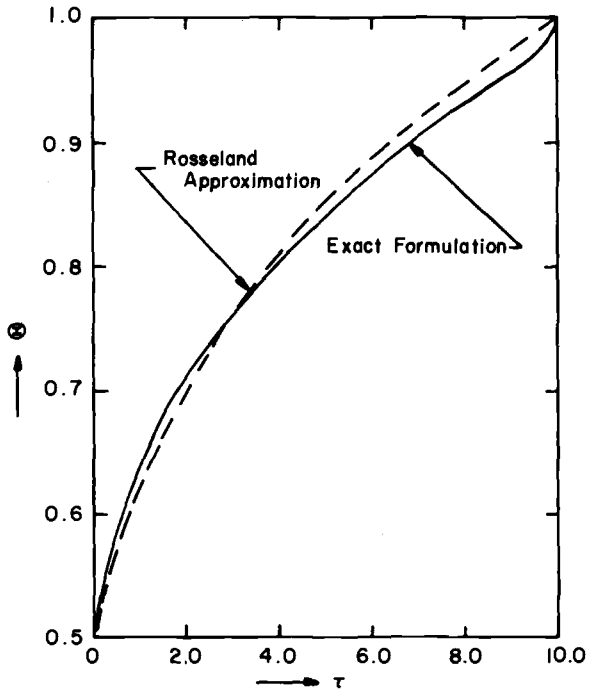

FIG. 1—*Dimensionless temperature, θ, versus the optical thickness, τ = αx, for* k_c = *0.093 W/m·K,* $\alpha = 328_m^{-1}$, $N = k_c\alpha/4\sigma T^3 = 0.02916$, *and* $\tau_0 = \alpha x_0 = 10$ *(from Ref 9).*

between black plates are in good agreement. However, the analysis of a hot-wire experiment for opaque specimens shows that the temperature profile in the region of material immediately adjacent to the hot-wire, that is, the hot surface, is of primary importance, for it is in this region that Eq 3 applies and it is through Eq 3 that the variation in the temperature of the hot wire is related to the thermal conductivity of the specimen.

The previous discussion was for planar geometry, while the geometry of interest in a hot-wire experiment is cylindrical. However, the cylindrical shell of material between the surfaces $r = b$ and $r = b + dr$ can be approximated as a plane for small values of dr. Thus, in this region a higher temperature gradient must also exist in a diathermanous material during a hot-wire experiment. Accordingly, for a given experiment in which the wire temperature and the rate of heat generation are measured, Eq 3 shows that for

$$\left(\frac{\partial T_s(b,t)}{\partial r}\right)_{\text{(actual)}} > \left(\frac{\partial T_s(b,t)}{\partial r}\right)_{\text{(predicted by Eq 12)}} \tag{13}$$

the measured thermal conductivity must always be *less than* the conduc-

tivity predicted by the approximate solution, that is, the effective thermal conductivity, when radiation heat transfer is of importance.

The thermal conductivity of amorphous silica has been measured by a variation of the hot-wire technique [*11*] and by a method similar to the guarded hot plate [*12*]; see Fig. 2. As expected, the results found by Wray and Connolly [*11*] using the hot-wire technique are always less than those found by Lee and Kingery [*12*]. Also, as would be expected, the results tend to converge at lower temperatures, where radiation heat transfer within the specimen diminishes.

Conclusions

For some materials, such as low-density fiber glass insulation, radiation heat transfer within the insulation is important at or below room temperature. For these materials, as well as for any diathermanous material in a temperature range where significant radiation heat transfer occurs, it must be concluded that the hot-wire technique will give a low value for the effective thermal conductivity of the material. The limit below which radiation is no longer important and below which the hot-wire technique will give valid results can be found only with the aid of the exact solution

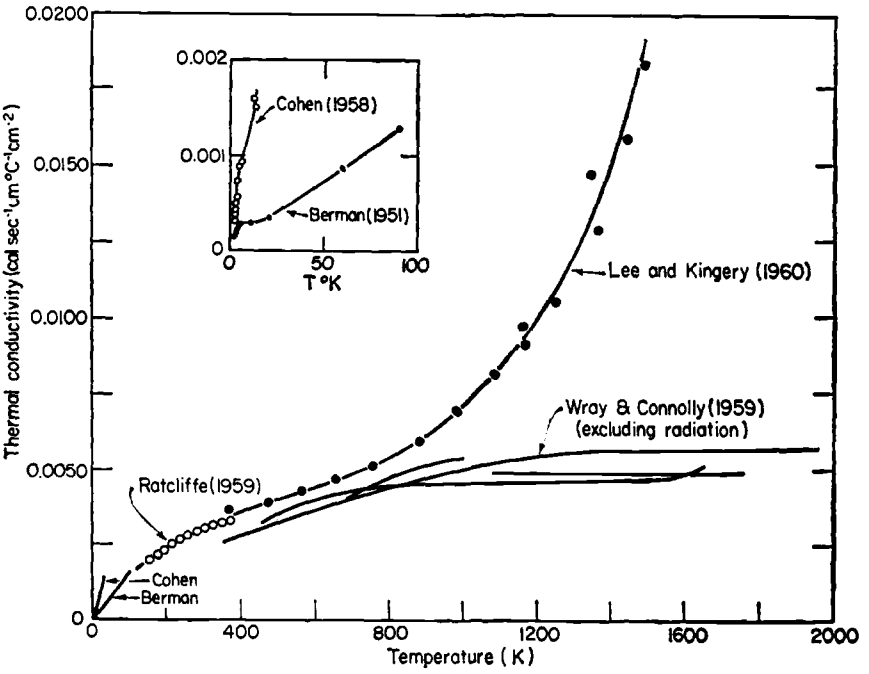

FIG. 2—*Thermal conductivity of amorphous silica (from Ref 13).*

to the combined heat-transfer problem. Without this solution, the technique should be used only on opaque materials, and an ASTM standard should not be developed for semitransparent materials.

References

[1] Tye, R. P., *Thermal Conductivity*, Academic Press, London, 1969, pp. 376–405.

[2] Fine, H. A. et al., "Thermal Properties of Adobe," *Ashrae Transactions*, American Society of Heating, Refrigeration and Air Conditioning Engineers, Vol. 83, 1977, pp. 80–88.

[3] Blackwell, J. H., *Journal of Applied Physics*, Vol. 25, No. 2, Feb. 1954, pp. 137–144.

[4] Seigel, R. and Howell, J. R., *Thermal Radiation Heat Transfer*, McGraw-Hill, New York, 1972, pp. 631–632.

[5] Rosseland, S., *Theoretical Astrophysics: Atomic Theory and the Analysis of Stellar Atmospheres and Envelopes*, Clarendon Press, Oxford, 1936.

[6] Kellett, B. S., *Journal of the Optical Society of America*, Vol. 42, No. 5, May 1952, pp. 339–343.

[7] Jackson, A. J., Adams, J., and Millar, R. C., this publication, pp. 154–171.

[8] Jeschke, P., this publication, pp. 172–185.

[9] Viskanta, R. and Grosh, R. J., *Journal of Heat Transfer*, Vol. 84, No. 1, Jan. 1962, pp. 63–72.

[10] Viskanta, R. and Grosh, R. J., *International Journal of Heat and Mass Transfer*, Vol. 5, 1962, pp. 729–734.

[11] Wray, K. L., and Connolly, T. J., *Journal of Applied Physics*, Vol. 30, No. 11, Nov. 1959, pp. 1702–1705.

[12] Lee, D. W., and Kingery, W. D., *Journal of the American Ceramic Society*, Vol. 43, No. 11, 1960, pp. 591–607.

[13] Kingery, W. D., *Journal of the American Ceramic Society*, Vol. 44, No. 7, 1961, pp. 302–304.

A. J. Jackson,[1] *J. Adams,*[1] *and R. C. Millar*[1]

Thermal Conductivity Measurements on High-Temperature Fibrous Insulations by the Hot-Wire Method

REFERENCE: Jackson, A. J., Adams, J., and Millar, R. C., **"Thermal Conductivity Measurements on High-Temperature Fibrous Insulations by the Hot-Wire Method,"** *Thermal Transmission Measurements of Insulation, ASTM STP 660*, R. P. Tye, Ed., American Society for Testing and Materials, 1978, pp. 154–171.

ABSTRACT: We have developed equipment to determine the "thermal conductivity" of insulating materials, in the temperature range 25° to 1600°C, by the hot-wire method. We have based our method on the German draft standard DIN 51046 and on the work of Padgett and Davis at the British Ceramic Research Association (BCRA). The method has been applied to measurements on polycrystalline alumina fibers, where the "thermal conductivities" range from 0.03 to 0.8 W/m·K. This paper gives details of our experiences with the hot-wire method and indicates some areas where we have found difficulties that are not completely covered in the specification.

In order to assess the value of "thermal conductivity" data obtained by the hot-wire method, we have, where possible, tried to compare our results with those obtained by parallel-plate methods. The dangers of making such a comparison are indicated, but the agreement between the results obtained by the two different methods gives us confidence in their reliability for insulation design.

KEY WORDS: thermal conductivity, fiber, standard, insulation, hot-wire method, linear heat source, transient, nonsteady state, high temperature, anisotropy, orientation, furnace, thyristor control, guarded hot plate, calorimetric parallel plate

The recent dramatic increases in fuel prices, together with the overwhelming need to conserve energy, have caused the operating efficiency of industrial furnaces to be examined more carefully. The trend in furnace insulation is toward inorganic fibrous materials where the low thermal capacity of the insulation enables considerable savings to be made compared with traditional brick-lined furnaces. Examples using Saffil[2] poly-

[1]Imperial Chemical Industries Ltd., Mond Division, Research & Development Department, The Heath, Runcorn, Cheshire, England.

[2]"Saffil" is a trademark of Imperial Chemical Industries (ICI) Ltd. for inorganic fibers.

crystalline alumina fibers in intermittent kilns in the pottery industry have shown that energy savings of over 40 percent can be achieved and production rates more than doubled by using fibrous insulations. Other advantages derive from the light weight and resilience of fibrous materials.

The temperature range of application of inorganic fibers as furnace insulations has been extended to 1600°C by the introduction of polycrystalline alumina fibers. The most economic insulation systems use several layers, where the more expensive material is limited to the hot face and may reduce the temperature only from, say 1600 to 1200°C. "Thermal conductivity" data are required in this temperature range to enable the required insulation thickness to be determined reliably. As far as we know, there are no parallel-plate test methods currently operating to mean temperatures of 1600°C;

Tye [*1*][3] has pointed out the dangers of extrapolating measured values to higher temperatures, and the parallel-plate measurements on Saffil alumina fiber, which are discussed later, highlight these dangers. A new method capable of operating to mean temperatures above 1400°C is therefore required.

The thermal conductivity, an intrinsic property of a material, is not strictly applicable in many cases—for example, when radiation is an important heat-transfer mode. The thermal conductivity is defined as the proportionality constant between heat flux and temperature gradient, and theory has shown that different values can be obtained for different conditions of measurement [*15,16*]. The theory has not yet been completely vindicated by experiment, but it does serve to show that significant errors can be introduced if this point is neglected; the magnitude of these differences will depend on the physical properties of the material and on the conditions of measurement. Data are presented which enable a comparison to be made between "thermal conductivity" values obtained under widely differing conditions. It is academic to consider errors of less than, say, 10 percent for the design of practical high-temperature furnace insulations, where the variability of other factors can easily exceed this level. In this context we have found that the "thermal conductivity" data obtained give a good basis for the design of effective insulations. It is in this context that the term "thermal conductivity" is used in this paper and it is enclosed in quotation marks to distinguish it from the academic concept of thermal conductivity. Ideally, the thermal conductance or resistance of every insulation should be measured under all the varying conditions of use, but this would add appreciably to the cost of producing an insulation.

The hot wire method is a means for determining the "thermal conductivity" k of insulating materials (that is, $k < 2$ W/m·K) up to 1600°C. The

[3]The italic numbers in brackets refer to the list of references appended to this paper.

temperature differentials employed are small (usually <25 K) and so data can be obtained with *mean* temperatures up to 1600°C. The practical details for operating the method are, in general, covered by the standard specification DIN 51046 (1973) [2]. This specification replaces the draft DIN 51046 (1969) and takes into account the comments made by many workers in the field. A summary of the work that went into constructing the standard is given by Lehmann and Schmidt [3]. Eschner et al [4] have studied the area of applicability of the method and Hayashi et al [5–7] have determined empirical relationships governing the size of specimen necessary for hot-wire measurements.

We have developed equipment to determine the "thermal conductivity" of insulating materials, in the temperature range 25° to 1600°C, by the hot-wire method. We have based our method on the German draft standard DIN 51046 [2] and on the work of Padgett and Davis [8] at the British Ceramic Research Association (BCRA). The method has been applied to measurements on polycrystalline alumina fibers, where the "thermal conductivities" range from 0.03 to 0.8 W/m·K. Many of the limiting conditions set out in the DIN 51046 specification are dependent on the "thermal conductivity" of the test material, and we have found that we can get accurate results without strictly complying with all the specifications, as the maximum "conductivity" that we measure is well below the limit of 2 W/m·K set in the standard. This paper gives details of our experiences with the hot-wire method and indicates some areas where we have found difficulties that are not completely covered in the specification.

In order to assess the value of "thermal conductivity" data obtained by the hot-wire method, we have, where possible, tried to compare our results with those obtained by parallel-plate methods, which are based on entirely different principles. The dangers of making such a comparison are indicated, but the agreement between the results obtained by the two different methods gives us confidence in their reliability as a basis for insulation design.

Theory

Theoretical Basis of the Hot-Wire Method

The first recorded work on the hot-wire method dates back to the nineteenth century, but it was first given a practical basis by Van der Held and Van Drunen [9] in 1949. Many authors have since discussed the theoretical formulation of the method [4,8,10–12].

An electric current is passed through a wire contained in a block of the specimen to be measured, giving rise to a cylindrical temperature field in the material (see Fig. 1). The rate of increase in the temperature of the center of the wire is related to the heat input and the "thermal conduc-

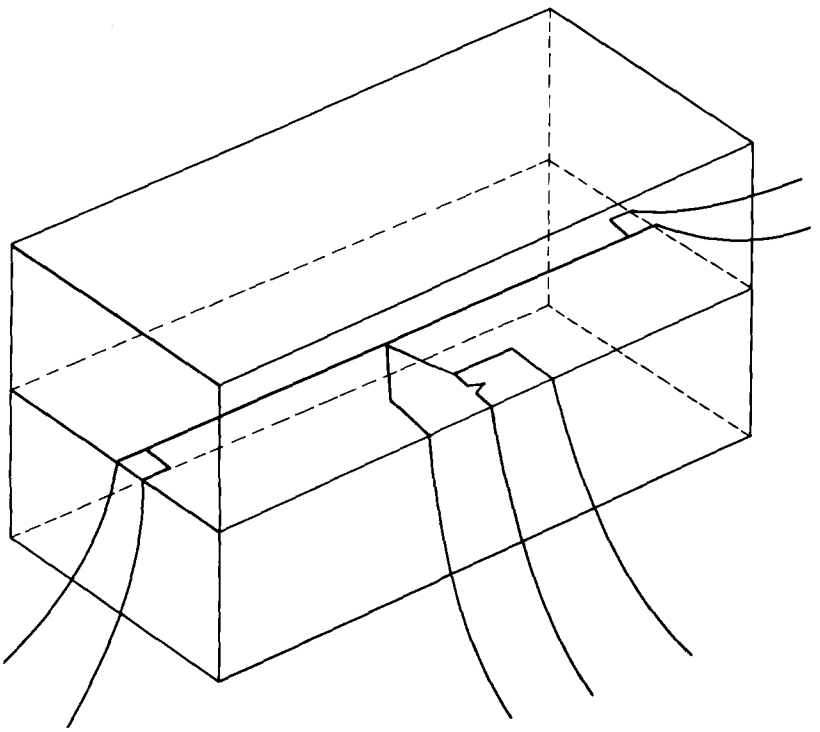

FIG. 1—*Specimen with wire assembly located between the two specimen halves. (See Fig. 5 for details of the wire assembly.)*

tivity" of the test block by the Fourier differential equation, which is detailed in Ref 9. The solution is of the form

$$\theta = \frac{q}{4\pi k}\left[-C - \ln\left(\frac{r_0^2}{4\,at}\right) + \left(\frac{r_0^2}{4\,at}\right) - \frac{1}{4}\left(\frac{r_0^2}{4\,at}\right)^2 + \ldots \right] \quad (1)$$

where

θ = temperature increase at center of wire,
q = constant heat input rate,
k = "thermal conductivity" of the specimen,
C = constant,
r_0 = radius of the wire,
a = thermal diffusivity of the specimen, and
t = time.

Van der Held and Van Drunen have studied this solution in detail and have shown that, by subtracting a constant time t_0 from t ($t_0 = -r_0^2/4a$

and can be obtained from the measurement), the error in neglecting the series expansion terms in Eq 1 is reduced to the order of $(r_0^2/4at)^2$. Equation 1 becomes

$$\theta = \frac{q}{4\pi k}\left[\ln (t-t_0) - C - \ln\left(\frac{r_0^2}{4a} \right) + \frac{1}{4}\left(\frac{r_0^2}{4a(t-t_0)} \right)^2 + \ldots \right] \quad (2)$$

When t is sufficiently large that the series terms can be neglected, the asymptotic form of Eq 2 is

$$\theta = \frac{q}{4\pi k}\left[\ln(t-t_0) + E \right] \quad (3)$$

where E is a constant. A graph of θ against $\ln(t-t_0)$ is a straight line with slope S given by

$$S = \frac{q}{4\pi k} \quad (4)$$

from which k can be determined.

By writing Eq 1 in terms of $(t-t_0)$, the time required for the asymptotic form to become valid can be significantly reduced (see Ref *9*).

The plot of θ against $\ln(t-t_0)$ gives a sigmoid curve, the initial curved portion being due to the series terms in Eq 2, which have been neglected in Eq 3. The upper curved portion results when the temperature front reaches the outside of the specimen block (or the cold junction of the differential thermocouple; see Experimental section). The extent of the lower curved portion is determined by the diffusivity of the material, and the onset of the upper curved portion is dependent on the "thermal conductivity" of the specimen, its geometric dimensions, and the heat input rate. The need for a linear portion of the curve sufficiently large that its slope can be measured dictates the limiting values of the latter two parameters. The range of values that we have experienced are detailed later.

The solution given in Eq 1 assumes an infinitely long heater of negligible radius. Van der Held and Van Drunen [*9*] have shown that the finite thermal capacity of the heating wire can also be taken into account by subtracting a constant time from the true time t; thus both sources of error can be allowed for in the t_0 correction.

The value of t_0 is obtained by plotting the inverse of the rate of increase in the temperature of the wire with time against the true time t. This can be understood by differentiating and inverting Eq 3, which gives

$$\frac{\partial t}{\partial \theta} = \frac{4\pi k}{q}\left(t - t_0 \right) \quad (5)$$

The linear portion of the curve can be extrapolated back to the time axis, where the intercept is $t = t_0$. For measurements on fibers with our wire system, we find t_0 to be about 1 s.

Fiber Orientation

In the design of practical fibrous insulations, it is necessary to know the "thermal conductivity" of the materials in the direction in which heat will flow in the given application.

Some fibrous materials, for example, ICI Saffil blankets, are laminar with fibers orientated randomly in the laminas but with few fibers perpendicular to them. The "thermal conductivity" $k_{//}$ in directions in the fiber planes is different from the value $k_\perp$, in a direction perpendicular to the planes, and the value of k in the general direction varies continuously between these two limits.

Most fibrous insulation designs are either "wallpapered" (fiber planes parallel to the furnace wall) or "edge-stacked" (fiber planes perpendicular to the furnace wall), and so it is sufficient to determine the two "conductivity" values $k_{//}$ and $k_\perp$.

In the derivation of Eq 1–5 it is assumed that heat flows cylindrically from the wire and that the "conductivity" k is independent of the cylindrical polar angle ϕ. If the hot-wire measurements are carried out with the wire perpendicular to the fiber planes (see Fig. 2*a*), the foregoing conditions are true and the "conductivity" obtained is simply $k_{//}$. However, the "conductivity" $k_\perp$ cannot be obtained directly from a single measurement. If the blankets are packed with the wire parallel to the fiber planes (PL orientation), the "conductivity" value obtained, k_{PL} is some kind of "average" value between the two extremes $k_{//}$ and $k_\perp$ (see Fig. 3*b*). Assuming their value to be the average value over the cylindrical polar angle, where the hot wire represents the axis of the cylinder, then

$$k_{PL} = \frac{1}{2\pi} \int_0^{2\pi} k\,(\phi) d\phi$$

and by symmetry

$$k_{PL} = \frac{2}{\pi} \int_0^{\pi/2} k(\phi) d\phi \tag{6}$$

for laminar materials. This formulation of the problem assumes that the temperature gradient in the radial direction is independent of the polar angle ϕ, which is not strictly true.

In the isotropic limit, $k(\phi)$ describes a circle as ϕ varies between 0 and 2π [$k(\phi)$ = constant] and, since $k_{//}$ and $k_\perp$ are extreme values of k by

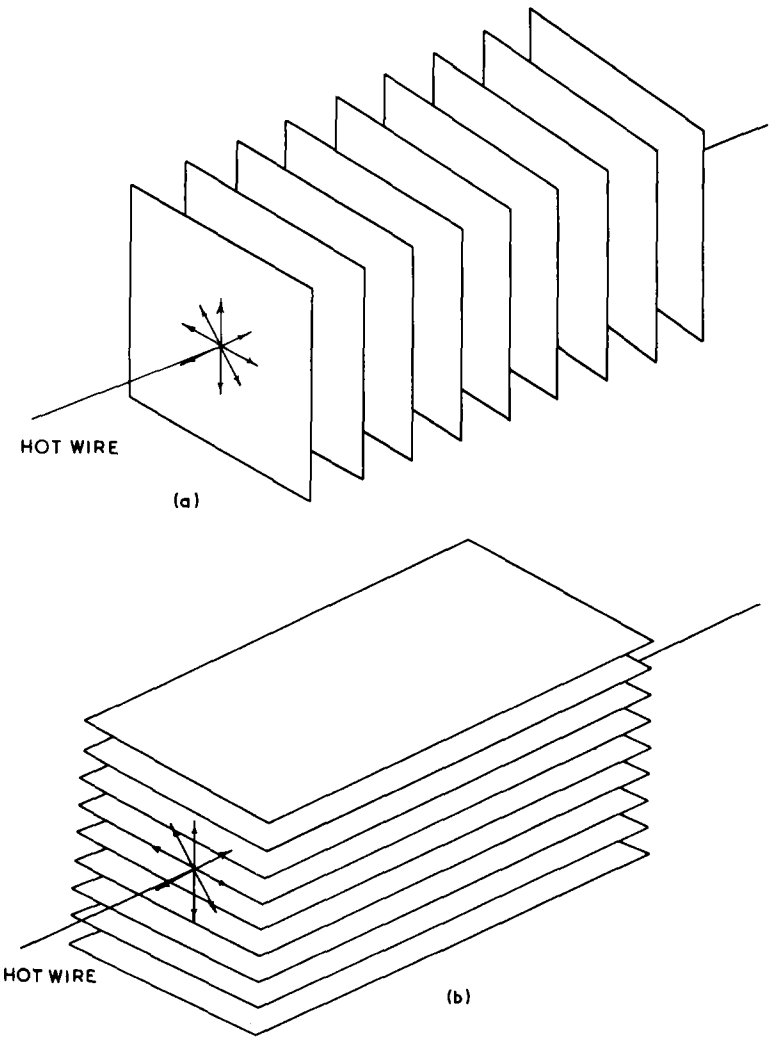

FIG. 2—*Schematic diagram showing the two orientations of laminar specimens: (a) hot wire perpendicular to the fiber planes; (b) hot wire parallel to the fiber planes (PL orientation).*

symmetry, an estimate of k_{PL} can be obtained by assuming that $k(\phi)$ varies elliptically with ϕ, with $k_{//}$ and $k_{\perp}$ the semimajor and semiminor axes, respectively. That is

$$k(\phi) = \left[\frac{\sin^2\phi}{k_{//}^2} + \frac{\cos^2\phi}{k_{\perp}^2} \right]^{-1/2} \tag{7}$$

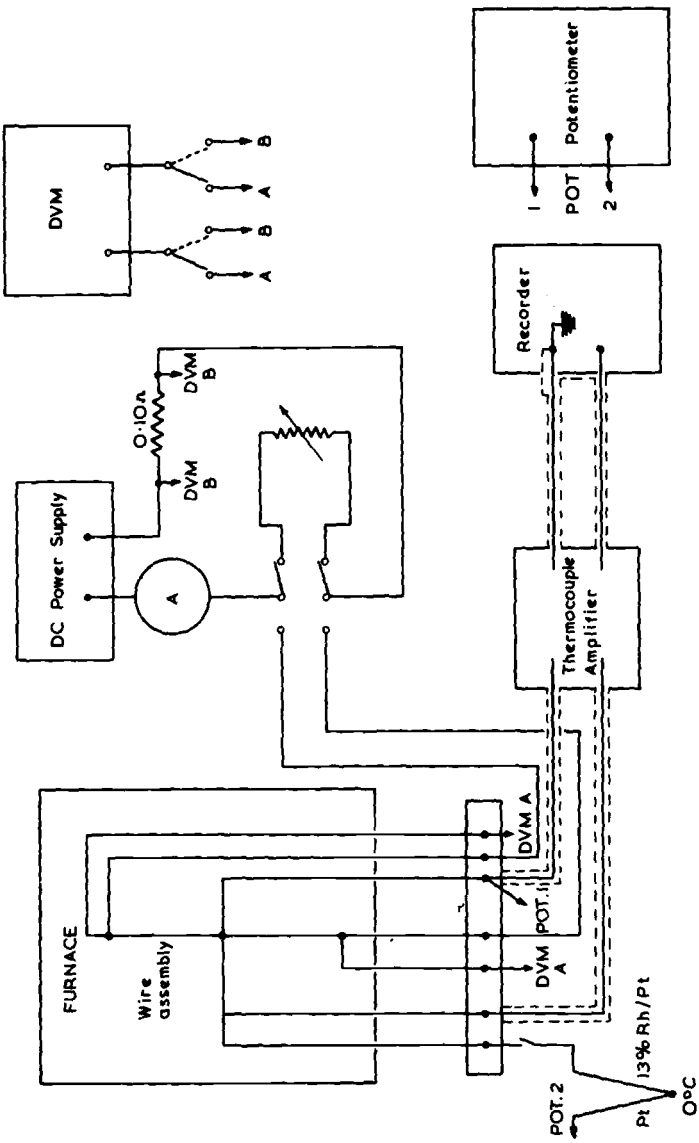

FIG. 3—*Experimental configuration.*

Substituting Eq 7 into Eq 6 and rearranging, we have

$$k_{PL} = \frac{2\,k_\perp}{\pi} \int_0^{\pi/2} (1 - m \sin^2\phi)^{1/2}\, d\phi \tag{8}$$

where

$$m = \left[\frac{k_{/\!/}^2 - k_\perp^2}{k_{/\!/}^2} \right]$$

The integral on the right-hand side (RHS) of Eq 8 is the standard elliptic integral $K(m)$, which is tabulated in Abramowitz and Stegun [*13*]. Having measured $k_{/\!/}$, the RHS of Eq 8 can be plotted as a function of $k_\perp$, and the value of $k_\perp$ for which the RHS equals the measured k_{PL} can be obtained. Thus, both $k_{/\!/}$ and an estimate of $k_\perp$ can be determined from two sets of measurements.

Experimental

The experimental equipment is shown in Fig. 3. The specimen is contained in an alumina box located in a small laboratory furnace. The wire system lies in a horizontal plane midway through the specimen (see Fig. 1). We have found negligible difference in the results obtained using a-c and d-c current to heat the wire, the magnitude of which is chosen to give a reasonable linear portion in the θ versus $\ln(t-t_0)$ plot. The maximum temperature differential depends on the heater current, but we have found that the "conductivity" values obtained are insensitive to the actual difference used [*4*].

The Wire System

The wire system is shown in detail in Fig. 4. A modification of the configuration due to Mittenbühler [*11*] has been adopted according to the recommendations of DIN 51046. The hot wire consists of about 160 mm of 33-SWG (0.254 mm diameter) 13 percent rhodium/platinum alloy wire; the alloy is used in order to minimize the variation in energy input to the wire, as the alloy has a lower temperature coefficient of resistance than the pure metals. Using this system, we find that the variation in the energy input during the run is less than 1 percent. Platinum wires of 32 SWG (0.274 mm diameter) are fused to the ends of the hot wire to serve as potential measuring leads. The differential thermocouple is made from 38-SWG (0.15 mm diameter) platinum and 13 percent rhodium/platinum wires, the thermojunctions being fused together. The measuring junction is welded to the midpoint of the hot wire by the capacitor discharge method

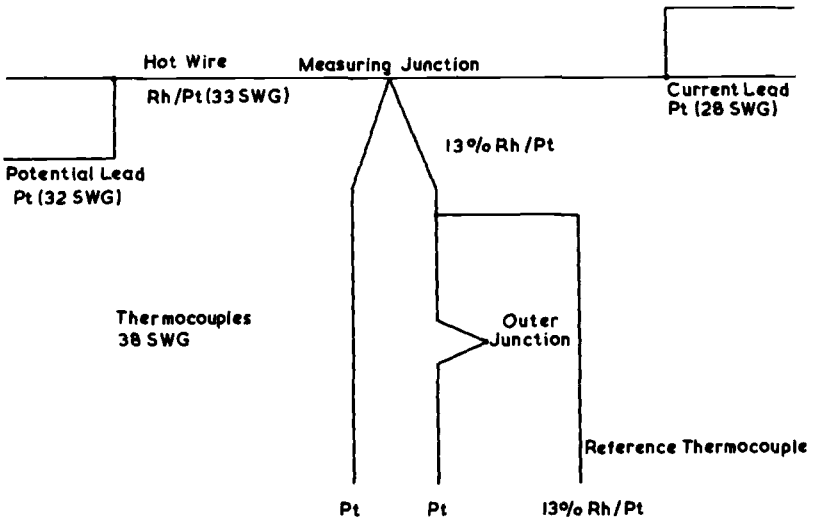

FIG. 4—*Wire assembly.*

[8]. All wires are led from the furnace through fine alumina conduits and are soldered to a thermally insulated tag strip.

The dimensions of the wire system that we have adopted satisfy the conditions set in DIN 51046, except that our hot wire is 160 mm long rather than 200 mm. We have tried varying the length of the hot wire by a small amount about the value 160 mm and have found that it makes no significant difference to the results obtained. Mittenbühler [11] argues that the finite heater length gives rise to a negligible disturbance of the radial temperature field, and heat losses along the wire are also negligible provided $(r/l)^{-1} \geqslant 200$, where r is the wire radius and l its length. Our case, $(r/l)^{-1} \geqslant 1200$, clearly satisfies this requirement. For convenience, therefore, we have continued to use a hot wire of 160 mm in length.

Both legs of the thermocouple circuit are taken from one side of the specimen rather than in the cross formation described in DIN 51046. By avoiding large loops in the wire system in this way, we have been able to reduce the interference pickup from the thyristor controller, which has been troublesome. The diameters of the thermocouple wires are considerably smaller than the limit set in DIN 51046, and so conduction of heat away from the center of the wire is still within the prescribed bounds.

The reference thermojunction relates to an external cold junction in ice and is used for measuring the absolute temperature of the center of the specimen at the start of the run. The potentiometer used for this measurement is disconnected from the wire assembly during the actual run, as it is susceptible to interference pickup, which finds its way into the

measuring circuits. All leads external to the specimen are kept as short as possible to minimize interference pickup.

From measurements made on Saffil alumina fiber boards at temperatures up to 1600°C, we found that after prolonged exposure at 1600°C a coating formed on the wire system which, on analysis in the electron microprobe, proved to be mostly alumina. The effect of this coating on the measurements is to give "conductivity" values which are higher than the "true" value. It is therefore necessary to replace the hot-wire system when such a coating is formed. It is worth stressing that care should be taken in all hot-wire measurements to ensure that the test material does not attack the wire assembly.

The Specimen and Specimen Container

The minimum specimen requirement of DIN 51046 is for two blocks each of 200 by 100 by 50 mm. Hayashi has made a study of the effects of specimen size on the results obtained by the hot-wire method and has derived some empirical relationships governing the minimum specimen size necessary. We operate with two specimen blocks of dimensions 193 by 153 by 35 mm, which exactly fill the alumina specimen container. Although these dimensions fall below the DIN 51046 limit, we have found them adequate for measurements on fibrous materials. This luxury is allowed because the "thermal conductivities" of our specimens seldom exceed 0.7 W/m·K, which is well below the limit of 2 W/m·K set in the standard. These dimensions satisfy Hayashi's criteria [5–7].

The specimens are contained in an alumina box with wall thickness 10 mm. An alumina lid is used to close the box completely and to cause a small amount of compression in the specimen, which helps to ensure good contact at the interface between the specimen halves.

The outer thermojunction is situated just inside the box so that the entire measuring circuit is shielded from temperature fluctuations in the furnace cavity by the high thermal mass of the box. Use of the alumina box has significantly reduced the fluctuations in the thermocouple trace.

Laminar blanket specimens can be packed in two orientations as described earlier (Fig. 2). Care must always be exercised to ensure good contact between the specimen halves; a large air gap near the wire allows convective and radiative heat loss from the wire, causing the measured "thermal conductivity" values to be too high. It has already been stated that putting specimens under slight compression by resting the alumina lid on top of them aids good contact. For fiber board specimens, the specimen halves are ground together to produce smooth surfaces which will contact well. Fibrous materials are well suited to the hot-wire method, since by their nature they are typically 95 percent air, and so small gaps near the wire are not entirely unrepresentative of the bulk material. For

brick specimens, grooves have to be cut for the wire systems and filled with cement made from the brick material.

The Furnace

Experiments are carried out in a small Saffil fiber-lined laboratory furnace. The furnace, the enclosure dimensions of which are 350 by 260 by 200 mm, is heated by five Kanthal molybdenum disilicide elements.

We adopted a thyristor controller for our furnace and have found that it gives rise to considerable noise in the measuring circuit which has been very difficult to remove. Eschner et al [4] have studied the interference caused by various controllers and have concluded that both thyristor control and two-point control methods are particularly susceptible to interference, but servo-control of the furnace does not suffer from this defect. This is a point worth very careful consideration when designing hot-wire equipment.

Electronics

It has been necessary to use platinum and rhodium/platinum alloy wires in the wire system described earlier, to enable measurements to be made up to 1600°C. The differential thermocouple output is amplified by a standard d-c amplifier and is simultaneously fed to a pen recorder and a digital computer. It is important that the amplifier has high common-mode rejection to keep the interference from the furnace controller out of the output display. We have found that earthing and screening are vitally important in keeping the noise level to a minimum. The configuration shown in Fig. 4 has proved to be the most successful. All measuring circuits are screened, except within the furnace enclosure, and a common earth point is taken at the pen recorder input stage.

Computerization

The digitalized amplifier output is stored directly in the computer and is smoothed by the procedures discussed by Savitzky and Golay [14]. Both $\partial t/\partial\theta$ against t and θ against $\ln(t-t_0)$ curves are plotted out directly, thus avoiding the laborious task of plotting them by hand.

Results and Discussion

Measurements have been made on polycrystalline alumina fibers in the form of blankets, boards, and low-density mats. We have found that the method is quick to operate; on one specimen, three runs can be obtained at each of seven temperatures within three days. Measurements on a

single test piece are capable of ±5 percent reproducibility over the temperature range, and, for a single material, repeatability between several test pieces is better than ±10 percent.

In trying to assess the reliability of the hot-wire method, we have compared our results, where possible, with results obtained on parallel-plate equipment, for example, with the guarded hot-plate method according to the standard ASTM Test for Steady-State Thermal Transmission Properties by Means of the Guarded Hot Plate (C 177-71). It is generally accepted that ASTM Method C 177 is accurate and reliable in its temperature range of application, even though Tye [*1*] has pointed out that results obtained by different workers, using equipment designed to the same standard, can differ by as much as 20 percent. These differences are attributed to the different operating conditions employed in each case, but they serve to highlight the dangers in drawing too strong conclusions from comparisons between different methods. Moreover, the temperature gradients developed in the hot-wire method are more complex than in the parallel-plate methods, and Tye has pointed out that the "thermal conductivity" results obtained may depend on the temperature gradient across the specimen, particularly at high temperatures, where radiation plays an important part in heat transfer. Having acknowledged the pitfalls in comparing our hot-wire data with parallel-plate data, we would point out that it still remains the most useful way of assessing the value of the data that we obtain.

It is also important to consider the effects of heat losses from the measuring equipment. Heat losses from the hot-wire equipment would cause the wire to heat up more slowly than in the ideal case, giving a conductivity value which is higher than the true value. Edge losses from the ASTM Method C 177 guarded hot-plate equipment, where the heat input is measured at the hot face, would cause the temperature gradient set up by a known heat flux to be too small, and thus an equivalent "conductivity" value which is again higher than the true value would be obtained. This conclusion is confirmed by Tye [*1*]. Edge losses from parallel-plate equipment, where the heat flux is measured calorimetrically from the cold face, would give rise to a too small heat flux for the temperature gradient that is set up, and so the "conductivity" values obtained would be smaller than the true values. However, measurements made using large temperature differentials are expected to give higher "thermal conductivity" values than isothermal measurements and this would, to some extent, compensate for the differences due to heat losses.

Eschner et al [*4*] find that hot-wire results are greater than calorimetric parallel-plate results obtained by the ASTM Tests for Thermal Conductivity of Refractories (C 201-47), Thermal Conductivity of Refractory Brick (C 202-47), Thermal Conductivity of Unfired Monolithic Refractions (C 417-72), and Thermal Conductivity of Insulating Firebrick (C 182-47).

Measurements have been made on our alumina blankets by four independent laboratories, each using a different form of the steady-state, parallel-plate type of equipment.

Figure 5 shows a comparison of data obtained using the ASTM C 177 guarded hot-plate technique with our hot-wire data for a 96-kg/m^3 (6 lb/ft^3) experimental, high-porosity-grade alumina blanket. The hot-plate measurements provide the value $k_\perp$ directly, but Fig. 5 compares these data with the hot-wire values for $k_\parallel$ and k_{PL}, and with the values for $k_\perp$ computed by the method described earlier. The agreement between the two sets of values is very good, particularly in view of the hazards in making the comparison that have been cited earlier. The divergence in the results above 800°C is probably due to structural changes in the blanket material. Conditioning these high-porosity fibers for long periods of time at temperatures above 800°C causes a reduction in the fiber porosity and consequently an increase in the blanket "conductivity." It is almost certain that the specimens were held at the high temperatures for a longer period of time during the hot-plate measurements, where thermal equilibrium is required, than during the hot-wire measurements, and this would explain the higher values obtained on the hot-plate equipment. Unfortunately, we have had no measurements made by ASTM Method C 177-71 on commercially available Saffil alumina fiber, whose porosity is reduced to a minimum during manufacture.

Figure 6 compares data obtained on a 96-kg/m^3 (6 lb/ft^3) Saffil alumina blanket by three alternative parallel-plate methods and the hot-wire method. In the first method (marked A in Fig. 6), the heat flow is determined from the calibrated heat losses from a mat-black brass plate. In the second (marked B) the heat flow is determined using a heat flowmeter at the cold face, and the third (marked C) is an extensively modified version of the ASTM Method C 201, where the heat flux is measured calorimetrically from the cold face.

The hot-wire results agree with the results from the different types of parallel-plate equipment as well as they agree between themselves, showing that, although the hot-wire and parallel-plate methods are conceptually different, the results obtained are reasonably consistent. The three parallel-plate curves are seen to diverge in going to higher temperatures, and the differences would be very large at, say, 1600°C. This shows the danger of following the practice whereby high-temperature "conductivity" values are obtained by extrapolating the curves obtained at lower temperatures. Tye [*1*] has observed this problem with data obtained by several workers, all using hot-plate equipment to measure the "conductivity" of fiberglass.

We have found that, if inadequate care is taken in setting the equipment up, the errors introduced into the "thermal conductivity" data invariably cause the measured values to be too large, and in most cases the error is so great as to be immediately obvious. The errors mentioned earlier,

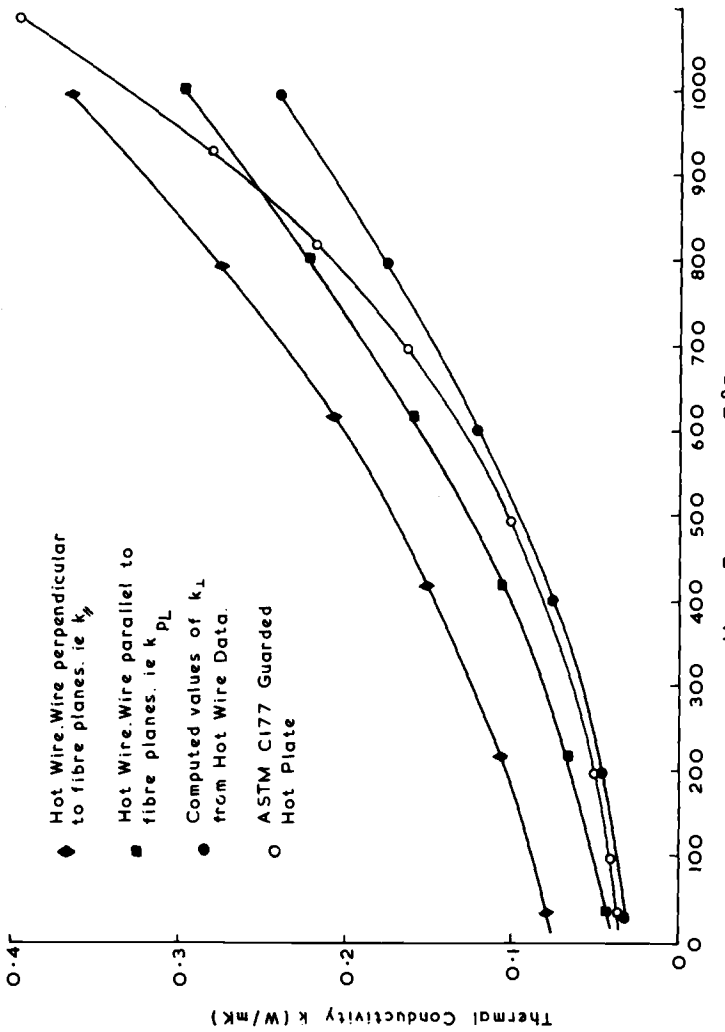

FIG. 5—*"Thermal conductivity" of Saffil experimental grade alumina blanket at 96 kg/m³ (6 lb/ft³). A comparison of Mond hot-wire measurements with Dynatech (United States) ASTM C 177 guarded hot-plate measurements.*

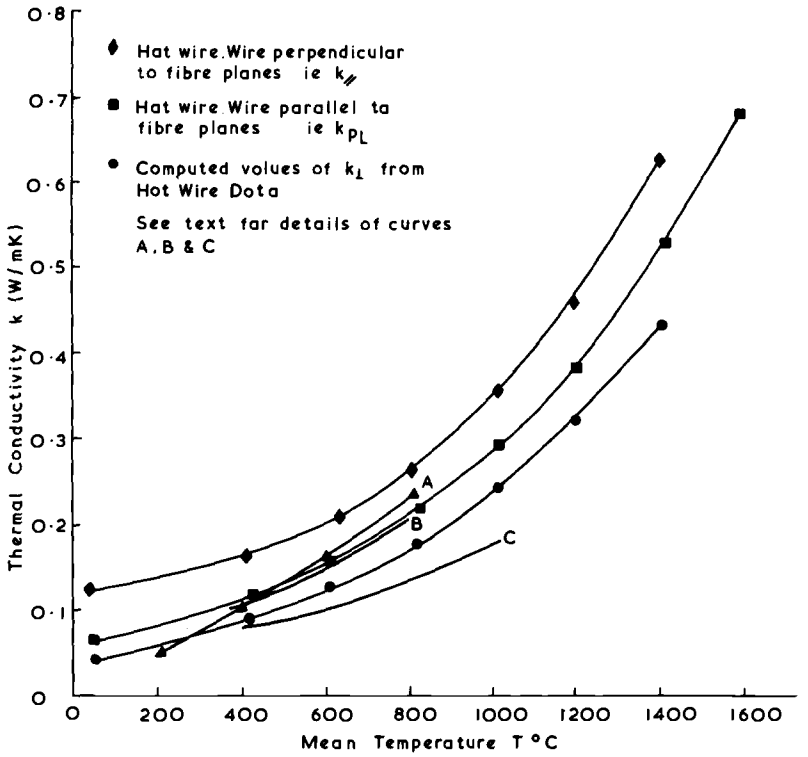

FIG.6—*"Thermal conductivity" of Saffil alumina blanket at 96 kg/m³ (6 lb/ft³). A comparison of Mond hot-wire measurements with three different parallel-plate methods.*

arising from the coating formed on the wire, also cause the measured values to be too high; in fact, we have never encountered any source of error which lowers the "conductivity" values obtained.

"Thermal conductivity" data on Saffil fibers, obtained by hot-wire and parallel-plate methods, correlate better to an exponential function of temperature T than to the T^3 expression predicted by theory [*15*]. A survey of published "thermal conductivity" data on a wide range of lightweight refractory insulations shows this to be typical. The temperature dependence of the radiation-scattering properties of fibers is extremely complex and it is clear that more work is necessary in this area to explain the observed effects. A paper will be published showing how, for lightweight refractories, "thermal conductivity" data obtained by different methods can be standardized and how they can be used in practical insulation design.

Conclusions

1. If sufficient care is taken, the hot-wire method provides a quick means of measuring the "thermal conductivity" of insulating materials at temperatures up to 1600°C and forms a good basis for practical insulation design.

2. The draft standard specification DIN 51046 (1973) provides a good framework on which to base "thermal conductivity" measurements by the hot-wire method, but additional guidance in the following four areas would be useful:

(*a*) the choice of furnace temperature control,

(*b*) the need for the electronic components and wiring to be designed in such a way as to effectively eliminate electrical interference from the measuring circuits, which is particularly troublesome with thyristor controlled furnaces,

(*c*) the need for special care when measuring the conductivity of materials which may attack the wire system, and

(*d*) the determination of the "thermal conductivity" in the principal directions for laminar materials.

3. Measurements made on Saffil fibers by the hot-wire method are consistent with measurements made on the same material with parallel-plate equipment.

Acknowledgments

We would like to thank the Research and Development Director of ICI Limited, Mond Division, for permission to publish this paper; also, our colleagues in the Research and Development Department, who have made numerous contributions to this work—in particular, P.M.L. Asher. We are also indebted to G. C. Padgett and W. R. Davis of the British Ceramic Research Association for introducing us to the hot-wire method.

References

[1] Tye, R. P., *Revue Internationale Des Hautes Températures Et Des Réfractaires*, Vol. 7, 1970, pp. 308–312.

[2] German Standards, Folio 1: "Testing of Ceramic Materials. Determination of Thermal Conductivity at Temperatures up to 1600°C by the Hot Wire Method", DIN 51046, 1973.

[3] Lehmann, H. and Schmidt, H-J., *Tonindustrie-zeitung*, Vol. 96, 1972, p. 12.

[4] Eschner, A., Großkopf, B., and Jeschke, P., *Tonindustrie-zeitung*, Vol. 98, 1974, pp. 212–219.

[5] Hayashi K. and Fukui, M., *Memoirs of the Faculty of Industrial Arts*, Kyoto Technical University, Science and Technology, Kyoto, Japan, Vol. 23, 1974, pp. 82–99.

[6] Hayashi, K., *Yogyo Kyokaishi*, Vol 82, No. 4, 1974, 202–208.

[7] Hayashi, K., Fukui, M., and Uei, I., *Yogyo Kyokaishi*, Vol. 81, No. 12, 1973, pp. 534–542.

[8] Davis, W. R., British Ceramic Research Association, Technical Note 224, 1974.
[9] Van der Held, E.F.M. and Van Drunen F. G., *Physica*, Vol. 15, No. 10, 1949, pp. 865–881.
[10] Hayashi, K., Fukui, M., and Uei, I., *Memoirs of the Faculty of Industrial Arts*, Kyoto Technical University, Science and Technology, Vol. 20, 1971, pp. 81–103.
[11] Mittenbühler, A., *Berichte Der Deutschen Keramischen Gesellschaft*, Vol. 39, No. 7, 1962, pp. 387–392.
[12] Mittenbülher, A., *Berichte Der Deutschen Keramischen Gesellschaft*, Vol. 41, No. 1, 1964, pp. 15–20.
[13] Abramowitz, M. and Stegun, İ., *Handbook of Mathematical Functions*, Dover Press, 1964.
[14] Savtizky, A. and Golay, M.J.E., *Analytical Chemistry*, Vol 36, No. 8, 1964, pp. 1627–1639.
[15] Larkin, B. K., Churchill, S. W., *American Institute of Chemical Engineers Journal*, Vol. 5, No. 4, 1959, pp. 467–474.
[16] *Heat Transmission Measurements in Thermal Insulations*, *ASTM STP 544*, American Society for Testing and Materials, 1973.

P. Jeschke[1]

Thermal Conductivity of Refractories: Working with the Hot-Wire Method

REFERENCE: Jeschke, P., **"Thermal Conductivity of Refractories: Working with the Hot-Wire Method,"** *Thermal Transmission Measurements of Insulation, ASTM STP 660*, R. P. Tye, Ed., American Society for Testing and Materials, 1978, pp. 172–185.

ABSTRACT: The German Standard Deutsche Industrie Norm (DIN) 51046 covers the measurement of thermal conductivity of refractories up to 1600°C by the hot-wire method. From the publishing of the first draft in 1969 to issuing the standard in 1976, several round-robin tests and other experimental work have shown that

1. the hot-wire method is safe to use for material up to $K = 2$ W/m·K, and under certain precautions may be used up to $K = 6$ W/m·K,
2. the simplified solution of the Fourier differential equation used in the standard can be safely applied if the thermal diffusivity is smaller than $a = 0.002$ m²/h,
3. for material with $a > 0.002$ m²/h, the recommended measuring time has to be reduced.
4. several recommendations can be given about the type of furnace and measuring equipment and suggestions can be made on how to avoid errors, and
5. the hot-wire method produces consistently higher values for thermal conductivity than other methods, including the ASTM procedure.

The hot-wire method has been adopted by the Féderation Européenne des Fabricants de Produits Réfractaires (PRE) as Recommendation 32 and has been submitted to the Technical Committee TC 33 of the International Standardization Organization (ISO).

KEY WORDS: thermal conductivity, hot-wire method, refractories, insulating brick, standardization

If a continuous line source is liberating heat at the constant rate q per unit time per unit length, the radial temperature distribution in the surrounding material can be calculated as follows

$$\frac{dT}{d \ln t} = \frac{q}{4 \pi K} \times e^{-\frac{r^2}{4at}} \tag{1}$$

[1]Manager, Research and Development, Didier Werke AG, Didier Research Institute, Wiesbaden, Germany.

where

T = temperature,
q = heat flow,
K = thermal conductivity,
r = radial distance from heating line,
t = time from beginning of heat liberation, and
a = thermal diffusivity.

From Eq 1, after inserting finite temperature and time differences, the thermal conductivity of the surrounding material can be computed from the temperature increase of the line source ($r = 0$)

$$K = \frac{q}{4\pi} \times \frac{\ln t_2 - \ln t_1}{T_2 - T_1} \tag{2}$$

where T_1 is the temperature of the line after time t_1 and T_2 is the temperature of the line after time t_2.

The apparatus is fairly simple and the following example shows a typical test procedure. The heat source is a platinum-rhodium wire of 0.175 mm radius, and the temperature increase is determined with a platinum-platinum-rhodium thermocouple welded on the wire. A reference junction is placed at the outside of the specimen. The specimen consists of two standard bricks with the wire-thermocouple unit sandwiched in between (Fig. 1).

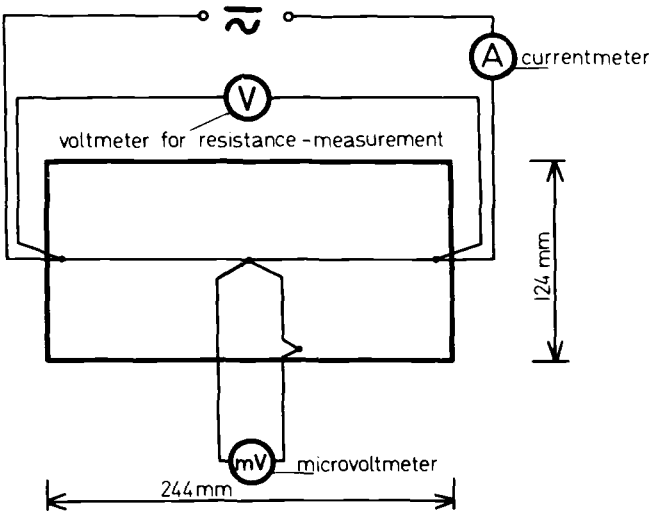

FIG. 1—*Hot-wire apparatus.*

At test temperature, the heating current is switched on and the temperature of the heating wire (rather, the voltage of the thermocouple) increases as shown in Fig. 2. The evaluation also is shown in Fig. 2 (correction of the variable wire resistance is left out). The main difficulty is to measure accurately a temperature increase of (in our example) 0.558 K at 965°C; this requires sensitive high-quality electronic equipment and careful execution of the tests.

History

Several authors [*2–5*][2] have used Eq 2 (or a similar equation) for determination of the thermal conductivity; Haupin [*6*] and Mittenbühler [*7*] applied the hot-wire method to refractories after eliminating possible sources of error and developing a suitable apparatus. In 1960, Haupin reported close agreement between his values and those determined by the

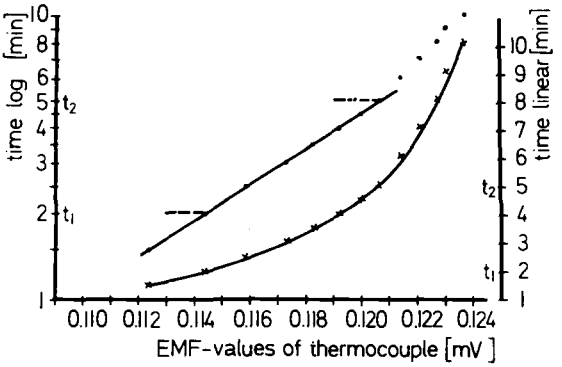

Test temperature :	965 °C
Thermocouple factor :	0.0113 mV/K
Length of wire : L =	0.342 m
Resistance measurement at 1 mA :	1.718 mV
Resistance of wire : $R = \frac{U/I}{L} =$	5.023 Ω/m
Heating current : I =	1.7525 A

$T_1 = 0.1144$ mV , $t_1 = 2$ min
$T_2 = 0.1207$ mV , $t_2 = 5$ min
$\Delta_T = 0.0063$ mV $\hat{=} 0.5575$K

$$K = \frac{I^2 R}{4\pi} \frac{\ln t_2/t_1}{T_2 - T_1} = 2.017 \text{ W/mK}$$

FIG. 2—*Temperature increase of heating wire and example of test evaluation.*

[2]The italic numbers in brackets refer to the list of references appended to this paper.

ASTM Test for Thermal Conductivity of Refractories (C 201-47); Mittenbühler agreed (1962) with the German Klasse method [*15*] where the conductivity is determined by comparison with a standard.

From 1962 to 1976, the method and its application to refractories were improved further. The permissible range of conductivities was defined, maximum diameter of the wire and minimum dimensions of the specimen were determined, and the evaluation was exactly specified [*7,9–11*].

Standardization

In 1974, an informal working group was formed within the Féderation Européenne des Fabricants de Produits Réfractaires (PRE), consisting of three laboratories:

BCRA—British Ceramic Research Association,

SFC—Société Française de Céramique, Centre National d'Etudes et Recherches Céramiques,

DFI—Didier Research Institute (for DIN committee B2a4), and two further consultants.

The working group was supposed to coordinate the work done on the hot-wire method in Britain, France and Germany and to write up a European Test Recommendation.

Great Britain

There exist the BS 2973 from 1961 and BS 1902 from 1966 using a modified ASTM apparatus. In 1974 the hot-wire method was tested at BCRA and compared favorably with the calorimeter method [*11*].

France

There is no standard method in France. Several procedures are in use which were evaluated in a report of the SFC [*12*] in 1962. The Paris institute of the SFC has then experimentally compared different methods. Among these were ASTM C 201-47, ASTM C 201-47 with a reduced test panel, a radial flux method [*13*], and the hot-wire method [*14*].

Germany

During the past 20 years, a comparative "disk method" after Klasse [*15*] was widely used. A DIN committee compared different methods from 1960 on, including the ASTM and hot-wire techniques. The Klasse procedure was not regarded as suitable for standardization because it is a comparative method and needs a master method for the calibration of the reference specimens. As early as 1968, the hot-wire method was selected

as German standard DIN 51046. After numerous round-robin tests and improvements of the apparatus, the first tentative standard was issued in 1969.

After SFC, BCRA, and DFI (for the DIN committee) agreed that the hot-wire method was to be recommended to the PRE as a European "Test Recommendation," the German DIN 51046 was issued in 1976—still called a preliminary standard to leave room for possible adjustments to the PRE recommendation to come.

PRE

After finishing the tests, the three institutes submitted in 1976 a mutual draft which has officially been accepted by the member countries and issued as PRE-recommendation 32.

ISO

The Technical Committee of the International Standardization Organisation (ISO), TC 33, has listed the thermal conductivity as a point of interest and an area of future work for Subcommittee SC 2. In 1973, the Netherlands submitted the cylinder method [*13*], and Germany submitted the hot-wire method in 1977.

Theoretical Aspects and Limitations

All authors and institutes involved agreed that the hot-wire method should for the time being be limited to material with low thermal conductivity. In the following, the reasons for this limitation are explained.

For the derivation of Eq 2 the following assumptions were made

1. The heat source is a line (heating wire) of infinitely small radius.
2. The coefficient of heat transfer between the wire and the surrounding medium is infinite.
3. The length of the wire is infinite.
4. The radius of the surrounding medium (cylinder) is infinite.

In the actual measurements, these conditions can be approached but never completely fulfilled, so that the possible errors, by not having ideal conditions, must be assessed.

Errors due to not fulfilling Assumptions 1 and 2 can be calculated using the following equation:

$$T = \frac{q}{4\pi K}\left[\, 2h + \ln\frac{4F_0}{C} - \frac{4h - W}{2WF_0} + \frac{W-2}{2WF_0} \times \ln\frac{4F_0}{C} + \ldots \,\right] \qquad (3)$$

where

T = temperature of (finite) heating wire,

F_0 = Fourier number, $\frac{at}{r^2}$

a = thermal diffusivity,

t = time from beginning of heat liberation,

r = radius of heating wire,

h = $2\pi K/H$,

H = coefficient of heat transfer from wire to surrounding medium,

W = $\frac{2 \times (\rho \times c_p) \text{ medium}}{(\rho \times c_p) \text{ wire}}$,

$\rho \times c_p$ = density · specific heat = heat capacity, and

C = 1.772 (= e^{γ} with γ = Euler's constant).

If the volume actually taken up by the wire consisted of the surrounding medium, the heat capacity ratio would be $w = 2$; for $H = \infty$ as ideally assumed, the coefficient h would be $h = 0$ and Eq 3 could be transformed into Eq 2.

To obtain practical results, calculations were made for which the maximum allowable error was defined as a 1 percent error in the temperature increase of the hot wire. For several materials, the allowable ranges were determined in which t_1 and t_2 could be chosen under this condition. The allowable range is characterized by a linear relationship between temperature and log time. The maximum allowable time for the end of the measurement is, of course, dependent upon specimen size. For a wire radius of 0.175 mm and a specimen "radius" of 57 mm (half width of a standard brick), the temperature increase of the reference junction is 1 percent of the temperature increase of the wire, if

$$t_{2\,\max} = \frac{1.97}{a}, \text{ s}$$

This maximum allowable time for the end of measurement $t_{2\,\max}$ depends only on the thermal diffusivity of the surrounding medium, that is, the refractory material. If the reference junction is closer to the heating wire, the maximum allowable time $t_{2\,\max}$ is less.

The beginning of the measurement, t_1, has to be chosen in such a way that the error is not more than 1 percent of the temperature increase of the wire between t_1 and $t_{2\,\max}$.

The coefficient of heat transfer between wire and refractory material (H) was determined experimentally. Values between 0.5 and 15 W/m^2·K were found, depending on the imbedding technique and other factors. For calculation of the earliest possible t_1, H = 0.5 W/m^2·K was assumed (Fig. 3).

It can be shown [*10*] that $t_{1\ min}$ depends on a, h, and w and that above $h = 50$ no measurement under the specified error conditions is possible. The results are given in Table 1. It can be seen that magnesite bricks have (theoretically) no allowable range for measurement.

These calculations (supported by experimental work) have shown limitations of the method which were included in the PRE and DIN standards as specifications of wire and specimen:

1. minimum specimen "radius" of 57 mm,
2. maximum wire radius of 0.175 mm,

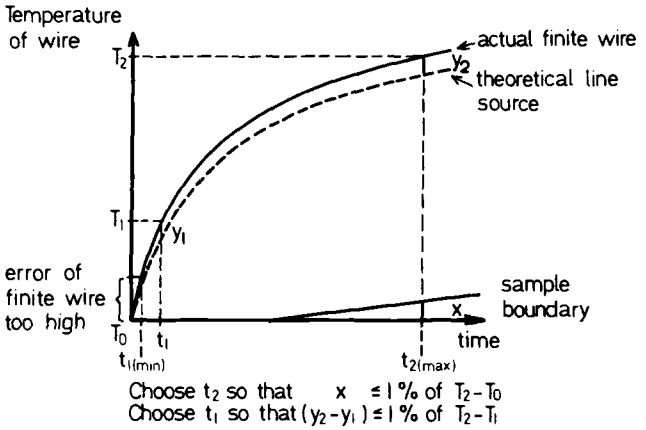

FIG. 3—*Assessment of errors.*

TABLE 1—*Permissible measuring ranges.*

Material	K	g	c_p	a			$t_{1(min)}$	$t_{2(max)}$
	[W/mK]	[kg/m³]	[kJ/kgK]	[m²/h]	h	w	min	min
Insulating brick	0.2	495	1.05	$1.62\ 10^{-3}$	2.513	0.314	2.84	20.3
Insulating brick	0.4	930	1.05	$1.72\ 10^{-3}$	5.026	0.605	1.07	19.06
Fireclay	1.0	2100	1.05	$1.90\ 10^{-3}$	12.566	1.260	0.68	17.22
Mullite	1.8	2500	0.97	$2.82\ 10^{-3}$	22.619	1.342	0.68	10.48
Forsterite	2.0	2700	1.05	$3.11\ 10^{-3}$	25.133	1.524	0.806	11.07
Chrome-Mag.	3.0	3000	1.13	$3.70\ 10^{-3}$	37.699	1.751	0.99	8.86
Magnesia	4.0	3000	1.18	$4.76\ 10^{-3}$	50.265	1.543	no measurement possible	
Magnesia	6.0	3000	1.18	$7.14\ 10^{-3}$	75.398	1.543		
Magnesia	10.0	3000	1.18	$11.90\ 10^{-3}$	125.663	1.543		

3. method of wire imbedding,
4. K_{max} of 2 W/m·K, and
5. a_{max} of 0.003 m²/h (check $t_{2\ max}$ if a is greater than 0.002 m²/h).

Within these boundary conditions, a correct determination of K is ensured. With an enlarged specimen size, smaller wire radius, and careful imbedding, higher K-values can be measured.

Apparatus, Practical Experience

Furnace

It is necessary to control the specimen temperature before the measurement to ± 0.05 K at the wire. This can be accomplished by using a furnace with a fairly high heat capacity and the conventional transformer-servomotor-control system which (once the temperature is established) does not change the transformer position any more.

Measuring Circuit

The microvoltage of the thermocouple can be measured by a millivolt recorder with a 0.1 to 0.2 mV range. A digital nanovoltmeter with a digital clock and printer is preferred. It is important that all input noise is completely filtered out.

Measuring Conditions and Accuracy

For a typical insulating brick of the 2300 class (K = 0.14 W/m·K), the amperage of the heating current was varied between 0.5 and 2.5 A and the diameter of the wire between 0.1 and 0.5 mm. No influence of these variations on the K-values was found. Furthermore, there was no difference noted using a-c or d-c current.

Ten consecutive measurements—each time the setup was completely taken apart and reassembled—had a standard deviation of less than 4 percent. The same standard deviation was found in 20 or more measurements when the two bricks of the test setup were turned around between measurements.

All these tests with the foregoing variations were carried out on the 2300-class insulating brick; the complete set of the total 100 tests had a mean of 0.142 W/m·K with a standard deviation of 0.0064 W/m·K, which is ± 4.5 percent. The maximum deviation of a single value from the average was 13.9 percent. These experiments covered the whole range of variation allowed in the DIN standard. DIN specifies that at each temperature level the measurement should be carried out three times. K is the arithmetic

mean of these values and no individual measurement may be more than 10 percent off this arithmetic mean.

The following is specified for the accuracy of the method:

Under repeat conditions (one observer, one instrument)	± 5 to 10 percent
Under comparison conditions (different observers, different instruments)	± 10 to 15 percent

Influence of Imbedding

To test this influence, the wire was imbedded in a 2300-class brick in extremely wide grooves, contradicting the standard procedure. The 0.5-mm notch, which usually takes up the heating wire, was replaced by a cylindrical hole of 20-mm diameter which was alternately filled with a lightweight powder and a magnesia powder or left unfilled. The result is given in Table 2. Although these values were obtained under completely unrealistic conditions, they show the importance of a correct imbedding technique. Using a 20-mm round hole for imbedding, the results deviated even more than for the cylindrical hole.

Measurement of High Thermal Conductivities

In Table 1 a theoretical limit of about 4 W/m·K was calculated. In practice, we have determined thermal conductivities up to 20 W/m·K (magnesite brick at room temperature), and reliable values could definitely be obtained up to about 6 W/m·K. Recommended is an increase in specimen dimensions to enlarge the maximum allowable time of measurement (Fig. 4).

TABLE 2—*Variation of imbedding technique.*

	Standard	20mm groove filled with		
		Air	MgO powder	lightweight powder
Number of measurements	10	10	10	10
K (average)	0.140	0.153	0.122	0.123
Standard deviation	2.9%	2.9%	2.2%	2.8%
Error	-	+9.3%	-13%	-12 %

Comparative Test

In the refractories field, the thermal conductivity is very important for insulating brick, so most determinations are made in the range of 0.1 to 1 W/m·K. After issuing the first tentative standard, the German DIN committee organized several round-robin tests which later included SFC and BCRA (Fig. 5–7). For the 2300- and the 2800-class insulating brick, the maximum deviation of a single laboratory from the average value was about 10 percent for the hot-wire method. The results of the hot-wire method are about 25 to 30 percent higher than the ASTM results.

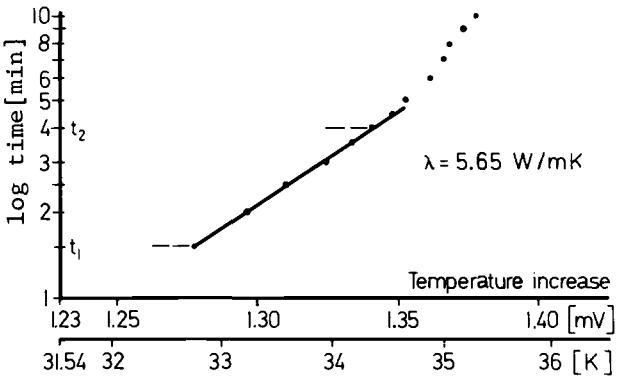

FIG. 4—*Determining* K *of a magnesia brick.*

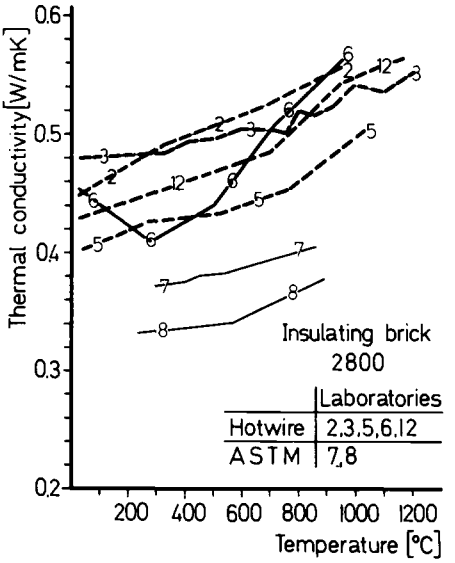

FIG. 5—*Comparative test.*

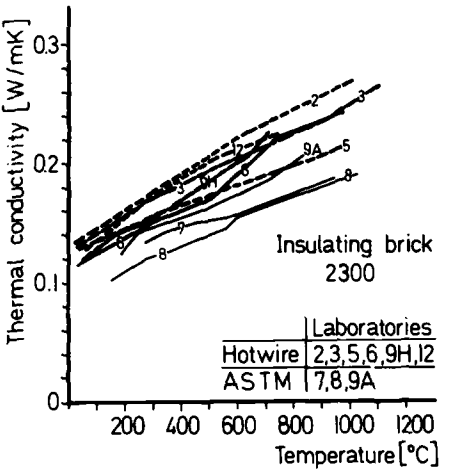

FIG. 6—*Comparative test.*

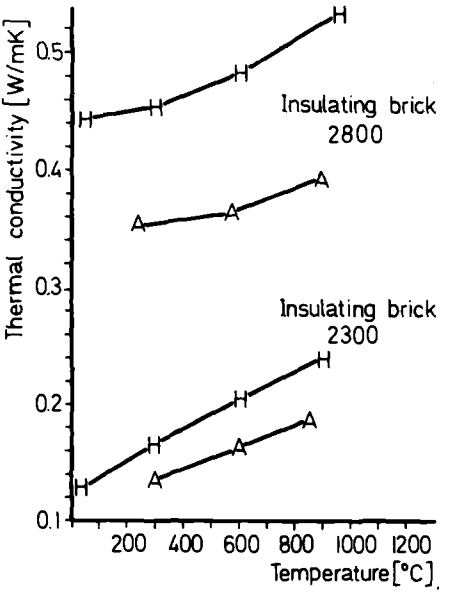

FIG. 7—*Average of hot-wire (H) and ASTM (A).*

Interestingly enough, the ASTM results obtained in the United States by the producer [7] and by an independent laboratory [8] were lower than the values obtained by a method similar to ASTM C 201-47 in Europe [9]. The results of laboratory 9 are the average of two measurements, one with and one without insulating material between the test specimen and the

calorimeter. There seems to be a difference in values between the two test setups; this, however, is not certain.

Other methods have been investigated in the round-robin tests, too. The experimental thermoconductivity values obtained by using the Klasse method lie between the values obtained by using the ASTM Method C 201-47 and the hot-wire method. The Klasse procedure relies on a standard whose thermal conductivity was defined in a test series between 1960 and 1965, relying mainly on ASTM values. Today, however, after Klasse, higher values are found than after ASTM. The radial flux procedure [*13*] (submitted to ISO by the Netherlands) is in accordance with the hot-wire method.

Discussion and Future Work

ASTM—Hot Wire; Comparison of Methods

The hot-wire apparatus is less expensive and the components are available off the shelf so that machining, fitting, and construction work is minimized. The apparatus lends itself favorably to automation and the man-hours per test are reduced. The tests may be run from room temperature up to 1500°C, possibly up to 1600°C; the specimen consists normally of two standard bricks. The method is faster—a test with six or seven temperature levels is carried out in two or three days. Three or four furnaces can be operated simultaneously with one measuring device. No unidirectional testing, however, is possible; the thermal conductivity is determined as the mean value of all directions. This makes measurements of fibrous material dubious, and of any other material where a variation of thermal conductivity in different directions is expected. The main disadvantage is the limitation to material below $K = 6$ W/m·K, officially in the DIN standard even below 2 W/m·K.

Further Development of the Hot-Wire Method

In Germany, several institutes are working on the measurement of high conductivities. First comparative tests have shown good agreement between two laboratories up to 12 W/m·K. It is expected that the standard will officially be extended to 6 W/m·K or even more within the next years.

In other trials, an additional thermocouple is imbedded a few millimetres beside the hot wire, allowing a measurement from the first second instead of from the first minute, which seems promising for high conductivities and for the simultaneous measurement of thermal diffusivity. Furthermore, trials are underway with no thermocouple at all, using the change

of the resistance of the hot wire for determination of the temperature increase.

International Standardization

The main difficulty to overcome in Germany in the course of standardization was the difference in values between hot-wire and ASTM methods for the insulating brick. The hot-wire method leads to higher K-values in the catalogs, and some companies, of course, foresee problems and complications in sales if all catalogs have to be rewritten.

After agreement was reached in Germany and, moreover, between the three involved European institutes, the same difficulties delayed the PRE work because one or more European producers wanted to adhere to the low ASTM values in their catalogs.

Before the ISO engages in a discussion on thermal conductivity, the ASTM and hot-wire methods should be compared with a few more ASTM-laboratories engaged and using three or four different refractory materials with K-values between 0.1 and 6 W/m·K. It should also be investigated if different values are obtained within the ASTM specifications by using polished or dull calorimeters and with or without spacers or insulating layers between the test brick and the calorimeter. It should be possible to find out why there is a difference between the ASTM and hot-wire procedures.

References

[1] Carslaw, H. S. and Jaeger, J. C., *Conduction of Heat in Solids*, 2nd ed., Oxford University Press, 1959.

[2] Van der Held, E.F.M. and Van Drunen, F. G., *Physica*, Vol. 15, No. 10, 1949, pp. 865–881.

[3] Hooper, F. C. and Lepper, F. R., *Transactions*, American Society of Heating and Ventilating Engineers, Vol. 56, 1950, pp. 309–324; *Heating, Piping and Air Conditioning Journal*, Section 22, 1950, pp. 129–135.

[4] Hooper, F. C. and Chang, S. C., *Heating, Piping and Air Conditioning Journal*, Section 24, 1952, pp. 125–129.

[5] Gupta, M. L., *Journal of Scientific and Industrial Research* (India), Vol. 19B, No. 7, 1960, pp. 240–243.

[6] Haupin, W. E., *American Ceramic Society Bulletin*, Vol. 39, No. 3, 1960, pp. 139–141.

[7] Mittenbühler, A., *Bérichte Der Deutschen Keramischen Gesellschaft*, Vol. 39, No. 7, 1962, pp. 387–392.

[8] Mittenbühler, A., *Berichte Der Deutschen Keramischen Gesellschaft*, Vol. 41, No. 1, 1964, pp. 15–20.

[9] Schwiete, H. E. and Dohm, K.-D., *Archiv für das Eisenhüttenwesen*, Vol. 38, No. 5, 1967, pp. 411–414.

[10] Eschner, A., Grosskopf, B., and Jeschke, P., *Tonindustrie-zeitung*, Vol. 98, No. 9, 1974, pp. 212–219.

[11] Davis, W. R., "The Determination of Thermal Conductivity of Refractory Insulating Materials by the Hot-Wire Method," BCRA Technical Note No. 224, British Ceramic Research Association, 1974.

[12] Halm, L., Bortaud, M., and Lapoujade, P., *Berichte Der Deutschen Keramischen Gesellschaft*, Vol. 39, No. 7, 1962 pp. 370–375.
[13] Van Konijnenburg, J. T., *Tonindustrie-zeitung*, Vol. 97, No. 4, 1973, pp. 89–94.
[14] Provost, G., "Conductivité thermique: Rappel de données théoriques, résumé d'essais comparatifs, conclusions pratiques," *Bulletin De La Societe Francaise Ceramique*, April, 17–23 June 1973.
[15] Klasse, F., Heinz, A., and Hein, J., *Berichte Der Deutschen Keramischen Gesellschaft*, Vol. 34, No. 6, 1957, pp. 183–189.

W. R. Davis[1]

Determination of the Thermal Conductivity of Refractory Insulating Materials by the Hot-Wire Method

REFERENCE: Davis, W. R., "**Determination of the Thermal Conductivity of Refractory Insulating Materials by the Hot-Wire Method**," *Thermal Transmission Measurements of Insulation, ASTM STP 660*, R. P. Tye, Ed., American Society for Testing and Materials, 1978, pp. 186–199.

ABSTRACT: The hot-wire line source technique has been applied to the measurement of the thermal conductivity of refractory insulating materials at temperatures up to 1000°C. The method is rapid and has a repeatability of better than 5 percent. Comparisons have been made with other methods.

KEY WORDS: ceramic fibers, fibrous insulation, heat flux, high-temperature research, high-temperature insulation, refractory materials, thermal conductivity

The work described herein formed part of a program, undertaken some years ago, to develop test methods for ceramic fibers. At the time, it was intended solely as an assessment of a possible rapid method for the determination of thermal conductivity, offering the possibility of carrying out a series of relatively inexpensive tests at temperatures up to and exceeding 1000°C in about half the time required for conventional tests.

Theory

The hot-wire method is a transient technique based on the measurement of the temperature rise at the midpoint of a heated wire embedded in the material under test. It may have the heater and thermocouple enclosed in a thin sheath—the probe type—or it may have an unenclosed straight resistance wire heater—the line-source type. It is assumed that the heat output is constant and uniformly distributed around and along the wire.

[1]Senior scientific officer, British Ceramic Research Association, Queens Road, Penkhull, Stoke-on-Trent, England.

The original method is attributed to Schieirmacher [*1*][2], but its practical application is due to Van der Held and Van Drunen [*2*], who first used the method to determine the thermal conductivity of liquids.

If a current is passed through a wire embedded in the test material, the wire will heat up. If the temperature at the midpoint of the heater is plotted against $\log_e$ of the elapsed time, a sigmoid curve (Fig. 1) is obtained. The initial portion of the graph is curved due to thermal diffusivity [*2*]. A linear portion follows, the length of which depends on the heat input and the conductivity of the specimen. The upper part of the graph is dependent on specimen size and end heat losses. Only the linear portion is used to determine the thermal conductivity.

The theory of the method has been developed in detail by Carslaw and Jaeger [*3*], Blackwell [*4*], and Hooper and Lepper [*5*], who have elaborated on the original Van der Held equations.

The basic equation for the temperature θ at a given time t at the midpoint of the heater wire is somewhat complex. It can be simplified by considering the *change* in temperature between two given times. This change in temperature $(\theta_2 - \theta_1)$ is given by

$$\theta_2 - \theta_1 = (q/4\pi\lambda) \log_e t_2/t_1 \tag{1}$$

where

q = heat input per unit length of wire,
θ_2 = temperature at time t_2,
θ_1 = temperature at time t_1, and
λ = thermal conductivity.

Temperatures θ_1 and θ_2 are chosen so that they lie on the linear portion of the curve. It should be noted that there is no thermal diffusivity term in this equation.

This expression assumes an infinitely long heater of negligible thickness. For practical purposes, a correction must be made for the finite size of the heater. This is done by evaluating a time interval t_0 which is subtracted from both t_1 and t_2 so that Eq 1 becomes

$$\theta_2 - \theta_1 = (q/4\pi\lambda) \log_e t_2 - t_0/t_1 - t_0 \tag{2}$$

where t_0 is evaluated by plotting $dt/d\theta$ at intervals of 1 s against the elapsed time for the first 15 to 20 s. The best straight line is drawn through the points, and the intercept on the time axis gives t_0.

If we now plot the temperature against $\log_e$ of the corrected time, we

[2]The italic numbers in brackets refer to the list of references appended to this paper.

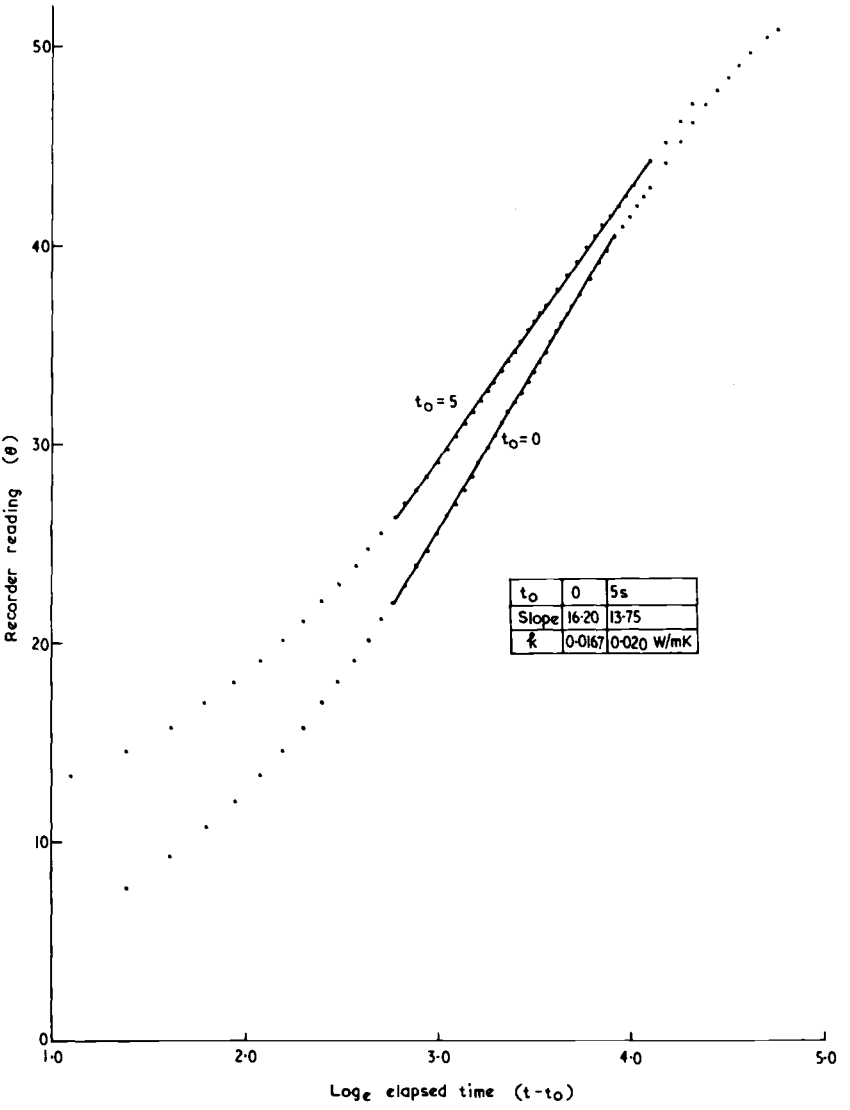

FIG. 1—*Determinaton of* λ *for ceramic fiber blanket: Haupin hot wire.*

should obtain a straight line whose slope is equal to $q/4\pi\lambda$. This is the basis of the hot-wire method.

Experimental Techniques

Thermal Conductivity Probes

Wechsler [6] has discussed fully the design and application of thermal conductivity probes. The advantages are simplicity of equipment and rapidity of measurement; under suitable conditions with a calibrated probe, only two temperature readings are required over a time interval which may lie between 150 s and 10 min. Accuracy may be as good as ± 5 percent. The disadvantages include difficulties in finding suitable material of known thermal conductivity and the fact that the probes must be individually calibrated and can be used with confidence only over the range of heater currents covered in the calibration. The temperature range is restricted to about 100°C, although probes can be used down to −200°C. Since the investigations were made at temperatures up to 1000°C, this technique was discarded and other hot-wire methods examined.

Line Heat Source Techniques

Haupin Type—The first method investigated is due to Haupin [7], where a butt-welded thermocouple is used as the heater. The two legs of the couple are of different resistance-alloy wires. Since these two alloys have differing resistivities, the resistance of each leg must be matched by using different wire gages. It was found that a batch of 22 B&S (0.643 mm) Nichrome-3 and 27 standard wire gage (SWG) (0.417 mm) Advance gave a good match up to 700°C, as shown by the following table:

Temperature, (°C)	20	100	200	300	400	500	600	700
Resistance match, percent	−3	−1	−0.7	+0.5	+1.6	+1.4	+0.4	+0.2

The butt weld was made by a capacitor discharge method. The couple was calibrated against a standard base-metal couple to 1000°C. The thermocouple electromotive force (emf)/temperature curve is not linear, as can be seen from the following:

Temperature, (°C)	50	100	200	300	400	600	800	1000
Emf, (mV)	2.04	4.27	9.32	14.98	21.00	33.42	46.78	60.26
μV/°C	44.6	49.2	55.2	59.6	61.0	64.0	68.4	67.0
Resistance, ohms/m	3.565	3.575	3.600	3.630	3.680	3.800	3.950	4.56

A heater-couple comprising platinum/platinum 13 percent rhodium was considered at this stage, but was discarded since the low thermo-emf would have required a stable d-c amplifier. Some difficulty had been experienced with interference from the furnace controller and nearby electrical equipment, and it was felt that in view of the limited scope of the tests too much time might be taken up with possible additional problems associated with the d-c amplifier. The upper temperature limit of 1000°C imposed by the base-metal combination was acceptable.

Since both the heater current and the thermoelectric current are flowing in the same wire, some means must be used to separate them. The original method used 60 Hz a-c to heat the wire, blocking the d-c thermo-emf with a large capacitor of low impedance to the a-c. In the thermocouple loop, the a-c was removed by a tuned filter comprising two large iron-cored inductors and two electrolytic capacitors. The present circuit (Fig. 2*a*) uses a similar setup. To reduce the filter components to a reasonable size, the frequency of the heater current is increased to 2200 Hz. A high-sensitivity oscilloscope was used to check the residual ripple present at the recorder input. With 0.7 A flowing, the residual ripple was less than 0.5 mV and became insignificant when a further filter comprising a 1-μF capacitor in parallel with a 1000-Ω resistor was placed across the recorder input.

The amplifier was a standard 15-W audio amplifier. This gave 1.5 A into a 6-Ω load before appreciable distortion was noticed. A 50- or 60-Hz

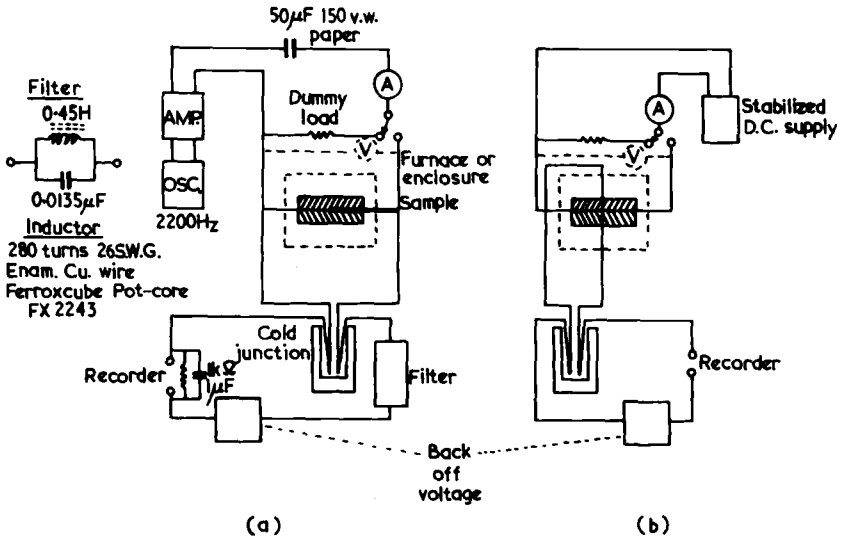

FIG. 2—*Schematic of hot-wire thermal conductivity apparatus:* (a) *a-c heating, Haupin type*; (b) *d-c heating, cross type.*

alternating current from a combination of a variable autotransformer and a fixed-ratio transformer can also be used provided the waveform has low distortion.

In the early tests, a first-grade analog a-c ammeter was used. This was later replaced by a digital multimeter. The final setup had a standard 0.100- or 1.00-Ω resistor in series with the heater. The voltage drop across the resistor was measured with a digital voltmeter. This meter could be switched to also measure the voltage drop between two wires spot-welded a measured distance apart on the heater. If a-c heating is used and there is appreciable distortion of the waveform, it is advisable to use a true root-mean-square (rms) voltmeter, or errors could arise.

A dummy load, equal in resistance value to that of the heater, was used to set the heater current to a known value and to check that the current was constant before switching to the heater.

The heater was sandwiched between two slabs of the test material. Where possible, these were 200 by 200 by 25 mm, but in some cases shortage of test material made it necessary to use 200 by 100 mm. In such cases the heater lay along the 200-mm direction. For bricks, the heater was sandwiched between the 220 by 110-mm faces.

At room temperature the test specimen was enclosed in a foamed polystyrene box to eliminate drafts and variations in ambient temperature. For the high-temperature measurements a sillimanite box fitted with a lid was used. This also acted as a heat sink and kept the specimen surroundings constant during a test run. It proved possible to maintain the temperature in the box constant to within 0.1°C over a 5-min period.

The high-speed recorder used had a maximum sensitivity of 250 μV full-scale deflection (fsd) (200-mm chart width), but for most of the tests the top speed of 600 mm/min was used with either the 0.5 or 1.0-mV sensitivity. The maximum temperature rise recorded was less than 20°C, being only 12 to 15°C for most of the tests. Because of the low cost of the wire, the heater-couple was discarded after a high-temperature run.

Although this method gave good results, it soon became apparent that a good butt weld could not be guaranteed. This affected the stability of the heater current and also the thermo-emf. Tests showed some variation in the temperature coefficient of the latter from one heater-couple to another, possibly due to the butt weld. Another disadvantage was the rapid rise in the resistivity of the heater above about 850°C. These disadvantages outweighed the convenience of the method.

Welded Heater-Thermocouple or Cross-Type Hot-Wire—This method has been used for some considerable time and is the basis of DIN 51046: 1973 [*8*], which is proposed as a standard test for refractory materials. It differs from the combined heater-couple in that a separate thermocouple is welded to the center point of the heater. In the present instance, the heater was a 22 B&S (0.643-mm) Nichrome-3 wire and the thermocouple

34-SWG (0.234 mm) T_1/T_2 alloys (Type K). The thermocouple size complies with DIN 51046.

The equipment layout was as in Fig. 2*b*. This is very similar to the combined heater-couple arrangement. Either d-c or 2200-Hz a-c could be used to heat the wire. In the case of the latter, the filter arrangement was unnecessary. Heavier-gage leads were used for the heater connections outside the box to minimize power requirements. The current was monitored throughout with the digital multimeter. It proved possible to maintain the current constant to better than 2 mA when 1 A was flowing. Checks were made to observe the effect of a deliberate variation in heater current during a run, and a change of 2 mA produced a measurable change in the slope of the curve.

Experimental Procedure

The specimen-heater-couple sandwich was assembled with the couple leads taken out at right angles to the heater and placed in the box. It was then allowed to reach thermal equilibrium, the couple being used to check. With the recorder on 1 mV fsd and the steady thermo-emf backed off, it was possible to detect changes of the order of 0.025°C. There was normally little difficulty in obtaining a temperature stability of 0.05°C over 5 min. When equilibrium was reached, the amplifier or power supply was switched on and the current set in the dummy load to a suitable value. As a rough guide, I^2R should be of the order of 5 to 8 W/m for a thermal conductivity of 0.1 W/m·K, where I is the heater current in amps (rms for a-c) and R the heater resistance in ohms per metre length (*not* the actual heater resistance). When the current had settled to a steady value, the recorder was zeroed, the chart drive engaged, and the current switched to the heater. A rapid initial rise in temperature is noted, followed by a leveling off to a steady rise, the rate of which slowly decreases. A typical run usually lasted 3 min.

The recorded trace has now to be replotted—recorder reading, θ—against $\log_e$ of elapsed time from the start of the run. Before this is done, however, the correction factor t_0 has to be evaluated to allow for the finite size of the heater wire. This was of the order of 5 s for 22 B&S wire or 1 s for 34-SWG wire. This value is subtracted for each time reading when plotting the graph. A typical corrected and uncorrected curve is given in Fig. 1. The graph is plotted on semilog paper.

The slope of the linear portion of the graph is then determined, the difference in recorder readings ($\theta_2 - \theta_1$) being converted to degrees (Celsius or Kelvin) by multiplying by the appropriate factor (degrees per millivolt). The thermal conductivity λ is then derived from the expression

$$\lambda = q/4\pi S \tag{3}$$

where S is the corrected slope.

The energy input q can be obtained from I^2R, in which case R must be corrected for variation with temperature. The necessary correction factor usually can be obtained from the manufacturer's literature. For the Nichrome-3 heater the factor is 1.123 at 1000°C. It should be emphasized that R is the resistance per metre length. An alternative method to obtain q is to measure the voltage V across the heater wire at the voltage takeoff points, preferably with a digital voltmeter. The power input is then given by VI/l, where l is the heater length in the specimen in metres. Both methods were used, there being little difference in the results obtained.

At least three determinations were made at each temperature, preferably with a range of heater currents. DIN 51046 suggests taking the temperature at 2 and 10 min. This simplified method can be used if a series of tests is being made on materials of roughly the same thermal conductivity or where the thermal conductivity does not vary greatly with temperature. If the variation of λ with temperature is large or unknown, it is advisable to plot the readings to ensure that there is a linear portion to the graph and that its position is known. Otherwise there is the risk that one or the other of the fixed time points may be off the linear portion, giving rise to serious errors. The time interval suggested is for insulating bricks or refractories and will be found to be excessive for ceramic fiber blankets, where a much shorter time interval is more appropriate.

The main difficulty at higher temperatures is in ensuring that the temperature of the specimen surroundings is steady both before and during the measurements. For this reason it is advisable to have the specimen in some form of refractory box to even out temperature fluctuations. Such variations during the measurement period will cause distortion of the curve. There may also be some trouble from interference pickup on the thermocouple leads, particularly if thyristor control of the furnace is employed. This can be minimized by a suitable disposition of the leads and thorough screening outside the furnace. It may be necessary to take the leads out parallel to each other rather than in the cross form.

It is essential that there be good contact between the heater wire and the specimen. With ceramic fiber blankets, slight loading of the upper slab may be necessary. With bricks, insulating or refractory, it will be necessary to smooth the contacting surfaces and cut a groove in the top surface of the lower brick. This groove should be of a width and depth only very slightly in excess of the diameter of the heater wire, which is cemented in place with a paste made from brick dust and a suitable organic binder.

Results

The preliminary tests were made at room temperature to establish repeatability and variation. Both a-c and d-c heating were used, there being little difference in the values obtained. A typical set of figures for a ceramic fiber blanket is

a-c Heating		d-c Heating	
Current, A	λ, W/m·K	Current, A	λ, W/m·K
0.544	0.0253	0.545	0.0252
0.590	0.0253	0.607	0.0254
0.646	0.0250	0.658	0.0255
0.677	0.0250	0.693	0.0253

The above figures for λ show a spread of about ± 1 percent. In these and the high-temperature tests, there was little difficulty in achieving the ±15 percent quoted in DIN 51046. The replotted curves of θ against $\log_e t$ were subjected to statistical analysis, and the straight-line portions of the graphs gave coefficients of variation ranging from 0.9995 to 0.99998.

Curves are given in Fig. 3 for two different crystalline-type fiber blankets (96 kg/m^3). The curves in Fig. 4 are for heavy-duty fiber blankets (128 kg/m^3) from two different manufacturers.

Comparison with Other Test Methods

Some time after these evaluation trials had started, the British Ceramic Research Association took part in a cooperative test organized by the German Standards Committee, DNA [*9*], in which a number of continental laboratories also took part, using a variety of methods with a 2300-Grade insulating brick as the test material (Fig. 5). In Fig. 5, the B.S. method refers to B.S. 1902: Part 1A: 1966, Section 12. The Klasse method is a comparative technique similar to the split-column method [*10*]. And the Radial-flow method uses thermocouples disposed radially at known distances from a central axial heater [*11*].

In this test, each laboratory tested two bricks from a selected batch, and there were therefore two sources of differences between laboratories: (1) differences due to experimental errors, both systematic and random, and (2) differences arising from test-piece variation. The overall spread of the hot-wire results is about ±25 percent. Nothing is known in this particular test of the variation in specimen conductivities, but an estimate of this may be made from data given by Cowling [*12*] which indicate that, if the test bricks were selected to have bulk density variations within ±8 kg/m^3, a spread of conductivities of about 15 percent of the mean value might be expected.

It is customary to label a conductivity value with the mean value of the temperature range over which it has been measured. If the conductivity/temperature relationship of the material departs from a straight line—as is the case for many ceramic fibers—the conductivity measured over a range of temperature will differ from the "true" or "actual" conductivity at the mean temperature of that range. This could lead to differences

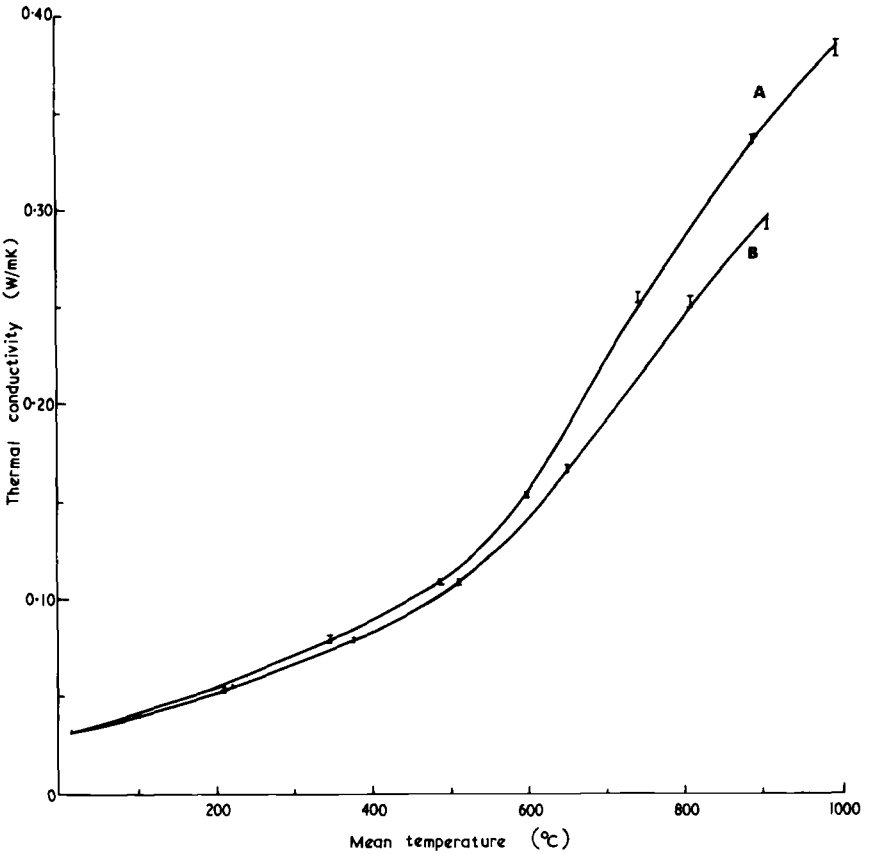

FIG. 3—*Variation of thermal conductivity with temperature: crystalline-type fiber blankets.* A: Al_2O_3 *fiber*; B: ZrO_2 *fiber (96 kg/m³).*

between methods employing small and large ranges such as the hot-wire and the B.S. methods.

Results of an early test on ceramic-fiber blanket are given in Fig. 6. The same 5-cm-thick (2 in.) blanket pads were measured by the ASTM Test for Steady-State Thermal Transmission Properties by Means of the Guarded Hot Plate (C 177-76), the B.S. 1902 method, and the hot-wire method, care being taken to maintain the same orientation and spacing. The B.S. method was used up to a hot-face temperature of 950°C and the hot-wire method between room temperature and 900°C. It can be seen that the B.S. method and ASTM Method C 177-76 do not cover the same range. The B.S. method operates with a cold-face temperature near the ambient level, giving a low mean temperature, whereas the supplementary

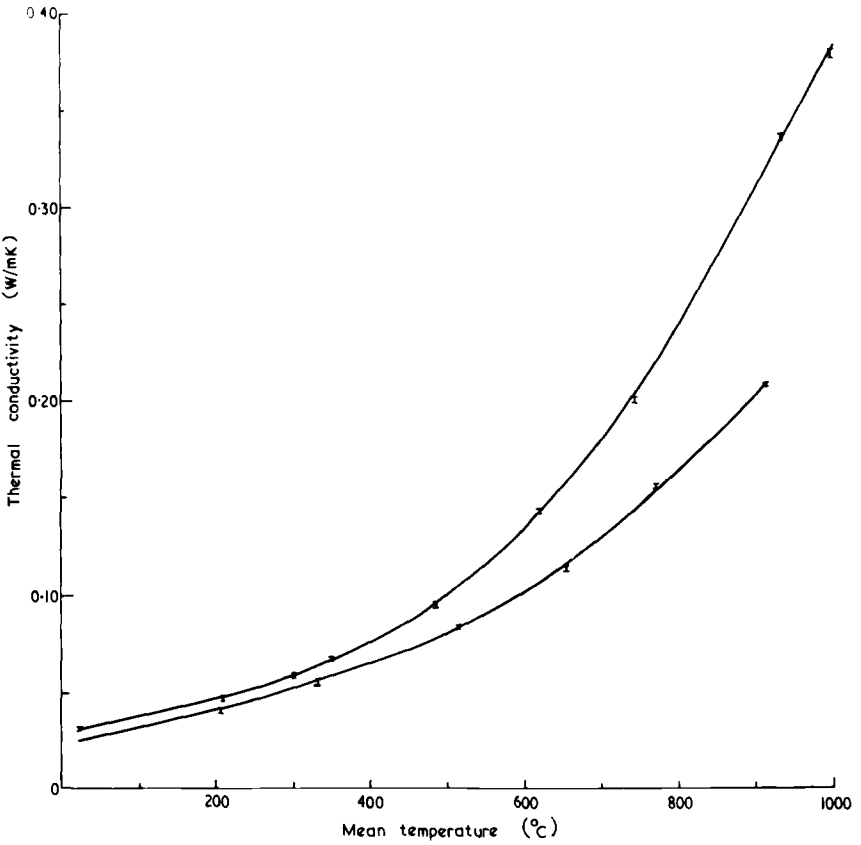

FIG. 4—*Variation of thermal conductivity with temperature: heavy-duty (128 kg/m³) ceramic fiber blankets, different manufacturers.*

heaters in the hot-plate apparatus bring the rear faces of the specimens to within about 100°C of the hot faces, giving a high mean temperature. These two methods produced lines of differing slope, meeting at about 500°C. The hot-wire points lie almost exactly on the two lines, suggesting almost perfect agreement.

Later tests on insulating bricks, however, gave results which were of the order of 10 to 20 percent higher than the B.S. method. One such comparison is given in Fig. 7 for a 2300-Grade insulating brick (500 kg/m³), where the difference is about 15 percent.

Conclusions

The hot-wire method offers the advantages of rapidity and relatively low cost. The temperature rise during a test is less than 20°C, so that the

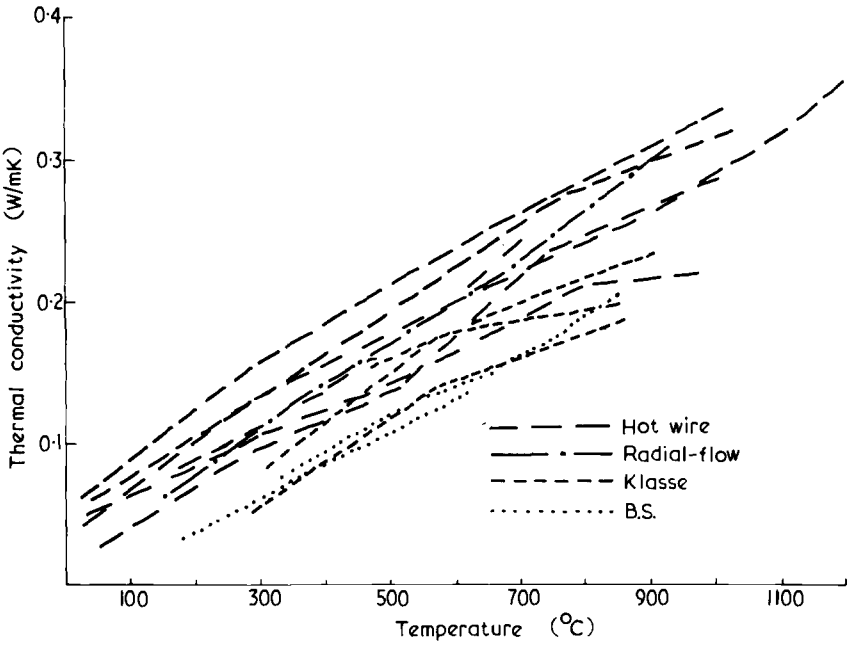

FIG. 5—*Cooperative measurements on 2300-Grade insulating brick.*

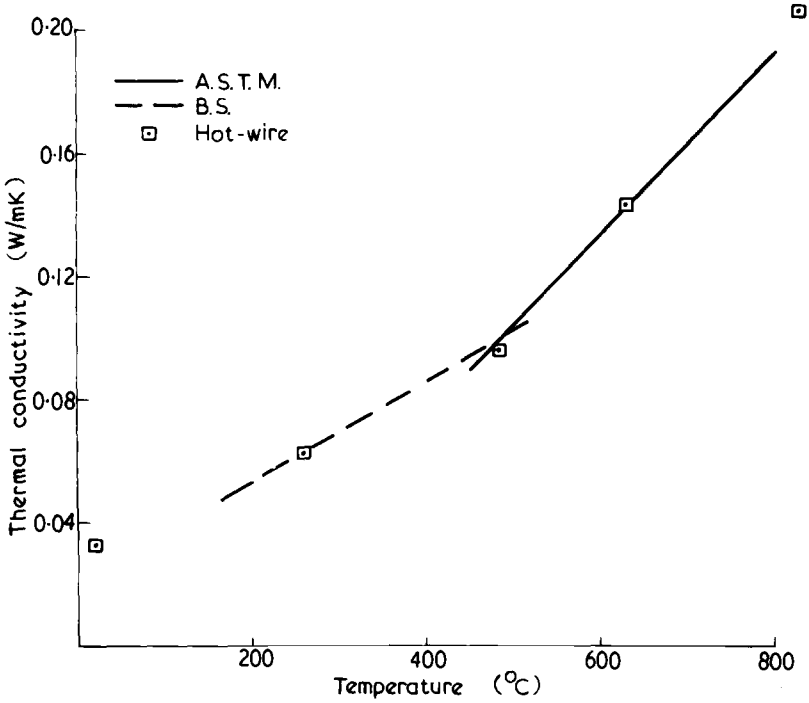

FIG. 6—*Cooperative measurements on ceramic fiber blanket (128 kg/m³).*

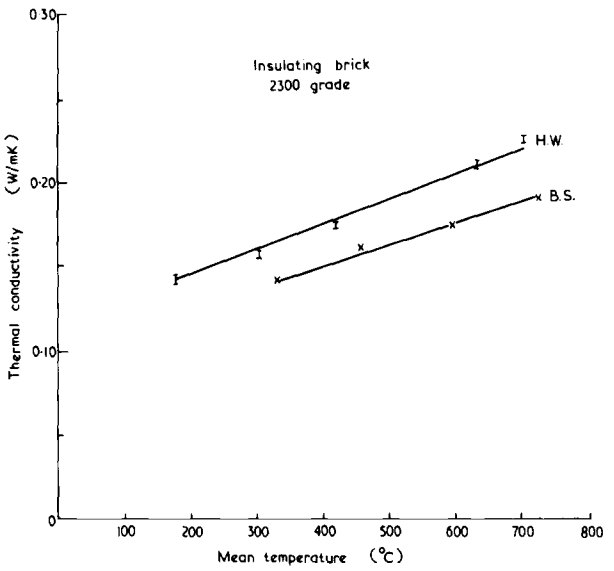

FIG. 7—*Comparative measurements on 2300-Grade insulating brick, HW = hot wire; B.S. = B.S. 1902.*

test can be regarded as isothermal compared with other methods, where a temperature gradient of several hundred degrees may exist. In the present instance it has been used at temperatures up to 1000°C. DIN 51046 gives 1600°C as the upper limit, with 2 W/m·K as the upper limit for the conductivity range. However, Eschner [*13*] shows that this limit can be raised to about 6 W/m·K.

The method is easily set up with standard laboratory equipment, the main expense being that of the furnace and temperature controller. It is readily adaptable to automatic working. The tedious curve plotting can be obviated by using an X-Y recorder with the X-axis fed from a linear ramp generator via a logarithmic amplifier. This will produce the necessary $\log_e t$ axis. If the heater wire has a diameter of 0.25 mm or less, the diameter correction will be about 1 s and can be ignored.

Although an early test with fiber blanket gave excellent agreement with the ASTM Method C 177-76 and the B.S. 1902 method, later results, particularly with insulating bricks, indicated that the hot-wire results tended to be some 10 to 20 percent higher than the other two methods. Private communications from other European workers have confirmed this, and it is suggested that further cooperative tests under standardized conditions be undertaken.

Acknowledgment

The author wishes to thank Mr. A. Dinsdale, O.B.E., director of research of the British Ceramic Research Association, for permission to publish this paper.

References

[1] Schieirmacher, A.L., *Wiedemann Annalen Physik*, Vol. 34, 1888.
[2] Van der Held, E.F.M. and Van Drunen, F.G., *Physika*, Vol. 15, No. 10, 1949, p. 865.
[3] Carslaw, H.S. and Jaeger, J.C., *Conduction of Heat in Solids*, 2nd ed., Oxford, University, Press, 1959.
[4] Blackwell, J.H., Journal of Applied Physics, Vol. 25, No. 2, 1954, p. 137.
[5] Hooper, F.C. and Lepper, F.R., *Transactions*, American Society of Heating and Ventilating Engineers, Vol. 56, 1950, p. 309.
[6] Wechsler, A.E., Cold Regions Research and Engineering Laboratories, Technical Report 182, U.S. Army Material Command, 1966.
[7] Haupin, W.E., *Bulletin of the American Ceramic Society*, Vol. 39, No. 3, 1960, p. 139.
[8] German Standards Committee, "Testing of Ceramic Materials, Determination of Thermal Conductivity to 1600°C by the Hot-Wire Method," DIN 51046, Aug. 1976.
[9] Lehmann, H., *Tonindustrie-zeitung*, Vol. 97, No. 10, 1973, p. 275.
[10] Klasse, F., Heinz, A., and Hein, *Berichte Der Deutschen Keramichen Gesellschaft*, Vol. 34, No. 6, 1957, p. 183.
[11] McElroy, D.L. and Moore, J.P. in *Thermal Conductivity*, Vol. 1, R.P. Tye, Ed., Academic Press, London, 1959.
[12] Cowling, K.W., Elliott, A., and Hale, W.T., *Transactions*, British Ceramics Society, Vol. 53, 1954, p. 461.
[13] Eschner, A., Grosskopf, B., and Jeschke, P., *Tonindustrie-zeitung*, Vol. 98, No. 9, 1974, p. 212.

Parameters Affecting Thermal Performance

T. J. Thirst[1] *and S. D. Probert*[1]

Heat Transfer Versus Pitch Angle for Nonventilated, Triangular-Sectioned, Apex-Upward Air-Filled Spaces

REFERENCE: Thirst, T. J. and Probert, S. D., "**Heat Transfer Versus Pitch Angle for Nonventilated, Triangular-Sectioned, Apex-Upward Air-Filled Spaces**," *Thermal Transmission Measurements of Insulation, ASTM STP 660*, R. P. Tye, Ed., American Society for Testing and Materials, 1978, pp. 203–210.

ABSTRACT: The optimal pitch angle of a nonventilated triangular-sectioned air space, corresponding to a minimum heat transfer ($\dot{Q}$) versus pitch angle (θ), was experimentally determined on a laboratory model to be 18 deg inclination for small values of temperature difference (ΔT) appropriate to those that would occur in roof spaces. In a more realistic roof cavity, this optimal pitch would be smaller; it is suggested that full-size nonventilated roofs be designed with pitches near 15 deg.

KEY WORDS: heat transfer, pitch angle, roof, thermal insulation, convection, triangular cavity, thermal conductivity

Nomenclature

$\dot{Q}$	Rate of heat transfer
T	Temperature of an inner surface of the triangular cavity ($T_1 < T_2$)
θ	Pitch of the roof
(*prefix*) Δ	Difference between
(*suffix*) 1	Referring to the pitched roof
(*suffix*) 2	Referring to the horizontal floor of the roof space
COND, CONV, RAD	Due to steady-state conduction, convection, and radiation, respectively, through the air under a fixed ΔT
(*suffix*) total	As measured experimentally

In an air-filled cavity having a vertical sectional form of an isosceles triangle, with cooled sloping sides, apex upward, and a heated horizontal base (Fig. 1), which is geometrically similar to the roof space of many

[1]School of Mechanical Engineering, Cranfield Institute of Technology, Bedford, MK43 OAL, England.

buildings, heat transfer to the sloping sides occurs by (1) radiation, (2) conduction, (3) convection (all through the contained air), and (4) conduction both across the contact between the eaves and the horizontal base as well as through the vertical end walls of the roof space (that is, perpendicular to the roof).

The aim of this project was to determine how the thermal resistance of the air in such a cavity, at atmospheric pressure, varies with the pitch angle of the identical sloping sides, and to determine the relative magnitudes of the heat transfer contributions (1–4) under a range of differing boundary temperatures.

Experimental Rig

It would have been propitious if a series of full-scale building roofs, identical except for roof pitch, had been accessible for experimentation. Unfortunately this was not so—there were unsystematic variations with respect to dimensions, shapes, and support structures, as well as different incursions (for example, chimneys) passing through the available roofs. In the initial series of tests, it was decided therefore to experiment upon a simple, model, roof space (Fig. 2) so that the only variable was the roof pitch angle, which could be appropriately selected in advance. It was recognized that any conclusions drawn might be susceptible to scaling errors if extrapolated to full-size systems.

All the walls of the cavity were chosen to be of polished copper (em-

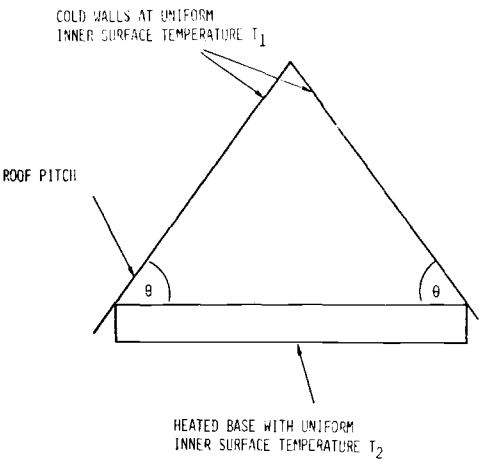

FIG. 1—*Representative cavity.*

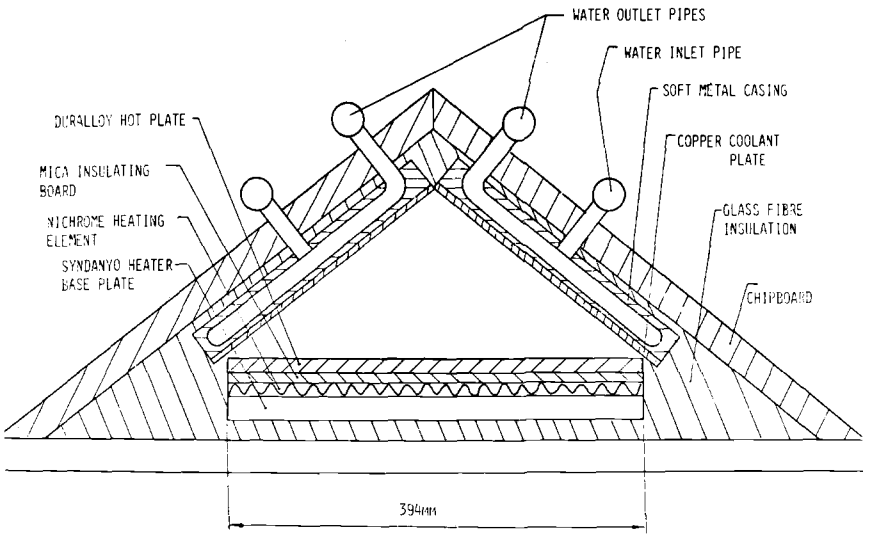

FIG. 2—*Schematic representative section through the experimental rig of lateral, horizontal dimension, 305 mm.*

issivity = 0.033±0.003). This reduced the radiant heat exchanges accordingly, and therefore convection became a relatively more important heat-transfer mechanism. In these circumstances any change (resulting from a change in roof pitch angle) in the convective contribution to the total rate of heat transfer became more apparent.

Experimental Measurements

For a horizontal, plane, parallel-walled cavity under small temperature differences, convection is virtually eliminated when the heat is required to flow downward even though vigorous convection ensues if the applied temperature difference is reversed.[2] Therefore, in a triangular cavity, apex downward, it is probable that a similar situation applies. This hypothesis was investigated with a 15-cm field-of-view Mach Zehnder interferometer employed in the infinite-fringe mode of operation so that the resulting interference lines represented isotherms. To limit any disruption of the internal flow in the horizontal-floored cavity, viewing was only via narrow vertical slots.

Typical interferograms for $\Delta T = 67°C$ are shown in Figs. 3 and 4 for the cavity with its apex downward and upward, respectively. From such

[2]Arnold, J.N., Bonaparte, P.N., Catton, I., and Edwards, D.K. in *Proceedings*, Heat Transfer and Fluid Mechanics Institute, Stanford University Press, 1974, pp. 321–329.

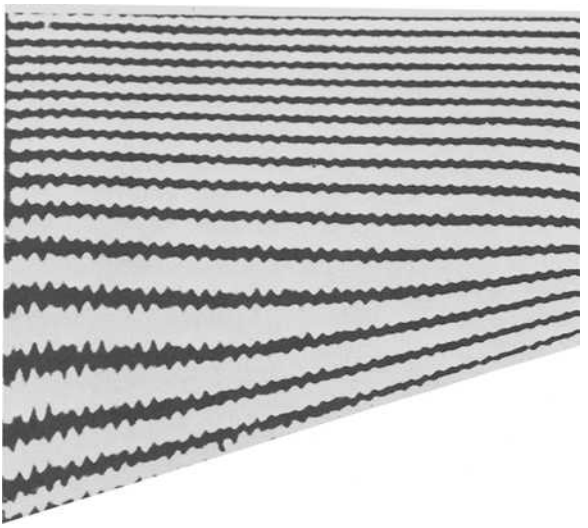

FIG. 3—*Temperature distribution in a slice through inverted 20-deg pitch cavity with* $T_1 = 20°C$ *and* $T_2 = 87°C$; *that is*; $\Delta T = 67°C$.

interferograms, especially those for low values of ΔT, it was seen that the hypothesis was corroborated, and also that the walls of the enclosure were truly isothermal as required. Therefore, for a given ΔT, the difference between the steady-state heat fluxes across the cavity with the apex upward and downward equals the convective heat transfer in the upright situation. [For large pitch angle cavities, at high values of ΔT (> 35°C), some convection ensued in the inverted case, and this technique therefore became less trustworthy for higher temperature differences.] For $\Delta T = 20°C$, the difference, that is, $\dot{Q}_{CONV}$, is plotted in Fig. 5, the maximum convective component occurring at a pitch of about 25 deg. The experimentally determined steady-state heat fluxes for a fixed ΔT across the upright cavity (see Fig. 6) revealed an optimal pitch angle corresponding to a minimum in the $\dot{Q}$-versus-θ graph at about 18 deg inclination for small values of ΔT, appropriate to those that would occur in roof spaces.

From experiments with 'Teledeltos' conducting paper, it was deduced that the conductive heat transfer through the air decreased with increasing roof pitch angle (see Fig. 5). The steady-state radiative heat transfer across the cavity was evaluated (for internal surfaces with emissivity 0.033). This together with the appropriate convective component can be summed and is shown in Fig. 5 together with $\dot{Q}_{total}$. This incorporates a solid conduction contribution, that is, Clause (4) of the initial paragraph of this paper. The difference between $\dot{Q}_{total}$ and the sum of

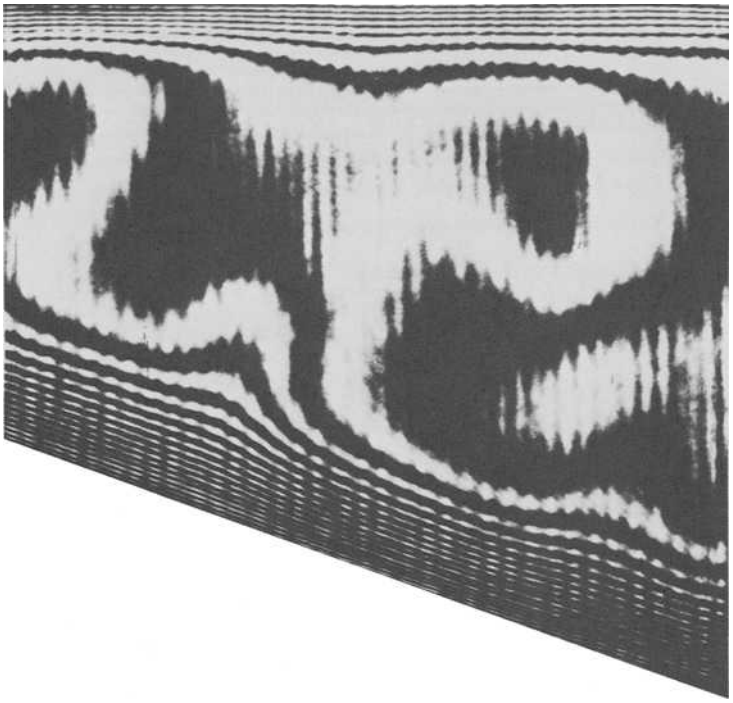

FIG. 4—*Isothermal map of the system used for Fig. 3 under identical boundary conditions, but with the cavity apex upward.*

$$\dot{Q}_{\text{CONV}} + \dot{Q}_{\text{RAD}} + \dot{Q}_{\text{COND}}$$

gave this contribution. It was remarkably consistent in view of the nine differing pitch arrangements involved and possible experimental error. The onset of free convection for $\Delta T \leqslant 20°C$ occurred at about 12-deg pitch angle, whereas the maximum in the rate of convection versus roof pitch angle decreased from 25 deg for $\Delta T = 20°C$ to 23 deg for $\Delta T = 80°C$.

The presented results are for the one-fifteenth scale cavity. In a more realistic roof cavity, the surface emissivities involved would probably be considerably higher (unless insulated by, say, aluminum foil), and thus the radiation contribution may become dominant and its decay-versus-pitch angle steeper. Thus the optimal pitch, corresponding to the minimum (or point of inflexion) in the $\dot{Q}_{\text{total}}$-versus-θ curve, would be smaller. It must be emphasized that the thermal resistance at the optimal pitch is less than that for very large pitch angles, but the extra costs and weights of these high-pitched roofs militate against them. Also, for the model tested, the use of an interim pitch up to about 35 deg is disadvantageous relative

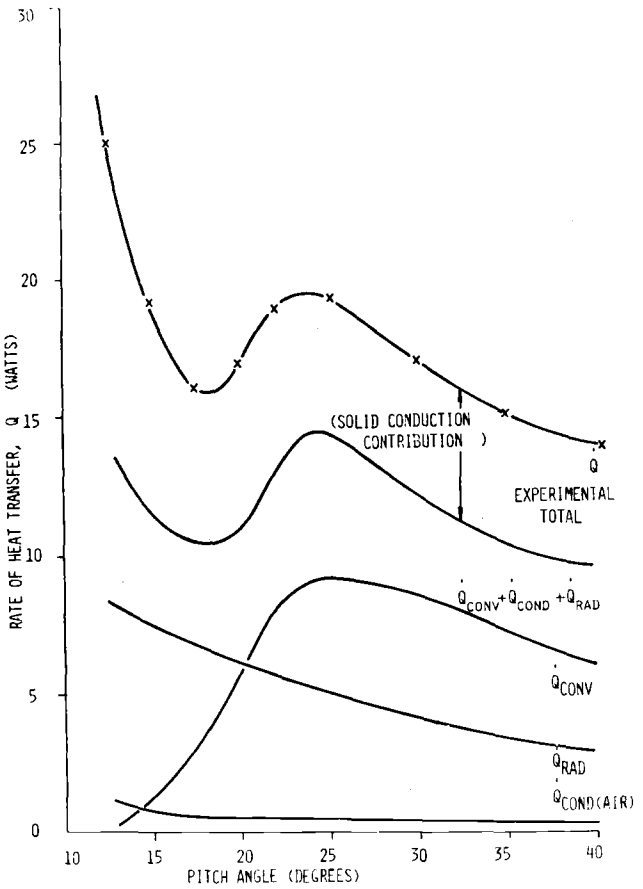

FIG. 5—*Component and total rates of heat flows across triangular-sectioned cavities, apex upward, for* $\Delta T = 20°C$.

to, say, 18 deg, not only because of the extra cost of the structure, but because it would also have a lower thermal resistance.

In a full-size roof cavity, the onset of convection for a given applied ΔT is likely to occur at smaller pitch angles than suggested by the model experiments, because of the larger vertical dimensions involved. It is therefore suggested that full-size roofs be designed with pitches near 15 deg, the exact value being dependent on the emissivities of the internal surfaces chosen.

Conclusions

Thermal insulation design involves selecting the most suitable shape, structure, and surface properties for the system, as well as the application

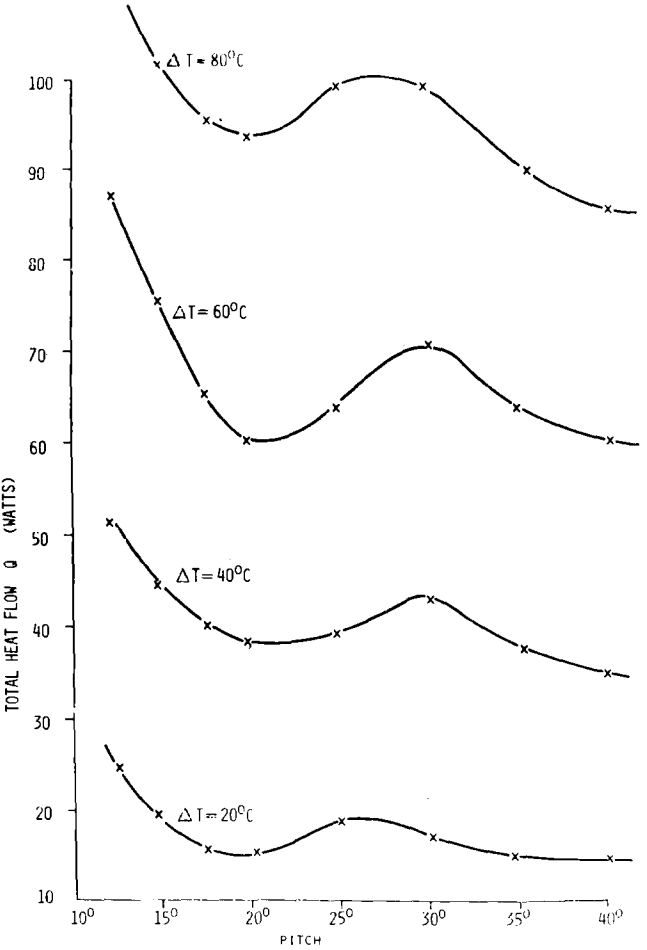

FIG. 6—*Steady-state total heat fluxes across the cavity.*

of the economically most favorable thickness of insulant (as evaluated over the proposed lifetime of the system, due allowance having been made for the future inflation of fuel costs). However, too often an insulant is applied to cover up mistakes due to careless design, incurring thereby an economic penalty.

It is suggested that further consideration be given to roofs of buildings having pitches of near 15 deg. This recommendation, however, must not be implemented in isolation from other design considerations; for example, restricting attic ventilation can lead to undesirable condensation within, and tiles on lower pitched roofs tend to have accelerated rates of deterioration.

Low-pitched (<30 deg) roofs are more commonplace in countries (for example, Switzerland) with higher annual snowfalls than the United Kingdom. The residence time for the snow on the smaller incline is likely to be longer and hence the insulation effect of the snow (when most needed) is advantageous. However, the roofs must then be appropriately stronger to withstand the increased weight of snow.[3] Also, in wind, the *suction* loads on roofs (especially around their perimeters) become more severe with decreasing roof pitch so that again increased strength is recommended.[4] Despite these problems, however, sufficient evidence is now available to suggest that, as energy becomes more expensive, further research into roof pitch (and building orientation) to achieve maximum thermal insulation, and simultaneous maximum benefit from solar radiation, in this commonly encountered construction is now overdue.

Acknowledgments

The authors wish to thank the Science Research Council for financial support of this project.

[3]Mitchell, G.R., "Snow Loads on Roofs," Building Research Establishment, Paper No. 33/76, H.M. Stationery Office, London, 1976.

[4]Eaton, K.J., Maynes, J.R., and Cook, N.J., "Wind Loads on Low-Rise Buildings—Effects of Roof Geometry," *Proceedings*, 4th International Conference on Wind Effects on Buildings and Structures, Brighton, U.K., 8–12 Sept. 1975.

M. Bomberg[1] *and C. J. Shirtliffe*[1]

Influence of Moisture and Moisture Gradients on Heat Transfer Through Porous Building Materials

REFERENCE: Bomberg, M. and Shirtliffe, C. J., "**Influence of Moisture and Moisture Gradients on Heat Transfer Through Porous Building Materials**," *Thermal Transmission Measurements of Insulation, ASTM STP 660*, R. P. Tye, Ed., American Society for Testing and Materials, 1978, pp. 211–233.

ABSTRACT: The total heat transfer through moist, porous building materials is the sum of a number of heat-transfer phenomena. This paper presents experimental data on heat transfer through specimens of moist aerated concrete and mineral fiberboard.

The aerated concrete specimens with known initial moisture distributions were exposed to a temperature gradient. This temperature gradient caused a redistribution of moisture which in turn changed the heat flow through the material. The changes were monitored by means of thermal probes, heat flowmeters, and thermocouples. The results of measurements were compared with calculations based on a simplified analytical model and with measurements made by other investigators.

A second series of tests was made on a moist specimen of high-density mineral fiberboard to demonstrate the extent of the dependence of the total thermal resistance on the distribution of moisture in the material.

KEY WORDS: thermal conductivity, thermal resistance, heat transfer, heat transmission, porous material, fibrous material, glass fiber, aerated concrete, moisture, moisture gradient, moisture effects, thermal conductivity probe, heat flowmeters

The primary objective in the solving of most thermal problems is to determine the heat flow through a given material or structure. To determine the rate of heat flow through a dry, one-dimensional solid material, the thermal conductivity is multiplied by the average temperature gradient. For fibrous or porous thermal insulations, in which radiation or convection plays a significant role in heat transfer, the rate of heat flow is calculated by dividing the temperature difference by the thermal resistance. The heat transferred through moist materials must be calculated as the sum of a

[1]Research officers, National Research Council of Canada, Division of Building Research, Ottawa.

number of components. In addition to transfer through the solid and gaseous phases of the material, heat is transferred through the liquid phase and by the movement of moisture in either the liquid or vapor phase [*1 – 3*].[2] If evaporation and condensation occur within the material, large exchanges of heat are involved. Thermal energy is stored or released by the solid phase and by air and also by liquid or gaseous water. The moisture is forced to move by the processes of evaporation, condensation, or capillary action.

Equations describing the simultaneous heat and mass transfer in porous bodies can be written, but they involve many physical properties of the material [*4*]. For specific boundary conditions and materials, some of the terms in these equations can be neglected. In some cases two terms can be grouped or approximated by a single term involving material characteristics. Few methods have been developed to measure these characteristics and, where they do exist, many measurements are required to determine one set of simplified characteristics for a single material. This has limited the use of the equations, especially for thermal insulating materials.

The simplified moisture flow equations have been verified for transient flows through building materials by Van der Kooi [*5*], Jenisch [*6*], Hens [*7*], Sandberg [*8*], and Bomberg [*9*]. Investigators have had less success in using simplified equations to predict heat flow through moist materials with either known moisture gradients or known average moisture contents.

This paper describes an attempt to use a particular set of simplified equations and to predict the heat flow through moist porous building materials with closed boundaries. The materials selected for study were an aerated concrete and a high-density mineral fiberboard. The aerated concrete was dense, which eliminated complicated radiation effects. It had a uniform cell structure and a high open cell content; the cell walls supported capillary action. This material represents a type of building material that is widely used in Europe and, to a lesser extent, in Canada. More important, it has been investigated extensively and many of its physical hygroscopic properties are well known. The mineral fiberboard represents a fibrous thermal insulation commonly used in roofs.

A closed system for moisture was used in tests on the two selected materials. The average moisture content of the specimens remained unchanged. Application of a thermal gradient caused redistribution of moisture which was initially placed in a part of the specimens. The experiment involved both a transient and a steady-state phase. Heat flow into each specimen of aerated concrete was measured with a heat flowmeter placed on the warm side. The apparent thermal conductivity[3] was measured at

[2]The italic numbers in brackets refer to the list of references appended to this paper.

[3]The capability for heat transfer through moist, porous materials, usually obtained from measurements, is called either the apparent thermal conductivity [*10*] or the effective thermal conductivity [*11,12*].

seven locations in this material with a double probe arrangement. Heat transfer across this material and at the seven points within it was calculated and compared with the measurements.

The dual system of measurement made it relatively simple to determine whether the discrepancies between the calculations and measurements were due to errors in the measurements or limitations in the model. The limitations of the simplified set of equations as well as the limitations of the dual probe method were illustrated by this study.

In the experiment on mineral fiberboard, two heat flowmeters were used, placed on both the cold and warm sides of the specimen.

Measurement of Simultaneous Heat and Moisture Transfer

The apparatus was designed to show how redistribution of moisture influences heat transfer through a specimen of porous material. Two cylindrical specimens of aerated concrete were tested. Each had a slightly different level of average moisture content and initial moisture distribution, and each consisted of two layers of aerated concrete (Fig. 1), with carefully ground surfaces ensuring good contact. The upper parts of the specimens were initially oven dry; the lower were initially water saturated. The dry and wet sections of each specimen were placed together and the assembly covered with an impermeable sealed membrane.

A temperature difference was imposed across the specimens by placing a heater under them and controlling the air temperature and heat-transfer coefficient above the top surface. The heat flow through the hot surface of each specimen was measured by an Organization for Industrial Research

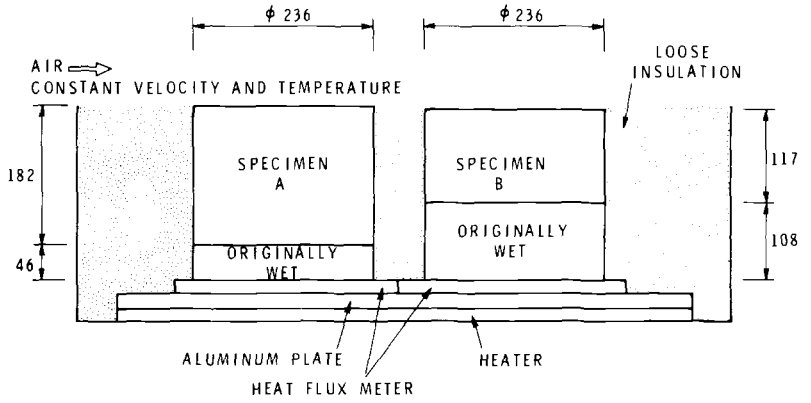

FIG. 1—*Test setup.*

(TNO)-produced heat flowmeter which consisted of a thermopile imbedded in polyvinyl chloride. The thermopile was formed from a helical coil of constantan wire, in which half of each wire was plated with copper. The helical coil was then spirally wound to produce a circular metered area. The windings of the coil produced high conductance paths from one surface of the metered area to the other.

The temperature gradient across the specimen accelerated the moisture equalization process and increased the rate of moisture flow from the bottom to the top section. Moisture could not escape from the upper surface or the sides of the specimens as these were sealed. Condensation therefore occurred in the cooler regions of the top section. Eventually a dynamic equilibrium was established: the flow of liquid in the downward direction counterbalanced the flow of vapor upward.

The heat flow in the specimen and through the hot and cold surfaces of the specimen was affected by the moisture redistribution process. The changes of heat flow and ability to transfer heat were measured by heat flowmeters, placed between the heater and specimens, and by the probes.

Two double-line thermal conductivity probes developed by Van Minnen and Vos [*13*] were inserted vertically in each specimen as described later, more or less symmetrically around the axis of revolution, and sufficiently distant from each other so that measurements could be made simultaneously without mutual interference. Each probe had two identical line sections. Thermocouples in one line section were used as temperature references. The other section acted as a line heat source for measuring the apparent thermal conductivity of the specimen at several points. The effect of the vertical temperature gradient imposed on the specimen in the testing apparatus was eliminated by this arrangement. The second set of probes was used to check the reproducibility of the measurements. The probes were inserted by drilling holes 4.5 mm in diameter through the specimens. A 4-mm glass tube was covered with adhesive and slipped into the hole. The probe, consisting of the heating wire and plastic shield (diameter 2.5 mm), was placed into the glass tube.

Owing to the small cross-sectional area of metal and glass in the probes, it was assumed that the heat flow along the probes would not introduce significant errors in the heat flowmeter measurements.

Thermocouples were placed on the sides of the specimens to measure the temperature at the surface and thus estimate the horizontal component of heat flow. Heat also flowed from the heater and aluminum plate to the surrounding insulation and then into the sides of the specimens. The net heat flow into the sides of the specimens was calculated from knowledge of the properties of this insulation. The airflow over the upper surfaces of the specimens was maintained at a temperature of approximately 25°C and a velocity of about 0.5 m/s. The temperature at the lower surface depended on the average heat flow through the specimen.

The dry density of the aerated concrete averaged 650 kg/m^3. The moisture contents of the lower sections of the specimens were 250 and 280 kg/m^3 (25 and 28 percent by volume) for Specimens A and B respectively.

Tests similar to those on aerated concrete were made on a specimen of a mineral fiberboard with a density of about 160 kg/m^3. The specimen, 50 mm thick and 300 mm square, had an average moisture content of 19.1 percent by weight. The specimen was enclosed in polyethylene film and placed between two heat flowmeters in a standard heat flowmeter apparatus to determine its apparent thermal resistance. The probes were not used in these tests because of the possibility of larger longitudinal heat flows.

Results of Tests on Aerated Concrete

The temperature and moisture distributions in the specimens changed after the two sections were placed in the apparatus. The rate of temperature change decreased with time. During the last two weeks of the test the temperature distribution changed very little. The temperature distribution on the sides at the end of the tests is shown in Fig. 2. Each point represents the average reading for two thermocouples. The temperature profile is nonlinear because of the nonuniform moisture content.

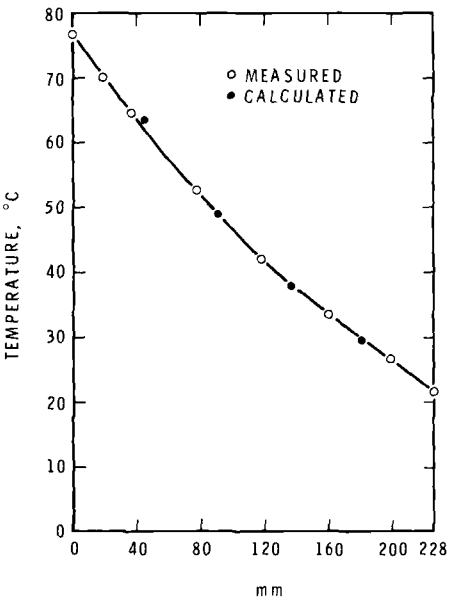

FIG. 2—*Temperature on side surfaces of aerated concrete Specimen A at end of test.*

Each specimen was assumed to be composed of nine layers of material. Layers 2 through 7 were 20 mm thick and were centered about the corresponding thermocouple in the probe; Layers 1 in Specimens A and B were 58 and 55 mm thick, respectively, and Layer 9 was 30 mm thick. The thermocouples were off-center in each of these layers. Each thermocouple was assumed to measure the temperature of that layer. The readings from the thermocouples at Layers 3 and 9 were erroneous and were discarded. The thicknesses of Layers 2, 4, and 8 were adjusted to account for the missing results from Layers 3 and 9.

The resistance of each layer was calculated from the thickness divided by the apparent thermal conductivity measured for that layer by the probe. The thermal resistance, R, of the total specimen was calculated as a sum of resistances of the layers

$$R_A = \frac{0.058}{\lambda_1} + \frac{0.030}{\lambda_2} + \frac{0.030}{\lambda_4} + \frac{0.020}{\lambda_5} + \frac{0.020}{\lambda_6} + \frac{0.020}{\lambda_7} + \frac{0.050}{\lambda_8}$$

$$R_B = \frac{0.055}{\lambda_1} \frac{0.030}{\lambda_2} \frac{0.030}{\lambda_4} \frac{0.020}{\lambda_5} \frac{0.020}{\lambda_6} \frac{0.020}{\lambda_7} \frac{0.050}{\lambda_8}$$

where λ_1 to λ_8 were measures of the ability to transfer heat in each of the layers. Layer 1 was the layer closest to the heater.

There was a large scatter in the probe measurements during the initial stages of the tests but this decreased after a considerable portion of the moisture had redistributed. About the 12th day of the test, the thermal resistance of the specimens could be calculated with some certainty. Figure 3 shows the readings from Points 1, 5, and 8 of Probe 1 in Specimen A. Point 1 was closest to the heater. The ability to transfer heat after 12 days was already close to the final value for that section of the specimen. The measurements from Point 8, which was next to the upper surface, show that the ability to transfer heat at that section remained almost constant during the whole test. Moisture had been forced to move away from the heater and condensation occurred nearer to the cold upper surface. Equilibrium also developed rapidly near the upper surface. The results from Point 5 in the middle of the specimen show that the amount of heat transferred was high at the beginning but decreased during the test due to moisture redistribution.

The overall thermal resistance of the specimen, calculated from the probe measurements, was comparable to the value obtained from the heat flowmeter measurements.

The total thermal resistance for Specimens A and B determined by both measuring methods is shown in Fig. 4. After about two weeks, the thermal resistance of both Specimens A and B as determined by the probe method was approximately the same as that determined with the heat flowmeter.

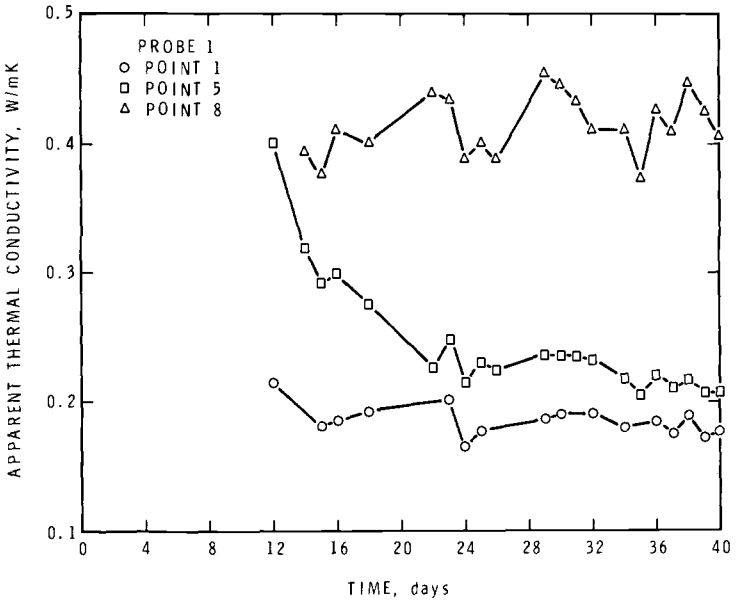

FIG. 3—*Apparent thermal conductivity measured on aerated concrete Specimen A with Probe 1. Point 1 is near the heater, Point 5 in the middle, Point 8 near the cold surface.*

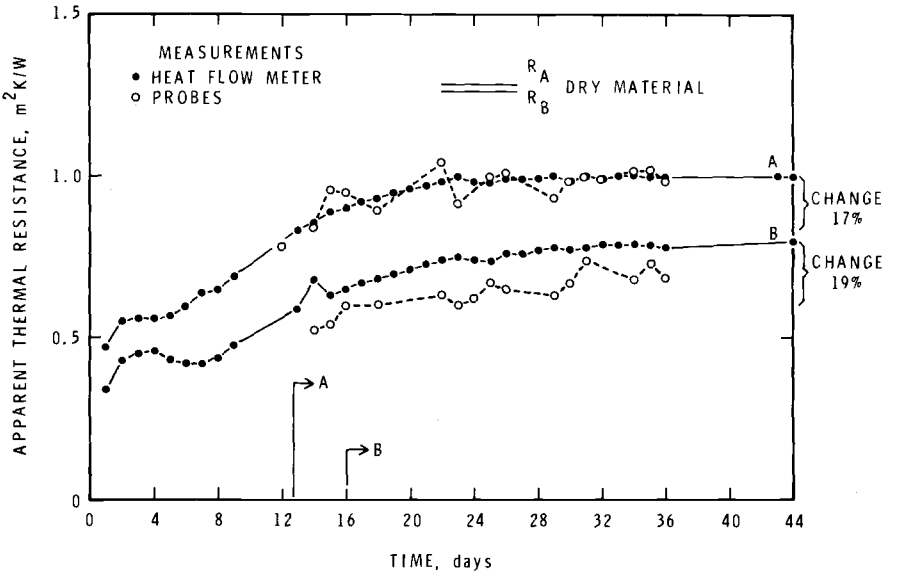

FIG. 4—*Thermal resistance determined by the two methods on aerated concrete, Specimens A and B. (Results of the heat flowmeters must be corrected for edge heat gains.)*

The scatter in measurements from single points on the probes was considerably larger than for the measurements made by the heat flowmeters. Daily variation in the total thermal resistances determined with the probes was large; for example, a 13 percent difference was found between the averages for Days 22 and 23 of the tests. The total thermal resistance determined with the heat flowmeters varied by less than 2 percent from day to day.

Average readings at Point 7 in the two probes placed in Specimen A differed by 16 percent in the period from Day 32 to Day 40. The difference between the two readings on any day during this period varied from 2 to 35 percent.

Each of the probe measurements was averaged over several days and the overall thermal resistance of the specimen was calculated. The averaged values agree reasonably well with the measurements made by the heat flowmeters.

The following were the averaged resistance values for Specimen A for the period between Days 34 and 40 of the tests

Probe 1	0.99 $m^2 \cdot K/W$
Probe 2	1.03 $m^2 \cdot K/W$
Heat flowmeter:	
uncorrected	1.00 $m^2 \cdot K/W$
corrected	0.95 $m^2 \cdot K/W$

The overall thermal resistance for Specimen B during this period was

Average from probes	0.70 $m^2 \cdot K/m$
Heat flowmeter:	
uncorrected	0.80 $m^2 \cdot K/m$
corrected	0.76 $m^2 \cdot K/m$

Figure 4 shows the ratio of the difference between the surface temperatures and the rate of heat flow at the lower surface of Specimens A and B measured with the heat flowmeter, as a function of time. When the heat transfer through the specimen reached a quasi-steady state, this ratio became equal to the apparent thermal resistance. Solvason [*14*] showed that after a sudden increase in the temperature of the hot surface of a moist material, the rate of heat flow at that surface might exceed the steady-state value. This effect increases the time required to establish the quasi-steady-state condition. The heat flow rate recorded for Specimen A reached a peak of 85.5 W/m^2 on the 4th day of investigation and decreased to 61.6 W/m^2 on the 14th day. For specimen B, it was 111.7 W/m^2 on the 7th day and decreased to 84.1 W/m^2 on the 14th day. (The tables of results can be obtained, on request, from the Division of Building Research, National Research Council of Canada.)

Results of Tests on Mineral Fiberboard

The specimen had a dry density of about 160 kg/m^3 and a thermal resistance R = 1.424 m^2·K/W. Moisture was added to the level of 19.1 percent by weight, that is, 30.5 kg/m^3, and the specimen was enclosed in sealed polyethylene film. The specimen was then left in the laboratory for a few days to allow the moisture distribution to become uniform; it was then placed into the heat flowmeter apparatus and heat fluxes recorded. The results are shown in Fig. 5 and Table 1.

After most of the moisture had been moved toward the cold side of the specimen, the specimen was reversed and the cold side placed in contact with the hot plate. The heat flowmeters remained at the same positions, and the temperatures of the plates were maintained constant throughout the test.

Heat fluxes at the surfaces were disrupted, but within half an hour came as close as 10 percent to each other. Within 2 h the difference in heat flux entering and leaving the specimen was less than 1 percent. This condition in which the level of mean heat flux passing the specimen was steady persisted for a few hours.

Inexperienced laboratory personnel might call this stage an established steady state. Later measurements showed that the thermal resistance of

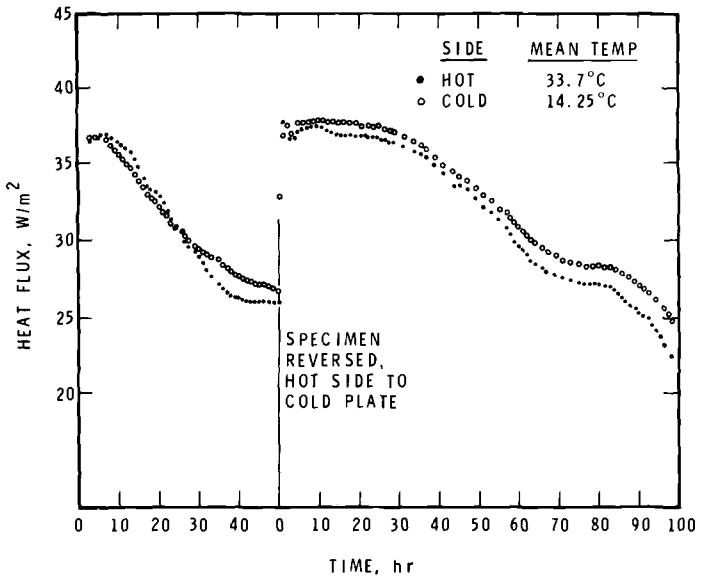

FIG. 5—*Heat fluxes as indicated by heat flowmeters placed on both sides of the moist, enclosed, high-density mineral fiberboard.*

TABLE 1—*Selected results from a test with a heat flowmeter placed on each side of the rigid, high-density mineral fiberboard insulation. (Thermal resistance of the dry specimen, R = 1.424 m²·K/W; thickness 50 mm.)*

Time from Start of Tests		Heat Flux, W/m², at Surface			Total Thermal Resistance
h	min	hot	cold	difference	m² · K/W
25	45	35.83	36.13	0.30	...
27	25	36.17	36.15	−0.02	0.447
27	55	36.24	36.06	−0.22	
28	25	36.16	35.98	−0.18	...
51	30	28.90	29.22	0.32	0.559
52	30	28.61	29.12	0.51	
71	00	25.88	26.43	0.55	0.619
71	30	25.83	26.40	0.57	
		Hot and cold sides of the tested specimen reversed			
0	00	46.47	32.47	−14.0	...
0	30	39.47	35.70	−3.77	...
2	00	36.29	36.94	0.65	...
4	00	36.29	36.43	0.14	...
8	00	36.55	37.20	0.65	...
25	00	36.03	36.82	0.79	0.444
47	00	32.84	33.36	0.52	0.489
96	00	22.54	24.66	2.12	0.686
98	00	22.29	24.47	2.18	

the specimen varies due to changes in moisture distribution and therefore this stage is only a quasi-steady state.

During the quasi-steady state, the heat flow recorded by the meter placed on the cold side was larger than that recorded by the meter on the hot surface. The difference between the two heat flows was about 2 percent during the later part of the first day and about 10 percent at the end of the test. The reason for this increase is probably due to the effect of condensation close to the windings on the thermopiles. Other experience with heat flowmeters having metal running through the metered area indicates that, when heat flowmeters are placed on the cold surface, a thermal damper such as a sheet of a dry standard thermal insulation a few millimeters thick must be placed between it and the surface to break the high-conductance paths.

The total thermal resistance of the high-density mineral fiberboard varied during the quasi-steady state. The thermal resistance at the end of the test was 50 percent higher than the value of the initial plateau. This demonstrates the extent of the dependence of the total thermal resistance on the distribution of moisture in the material.

Calculations of Simultaneous Heat and Moisture Transfer

The calculation of moisture flow due to a temperature gradient and heat flow due to a moisture gradient is discussed elsewhere [*15, 16*]. The following set of equations for heat and moisture flow, each being the sum of a moisture gradient and a temperature gradient term, were derived

$$q_e = -\lambda\frac{dT}{dx} - \lambda_m\frac{dp_c}{dx} \tag{1}$$

$$q_m = -k\frac{dp_c}{dx} - K_T\frac{dT}{dx} \tag{2}$$

where

q_e = rate of heat flow, W/m^2,
q_m = rate of moisture flow, kg/m^{2}s,
T = temperature, K,
p_c = capillary suction, Pa,
λ = thermal conductivity, W/(m·K),
k = moisture conductivity, s,
K_T = moisture conductivity due to temperature gradient, kg/(m·K·s), and
λ_m = heat conductivity due to moisture gradient, J·s/(kg·m).

Transport coefficients in Eqs 1 and 2 hold the following relations to the phenomenological coefficients used in the theory of irreversible thermodynamics

$$\lambda = \frac{1}{T^2}\cdot L_{qq},\ k = \frac{\rho}{T}\cdot L_{mm},\ \lambda_m = \frac{\rho}{T}\cdot L_{qm},\ K_t = \frac{1}{T^2}\cdot L_{mq}$$

where ρ is the pore-water density in kg/m^3.

Onsager's reciprocal relation for the transport coefficient states that $L_{mq} = L_{qm}$. This allows calculation of the λ_m-coefficient from the K_T when all other gradients and transport coefficients are known.

The term describing the energy flow due to a moisture gradient was calculated and its magnitude shown to be negligible under the conditions of these tests.

The computer program used for the calculation of moisture transport in porous materials has been described by Bomberg [*9*]. The temperature field was calculated from a heat flow model in which the thermal capacity effects were neglected. The calculated temperature gradients were used as driving forces in calculating the moisture flow, which was made using a transient-state flow model.

Eliminating the thermal capacitance from the heat-transfer calculations resulted in a rapid establishment of the final temperature gradient for given steady boundary conditions. As a result, the calculated moisture flows

should be somewhat greater than the actual moisture flows. The errors in the calculation of moisture movement caused by neglecting the short-term temperature gradients were found by Sandberg [*8*] to be negligible. Other researchers [*5, 17*] have also used this simplification with success. In general, this means that it is the difference in temperature between the two boundaries that has the major effect on the local moisture and thermal flows.

Heat flow and moisture transport in a porous body can be calculated only if the approximate dependence of the material properties on the moisture content is known. The thermodynamic potential for moisture, the moisture conductivity, and the apparent thermal conductivity must be known for all values of moisture content. The material characteristics of aerated concrete used for the computer calculation are discussed in the Appendix.

Comparison of Calculations with Measurements (Aerated Concrete)

The temperature gradient in the thermal insulation surrounding the tested specimens was almost linear. The temperature gradient measured at the side of the specimens was nonlinear because the apparent thermal conductivity varied from point to point in the concrete. The difference in gradients caused an exchange of heat between the specimens and the surrounding insulation. The heat flows through the side of the cylinder and the temperature gradient were computed with the finite-element program described by Konrad and Silvester [*18*]. Figure 2 shows that there was good agreement between the calculated and measured temperature gradients. The effect of lateral heat flow on the heat flow through the hot surface of the specimens was calculated and this value was used to correct the measurements of the steady-state flux through the hot surface obtained with the heat flowmeters. The correction for Specimen A was only 5.6 percent (any error in this estimate would be of second-order magnitude).

The distribution of moisture in the specimens was measured at the beginning and end of the test series and was also calculated with the program. Figure 6 shows that there is good agreement between the measured and calculated distribution of moisture content at the end of the test. Each point in the figure represents the mean of four measurements. The apparent thermal conductivity measured by the two probes in the specimens is also plotted in Fig. 6. The curve has the same shape as the curve for moisture content.

The main components of heat and moisture transfer in Specimen A determined with the computer program are given in Table 2. The results given for ten equal layers, different from those assumed in the probe measurements, are

1. heat flux due to moisture gradient.

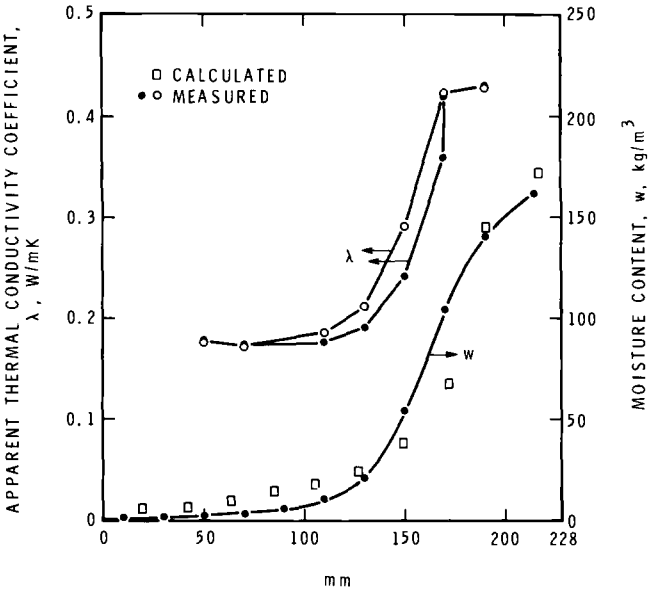

FIG. 6—*Measured and calculated moisture content distribution in aerated concrete Specimen A and the apparent thermal conductivity measured with the two probes at the final stages of the tests.*

2. apparent thermal conductivity calculated for the specified mean moisture content and the moisture gradient.

3. apparent thermal conductivity calculated for the specified mean moisture content and no gradient of moisture, and

4. mean moisture content of the layer.

The quantity of heat transported by moisture flow can be significant when heat is extracted from one place, carried through a significant distance, then released. Table 2 and Fig. 7 give the results of the calculations for the quantity of heat transported by moisture flow. In the 4th layer, the heat flow caused by the moisture content gradient alone during the 1st day was about 30 percent of the heat flow during the steady state. The flow decreased rapidly and in the later stage of the test was in the opposite direction. In the final stage of the measurements, the heat flow caused by the moisture gradient in Layers 7 and 8 was about 10 percent of the level measured with the heat flowmeter placed at the surface. These flows occur only within a narrow portion of the material and do not cause significant errors in the calculation of the overall thermal resistance. The difference between the local apparent thermal conductivities was slight, whether moisture gradients had been taken into account in calculations or not, and the total thermal resistance may be calculated without regard to heat flow caused by moisture gradients.

TABLE 2—*Calculated properties:* (a) *Heat flux due to moisture content gradients*, (b) *apparent thermal conductivity*, (c) *apparent thermal conductivity in absence of the moisture gradient, and* (d) *mean moisture content for consecutive layers.*

Day	Calculated Property		Layers									
	Designation	Unit	1	2	3	4	5	6	7	8	9	10
1	a	W/m^2	0.0	0.1	0.3	16.0	0.5	0.0	0.0	0.0	0.0	-0.1
	b	W/(m·K)	0.387	0.362	0.230	0.189	0.180	0.180	0.180	0.180	0.180	0.182
	c	W/(m·K)	0.372	0.352	0.306	0.200	0.186	0.182	0.182	0.182	0.184	0.189
	d	kg/m^3	175	158	118	21	8	4	4	4	5	10
3	a	W/m^2	0.0	0.1	0.2	7.8	5.4	0.3	0.0	-0.1	-0.6	-1.0
	b	W/(m·K)	0.345	0.331	0.294	0.181	0.175	0.183	0.182	0.183	0.188	0.198
	d	kg/m^3	150	138	108	39	14	9	7	8	12	22
5	a	W/m^2	0.1	0.1	0.2	4.1	7.4	0.3	-0.1	-0.4	-1.4	-3.9
	b	W/(m·K)	0.327	0.313	0.283	0.205	0.167	0.186	0.186	0.190	0.200	0.221
	d	kg/m^3	135	124	99	45	15	11	11	13	20	34
7	a	W/m^2	0.1	0.1	0.3	3.6	8.5	0.3	-0.2	-0.8	-2.4	-7.9
	b	W/(m·K)	0.313	0.301	0.273	0.210	0.165	0.188	0.189	0.195	0.209	0.259
	d	kg/m^3	123	113	90	46	16	13	14	17	26	48
13	a	W/m^2	0.1	0.3	0.6	7.6	5.6	0.1	-0.7	-2.5	-6.1	-4.4
	b	W/(m·K)	0.281	0.267	0.242	0.188	0.176	0.194	0.198	0.215	0.246	0.305
	d	kg/m^3	95	85	63	32	21	18	20	27	42	104
15	a	W/m^2	0.1	0.2	1.5	10.6	2.0	0.2	-1.2	-2.9	-6.4	-3.4
	b	W/(m·K)	0.270	0.258	0.230	0.171	0.187	0.194	0.202	0.219	0.251	0.329
	d	kg/m^3	87	76	55	26	21	20	22	29	46	127
21	a	W/m^2	-0.1	2.2	7.7	3.9	0.2	-0.7	-1.6	-5.4	-5.6	-1.0
	b	W/(m·K)	0.241	0.221	0.183	0.181	0.194	0.199	0.207	0.238	0.277	0.373
	d	kg/m^3	60	49	28	21	19	20	26	37	71	177
28	a	W/m^2	1.7	0.2	0.5	-0.2	-0.2	-1.1	-3.4	-6.2	-3.8	-0.3
	b	W/(m·K)	0.194	0.193	0.192	0.192	0.195	0.199	0.219	0.249	0.319	0.413
	d	kg/m^3	20	18	17	16	17	21	28	44	117	208
35	a	W/m^2	0.9	-0.1	-0.4	-0.4	-0.9	-1.7	-5.6	-6.2	-1.3	-0.1
	b	W/(m·K)	0.181	0.185	0.188	0.190	0.196	0.205	0.236	0.271	0.352	0.379
	d	kg/m^3	8	9	10	12	16	22	34	62	152	181
44	a	W/m^2	0.6	-0.3	-0.1	-0.5	-0.9	-1.7	-6.4	-5.8	-0.9	-0.1
	b	W/(m·K)	0.180	0.185	0.185	0.190	0.196	0.205	0.243	0.278	0.349	0.372
	c	W/(m·K)	0.185	0.185	0.188	0.191	0.195	0.202	0.238	0.252	0.345	0.376
	d	kg/m^3	7	7	9	12	16	23	36	69	152	177

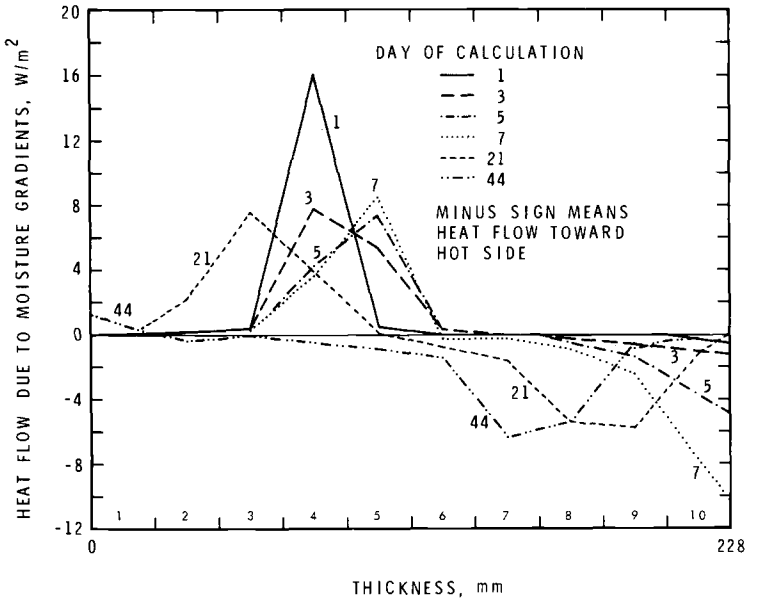

FIG. 7—*Calculated distribution of the heat flows due to moisture gradient in aerated concrete Specimen A.*

The heat flow caused by transient moisture flows may result in significant errors in values of the apparent thermal resistance measured by heat flowmeters placed next to the condensation zone [*19*]. It will not cause errors in the measurements made by the heat flowmeters placed on the hot side of the specimen. After a sudden temperature change, however, the heat flux measured at the hot surface may greatly exceed the heat flux that would occur under steady-state conditions. In these tests the heat flux measured by the heat flowmeter placed at the hot surface did not equal the average value of heat flux through the specimen during the first two weeks.

Prediction of Heat Flow Through a Porous Material with Known Moisture Distribution

In calculating the heat flow during the period of quasi-steady state, the flow of moisture through a closed system can be disregarded. The presence of moisture increases the heat conduction in the specimen. The equation for heat flow can be approximated by the first term of Eq 1 for q_e and an apparent thermal conductivity can be used to calculate heat flow.

Figure 8 illustrates a simple model of the interactions between the different modes of conductive heat transfer in a porous body based on

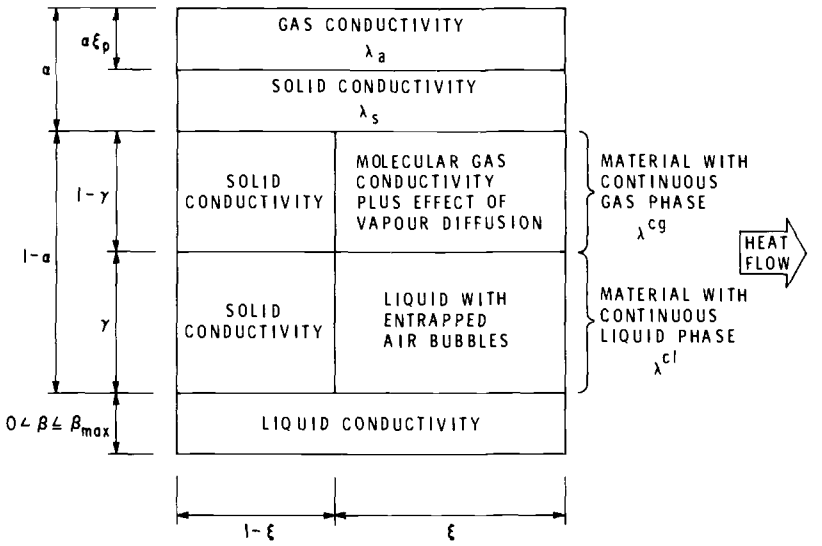

FIG. 8—*Model of interaction of different modes of conductive heat transfer in a porous body.*

work of Verschoor and Greebler [*20*], Krischer [*21*], Pelanne [*22*], and Bankvall [*23*]. Heat can be conducted either in a single phase, or it can be transferred from one phase to another and back again—for example, from the solid phase to the pore air and back to solid phase. Simple apparent thermal conductivities can be used to describe the flow of heat

1. conducted through the solid phase only,
2. conducted through the continuous gas phase only, or
3. conducted through the continuous liquid phase only.

"Composite" thermal conductivities can be used to describe the heat

1. transferred from the solid to the gas phase and back to the solid phase, or
2. transferred from the solid to the liquid phase and back to the solid phase.

The thermal conductivity of the gas phase is the sum of the apparent gas conductivity and the energy that is transferred by the diffusion of water vapor.

The thermal conductivity of the liquid phase can be treated as a sum of series and parallel paths. Heat will be transferred both through a water film adsorbed by the pore walls and a series-transport through the entrapped air bubbles. It can flow from the liquid phase to the gas phase and back to the liquid phase. The contribution of the absorbed and adsorbed water to the transfer of heat depends on the moisture content of the material. The heat flow occurs through both liquid and solid; that is,

a "composite" solid and liquid heat transfer mechanism occurs. The apparent thermal conductivity of the aerated concrete was calculated using such models. A series model was used to calculate the thermal conductivity of that portion of the material with a continuous gas phase; that is

$$\lambda^{cg} = \lambda_a \cdot \lambda_s / [\lambda_s \epsilon + \lambda_a (1 - \epsilon)] \quad (3)$$

Using a total open porosity, ϵ, of 0.70, an air conductivity $\lambda_a = 0.026$ W/(m·K), and a solid phase conductivity $\lambda_s = 2.5$ W/(m·K), yields a λ^{cg} of 0.037 W/(m·K). Equation 3 does not include effects of evaporation, diffusion, and condensation on the thermal conductivity of air [*12*].

The calculated thermal conductivity will be low for the range of moisture contents where phase changes play an important role in the total moisture transfer. The quantity of heat transferred through the air phase is negligible even though the porosity of the aerated concrete is 70 percent. The difference between the measured thermal conductivity of a dry material and the series conductivity of that portion of the material containing the continuous air phase is the solid-phase conductivity

$$\lambda^{cs} = \lambda_{dry} - \lambda^{cg}, \quad \lambda_{dry} = 0.176 \text{ W/(m·K)}, \lambda^{cg} = 0.037 \text{ W/(m·K)}, \lambda^{cs} = \lambda_{dry} - \lambda^{cg} = 0.139 \text{ W/(m·K)}$$

The solid phase conductivity is not influenced by the moisture content. The effect of the moisture can be added to the series conductivity by using the conductivity of the air-water mixture for the gas conductivity. The thermal conductivity of the continuous water phase with entrapped air bubbles can be calculated using Maxwell's model [*24*]

$$\lambda_m = \lambda_c (\lambda_d + 2\lambda_c - 2P_d [\lambda_c - \lambda_d])/(\lambda_d + 2\lambda_c + P_d [\lambda_c - \lambda_d]) \quad (5)$$

where

λ_m = conductivity of the mixture,
λ_c, λ_d = conductivity of continuous and disperse phases, respectively, and
P_d = volume fraction of the disperse phase.

The following example will illustrate how this formula can be used in calculations for an aerated concrete with the following properties: moisture content, $\omega = 180$ kg/m^3 (18 percent by volume); total porosity, $\epsilon = 0.70$; and degree of saturation, $S = 0.257$ (P_d is 0.743). The thermal conductivity of the continuous water phase with a disperse air phase becomes $\lambda_m = \lambda^{cw} = 0.132$ W/(m·K).

The apparent thermal conductivity of the system can be calculated from

$$\lambda_{app} = \lambda^{cs} + \lambda^{cw} \cdot \lambda_s / (\lambda_s \cdot \epsilon + \lambda^{cw} [1 - \epsilon]) \quad (6)$$

or substituting in Eq 6

$$\lambda_{app} = 0.139 + 0.216 = 0.355 \text{ W/(m·K)}$$

The results of the calculations for Specimen B are given in Table 3a. The corrected value of the total thermal resistance of the specimen determined by the heat flowmeter was 0.76 $m^2 \cdot K/W$. The probe measurements gave a thermal resistance about 8 percent lower. The thermal resistance determined from the calculated apparent thermal conductivity was about 8 percent higher (Table 3*b*).

The model of apparent thermal conductivity used in these calculations does not accurately describe the moisture-air interaction. The effects of evaporation, diffusion, and condensation have also been neglected. As a result, the calculated thermal resistance is somewhat higher than it should be, but even this crude model gives an accuracy comparable to the measurements made by the probe. More refined computational models could be used for apparent thermal conductivity determination and would doubtless give even better results.

TABLE 3*a*—*Thermal resistance of Specimen B calculated on the basis of measured moisture content distribution and calculated apparent thermal conductivity.*

Layer, mm	Moisture[a] Content, kg/m^3		Thermal Resistance, m^2 K/W
0 to 20	3		0.112
20 to 40	5		0.111
40 to 60	8		0.110
60 to 80	23		0.101
80 to 100	41		0.091
100 to 120	151		0.061
120 to 140	247		0.047
140 to 160	253		0.046
160 to 180	254		0.046
180 to 200	256		0.046
200 to 225	257		0.052
		Total	0.82

[a]Moisture content 1 percent by volume = 10 kg/m^3.

TABLE 3*b*—*Thermal resistance of Specimen B determined by different methods.*

	Total Resistance	Ratio to Corrected HFM[a]
Calculated (Table 3*a*)	0.82	1.08
Probe measurements	0.70	0.92
Heat flowmeter measurements	0.80	1.05
Corrected heat flowmeter measurements	0.76	1.0

[a]Heat flow measurements.

The computational model developed has been used also to calculate the thermal resistance of the aerated concrete under the same conditions as were found in measurements made by Künzel [*25*]. He measured a thermal conductivity of 0.14 W/(m·K) for dry aerated concrete and 0.74 W/(m·K) for the same material with a moisture content of 820 kg/m^3. Measurements by Künzel showed that the thermal conductivity of the material increased linearly with the moisture content and that at a moisture content of 160 kg/m^3 the thermal conductivity was 0.24 W/(m·K). Using Eqs 3–6, an apparent thermal conductivity, λ_{app} = 0.78 W/(m·K) was calculated for a moisture content of 820 kg/m^3 and a value of λ_{app} = 0.24 W/(m·K) for a moisture content of 160 kg/m^3. The difference between the measured and calculated values is 5.4 and 0 percent, respectively. these values further validate these equations.

The apparent thermal conductivity of the aerated concrete used in this test was calculated with Eq 6 and is plotted versus moisture content in Fig. 9. The results of the probe measurements are also shown. The accuracy of the probe measurement is good at low moisture contents but poor at high moisture contents.

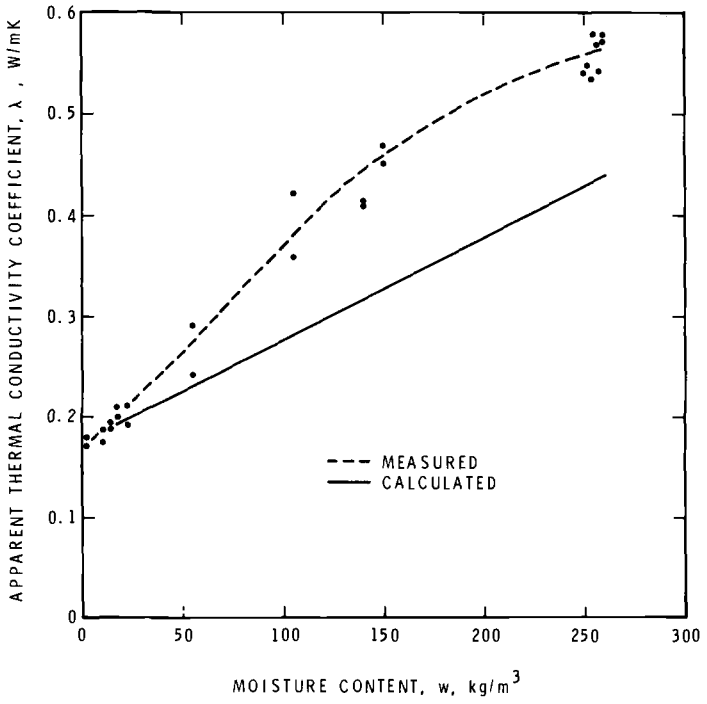

FIG. 9—*Comparison of apparent thermal conductivities measured with the probe technique with calculated values.*

Conclusions

A number of conclusions regarding the effects of moisture on heat transfer in a closed system can be made. The heat flows due to moisture gradients are significant during the initial stages of the moisture redistribution process. When moisture is prevented from leaving the material, condensation will usually occur at the colder surfaces. The vapor that is transferred to and condenses in this region carries heat with it. This reduces the temperature gradient through a part of the specimen during the moisture redistribution process and thereby temporarily reduces the heat conduction component of the total heat flow.

Increasing the moisture content increases the time required to reach the quasi-steady-state condition, that is, the condition where heat flow measured at the hot surface would equal the mean heat flow through the specimen. Only after the quasi-steady state in heat flow is reached do the measurements from both the heat flowmeters and probes give values of the average heat flow through the specimen and therefore of the average apparent thermal conductivity. The results show that under quasi-steady-state conditions the net effect of the moisture gradient on heat transfer through a closed system becomes negligible, and that the total thermal resistance depends on the distribution of moisture in the material. Changes in the total thermal resistance of aerated concrete as large as 19 percent occurred between Day 13 and Day 44 for Specimen A and between Day 16 and Day 44 for Specimen B because of the moisture redistribution. Measurements taken during this period using both techniques agreed reasonably well.

The apparent thermal conductivity of moist aerated concrete can be calculated on the basis of the interactions of different modes of heat transfer and material structure to an accuracy comparable with that obtained with current measurement techniques. Such calculations require the knowledge and use of material properties that are not usually measured by material manufacturers.

The apparent thermal conductivity indicated by the probe changes with the magnitude of the temperature and moisture gradients in the material surrounding the probe. When used in the normal manner, probes are not an accurate means of measuring apparent thermal conductivity when large thermal and moisture gradients are present. The conclusions of this study are in agreement with those of Joy [*26*].

The observations made from this study are valid only for aerated concrete and mineral fiberboard, the materials tested. Aerated concrete was specifically chosen for investigation since it had one of the worst combinations of factors influencing the time to establish quasi-steady-state conditions. The material is dense, has a high open micropore and macropore content, and a high capability for capillary liquid transport to counteract the moisture transported in the vapor phase.

Acknowledgments

The authors wish to express their appreciation to Dr. Bob H. Vos of the Institute for Building Materials and Building Structures, the Organization for Industrial Research (TNO) in Rijswijk, Holland, who initiated and acted as consultant on the series of tests discussed in this paper. They were performed by M. Bomberg when he held a fellowship at the TNO laboratory in 1967. Thanks are also accorded to Dr. Charles P. Hedlin for comments and discussions of the problem and to Dr. A. (Bela) Konrad who modified one of his element computer programs to make it applicable to this research.

This paper is a contribution from the Division of Building Research, National Research Council of Canada, and is published with the approval of the director of the Division.

APPENDIX

Hygrothermal Characteristics of Aerated Concrete

The following material properties were used in the calculations:

1. The moisture retention curve, which describes the variation of thermodynamic moisture potential with moisture content, was taken from Van der Kooi [*5*] for equilibria conditions below 98 percent and from Bomberg [*9*] for equilibria at higher moisture contents.
2. The moisture diffusivity curve, which describes the variation of the dynamic transport coefficient for moisture flow within a porous body, was derived from two sources: The isothermal moisture diffusivity curve was taken from the drying experiments of Van der Kooi [*5*]. This curve is discussed by Nielsen [*17*]. The thermal moisture diffusivity was assumed constant at 0.32×10^{-8} kg/(m·s·K) when the moisture content was between 20 and 260 kg/m^3. At moisture contents below and above this region, it decreased to a nonsignificant level. (A detailed discussion is included in Ref *9*.)
3. The thermal conductivity for the dry material was assumed to be 0.176 W/(m·K). The apparent thermal conductivity of the wet material was calculated using a series and parallel heat flow model of the air, water, and solid phases. A term was added to account for the energy flow due to the moisture gradient. The following values were used in the calculations of the dry and wet thermal conductivities:

$$\lambda_s = 2.5 \text{ W/(m·K) for solid phase of the material}$$

$$\lambda_a = 0.026 \text{ W/(m·K) for moist air in pores, that is, the gaseous phase}$$

$$\lambda_e = 0.58 \text{ W/(m·K) for water, that is, the liquid phase}$$

The average density of the material was 650 kg/m^3; the total open porosity was not measured but could safely be assumed to be 70 percent.

Hygrothermal properties of aerated concrete have been reported by Sandberg [*8*], Vos [*27*], Lund-Hansen [*28*], Nicolajsen [*29*], and Künzel [*30,31*]. Paljak [*32*] measured the apparent thermal conductivity of moist materials by transient and steady-state methods.

References

[1] Hutcheon, N.B. and Paxton, J.A., *Heating, Piping and Air Conditioning*, April 1952, pp. 113–121.

[2] Kuzmak, J.M. and Sereda, P.J., *Soil Science*, Vol. 84, No. 4, 1957, pp. 291–299, and No. 5, 1957, pp. 419–422.

[3] Woodside, W. and Kuzmak, J.M., *Transactions*, American Geophysical Union, Vol. 39, No. 4, 1958, pp. 676–680.

[4] Comini, G. and del Giudice, S., "Finite Element Analysis of Heat and Mass Transfer in Buildings," International Centre for Heat and Mass Transfer, Dubrovnik, Yugoslavia, Session 1, 29 Aug.–3 Sept. 1977.

[5] Van der Kooi, J., "Moisture Transport in Cellular Concrete Roofs," Ph.D. Thesis, Delft University, Wahlman, Delft, The Netherlands, 1971.

[6] Jenisch, R., "Beitrag zum Problem der wasserdampfdiffusion durch Aussenwände von Gebäuden (Kondensations- und Austrockgungs-verhältnisse abhängig vom Aussenklima)," On the Problem of Water Vapor Diffusion Through Exterior Building Partitions (Condensation and Drying Behaviour in Relation to the Outdoor Climate), Ph.D. Thesis, University of Stuttgart, West Germany, 1970.

[7] Hens, H., "Teoretische en Experimentele Studie van het Hygrotermisch Gedrag van bouw- an Isolatiematerialen . . ." (Theoretical and Experimental Study of the Hygrothermal Behavior of Building and Thermal Insulating Materials in Internal Condensation and Drying Processes with Application to Flat Roofs), Ph.D. Thesis, University of Leuven (KUL), 1976. (A detailed summary, in English, regarding condensation problems, is obtainable from the Laboratory for Acoustics and Heat Transfer, KUL, Leuven, Belgium.)

[8] Sandberg, P.I., "Byggdelars Fuktbalans i Naturligt Klimat (Moisture Balance in Building Elements Exposed to Natural Climatic Conditions)," Report 43, Division of Building Technology, Lund Institute of Technology, Sweden, 1973.

[9] Bomberg, M., "Moisture Flow Through Porous Building Materials," Report 52, Division of Building Technology, Lund Institute of Technology, Lund, Sweden, 1974.

[10] Harmathy, T.Z., *I & EC Fundamentals*, Vol. 8, No. 1, Feb. 1969, pp. 92–103.

[11] Palosaari, S.M., "Steady State Effective Thermal Conductivity of Wetted Closed Porous Systems," Ph.D. Thesis, London University, Department of Chemical Engineering, Imperial College of Science and Technology, London, 1972.

[12] Palosaari, S.M. and Cornish, A.R.H., *Acta Polytechnica Scandinavica*, Helsinki, Chapter 125, 1975, pp. 1–34; Chapter 126, 1975, pp. 1–24; and Chapter 128, 1975, pp. 1–38.

[13] Van Minnen, J. and Vos, B.H., "Determination of Water Content, Water Distribution and Heat Resistance of Walls," Report II-4/23N5, Organization for Industrial Research, Institute for Building Materials and Building Structures, Delft, The Netherlands, 1965.

[14] Solvason, K.R., *ASHAE Journal*, Section, *Heating, Piping and Air Conditioning*, American Society of Heating and Air Conditioning Engineers, Vol. 27, No. 11, 1955, pp. 137–142.

[15] de Groot, S.R., *International Journal of Heat and Mass Transfer*, Vol. 4, 1961, pp. 63–70.

[16] Cary, J.W. and Taylor, S.J., in *Proceedings*, Soil Science Society of America, 1962, pp. 413–416.

[17] Nielsen, A.F., "Fugtfordelinger i Gasbetong under Varme- og Fugttransport" (Moisture Distribution in Cellular Concrete During Heat and Moisture Transfer), *Meddelelse*, No. 29, Thermal Insulation Laboratory, Technical University of Denmark, 1974.

[18] Konrad, A. and Silvester, P., in *Computer Physics Communications 5*, North Holland Publishing Co., 1973, pp. 437–455.

[19] Samuelsson, I., "Fukt: Utvändigt Isolerade Plottak" (Moisture Transfer in Steel Decks), Report 67, Division of Building Technology, Lund Institute of Technology, Sweden, 1975.

[20] Verschoor, J.D. and Greebler, P., *Transactions*, American Society of Mechanical Engineers, Vol. 74, No. 6, Aug. 1952, pp. 961–968.

[21] Krischer, O., *Die Wissenschaftlichen Grundlagen der Trocknungtechnik* (The Scientific Basis of the Drying Technology), Springer-Verlag, Berlin, 1956.

[22] Pelanne, C.M., in *Proceedings*, Eighth Conference on Thermal Conductivity, Plenum Press, New York, 1969, pp. 897–911.
[23] Bankvall, C.G., *Journal of Testing and Evaluation*, Vol. 1, No. 3, May 1973, pp. 235–243.
[24] Cheng, S.C. and Vachon, R.I., *International Journal of Heat and Mass Transfer*, Vol. 13, 1970, pp. 537–546.
[25] Künzel, H., "The Dependence of Thermal Conductivity on Moisture Content," Communication to CIB W-40 Working Group, Institute für Technische Physik, Stuttgart, West Germany, 1969.
[26] Joy, F.A. in *Symposium on Thermal Conductivity Measurements and Applications of Thermal Insulations, ASTM STP 217*, American Society for Testing and Materials, 1957, pp. 66–79.
[27] Vos, B.H., *Gesundheits-Ingenieur*, Vol. 11, 1969, pp. 334–342.
[28] Lund-Hansen, P., "Fugttransport i Byggematerialer" (Moisture Transfer in Building Materials), *Meddelelse*, No. 15, Technical University of Denmark, 1967.
[29] Nicolajsen, A., "Fugttransportkoefficienter for Gasbeton" (Moisture Transfer Coefficients of Cellular Concrete), Meddelelse, No. 25, Thermal Insulation Laboratory, Technical University of Denmark, 1973.
[30] Künzel, H., *Gasbeton, Wärme- und Feuchtigkeitsverhalten* (Aerated Concrete, Heat and Moisture Aspects), Bauverlag GmbH, Wiesbaden and Berlin, 1971.
[31] Schüle, W. et al, *Gesundheits-Ingenieur*, 1/2 Jan./Feb. 1976, pp. 17–18, 23–26.
[32] Paljak, I., *Swedish Journal of Building Technology*, No. 6, 1973, pp. 20–22.

F. J. Dechow[1] *and K. A. Epstein*[1]

Laboratory and Field Investigations of Moisture Absorption and Its Effect on Thermal Performance of Various Insulations

REFERENCE: Dechow, F. J. and Epstein, K. A., "**Laboratory and Field Investigations of Moisture Absorption and Its Effect on Thermal Performance of Various Insulations,**" *Thermal Transmission Measurements of Insulation, ASTM STP 660*, R. P. Tye, Ed., American Society for Testing and Materials, 1978, pp. 234–260.

ABSTRACT: Much work has been done in Europe, Canada, and the United States with respect to the effect of moisture on the thermal efficiency of various insulations. However, very little research has been done to orient the laboratory test methods to the actual field conditions in which the various insulations will be used.

This paper reports on the moisture performance characteristics of various thermal insulations under laboratory conditions and under actual field conditions. The various moisture effects, such as freeze-thaw cycling in the presence of water, water absorption, and water vapor transmission, which occur in insulations in upside-down roof systems and below-grade applications, reduced the thermal efficiency of all insulations tested. This loss of thermal resistance of the common insulating materials using both laboratory methods and field data is related to the volume of water present in the insulations. The minimum performance criteria for insulations exposed to the various laboratory test methods and to actual field conditions are also discussed. The insulations investigated include fiber glass, fiberboard, expanded (bead) polystyrene, extruded polystyrene, polyurethanes, and cellular glass. The effect of various top coverings for upside-down roof applications on the thermal resistance performance of insulations is also discussed.

KEY WORDS: below-grade insulation, cellular plastic, heat transmission, highway insulation, insulation, moisture content, thermal insulation, thermal measurements, thermal conductivity, upside-down roof

In this paper several modes of moisture entry into thermal insulations have been studied and analyzed for relevance to the moist environment commonly found in upside-down (USD) roofs and below-grade (perimeter and highway) applications.

[1]Senior research chemist and research specialist, respectively, The Dow Chemical Company, Granville, Ohio 43023.

The protected membrane or USD roof system places the membrane on the deck and then places the insulation above the membrane so that the membrane remains very close to room temperature at all times (see Fig. 1). The insulation must be highly resistant to water in all forms since it is placed above the membrane. The two measures of this resistance are the measurement of water transport into the foam and the measurement of the resistance to freeze-thaw action. The USD roof system has possibly the most severe combination of water conditions: (1) a large temperature differential across the insulation and (2) a constant source of high humidity at both the membrane level and above the insulation. There are over 10 000 USD roofs in the United States, Canada, Europe, Japan, and the Middle East (Saudi Arabia).

Applications such as below-grade perimeter and below highways also subject insulations to similar severe moisture environments. Although the authors feel that these environments are not as severe as those found in the USD roof applications, both a temperature differential and constant source of high humidity on both sides of the insulation do exist.

Insulations are used under highways primarily for reduction of heaving of the pavement due to moisture vapor pressure and freeze-thaw cycling. This insulation application is widely used in Alaska, Canada, and the Scandanavian countries.

Insulations have been used in below-grade perimeter applications on commercial and on some residential buildings for many years to reduce heat loss and to protect the building components from thermal cycling. However, only recently has any concern been expressed about the loss in thermal efficiency of the insulation due to its exposure to the moist environment.

Table 1 describes the insulations investigated in this work.

Water Absorption with a Concentration Gradient

The water absorbed by a slab of foam is determined in ASTM Test for Water Absorption of Rigid Cellular Plastics (D 2842-69) by measuring the

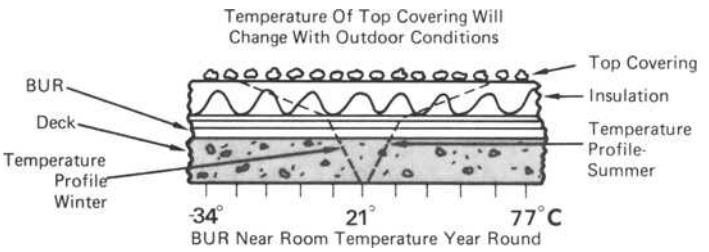

FIG. 1—*Temperature profile of a USD Roof System.*

TABLE 1—*Insulation nomenclature.*

Cut Cell Extruded Polystyrene—This polystyrene is continuously extruded into thick billets and then cut to desired thickness.
Extruded Polystyrene Skinboard—This polystyrene is continuously extruded to the desired thickness. A high-density polystyrene skin is formed on the top and bottom of this product during extrusion.
Cut Cell Molded Bead Polystyrene—This polystyrene is molded into thick billets and then cut to desired thickness.
Molded Bead Polystyrene—This polystyrene is molded to the desired thickness.
Polyurethane/Polyisocyanurate (without skins)—These products are made into thick billets and then cut to desired thickness.
Polyurethane/Polyisocyanurate Laminated with Paper or Aluminum Foil—These products are continuously made to desired thickness. The paper (or aluminum foil) facing on the top and bottom of these products is placed on the products as the products are being made.
Polyisocyanurate Laminated with Aluminum Foil and Containing Glass Fibers—This product is continuously made to desired thickness. The aluminum facing is placed on the product as the product is being made. The glass fibers are interspersed throughout the polyisocyanurate core as the product is made.
Cellular Glass—This inorganic product is made in billets and is cut to desired thickness.
Fiberglass—This rigid board contains glass fibers held together with a binder and topped with an asphalt-saturated felt on one side.
Fiberboard—This product contains perlite, vermiculite or other inorganic particles held together with a binder.

change in buoyant force resulting from the insulation's immersion under a 5.08-cm (2 in.) head of water for 96 h. In general, multilaboratory test results for this method had a reproducibility to within ± 1.0 volume percent at two standard deviations. However, the test specifies measuring the volume of the specimen after completion of the immersion, for computing the volume percent of absorbed water. Since some of the foam specimens (the polyurethanes) increase in volume when immersed in water, the cal-

culated volume percent of water absorbed would be lower than actual. Also, this test penalizes the insulations that are covered with paper or aluminum because the specimen size is small enough that the unprotected edges of the insulation represent a larger exposed area of the specimens than they would in actual field applications.

The water absorption data are presented in Fig. 2. Because it is believed that the submersion time in the applications mentioned can be for longer than 96 h, the test was actually run for 500 h (21 days). Each point

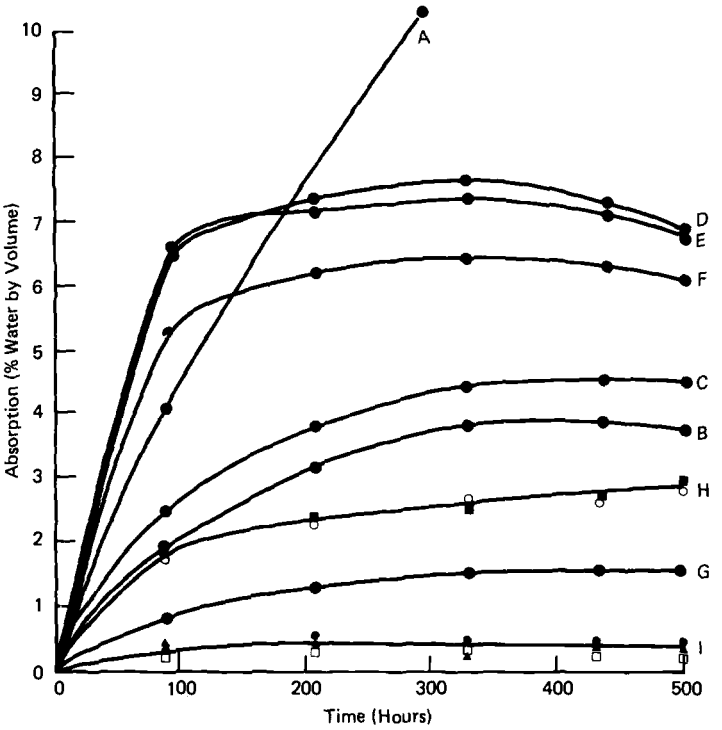

Curve A - 2.54 cm thick fiberboard, 169.8 kg/m^3
Curve B - 2.54 cm thick bead polystyrene, 26.2 kg/m^3, 31% void
Curve C - 5.33 cm thick bead polystyrene, 26.8 kg/m^3, 27% void
Curve D - 3.56 cm thick bead polystyrene, 21.3 kg/m^3, 27% void
Curve E - 5.08 cm thick bead polystyrene, 19.7 kg/m^3, 37% void
Curve F - 5.08 cm thick bead polystyrene, 16.5 kg/m^3, 27% void
Curve G - 5.08 cm cellular glass, 133.9 kg/m^3
Curve H - ■ 5.08 cm thick polyurethane, 50.1 kg/m^3, aluminum skins
o 2.54 cm thick polyisocyanurate, 41.3 kg/m^3, aluminum skins, glass reinforced.
Curve I - • 5.08 cm thick German bead polystyrene, 35.6 kg/m^3, 10% void
▲ 3.56 cm thick extruded polystyrene skinboard, 36.5 kg/m^3
□ 3.81 cm thick extruded polystyrene skinboard, 46.5 kg/m^3

FIG. 2—*This test measures the percent volume of water absorbed per unit volume of foam. The 96-h test is described in ASTM Method D 2842-69. Since longer periods of submersion can occur in the USD application, the test was run for 504 h (21 days).*

represents the average of three specimens of each insulation with measurements taken every 100 h.

The 2.54-cm-thick (1 in.) fiber glass specimens with a density of 221.32 kg/m^3 (13.82 lb/ft^3) absorbed so much water that they sank within 2 h and thus their water absorption could not be measured. The fiberboard specimens (Curve A of Fig. 2) absorbed over 20 percent by volume water by 500 h. The bead polystyrene specimens in 500 h absorbed from 0.3 to 7.0 percent water, depending on foam thickness, density, and void volume. The cellular glass, Curve G, absorbed 1.3 percent water; the aluminum-covered polyurethane or polyisocyanurate specimens, Curve H, absorbed 2.7 percent water; and the extruded polystyrene skinboard specimens, Curve I, absorbed 0.3 percent water after 500-h exposure. Note that the relative performance of the materials evaluated, with the exception of fiberboard, is not changed by extending the test from 96 to 500 h.

Water Absorption with Both Thermal and Concentration Gradients[2]

This test is defined under Paragraph 2.242 of the standard "Dämmschichten als Frostschutz" from the Research Association for Highways at Cologne, West Germany ("Forschungsgesellschaft für das Strassenwesen e. V.," Köln). In the test, both a temperature gradient [minimum 10°C per centimetre thickness (45.7°F per inch)] and a water-saturated environment are used to drive water into the specimens.

Insulation specimens, 500 by 500 mm (19.68 by 19.68 in.), of various thicknesses were subjected to the water vapor partial pressure gradient which exists when an insulation is placed between a cooling plate at 1°C (33.8°F) and a water bath whose temperature is regulated between 40 and 60°C (104 and 140°F) to maintain a 10°C per centimetre (45.7°F per inch) thickness temperature gradient across the foam. The specimens were turned daily as specified by the test to achieve a uniform moisture distribution. The test is run for a minimum of 28 days.

High-density bead polystyrenes (molded and cut), low-density bead polystyrene, extruded polystyrene skinboard, a polyurethane laminated with paper skins, and a polyurethane without skins were subjected to these test conditions for 28 days. Although the reproducibility of this test has not been determined by multilaboratory testing, the values for the five specimens of extruded polystyrene skinboards agreed to within ± 0.15 volume percent. The water absorbed on a volume percent basis is presented in Fig. 3. The points on Curve F (extruded polystyrene skinboard) represent the average water absorption values for five specimens. The water absorption for five specimens of cut cell molded bead polystyrene were averaged to define the points on Curve D. The amounts of water

[2]This study was performed at the Dow Laboratory in Horgen, Switzerland.

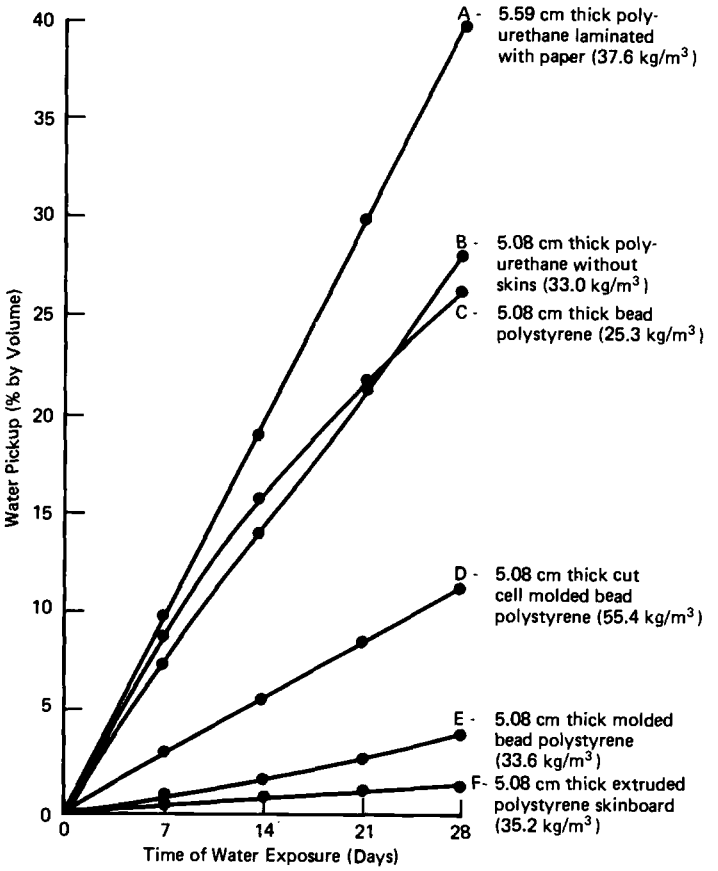

FIG. 3—*Water pickup (percent by volume) versus time (days). German water absorption test by diffusion (temperature gradient of 10°C per centimetre thickness). The Dow Chemical Co., Horgen, Switzerland (1976).*

absorption for two specimens of molded bead polystyrene were averaged to give the points for Curve E. Curves A (polyurethane), B (polyurethane without skin), and C (low-density bead polystyrene) each represent the water absorption data points from one specimen. The extruded polystyrene skinboards (Curve F) picked up less than 2 percent water by volume. The molded bead polystyrenes performed well in this test with one specimen (Curve E) picking up only 4.2 percent water by volume. The high-density cut bead polystyrenes (Curve D), with water absorptions of 11 to 12 percent by volume, performed much worse than the extruded and molded polystyrenes, but performed better than the low-density bead polystyrene or the polyurethane foams, which absorbed over 25 percent water by volume.

The greater moisture driving force of this test method over that described earlier in this paper can be seen by comparing Fig. 3 with Fig. 2. The stronger moisture driving force differentiates the moisture resistance of the extruded polystyrene skinboard (Curve F) from the high-density bead polystyrene (Curves D and E). Curve C on each graph corresponds to a 5.0-cm-thick (2.0 in.) bead polystyrene with a density about 25 kg/m^3 (1.6 lb/ft^3). The severity of this test is illustrated by this specimen absorbing over 25 percent water by volume, whereas in the previous test only 4 percent water by volume had been absorbed.

Freeze-Thaw Water Absorption

Regional Climate Conditions

L. Williams of the U. S. Army Natick Laboratory discussed [*1*][3] where freeze-thaw cycles occur in North America. Williams defined −2.22°C (28°F) as the freeze temperature and 1.11°C (34°F) as the thaw temperature. When the temperature drops from 1.11 to −2.22°C (34 to 28°F) or below, he considers conditions to be conducive to freeze water. Conversely, when the temperature rises from −2.22 to 1.11°C (28 to 34°F) or above, he considers conditions to be conducive to melt frozen water.

Williams states that any establishment of temperature levels for freeze-thaw with the implication of their effectiveness is rather subjective on the basis of readily available temperature data. Earlier work by Russell [*2*], and Alpert's determination of freeze-thaw cycles for 24 cities in the United States [*3*], used −2.22°C (28°F) (Russell) or −0.6°C (31°F) (Alpert) as the freezing temperature and 0°C (32°F) (Russell) or 0.6°C (38°F) Alpert) as the thawing temperature. Thus William's studies are conservative relative to the number of freeze-thaw cycles found in any one locality.

The freeze-thaw activity description by Williams is included in this paper because his data allow the laboratory freeze-thaw results presented in the later subsections to be correlated with actual freeze-thaw cycles occurring in different locations in North America. Figure 4 and Table 2 give freeze-thaw data on different locations in North America. The geographical region numbers divide North America into regions based on the number of freeze-thaw cycles per year, the duration of a freeze, the severity of a freeze, and the months when the cycles occur. Representative cities for each region are listed.

[3]The italic numbers in brackets refer to the list of references appended to this paper.

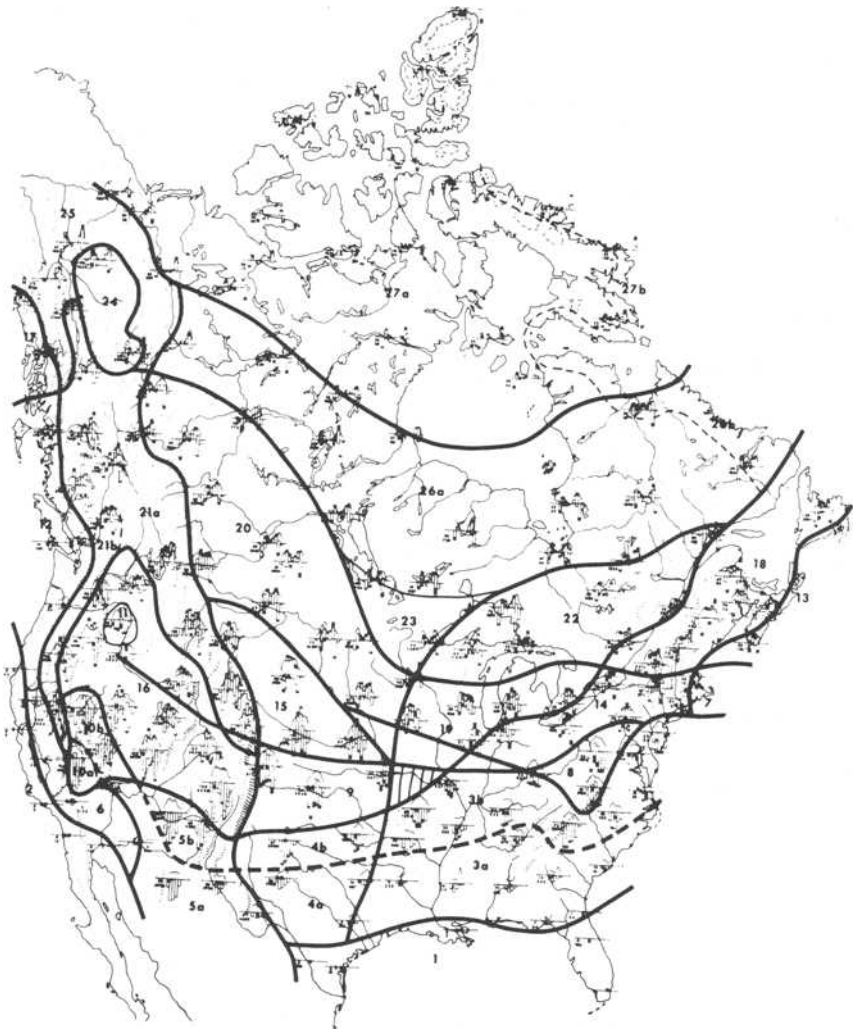

FIG. 4—*Freeze-thaw regions based on frequency, duration, and severity of freeze-thaw activity* [2].

U. S. Army Cold Regions Research and Engineering Laboratory (CRREL) Study

The objective of this CRREL study [*4*], which presented data on the effect of freeze-thaw cycling on various insulations, was to expose different thermal insulating materials for use under highway pavement to a wet environment and numerous freeze-thaw cycles, to simulate conditions

TABLE 2—Freeze-thaw cycle for various regions.

Geographical Region No. from Fig. 4	Freeze-Thaw Cycles/Year
1 (Miami, Fla.)	0
2 (San Francisco, Calif.)	0
3a (Macon, Ga.)	15
3b (Bowling Green, Ky.)	54
4a (Big Springs, Tex.)	26
4b (Amarillo, Tex.)	67
5a (El Paso, Tex.)	28
5b (Albuquerque, N.M.)	68
6 (San Bernadino, Calif.)	6
7 (Boston, Mass.)	42
8 (Elkins, W. Va.)	85
9 (Garden City, Kans.)	96
10 (Tonopah, Nev.)	103
11 (Pendleton, Ore.)	46
12 (Portland, Ore.)	15
13 (Yarmouth, N. S., Canada)	52
14 (Akron, Ohio)	63
15 (Ogallala, Neb.)	111
16 (Elko, Nev.)	137
17 (Juneau, Alaska)	52
18 (Millinockel, Me.)	71
19 (Grand Rapids, Mich.)	63
20 (Fort Peck, Mont.)	69
21 (Cranbrook, B. C., Canada)	103
22 (Val d'Or, P.Q., Canada)	49
23 (Winnipeg, Man., Canada)	46
24 (Mayo Landing, Y. T, Canada)	58
25 (Dawson, Y. T., Canada)	47
26 (Trout Lake, Ont., Canada)	36
27 (Baker Lake, N. W. T., Canada)	28

in any given winter. Eight extruded polystyrene foams, one bead polystyrene, three urethanes, one perlite, and one cellular glass insulation board were tested.

Two 12.7-cm (5 in.) square specimens of each insulation were oven-dried and submerged in water for seven days prior to freeze-thaw experiments. After the seven-day soak, the 28 specimens were removed and submerged flat in shallow metal trays, nine to a tray. One specimen of each insulation was then subjected to 15 freeze-thaw cycles and a second specimen to 30 freeze-thaw cycles. The trays generally took 1½ h to freeze and about 3 h to thaw.

At the completion of each series, the specimens were trimmed and sliced and the gain in water content of each section determined. The internal moisture distributions for each material have been plotted in Fig. 5 for comparison of (1) zero pressure—seven day soaking; (2) 1.03×10^5 N/m^2 (15 psi) pressure immersion tests; (3) 15 freeze-thaw cycles; and (4) 30 freeze-thaw cycles.

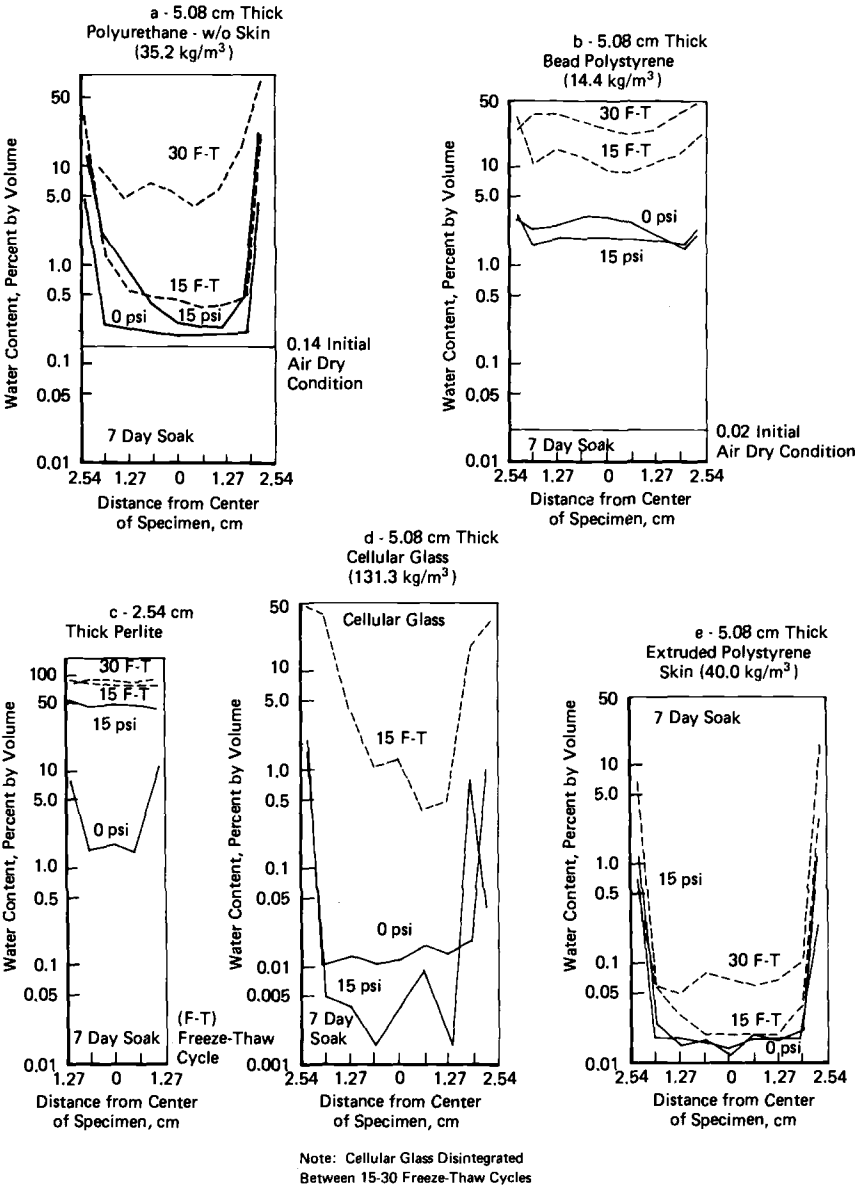

FIG. 5—*Moisture distribution in insulations after freeze-thaw cycling* [4].

Conclusions reached in the CRREL report were that (1) the freeze-thaw test had destructive results on highly absorbant systems; (2) the internal water content increased in practically all specimens; and (3) the cellular glass disintegrated before it could be weighed after 30 cycles, thus deteriorating more rapidly in wet freeze-thaw tests than other insulations.

The basic recommendation of the CRREL report is that "selection of rigid insulations for applications under wet conditions with anticipated periodic freezing and thawing temperatures should be based on results of tests with 30 or more freeze-thaw cycles." That more laboratory freeze thaw cycles are required to model field results for some geographic regions was demonstrated in a subsequent CRREL report [5], which showed that extruded polystyrene skinboard in USD roof systems in Alaska picked up 1.0 to 1.7 percent moisture by volume after 36 months. This is more moisture absorption than is indicated in Fig. 5*e* by the results for extruded polystyrene skinboard after 30 freeze-thaw cycles. The authors found that the report's data also supported the conclusion that extruded polystyrene foam performed best in these tests. The polyurethane foam (no skins) and bead polystyrene foams performed worse than the extruded polystyrene foams, but better than the cellular glass and perlite insulations.

Dow Study

The Dow freeze-thaw study measured the water absorbed by a slab of foam which was subjected to alternating cycles of freezing and thawing. This test was a variation on the ASTM Tests for Resistance of Concrete to Rapid Freezing and Thawing (C 666-73). The procedure used was freeze in air (at −17.8°C or 0°F) and thaw in water (at 4.4°C or 40°F). Each cycle lasted 4 h and the weight of each specimen was determined approximately every 50 cycles. The increases in weight were taken as the amount of water absorbed and this is reported as the percent water per unit volume of foam. Two specimens each of various insulations such as cellular glass, fiberboard, fiber glass, polyurethane, polyisocyanurate, bead polystyrene foam, and extruded polystyrene foam were tested for more than 1000 freeze-thaw cycles. The specimen size was a 10.2 cm (4 in.) square but the thicknesses varied.

This freeze-thaw method does take into consideration the changes in external environment (from 4.4 to −17.8°C) (40 to 0°F), but does not allow the interior (bottom of foam) environment to remain constant as it would in the USD roof system. Thus, the entire thickness of insulation goes through these cycles. In actual fact, this method may not be as severe for water absorption as actual roofing conditions because there is not as great a thermal driving force for water vapor to be driven into the insulation. Rather, this test method just provides a way to separate those insulations which have the physical integrity to withstand the harsh environment in

which they will find themselves. This test method does indicate some insulations which will be more sensitive to the combination of water absorption and freeze-thaw conditions.

The data on the various insulations after 1000 freeze-thaw cycles are presented in Fig. 6. Several pieces of data should be noted. First, the critical number of freeze-thaw cycles where the moisture resistance of many of the insulations begins to deteriorate rapidly seems to be between 300 and 700. The behavior of an insulation throughout this freeze-thaw cycle region will give a good indication of its applicability in a freeze-thaw environment, because it has been shown [1] that many of the North American locations will have over 500 freeze-thaw cycles in 10 years. Note the deterioration of even the 35.24-kg/m^3 (2.2 lb/ft^3) German bead polystyrene in Fig. 6 (Curve G) by 500 cycles.

Secondly, thickness of the insulation sometimes influences the water

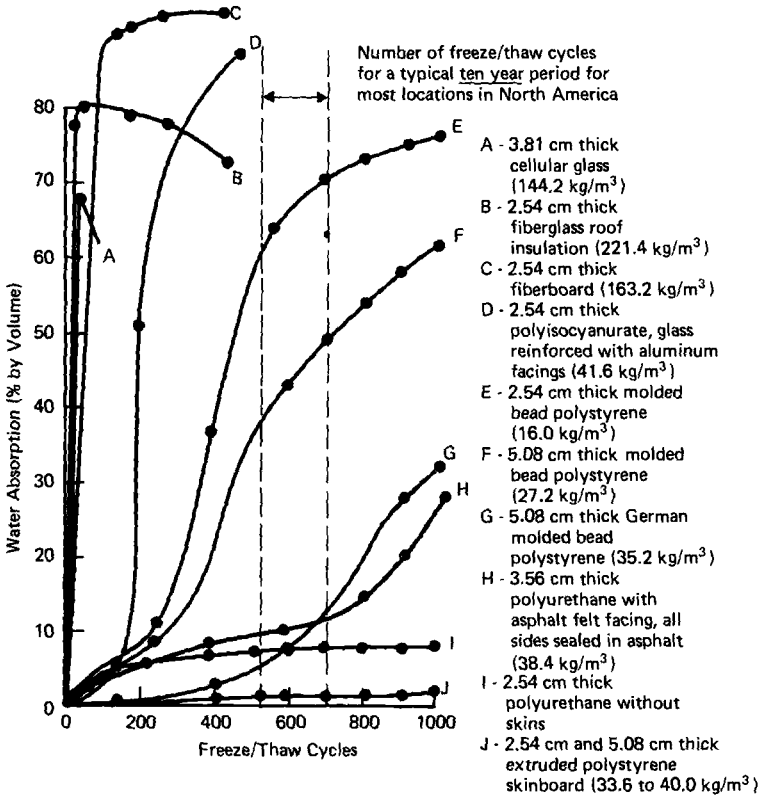

FIG. 6—*The water absorption of various insulations after freeze-thaw exposure following ASTM Method C 666-73 (freeze in air, thaw in water). The Dow Chemical Company, Midland, Mich. 1976.*

pickup. The amount of water available is the same no matter what the thickness; so the thicker the insulation, the lower the water pickup (assuming the insulation does not physically deteriorate in the freeze-thaw cycle testing).

Thirdly, the extruded polystyrene skinboards performed much better than the other insulations tested. Several insulations did not survive for 1000 cycles. The fiber glass (Curve B) and fiberboard (Curve C) insulations started to break up after 400 freeze-thaw cycles. These specimens were taken out of the chamber at that time. The polyisocyanurate foam with reinforcing glass fibers and aluminum skins on the top and bottom (Curve D) of the insulation lasted 458 cycles before it began to deteriorate and had to be removed from the chamber. The cellular glass specimens (Curve A) fell apart before 100 freeze-thaw cycles, which supports the data shown in the CRREL report.

One more note relative to the data shown in Fig. 6: cut cell unfaced polyurethane (Curve I) performed better than felt-faced, asphalt-coated polyurethane (Curve H) and much better than aluminum foil laminated, glass-reinforced polyisocyanurate foam (Curve B) in this freeze-thaw cycle testing.

Laboratory Measurements of Thermal Resistance versus Moisture Content of Insulations

The previous sections have shown the extent to which moisture may get into insulation materials by moisture transport and freeze-thaw action. The specific effect of moisture on the thermal resistance of various insulations will now be illustrated.

Since liquid water conducts 25 times more heat than the air it replaces, open-celled or porous materials are affected to a much greater degree by moisture than closed-cell materials in which any moisture is primarily in the vapor phase. If the insulation is in a freezing environment, the ice trapped in the insulation will conduct over 100 times more heat than air would.

Thorsen Study

S. H. Thorsen has performed a laboratory study [6] of the effect of moisture on the thermal conductivity of extruded polystyrene foam of 33.96 kg/m^3 (2.12 lb/ft^3), polyurethane foam of 30.44 kg/m^3 (1.90 lb/ft^3), and bead polystyrene foams of densities from 17.30 to 19.22 kg/m^3 (1.08 to 1.20 lb/ft^3).

Thorsen drove the moisture into the specimens by using them as part of the walls of a box housing an immersion heater in a saturated-salt

solution maintained at 70°C (158°F) and having an internal constant relative humidity of about 75 percent. This box was placed into a thermostatted chamber where the temperature was kept constant at 20°C (68°F) and the relative humidity was 50 percent. The specimens were of 45 by 45-cm^2 (17.72 by 17.72 in.^{2}) size with the same nominal thickness of 5 cm (1.97 in.). The moisture absorption tests lasted for three months. The thermal conductivity coefficients for the specimens were determined at a mean temperature of 10°C (50°F) in a Lang device calibrated with two standard specimens.

Thorsen's results for specimens both without and with a wax moisture barrier on their cold side are shown in Fig. 7 and 8, respectively. He points out that the dependence of the thermal conductivity on moisture content exhibits a parabolic dependence for the polyurethane foam and the bead polystyrene foam. Only the extruded polystyrene foam exhibits linear dependence of the thermal conductivity on moisture content. The presence of the moisture barrier on the cold side of the insulation more than doubled the moisture absorption of each of the insulations.

Dow Study

In another laboratory study conducted at the Dow Chemical Co., 20 different insulation materials were examined for the effect of moisture on their thermal resistance. These materials included extruded polystyrene foam, molded and cut cell bead polystyrene foam, urethane foam, and fiber glass insulation.

Water was driven into the specimens by placing them on top of a pan containing 50°C (122°F) water whose temperature was controlled with a hot plate. A towel, acting as a porous wick, was placed over the specimen

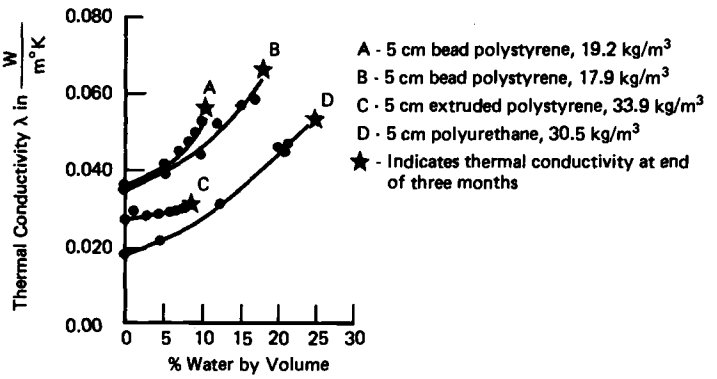

FIG. 7—*Effect of moisture absorption on thermal efficiency of insulation without a moisture barrier. Mean temperature of 10°C with a 20°C temperature gradient. Study performed by Thorsen* [6].

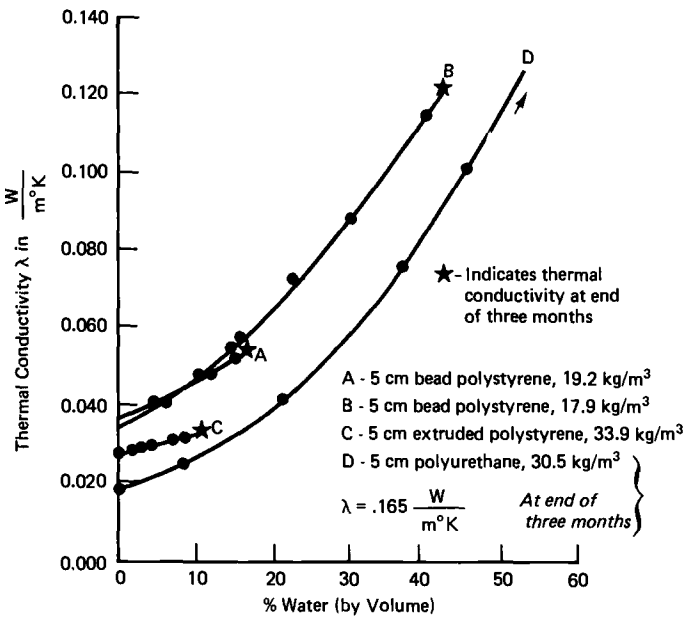

FIG. 8—*Effect of moisture absorption on thermal efficiency of insulation with a wax moisture barrier on the cold side of the insulation* [6].

so that evaporation of water would keep the top of the specimen cool to maintain a driving force for the moisture to enter it.

The thermal resistance was measured using a K-matic instrument which was produced by Dynatech R/D Co. and which was calibrated using two standard specimens. The mean temperature of the test was 23.9°C (75°F) with a 27.78°C (50°F) differential across the specimen. This temperature differential causes relocation of the water in the closed cell specimens. For open-cell or fibrous materials with no moisture barrier, the temperature differential may cause the water to be driven out of the specimen during the test. The specimens were wrapped in polyethylene film to prevent moisture condensation in the measurement apparatus. Before and after their thermal resistance was measured, the specimens were weighed without the polyethylene film wrap to determine whether any moisture had been driven from the specimen during the measurement. The before and after weights of the specimens agreed to within 6 g (0.21 oz), which is a 5 percent maximum difference. At times it took as long as 16 h for the specimen to attain a quasi-equilibrium value in the K-matic. The quasi-equilibrium value was determined by there being less than 1 percent change in the thermal resistance of a specimen for one hour.

The parameter k versus moisture content (percent by volume) for these specimens is illustrated in Fig. 9. This accelerated laboratory test does

not simulate the amount of water that an insulation will pick up in an end-use application. The amount of moisture driven into the insulation as a function of time varies depending on the physical and chemical properties of the insulations. This point is illustrated in Fig. 10, which shows the length of time required for insulations to pick up various levels of moisture (percent by volume) with this test.

The dependence of the thermal resistance of these insulations on moisture content shows the same trends as the results obtained by Thorsen

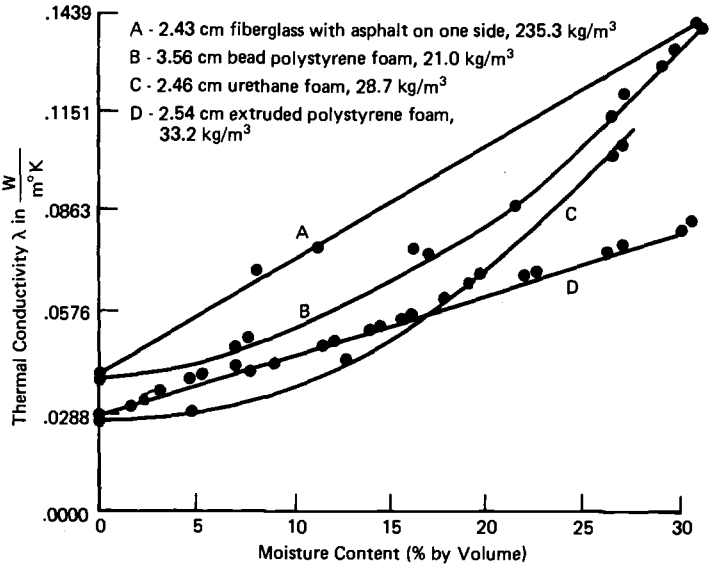

FIG. 9—*Thermal conductivity as a function of moisture content for insulation materials. Mean temperature is 22°C. The temperature differential to drive the water into the specimens was 30°C. These are laboratory results and do not illustrate the moisture resistance of an insulation, but illustrate only the effect of absorbed moisture on the thermal conductivity of the insulation.*

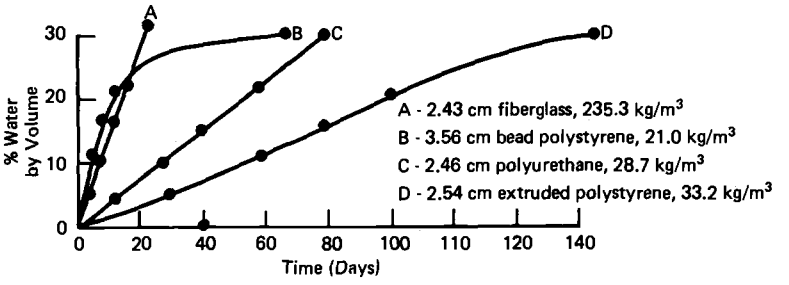

FIG. 10—*Moisture absorption as a function of time for various insulations.*

[6] (Figs. 7 and 8) and by Paljak [7]. The following equations describe this dependence on moisture content for 0 to 30 percent volume percent water. Similar equations, with slightly different coefficients, were obtained in studies by Levy [8], Mittasch [9], and Achtziger [10]. These equations do not indicate *how much* water a particular insulation will pick up in an actual end-use application, but they do indicate what the effect of a certain water percentage (by volume) will be on the long-term thermal efficiency of the insulation in question.

In the equations for the thermal conductivity (λ or k), V is the percent moisture by volume, the units on λ are W/m·K, and the units on k are Btu.·in./h·ft²·deg. F.

Polyurethane/Polyisocyanurate(u)

$$k_{u\ \text{wet}} = k_{\text{dry}}{}^{*} + 0.008\,(V) = 0.16^{*} + 0.008\,(V)$$

(0 to 10% by volume water) $\lambda_{u\ \text{wet}} = 0.0231^{*} + 0.00115\,(V)$

$$k_{u\ \text{wet}} = k_{\text{dry}}{}^{*} + 0.0055(V) + 0.00028(V)^2 = 0.16^{*} + 0.0055(V) + 0.00028(V)^2$$

(10 to 30% by volume water) $\lambda_{u\ \text{wet}} = 0.0231^{*} + 0.00079(V) + 0.000041(V)^2$

Low-Density Molded Bead Polystyrene (bd bd)***

$$k_{bd\ bd\ \text{wet}} = k_{\text{dry}}{}^{*} + 0.0122(V) = 0.28^{*} + 0.0122(V)$$

(0 to 10% by volume water) $\lambda_{bd\ bd\ \text{wet}} = 0.0403^{*} + 0.00175(V)$

$k_{bd\ bd\ \text{wet}}$ = artificial factor** + $0.0167(V) = 0.225^{**} + 0.0167(V)$

(10 to 30% by volume water) $\lambda_{bd\ bd\ \text{wet}} = 0.0325^{**} + 0.00240(V)$

High Density Molded Bead Polystyrene (bd bd)****

$$k_{bd\ bd\ \text{wet}} = k_{\text{dry}} + 0.015\,(V) = 0.24^{****} + 0.015(V)$$

(0 to 30% by volume) $\lambda_{bd\ bd\ \text{wet}} = 0.0346^{***} + 0.00216(V)$

Fiber Glass (FG)

$$k_{\text{FG wet}} = k_{\text{dry}}{}^{*} + 0.082(V) = 0.25^{*} + 0.082(V)$$

(0 to 2% by volume water) $\lambda_{\text{FG wet}} = 0.036^{*} + 0.0118(V)$

$k_{\text{FG wet}}$ = artificial factor** + $0.006\,(V) = 0.41^{**} + 0.006(V)$

*Assumed aged value of at least one year using American Society of Heating, Refrigeration and Air-Conditioning Engineers (ASHRAE) (1972) table.

**Artificial factor determined by experimental data.

***These equations apply only to bead polystyrenes with densities at or below 28.83 kg/m³ (1.8 lb/ft³).

****This equation applies only to bead polystyrenes with densities greater than or equal to 33.64 kg/m³ (2.11 lb/ft³). The published k-factor of European high-density beadboards varies between 0.0326 and 0.0366 W/m·K.

(3 to 10% by volume water) $\lambda_{FG\ wet} = 0.059^{**} + 0.00086(V)$

$$k_{FG\ wet} = k_{dry}^{*} + 0.0217(V) = 0.25^{*} + 0.0217(V)$$

(10 to 30% by volume water) $\lambda_{FG\ wet} = 0.036^{*} + 0.00312(V)$

Extruded Polystyrene (EP)

$$k_{EP\ wet} = k_{dry}^{*} + 0.008(V) = 0.20^{*} + 0.008(V)$$

(0 to 30% by volume water) $\lambda_{EP\ wet} = 0.0288^{*} + 0.00115(V)$

Field Experience of Thermal Resistance Versus Moisture Content of Insulations

Moisture Content and Thermal Resistance Measurement Considerations

The field insulation specimens were removed from the installation as 35 by 35 cm (14 by 14 in.) specimens and were immediately sealed in a polyethylene bag and delivered to the laboratory. At the laboratory, surface dirt was carefully removed from the specimens, which were weighed and their thermal resistance determined using the procedure described in the foregoing for insulations with moisture content. After the quasi-equilibrium thermal resistance had been established, the specimens were dried at 60°C (140°F) until constant weight was achieved. The moisture content of the specimens was determined from the weight loss due to drying.

The measured parameter k-values may be compared with the values calculated using the equations of the previous section in Tables 3 and 4.

Upside-Down Roofs

USD roofs have been in use for the past eight years. Data from some of these field installations can be found in Table 3 for the following insulations: (1) molded bead polystyrene, (2) extruded polystyrene skinboard, and (3) polyurethane (without skins). Data on the performance of polyurethane insulation are limited because of its limited use in USD roofs.

The data reported in Table 3 are restricted to roofs with slopes of less than or equal to 1.25 cm per 30.48 cm (0.5 in. per 12 in.). The top covering in all cases is stone. Data for specimens taken from ponded areas are footnoted in Table 3.

When a specific amount of thermal resistance is required by the architect and the owner of an installation, it is important for them to know how much the thermal resistance may be reduced during a given life span of the installation. The authors think it is reasonable to expect an insulation to retain at least 80 percent of its specified thermal resistance after 10

TABLE 3—*Field performance of various insulations used in stone-covered USD roofs [low slope, 1.27 cm (½ in.) per foot].*

Location	Thickness, cm (in.)	Density, kg/m³ (lb/ft³)	Time in Service, years	Properties of Insulations After Years in Service: Water Pickup, % by volume	Properties of Insulations After Years in Service: λ W/m·K K, Btu·in./h·ft²·deg F	Published λ, W/m·K K, Btu·in./h·ft²·deg F
A. EXTRUDED POLYSTYRENE SKINBOARD						
1. Braunschweig, Germany	5.08 (2)	#	2	0.09%	0.0288* (0.20*)	0.0288 (0.20)
2. Stahlton Frick, Switzerland	5.08 (2)	#	2.5	0.17%	0.0288* (0.20*)	0.0288 (0.20)
3. Neuheim, Switzerland	4.06 (1.6)	#	2.8	1.1%**	0.0303* (0.21*)	0.0288 (0.20)
	4.06 (1.6)	#	3	0.72%**	0.0303* (0.21*)	0.0288 (0.20)
4. Lausanne, Switzerland	4.06 (1.6)	36.04 (2.25)	3.3	0.03%	0.0288* (0.20*)	0.0288 (0.20)
5. Montreal, Canada	3.81 (1.5)	#	5	0.11%	0.0317 (0.22)	0.0288 (0.20)
6. Quebec, Canada	5.08 (2)	#	5	0.02%	0.0303 (0.21)	0.0288 (0.20)
7. Quebec, Canada	5.08 (2)	#	5	0.29%	0.0317 (0.22)	0.0288 (0.20)
8. Edmonton, Canada	3.81 (1.5)	#	5	0.01%	0.0303 (0.21)	0.0288 (0.20)
9. Midland, Mich., (USA)	2.54 (1)	#	6.4	0.13%	0.0317 (0.22)	0.0331 (0.23)
	2.54 (1)	38.92 (2.43)	6.4	0.32%	0.0317 (0.22)	0.0331 (0.23)
	2.54 (1)	41.49 (2.59)	6.4	0.24%	0.0317 (0.22)	0.0331 (0.23)
10. Hannheim, Germany	4.06 (1.6)	38.92 (2.43)	7.2	0.62%	0.0288 (0.20)	0.0331 (0.23)
B. MOLDED BEAD POLYSTYRENE						
1. Sarnia, Canada	3.18 (1.25)	28.19 (1.76)	0.8	21.4%	0.0749 (0.52) (0.58*)	(0.26 to 0.24) 0.0346 to 0.0375
2. Zug, Switzerland	5.08 (2)	37.00 (2.31)	1	5.6%	0.0461 (0.32*)	(0.26 to 0.24) 0.0346 to 0.0375
3. Zug, Switzerland	5.08 (2)	37.00 (2.31)	5	30%	0.0995 (0.69) (0.69*)	(0.26 to 0.24) 0.0346 to 0.0375
4. Toronto, Canada	8.89 (3.5)	31.24 (1.95)	1	16.0%	0.0764 (0.53) (0.48*)	(0.26 to 0.24) 0.0346 to 0.0375

5. Sarnia, Canada	5.08 (2)	24.35 (1.52)	1.1	26.5%	0.0720 (0.50) (0.67*)	(0.26 to 0.24) 0.0346 to 0.0375
	5.08 (2)	24.35 (1.52)	2.1	38.6%**	0.1010 (0.70) (0.87*)	(0.26 to 0.24) 0.0346 to 0.0375
6. Quebec Province, Canada	5.08 (2)	29.15 (1.82)	2	57.9%**	0.2336 (1.62) (1.19*)	(0.26 to 0.24) 0.0346 to 0.0375
7. Heidelburg, Germany	6.10 (2.4)	28.03 (1.75)	not known	18.7%	0.0591 (0.41) (0.54*)	(0.26 to 0.24) 0.0346 to 0.0375
8. Zaandam, Holland	4.06 (1.6)	40.04 (2.5)	3.5	17%	0.0720 (0.50*)	(0.26 to 0.24) 0.0346 to 0.0375
9. Midland, Mich. (USA)	2.54 (1)	24.99 (1.56)	7.3	8.6%	0.0490 (0.30) (0.38*)	(0.26 to 0.24) 0.0346 to 0.0375
	2.54 (1)	25.15 (1.57)	7.3	15.9%	0.0620 (0.43) (0.48*)	(0.26 to 0.24) 0.0346 to 0.0375
	2.54 (1)	28.03 (1.75)	7.3	17.2%	0.0562 (0.39) (0.51*)	(0.26 to 0.24) 0.0346 to 0.0375
C. POLYURETHANE (without skins)						
1. Braunschweig, Germany	5.08 (2)	33.48 (2.09)	2	1.72%	0.0245 (0.17*)	(0.16 to 0.13) 0.0187 to 0.0230
2. Saskatoon, Saskatchewan, Canada	5.08 (2)	32.04 (2)	4	4.5%***	0.0303 (0.21*)	(0.16 to 0.13) 0.0187 to 0.0230
	5.08 (2)	32.04 (2)	4	12.0%****	0.0389 (0.27*)	
3. Saskatoon, Saskatchewan, Canada	5.08 (2)	32.04 (2)	5	5.1%***	0.0317 (0.22*)	(0.16 to 0.13) 0.0187 to 0.0230
	5.08 (2)	32.04 (2)	5	17.0%****	0.0476 (0.33*)	(0.16 to 0.13) 0.0187 to 0.0230

Not measured, but ranges from 33.64 to 41.65 kg/m³ (2.1 to 2.6 lb/ft³).
* k calculated by using formulas given in text.
** Continuously ponded area.
*** Average of three specimens.
**** Maximum water pickup of specimens.

TABLE 4—*Field performance of various insulations used in below-grade applications.*

Insulation	Application	Thickness cm (in.)	Density, kg/m³ (lb/ft³)	Time in Service, years	Properties of Insulations After Years in Service: Water Absorption % by volume	Properties of Insulations After Years in Service: W/m·K K, Btu·in./h·ft²·deg F	Published λ, W/m·K K, Btu·in./h·ft²·deg F
A. EXTRUDED POLYSTYRENE SKINBOARD							
1. Midland, Mich.	highway insulation	2.54 (1)	40.04 (2.50)	10	4.24%	0.0311 (.220) (0.234*)	0.0288 (0.20)
2. Midland, Mich.	highway insulation	2.54 (1)	40.04 (2.50)	1.7	0.26%	0.0292 (.202) (0.202*)	0.0288 (0.20)
3. Ontario, Canada	soil insulation	5.08 (2)	38.28 (2.39)	5	0.36%	0.0303 (.210) (0.203*)	0.0288 (0.20)
4. Ontario, Canada	soil insulation	3.81 (1½)	42.45 (2.65)	5	0.44%	0.0318 (.221) (0.204*)	0.0288 (0.20)
5. Midland, Mich.	below-grade perimeter insulation	3.81 (1½)	33.00 (2.06)	2	0.56%	0.0297 (.206) (0.204*)	0.0288 (0.20)
6. Midland, Mich.	below-grade perimeter insulation	5.08 (2)	33.64 (2.10)	4	1.10%	0.0307 (.213) (0.209*)	0.0288 (0.20)
7. Midland, Mich.	below-grade perimeter insulation	3.81 (1½)	35.40 (2.21)	6	1.20%	0.0333 (.231) (0.210*)	0.0288 (0.20)
8. Midland, Mich.	below-grade perimeter insulation	3.81 (1½)	39.72 (2.48)	7	1.20%	0.0318 (.221) (0.210*)	0.0288 (0.20)
9. Midland, Mich.	below-grade perimeter insulation	3.81 (1½)	33.48 (2.09)	8	0.70%	0.0317 (.220) (0.206*)	0.0288 (0.20)

B. Molded Bead Polystyrene							
1. Midland, Mich.	highway insulation	2.54 (1)	20.02 (1.25)	1.7	0.41%	0.0371 (.257) (0.245*)	0.0346 (0.24)
2. Midland, Mich.	highway insulation	2.54 (1)	20.34 (1.27)	10	9.55%	0.0507 (.351) (0.356*)	0.0346 (0.24)
C. Polyurethane (without skins)							
1. Midland, Mich.	highway insulation	2.54 (1)	30.43 (1.90)	1.7	4.2%	0.0343 (0.238) (0.194*)	(0.13–0.16) 0.0187 to 0.0230
2. Midland, Mich.	highway insulation	2.54 (1)	30.27 (1.89)	10	20.31%	0.0484 (0.336) (0.387*)	(0.13–0.16) 0.0187 to 0.0230
3. Midland, Mich.	highway insulation	2.54 (1)	30.43 (1.90)	15	17.08%	0.0629 (0.436) (0.336*)	(0.13–0.16) 0.0187 to 0.0230

*k calculated by using formulas given in text.

years of service. The equations of the previous section describing the thermal resistance as a function of moisture content were used to calculate the moisture absorption each insulation type requires to decrease its thermal resistance by 20 percent. The limit on the amount of moisture absorption is 5.0 percent for polyurethane, 5.7 percent for low-density bead polystyrene, 4.0 percent for high-density bead polystyrene, 0.8 percent for fiber glass, and 6.2 percent for extruded polystyrene.

The time in service for the extruded polystyrene samples in Table 3 ranged from 2 to 7.2 years. In each case, even when the insulation specimen was from a continuously ponded area, the insulation maintained 90 percent or more of its thermal resistance. Only in the continuously ponded case in Switzerland (A-3 in Table 3) did a specimen pick up more than 1.0 percent water by volume. For those cases where both the water pickup and the thermal resistance were measured, the relationship between them can be described to within ± 10 percent by the equation of the previous section for extruded polystyrene.

As the specimens from this ponded roof show, the moisture content of insulation specimens in the USD roofs varies with the time of year. Insulation specimens taken in the spring will show higher water absorption than specimens taken in late summer. This phenomenon is illustrated in Fig. 11 for an extruded polystyrene foam and a bead polystyrene foam

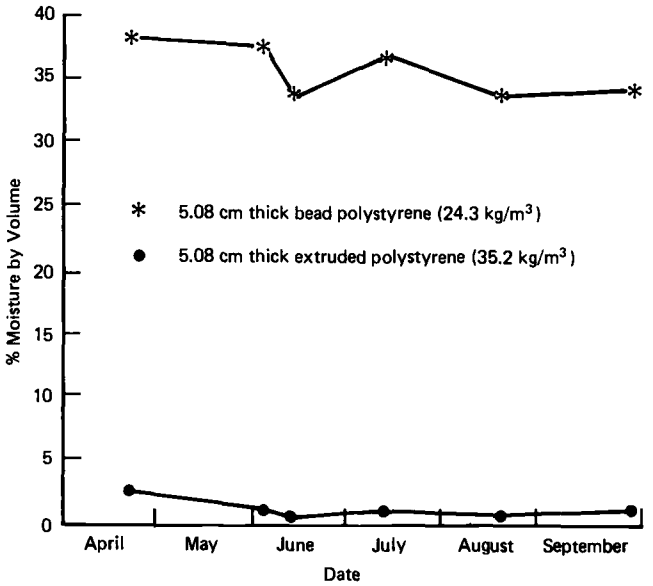

FIG. 11—*Fluctuation in absorbed moisture for extruded polystyrene and bead polystyrene insulation in USD roof in its third year after installation. The extruded polystyrene almost dries out completely by the end of the summer, but the bead polystyrene still retains over 30 percent water by volume.*

which were in their third year on the roof when the measurements were made.

The amount of water absorbed after seven years in the nonponded roofs with extruded polystyrene was equivalent to the water absorbed by 21 days in the water absorption test with the specimen subjected to both a concentration and a temperature gradient (Fig. 3, Curve E). The amount of water picked up by the insulation specimen from the ponded roof corresponded to the laboratory test results for 28 days.

The time in service for the bead polystyrene specimens in Table 3 ranged from 0.8 to 7.3 years. The nonponded roofs picked up from 8.6 to 17.2 percent water by volume after 7.3 years. The thermal resistance of these foams had decreased by 30 percent for the 8.6 percent water pickup and had decreased by 65 percent for the 15.9 percent water pickup. The measured thermal resistance of the nonponded insulations agreed to within 14 percent with the values calculated using the equations of the previous section for low-density [less than 32.0 kg/m^3 (2.0 lb/ft^3)] and high-density [greater than 32.0 kg/m^3 (2.0 lb/ft^3)] bead polystyrene. The measured thermal resistances of the ponded insulations, of the specimen from Heidelburg, Germany, and of the specimen from Midland, Michigan, which picked up 17.2 percent water by volume, did not agree as well with their calculated values. The equations for the dependence of the thermal resistance of insulations on moisture content possibly could be refined by including factors involving thickness, density, the size of the voids, the number of voids, and the location of the moisture in the insulation.

The 28-day laboratory water absorption test (Fig. 3, Curve B) in which the specimen is subjected to both a temperature and a concentration gradient did not cause the high-density bead polystyrenes to absorb as much moisture as the field specimens absorbed in just two years. Although this laboratory test does not cause the same amount of water absorption as field conditions, it is useful in screening potential insulations for moist-environment applications. Those insulations which absorb less than 5 percent moisture by volume in this 28-day test *and* which absorb less than 5 percent moisture by volume after 700 freeze-thaw cycles should perform well in moist-environment applications.

The time in service for the polyurethane specimens in Table 3 ranged from 2 to 5 years. By five years, the polyurethanes had picked up an average of over 5 percent water by volume, with one specimen absorbing 17.0 percent water by volume. The average level of absorption corresponds to the amount of water absorbed by the laboratory specimen (Curve I of Fig. 6) after 200 freeze-thaw cycles. More field data must be collected to determine whether the amount of moisture in the field specimens will level out as the laboratory freeze-thaw specimens did. The thermal resistance of these polyurethanes was calculated to have deteriorated by 38 percent on the average (in one case, by 106 percent) after five years in service.

The top covering, normally stones, in the USD roof system provides the buoyancy resistance, the burning-brand fire protection, and the ultraviolet shield for the insulations. However, the top covering can also cause disadvantages with respect to the long-term thermal performance of insulations. Concrete paving blocks placed directly on top of an insulation in a USD roof system may retard the water vapor from escaping from the insulation in winter, thus causing water absorption in the insulation. Due to the mass and thickness of the block and the surface tension of water on the block, the patio block could also act as a barrier and reduce evaporative drying of the top surface of the insulation. The overall result would be some loss in thermal resistance of the insulation depending on the type and thickness of insulation used and the location (that is, Montreal or Miami) of the roof application. A recommended way to use concrete paving blocks to avoid any potential thermal resistance loss is the use of spacers or gravel between the insulation and the concrete paving blocks.

Below-Grade Perimeter Installations

The thermal performance of various types of insulations exposed to actual highway conditions have been monitored for the past 15 years. Most of these data are for extruded polystyrene foam since it was selected for field use on the basis of its laboratory performance in moisture absorption and freeze-thaw testing. A few field specimens of other types of insulation were available. These data are given in Table 4. Data from soil insulation tests and below-grade perimeter insulation are also given in Table 4. The field results for the relative susceptibility of the different types of insulation to moisture absorption correspond to the results obtained in the laboratory studies discussed in the foregoing. The effect of this moisture absorption on the thermal resistance of the insulations in the field environment also follows the trends noted in the laboratory studies. The amount of water absorbed by the insulations in the below-grade applications are less for the same time periods than in the USD roof application. Extruded polystyrene foam performs better than molded bead polystyrene and polyurethane without skins in terms of moisture absorption resistance and retention of thermal resistance in below-grade applications.

Conclusions

1. As the water content of an insulation increases, the thermal resistance of the insulation decreases. The overall performance of the insulations have been dependent on the type used. The extruded polystyrene skinboard is the most widely used in the applications discussed and has demonstrated excellent thermal performance because of its resistance to water

absorption in field applications as compared with other insulations. The specific long-term performance of the various insulations most commonly used in USD roofs can be found in Table 3. The field performance of the insulations correlates favorably with the laboratory studies on the effect of moisture on thermal resistance described in this paper. Better correlation may be attainable by including factors such as thickness, density, size of voids, number of voids, and location of the moisture in the insulation.

2. As a minimum criterion for insulations being considered for applications where water is present, the authors recommend that these insulations retain at least 80 percent of their thermal resistance for a 10-year period.

3. Water absorption tests without a thermal driving force (ASTM Method D 2842-69), even those run for long durations such as 504 h, are inadequate for screening insulations for wet environmental applications. The best water absorption test for screening thermal insulations is where there is a water vapor driving force through the insulation (from bottom to top). This test should have both a temperature gradient [minimum 10°C per centimeter (45.7°F per in.) thickness] and a water-saturated environment and should be run for a minimum of 28 days. A good water pickup limit for screening with this type of test would be 5 percent by volume water after 21 days. If the insulation has a higher water pickup than this limit, it should not be considered for wet environments (below-grade perimeter insulation, highway insulation, or USD roof insulation).

4. The relevance of the freeze-thaw test as a laboratory screen for insulations to be used in wet environmental applications is determined by the geographic location of the installation. It is not only the number of freeze-thaw cycles in a particular geographic region that must be considered, but also the severity of the freeze, the duration of the freeze, and the temperature gradient across the insulation. For most areas of North America, a minimum criterion for a laboratory freeze-thaw test would be 500 to 700 freeze-thaw cycles with a water pickup limit of not more than 5 percent (water by volume). This test should be used in conjunction with the water absorption test employing both thermal temperature and concentration gradients as moisture driving forces.

Acknowledgment

Although the authors are responsible for assembling the information in this paper, the data have been generated through the cooperation and effort of many people in several Dow locations, including Horgen, Switzerland, Sarnia, Canada, and Midland, Michigan.

References

[1] Williams, Llewelyn, "Regionalization of Freeze-Thaw Activity," U. S. Army Natick Laboratories, *Annals of Association of American Geographics*, Vol. 54, No. 4, Dec. 1964.

[2] Russell, R. J., *Transactions*, American Geographical Union, 1943, p. 125.

[3] Alpert, L., "Adhesion Type Ceramic Veneer," Structural Clay Products Institute, *Technical Notes on Brick and Tile Construction*, Vol. 4, May 1953.

[4] Kaplar, Chester W., "Moisture and Freeze-Thaw Effects on Rigid Thermal Insulations," U. S. Army Cold Regions Research and Engineering Laboratory, Hanover, N. H., Technical Report 249, April 1974.

[5] Schaefer, David, "Water Absorption of Insulation in Protected Membrane Roofing Systems," U. S. Army Cold Regions Research and Engineering Laboratory, Hanover, N. H., CRREL Technical Note, Jan. 1974.

[6] Thorsen, Sven-Hakan, "Determination of the Expansion Coefficient, Water Absorption, Moisture Diffusivity, As Well As Thermal Conductivity at Different Moisture Contents for Polystyrene and Urethane Cellular Plastics," Institute for Building Technology, Chalmers Technical University, Goteborg, Sweden, Aug. 1973.

[7] Paljak, Ivar, National Swedish Institute for Material Testing, *Materiaux et Constructions*, Vol. 6, No. 31, 1973, p. 53.

[8] Levy, M. M., *Journal of Cellular Plastics*, Jan. 1966, p. 37.

[9] Mittasch, H., *Plaste und Kautschuk*, Vol. 16, No. 4, 1969, p. 268.

[10] Achtziger, J., *Kunststoffe Im Bau*, Vol. 23, 1971, p. 3.

[11] Hedlin, C. P., "Moisture Attack on Insulation in Protected Membrane Roofing," Division of Building Research, National Research Council of Canada, Ottawa, Ont., Research Paper No. 634, 1974.

[12] Hedlin, C. P. in *Roofing Systems, ASTM STP 603*, American Society for Testing and Materials, 1976, pp. 36–50.

[13] Aamot, H.W.C. and Schaefer, D., "Protected Membrane Roofs in Cold Regions," Corps of Engineers, U. S. Army, Hanover, N. H., March 1976.

[14] Baker, M. C. and Hedlin, C. P., "Protected Membrane Roofs," Canadian Building Digest No. 150, Division of Building Research, National Research Council of Canada, Ottawa, Ont., June 1972.

[15] "Performance of Membrane Roofing Systems," Division of Building Research Seminar Workshop, National Research Council of Canada, Ottawa, Ont., 1975.

[16] Jespersen, H. B., "The Effect of Moisture on Insulating Materials Made of Plastic Foam, Impregnated Mineral Wool, Vermiculite and Concrete Cylinders," Denmark Technological Institute, 1960.

[17] Kaplar, C. W., "Studies of Moisture Effects on Thermal Conductivity of Rigid Insulations," U. S. Army Cold Regions Research and Engineering Laboratory, Hanover, N. H., CRREL Internal Report No. 207, 1969.

Heat Transmission Models and Measurements

C. M. Pelanne[1]

Light Transmission Measurements Through Glass Fiber Insulations

REFERENCE: Pelanne, C. M., "**Light Transmission Measurements Through Glass Fiber Insulations,**" *Thermal Transmission Measurements of Insulations, ASTM STP 660*, R. P. Tye, Ed., American Society for Testing and Materials, 1978, pp. 263–280.

ABSTRACT: As part of a study to define the structure of glass fiber insulations, light transmission was measured through a number of insulations made by different manufacturing processes.

A significant relationship was observed between light transmitted normal to the plane of the insulation and the apparent thermal conductivity. This relationship suggests a possible application for the continuous monitoring of glass fiber insulation being manufactured.

The light transmission measurement allows us to see the laminar structure of glass fiber insulations as well as the preferred orientation of the fibers resulting from manufacturing process characteristics.

The light transmission measurements also may provide an indirect way of estimating the apparent thermal conductivity in the plane of the insulation, as well as a way of evaluating heat flow in tailor-made glass fiber specimens.

KEY WORDS: thermal insulation, glass fibers, structure of insulation, light transmission, radiation, thermal conductivity

While the mechanisms of heat transport through a glass fiber insulation are complex, as has been discussed extensively in a number of papers ([*1–9*][2], and others), it has been demonstrated that "radiation transmission" is the controlling influence of the upward shape of the k-versus-density curve as it goes from high to low densities [*7*]. As discussed in the aforementioned papers, the radiation transmission component of heat transport in glass fiber insulation is part of the total radiation transfer between the hot and cold faces of the insulation. Thus, the "radiation transmission" is influenced by radiation laws.

For a given temperature, the total radiant energy is the integration of

[1]Senior research specialist, Johns-Manville Research and Development Center, Denver, Colo. 80217.

[2]The italic numbers in brackets refer to the list of references appended to this paper.

the energy distribution over a wide band of wavelengths dominated at the peak by one wavelength. As shown in Fig. 1, this peak is displaced toward the shorter wavelengths as the temperature increases (Wien's displacement curve). Also shown in Fig. 1 is the span of the visible spectrum (0.4 to 0.7μm), the region within which these experiments were performed. Except at high temperatures, there is relatively little visible energy emitted from a body. At the temperatures at which much of the glass fiber insulation is used (24°C mean temperature), between 38°C and 10°C the major portion of the energy (~70 percent) is generated between 3 and 20 μm with the peak occurring at approximately 9.7 μm. The curves for this temperature range are shown in Fig. 2.

Glass, as shown by the greenhouse effect, is practically transparent at the shorter wavelengths in the visible spectrum 0.4 to 0.7 μm (solar energy) and is opaque to the long wavelengths at the infrared region beyond 2.5 μm generated by low-temperature surfaces. Thus, as insulating fibers, the glass performs its primary insulating function by absorbing and scattering the infrared radiation. Since the absorbing and scattering characteristics are a function of fiber diameter, correlation of light transmission with the heat transmission was not the object of this investigation.

This study was conducted as a part of a basic research project sponsored by the Johns-Manville Corp. The principal objective was to relate the structure of glass fiber insulations to the heat flow mechanisms involved in the insulating process. In this phase, we measured the light transmitted

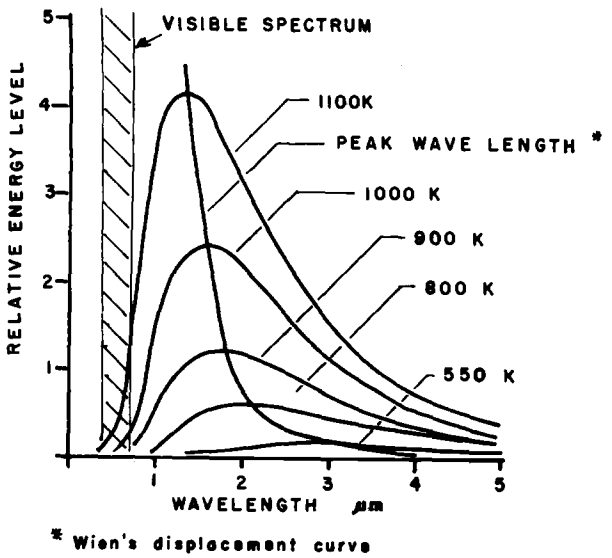

FIG. 1—*Radiant energy distribution curves at high temperatures.*

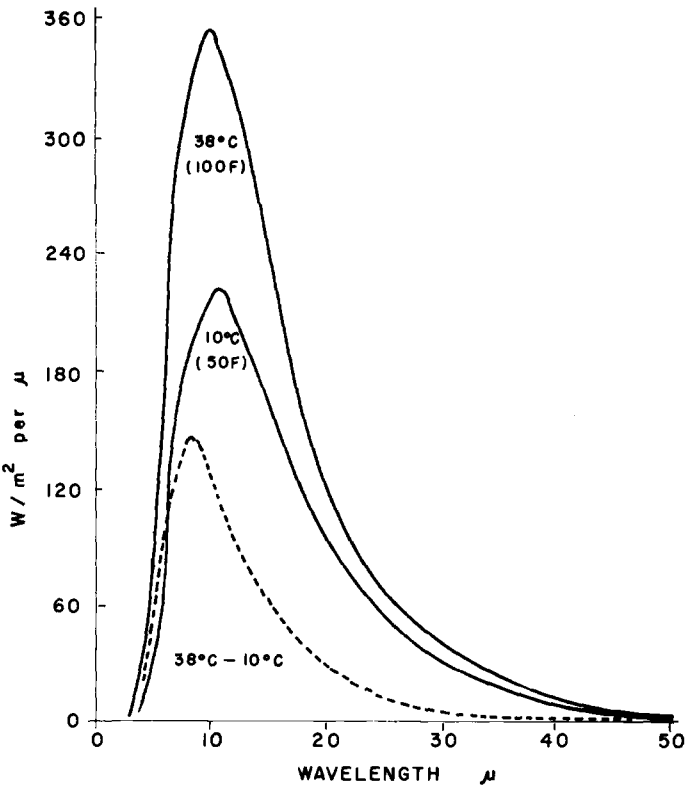

FIG. 2—*Radiant energy distribution at heat meter test conditions. (Net energy transfer between 38 and 10°C shown by dashed line.)*

through the three major axes of 25.4-mm (1 in.) cubes of a number of glass fiber insulation specimens and observed a significant relationship between the light transmitted in the direction normal to the plane and the apparent thermal conductivity of the specimens. This paper discusses only this observed relationship and its possible application for product performance control.

Discussion

Materials and Specimen Preparation

The insulations used for these experiments were representative of two manufacturing processes in use by Johns-Manville when this research was carried out (1970–1971) and a specimen from another manufacturer. The two manufacturing processes are referred to as Pot and Marble (A and AA) and Rotary (B and C). As will be demonstrated, the two processes

result in a different lay of the fibers, resulting in different heat flow characteristics. The experiments involved a wide range of product densities, 6 to 25 kg/m (0.375 to 1.6 lb/ft^3), and average fiber diameters (2.2 to 7.2 μm, by airflow measurement technique).

From each sample lot, six 305 by 305 by 25.4-mm (12 by 12 by 1 in.) specimens were cut, their densities determined and their apparent thermal conductivites k measured with a heat flowmeter apparatus [ASTM Test for Steady-State Thermal Transmission Properties by Means of the Heat Flow Meter C 518-76] [6]. One specimen from the six was picked on the basis of representation of the lot population and its position with respect to the average k-versus-density curve. The k and densities of these specimens are given in Table 1 and plotted later in Fig. 6.

Out of the center 152 by 152-mm (6 by 6 in.) square (heat flowmeter measurement area), nine 25.4-mm (1 in.) cubes were cut as shown in Fig. 3. The preparation of the 25.4-mm (1 in.) cubes proved to be much more difficult than anticipated. They were rough cut, placed in a jig, and trimmed with an electric hair clipper set for a very close cut. Even with this setup, the variations in density through the thickness of the piece caused some irregularities in the shape of the cubes. The densities were determined for both the 152 by 152-mm (6 by 6 in.) square and the individual cubes. The k values were plotted against the density of the 152 by 152-mm (6 by 6 in.) squares and the average light transmission against the average density of the nine cubes. A small dot of paint was placed on the top face of each cube as shown in Fig. 3. This dot was used as reference when positioning the cube in the test apparatus.

Light Transmission Measurements

Instrumentation—The light transmission measurements were performed with a Brice-Phoenix Universal Light Scattering Photometer 1000 series, which is described as "a versatile instrument especially designed for the measurement of micro-scattering, micro-fluorescence, micro-luminescence and very low transmittance and reflectance of dark materials." As shown in Fig. 4, the apparatus consists of a constant-intensity light source (mercury vapor lamp), a collimating tube through which the light is directed into a black measurement compartment, a specimen support stage located at the center of the compartment, and a photomultiplier tube attached to a graduated disk indicating the angle at which the tube is viewing the incident beam. This arrangement allows the photomultiplier tube to rotate on a 270-deg arc about the stage. The light transmission measurements were taken with the photomultiplier tube directly in line with the light beam and the center of the specimen. Scattered light measurements were taken at a 90-deg angle.

The light is collimated to form a 6.35 by 3.81-mm (0.25 $\times$ 0.15 in.) beam

TABLE 1a—*Test results—SI units.*

Ident. No. Lot Sample	Micronaire Fiber Diameter μ	Binder Content %	Density, pcf 12" x 12" pcf	Density, pcf 6" x 6" pcf	Apparent Thermal Conductivity Btu in./ft^2·F·hr	Cube Density Avg 9 Cubes pcf	Light Transmission Normal Avg. 1 & 3	Light Transmission Cross Machine 2	Light Transmission Machine 4	Scattered Light Avg. 1 & 3
Pot and Marble Process							x 10^{-4}% of Incident Light			
A-1-9	3.96	16.3	0.722	0.804	0.274	0.841	9.85	43.1	135.0	53.5
A-1-8	4.80	14.3	1.282	1.332	0.247	1.371	2.20	6.88	27.7	16.1
A-1-7	4.12	16.7	0.640	0.677	0.289	0.692	15.49	111.7	485.9	42.6
A-1-2	4.10	7.7	0.637	0.581	0.304	0.590	36.6	120.8	473.5	84.6
A-1-5-a	4.20	18.2	0.473	0.476	0.345	0.475	273.3	584.7	618.1	85.6
A-1-5-b	3.93	14.5	0.566	0.592	0.297	0.604	24.3	150.2	330.3	78.3
A-1-7	4.65	11.2	1.485	1.607	0.237	1.664	0.098	1.85	3.55	3.18
A-1-3	4.23	8.2	0.737	0.782	0.281	0.828	10.03	190.8	368.2	86.2
A-1-2-a	4.05	13.7	0.875	0.899	0.267	0.979	3.00	50.5	118.5	47.1
A-1-2-b	4.14	5.8	0.468	0.486	0.322	0.487	73.8	456.7	644.9	85.1
A-1-9	4.03	8.0	0.333	0.350	0.372	0.342	452.8	661.0	676.6	126.3
AA-1-1	2.2	19.3	0.539	0.550	0.253	0.608	0.112	1.37	3.50	3.23
Rotary Process										
B-1-1	5.5	7.1	0.791	0.814	0.302	0.778	32.5	321.8	307.8	88.5
B-2-5-a	4.1	11.4	0.862	0.835	0.295	0.882	14.8	108.7	106.6	40.4
B-2-5-b	3.7	13.2	0.981	0.994	0.278	1.070	4.15	30.7	28.1	23.2
B-2-5-c	4.45	9.1	1.385	1.374	0.255	1.477	1.91	9.90	9.84	14.4
C-2-1	7.15	4.4	0.650	0.719	0.328	0.741	186.5	391.5	437.9	55.3

TABLE 1*b*—*Test results—U.S. customary units.*

Ident. No. Lot Sample	Micronaire Fiber Diameter μ	Binder Content %	Density kg/m^3 305 x 305 mm	Density kg/m^3 152 x 152 mm	Apparent Thermal Conductivity W/m·k	Cube Density Avg 9 Cubes kg/m^3	Light Transmission Normal Avg. 1 & 3	Light Transmission Cross Machine 2	Light Transmission Machine 4	Scattered Light Avg. 1 & 3
Pot and Marble Process							x 10^{-4}% of Incident Light			
A-1-9	3.96	16.3	11.6	12.9	0.0395	13.5	9.85	43.1	135.0	53.5
A-1-8	4.80	14.3	20.5	21.3	0.0356	22.0	2.20	6.88	27.7	16.1
A-1-7	4.12	16.7	10.3	10.8	0.0417	11.1	15.49	111.7	485.9	42.6
A-1-2	4.10	7.7	10.2	9.3	0.0438	9.5	36.6	120.8	473.5	84.6
A-1-5-a	4.20	18.2	7.6	7.6	0.0498	7.6	273.3	584.7	618.1	85.6
A-1-5-b	3.93	14.5	9.1	9.5	0.0428	9.7	24.3	150.2	330.3	78.3
A-1-7	4.65	11.2	23.8	25.7	0.0342	26.6	0.098	1.85	3.55	3.18
A-1-3	4.23	8.2	11.8	12.5	0.0405	13.3	10.03	190.8	368.2	86.2
A-1-2-a	4.05	13.7	14.0	14.4	0.0385	15.7	3.00	50.5	118.5	47.1
A-1-2-b	4.14	5.8	7.5	7.8	0.0464	7.8	73.8	456.7	644.9	85.1
A-1-9	4.03	8.0	5.3	5.6	0.0536	5.5	452.8	661.0	676.6	126.3
AA-1-1	2.2	19.3	8.6	8.8	0.0365	9.7	0.112	1.37	3.50	3.23
Rotary Process										
B-1-1	5.5	7.1	12.7	13.0	0.0436	12.5	32.5	321.8	307.8	88.5
B-2-5-a	4.1	11.4	13.8	13.4	0.0425	14.1	14.8	108.7	106.6	40.4
B-2-5-b	3.7	13.2	15.9	15.9	0.0400	17.1	4.15	30.7	28.1	23.2
B-2-5-c	4.45	9.1	22.2	22.0	0.0368	23.7	1.91	9.90	9.84	14.4
C-2-1	7.15	4.4	10.4	11.5	0.0473	11.9	186.5	391.5	437.9	55.3

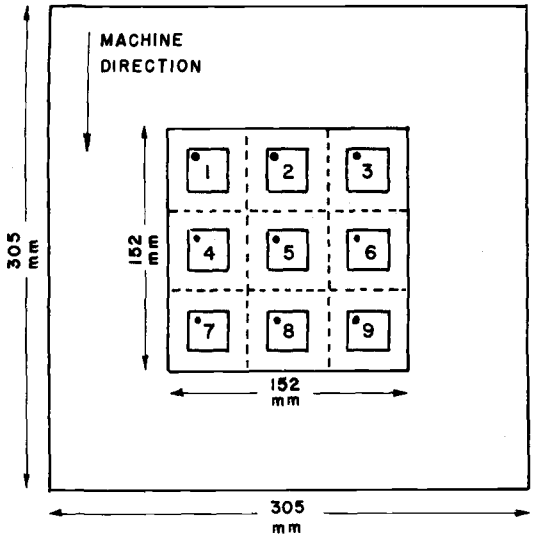

FIG. 3—*Diagram of specimen preparation: Heat meter test specimen, 305 by 305 mm (12 by 12 in.); heat meter measurement, 152 by 152 mm (6 by 6 in.); light transmission specimens, nine 25.4-mm (1 in.) cubes. (Dots on corners serve for positioning of cubes.)*

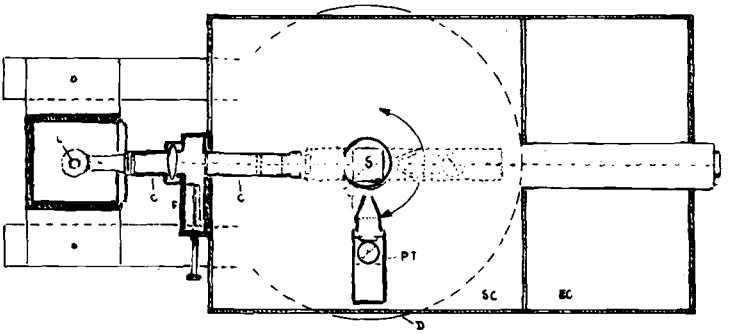

FIG. 4—*Brice-Phoenix light-scattering photometer optical system diagram (top view). L = light source (mercury vapor lamp); F = neutral filters; C = collimating tube; D = graduated disk (photocell positioning); S = stage—specimen position; PT = photomultiplier tube; EC = amplifier; SC = scattering compartment.*

striking the surface of the specimen. This incident beam when unobstructed by a specimen or light filter is too intense to be viewed by the highly sensitive photomultiplier tube. Therefore, the equipment was calibrated with neutral-density filters in terms of millivoltage output from the amplifier.

An opal reference standard was calibrated and, during the measurements, inserted periodically into the beam to check the amplifier and the calibration of the precision recorder used to collect the data.

Measurement Procedure—Each of the nine cubes of each specimen was positioned on the specimen stage in four different positions as shown in Fig. 5. The light measurements were taken as indicated in the following table:

Position	Light Transmission	Light Scattered
1	[3]normal to plane	[3]machine direction
2	[3]cross-machine direction	machine direction
3	[3]normal to plane	[3]cross-machine direction
4	[3]machine direction	cross-machine direction

In order to duplicate the positioning of the cube, it was placed against a cornering stop fixed to the specimen stage. Only the scattered light measurements taken from the cube side placed against the stop were used for this study, in this way ensuring a constant through-specimen distance of light travel.

From duplicate testing of two groups of specimens, we concluded that the tests were reproducible. The scatter of the individual measurements as shown later in Fig. 10 was repeated despite the visible irregularities of the matrix within the 25.4-mm (1 in.) cube. Because of this scatter, it was decided that for this phase the average of the nine measurements (in the case of the normal-to-plane measurements, the average of 18) would be

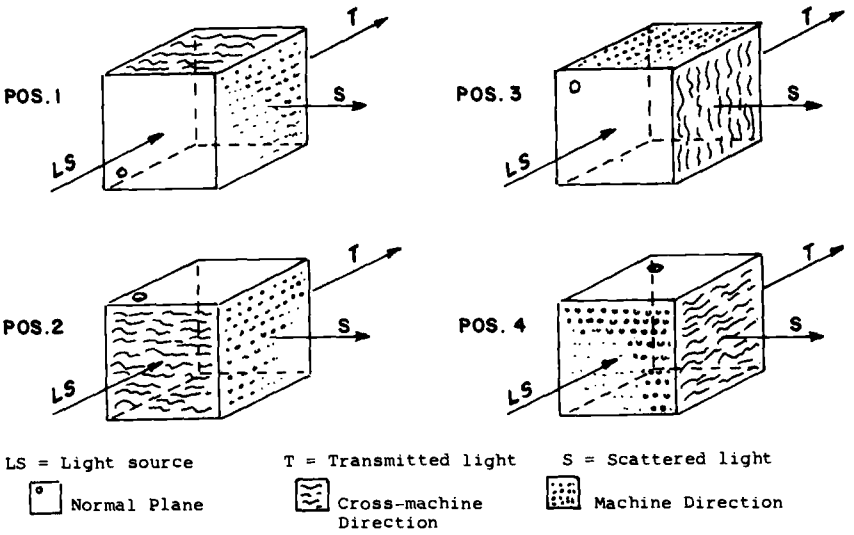

FIG. 5—*Specimen positions and light measuring pattern.*

[3]Data referred to in this paper.

reported; see Table 1. It is anticipated that the individual values could help define better the character of the insulation structure if the data are analyzed further. (One hundred and eight individual measurements were taken on each insulation specimen for which a single k-value was obtained.)

Results (See Table 1)

Apparent Thermal Conductivity Versus Density—Fig. 6

The apparent thermal conductivity measurements, k, were made on 25.4-mm-thick (1 in.) specimens with a rapid heat flowmeter apparatus [*10*] (ASTM C 518-76). The k-versus-density of the Pot and Marble (A)

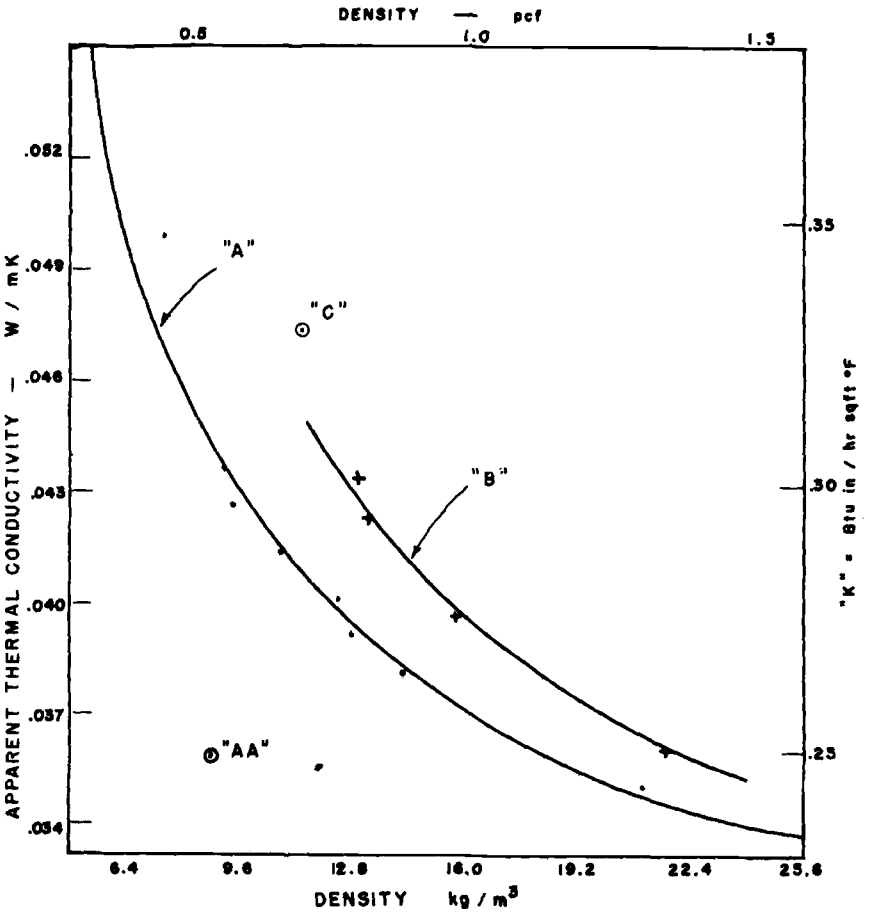

FIG. 6—*Apparent thermal conductivity versus density of glass fiber insulation [density = 305 by 305 mm (6 by 6 in.), center of test specimen].*

and Rotary (B) products form two curves as expected. The AA fiber point is significantly separated from these two populations.

Light Transmission Versus Density—Fig. 7

The results of the light transmission measurements normal to the plane of the insulation when plotted against the average cube density on semilog paper also show separate curves for the A and B products. Both the AA fiber and C specimens are significantly separated from the two populations.

We observe a little more scatter than appeared in the k-versus-density curves. This is not too surprising when we consider the relative areas of

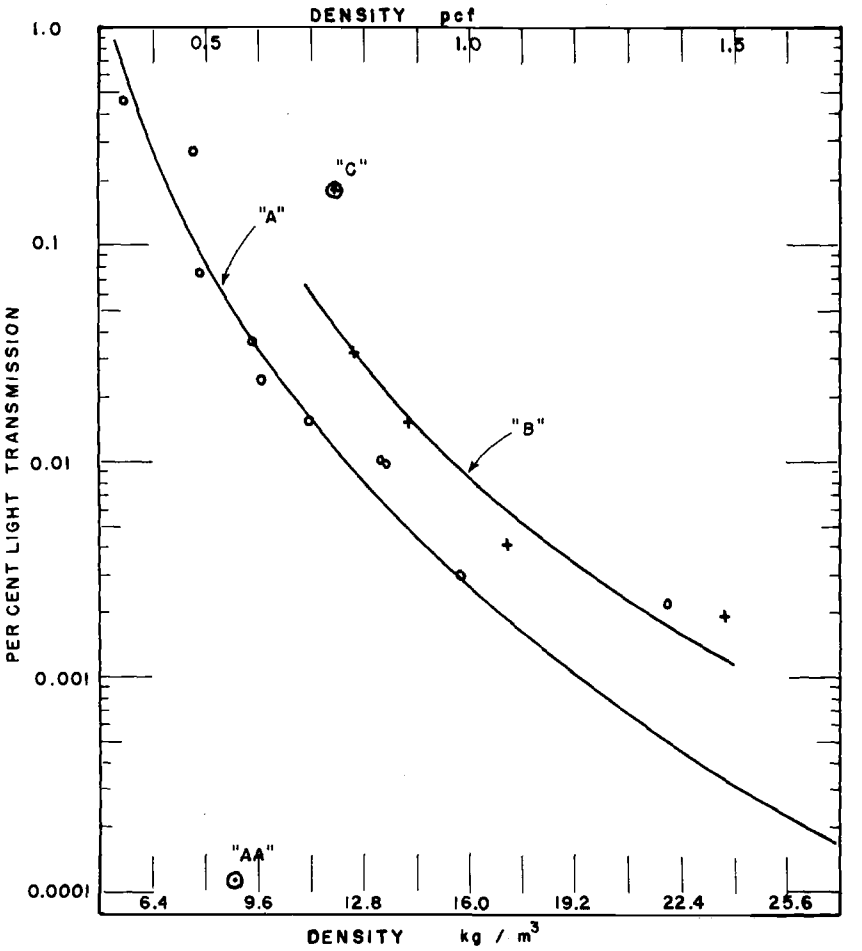

FIG. 7—*Light transmission versus density.* [*The density, as a percentage of incident light, is the average of nine 25.4-mm (1 in.) cubes.*]

the measurement and the representative density against which the data are plotted. The *k*-data are based on a 232-cm^2 (36 $in.^2$) test area and are plotted against the density of the same area of the specimen. The light transmission measurements are the average of two sets of nine measurements representing a total area of 4.36 cm^2 (0.675 $in.^2$) (24.2 mm^2 by 18), which is only 7.5 percent of the area used to determine the density, 58 cm^2 (9 $in.^2$).

It is very important to remember that light density fibrous insulations are not homogeneous. Referring to Fig. 12, the nonhomogeneity at the scale of these measurements (24.2 mm^2) (0.0375 $in.^2$) can be visualized when considering that the measurements shown in Fig. 12 represent the integration of the light over a 182.41 cm^2 (28.3 $in.^2$) and 5.07 cm^2 (0.785 $in.^2$) area, respectively.

Light Transmission Versus k—*Fig. 8*

When the light transmission normal to the plane of the insulation is plotted against the apparent thermal conductivity of the specimen from which the cubes were cut, we observe a very good correlation. Of the 17 points, we observe that 70 percent fall within ±2 percent of the curve in terms of apparent thermal conductivity. Even the very significantly different AA fiber specimen is less than 7 percent away from the average curve. This agreement is particularly surprising since the light measurement area represents less than 2 percent of the heat flow measurement area.

Light Transmission Versus Density and Cube Orientation—Fig. 9

The light transmitted through the three axes of the cubes demonstrates some very significant differences in the structure of the insulations. From Fig. 9 we observe that more light travels through the horizontal plane of the insulation. In the case of the B insulation, we observed that the two horizontal planes, machine and cross-machine direction, offered the same resistance to light transmission, indicating a laminar but not preferably oriented array of fibers. This was not the case with the A insulation, which showed a preferred orientation of the fibers in the direction of fabrication. This preferred orientation is less observable as the density is lessened, because of the more open fiber network. It might be expected that the three curves would also converge at higher densitites as they do at the lower densities.

A typical set of individual cube measurements is shown in Fig. 10. From this plot we observe a wide scatter of the points representing the light transmission through the two horizontal planes. This scatter can be attributed to the irregularities in density within the individual cubes. A better

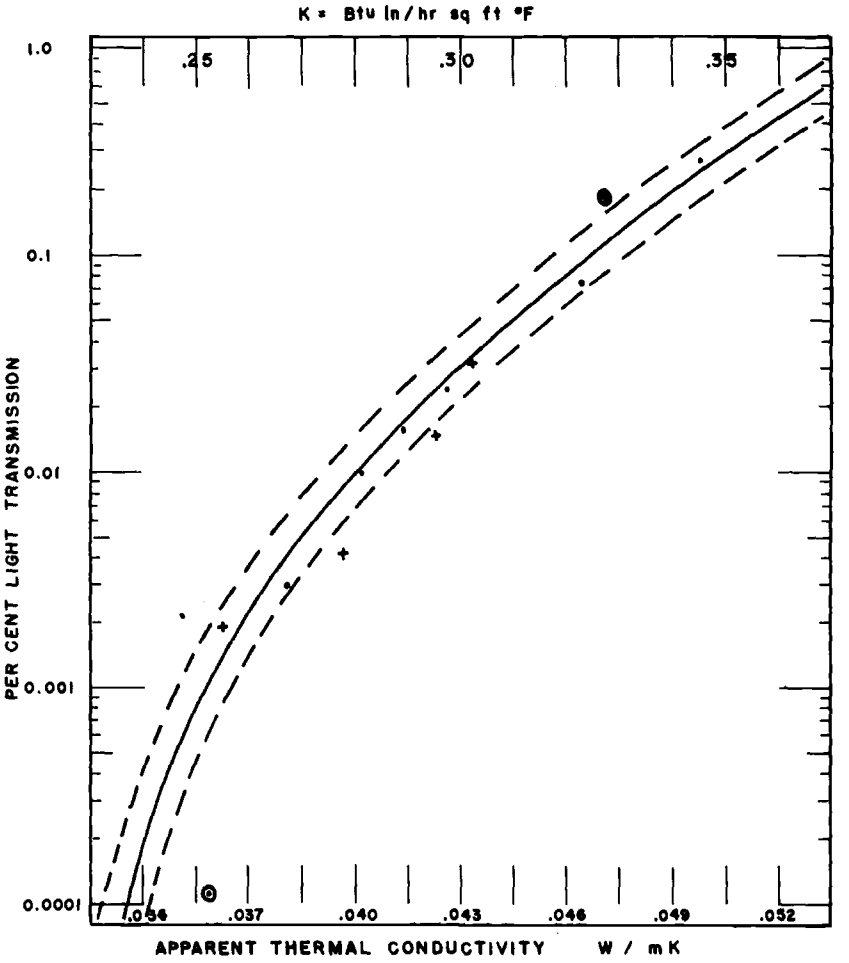

FIG. 8—*Light transmission through the normal plane of the insulation versus the apparent thermal conductivity of the same specimens.*

agreement might be obtained if a more precise determination of the density in the path of the light beam could be obtained. The beam represents only 3.7 percent of the cross-sectional area of the cube.

Scattered Light and Light Transmission Versus Density—Fig. 11

Figure 11 shows the percentage of light transmitted and scattered light which exists at the center of the lateral surfaces of the cube, at 90 deg to

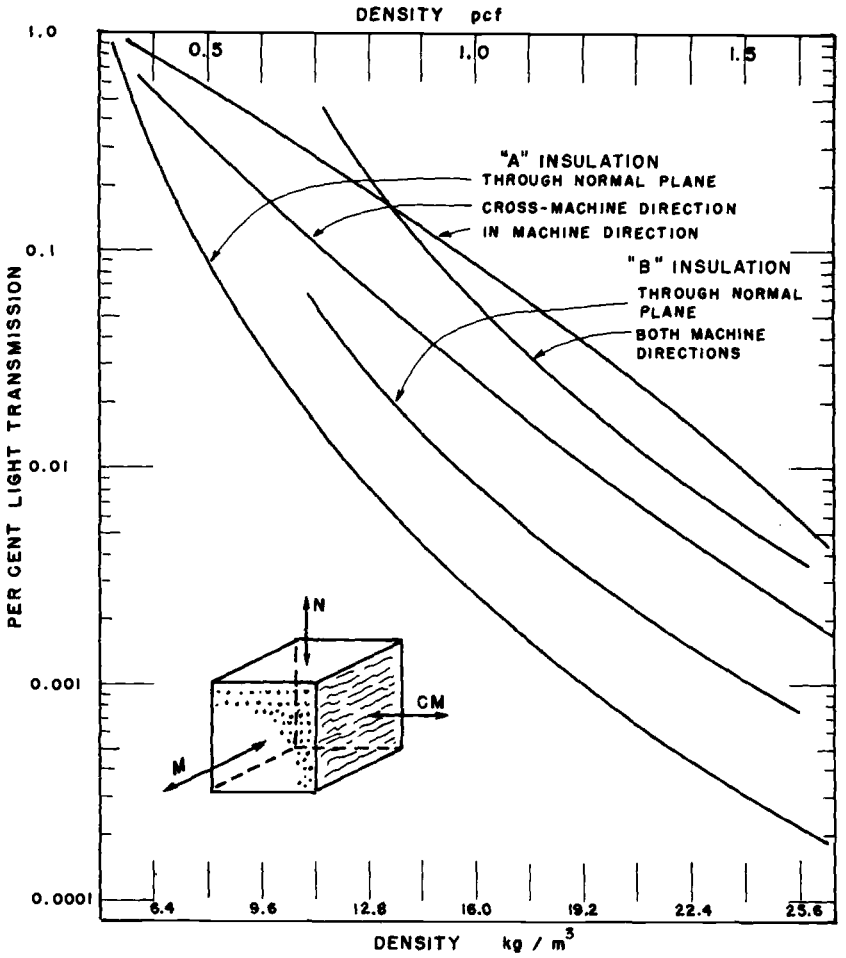

FIG. 9—*Light transmission versus density and cube orientation as a percentage of incident light. N = normal to the plane; M = machine direction; CM = cross-machine direction.*

the incident beam. The plot of scattered light represents the data for both A and B insulation products. The common curve for both products seems to indicate that, despite the marked difference in the fiber orientation characteristics, both products have the same average light scattering. This indicates that at that direction the products behave similarly.

The intersection of the light transmission and scattered light curves at lower densities is to be expected since the light transmission goes to a maximum and the scattered light goes to a minimum with zero density. The curves will also converge to a minimum when the insulation reaches

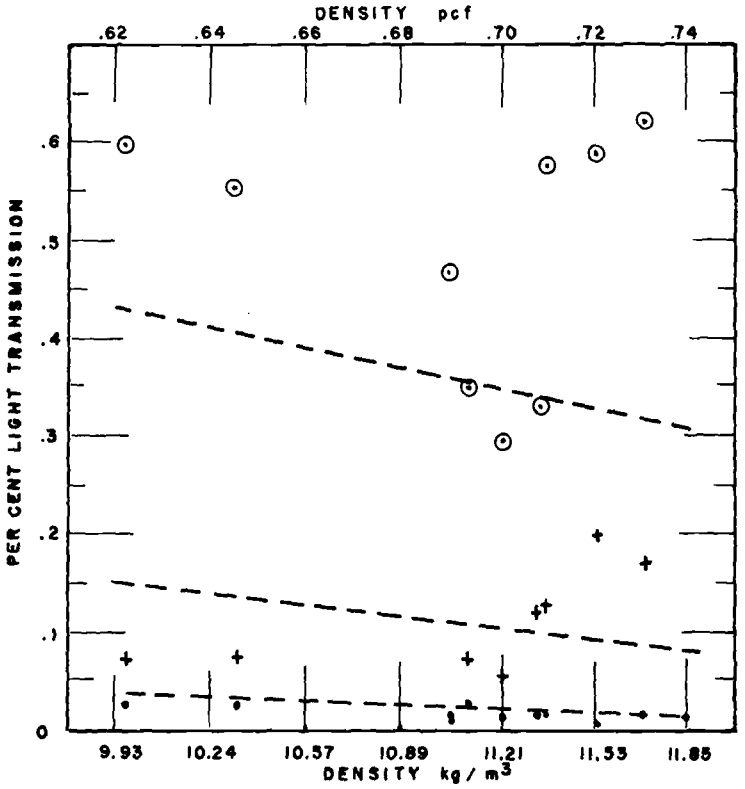

FIG. 10—*Typical light transmission through the three axes of the nine individual cubes of one specimen (Specimen "A"-1-7). · normal plane; + cross-machine direction; · machine direction. Dashed lines represent the average curves for all the specimens as shown in Fig. 9.*

a maximum density, allowing no light to penetrate: see insert on graph, Fig. 11.

Conclusions and Implications

1. The most significant practical observation derived from this investigation, so far, is the unexpected correlation of the light transmitted through the normal-to-plane direction of the glass fiber insulation and its apparent thermal conductivity. This observation has led us to describe the possible use of this relationship for the continuous monitoring of the thermal resistance of the glass fiber blanket on the production line. Patent No. 3,987,660, Method of Determining Thermal Conductivity of Fiber Insulation, was issued 26 Oct. 1976.

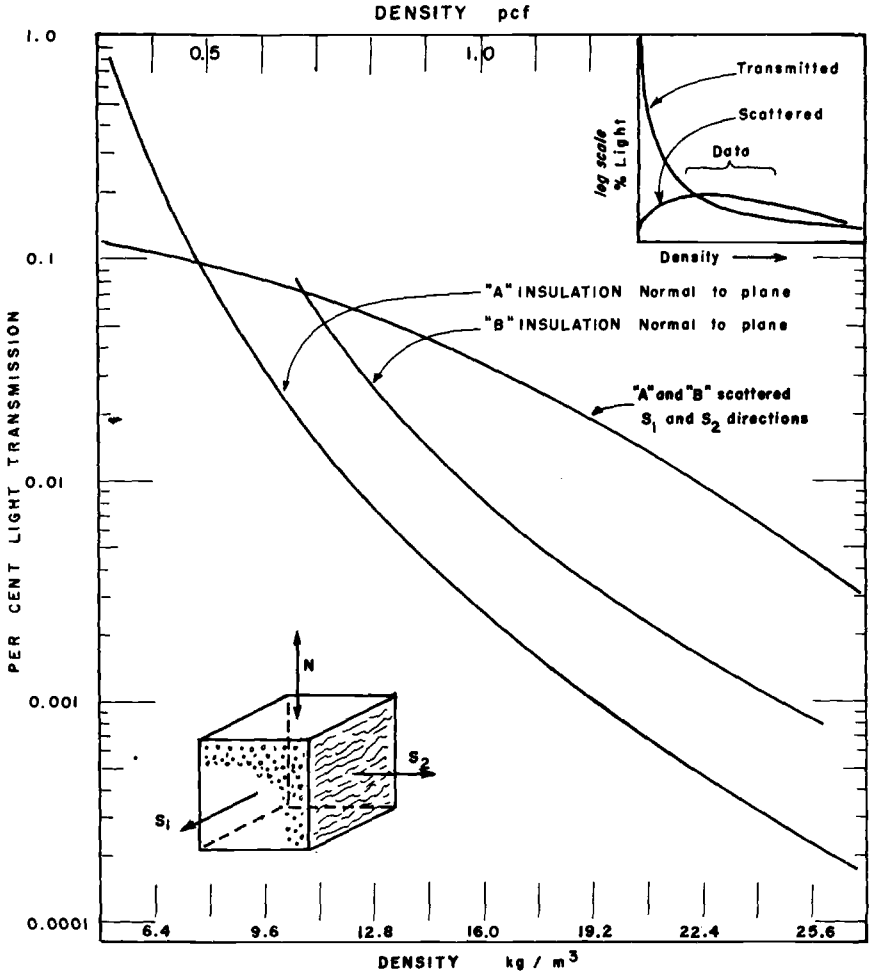

FIG. 11—*Light transmission and average scattered light versus density. (The scattered light is the average of* S_1 *and* S_2.)

Earlier, we had considered the possibility of monitoring production with infrared radiation but this approach had two major drawbacks. First, the level of energy available at the temperatures of interest was very low, making sensitive detection difficult; second, the temperature of the blanket would be difficult to keep constant enough so as not to mask the monitored radiation with the variable radiation emanating from the blanket.

The use of light overcomes both of these problems. Light is available at a high energy level (intensity) with only negligible effect on the blanket temperature. Also, the infrared energy emanating from the blanket remains

undetected by the light-sensitive detector. Only a relatively simple shielding for extraneous light is necessary.

Since our measurements showed that the transmitted light through a 25.4-mm (1 in.) thickness was only a very small percentage of the incident light, our first objective in evaluating the practicality of the method was to determine if we could accurately measure the light transmitted through thick blankets. The results of our first step is shown in Fig. 12. The upper

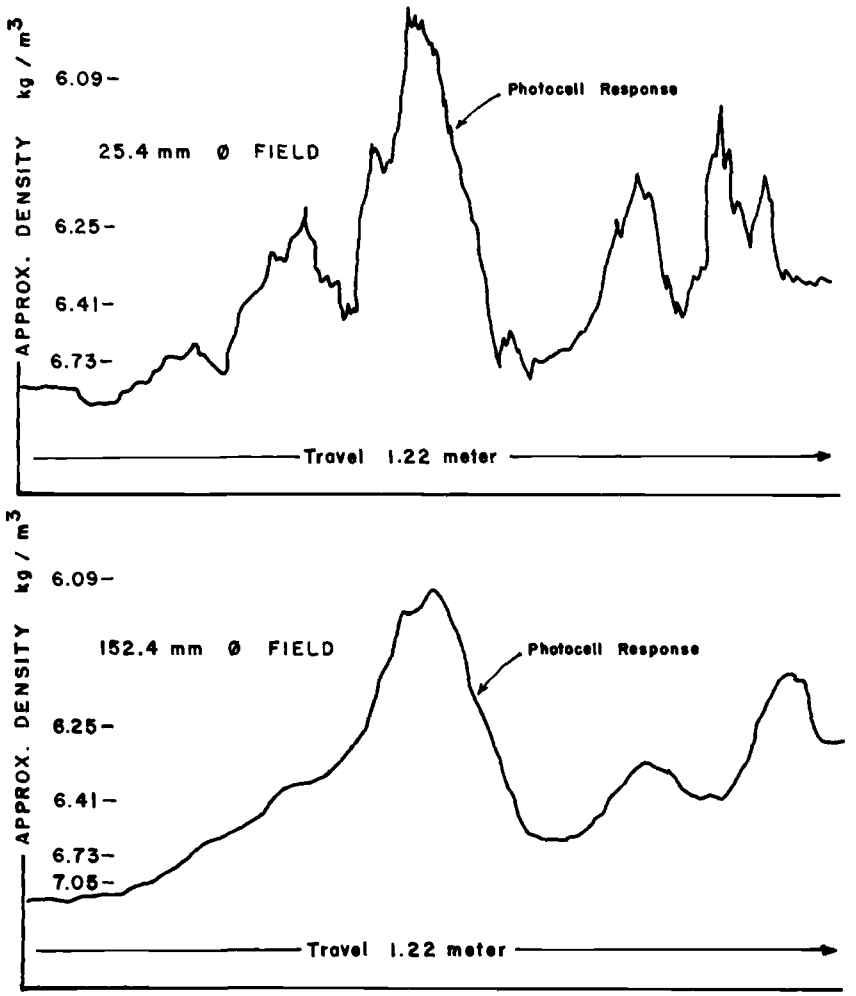

FIG. 12—*Light transmission along a 1.22-m (4 ft) length of building insulation compressed to 0.165 m (0.541 ft) thickness. [The photocell followed the same course, viewing a 2.5-cm-diameter (1 in.) field in the first case and a 15.2-cm-diameter (6 in.) field in the second case.]*

trace shows the recorded output of a 25.4-mm-diameter (1 in.) photomultiplier tube under which a 1.22-mm (48 in.) length of thick building insulation was drawn on a straight path. The blanket was compressed to a uniform 165-mm (6.5 in.) thickness (the application design thicknesses). In this instance, the photomultiplier tube orifice was placed in direct contact with the blanket surface. The photomultiplier tube viewed many small as well as several major irregularities in the blanket density. The lower trace shows the output of the same photomultiplier tube viewing a 152-mm-diameter (6 in.) area of the blanket over the same course as the 25.4-mm (1 in.) measurement. The photomultiplier tube was located at the top of a 457.2-mm-high (18 in.) cone with a 152-mm-diameter (6 in.) opening in contact with the blanket surface. The smoother trace, as shown, is the integration of the many variations indicated by the upper trace. The major variations in density remain apparent. The approximate density scale shown on the side is based on density measurements of several pieces cored from along the length of the blanket. These determinations were correlated with the light transmission measurements taken at the same positions in the blanket.

2. The light transmission measurements are of significance since they provide a quantitative measure of certain characteristics of the insulation structure. The laminar structure of both types of glass fiber insulations as well as the preferred orientation of the fibers in the Pot and Marble products have been clearly shown by the light transmission measurements. The wide scatter in the light transmission in the machine and cross-machine directions indicates great variations in density within the small scale of the measurement.

3. As a method for the study of glass fiber insulation, light transmission suggests some new investigative possibilities.

(*a*) A method for the evaluation of the thermal conductivity along the three axes of the insulation.

(*b*) A method for the evaluation of tailor-made structures to assess the most effective configurations of the fiber array.

References

[1] Allcut, E. A., *The Engineering Journal*, Vol. 35, Aug. 1952, pp. 836–841.

[2] Bankvall, Claes G., "Heat Transfer in Fibrous Materials," Document D-4, The National Swedish Institute for Building Research, 1972.

[3] Brailey, R. H. E., "Heat Flow Through Insulations Used in the Chemical Process Industry," *Proceedings*, Symposium on Glass and Related Materials, Part II, Preprint 32E, American Institute of Chemical Engineers, Philadelphia, 31 March–14 April 1968.

[4] Hager, N. E. and Steere, R. C., Journal of Applied Physics, Vol. 3, No. 12, 1967, pp. 4663–4668.

[5] Larkin, B. K. and Churchill, S. W., *Journal of the American Institute of Chemical Engineers*, Vol. 5, No. 4, 1959, pp. 467–474.

[6] Pelanne, C. M. in *Proceedings*, Eighth Conference on Thermal Conductivity, Plenum Press, New York, 1969, pp. 897–911.
[7] Pelanne, C. M., "Thermal Insulation—What is it?—How does it work?," Society of Mining Engineers of AIME, American Institute of Mining Engineers, Publication 76-H-301, Sept. 1976.
[8] Tye, R. P. and Pratt, A. W., "Heat Transmission in Low Conductivity Materials," *Thermal Conductivity*, Vol. 1, Academic Press, London, 1969.
[9] Verschoor, J. D. and Greebler, P., *Transactions*, American Society of Mechanical Engineers, Vol. 74, No. 6, Aug. 1952, pp. 961–968.
[10] Pelanne, C. M. and Bradley, C. B., *Materials Research and Standards*, Vol. 2, July 1962, pp. 549–552.

C. R. King[1]

Fibrous Insulation Heat-Transfer Model

REFERENCE: King, C. R., "**Fibrous Insulation Heat-Transfer Model,**" *Thermal Transmission Measurements of Insulation, ASTM STP 660*, R. P. Tye, Ed., American Society for Testing and Materials, 1978, pp. 281–292.

ABSTRACT: A mathematical model has been developed for the transfer of heat through fibrous insulating materials. Model development was an outgrowth of a study of heat transfer mechanisms and insulating material efficiencies.

This paper describes the mathematical derivation of the model based upon fundamental concepts of heat transfer and certain simplifying assumptions. It is shown that the efficiency of a fibrous insulation may be characterized by three model constants. One constant is calculated from fiber emissivity data and the other two may be determined from measurement of the "apparent" thermal comductivity at two different temperatures by the ASTM Test for Steady-State Thermal Transmission Properties by Means of the Guarded Hot Plate, (C 177-76). Actual test data are included to indicate the model's validity throughout the temperature ranges of practical interest for the materials investigated.

In one form, the model may be used to estimate the "apparent" thermal conductivity of a material for various combinations of hot-face and cold-face temperatures. The model may also be used to calculate heat losses and corresponding temperature profiles through insulated systems under known or assumed boundary conditions without relying upon the concept of "mean" temperature.

KEY WORDS: mathematical model, heat transfer, insulation, thermal conductivity, calculation, (material) characterization, physical properties, (temperature) profile

Heat is transferred by the primary modes of conduction, convection, and radiation. Studies of the radiation mechanism have led to development of a simplified mathematical model for transfer of heat through fibrous insulations.

Radiation studies were prompted by interest in the possibility that variations in apparent thermal conductivity (or "apparent k") of fibrous insulations with temperature might be primarily attributable to changes in radiant heat transfer rates. An academic exercise designed to test this supposition evolved into the proposed simplified model. Studies first led

[1]Research engineer, Eagle Picher Industries, Inc., Joplin, Mo. 64801.

to the startling discovery that radiant heat transfer coefficients of fibrous insulations could, under certain conditions, be expressed by a mathematical function containing hot-surface and cold-surface temperatures as the only variables. The simplified model resulting from this discovery appears to predict rather well the performance of a variety of industrial fibrous insulations. This observation has raised the possibility that the proposed model could be of more than academic interest.

Development of the current model was the result of initial efforts in a new field and without benefit of prior knowledge of extensive work by others in thermal modeling. Subsequent comparisons made with other work tend both to reinforce and to contradict the validity of the proposed model. An effort has been made to discuss these comparisons at appropriate points in the text. However, the author's lack of experience has precluded the type of exhaustive comparison that would normally be expected in a contemporary paper on this subject.

Discussion

Basic Assumptions

Two simplifying assumptions were basic to development of the current model. First, it was assumed that the coefficients of conductive and convective heat transfer are constant with temperature. Based upon this assumption, the two may be combined into a single term referred to as a "conductivity coefficient." The second assumption was that radiant heat transfer through fibrous insulations may be considered as occurring between equally spaced hypothetical planes in a manner analagous to the concept of mass transfer on "theoretical" plates in packed columns. The spacing of these hypothetical planes would be a physical constant for each insulation type and dependent upon properties affecting the absorption and scattering of radiation. Examples of such properties would include insulation bulk density, fiber diameter, and orientation of fiber within the insulation.

The boldness of the first assumption was recognized at the outset in view of its conflict with published thermal conductivity data for air. Hence, the modeling exercise was undertaken merely to obtain a general idea of the applicability of the second assumption to the phenomenon of radiant heat transfer.

Mathematical Derivation

The fundamental theory upon which model derivation is based may be applied to various geometric shapes. However, in the interest of simplicity, it will be assumed that insulation specimens are such that their cross-

sectional area does not vary with thickness (that is, that they are flat slabs). The conceptual model of layer-to-layer heat transfer through flat insulations is depicted in Fig. 1.

Under equilibrium conditions, the heat transferred from each hypothetical layer to the next succeeding layer is a constant. Based upon the foregoing assumptions, this equilibrium rate of heat transfer may be expressed in terms of a conduction component and a radiation component as follows

$$\frac{q}{A} = \text{Conduction component} + \text{radiation component} \qquad (1)$$

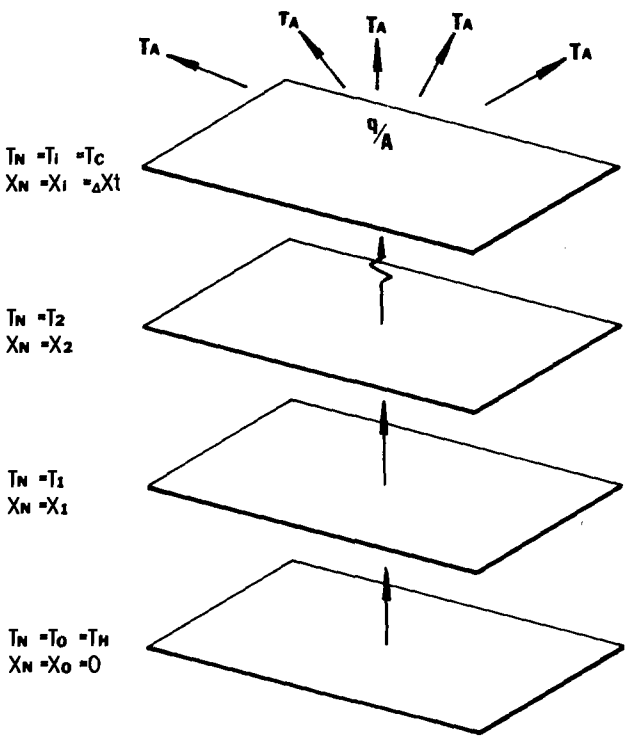

WHERE $\frac{q}{A}$ = LAYER-TO-LAYER HEAT TRANSFER, W/mK
T_N = TEMPERATURE OF N th LAYER, K
T_H = HOT SURFACE TEMPERATURE, K
T_c = COLD SURFACE TEMPERATURE, K
T_A = AMBIENT TEMPERATURE, K
X_N = DISTANCE OF N th LAYER FROM HOT SURFACE, m
ΔX_t = TOTAL INSULATION THICKNESS, m
i = TOTAL NUMBER OF TRANSFERS BETWEEN HYPOTHETICAL LAYERS

FIG. 1—*Conceptual heat-transfer model.*

or
$$\frac{q}{A} = \frac{k\,(T_n - T_{n+1})}{(X_{n+1} - X_n)} + \sigma e_{\text{eff}}\,(T_n^4 - T_{n+1}^4) \tag{2}$$

where

q = heat flow, J/s,
A = cross-sectional area, m^2,
k = conductivity coefficient, W/m·K,
T_n = temperature of nth layer, K,
T_{n+1} = temperature of next succeeding layer, K,
X_n = distance of nth layer from hot surface, m,
X_{n+1} = distance of next succeeding layer from hot surface, m,
σ = Stefan-Boltzmann constant = 5.727×10^{-8}/(W/m^{2}K^4), and
e_{eff} = effective layer-to-layer emissivity.

Since, by definition, layers are equally spaced

$$(X_{n+1} - X_n) = \frac{(X_o - X_i)}{i} = \frac{\Delta X_t}{i} \tag{3}$$

where

i = number of radiant heat transfer occurring between parallel planes. (Note: the number of transfers is equal to the number of hypothetical insulation layers as long as any cold-surface boundary effects may be neglected), and
ΔX_t = total insulation thickness, m.

Substituting for $(X_{n+1} - X_n)$

$$\frac{q}{A} = \frac{(ki)}{(\Delta X_t)}\,(T_n - T_{n+1}) + \sigma e_{\text{eff}}\,(T_n^4 - T_{n+1}^4) \tag{4}$$

Expanding and rearranging terms

$$\frac{(ki)}{(\Delta X_t)}\,(T_{n+1}) + \sigma e_{\text{eff}}\,(T_{n+1}^4) = \frac{(ki)}{(\Delta X_t)}\,(T_n) + \sigma e_{\text{eff}}\,(T_n^4) - \frac{q}{A} \tag{5}$$

Layer-to-layer calculations by Eq 5 enable determination of succeeding layer temperatures from known originating layer temperatures and the as-yet unknown constant rate of heat transfer per unit area. Assuming that the effective emissivity for all layer-to-layer transfers is constant, it will be observed that each succeeding layer temperature is derived from an identical function of originating layer temperature less the constant, q/A. Thus, after i transfers from T_H to T_c, Eq 5 may be expressed in terms of hot-surface and cold-surface temperatures as follows

$$\frac{(ki)}{(\Delta X_t)}\,(T_C) + \sigma e_{\text{eff}}\,(T_C^4) = \frac{(ki)}{(\Delta X_t)}\,(T_H) + \sigma e_{\text{eff}}\,(T_H^4) - i\,\frac{(q)}{(A)} \tag{6}$$

where

T_H = hot-surface temperature, K, and
T_C = cold-surface temperature, K.

Solving again for q/A

$$\frac{q}{A} = \frac{(k)}{(\Delta X_t)}(T_H - T_c) + \frac{\sigma e_{\text{eff}}(T_H{}^4 - T_C{}^4)}{i} \tag{7}$$

Also, in terms of "apparent k,"

$$\frac{q}{A} = (\text{Apparent } k)\frac{(\Delta \text{ Temperature})}{(\Delta \text{ Thickness})} = (\text{Apparent } k)\frac{(T_H - T_C)}{(\Delta X_t)} \tag{8}$$

Equating Eqs 7 and 8 and solving for apparent k,

$$\text{Apparent } k = k + \frac{(\Delta X_t)}{(i)}\frac{(1)}{(T_H - T_C)}\sigma e_{\text{eff}}(T_H{}^4 - T_C{}^4) \tag{9}$$

The foregoing terms are known from determinations of apparent k according to ASTM Test for Steady-State Thermal Transmission Properties by Means of the Guarded Hot Plate (C 177-76) except for k, i, and e_{eff}. The term e_{eff} can be calculated from the total hemispherical emissivity of the insulating fiber. The constants k and i may be determined for a given insulation specimen if apparent-k data are available from tests at two different temperature conditions by the simultaneous solution of two equations in two unknowns. Once k and i have been established, apparent k may be estimated for conditions other than those under which guarded hot-plate determinations were made.

Model Testing

Model validity has been tested by using ASTM Method C 177-76 data at two relatively low temperature levels to establish the constants k and i and then comparing model predictions with actual measurements of apparent k at higher temperature levels. Six specimens have been studied to date, five mineral wool insulations and one ceramic fiber insulation. Results are given in Table 1. As noted in the table, published emissivity values for the materials comprising the insulations were used in the absence of actual emissivity data for the specimens tested. Effective emissivities were calculated from the equation

$$e_{\text{eff}} = (e_1\, e_2) / [(e_1 + e_2) - (e_1\, e_2)]$$

for radiant heat transfer between infinite parallel planes [*1*].[2]

Perhaps the first observation that one might make in examining the validity test results is that model predictions are generally within accepted error limits of the measured apparent-k values. Discrepancies between calculated and measured values are less than 2 percent for three of the

[2]The italic numbers in brackets refer to the list of references appended to this paper.

TABLE 1—*Model validity test results.*

Insulation			Model Constants		Temperatures			Apparent k,	
Type	Density, Kg/m³	Thickness, ΔX_t, m	i[a]	k,[b] W/m·K	Hot Surface, T_H, k	Cold Surface, T_C, K	e[c]	Calculated[d] W/m·K	Measured, W/m·K
Mineral wool 1	101	0.0249	10.9	0.0262	307	286	0.90	...	0.038
Mineral wool 1	101	0.0249	10.9	0.0262	516	494	0.90	...	0.082
Mineral wool 1	101	0.0249	10.9	0.0262	681	664	0.90	0.157	0.150
Mineral wool 2	134	0.0249	11.5	0.0261	307	286	0.90	...	0.037
Mineral wool 2	134	0.0249	11.5	0.0261	516	496	0.90	...	0.080
Mineral wool 2	134	0.0249	11.5	0.0261	683	661	0.90	0.150	0.140
Mineral wool 3	149	0.0508	38.0	0.0373	396	351	0.90	...	0.050
Mineral wool 3	149	0.0508	38.0	0.0373	487	409	0.90	...	0.061
Mineral wool 3	149	0.0508	38.0	0.0373	558	488	0.90	0.074	0.074
Mineral wool 4	186	0.0434	29.0	0.0343	394	352	0.90	...	0.049
Mineral wool 4	186	0.0434	29.0	0.0343	487	409	0.90	...	0 061
Mineral wool 4	186	0.0434	29.0	0.0343	559	487	0.90	0.075	0.074
Mineral wool 5	237	0.0259	21.0	0.0360	307	286	0.90	...	0.042
Mineral wool 5	237	0.0259	21.0	0.0360	514	496	0.90	...	0.066
Mineral wool 5	237	0.0259	21.0	0.0360	682	662	0.90	0.107	0.105
Ceramic fiber	243	0.0259	7.0	0.0399	307	286	0.70	...	0.052
Ceramic fiber	243	0.0259	7.0	0.0399	514	496	0.56	...	0.082
Ceramic fiber	243	0.0259	7.0	0.0399	1152	1136	0.25	0.222	0.250

[a] A constant representing the number of hypothetical insulation layers.
[b] A constant representing the conductivity coefficient of heat transfer.
[c] Assumed emissivity of insulating fiber based upon published data for the various material types.
[d] Calculated value based upon the equation

$$\text{Apparent } k = \frac{(\Delta X_t)}{(i)} \frac{(l)}{(T_H - T_C)} (\sigma) (e_{\text{eff}}) (T_H^4 - T_C^4) + (k)$$

where

$$e_{\text{eff}} = \frac{(e_1 e_2)}{(e_1 + e_2) - (e_1 e_2)}$$

mineral wool specimens. The discrepancy between calculated and measured apparent-k values for the ceramic fiber specimen is greater, but this is not surprising considering the use of assumed emissivity data and the degree of extrapolation involved (that is, from mean temperatures of 23 and 232°C for establishing constants to a mean temperature of 871°C for validity testing).

It is very interesting to note that reasonable predictability of ceramic fiber insulation apparent-k values could be achieved only when emissivity factors were varied with temperature. This is consistent with known material behavior and emphasizes the theoretical basis for the simplified model as opposed to a strictly empirical modeling approach. One might suspect that use of actual emissivity data at the various temperatures would have improved predictability of the model for the ceramic fiber insulation specimen.

Another interesting observation at this point is that the value of emissivity used in the calculation of effective emissivity has no bearing on model predictability as long as emissivity may be assumed to be constant with temperature. This is in view of the fact that e_{eff}/i under conditions of constant emissivity is a constant, although of less obvious physical significance than that of either e_{eff} or i considered separately. Thus, incorrect values for constant emissivity introduce errors into calculated values of i, but do not affect calculated values of apparent k. Of course, if emissivity varies significantly over the temperature range in question, accurate predictions are possible only if the actual emissivity values are known.

Model Analysis

Conduction Component—Components of the "conductivity coefficient" as defined in the model are gas convection, solids conduction, and gas conduction. Gas convection in fibrous insulations of moderate density (that is, greater than about 16 kg/m^3) has been reported to be of negligible value by various investigators [*2–4*]. The contribution of solids conduction to heat transfer through porous fibrous insulations is, likewise, reported to be relatively insignificant [*5*]. Thus, these components should have little effect upon the conductivity coefficient with variations in temperature, and the assumption of its constancy would appear justified.

Still unexplained, however, is the apparent lack of effect from ignoring the accepted increase in thermal conductivity of air with temperature. At least two possibilities might be suggested in addition to the possibility of a fortuitous coincidence of compensating errors. First, taking due consideration of the difficulties associated with its determination, the variation in thermal conductivity with temperature for air may not be so great as current measurements indicate. The historical trend in published thermal

conductivity for air would appear to support this possibility. Presumably, this trend may be due to improvements in techniques for separating convective and radiative effects from the property being measured. Secondly, it is possible that the model "radiation coefficient" for fiber-to-fiber heat transfer may unwittingly include compensation for potential radiative heat transfer within the gas medium. Exploration of these possibilities is beyond the scope of this paper.

Radiation Component—The complexity of radiant heat transfer within a fibrous medium is an almost insurmountable barrier to development of a model that is both practical and capable of withstanding a rigorous theoretical analysis. Several different approaches have been taken with varying degrees of success. Using the concept of layer-to-layer transfer presented in this paper, one investigator has derived an expression for a radiation coefficient similar to the one contained in the proposed model [*6*]. However, the expression applies only to transfers between two adjacent layers. It is neither suggested nor at all obvious in the form presented that the expression might apply to the total insulation thickness. Another investigator using a different approach has developed an expression for layer-to-layer radiation heat transfer applicable to full insulation thickness [*7*]. Model development assumes that radiation from layer to layer is constant with no allowance for the influence of decreasing temperature level on the relative contribution of radiant heat transfer to the constant total heat transfer. The model, which was tested in the ambient temperature range, is said to apply for moderate temperature differentials across fibrous insulating materials. Still another approach toward modeling of radiant heat transfer has been based upon infrared transmission measurements [*8*]. The net radiative heat transfer is treated as the difference between radiant fluxes in the forward and backward directions. Two-flux and four-flux models are described, both of which are primarily applicable to materials with low radiation absorptivity.

Perhaps the most notable aspect of the proposed model's radiation coefficient in comparison with those of other models is its simplicity. The assumed lack of restrictions, other than that the layer-to layer emissivity must be essentially constant, is also in contrast with other radiation models.

General—The heart of the proposed model is its derived empirical constants, k and i. Although empirical, the values of these constants are generally in accordance with expectations based upon theoretical considerations. For example, values for k in Table 1 approximate the thermal conductivity of air at normal ambient temperature and tend to increase with specimen density. Also, the values for i in Table 1 tend to increase with both thickness and density, except for that of the ceramic fiber specimen. The ceramic fiber's i value is much lower than its comparative density would suggest. This difference between the mineral wool speci-

mens and the ceramic fiber specimen may be attributable to a basic difference in the mechanisms of radiant heat transfer.

Potential Applications

Material Characterization—Studies to date suggest that fibrous insulations of a particular type may be characterized by performance constants in the simplified mathematical model for apparent k (that is, k, i, and e_{eff}). Although only fibrous insulations have been tested, there is reason to believe that the model could also apply to other types of insulations that depend upon the creation of numerous tiny air cells for their insulating efficiency.

It is known that apparent k is a function of the temperatures producing a given mean and not of the mean temperature itself. This fact is apparently accounted for by model predictions of different values for apparent k for different combinations of temperatures resulting in the same mean temperature. The trend is toward higher values of apparent k as the deviation of test temperatures from the mean is increased, which is as one might expect.

Assuming at least the qualitative accuracy of estimated temperature effects, the model suggests an explanation for different apparent-k values for flat-slab insulations and pipe insulations of the same material. Flat-slab tests by ASTM Method C 177 are usually run with relatively low temperature differentials. Pipe insulation tests by ASTM Test for Thermal Conductivity of Pipe Insulation (C 335-75) are usually conducted with the cold surface near ambient temperature and the hot surface at the temperature required to produce the desired mean. The resulting higher temperature differential for ASTM Method C 335 would, by the model's prediction, result in an observed tendency toward higher apparent k values for pipe insulations than for supposedly identical flat-slab insulations tested by ASTM Method C 177.

The physical significance of the empirical constant, i, in the model suggests a further explanation for differences in values from ASTM Method C 177 and C 335. It was stated in the model's derivation that i, the number of hypothetical radiation transfers, is equal to the number of hypothetical insulation layers as long as any cold-surface boundary effects may be neglected. This is not the case in ASTM Method C 177, since emissivity of the guarded hot-plate cold surface is always less than 1.0. On the other hand, cold surfaces of pipe insulations tested by ASTM Method C 335 usually radiate into an open room that may approximate a black body. Thus, the additive effect of the hindrance to radiant heat transfer presented by the guarded hot plate's cold surface would be expected to result in a lower apparent k by ASTM Method C 177 than for an identical insulation tested by ASTM Method C 335. An extension of

this reasoning could also at least partially explain and help quantify the observed thickness dependency of apparent k when insulations are tested by ASTM Method C 177.

Heat Loss Estimation—Preliminary work indicates that model characterization of insulating materials would afford a convenient approach to heat loss calculations. This is particularly true of those materials exhibiting a relatively constant emissivity over a specified temperature range, although special treatment would permit calculations for materials with variable emissivity.

In order for this approach to be of any practical value, the number of hypothetical layers in a particular type of insulation must be directly proportional to insulation thickness. Limited testing of varying thicknesses of the same insulation type shows this trend, which should not be surprising if one considers the fundamental physical properties thought to influence the spacing of hypothetical layers. If the number of hypothetical layers is indeed proportional to thickness, a new insulation characteristic constant may be introduced as defined by

$$L = \frac{(i)}{(\Delta X_t)} \tag{10}$$

where

L= hypothetical layers per unit thickness (for example, layers/m) of a particular insulation type,
i= layers in guarded hot-plate test specimen of insulation type, and
ΔX_t= thickness of guarded hot-plate test specimen of insulation type.

Then, the number of hypothetical layers in varying thicknesses of an insulation type follows as

$$i = (L)\,(\Delta X_t) \tag{11}$$

where

i= layers in installed insulation, and
ΔX_t= installed insulation thickness.

Referring to the mathematical derivation of apparent k, it was shown in Eq 7 that for flat slabs

$$\frac{q}{A} = \frac{(k)}{(\Delta X_t)}(T_H - T_C) + \sigma e_{\text{eff}} \frac{(T_H^4 - T_C^4)}{(i)} \tag{12}$$

Substituting for i

$$\frac{q}{A} = \frac{(k)}{(\Delta X_t)}(T_H - T_C) + \sigma e_{\text{eff}} \frac{(T_H^4 - T_C^4)}{(L)\,(\Delta X_t)} \tag{13}$$

Solutions for the foregoing equation are possible through utilization of the knowledge that equilibrium heat flow through an insulation must equal

the rate of heat dissipation from the insulation surface. Mathematical expressions have been developed for rates of heat dissipation from various surfaces in terms of certain constants, T_C, and T_A (where T_A is the ambient temperature). Where surface loss equations apply, and if k, ΔX_t, T_H, e_{eff}, L, and T_A are known, the equality of insulation heat flow with surface heat dissipation may be expressed in terms of a single unknown, T_C. This equation can be easily solved for T_C and the corresponding value for q/A.

It can be shown that a similar approach may be used for estimation of heat losses through cylindrical insulations if the characterizing constants are known for the insulation type in question. In this case, concentric cylindrical surfaces are hypothesized instead of parallel planes. Calculations are complicated by variation in areas of these hypothetical surfaces with distance from the pipe surface. However, solutions may be readily obtained by computer through iterative calculation procedures.

Insulation Temperature Profile Estimation—Since heat loss estimations based upon the simplified mathematical model involve layer-to-layer calculations, intermediate results may be used to predict insulation temperature profiles. An example of temperature profile predictions is shown in Fig. 2.

In developing the temperature profile data of Fig. 2, insulation characteristic constants for mineral wool-Specimen 3 were assumed to apply for a thickness of 2.54-cm (1-in.) over either a flat surface or 7.62-cm (3-in.) pipe (that is, $k = 0.0373$, $L = 38/0.0508 = 748$, and $e = 0.90$). The hot surface and ambient temperatures were taken to be 616 and 300 K, respectively. Insulation heat flow rates were adjusted by trial and error

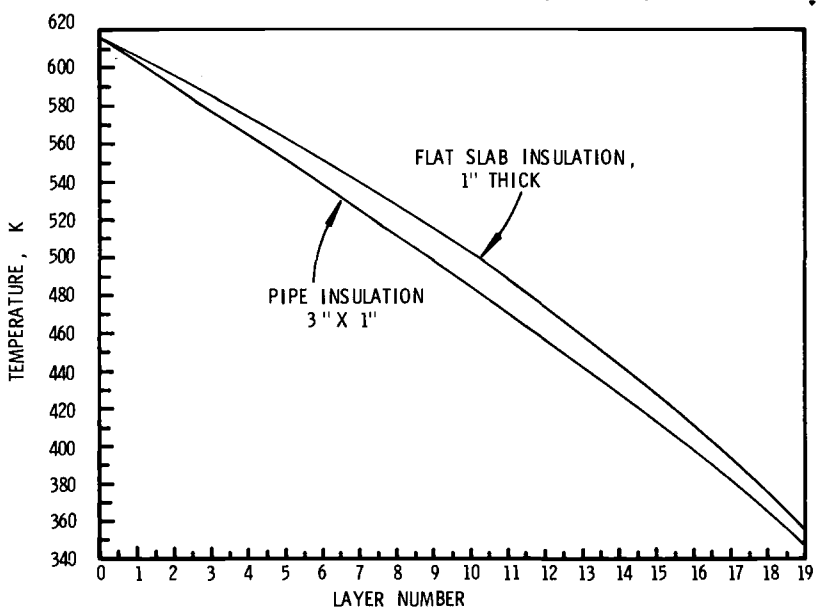

FIG. 2—*Heat-transfer model generated temperature profiles.*

to obtain equality with estimated rates of surface heat dissipation at model-predicted cold-surface temperatures.

The temperature profile curves are concave downward for both the flat surface and pipe insulations. This is the result of a model-predicted predominance of radiant heat transfer at relatively low temperature differentials between hypothetical layers closest to the hot surfaces. The effect is less pronounced in the pipe insulation because of the offsetting influence of decreasing heat flux as the distance of hypothetical layers from the hot surface is increased.

No attempt has been made to verify predicted temperature profiles due to the virtual impossibility of measuring internal insulation temperatures at the required close intervals without distorting thermal performance. If the predicted temperatures are reasonably accurate, model-generated temperature profiles could promote an understanding of difficulties encountered in assuming linear profiles for estimation of mean temperatures and corresponding apparent-k values of insulating materials.

Conclusions

A simplified mathematical model has been used to generate apparent-k data for a variety of fibrous insulations over a wide temperature range. The model has also been adapted for use in the estimation of heat flow rates through various insulation shapes without relying upon the concept of mean temperature. Although absolute validity has not been established, limited verification tests demonstrate a surprising degree of predictability in view of the simplifying assumptions made in the model's derivation. Subject to further verification and possible refinements, the model could afford a practical solution to the problem of representing thermal insulation performance through its characterizing constants for different insulations.

References

[1] Wilkes, G.B., *Heat Insulations*, Wiley, New York, 1950, p. 19.

[2] Bankvall, C.G. in *Heat Transmission Measurements in Thermal Insulations*, *ASTM STP 544*, American Society for Testing and Materials, 1974, p. 43.

[3] Brendeg, E. and Frivik, P.E. in *Heat Transmission Measurements in Thermal Insulations*, *ASTM STP 544*, American Society for Testing and Materials, 1974, p. 156.

[4] Fournier, D. and Klarsfield, S. in *Heat Transmission Measurements in Thermal Insulations*, *ASTM STP 544*, American Society for Testing and Materials, 1974, p. 237.

[5] Verschoor, J.D. and Greebler, P., *Transactions*, American Society of Mechanical Engineers, Aug. 1952, p. 964.

[6] Jakob, M., *Heat Transfer*, Vol. 1, Wiley, New York, 1949, p. 87.

[7] Bankvall, C.G., *Journal of Testing and Evaluation*, American Society for Testing and Materials, Vol. 1, No. 3, May 1973, p. 235.

[8] Linford, R.M.F., Schmitt, R.J., and Hughes, T.A. in *Heat Transmission Measurements in Thermal Insulations*, *ASTM STP 544*, American Society for Testing and Materials, 1974, p. 68.

A. H. Striepens[1]

Heat Transfer in Refractory Fiber Insulations

REFERENCE: Striepens, A. H., "**Heat Transfer in Refractory Fiber Insulations**," *Thermal Transmission Measurements of Insulation, ASTM STP 660*, R. P. Tye, Ed., American Society for Testing and Materials, 1978, pp. 293–309.

ABSTRACT: Test results are presented for the thermal conductivity, over a broad range of temperatures and pressures, of two refractory blown fiber insulations. The data, which were obtained for several bulk densities of each material, are compared with predictions from a theoretical expression that accounts for radiation transmission as well as solid and gas conduction contributions to the effective conductivity. The simple model utilized provides a remarkably accurate prediction of insulation performance for the materials of interest and, therefore, represents a useful tool for design purposes, minimizing the amount of actual testing necessary to characterize candidate materials. Criteria are indicated by which it is possible to determine whether the model will be applicable to a given fiber insulation. This study was accomplished over a two and one-half year period, in support of the Space Shuttle thermal protection system design.

KEY WORDS: fibrous insulation, thermal insulation, heat transmission, thermal conductivity, guarded hot plate, infrared transmission, high-temperature tests

Nomenclature

- C Constant
- D Effective fiber diameter
- f Fiber volume fraction
- k_{cd} Effective conductivity attributable to combined solid and gas conduction
- k_{cv} Effective conductivity attributable to heat transfer by convection within the insulation
- k_{eff} Effective thermal conductivity
- k_F Thermal conductivity of fiber material
- k_g Thermal conductivity of the free gas
- k_G Thermal conductivity of the gas within the pores of the insulation
- k_{rt} Effective conductivity attributable to radiation transmission
- k_{scd} Effective conductivity attributable to series solid and gas conduction
- k_{ssc} Effective conductivity attributable to solid and solid-to-solid contact conduction
- L Thickness of the insulation

[1]Member of technical staff, Rockwell International, Space Division, Downey, Calif., 90241.

L_F Effective pore size
L_G Mean free path of the gas
M Extinction cross section
N Bulk density-independent backscattering cross section
N' Bulk density-dependent backscattering cross section
p Pressure
P Absorption cross section
q Rate of heat flow per unit area; heat flux
T Absolute temperature
α Porosity parameter
ϵ Emittance
λ_R Mean free path for photon-fiber collisions
ρ Bulk density
ρ_s Surface density of insulation specimen
σ Stefan-Boltzmann constant
ϕ_p, ϕ_s Porosity parameters

In the Space Shuttle thermal protection system, the airframe structure will be shielded from excessive temperature in places through the use of refractory fiber insulation blankets. Preliminary screening resulted in the selection of two commercially available aluminosilicate fiber felts, one with chromia addition. Selection of densities and thicknesses for specific applications necessitated thorough characterization of the thermal performance of several densities of each material at temperatures as high as 980°C (1800°F) and pressures as low as 1.33 Pa (10^{-2} torr). Principal among the properties required for design and thermal analysis was thermal conductivity. Direct measurement with conventional guarded hot-plate apparatus was capable of providing fairly reliable atmospheric and reduced pressure data at temperatures to approximately 430°C (800°F). However, uncertainty in guard-to-test-area heater temperature balance was a persistent problem encountered when operating the ceramic core heaters above 430°C (800°F) at all pressures. The resultant systematic errors made it difficult to obtain reproducible and reliable high-temperature data. In the course of the material characterization, it was also observed that the test results at elevated temperatures were consistently higher than values suggested by the manufacturer (available for atmospheric pressure only). The theoretical estimation of the effective conductivity of these materials was therefore attempted in order to resolve the discrepancy between experimental results and expected behavior at elevated temperatures and, further, to minimize high-temperature testing at both atmospheric and reduced pressures. Temperatures in excess of 700°C (1300°F) were particularly severe for the heaters, and excessive time had to be devoted to repairs. Existing theoretical models and expressions for prediction of heat transfer in porous materials, particularly fiber systems, were scrutinized and a composite expression, which seemed appropriate to the materials of interest, was adopted for use. The necessary physical data for the fibers was obtained, either from the manufacturer or by direct experimental determination. Finally, predictions based on the theoretical model were

compared with the experimental results at both atmospheric and reduced pressures.

Review of Available Data

Both of the materials evaluated consist of resin-bonded aluminosilicate refractory fibers, so-called because of their usefulness at temperatures as high as 1260°C (2300°F) for the TF material and 1480°C (2700°F) in the case of the DF felt. The latter includes about 4.5 percent chromia addition to the fiber composition. Physical data for the fibers are given in Table 1. The as-received materials contain as much as 12 percent by weight of thermosetting organic binder (depending on the bulk density) as well as significant amounts of "shot," approximately globular particles said to be characteristic of blown fibers. The fibers in these felts are present in a rather wide range of diameters.

Existing literature relating to the thermal conductivity of the refractory fiber insulations is sparse. The earliest work is attributable to Verschoor and Greebler [*1*],[2] who tested an experimental ceramic fiber insulation (mean diameter 2.6 μm) at temperatures up to 150°C (300°F). They developed a suitable model for estimating the heat transfer attributable to gas conduction in such insulation, as well as an expression for the radiation transmission, and were able to successfully predict the effective conductivity by combining these contributions, while neglecting convection and fiber contact conduction. Subsequently, Greebler [*2*] reported on the results of extensive conductivity testing of an aluminosilicate fiber felt at temperatures up to 590°C (1100°F) and densities ranging from 32 to 192 kg/m^3 (2 to 12 lb/ft^3). Based on the reported data, Greebler derived a semi-empirical expression for the radiation contribution to the effective conductivity, as well as a wholly empirical expression for the contribution

TABLE 1—*Fiber properties.*

Designation	TF	DF
Composition	Al_2O_2 SiO_2 ...	Al_2O_3 SiO_2 Cr_2O_3
Temperature limit, deg C	1260	1480
Specific gravity	2.6	2.4
Mean diameter, μm	3.7	3.7
Effective diameter, μm	6.7	4.8

[2]The italic numbers in brackets refer to the list of references appended to this paper.

due to solid and solid-to-solid contact conduction. The material Greebler studied appears to be similar to the TF insulation. Thigpen and Short [3] also tested material similar to the TF insulation at temperatures to about 340°C (650°F). They compared their experimental results and manufacturer's data with predictions from a theoretical model for temperatures up to 540°C (1000°F) and demonstrated the effect of density and pressure on the effective conductivity, as had Verschoor and Greebler. Rolinski and Purcell [4] accomplished conductivity measurements of 128 kg/m^3 (8 lb/ft^3) material similar to the DF felt at temperatures up to 1290°C (2350°F) in air and 1070°C (1950°F) in vacuum. They made use of the so-called two-flux radiation transmission model and determined the infrared transmission characteristics of several insulation materials, but unfortunately did not report the necessary optical data for the material of interest. Furthermore, large guard-to-test-area heater temperature unbalances in much of their conductivity testing undoubtedly led to serious errors at the higher temperatures. Most recently, Dickson [5], in a study of evacuated load-bearing insulations, tested an aluminosilicate fiber blanket of high density (288 kg/m^3) (18 lb/ft^3) over a range of pressures from 13.3 to 10^5 Pa (0.1 to 760 torr), at a mean temperature of 390°C (734°F). He indicates the fiber diameter was about 2 μm. In these tests, the insulation thickness was reduced by compression under atmospheric pressure as the material was evacuated. Therefore the density was not constant throughout the test.

The available data relate to materials of several different, though similar, fiber types and sizes, and proved to be of little use in resolving the differences between our test data and the manufacturer's recommended values. Therefore, it was necessary to attempt a theoretical prediction of the material behavior, based on existing knowledge of the mechanisms of heat transfer in fiber insulations.

Theory

It is well known that heat is transferred through highly porous materials by a combination of mechanisms—namely, solid conduction, gas conduction, and radiation transmission. In fibrous insulation at elevated temperature, gas conduction and radiation have been shown to be the major contributors. In vacuum, gas conduction and convection are absent, of course, and radiation is the principal mode of heat transfer at high temperatures. When a material is tested under conditions in which radiation or convection or both are known to contribute to the measured heat flux, it has been recommended [6] that the derived proportionality constant relating heat flux and temperature gradient be referred to as an apparent or effective conductivity. It would clearly be desirable if this effective conductivity could be estimated as a simple summation of effective con-

ductivities attributable to the various modes of heat transfer, according to the relation

$$q_T = k_{eff}\frac{\Delta T}{L} = (k_{cd} + k_{cv} + k_{rt})\frac{\Delta T}{L} \tag{1}$$

Here, q_T is the combined heat flux and k_{cd}, k_{cv}, and k_{rt} are the effective conductivities due to combined solid and gas conduction, convection, and radiation transmission, respectively. This simplification of the heat-transfer process in porous insulation permits each mode to be analyzed separately. A rigorous approach would require a simultaneous solution for all the modes, since each mode is dependent upon the temperature gradient, which is controlled by the total heat transfer.

Theoretical expressions for estimating the magnitudes of the components of the effective conductivity have been derived by numerous investigators. These are based on the employment of idealized conceptions or models of the insulation structure. For most fiber batts, this structure is approximated by randomly oriented fibers with the majority of them arranged in more or less parallel planes which, in turn, are perpendicular to the usual direction of heat flow. Generally, therefore, a series model, or perhaps a combined series and parallel arrangement of lumped thermal resistances, has been assumed to approximate the effective thermal resistance of the insulation. Utilization of the derived expressions requires the knowledge or estimation of fiber mechanical, thermal, and optical properties as well as certain insulation structural parameters, any of which may be difficult or impossible to determine by direct experimentation. Examples are the photon mean free path and effective pore size in the insulation, and the thermal conductivity, emittance, and elastic modulus of the fibers. These difficulties have undoubtedly limited the application of some of the expressions, particularly those for the effective conductivity due to solid and solid-to-solid contact conduction. It remains, therefore, to assess the suitability of the existing relations for predicting the behavior of the refractory fiber insulations.

Conduction (k_{cd})

A thorough analysis of the combined conduction heat transfer in fiber insulations must take into account both parallel and series paths for fiber and gas conduction. This approach requires knowledge of the distribution of solid and gas phases in the fiber batt. Thigpen and Short [3], who utilized a geometrically regular array of square fibers as their structural model, were able to express the distribution in terms of the fiber volume fraction (an easily determined parameter). Using their approach, but neglecting radiation, one can define a unit cell in the insulation and arrive at the following expression

$$k_{cd} = f^2 k_F + \frac{4f(1-f)}{\frac{1}{k_G} + \frac{1}{k_F}} + (1-f)^2 k_G \tag{2}$$

where f is the fiber volume fraction and k_F and k_G are the fiber and gas conductivities, respectively. The first term represents direct (parallel) solid conduction, assuming perfect contact between the fibers. The second term represents the series solid and gas conduction, and the last term the direct (parallel) gas conduction. Bankvall [7] has analyzed the situation in a more general manner, defining arbitrary structural (porosity) parameters that indicate the proportions of the condensed phases in series and parallel combination. Bankvall derived the expression

$$k_{cd} = (1-\phi_p)\, k_F + \frac{(1-\alpha)\, k_F\, k_G}{\phi_s k_F + (1-\phi_s)\, k_G} + \alpha\phi_p k_G \tag{3}$$

where the porosity parameters α, ϕ_p, and ϕ_s are related to the total porosity $(1-f)$ by the relation

$$(1-f) = (1-\alpha)\,\phi_s + \alpha\phi_p \tag{4}$$

The similarity between Eqs 2 and 3 is apparent. If Bankvall's porosity parameters are expressed in terms of the geometrical factors for the Thigpen and Short model, the expressions are found to be identical. Bankvall, however, did not deduce the values of the porosity parameters from consideration of a structural model, but instead determined them empirically from measurements of effective conductivity of a particular glass fiber insulation. While this approach may well serve to interpret the behavior of a given insulation for which conductivity data are available, the empirically determined values of the porosity parameters can be no more accurate than that data, and cannot be assumed to be typical of other fiber insulations.

An effective conductivity due to series solid and gas conduction (k_{scd}) may also be derived from consideration of a simple, condensed fiber model in which the fiber batt is represented by parallel layers of solid separated by layers of gas. This approach was used by Verschoor and Greebler [1] and Hager and Steere [8]. Calculation of the effective conductivity of a slab of solid (fiber) in series with a slab of gas phase, when the fiber conductivity greatly exceeds that of the gas and the fiber volume fraction is very small, leads to the straightforward approximation

$$k_{scd} = \frac{k_G}{(1-f)} \tag{5}$$

Here k_G is the conductivity of the gas within the pores of the insulation. This has been demonstrated to be a function of the effective pore size,

L_F, and mean free path of the gas, L_G, at the temperature and pressure of interest [*1, 7, 9*]. Thus

$$k_{scd} = \frac{[k_g]T}{(1-f)}\left(\frac{L_F}{L_F + L_G}\right)_{p,T} \tag{6}$$

Here k_g is the conductivity of the free gas at temperature T. The effective pore size, which may be thought of as a mean free path for molecule-fiber collisions, is given as

$$L_F = \frac{\pi D}{4f} \tag{7}$$

D, the effective diameter, is defined as the ratio of the mean square diameter to the mean diameter. This quantity is said to give a truer value of the effective pore size than would the mean diameter, for insulation with a wide range of fiber diameters. The fiber volume fraction, f, is readily calculated as the ratio of the insulation bulk density to the fiber density. Thus it appears that Eq 6 requires the knowledge only of readily obtainable insulation structural parameters, and the gas conductivity. It should be noted that for a typical fiber insulation with high porosity, the expression $L_F/(L_F + L_G)$ approaches unity at atmospheric pressure. At this pressure, the value of k_{scd} can exceed the conductivity of the free gas. This results from the influence of the high series conductance due to the fibers, which make up part of the conduction path.

In spite of several fairly sophisticated analyses typified by that of Strong et al [*9*], no really satisfactory theoretical expression exists for predicting the solid and solid-to-solid contact conduction. k_{ssc}. The problem with many of the existing expressions is that they require knowledge of the load per contact as well as fiber mechanical properties such as the modulus of elasticity and Poisson's ratio, while all require knowledge of the fiber conductivity. Qualitatively, the behavior is predictable. One would certainly expect k_{ssc} to increase with the bulk density or fiber volume fraction. One would also expect the fiber conductivity to directly influence k_{ssc}, but here the problem of the contact resistance arises. In the uncompressed, binder-free condition, the fiber conductivity probably has a limited effect on the value of k_{ssc}. Assuming perfect contact, Hager and Steere [*8*] arrived at

$$k_{ssc} = 4f^3 k_F \tag{8}$$

which would lead to the conclusion that direct conduction through the fibers is negligible for insulations with greater than 90 percent porosity. As was already noted (Eq 2), Thigpen and Short, similarly assuming perfect contact, concluded that

$$k_{ssc} = f^2 k_F \tag{9}$$

Some authors have taken an empirical approach, deducing k_{ssc} from experimental conductivity data. Greebler [2] found that for an aluminosilicate fiber insulation ($D = 3.6\ \mu$m), the relation

$$k_{ssc} = 4.5 \times 10^{-5}\, \rho\ w/(m \cdot K) \tag{10}$$

satisfactorily represented the data for densities up to 192 kg/m^3 (12 lb/ft^3) if the density is expressed as kg/m^3.

Convection (k_{cv})

Considering the fact that the lowest material density of interest in this study was 96 kg/m^3 (6 lb/ft^3), and the minimum temperature was 38°C (100°F), heat transfer by convection may safely be assumed to make no measurable contribution. In the interest of brevity, consideration of the theoretical basis for estimating k_{cv} is not included in this presentation.

Radiation Transmission (k_{rt})

The processes that have been recognized as determining the magnitude of the radiation heat transfer through fiber insulations are (1) direct transfer of radiation from the hot to cold faces of the material by a series of scattering reflections at the fiber surfaces, (2) a process of absorption and reemission by the fibers, resulting in a net transfer of heat, and (3) direct transmission of radiation through the voids and fiber material; for typical high-temperature fiber insulations, however, direct transmission is usually negligible. Although the scattering and absorption processes may both be present in a given material, often one or the other dominates. The effective conductivity for any or all of these processes may be referred to as the conductivity due to radiation transmission, k_{rt}. Many approaches have been taken in order to derive expressions for estimating k_{rt}. The simplest of these require knowledge only of the effective pore size in the insulation, since they assume the fibers are effectively black. Jakob, for example, considered absorption and reemission through a porous material whose structure may be approximated as a series of opaque plates [*10*]. He concluded that the conductivity due to radiation varies as the cube of the absolute (mean) temperature, and the spacing between the plates. This approach has been refined by several authors, who attempted to compute the radiant transfer between nonblack fibers, also taking into account fiber orientation [*1, 2, 8, 9*]. If it is assumed that the ΔT is small with respect to the absolute mean temperature, the resulting expressions tend to be of the form

$$k_{rt} = 4\, \sigma\, T^3\, \lambda_R \tag{11}$$

where λ_R may be thought of as an effective mean free path for photon-

fiber collisions. The value of λ_R depends upon the theoretical and structural model used by the various authors. It is related to L_F, the mean free path for molecule-fiber collisions discussed earlier, and expressions for k_{rt} often incorporate L_F or the ratio D/f. Equation 11 serves to qualitatively describe the heat transfer by radiation, showing it to be dependent on the cube of the absolute temperature and the fiber structural parameters, which partly determine λ_R. Insofar as λ_R includes the optical behavior or radiational properties of the fibers, the usefulness of the various theoretical expressions hinges on availability or experimental determination of data for these properties. Hager and Steere [8], whose work involved fibers with diameters larger than the dominant wavelengths, have pointed out that for common fiber insulations where the fibers have diameters less than or equal to the dominant infrared wavelengths (2 to 5 μm), the concept of a fiber "emittance" becomes theoretically questionable.

A different approach considers the phenomena of both scattering and absorption in the insulation, analyzing the radiant transfer in terms of integrodifferential equations describing the directed radiation fluxes, together with a differential energy balance with appropriate boundary conditions. The so-called two-flux model was originally utilized by Hamaker [11] and has been further applied and developed by others [12–15]. This model leads to differential equations expressing the radiant fluxes in the forward and backward directions in terms of the backscattering cross section, N, the absorption cross section, P, and the interception cross section, $M(=N+P)$. For material in which scattering is the dominant mechanism ($N \gg P$), the differential equations were solved by Larkin [12] to yield an expression for the heat flux due to radiation transmission in terms of the boundary conditions and N' as follows

$$q_{rt} = \frac{\sigma\,(T_0^4 - T_L^4)}{1/\epsilon_0 + 1/\epsilon_L - 1 + N'L} \tag{12}$$

This expression supposes N' to be independent of wavelength (or source temperature), a condition that is reasonably approximated when N' varies only weakly with temperature and the temperature difference $(T_o - T_L)$ is small. The last restriction also permits the assumption $\epsilon_0 = \epsilon_L$ when the boundary surfaces are of the same material. It can be shown that when $(T_o - T_L) \ll T$, the difference in the fourth powers of the temperature can be approximated by $4\,T^3\,\Delta T$. Defining a conductivity due to radiation transmission by the expression $q_{rt} = k_{rt}\,(\Delta T/L)$ and equating the two expressions for the heat flux leads to the following solution for k_{rt}

$$k_{rt} = \frac{4\,\sigma\,T^3 L}{2/\epsilon - 1 + N'L} \tag{13}$$

Equation 13 may be further simplified if $(2/\epsilon - 1) \ll N'L$ to yield finally

$$k_{rt} = \frac{4\sigma T^3}{N'} \tag{14}$$

The similarity to Eq 11 is obvious. λ_R being equivalent to $(N')^{-1}$.

Estimation of Effective Conductivity (k_{eff})

Based on the considerations outlined previously, it remains to select appropriate expressions for k_{cd} and k_{rt} to incorporate into Eq 1 for prediction of the effective conductivity. For estimating the magnitude of the combined solid and gas conduction term, k_{cd}, the general expression attributable to Bankvall (Eq 3) presents difficulties since data are not available for either the fiber conductivity or porosity parameters for the insulations of interest. The related expression derived by Thigpen and Short requires only the assumption of values for k_F, but is subject to the limitations of the highly simplified model that they utilized. A much simpler approach is to combine the Verschoor and Greebler expression for k_{scd} (Eq 6) with a correction term for the solid and solid-to-solid contact conduction. For the added correction, Greebler's empirical relation seems appropriate. The assumption that k_{ssc} is constant over a broad temperature range will result in little error since this represents such a small part of the effective conductivity. Thus the conductivity due to combined solid and gas conduction can be calculated from the expression

$$k_{cd} = \frac{k_g}{(1-f)}\left(\frac{L_F}{L_F + L_G}\right) + C\rho \tag{15}$$

Alternatively k_{cd} can be estimated from Eq 2 if values for k_F are assumed. Melonas et al [*16*] present conductivity data for an aluminosilicate glass over the temperature range 70°C to 530°C (160°F to 980°F). The data indicate a weak temperature dependence. Assuming their values are applicable to the TF fibers, k_{cd} was calculated for 96 to 384 kg/m^3 (6 to 24 lb/ft^3) material, over the temperature range of 38°C to 480°C (100°F to 900°F). Values calculated from Eq 2 were in good agreement with those calculated from Eq 15. The simplicity of the latter, and the uncertainties in the use of the former, recommend Eq 15 for engineering calculations.

For fiber materials for which backscattering and absorption cross sections have been determined experimentally, backscattering is usually found to be the governing mechanism for radiation attenuation. Schmitt et al [*14*] have reported measurements on Mullite fibers ($3Al_2O_3 \cdot 2SiO_2$) that indicate N is more than two orders of magnitude greater than P for that material, in the range of fiber sizes from 2.5 to 6 μm. Thus it appeared to be a reasonable assumption that the aluminosilicate refractory fibers of interest would behave similarly. On this basis, it was decided that measurements of the cross sections for the refractory fibers would be

worthwhile, and Eq 13 was selected for use in estimating the effective conductivities. The assumptions on which this expression is based happen to correspond very well to the conditions that prevail in the thermal conductivity testing using the guarded hot plate. These assumptions are (1) that ΔT is small in comparison with T, and (2) that boundary surfaces of essentially identical emittances behave as gray radiators. Furthermore, it was found, upon experimental determination of the infrared transmittances and the cross sections for the fiber felts, that the remaining conditions, namely $N \gg P$ and N constant with temperature over the range T_O to T_L, are also sufficiently satisfied.

The theoretical expression for the effective conductivity can now be completed by combining Eq 13 and 15 to obtain

$$k_{eff} = \frac{4 \sigma T^3 L}{2/\epsilon - 1 + N'L} + \left[\frac{k_g}{(1-f)} \left(\frac{L_F}{L_F + L_G} \right) \right]_{P,T} + C \rho \qquad (16)$$

This expression demonstrates several established and important aspects of the behavior of fiber insulations. The first term (k_{rt}) indicates that the effective conductivity may be a function of the batt thickness as well as the emittance of the bounding surfaces. The second term (k_{scd}) defines the pressure dependence of the effective conductivity, based on the variation of the mean free path of the gas within the insulation, while the third term (k_{ssc}) reflects the dependence of the solid and solid-to-solid contact conductance contribution on the fiber volume fraction, which varies directly as the bulk density. The first two terms, which account for the largest part of the effective conductivity at atmospheric pressure and at moderate to elevated temperatures, are well founded in theory and have been verified experimentally for many materials. The third term, although empirical, represents only a small fraction of k_{eff} at atmospheric pressure.

Test Procedure

All thermal conductivity test data were obtained with guarded hot-plate assemblies operated in strict accord with the ASTM Test for Thermal Conductivity of Materials by Means of the Guarded Hot Plate (C 177-71). The specimens were tested in most cases in the binder-free condition and were 200 mm (8.0 in.) in diameter and 10 to 13 mm (0.4 to 0.5 in.) thick. Temperature gradients were held at low levels (1.5 to 5.5 deg C/mm) but well above the limit recommended by the ASTM procedure, for testing of good insulators. The temperature differences across the specimens were calculated from the indications of Awg No. 30 thermocouples embedded in the surface plates of the hot- and cold-side heaters.

The radiation transmission parameters were obtained from room temperature total infrared transmittance measurements on specimens of sev-

eral thicknesses for each of the materials, much as described in Ref *15*. The blackbody source temperature was varied from 480 to 980°C (900 to 1800°F) with the specimens at essentially room temperature. Infrared transmittance data as a function of surface density for a given source temperature can be correlated using the two parameters, the backscattering cross section, N, and the interception cross section, M, in accordance with the relation

$$\tau = \frac{2\sqrt{M^2-N^2}}{M+\sqrt{M^2-N^2}} e^{-\rho_s \sqrt{M^2-N^2}} \left[\sum_{n=0}^{n=\infty} (-1)^n \left(\frac{M-\sqrt{M^2-N^2}}{M+\sqrt{M^2-N^2}} \right)^n e^{-2n \rho_s \sqrt{M^2-N^2}} \right]$$

where τ is the total infrared transmittance of a specimen with surface density ρ_s.

Experimental Results

The total infrared transmittance determinations were made on binder-free specimens of each material, using the 96 kg/m³ (6 lb/ft³) density. The transmittance is determined as a function of surface density and the data are therefore applicable to any bulk density of a material so long as the fibers are the same for all bulk densities. The necessity of using very thin specimens results in considerable data scatter due to the inhomogeneities in the specimens. Energy-limiting effects at the lowest source temperature also rendered that particular set of data doubtful. Figure 1 presents the experimentally determined (density-independent) backscattering cross sections as a function of source temperature for both refractory fiber

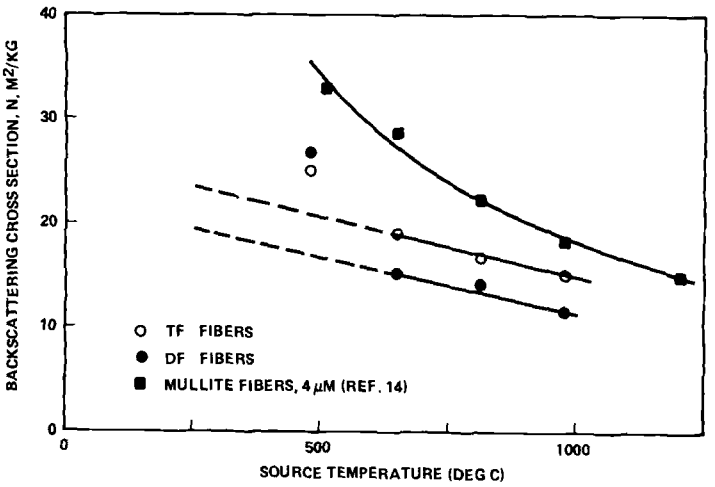

FIG. 1—*Backscattering cross section versus source temperature for several refractory fibers.*

materials. For use in the expressions for k_{rt}, these values must be multiplied by the bulk density. The extrapolations to the lower temperatures result in better fits to the experimental conductivity data, while the experimental N values at 430°C (806°F) seem somewhat improbable. The absorption cross sections did not in any case exceed 6 percent of the backscattering cross sections.

Effective conductivity data were obtained for 96, 128, 160, and 384 kg/m^3 (6, 8, 10, and 24 lb/ft^3) refractory fiber felts at temperatures from 38°C (100°F) to 930°C (1700°F) and pressures from 1.33 to 10^5 Pa (0.01 to 760 torr). These data as a whole agreed well within 10 percent of values calculated from Eq 16. Selected experimental results are compared in Figs. 2 through 4 with estimated values given by the solid curves. In Figs. 2 and 3, two curves are given for k_{eff} because of the differences in the estimated values for k_{rt} for the two materials. The predicted difference in k_{eff} was not confirmed by the test data since the differences at the lower temperatures were of the same order of magnitude as the accuracy of the conductivity test data (±10 percent), while the high-temperature test data are too limited and subject to too great an uncertainty due to systematic errors to be useful in critically evaluating the predictive model. The expectation is, however, that if reliable conductivity data could be obtained for temperatures above 700°C (1300°F), the predictive model and the backscattering cross-section data would be confirmed.

As is evident from Fig. 4, the agreement between the predicted behavior and conductivity test results at ambient and reduced pressures for the 96 kg/m^3 (6 lb/ft^3) TF felt is not very good. The explanation is likely to be

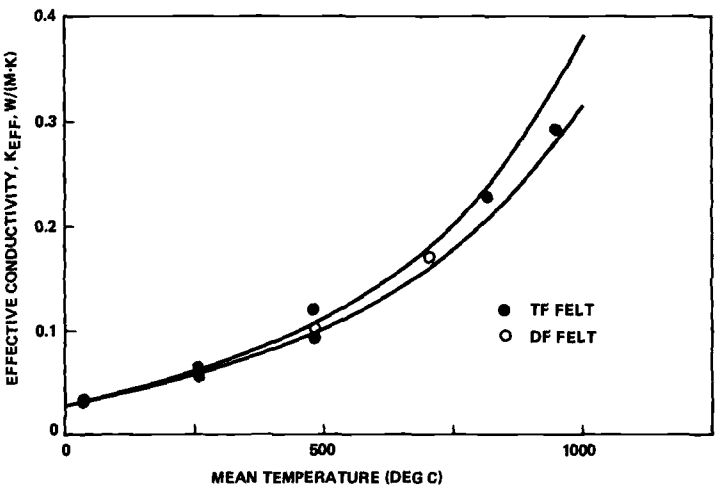

FIG. 2—*Effective thermal conductivity versus temperature; 128 kg/m^3 (8 lb/ft^3) refractory fiber felts.*

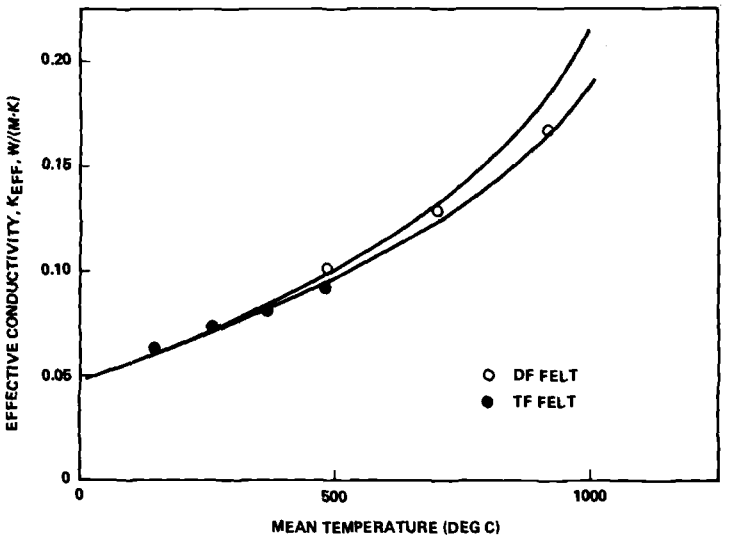

FIG. 3—*Effective thermal conductivity versus temperature; 384 kg/m³ (24 lb/ft³) refractory fiber felts.*

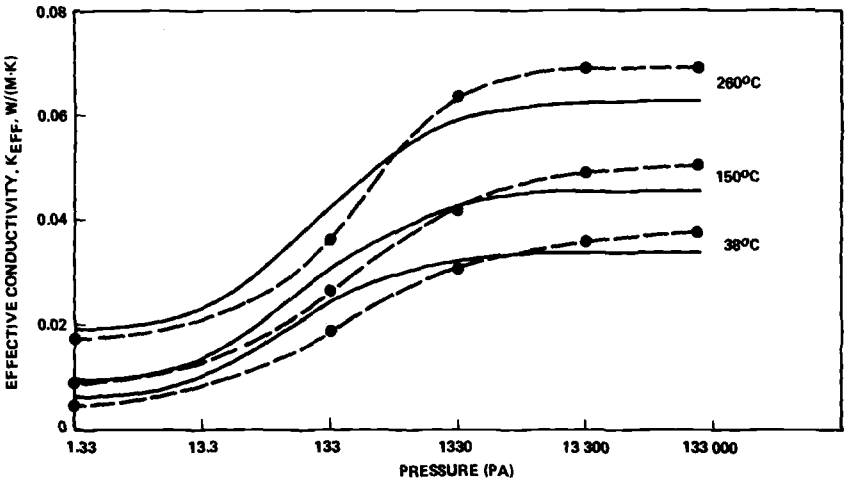

FIG. 4—*Effective thermal conductivity versus pressure; 96 kg/m³ (6 lb/ft³) TF felt.*

found in one or more of the following factors; (1) Uncertainty in pressure measurement. The vacuum system often must be held in a state of dynamic equilibrium at a given pressure. Pressure gradients therefore exist within the test chamber. (2) Uncertainity in estimation of the effective pore size, L_F, which depends on the value used for the effective diameter. This is

difficult to measure, and may vary for different specimens of the same material. (3) Changes in heater performance due to increase in interface resistances upon evacuation. This is a problem particularly with the high-temperature heaters, due to the construction. (4) The 96 kg/m^3 material may be porous enough to permit limited convection at the lower temperatures. This would be relevant to the data for the highest pressure only.

Discussion

The suitability of the theoretical model having been verified by the experimental results, limited as they may be, one is now in a position to exploit the model for predicting the performance of a wide range of densities, temperatures, and pressures. A single example will suffice to demonstrate the applications. In Fig. 5, a set of curves for the TF felt is given which has been generated by the application of Eq 16 through a computer program. For the moderately elevated temperature, it is apparent that the effective conductivity at ambient pressure is strongly influenced by radiation transmission for the lower bulk densities; for the high densities, gas conduction is the principal contributor. The curves also indicate a likely optimum density (for minimum k_{eff}) above which no further reduction of k_{eff} is to be expected. The effective conductivity in vacuum, however,

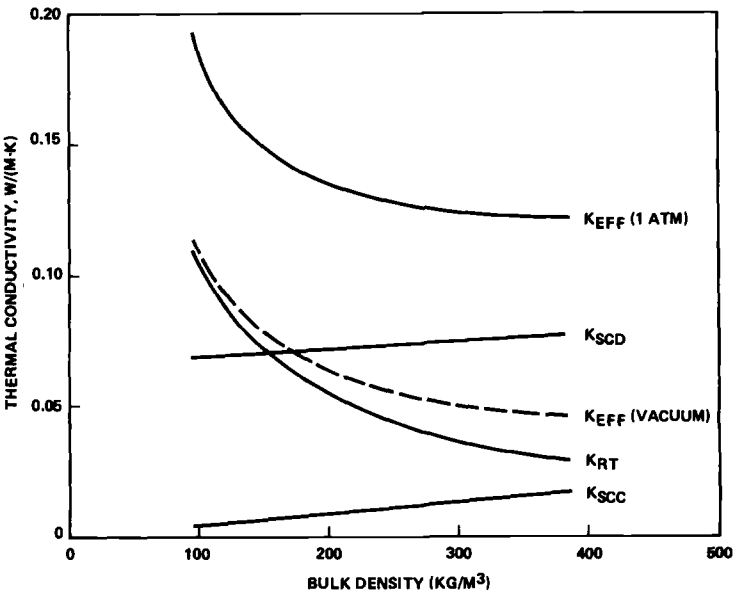

FIG. 5—*Thermal conductivity versus bulk density; TF felt at 700°C (1292°F) mean temperature.*

is shown to be principally determined by k_{rt} with solid conduction playing a significant role at the highest densities.

The criteria for determining whether the model represented by Eq 16 is appropriate for predicting the behavior of a given fiber insulation will now be reviewed.

1. The structure of the material should be such that the fibers are randomly oriented in planes that are normal to the direction of heat flow. This is the usual situation for commercial fiber felts and batting.

2. The fiber volume fraction must be large enough that convection does not contribute to heat transfer at the temperatures of interest. On the other hand, the fiber volume fraction should not be so large that the approximation on which Eq 5 is based is not valid. The appropriate range for f appears to be between 3 and 30 percent for fiber with specific gravity of the order of 2.5

3. The material must absorb radiation only weakly, and transmission of radiation should be governed primarily by scattering ($N \gg P$). This behavior seems to be the rule for the glass and ceramic fibers for which data are available.

4. The temperature drop across the insulation should be small compared with the absolute mean temperature, and the material situated between opaque surfaces that behave as gray radiators. These conditions prevail generally in guarded hot-plate testing. However, for prediction of performance in a specific design application, where large ΔT's could exist, the simplifications inherent in Eq 13 may lead to significant errors.

Conclusions

The agreement between the test results and estimates from the theoretical model represented by Eq 16 is of considerable significance to aerospace engineers involved in the areas of thermal design and analysis. Since the model suits many commercial refractory fiber batts for which reliable high-temperature thermal conductivity data, particularly at reduced pressure, are not likely to be abundant, the model provides an independent device for critically reviewing and extrapolating available data. The generation of infrared transmission data, though not without difficulty in the area of specimen preparation, is far speedier and less costly than performing many thermal conductivity measurements by the guarded hot-plate technique. Transmission measurements can also be carried out to temperatures well beyond the limit for practical conductivity testing. Guarded hot-plate testing of low-conductivity materials at elevated temperatures remains full of pitfalls for the unwary or inexperienced experimenter, and suitable standard materials are still unavailable. Although these circumstances tend to limit the reliability of such conductivity data,

the state of theoretical understanding of the behavior of fiber insulations would appear adequate to permit individuals to assess the quality or reasonableness of their own data at little added cost and effort, through the application of suitable models of the type that has been described.

Acknowledgments

The author wishes to acknowledge the contribution of R.J. Schmitt, of the McDonnell Aircraft Co., who was responsible for the infrared transmission measurements. Credit is also due to R.G. Ivy, Rockwell International, Space Division, who accomplished the majority of the thermal conductivity measurements while contending with numerous test difficulties.

References

[1] Verschoor, J.D. and Greebler, P., *Transactions*, American Society of Mechanical Engineers, Vol. 74, 1952, pp. 961–968.

[2] Greebler, P., *Jet Propulsion*, Nov.–Dec. 1954, pp. 374–378.

[3] Thigpen, J.J. and Short, B.E., ASME Paper No. 59-A-293, American Society of Mechanical Engineers, 1959.

[4] Rolinski, E.J. and Purcell, G.V., "Investigation of Radiation and Conduction Heat Transfer in Fibrous High Temperature Insulation," USAF (AFML) TR-67-251, Air Force Materials Laboratory, Dayton, Ohio, Dec. 1967.

[5] Dickson, D.J. in *Heat Transmission Measurements in Thermal Insulations, ASTM STP 544*, American Society for Testing and Materials, 1974, pp. 243–255.

[6] ASTM Subcommittee C16.30 in *Heat Transmission Measurements in Thermal Insulations, ASTM STP 544*, American Society for Testing and Materials, 1974, pp. 5–12.

[7] Bankvall, C., *Journal of Testing and Evaluation*, Vol. 1, No. 3, May 1973, pp. 235–243.

[8] Hager, N.E., Jr. and Steere, R.C., *Journal of Applied Physics*, Vol. 38, No. 12, 1967, pp. 4663–4668.

[9] Strong, H.M., Bundy, F.P., and Bovenkerk, H.P., *Journal of Applied Physics*, Vol. 31, No. 1, 1960, pp. 39–50.

[10] Jakob, M., *Heat Transfer*, Vol. I, Wiley, New York, 1949, p. 87.

[11] Hamaker, H.C., *Phillips Research Report*, Vol. 2, 1947, pp. 55–67, 103–111, 112–125, and 420–425.

[12] Larkin, B.K., "A Study of the Rate of Thermal Radiation Through Porous Insulating Materials," Ph.D. Thesis, University of Michigan, Ann Arbor, Mich., 1957.

[13] Larkin, B.K. and Churchill, S.W., *Journal of the American Institute of Chemical Engineers*, Vol. 5, No. 4, Dec. 1959, pp. 467–474.

[14] Schmitt, R.J., Linford, R.M.F., Dillow, C.F., and Hughes, T.A., *AIAA Progress in Astronautics and Aeronautics Series*, R.G. Hering, Ed., Vol. 35, the M.I.T. Press, Cambridge, Mass., 1974, pp. 183–204.

[15] Linford, R.M.F., Schmitt, R.J., and Hughes, T.A. in *Heat Transmission Measurements in Thermal Insulations, ASTM STP 544*, American Society for Testing and Materials, 1974, pp. 68–84.

[16] Melonas, J.V., Covington, P.C., and Pears, C.D., "Measurement of Some Thermal Properties of Three Glasses," WADC TR 58–129, Southern Research Institute, Birmingham, Alabama, 1958.

S. H. Jury,[1] *D. L. McElroy,*[1] *and J. P. Moore*[1]

Pipe Insulation Testers*

REFERENCE: Jury, S. H., McElroy, D. L., and Moore, J. P., "**Pipe Insulation Testers,**" *Thermal Transmission Measurements of Insulation, ASTM STP 660*, R. P. Tye, Ed., American Society for Testing and Materials, 1978, pp. 310–326.

ABSTRACT: The steady-state temperature distribution of two pipe insulation testers was modeled using the HEATING5 computer code available in the computers at Oak Ridge National Laboratory. One pipe tester, which conformed to the ASTM Test for Thermal Conductivity of Pipe Insulation (C 335-69) specification, had the core heater mounted inside a pipe around which the test insulation was placed. Guard heaters were employed to reduce unwanted axial heat conduction. Computer modeling showed that adjustment of the guard heaters was critical for short testers but not for long ones. A second tester, called an ideal tester, had no guard heaters, and only a simple, resistively heated core heater. The modeling results showed that there is a minimum length-to-thickness (L/S) ratio that will lead to a correct value of thermal conductivity calculated at the midplane of the tester. A peripheral heater with backup insulation can be added to the ideal tester to permit selection of the mean temperature of the test insulation. The ideal tester has the advantage over the ASTM design in that no balancing of heater power is required.

A mock-up of the ideal tester was constructed and tested with calcium silicate pipe insulation. The core heater was a stainless steel screen, whose low thermal conductivity reduces end losses and permits use of a short tester (~0.9 m). Measured values on asbestos-free calcium silicate show reasonable agreement with the data of others that contain asbestos.

KEY WORDS: thermal conductivity, pipe insulation tester, calcium silicate insulation, thermal insulation, heat transmission, thermal modeling, computer simulation, radial heat flow, screen heater

Nomenclature

A	Effective screen cross-sectional area normal to current flow, m^2
a_i	Coefficients in power series expansion of E
b_j	Coefficients in power series expansion of λ
E	Voltage at location X on heater, V
I	Current through heater, A
λ	Thermal conductivity, W/m·K

*Research sponsored by the Department of Energy under contract with the Union Carbide Corporation.

[1]Consultant, University of Tennessee and metallurgists, Metals and Ceramics Division, Oak Ridge National Laboratory, Oak Ridge, Tenn. 37830.

L Specimen length, m
P Power, W
r Radial position in general, m
r_1 First radial position in specimen, m
r_2 Second radial position in specimen, m
X Longitudinal position in pipe tester, m
ΔX Incremental length of pipe tester, m
ρ Specific electrical resistivity, ohm·m
T Temperature, °C
T_1 Temperature at radius, r_1, °C
T_2 Temperature at radius r_2, °C
ΔT Temperature difference, °C
D Specimen outside diameter, m
S Specimen thickness, m
Z X; Z is used in HEATING5

The desire to conserve energy has focused attention on the heat flow characteristics of insulation and the methods for determining this property. In steam generating plants and their distribution systems the need for high-quality pipe insulation is obvious. The same is true in the chemical process industry where process streams flow long distances and range in temperature from the cryogenic to the ultrahigh.

Various testing laboratories and the American Society for Testing Materials (ASTM) are engaged in the development of testing equipment and its application to specific insulation problems. ASTM Committee C16 is engaged in the development of test methods. This paper focuses on two pipe testers that were modeled and simulated at the Oak Ridge National Laboratory (ORNL). The details of this analysis and some test results from an apparatus are reported.

Two Pipe Tester Systems

Descriptions

The first pipe tester, shown in Fig. 1, is designed to meet the ASTM Test for Thermal Conductivity of Pipe Insulation (C 335-69) [*1–2*][2]. It consists of a cylindrical core heater with cylindrical guard heaters placed one at each end of the core heater. This assembly is spaced by brick insulating rings and positioned inside Schedule 40 type 304 stainless steel pipe [8.89 cm (3½ in.) outside diameter]. This pipe has disks of transite 0.0381 m (1½ in.) thick by a 0.254 m (10 in.) outside diameter mounted on either end. The main test active length is 0.914 m (3 ft) and it is 1.60 m (5 ft-3 in.) long, including guard heated lengths. Fiberfrax[3] ceramic fiber

[2]The italic numbers in brackets refer to list of references appended to this paper.
[3]Fiberfrax is a tradename for a ceramic insulation manufactured by Carborundum Corp.

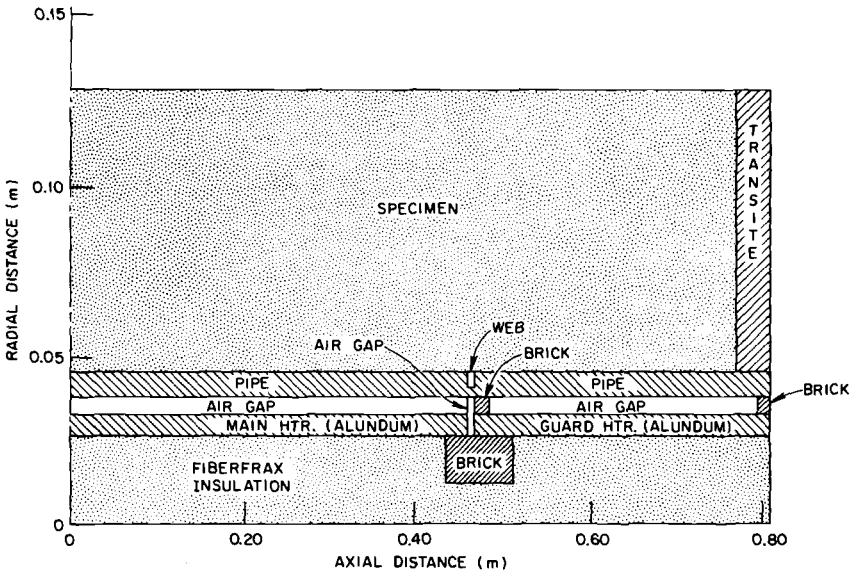

FIG. 1—*Cross-sectional model of ASTM pipe tester.*

insulation is used to fill the alundum tube on which the heater is wound. The specimen insulation to be tested is fitted around the pipe and up to the transite ends. The pipe has grooves (webs) cut at the ends of the active test length to minimize heat loss from the main test section to the guarded sections. The pipe and insulation specimen are fitted with thermocouples for determining the steady-state temperature differential across the specimen (preferably at its midplane). The apparent thermal conductivity is calculated from the formula

$$\lambda = (P \ln r_2/r_1)/(2\pi L \Delta T) \quad (1)$$

The apparent λ-value becomes the effective λ-value when it is known that the longitudinal temperature profile is flat over some reasonable length which includes the midplane and is reasonably representative of the specimen. Equation 1 is strictly applicable only to the radial flow of heat with constant thermal conductivity. In this case the radial ΔT is constant along L and is the effective value for the insulation. When Eq 1 is applied to a heat flow that has a longitudinal component, then the longitudinal temperature profile is not flat and ΔT measured at the midplane is different from that for a flat profile. The λ calculated under these circumstances is referred to here as an apparent (or fictitious) λ-value.

If we continue to apply Eq 1 to materials for which the thermal conductivity is not constant but is a function of temperature, then the effective λ-value obtained applies only to the range of the radial temperatures

involved in the measurement. The effective λ-value as a function of temperature is determined by methods discussed later in this report. Alternatively, one can make measurements over a series of narrow temperature bands.

The purpose of the guard heaters is to flatten the specimen longitudinal temperature profile by supplying heat lost from the ends of the pipe tester as well as peripheral heat losses from the guarded sections. The term "adjusting the guarding" will be used to indicate adjustment of guard heater power level necessary to produce the flat longitudinal temperature profile in the specimen.

The second pipe tester, called an "ideal" pipe tester, was an outgrowth of some ideas for simplification and a desire for a simple test geometry to check the computer code being used for simulation purposes. In concept the ideal tester involved two regions, that is, an outer cylinder of pipe insulation and an inner cylinder in which resistive-type volume heating occurred as shown in Fig. 2. Thermocouples were envisioned for measuring the ΔT across the insulation, and Eq 1 would be used to calculate the apparent thermal conductivity.

Although for calculation purposes we focus attention on the midplane, our real purpose here is the same as that covered by the ASTM Method C 335-69, that is, to establish a flat longitudinal temperature profile over some reasonable length of the specimen. Real specimens may contain

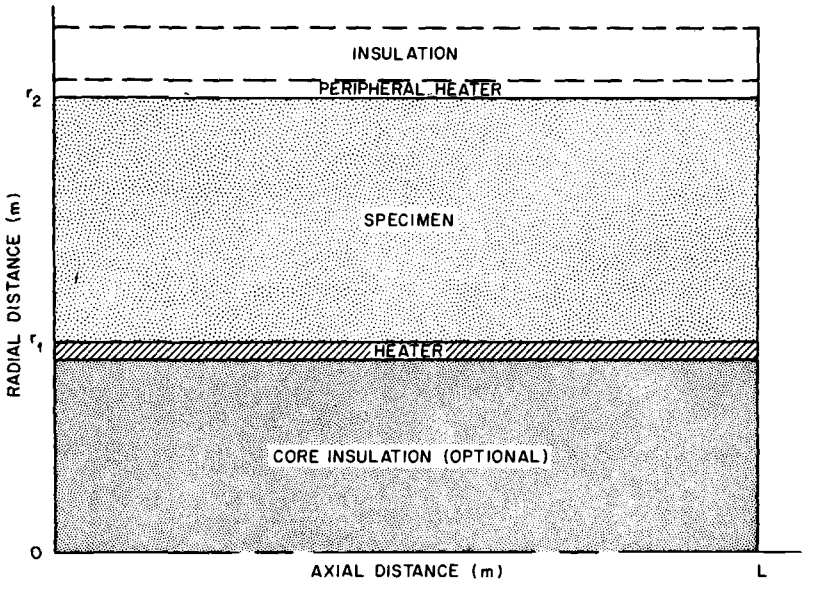

FIG. 2—*Cross-sectional model of ideal pipe tester (peripheral heater and insulation shown dotted).*

inhomogeneities or anisotropic effects. These tend to interact over the length of the test region and will therefore effect the midplane temperature distribution. Consequently these effects are reflected in the midplane calculations. Thus the calculated effective thermal conductivity for real materials based on midplane measurements is closer to reality than might be anticipated.

Models

In both pipe testers it is assumed that there is no azimuthal heat flow, nor is there any flow across the plane midway between the two ends of the tester. Thus one need only simulate the two-dimensional heat flow in the *r-Z* plane formed by simply cutting a half-cylinder from its periphery along a radius to its longitudinal axis. It should be noted that in this work the thermal conductivity of the insulation specimens is considered to be isotropic.

Computer Code for Simulation—HEATING5

HEATING5 is the latest revision of "The Heating Program," where HEATING is an acronym for Heat Engineering and Transfer in Nine Geometries [*3*]. It is designed to solve steady-state or transient heat conduction problems or both in one, two or three-dimensional cartesian or cylindrical coordinates or one-dimensional spherical coordinates. It is a multiregion program that solves numerically the system of simultaneous conduction equations that govern the heat transfer involved in the model. The program permits solving nonlinear conduction problems involving radiative transfer, properties variable with temperature, and moving boundaries, among others. HEATING5 is a very versatile code (program) available on the ORNL computer,[4] and is suited for describing the two-pipe tester models and solving for the steady-state temperature distribution. From this solution or temperature map, one can compute the specimen apparent thermal conductivity at any location, and this property is of principal interest here.

ASTM Pipe Tester Analysis

Simulation

HEATING5 was used to calculate the temperatures for 1363 nodes in the diagram in Fig. 1. The values used for the material thermal conductivity are given in Table 1. In these calculations, some of the materials and their

[4]Computers at Oak Ridge National Laboratory include IBM 360/65 and IBM 360/91.

TABLE 1—*Temperature-independent thermal conductivity of various pipe tester materials.*

Material Number	Material	λ, W/m·K
1[a]	Fiberfrax core	0.03461
2	brass pipe	159.25
3*a*	stainless steel 304	16.27
3*b*	stainless steel 304 pipe	4.153
4	transite ends	0.7442
5	brick rings	1.004
6[a]	alundum core	3.461
7[a]	specimen	0.03461
8	air	0.03116
9*a*	web	16.27
9*b*	web	1.627

[a]Ideal tester components.

properties were intentionally changed to study effects of alternative constructions on the pipe tester thermal behavior. Although the selection of temperature-independent properties may seem unrealistic, it provided a useful basis for comparison of results. In the case of the specimen, the midplane thermal conductivity λ could be calculated from the radial temperature profile and the main heater power density using Eq 1. The result could be compared with the input value of 0.0346 W/m·K [0.02 Btu·ft/(h·ft²·°F)]. In Eq 1, $\Delta T = T_1 - T_2$, where the two temperatures are calculated by HEATING5 at two radii, r_1 and r_2, respectively.

The general goal of these calculations was to evaluate the system performance for various input conditions. The main goal of any radial heat-flow measurement system is to obtain pure radial heat flow as opposed to radial flow with an unwanted axial heat flow component which would yield an incorrect specimen thermal conductivity. For instance, if the guard power density is too low, the system ends run cold and some of the main power is leaked axially. This axial leakage reduces the radial heat flow, so the resulting radial temperature difference is decreased and the calculated thermal conductivity is too high. Similarly, if the guarding is excessive, axial heat flow adds to the main power, increases the radial temperature difference, and the calculated thermal conductivity is too low.

Because of the effect on λ described in the foregoing, the initial calculation task was to obtain the proper guard power density for a given main power density. For the HEATING5 calculations to be meaningful, the program convergence must be adequate, and in this work we used 5×10^{-8}.

Results

During the course of 38 simulation runs, we investigated (1) the effect of replacing the red brass pipe with 304L stainless steel, (2) the effect of main heater/guard heater power ratio, (3) the effect of changing the degree of isolation between sections of pipe in the main region and in the guarded regions, (4) the effect of air in gap regions, and (5) the effect of the pipe thickness. All of this was done while simulating a hypothetical nominal 0.0762-m (3 in.) pipe insulation (actually 88.9 mm or 3.5 in.) with a 0.0825 m (3¼ in.) thickness and $\lambda = 0.0346$ W/m·K (0.02 Btu/h·ft·°F).

In general we found that a reduced longitudinal heat conduction lowered the guard power required to produce a flat temperature profile in the main section. Perhaps the most significant conclusion from this work was that the guard heater does not have to be in exact balance. A typical illustration of this is based on the results from Run 38, where Fig. 3 shows the temperature of the stainless steel wall as a function of distance. There is a temperature difference of 16.6°C (30°F) between the stainless steel midplane and web section, and yet, at the midplane, $(\lambda_{apparent}/\lambda_{real}) \times 100 = 99.74$ percent. The 1600°C range of temperatures shown in Fig. 3 indicates that we used more power than practical with stainless steels but that it was all right for simulation purposes. Another more subtle conclusion is that guard heating is unnecessary if the core heater and length of the pipe tester are properly designed.

Ideal Pipe Tester Analysis

Simulation

As shown in Fig. 2, the ideal pipe tester had only three regions involved in contrast to the 20 required to model the ASTM pipe tester. A second cylindrical heater, backed up with insulation, was added in some later calculations. The simple ideal tester fitted in this, so that the general level of the thermal distribution in the specimen could be controlled. This addition to the ideal tester is shown dotted in Fig. 2.

Results

Thirty-five calculations were made on the ideal tester to show the effect of (1) length, (2) diameter, (3) heater power level, and (4) adding peripheral heat. It was found that adding peripheral heat and reducing core heat permitted smaller temperature gradients radially across the specimen at any temperature level desired. The higher the peripheral heat, the higher the temperature level. The more core heat, the greater the temperature gradient across the specimen.

An *L/D* or *L/S* effect was observed. If the specimen inside diameter

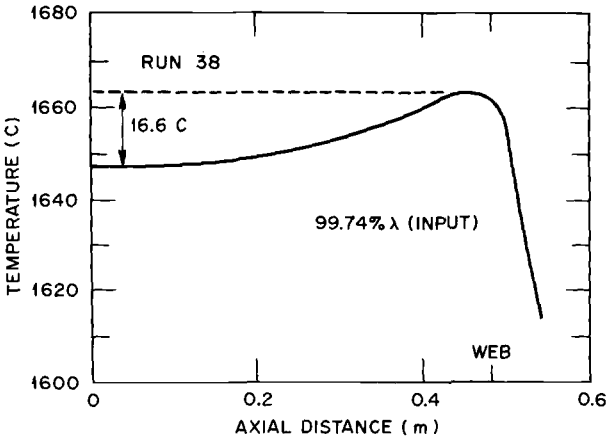

FIG. 3—*Temperature of stainless steel pipe wall with main and guard heaters nearly balanced.*

was held constant and the outside diameter varied, then the pipe tester length required to give results within the 1 percent level was related to the *L/D*. If length, outside diameter, and inside diameter were varied, then the effect was related to *L/S* where *S* is the specimen wall thickness. The *L/S* effect can be observed in Figs. 4–7. Figure 4 shows the temperature of the heater/specimen interface as a function of axial position for several system lengths. A 0.914-m half-length system yields 0.20-m isothermal zone, and Fig. 5 shows that the λ-error for this region is less than 1 percent. Similarly, Figs. 6 and 7 show that for a larger-specimen diameter of the same thickness, longer systems are needed.

Ideal Pipe Tester Tests

Description

Based on the results of the computer models, we decided to build a pipe tester modeled after the ideal tester. As an initial step, we decided to build a mock-up of the ideal tester before building a full-scale one. The design of the apparatus is shown in Fig. 8. A crucial aspect of the design of the ideal pipe tester is dependent on selection of a core heater with a low thermal conductivity. Various heater designs were considered, including wire wound in a spiral groove in alundum, a resistively heated tube, spiral ribbon heaters, and clad heaters. Electrical transformer matching, d-c power measurements, ease of instrumentation, ease of fabrication, costs, and availability were considered and suggested either a perforated metal tube or a tube formed from a metal screen. Finally, a 40 by 40 mesh (per inch) 316 stainless steel screen made with 0.25-mm-diameter (0.010

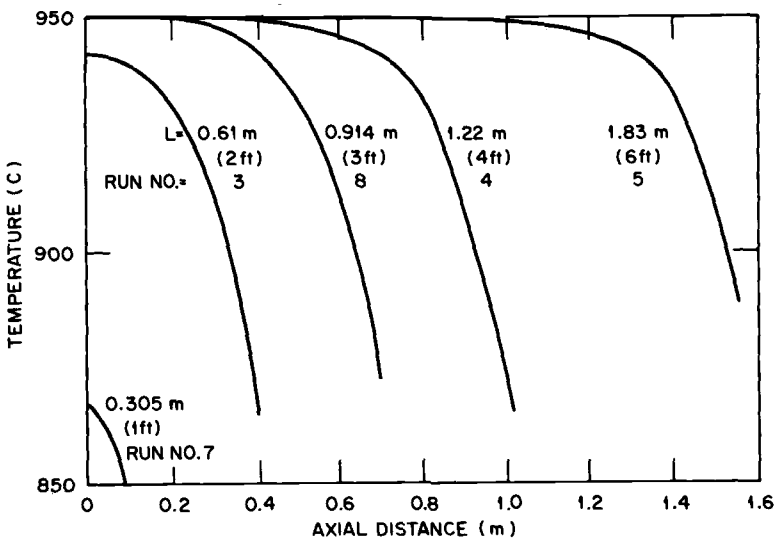

FIG. 4—*Ideal tester axial temperature distribution along interface between pipe and specimen (specimen ID = 0.0889 m and thickness = 0.0825 m).*

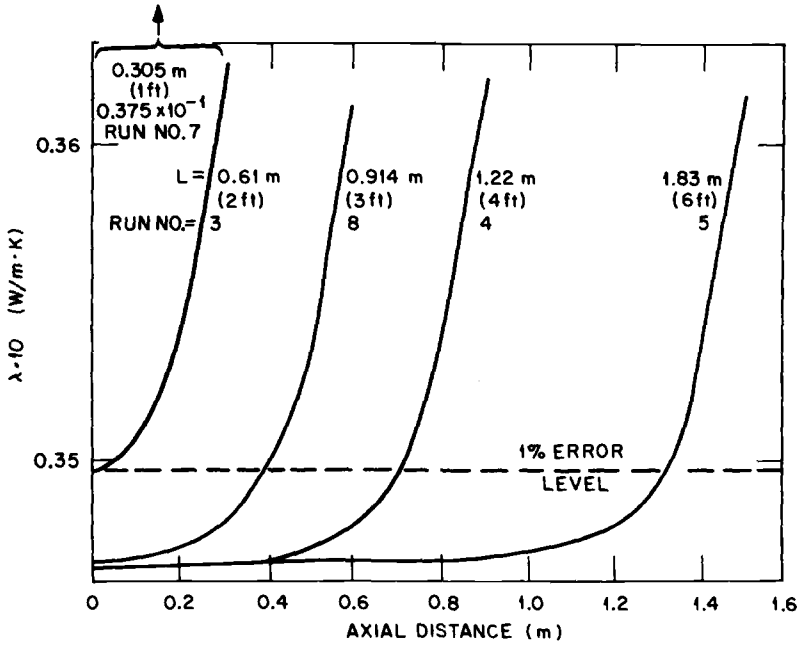

FIG. 5—*Apparent thermal conductivity of specimen as a function of axial distance from midplane (specimen ID = 0.0889 m and thickness = 0.0825 m).*

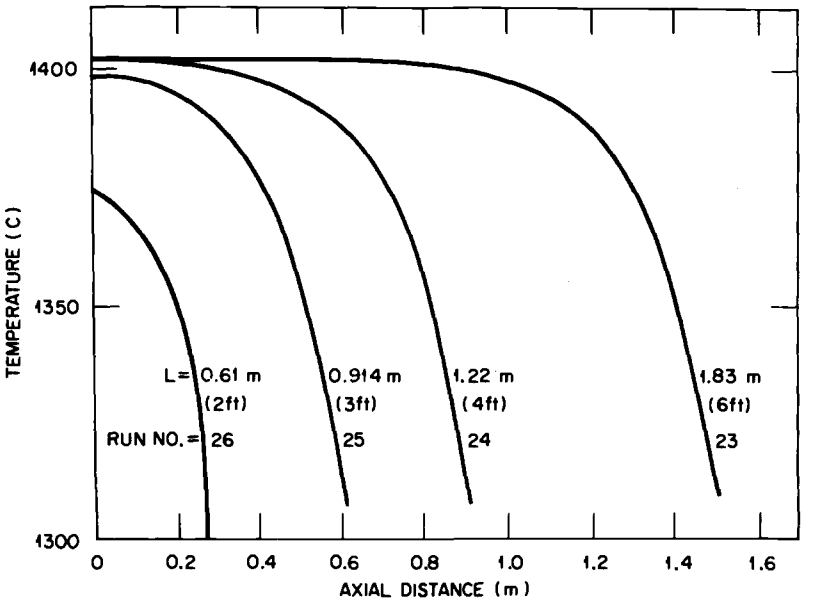

FIG. 6—*Axial temperature distribution along interface between pipe and specimen (specimen ID = 0.324 m and thickness = 0.0825 m).*

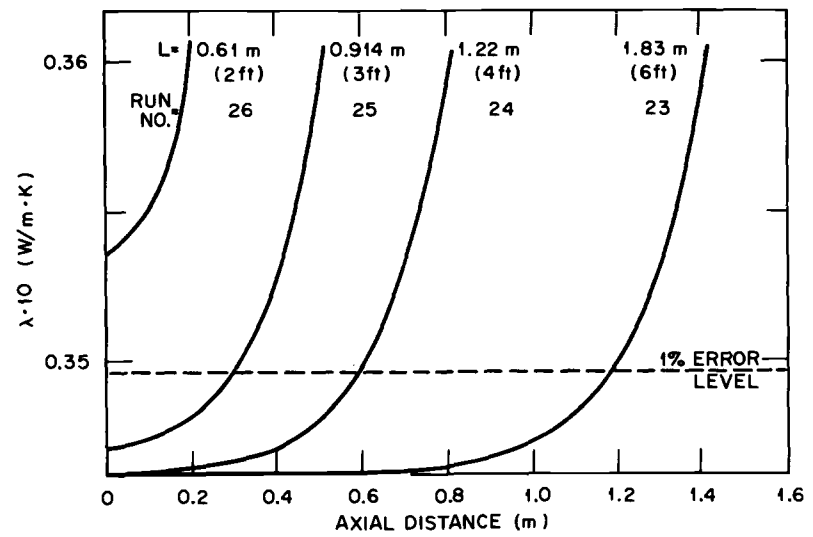

FIG. 7—*Apparent thermal conductivity of specimen as a function of axial distance from midplane (specimen ID = 0.324 m and thickness = 0.0825 m).*

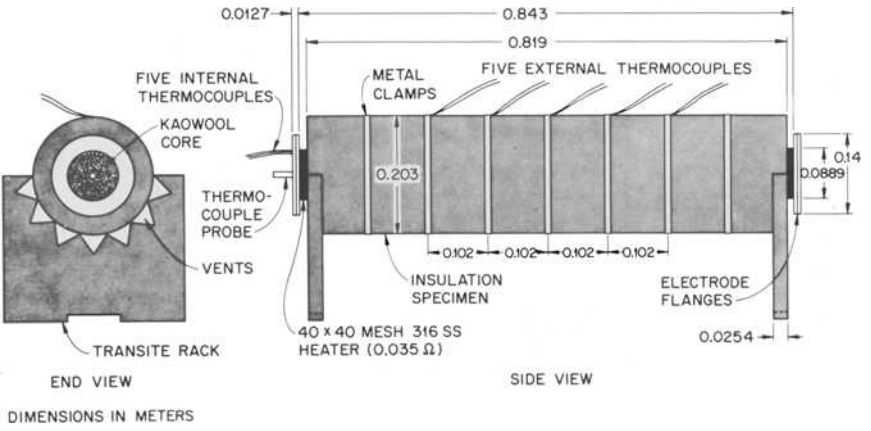

FIG. 8—*Mock-up of ideal pipe tester design.*

in.) wire appeared to be near ideal and work proceeded based on this selection.

Nominal 7.62-cm-diameter (3 in.) calcium silicate pipe insulation 0.0508 m (2 in.) thick and 0.914 m (36 in.) long was shortened to 0.819 m (32¼ in.) to fit between two sets of brass electrode flanges and around an 0.089-m-diameter (0.29 ft) cylindrical heater fabricated from 316 stainless steel screen (40 by 40 mesh/inch) as shown in Fig. 8. This assembly was placed in a transite rack that was equipped with vents around the insulation periphery to permit the free passage of air and thus to minimize thermal distortion at the ends of the test specimen. Five metal straps [approximately 0.0127 m (0.0416 ft) wide] were used to clamp the assembly at 0.1016-m (4 in.) intervals. Each strap had a platinum 10 percent rhodium versus platinum thermocouple welded to its inside surface adjacent to the specimen.

The screen was instrumented with five platinum 10 percent rhodium versus platinum thermocouples welded to the screen at longitudinal positions to match the outer thermocouples. Originally the junctions were welded directly to the screen, but later they were welded to one end of a short length of platinum wire which was welded to the screen. This modification removed the thermocouple junction from the path of heater current and prevented thermocouple error from voltage pickup (IR drop). The ends of the screen were notched 0.0254 m (1 in.) deep so that the resulting tabs could be folded for clamping between pairs of brass electrode flanges shown in Fig. 8.

The instrumented screen was formed around disks of Kaowool. A movable platinum 10 percent rhodium versus platinum thermocouple was placed in an axially located quartz tube for determining the axial tem-

perature profile. All 11 thermocouples extended to a 0°C ice-water reference bath. All thermal emfs were measured with an L&N-type K-5 potentiometer.[5]

A Varian d-c power supply[6] provided direct current to the screen via copper wires connected to the brass electrodes. The current in this circuit could be reversed and passed through 0.001 and 0.01 Ω standard resistors for current determination with the L&N-type K-5 potentiometer. The five platinum wires attached to the screen as part of the thermometry also allowed the screen voltage drop to be measured along its length.

The flange-to-flange electrical resistance of the screen heater was 0.035 Ω. A water-cooled ballast resistor was added in series to bring the total resistance to 0.25 Ω, which is the rated load for the Varian d-c power supply.

Simulation

HEATING5 was used to simulate the mock-up, and results from Runs 28–35 are plotted in Figs. 9–11. Various heater lengths (Fig. 9; 0.409 and 1.83 m), power levels (Fig. 10; 0.2×10^6 to 4.7×10^6 W/m^3), core materials, and specimens (Fig. 11) were investigated. It is quite obvious that the thin

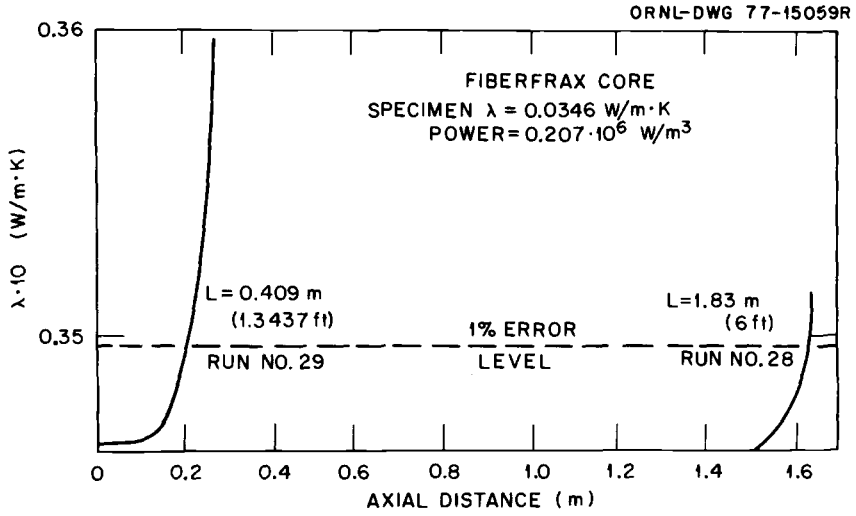

FIG. 9—*Apparent thermal conductivity of specimen as a function of axial distance from midplane. Comparison of short (0.41 m) ideal tester 40 × 40 mesh screen heater) with a longer tester (1.82 m) (specimen ID = 0.0825 m and thickness = 0.0508 m).*

[5]Leeds & Northrup Co. Model 7555 type K-5 potentiometer; uncertainty ± 0.005 percent of reading plus 0.1 μV.

[6]Varian V-2608 regulated magnet power supply rated for 4.5 kW at 32 V dc and 140 A dc.

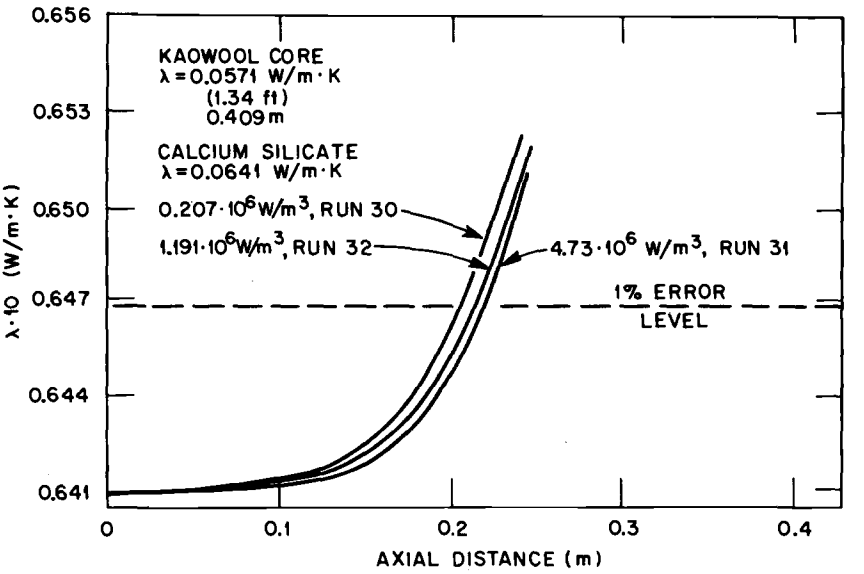

FIG. 10—*Apparent thermal conductivity of calcium silicate specimen as a function of axial distance from midplane. Comparison of different heat levels in mock-up equipped with 40 × 40 mesh (per inch) screen heater (specimen ID = 0.0889 m and thickness = 0.0508 m).*

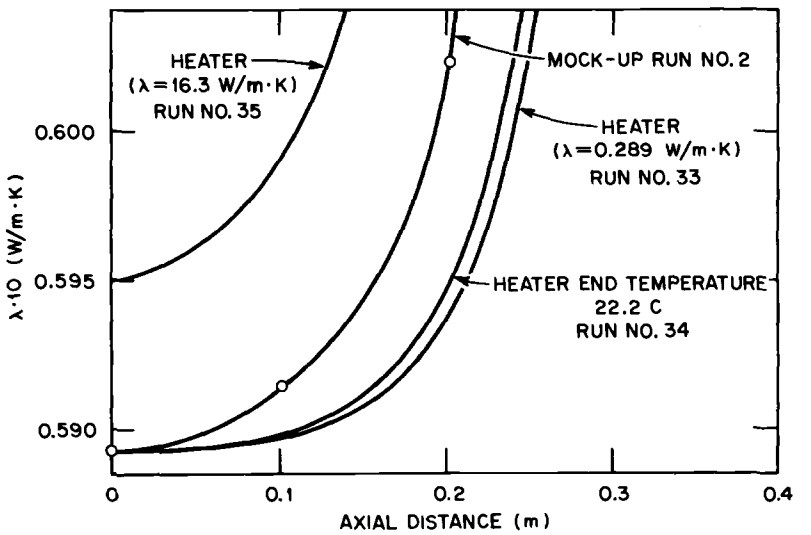

FIG. 11—*Comparison of results obtained from the ideal tester and its simulations.*

0.533-mm (0.021 in.) mesh heater with its lower thermal conductivity tends to produce curves that are much flatter than those shown earlier. As a consequence, a pipe tester 0.864 m (34 in.) in overall length is more than adequate to produce results which are accurate to 1 percent. The screen thermal conductivity was estimated as suggested by Koh and Fortini [4], and this was used in Runs 33 and 34. In the latter, we simulated the effect of the flanges by holding the heater ends at ambient temperature (22.2°C) (72°F). In Run 35 we treated the heater as though it were solid stainless steel. Figure 11 shows that the flange temperatures make only a small difference. Increasing λ, however, shifts the curve to much greater λ-distance sensitivity. For this reason it appears that the λ of the screen used in the experimental mock-up might be a little higher than the value [4] assumed for the computer models.

Another important point is that the computer models suggest that the axial temperature is essentially the same as the screen heater temperature for a given axial location in the mock-up pipe tester. At the midplane in Run 32, for example, the axis temperature was 452.73°C (846.91°F) and 452.75°C (846.95°F) at the screen. The temperature drop across the screen was 0.59°C (1.06°F). The latter drop should be less in the actual mock-up because the screen can see various parts of itself through the holes in the screen, and this has a temperature-smoothing effect, particularly since the heat flux is so low.

Experimental Test Results

The initial run used a screen current of 15 A and reached steady state overnight. The midplane heater and core temperature rose to about 54.5°C (130°F) while the corresponding outer strap temperature was 23.33°C (74°F), and Eq 1 yielded a λ of 0.0544 W/m·K. During this initial run we suspected that the flow direction of current in the heater might be affecting the thermocouple readings and this was confirmed by reversing the current. Therefore, in Run 2 the current was reversed as a routine part of data acquisition. (Subsequent use of the short platinum connecting wire removed this current reversing effect.) The averaged λ-results are plotted in Fig. 11 and compare well with the results from the simulation using HEATING5.

In the simulations, the specimen λ was forced to be a constant, but the thermal conductivity of the specimen does in fact vary with temperature. Therefore we have used the following in the ideal pipe tester analysis. For radial heat flow, P, through a specimen increment ΔX long

$$P = \lambda\, 2\pi r\, \Delta X\, dT/dr \tag{2}$$

where in general λ is a function of temperature, as

$$\lambda = b_0 + b_1 T + b_2 T^2 + \ldots \tag{3}$$

which can be truncated after the second-order term. The current in the heater is

$$I = (A/\rho)\, dE/dX \tag{4}$$

so

$$P = I^2 \rho \Delta X/A = I \Delta X\, dE/dX \tag{5}$$

Now λ can be eliminated between Eqs 2 and 3 and P between the result and Eq 5. After integration along r, one finds that

$$I(dE/dX)\,(\ln r_2/r_1)/2 = b_0(T_2 - T_1) + b_1/2(T_2^2 - T_1^2) + (b_2/3)\,(T_2^3 - T_1^3) \tag{6}$$

Thus if we make three runs with $(T_2 - T_1)$'s spanning the temperature range of interest, we can substitute in Eq 6 and solve the three equations simultaneously for the coefficients b_0, b_1, and b_2 and then put them into Eq 3 to obtain our result for λ. The dE/dX for each run is obtained by fitting

$$E = a_1 X + a_2 X^2 + a_3 X^3 + \ldots \tag{7}$$

to the voltage data measured along the heater at three points and then

$$dE/dX = a_1 + 2a_2 X + 3a_3 X^2 \ldots \tag{8}$$

In our experiments these data were plotted and found to be virtually linear, so that the coefficient, a_1, was adequate to represent dE/dX.

We made three runs over the temperature range 39.16 to 458.7°C and found by the foregoing procedure that

$$\lambda = 0.5485 \times 10^{-7} + 0.4655 \times 10^{-5} \times T + 0.1808 \times 10^{-6} \times T^2 \,(W/m \cdot K) \tag{9}$$

where T is in C. Typical calculated results are presented in Fig. 12 labeled "ORNL λ(T)." At the lower temperatures, these results are about the same as those available in the literature [5]. The "ASTM EQ." in Fig. 12 is

$$\lambda = 0.400 + 0.105 \times 10^{-3} \times T + 0.286 \times 10^{-6} \times T^2$$

where, in this case, T is the temperature, F, and λ the thermal conductivity, Btu·in./(h·ft²·°F).

At the higher temperatures, our results are about 10 percent lower. This is quite remarkable considering that the literature values are for older specimens which contained asbestos and our specimens are of the new asbestos-free variety. This material has a measured density of 0.1977 to 0.2106 mg/m³ (12.34 to 13.14 lb/ft³). The apparent λ-values previously plotted are related to the coefficients in Eq 3, or Eq 9; thus

$$\lambda_{\text{apparent}} = b_0 + (b_1/2)\,(T_2 + T_1) + (b_2/3)\,(T_2^3 - T_1^3)\,(T_2 - T_1) \tag{10}$$

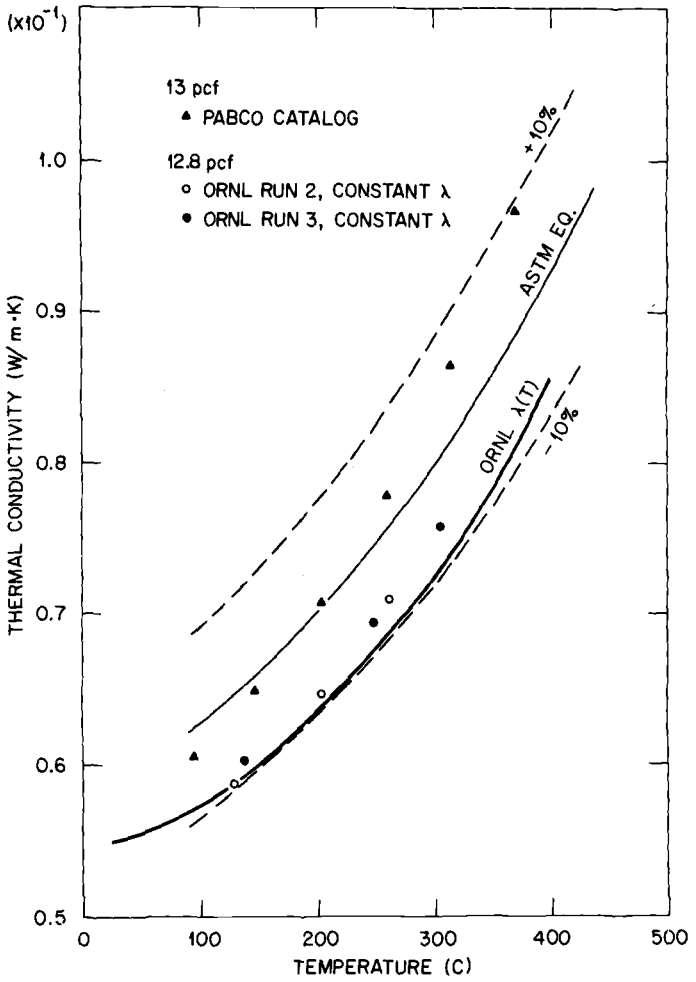

FIG. 12—*Thermal conductivity of calcium silicate insulation specimen.*

Conclusions

As a result of our computer modeling and tests we have concluded as follows:

1. The HEATING5 model of the ASTM pipe tester system shows that the calculated specimen thermal conductivity agrees with the input specimen thermal conductivity to within 0.3 percent for a 16.6°C (30°F) temperature difference between the stainless steel midplane and web section [0.4572 m (1.5 ft) from midplane]. A 3 percent λ-difference was noted for a 65.6°C (150°F) temperature difference. This is a very favorable result and suggests a useful operational control specification.

2. HEATING5 calculations show that in some cases the ASTM pipe tester could be replaced by a simplified version which is simpler to construct and control because no guard power is necessary.

3. An *L/S* effect is apparent in the ideal pipe tester, which suggests a half length of more than 0.915 m (3 ft) to maintain the 0.3 percent or less deviation from the correct thermal conductivity value. A screen heater reduces this half length to about 0.41 m (16 in.) due to the much lower thermal conductivity of the screen.

4. Peripheral heat can be added to the ideal pipe tester with minimal complication to allow the measurement of thermal conductivity over a narrow specified temperature range.

5. The mock-up tests confirm our simulation results for the ideal pipe tester.

Acknowledgments

The authors are grateful to T. G. Godfrey and R. K. Williams for reviewing the manuscript, to F. J. Weaver for performing some of the measurements, and to Sharon Buhl for her careful typing.

References

[1] ASTM C 335-69, *1974 Annual Book of ASTM Standards*, American Society for Testing and Materials, Part 18, 1974, pp. 75–80.

[2] System designed for York Research Corporation by Sparrell Engineering Corporation; private communication, Lampert, A. D. and Laube, A. H., York Research Corporation, to McElroy, D. L. and Moore, J. P., Oak Ridge National Laboratory, 14 Dec. 1976.

[3] Turner, W. D., Elrod D. C., and Siman-Tov, I. I., "HEATING5—An IBM 360 Heat Conduction Program," ORNL/CSD/TM-15, Oak Ridge National Laboratory, Oak Ridge Tenn., 1977

[4] Koh, J.C.Y. and Fortini, A., "Prediction of Thermal Conductivity and Electrical Resistivity of Porous Metallic Materials," *International Journal of Heat Mass Transfer*, Vol. 16, 1973, pp. 2013–2021.

[5] ASTM C 680-71 Standard Recommended Practice for Determination of Heat Gain or Loss, and Surface Temperatures of Insulated Pipe and Equipment Systems by the Use of a Computer Program and Pabco High Temperature Insulation Systems Catalog, Fibreboard Corp., Fruita Co.

Systems Evaluation

R. G. Miller,[1] *E. L. Perrine,*[2] *and P. W. Linehan*[2]

A Calibrated/Guarded Hot-Box Test Facility

REFERENCE: Miller, R. G., Perrine, E. L., and Linehan, P. W., "**A Calibrated/Guarded Hot-Box Test Facility,**" *Thermal Transmission Measurements of Insulation, ASTM STP 660*, R. P. Tye, Ed., American Society for Testing and Materials, 1978, pp. 329–341.

ABSTRACT: A hot-box test facility was fabricated by Wiss, Janney, Elstner and Associates for Jim Walter Research Corp. The equipment is capable of operating in either a calibrated or a guarded mode. When operating in the guarded hot-box mode, the equipment is in accordance with the ASTM Test for Thermal Conductance and Transmission of Built-Up Sections by Means of the Guarded Hot Box (C 236–66). When operating in the calibrated hot-box mode, the equipment is in accordance with the proposed ASTM Test for Thermal Performance of Building Assemblies by Means of a Calibrated Hot Box, which is presently being written by ASTM Subcommittee C16.30 and for which input has been provided from this facility. The basic design consists of a separate cold box, hot box, specimen frames, refrigeration unit, control and data-acquisition panel, and metered box. Both the hot and cold boxes are insulated with low-density polyurethane foam, with an overall minimum thickness of 30.5 cm (12 in.). The attitude of the test facility can be varied to provide upward, downward, or horizontal heat flow. Both the hot and cold boxes can provide variable air velocities parallel to the specimen face.

The following is a summary of the operating characteristics of the test facility:

Test specimen area dimensions: 2.4 by 2.4 m (8 by 8 ft)
Guarded mode metering area: 1.8 by 1.8 m (6 by 6 ft)
Cold side: normal temperature range: 27 to −23°C (80 to −10°F)
special temperature range: to −46°C (to −50°F)
air velocity: 0.8 to 24 km/h (0.5 to 15 mph)
Hot side: temperature range: 2 to 71°C (35 to 160°F)
air velocity: 0.8 to 24 km/h (0.5 to 15 mph)

KEY WORDS: thermal insulation, heat transmission, calibrated hot box, guarded hot box, thermal resistance, thermal conductance, thermal conductivity, large-scale thermal testing

With the current fuel shortage and the increasing cost of fuel, more efficient thermal insulation systems are required. From a testing point of

[1]Senior research engineer, Jim Walter Research Corp., St. Petersburg, Fla. 33702.
[2]Manager of Environmental Engineering Services and senior engineer, respectively, Wiss, Janney, Elstner and Associates, Inc., Northbrook, Ill. 60062.

view, in order to provide accurate and reliable data on these new systems, *large-scale* thermal testing is needed. One such method is the calibrated hot box.[3]

The current test method, ASTM C 236-66, Thermal Conductance and Transmittance of Built-Up Sections by Means of the Guarded Hot Box, is difficult to utilize when large building sections must be tested. The size of the test apparatus becomes unwieldy because guard areas are needed, and test panel construction is complicated by the need to isolate the metered area from the guarded area. The calibrated hot box avoids these problems. As Mumaw[3] states:

> The calibrated hot box is a heat transfer apparatus similar in construction and operation to the ASTM guarded hot box, with the exception that there is no guard chamber surrounding the hot side metering box. The calibrated hot box is generally operated in a conditioned laboratory space free from localized hot and cold sources; thus, in principle, the laboratory space acts as a guard. The unit obtains its accuracy through careful analysis of the metering chamber wall heat transfer mechanism. This analysis includes the use of a calibrated standard section, having known thermal characteristics; thus, the name calibrated hot box.

General Description of the Calibrated/Guarded Hot Box

The Jim Walter Research Corp. (JWRC) hot-box test facility is capable of operating in either a calibrated or guarded mode. When operating in the guarded mode, the apparatus is in accordance with ASTM C 236–66. The orientation of the hot box may be varied to provide horizontal, upward, or downward heat flow. When providing horizontal heat flow, the facility is capable of testing vertical constructions, such as walls. When providing vertical heat flow, floors/ceilings/roofs may be tested, with the added advantage of being able to simulate either winter (cold-box top/hot-box bottom) or summer (hot-box top/cold-box bottom) conditions. Both boxes can provide variable air velocities parallel to the specimen face.

In order to simulate a wide range of naturally occurring conditions in the United States, the JWRC hot-box test facility was designed with the following operating characteristics: (1) hot-side chamber, 2 to 71°C (35 to 160°F) and 0.8 to 24 km/h (0.5 to 15 mph) air velocities; and (2) cold-side chamber, −46 to 27°C (−50 to 80°F) and 0.8 to 24 km/h (0.5 to 15 mph) air velocities.

Figures 1 and 2 show schematics of the JWRC hot-box test facility in the wall mode and floor/ceiling/roof mode, respectively.

[3]Mumaw, J. R. in *Heat Transmission Measurements in Thermal Insulations, ASTM STP 544*. American Society for Testing and Materials, 1973, pp. 193–211.

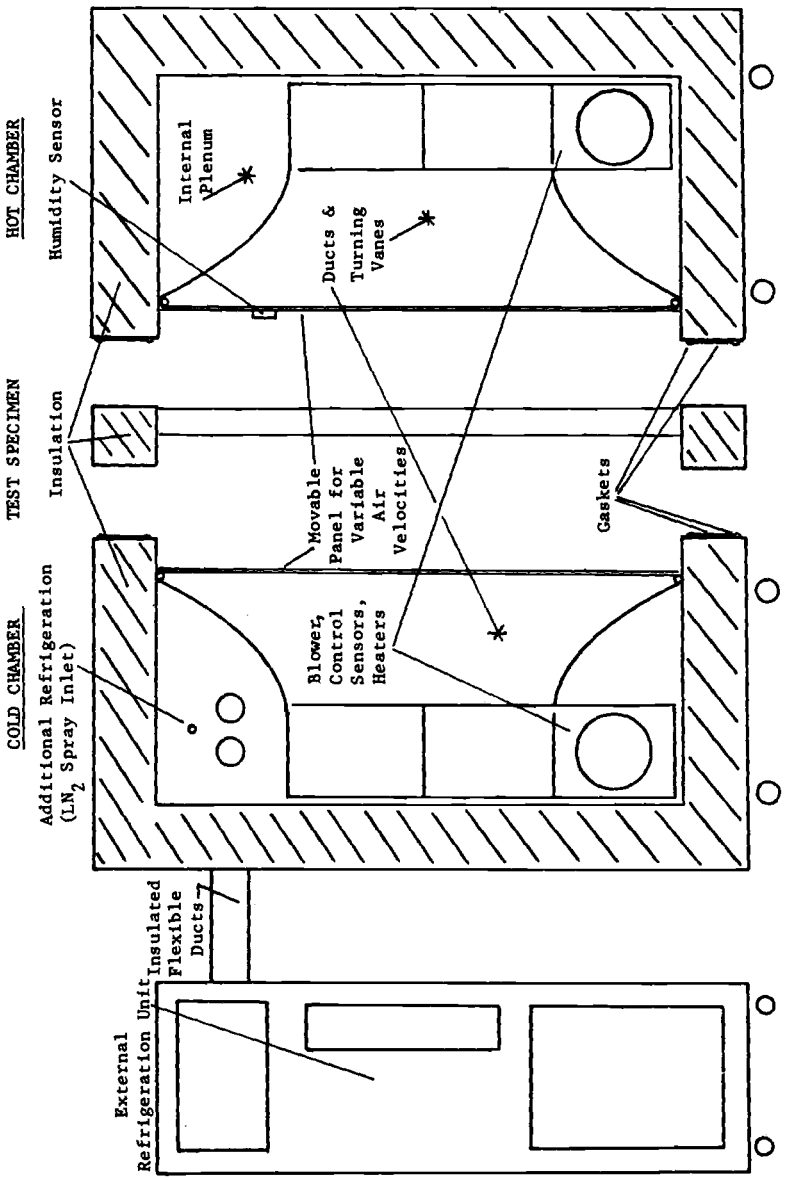

FIG. 1—*Schematic of JWRC hot-box test facility in horizontal heat flow mode.*

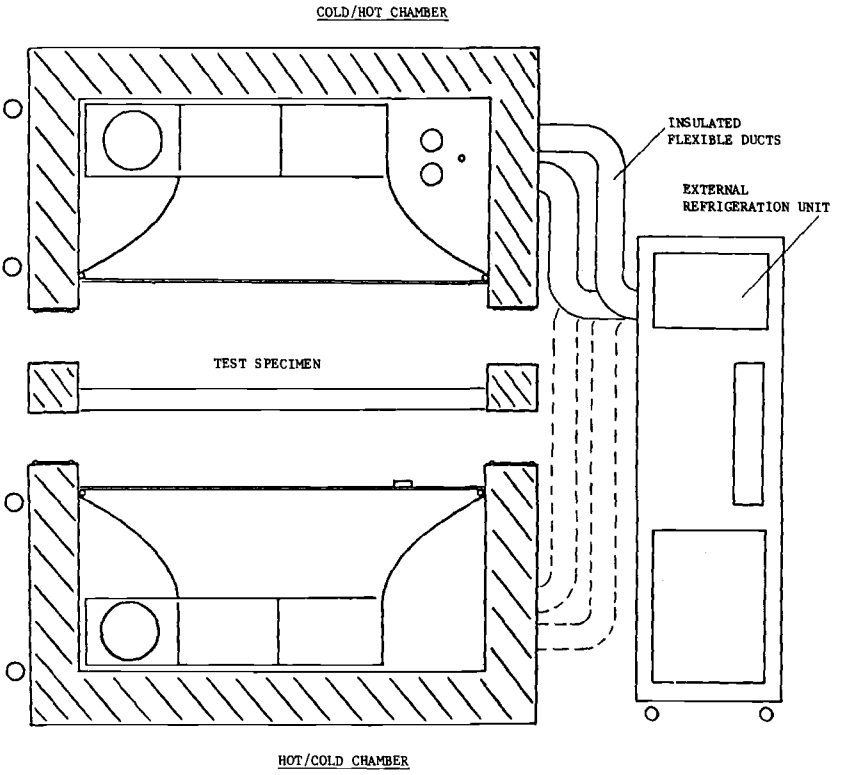

FIG. 2—*Schematic of JWRC hot-box test facility in vertical heat flow mode.*

Construction of Hot and Cold Test Chambers

The hot and cold test chambers are nearly identical in construction. The inner and outer shells of both boxes were constructed of 19-mm (3/4 in.) plywood. Wood and steel reinforcements were used at corners and additional plywood and steel plates were used for reinforcement at lift points. The chamber walls were insulated with five layers of 63.5-mm (2.5 in.) Celotex TF-730 (a polyurethane foam with aluminum foil facers on both sides). Edges of the foam layers were covered with tape to seal in the blowing agent. Contact adhesive was used to attach the successive layers of insulation. The inside dimensions of the boxes are 2.7 m wide by 2.4 m high by 1.4 m deep (9 by 8 by 4.5 ft) and the outside dimensions are 3.5 m wide by 3.2 m high by 1.7 m deep (11.5 by 10.5 by 5.7 ft). It is estimated that the total thermal resistance of the chamber construction is approximately 17.6 m^2 K/W (100 h·ft^2·deg F/Btu).

The faces of the test chamber openings were constructed of 13-mm (1/2

in.) plywood. Thickness was selected to give the needed strength yet offer a minimum cross section for heat loss. In order to provide an airtight seal between the faces of the test chamber and the test specimen frames, the face of each test chamber has a gasket located near its inner and outer edges. The space between the gaskets contains a flexible urethane foam to prevent convection of air in the space between test frame and chamber opening. Lever clamps secure the test frame to the hot and cold test chambers.

Both test chambers are mounted on casters for maneuverability. Lifting pins on the chambers are used in conjunction with a yoke and overhead crane to rotate the boxes from a wall testing mode to a roof testing mode.

Construction of Test Specimen Frames

Test specimen frame construction was similar to that of the test chambers. Outer and inner faces were constructed of 19-mm (¾ in.) plywood and the faces which contact the test chambers were constructed of 13-mm (½ in.) plywood. The inner faces of the frame, on which the test specimens are mounted, were attached with screws so that they might be replaced after long use. All other connections were made with both glue and screws. The frames also contained lifting pins for ease of exchange of test specimens.

Six test specimen frames were constructed. Five are 30.5 cm (12 in.) deep and the sixth is 61 cm (24 in.) deep. Two of the 30.5-cm (12 in.) frames contain standard test specimens for calibration of the hot box. The remaining three are used mainly for testing of wall constructions. The larger frame is used for testing of roof constructions.

The inside dimensions of the test specimen frame are 2.4 by 2.4 m (8 by 8 ft), which is the metering area in the calibrated hot-box mode. The outside dimensions are identical to the test chambers, that is, 3.5 m wide by 3.2 m high (11.5 by 10.5 ft).

Airflow Details—Hot and Cold Test Chambers

The hot and cold test chambers have independent interior air-circulation fan systems capable of providing air velocities parallel to the test specimen of 0.8 to 24 km/h (0.5 to 15 mph). The airflow in the chambers is in a "counterflow heat exchanger" configuration in order to maintain approximately the same temperature differential across any section of the test specimen.

The high-velocity mode of 24 km/h (15 mph) in conjunction with a minimum-flow cross-sectional area adjacent to the test specimen of 25.4 mm by 2.4 m (1 in. by 8 ft) requires a fan system with a capacity of

approximately 0.42 m^3/s (900 ft^3/min). A fan system which would give this flow with minimum heat dissipation was considered crucial to the design. Well-insulated test specimens can be expected to produce relatively large temperature differences with small input power requirements. Therefore, the minimum power generated in the hot box, as a result of fan operation, dictates the minimum temperature that can be obtained on the specimen's hot face with a fixed cold-face temperature. Low fan power also reduces the refrigeration load on the cold side.

A backward-inclined-airfoil centrifugal fan was chosen for each box as this type of fan exhibits high-efficiency characteristics. Each fan is powered by a 0.186-kW (¼ hp) motor via a variable-diameter pulley. The actual power drawn at ambient conditions is approximately 125 W (426 Btu/h) per fan.

The transition losses to the ultimate test panel velocity were minimized by the use of an exponential duct with turning vanes. A photograph of the fan and duct system, as located in the hot test chamber, is shown in Fig. 3.

The air velocities parallel to the hot and cold faces of the test specimens are varied by adjusting the location of a movable panel in each box (Fig. 1) and are determined from a curve of air velocity versus distance (between

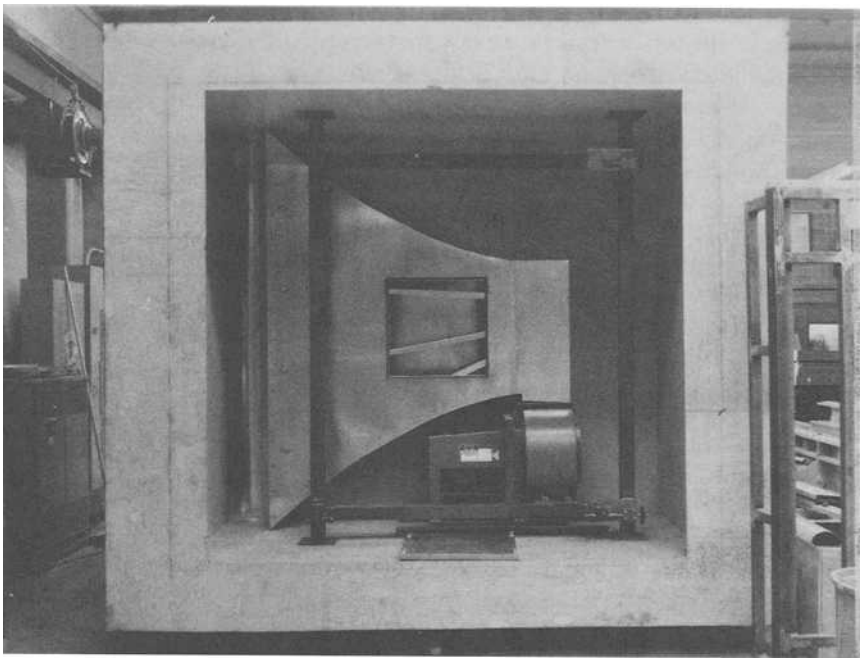

FIG. 3—*Photograph of air handling system.*

the movable panel and test specimen face) supplied by Wiss, Janney, Elstner and Associates (WJE). Velocity probes will be added in the near future for direct measurement of air velocity. The movable panel forms one perimeter face of the air discharge across the test specimen in each box and is manually positioned by three screw jacks. The screw jacks in each box are mechanically driven by a chain-and-sprocket assembly activated by a steel crank coupled to the system through a port on the side of each box. Each movable panel can be moved over a total distance of 30.5 cm (12 in.). A mechanical linkage couples the baffle on the inlet duct of the circulation fan to the movable panel, thereby throttling the inlet air as the movable panel is retracted. The overall effect is a reduced airflow as the panel is retracted. This technique is necessary in order to provide low-velocity gradients across the test section and over the full test panel height.

Refrigeration Equipment

A low-temperature capability to −46°C (−50°F) was a design requirement for the test facility; however, the majority of tests did not require temperatures below −23°C (−10°F). Based on this consideration, a mechanical refrigeration system was chosen for temperatures of −23°C, and an (liquid nitrogen) LN_2 injection system operating in conjunction with the mechanical refrigeration unit was chosen for temperatures below −23°C. The limitation with the LN_2 system is the temperature limit of the grease used in the cold-chamber fan, −46°C.

The Thermotron Model F-8-CH-2-S Temperature Environmental Test Chamber was chosen for the test facility. This unit is a remote mechanical refrigeration system coupled to the cold-test chamber via two 15-cm (6 in.) insulated flexible ducts, which are used for the forced-air supply to the cold chamber and return air to the refrigeration system plenum. The air circulation between the Thermotron and the cold chamber is approximately 0.12 m^3/s (250 ft^3/min). The unit uses R-502 refrigerant and has a cooling capacity of 1025 W (3500 Btu/h) at −23°C (−10°F).

Temperature control is obtained with a bypass circuit, which shuts the evaporative coil of refrigerant gas when activated by the temperature control of the refrigeration system. The refrigeration system control is capable of maintaining the temperature of the cold chamber to within ±0.7 deg C (±1.25 deg F) of the set-point temperature. However, finer control of the cold chamber temperature is attained with the Leeds and Northrup (L&N) controller-heater system (see Instrumentation section) operating in tandem with the refrigeration system controller.

The normal mode of operation consists of initial temperature stabilization of the cold chamber at a temperature slightly lower than the final desired temperature. The refrigeration system controller alone is opera-

tional during this initial stabilization period. The L&N temperature controller-heater system is then activated with the controller set-point adjusted slightly higher than the refrigeration system set-point temperature. The fast reaction time of the L&N controller-heater system, working in tandem with the refrigeration system controller, results in a fine temperature control of the cold chamber to less than ±0.08 deg C (±0.15 deg F) of the set point temperature.

Cold-chamber temperatures below −23°C (−10°F) are attained with the assistance of an LN_2 injection system. A solenoid valve is used for injection of LN_2 into the chamber. This LN_2 solenoid valve, as well as the mechanical refrigeration system, are activated by the refrigeration system controller. The L&N controller-heater system continues to operate as the fine control for the cold-chamber temperature.

Instrumentation for the Hot-Box Facility

One of the main requirements for reliable and accurate test results is accurate data acquisition and control equipment. The following paragraphs describe the control equipment and instrumentation for the JWRC test facility.

The hot and cold test chambers have identical heater-controller systems. Each system consists of an L&N Electromax IV Temperature Controller which energizes heaters located in each box via a silicon-controlled rectifier (SCR). Both L&N controllers use as sensors Type T thermocouples located in the circulation fan discharge ducts. The controllers include adjustments for proportional band, reset, rate, and approach. A primary guide in choosing these controllers was the stability characteristics. A ±10 percent line voltage variation results in a calibration shift of less than 0.06 percent of the setting. The temperature stability of the controllers is less than ±0.05 percent/deg C change in room ambient temperature.

The output signal from the temperature controllers controls the heater power via the SCR. The SCR's give a steady draw to the heaters, minimizing temperature changes. A zero-firing-type SCR unit was chosen in order to minimize metering errors (voltage and current). This type of unit also eliminates electrical interference problems normally present with relay circuitry. The L&N temperature controller-heater system provides fine temperature control for both hot and cold chambers to less than ±0.08 deg C (±0.15 deg F) of the set-point temperature.

Heaters are located in the circulation fan inlet duct in each box. Each system uses three heaters with capacity ratings of 100, 200, and 400 W, (341, 682, and 1364 Btu/h), energized from the control panel. Each of the heaters can be switched into the heater control circuit, giving seven increments of heater power for optimum temperature control. Bare nichrome

wire heaters were chosen because of their fast temperature response characteristics.

All temperatures (hot air, hot surface, cold air, cold surface, and inside and outside surfaces of the hot-test chamber) are measured with 24-gage multistrand Type T thermocouples. The thermocouples are fabricated to the ANSI special limits of ±0.4 deg C (±0.7 deg F).

The data-acquisition system chosen was a Kaye 8000 System consisting of a 30-channel skip controller, 150 Type T thermocouple channels, and 10 voltage channels interfaced with an Automatic-Send-Receive (ASR) Type 33 Teletype printer and punch. The primary criterion used in selecting this system was the accuracy of the temperature measurements. The Kaye 8000 has an absolute accuracy of ±0.17 deg C (±0.3 deg F) and differential accuracy of ±0.06 deg C (± 0.1 deg F). The system provides the capability for selecting six sample interval times (0.3, 0.5, 1,2,5, and 10 s) and 11 scan interval times (1, 2, 5, 10, 20, and 30 min; 1,2,4,8, and 24 h). The data are presented in two forms—a digital display and a printed output. The printed output contains the date, time, channel or thermocouple number, temperature in degrees Fahrenheit, and energy in kilowatt-hours. A punched paper tape may also be obtained which acts as the input to a computer data analysis program. This program is being developed.

The cumulative watt-hours of electrical energy are measured using an Ohio Semitronics Watt-Hour meter. This instrument utilizes two Hall-effect watt transducers; one measures the SCR heater power, the other the fan power. The watt-hour meter develops a voltage output which is proportional to the cumulative watt-hours of electrical energy developed by the fan and heaters and which is measured using a voltage channel on the Kaye 8000 data acquisition unit. The accuracy of the watt-hour meter is ±0.5 percent.

There are several additional components in the instrumentation system. Power for all instrumentation is brought from a constant-voltage isolation transformer, minimizing line voltage variations. The hot and cold test chambers each incorporate temperature-limit alarms which are independent of all control action. Temperatures above a preset limit in either the hot or cold chamber will activate the respective alarm and shut down all system power. The instrumentation system also includes two temperature recorders. Each recorder uses a thermistor transducer to measure the temperature in the circulation fan discharge ducts in the hot and cold chambers. The primary function of the recorders is to give the operator a quick status check on the test temperature conditions.

Guarded Hot-Box Test Mode

Instrumentation and controls are the same in the guarded mode as in the calibrated mode except as noted in the following.

The JWRC hot-box test facility can be operated in a guarded hot-box mode in accordance with ASTM C 236–66. The metered box was designed and fabricated to be located inside the hot chamber, the hot chamber then serving as the guarded box. The metering area is 1.8 by 1.8 m (6 by 6 ft).

The metered box includes heater banks from 70 to 650 W (239 to 2218 Btu/h). The amount of power needed is chosen prior to the starting of the test.

A circulation fan having a capacity rating of approximately 0.07 m^3/s (150 ft^3/min) is used for recirculation of the air across the test section through the heater plenum. The air velocity direction is that of natural convection and is approximately 0.8 km/h (0.5 mph). The fan power is the minimum power available in the metered box and is approximately 30 W (102 Btu/h).

The metered box is mounted on the hot chamber movable panel, using angle-iron support brackets which are mounted on the movable panel. Type T thermocouples on the inside and outside faces of the metered box are wired as a thermopile. A differential temperature across the insulated face of the metered box generates a differential voltage output, which is measured and used to control the hot chamber (guard area) via an L&N Electromax III differential voltage controller. The output control signal from the differential controller is used to control the amount of heat in the hot chamber (guard area), minimizing the temperature differential between the inside and outside surfaces of the metered box. The differential controller is wired to the SCR for this test mode, and the SCR in turn is used to control the amount of heat in the guard box.

Power for the metered box is derived from the constant-voltage isolation transformer and routed to the metered box via the watt-hour transducer in order to measure the watt-hours of electrical energy. Thus the technique consists of a fixed amount of power to the metered box, with the differential controller-heater system minimizing the temperature difference between the metered box and hot chamber (guarded area).

Standard Test Panels and Hot-Chamber Calibration

In order for the calibrated hot box to be an effective tool for measuring the thermal resistance of large-scale systems, calibrated test specimens must be used for proper calibration of the hot test chamber.

Two of the six test frames incorporate standard test panels. These panels were fabricated using high-density molded glass fiber board supplied by Owens-Corning Fiberglas Corporation. One panel consisted of two 1.2 by 2.4 m (4 by 8 ft), 206 kg/m^3 (12.89 lb/ft^3) boards with an average thickness of 26 mm (1.03 in.). The other panel contained two 1.2 by 2.4 m (4 by 8 ft), 204 kg/m^3 (12.73 lb/ft^3) boards with an average thickness of 51 mm

(2.02 in.). All boards were covered with vinyl tape to form a vapor barrier on each side and to prevent air circulation through the insulation.

An additional board of each thickness was fabricated by Owens-Corning in order to measure the thermal conductance at each thickness. The measurements were performed by the ASTM Test for Thermal Conductivity of Material by Means of the Guarded Hot Plate (C 177–71) at various mean temperatures. These data were then used in the heat-transfer analysis of the calibrated hot box.

Several preliminary calibration tests were performed by WJE prior to shipment of the hot-box facility to JWRC. These tests were performed with the nominal 51-mm (2 in.) glass fiber panel and included calibrated and guarded hot-box modes. The data from the calibrated hot-box tests provided heat loss factors which could be used to calculate the thermal resistance of unknown test panels within 5 percent. The data obtained in the guarded mode showed correlation with the guarded hot-plate tests within 5 percent. Testing is presently under way at JWRC to further reduce this deviation.

Test Results

Before discussing some of the test results from the JWRC hot-box test facility, a brief description of the testing procedure is in order.

After completing construction of the test specimen in the frame, the frame is inserted between the hot and cold test chambers. If the test is to be conducted in the calibrated mode, the necessary electrical connections are made and the thermocouples are attached to the test specimen for measuring both air and surface temperatures. The movable panels are then positioned for the desired air velocities. The test specimen frame is then securely attached to the test chambers by means of the four lever clamps. The refrigeration system and the hot-side and cold-side fans are switched on, and the power to the hot and cold sides is manually adjusted by means of the controllers to obtain the desired surface temperatures. Once steady state has been reached, test data are normally taken every hour over a 16-h period. The data are reported if the thermal resistance values of two 8-h periods agree within 1 percent. Test duration ranges from two to seven days depending on type of specimen construction and temperatures selected.

If the test is to be conducted in the guarded mode, the 1.8 by 1.8 m (6 by 6 ft) metering box is placed on the movable panel in the hot-test chamber. The power needed is chosen prior to the test and is obtained by wiring the appropriate heaters from the metering box heater bank. After making the necessary electrical connections and attaching the thermocouples to the specimen, the box is closed and securely latched. The test procedure now follows the calibrated-mode test procedure except

that the hot-side controller is not used; instead, the hot-side temperature is allowed to find its equilibrium value, while the differential controller maintains essentially a zero temperature differential across the metered box by adjusting the power in the hot chamber (guard area).

The absolute accuracy of the hot-box test facility equipment was estimated based on the following rule from Schenck[4]: "When the result is a function of quotients and/or products of a series of measurements, the square of the percent error of the result is equal to the sum of the squares of the percent errors of the individual measurements." From this mathematical rule, the maximum error was calculated as approximately 0.70 percent. Under extreme conditions the maximum error was calculated to be approximately 1 percent.

Figure 4 presents the results of guarded hot-box tests on four different insulation boards. The data were obtained at two mean temperatures, namely, 4°C (40°F) and 24°C (75°F), from the JWRC test facility and from two independent testing laboratories. The average overall error is within 4 percent. This agreement is excellent considering the large differences in guarded hot-box test facilities.

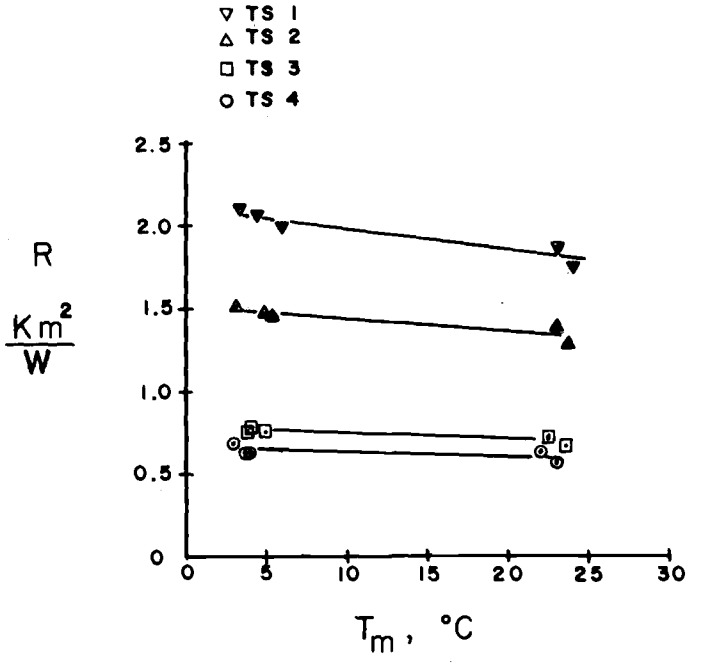

FIG. 4—*Interlaboratory guarded hot-box test results.*

[4]Schenck, H., Jr., *Theories of Engineering Experimentation*, 2nd ed., McGraw-Hill, New York, 1968, p. 47.

Correlation tests between the guarded mode and the calibrated mode have been conducted at JWRC. The calibrated mode has been correlated to within approximately 5 percent of the guarded-mode results, which is the present accuracy of the heat loss factors for the calibrated mode. Tests have also been run between the guarded hot plate (GHP) and guarded hot box (GHB), and guarded hot plate (GHP) and calibrated hot box (CHB). The results of the GHP/GHB tests have correlated within 3 percent, while the results of the GHP/CHB tests have correlated within 5 percent.

Conclusions

It is believed that the calibrated hot box is an accurate and reliable method for obtaining thermal resistance values on large-scale systems. The JWRC hot-box test facility, which includes both guarded and calibrated modes, has been shown to correlate well with independent testing laboratories, with guarded hot-plate tests, as well as with itself (guarded-calibrated). Testing is underway to further improve the accuracy, mainly by determining more accurately the heat loss factors for the calibrated mode.

Improvements are also being made to the facility—namely, the total automation of the calibrated hot box. This will shorten total test time, as well as improve data handling capability. With automation, transient heat-transfer tests and diurnal cycle tests, more accurately simulating natural conditions, will be possible.

It is hoped that in the near future more such facilities are constructed in order to provide the *large-scale* thermal testing capabilities needed in the United States.

H. W. Wahle[1], *D. A. Rausch*[2] *and*
B. A. Allmon[1]

New High-Temperature Guarded Hot-Box Facility for Reflective Insulation

REFERENCE: Wahle, H. W., Rausch, D. A. and Allmon, B. A., "**New High-Temperature Guarded Hot-Box Facility for Reflective Insulation,**" *Thermal Transmission Measurements of Insulation, ASTM STP 660*, R. P. Tye, Ed., American Society for Testing and Materials, 1978, pp. 342–356.

ABSTRACT: All-metal reflective insulation, used to insulate commercial nuclear power plants, requires special test considerations because of its nonhomogeneous nature. Internal convection and conduction paths that exist in the field must be preserved in the laboratory if the results are to be representative of field performance. The existing guarded hot-box method, ASTM Test for Thermal Conductance and Transmittance of Built-Up Sections by Means of the Guarded Hot Box (C 236–66), although intended for testing nonhomogeneous structures, does not properly consider these effects which could result in large measurement errors. A modified high-temperature guarded hot box, constructed for testing reflective insulation panels, can test one full-size, 914-mm (36 in.) square, flat panel up to 203 mm (8 in.) thick. This facility can operate at hot surface temperatures up to 811 K (1000°F) and can be rotated to test a panel in either the horizontal or vertical orientation. The facility was verified for testing both homogeneous and nonhomogeneous insulations, and data are presented to illustrate the effect that internal convection and orientation can have on heat loss. Large-scale experiments are planned to verify the performance of individual units of insulation in a system environment.

KEY WORDS: thermal insulation, reflective insulation, insulation, testing, test methods, high-temperature tests, test facilities, thermal conductivity

All-metal reflective insulations are currently being used to insulate commercial nuclear power plants and industrial piping. For the nuclear application, this includes both pressurized and boiling-water reactors operating at surface temperatures up to 616 K (650°F) in 310 K (100°F) ambient air. Equipment inside the containment building that typically is insulated with all-metal reflective insulation includes the reactor vessel, steam generators, pressurizer, pumps, and piping. Much of the insulation

[1]Babcock & Wilcox Company, Research and Development Division, Alliance, Ohio 44601.
[2]Mirror Insulation Unit of Diamond Power Specialty Co., Lancaster, Ohio 43130.

is individual units of pipe insulation. However, insulation for the larger pieces of equipment, such as the reactor vessel and steam generators, is composed of large curved panels that are normally 914 mm (36 in.) square. For a boiling-water reactor vessel, for example, the radius of curvature for the insulation panels is about 3 m (10 ft) and the performance is similar to that of a flat panel.

The unique construction of reflective insulation makes it difficult to measure the true field performance in a laboratory test. Existing test methods for nonhomogeneous insulation panels, if used without special precautions, may yield test results that do not represent field performance.

This paper presents the problems associated with testing reflective insulation panels and then describes a modified high-temperature guarded hot box designed for this purpose. Test results are presented that verify the new facility for use with both homogeneous materials and nonhomogeneous reflective insulation panels.

A large-scale experiment is described that can be used to measure panel heat loss in a real system environment.

Insulation Construction

A reflective insulation system is composed of prefabricated units. Each unit, in either pipe or panel form, is a rigid, self-contained, metal construction comprising an inner and outer casing and one or more spaced reflective liners. Figure 1 shows a typical 914-mm (36 in.) square reflective panel, and two types of construction are shown schematically in Fig. 2. The definition of terms is consistent with the proposed revision to the ASTM Recommended Practice for Prefabricated Reflective Insulation Systems for Equipment and Pipe Operating at Temperatures Above Ambient Air (C 667–72). The construction is all metal and 304 stainless steel is normally used. However, aluminum liners have been used for some applications. The liners are thin-metal foils laid parallel to the insulated surface and are spaced to form alternate layers of foil and air. Liners can be either supported flat parallel sheets or can be formed to provide contact points for spacing. Thermal efficiency depends, in part, on minimizing the thermal radiation between liners by using metals of high reflectance and low emittance. A small liner spacing is also designed to minimize natural convection within the enclosed air spaces. Conduction paths can also exist because of the nonhomogeneous structure, and can include metal-to-metal contact at liner support points and at end supports (see Fig. 2.). End supports can be either completely closed to eliminate panel-to-panel convection paths, or can be partially open to reduce the through-conduction paths.

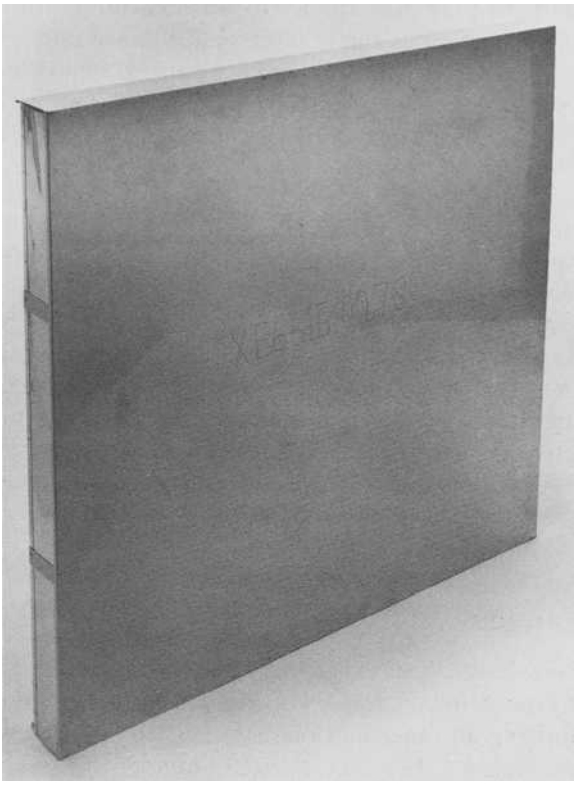

FIG. 1—*Reflective insulation panel.*

Measurement Problems

Heat loss data for reflective insulation panels are needed for design and for verification of mathematical models used to predict the performance of the insulation. The nonhomogeneous construction, however, causes problems when true field performance is to be determined by a laboratory experiment. Internal convection and conduction paths within an insulation panel have a strong effect on heat loss, and their heat transfer mechanisms must not be modified in a laboratory test. Natural convection is strongly dependent upon geometry. The possible flow paths are illustrated in Fig. 3 for two orientations of a reflective insulation panel. The two types of convection that exist are the cellular form between adjacent liners and a gross convective cell within a panel. These convective cells can also exist for contacting liners; parallel liners were shown in Fig. 3 for ease of illustration. Both types of convection must be preserved in the laboratory test if the heat loss results are to be meaningful.

Previous tests on reflective pipe insulation have clearly demonstrated the effect of orientation, and thus internal convection, on heat loss. Pipe tests were conducted in the horizontal orientation using the ASTM Test for Thermal Transference of Nonhomogeneous Pipe Insulation at Temperatures Above Ambient (C 691–77). The same facility and test procedure were used for the vertical orientation. A comparable standard does not exist for the vertical orientation; however, a task group of ASTM Subcommittee C16.30, Thermal Measurements, is currently working on a test method for vertical reflective pipe insulation. The effect of orientation on heat loss will be shown later for a piece of flat panel insulation.

Facility Design

Field boundary conditions, panel size, and orientation must be duplicated as closely as possible in the laboratory if true field performance is to be determined. A desirable experiment should include the following features:

1. Test at least one full-sized panel from edge to edge so that internal conduction and convection paths are not disturbed.

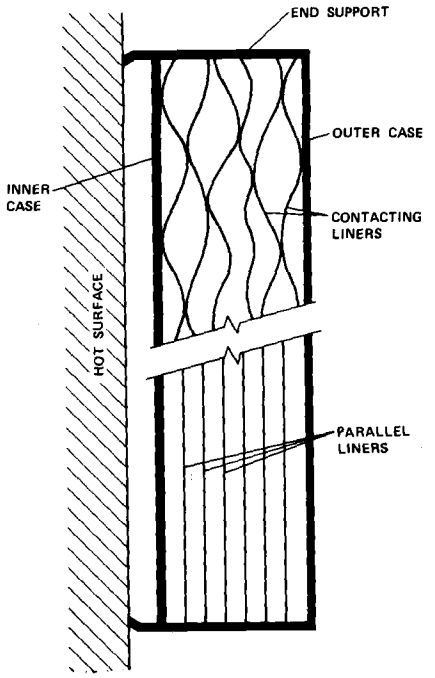

FIG. 2—*Reflective insulation panel construction.*

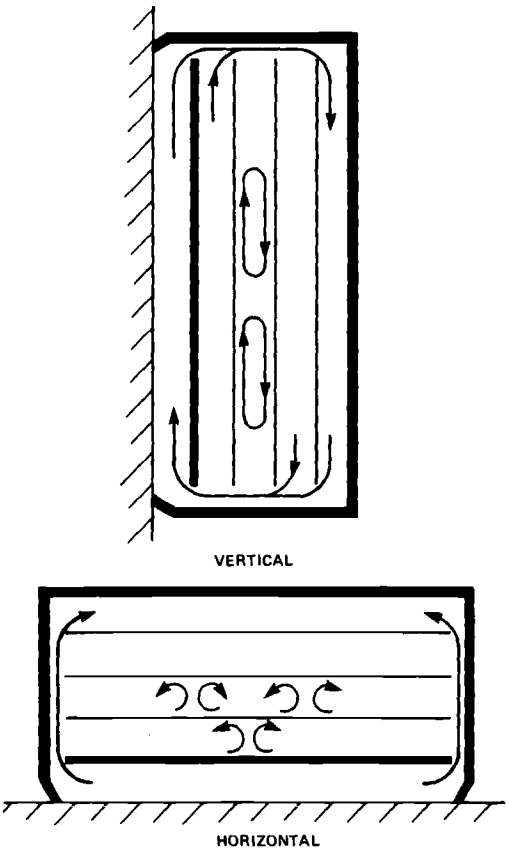

FIG. 3—*Internal convection can affect heat loss.*

2. Simulate the hot equipment surface on one side and ambient air on the cold side.

3. Test in both horizontal and vertical positions because performance is affected by orientation.

4. Provide hot surface temperatures up to 616 K (650°F).

Based on these requirements, it was decided that a "guarded hot box" method would be the best for use with reflective panels. Figure 4 shows the guarded hot box facility as described in the ASTM Test for Thermal Conductance and Transmittance of Built-Up Sections by Means of the Guarded Hot Box (C 236–66). This test method was designed for non-homogeneous panels such as wall, roof, and floor constructions used in buildings. The use temperatures for these facilities are low because of the type of construction tested. The facility consists of a test panel between a cold box and a hot guard box. Only the central region of the test panel

is tested via a metering box while the remainder of the test panel serves as guard insulation. Fans are used to provide a forced convection boundary on both the hot and cold sides of the test panel.

The ASTM C 236 apparatus in Fig. 4 is not suitable for testing reflective panels because of the panel's nonhomogeneous construction. The existing method only meters the central area of a test panel, yet, as discussed in the foregoing, reflective panels can have through-conduction paths and internal convection in the air cavities, both of which can exist outside the central metering area. This is illustrated by the test panel in Fig. 4, which shows internal convection paths that extend beyond the central metered area into the guard area. The existing method, although intended for nonhomogeneous structures, permits blocking internal convection and conduction paths at the boundary of the metered area. Notice also in Fig. 4 that the top and bottom edges of the test panel are sealed with edge insulation. This would prevent any convective interchange between stacked panels for those reflective designs with partially open end supports. Testing only a central area and intentionally modifying real heat-transfer mechanisms ensures that the test results will *not* represent true field performance.

Facility Description

The modified guarded hot-box facility is shown schematically in Fig. 5, and it consists basically of only the hot side of the typical facility shown in Fig. 4. The major design features required for testing reflective insulation panels include the following:

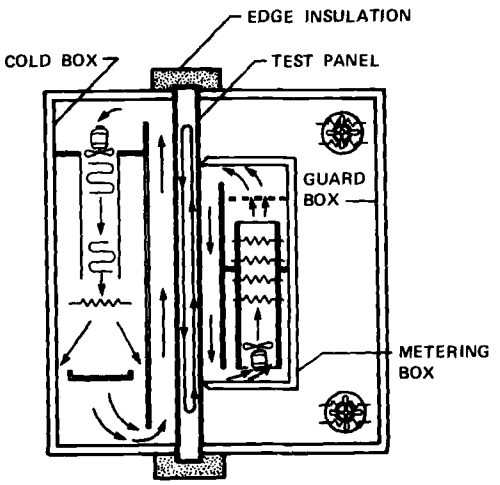

FIG. 4—*Low-temperature ASTM C 236 guarded hot-box facility.*

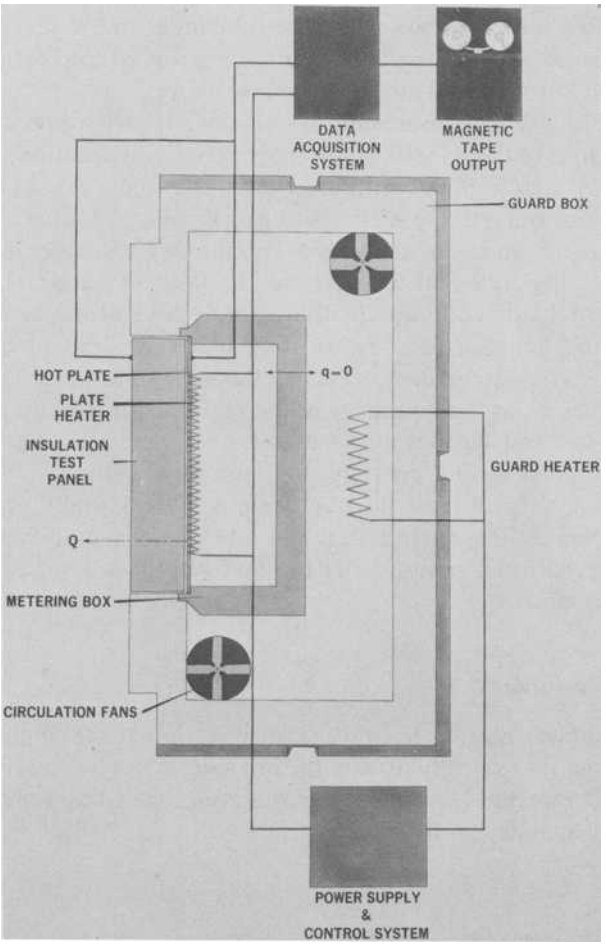

FIG. 5—*Schematic of high-temperature guarded hot box.*

1. The test panel does not extend beyond the metering area, which is sized to accept one full-sized 914-mm (36 in.) square panel up to 203 mm (8 in.) thick. Homogeneous insulation surrounds the edges of the test panel and acts as guard insulation. The test panel edge boundary condition is important and will be discussed later. All of the internal through-conduction and convection paths that exist in the field also exist in the test panel. Internal panel modifications are not required.
2. The cold side of the box has been eliminated to expose the cold surface of the test panel to ambient air. This allows a natural convection boundary condition on the cold side of the test panel.
3. The forced-convection boundary on the hot side of the test panel

has been replaced with a constant-temperature hot surface. This heated plate simulates the hot equipment surface.

4. The entire guarded hot box can be rotated to a position anywhere between vertical and horizontal. In the horizontal position the panel is bottom-heated and the heat flow is upward.

5. Hot surface temperatures up to 811 K (1000°F) can be achieved on the heated surface.

Figure 6 shows the facility in the vertical position. A brief description of the major facility components follows:

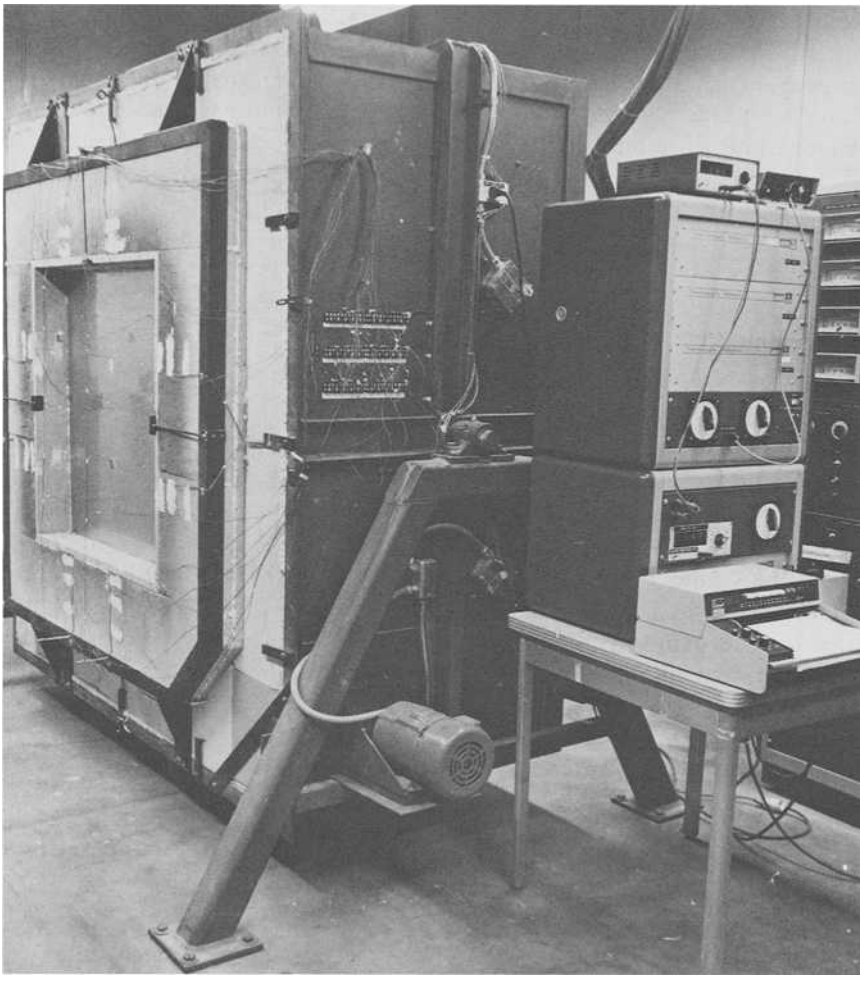

FIG. 6—*New high-temperature guarded hot-box facility.*

Guard Box

The guard box consists of a structural steel frame insulated with 152 mm (6 in.) of calcium silicate block insulation on the inner surface. Air in the guard box is circulated by two fans after being heated by tubular electric heaters in circular ducts. The temperature in the guard box is automatically controlled to maintain a near-zero temperature difference across the metering box walls.

Metering Box

The metering box walls are 102 mm (4 in.) thick and constructed from four layers of 25-mm-thick (1 in.) structural insulation board. The layers are fastened together by stainless wood screws staggered between layers to prevent any through-conduction paths. The inner surface of the metering box is painted with a high-emittance paint to increase radiation interchange and to minimize temperature differences within the box cavity. The five metering box walls are instrumented with a thermopile consisting of 21 pairs of thermocouples between the inner and outer surfaces. This thermopile is used to control the guard box heaters and also to make a heat flow correction for the metering box. Several independent thermocouples are also installed on the inner and outer surfaces for measuring local temperature imbalances.

Hot Plate

The plate size is 914 mm (36 in.) by 914 mm (36 in.) by 13 mm (0.50 in.) and was fabricated by screwing together two thin stainless steel sheets. A heater wire, insulated with ceramic beads and cement, is imbedded in a machined groove in one of the plates. This groove forms a squared spiral from the center out to the edges of the plate. The second thin stainless plate covers the heater wire and is painted with a high-emittance paint on the surface exposed to the test panel. The back side of the assembled plate (toward the metering box) is also coated with a high-emittance paint.

Power Supply and Controls

Both the hot plate and the guard box power supplies are automatically controlled. Plate power is dc and is controlled to provide the desired plate temperature. Guard box power is ac and is controlled to maintain a near-zero temperature difference across the metering box walls.

Data Acquisition and Reduction

Data from the facility includes thermocouple and plate power measurements. These d-c voltage signals are recorded on magnetic tape via

a Hewlett-Packard 2100A computer-controlled digital data acquisition system. The primary data reduction and analysis is performed with this tape on a Control Data Corp. 7600 computer.

Test Panel Edge Boundary

As mentioned in the foregoing, the edge boundary condition for the test panel is important and requires special consideration. The new facility was designed to test only reflective panels with end supports (see Fig. 2) that are *completely closed*. A closed end support assures that there is no direct convection path between stacked panels, and conduction between adjacent end supports is the only mechanism for panel-to-panel heat transfer. If the end supports are partially open, a convection path would exist between vertically stacked panels and a test on several stacked panels would be the only way to measure the true heat loss.

Because the facility was designed to test panels with completely closed end supports, any heat conducted in or out of the panel edges will affect measured performance and must be included in the data analysis. A two-dimensional conduction heat-transfer model was developed to calculate the heat flow through the edges of the test panel. This finite-difference conduction model includes the region of homogeneous insulation that forms the test cavity and that portion of the metering box adjacent to the edges of the hot plate. Heat flows through these modeled regions can be determined quite accurately if the boundary temperatures can be defined. Approximately 100 thermocouples are installed on the surfaces of these regions, and these temperature measurements provide the steady-state boundary conditions for the conduction model. The calculated edge heat flow is then either added or subtracted, depending on its direction, to that generated in the hot plate. Typically, the magnitude of this edge heat flow correction is only about 7 percent of the power generated in the hot plate.

Facility Verification

It was desired to verify the panel facility by testing a reflective insulation panel at an independent laboratory. However, other facilities were not available that could test a 914-mm (36 in.) square panel with the same boundary and temperature conditions. Instead, two 914-mm (36 in.) square *homogeneous* panel specimens were tested in the horizontal position on the guarded hot box. High-temperature rigid fibrous block insulation was used. After testing on the guarded hot box, two 610-mm (24 in.) square specimens were cut and sent to an independent laboratory (Dynatech R/D Co.) for testing via the ASTM Test for Steady-State Thermal Transmission Properties by Means of the Guarded Hot Plate (C 177–76). Two identical

specimens were required and testing was done in the horizontal orientation. The results from these tests (Fig. 7) show the measured thermal conductivity obtained from two independent laboratories using different test methods. Agreement between the two data sets is very good, with the total spread averaging approximately 3.5 percent.

It was still desired to verify the facility for reflective insulation panels. Since a suitable independent facility that could test panels did not exist, a pseudo-verification was performed. With reflective panels in the vertical orientation, heat flux was measured from the exposed surface of the test panel. A single heat flux meter was moved from position to position to measure the cold surface heat flux at 48 grid locations as shown in Fig. 8. Grid locations were closely spaced in regions of higher heat flux gradients based upon temperature measurements on other panels. A commercial heat flux meter was specially modified by attaching a lightly oxidized stainless steel metal foil on the exposed (or cold) surface of the meter. The emittance of this metal foil was selected so that the thermal resistance from the insulation outer surface to the ambient air did not change when the heat flux meter was applied. Flux readings from the 51-mm (2 in.) square meter were area-weighted and averaged to provide a heat flux for comparison with that measured by the guarded hot box facility. Results from tests on two panels are shown in Fig. 9, and the agreement is quite good. The heat flux meter gave results that were 4.9

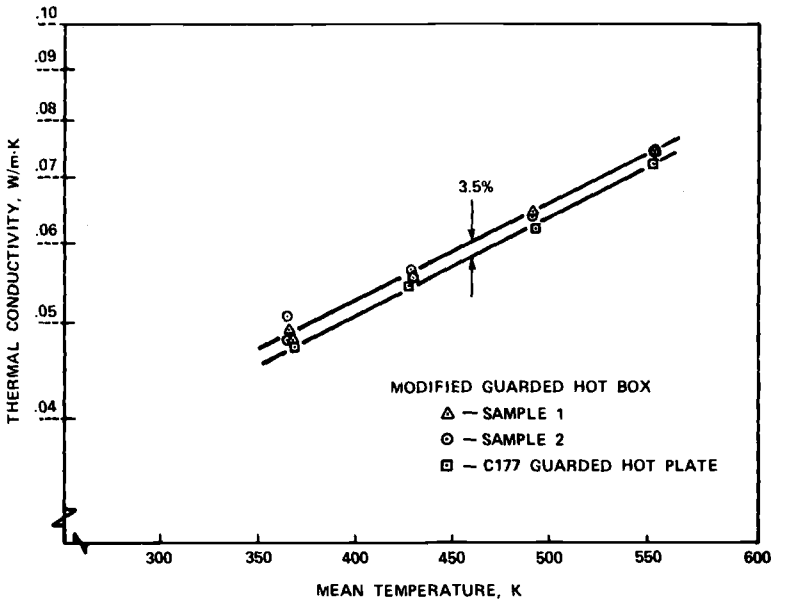

FIG. 7—*Verification tests with homogeneous insulation.*

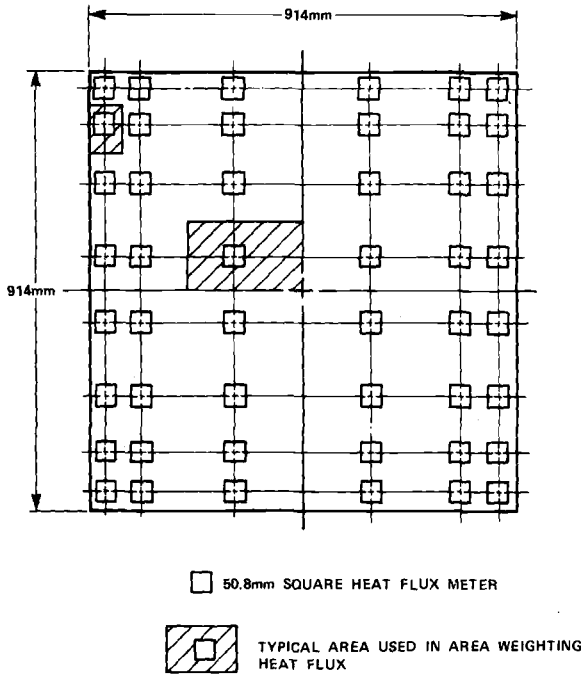

FIG. 8—*Heat flux measurement array on cold surface of a reflective insulation panel.*

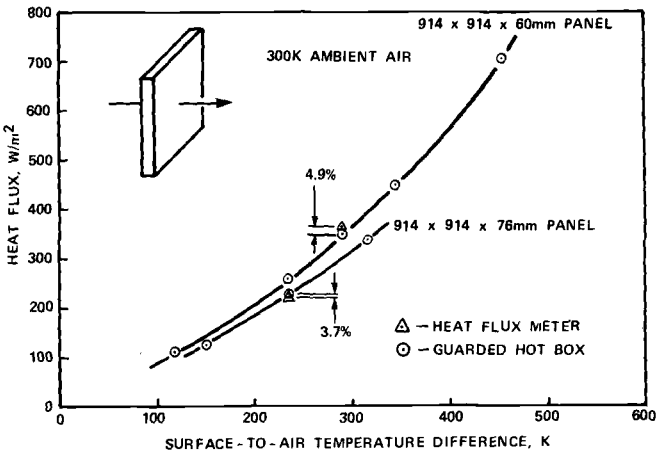

FIG. 9—*Verification test with reflective insulation.*

percent greater than the hot-box facility for one panel, and gave results that were 3.7 percent lower for the other panel.

Convection Effects

As discussed in the foregoing, internal convection can affect the heat flow from a reflective insulation panel. If it does exist to a significant degree, the effects will be a higher heat loss and a nonuniform heat flux on the outer surface. This is illustrated by heat flux profiles obtained during the foregoing verification tests. Figure 10 shows the vertical and horizontal heat flux profiles along the outer surface of a reflective panel in the vertical position. The nonuniform vertical profile clearly shows that internal convection does exist within this particular panel. The horizontal heat flux profile is almost flat, as expected, since the buoyancy force acts only in the vertical direction.

The heat flux profiles shown in Fig. 10 were measured on a panel with contacting "dimpled" liners. Liners were spaced by the dimples, which were a regular array of bumps formed in the liners. Similar heat flux profiles were measured for panels with parallel smooth liners and for random "crinkled" lines. Crinkled liners were spaced by a random pattern of deformations over the entire liner surface. Similar heat flux profiles

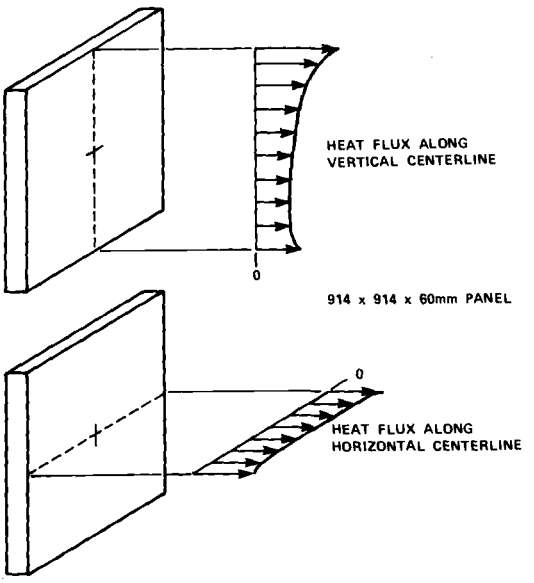

FIG. 10—*Heat flux distributions illustrate internal convection.*

means that internal convection did exist in each of the test panels with different liner spacing designs.

Orientation affects internal convection and, therefore, heat loss from a reflective panel. This is shown in Fig. 11, by transference data for a panel with significant internal convection which was tested in the vertical and horizontal positions. Transference is an overall heat-transfer coefficient from the hot surface to the ambient air. The only difference between the two sets was orientation, and the heat loss for the vertical position was greater than that for the horizontal position. Internal convection was the only heat-transfer mode affected by the orientation change. Notice in Fig. 11 that the two performance curves tend to converge at the higher temperatures. This is caused, in part, by the effect of increasing radiation heat transfer, which becomes dominant at higher temperatures. Natural convection within the panel is also greatly reduced at higher temperature levels. In the air gaps near the hot surface, for example, the Grashof number is reduced by about a factor of ten from the lowest to the highest temperature test points. The Grashof number is a dimensionless number used to characterize the driving force for natural convection.

System Heat Loss

A new guarded hot-box facility has been described for testing one flat panel of reflective insulation under simulated field boundary conditions.

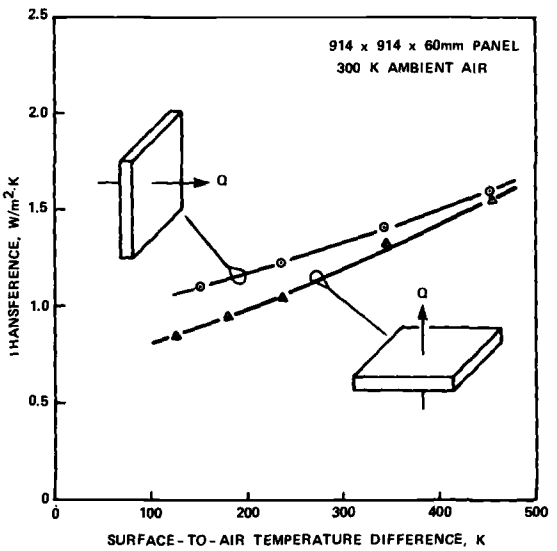

FIG. 11—*Heat loss through reflective insulation is affected by orientation.*

This facility can be used to measure the effects of insulation thickness, number of reflective liners, panel orientation, panel construction, panel-to-panel joints, and hot surface temperature. All of these parameters must be considered when designing a complete reflective insulation system. However, it is difficult to exactly duplicate true field boundary conditions in a laboratory experiment. Therefore, it is still desirable to verify the installed performance of an insulation system.

A field test of an insulation system on an operating commercial nuclear reactor is not practical for many reasons. The primary technical difficulty is caused by the number of systems within the containment building and the equipment size and complexity. The heat loss from the insulated equipment is only a portion of the total containment heat load and cannot be isolated from the total.

A reasonable compromise between a single-unit laboratory test and a system test on a nuclear reactor would be a controlled large-scale experiment consisting of several panels of reflective insulation assembled into a "system." One such test that is being considered consists of a 3-panel-wide by 4-panel-high array of full-size flat panels installed on a vertical hot surface. The hot-surface boundary would be the furnace wall of a fossil boiler operating at a temperature of about 561 K (550°F). The heat loss of individual panels in the array would be determined by the heat flux mapping technique described earlier. This should provide heat loss data for a "system" of reflective panels tested with hot surface, cold surface, and edge boundary conditions identical to those expected in service.

Summary

Reflective insulation requires special test considerations because of its nonhomogeneous construction, and the existing ASTM C 236 method can yield invalid results relative to true field performance. A new high-temperature guarded hot-box facility was constructed to test full-sized flat reflective insulation panels in both the vertical and horizontal orientations. Tests by an independent laboratory, using a different ASTM test method, have verified the facility for testing homogeneous insulations. Verification tests on vertical reflective insulation panels, using heat flux measurements on the exposed surfaces, have shown good agreement with data from the panel facility. An *in situ* system heat loss verification test is desirable, but not practical. A large-scale experiment, consisting of several panels metered for heat flux on their cold surface, is proposed to verify that reflective insulation systems can be accurately designed from tests on individual units of insulation.

T. L. Lauvray[1]

A Calibrated Hot-Box Approach for Steady-State Heat-Transfer Measurements in Air Duct Systems

REFERENCE: Lauvray, T. L., "**A Calibrated Hot-Box Approach for Steady-State Heat-Transfer Measurements in Air Duct Systems,**" *Thermal Transmission Measurements of Insulation, ASTM STP 660*, R. P. Tye, Ed., American Society for Testing and Materials, 1978, pp. 357–373.

ABSTRACT: The paper describes a procedure for measurement of steady-state heat transfer through the walls of air duct systems under actual operating conditions and configuration. The procedure uses two independent measurement techniques. A calibrated hot box is the primary measurement technique and an airstream temperature-drop measurement provides a secondary technique.

The calibrated hot box is a heavily insulated box which is sealed around a duct conveying cold air. A temperature controller and electric resistance heaters maintain the box temperature as close as possible to ambient temperature. Thus, the laboratory space acts as a guard for the box. The energy input to the box is measured with a watt-hour meter. The total energy input, corrected for the heat transfer through the box wall, represents the heat transfer through the test system.

The temperature-drop technique uses thermocouples to measure the temperature difference betweeen two stations in the test duct and orifice plates to measure airflow. The heat transfer from this technique is compared with calibrated hot-box measurements.

An automatic data collection system is used so that tests can be conducted over a long period of time to assure steady-state conditions and to determine reproducibility.

Verification of the calibrated hot-box technique is achieved by testing a specially constructed section of duct whose heat transfer can be readily calculated. Experimental and calculated data are presented for this duct section.

KEY WORDS: air ducts, calibrated hot box, heat transfer, thermal transmission, thermal conductivity

Nomenclature

- U Thermal transmittance based on outside surface area, W/m^2K, $(Btu/h \cdot ft^2 °F)$
- q Heat flow through test specimen, W, (Btu/h)
- A_o Outside surface area of test specimen, m^2, (ft^2)

[1]Senior engineer, Owens/Corning Fiberglas Corp., Granville, Ohio 43023.

T_a Average temperature around the test specimen, K, (°F)
T_d Average air temperature of ducted airstream in test specimen, K, (°F)
M Mass flow rate in flow loop, kg/s, (lb/h)
C_p Specific heat of airstream, J/(kgK), [Btu (lb°F)]
t_1 Bulk mean fluid temperature at upstream section of test specimen, K, (°F)
t_2 Bulk mean fluid temperature at downstream section of test specimen, K, (°F)
P Measured energy input to calibrated hot box, W, (Btu/h)
F_b Box correction factor or heat flow through box walls per degree, W/K, (Btu/(h·°F))
T_b Average temperature in calibrated hot box, K, (°F)
T_{am} Ambient temperature surrounding calibrated hot box, K, (°F)
D_i Outside diameter of metal pipe used for standard duct, m, (ft)
h_i Inside film heat-transfer coefficient, W/ (m²K), [Btu/(h·ft²°F)]
D_o Outside diameter of insulated standard duct, m, (ft)
λ Apparent thermal conductivity of insulation material used on standard duct, W/(m·K), [Btu/(h·ft°F)]
h_o Outside film heat-transfer coefficient, W/(m²K), [Btu/(h·ft²°F)]
λ_f Thermal conductivity of air, W/(m·K), [Btu/h·ft°F)]
Re Reynolds number
Pr Prandtl number
f Frictional drag coefficient of standard duct
h_c Convection outside film coefficient, W/(m²K), [Btu/(h·ft°F)]
Gr Grashof number
g Gravitational acceleration constant, m/s², (ft/s²)
ρ Air density, kg/m³, (lb/ft³)
β Coefficient of thermal expansion, 1/K, (1/R)
T_s Temperature of duct surface, K, (°F)
μ Viscosity of air, kg/(s·m), [lb/(s·ft)]
$\in$ Emittance of duct surface
ν Nusselt number
h_r Radiant outside surface coefficient, W/(m²K), [Btu/(h·ft²°F)]

The severe winter of 1977 has accented our energy problems and has every segment of society seeking solutions. Obviously, conservation will play a key role whatever the solution. Standards and codes requiring minimum performance levels for building energy-system components will help to encourage conservation. Without accurate procedures for measuring the performance of the components, however, such standards will be meaningless.

Insulation requirements for air duct systems exemplify the need for improved measurement procedures. The American Society of Heating, Refrigeration, and Air-Conditioning Engineers (ASHRAE) Standard 90-75 contains a thermal resistance requirement for air duct systems. In the most straightforward approach to determining compliance, the insulation thickness is divided by the thermal conductivity of the insulation material. Manufacturers of air duct insulation and preinsulated air duct systems provide thermal conductivity data with their products as measured by the ASTM Test for Steady-State Thermal Transmission Properties by Means of the Guarded Hot Plate (C 177-76), or ASTM Test for Steady-State Thermal Transmission Properties by Means of the Heat Flow Meter (C 518-76).

However, the construction of some products suggests that thermal resistance based on thermal conductivity data may not represent thermal

performance under actual operating conditions and configurations. Specifically, products that have a porous insulation material in contact with the ducted airstream may have poorer thermal performance than expected. A small airflow within the insulation can adversely affect thermal performance. Joints are another possible cause of unpredicted energy loss. Thus, the traditional approach for measuring thermal resistance may be unsuitable in some cases.

Little thermal performance data exist on air duct systems tested under actual operating conditions and configurations. This paper describes a procedure which can be used to generate the needed data at accuracies within 5 percent. This procedure utilizes a calibrated hot box to provide the primary measurement technique. Temperature-drop measurement serves as a secondary technique and provides a rough check on calibrated hot-box results.

General Description of Procedure

Thermal transmittance, U, for a test duct specimen under steady heat flow conditions can be computed from

$$U = q/[A_o\,(T_a - T_d)] \tag{1}$$

The calibrated hot-box test procedure is designed to measure the independent variables of Eq 1.

To generate a temperature difference, cold air at a controlled temperature is circulated through a closed-loop air duct system. The test duct specimen forms one section of the loop. The rest of the loop is an integral part of the test apparatus and contains a fan, an air metering duct, refrigeration equipment, heaters, temperature controls, and connecting ducts.

The heavily insulated calibrated hot box is equipped with an air-circulation system, electrical heaters, and temperature controls. The box is sealed around a section of the air duct test specimen. A watt-hour meter is used to measure total energy input to the box. Ideally, heat exchange between the box and ambient space is negligible and energy input to the box equals the heat flow, q, between the box and the section of test specimen within it. This ideal condition is approximated by locating the box in a temperature-controlled laboratory and keeping the box temperature as close as possible to the laboratory temperature. The insulation on the box walls further reduces heat exchange.

Nevertheless, there is still some heat exchange between the box and laboratory. Since the box wall area is considerably greater than the test specimen area, only a small temperature difference between the box and laboratory can result in an undesirably large heat exchange between the

box and laboratory. In practice, the laboratory temperature fluctuates a few degrees from its control point, which makes a zero-degree temperature difference impractical. For these reasons it is necessary to measure the thermal transmittance of the box in order to correct the test results. This is done by maintaining the box temperature several degrees above ambient and metering the energy input. The box area is fixed for all tests, so heat transfer between the box and laboratory is a function of temperature difference only. Thus, once the box transmittance is measured, a correction can be applied to all tests.

With the design considerations and correction just described, the heat flow through the test specimen can be measured with sufficient accuracy. The calibrated hot box and flow loop combine to generate a stable temperature difference and, thus, steady heat flow. The specimen area and temperature difference can be readily measured, so thermal transmittance of the test specimen can be computed using Eq 1.

Thermal transmittance is also measured by a temperature-drop technique. Steady heat transfer occurs between the laboratory space and the test specimen portion of the flow loop. The heat flow can be computed from Eq 2 by measuring the mass flow, m, and the temperature difference, (t_1-t_2), between two stations in the test duct

$$q = MC_p\,(t_1-t_2) \tag{2}$$

Again the temperature difference and specimen area are readily measured, so Eqs 1 and 2 can be used to compute the thermal transmittance of the test specimen.

This approach is less accurate than the calibrated hot-box approach. The temperature difference between two stations in the test duct is very small and difficult to measure accurately. Laboratory temperature variations cause fluctuation in heat flow. Despite these limitations, the temperature-drop technique serves, with little additional effort, as a rough check on calibrated hot-box results. It also can be used to test specimens with the heat flow reversed, by testing with duct temperatures above ambient.

Test Apparatus

Flow Loop

Figure 1 is a schematic arrangement of the major elements of the test apparatus. This is a convenient arrangement that fits within laboratory space constraints while meeting requirements for proper test procedures.

Two considerations need to be addressed regarding airflow. The fan must have sufficient capacity to provide the desired air velocity in the largest duct specimen to be tested. The chosen fan has a capacity of 2.36

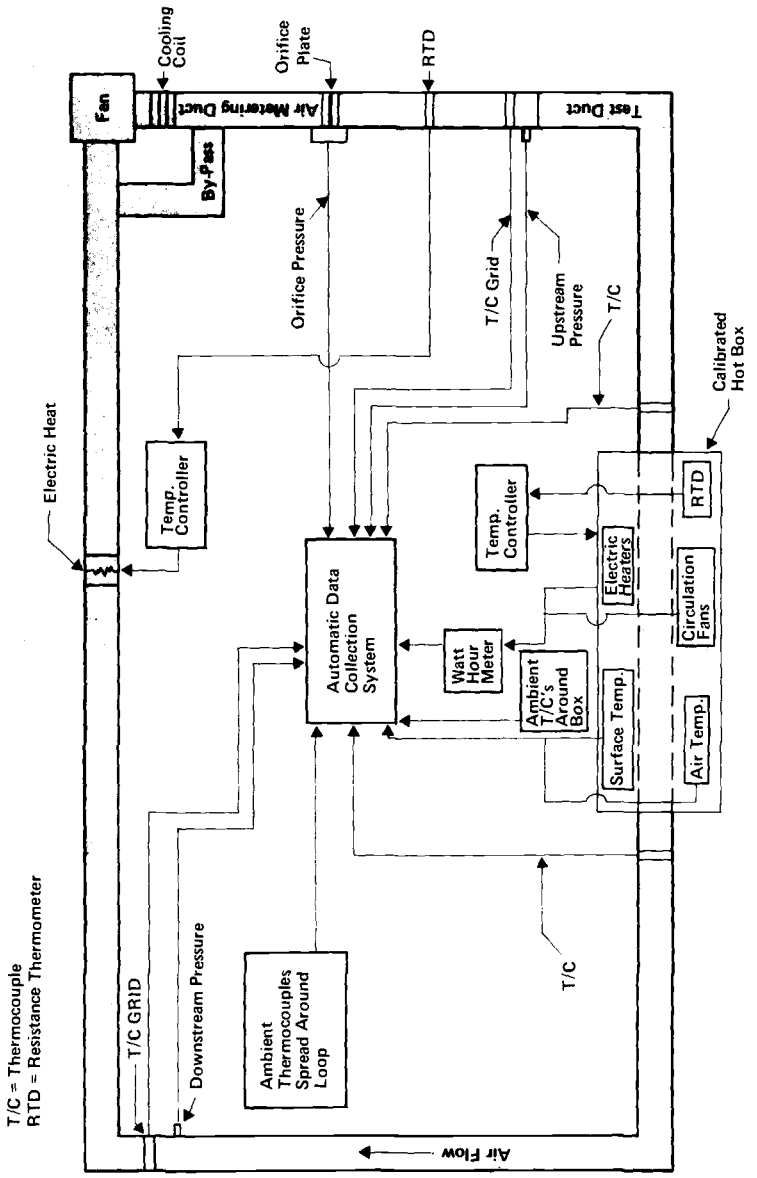

FIG. 1—*Diagram of test apparatus.*

m^3/s (5000 ft^3/min) at a total pressure rise of 1494 N/m^2 (6 in. of water). Second, and equally important, is the ability to control airflow. The desired flow in the test specimen must be obtained while at the same time maintaining a minimum airflow across the coil to prevent frost buildup. This is accomplished by a combination of variable inlet vanes on the fan and a bypass air duct after the coil. Damper adjustment proportions the total flow between the test loop and bypass loop.

An air metering duct meters the airflow through the test loop. This duct is designed according to the 1959 edition of *Fluid Meters*, published by the American Society of Mechanical Engineers (ASME). The primary flow metering devices are concentric orifice plates. Three different-size orifice plates provide metering capability over a wide range of flows. The entire metering duct is constructed of stainless steel. Gaskets and angle-iron flanges are used for transverse joints. Straightening vanes 2.7m (9.0 ft) upstream of the orifice plate minimize flow distortions. Four equally spaced sidewall pressure taps are located one diameter upstream and one-half diameter downstream of the orifice plate.

Use of ASME design parameters allows ASME published orifice flow coefficients to be used to compute airflows. This eliminates the need for orifice plate calibration, which is very difficult for the desired range of Reynolds number. ASME claims accuracies within 1 percent for properly designed metering sections. A comparision of the metering duct with a carefully conducted pitot-static tube traverse showed agreement within 3 percent over the range of airflow rates. Orifice plates have a distinct advantage over venturi-tubes or flow nozzles. They can easily be replaced with different-size plates to cover a wide range of airflows.

A cooling coil supplied by a cold-water chiller cools the air circulating through the flow loop. The chiller has a 4.5-tonne(t) (5 ton) refrigeration capacity at a leaving coil temperature of 266 K (20°F).

Normally, it is desirable to run the test with loop air temperature as low as possible. This condition is desirable to minimize the percentage of calibrated hot-box correction to heat flow and to maximize loop temperature change. For some types of ducts, however, air temperatures of 266 K (20°F) result in surface condensation, a condition causing errors in thermal transmittance measurements. To avoid this, the test specimen surface temperature must be maintained above the surrounding air dew point. This is achieved by varying the test loop temperature.

Coarse temperature control is achieved by bypassing a portion of the fluid from the coil back to the chiller. The use of a chilled fluid rather than direct refrigeration is more compatible with a bypass system.

Fine temperature control is achieved with electric resistance heaters coupled with a temperature controller. The total reheat capacity is 4000 W—3000 W fixed and 1000 W control. The temperature controller consists of fine nickel wire and forms one leg of a Wheatstone bridge circuit. The

nickel wire is strung on a frame with the same internal diameter as the duct into which it is mounted. This approach serves to control the average air temperature.

Connecting air ducts in the flow loop are constructed from galvanized metal. All joints are carefully sealed. To minimize condensation, 2.54-cm (1 in.) fibrous glass with an aluminum foil vapor barrier is applied to the exterior walls of the loop air ducts. Insulation joints are covered with aluminum-foil tape to ensure a continuous vapor barrier.

Calibrated Hot Box

Figures 2 and 3 are schematic diagrams of the calibrated hot box. The diagrams show the arrangement and relative size of the various elements.

The box is constructed of 12.7-mm (1/2 in.) plywood and is insulated with 152-mm (6 in.) urethane foam. The resulting thermal resistance is greater than 5.3 m^2K/W (30 $h \cdot ft^{2\circ}F/Btu$). The surface of the foam insulation is protected with an elastomeric coating. Blocks of foam insulation 76 mm (3 in.) were cut and fitted to insulate the box. All joints were offset to minimize heat transfer through cracks in the insulation.

The box contains two independent sections, which allows either straight duct sections or elbows to be tested. Each section has one removable end

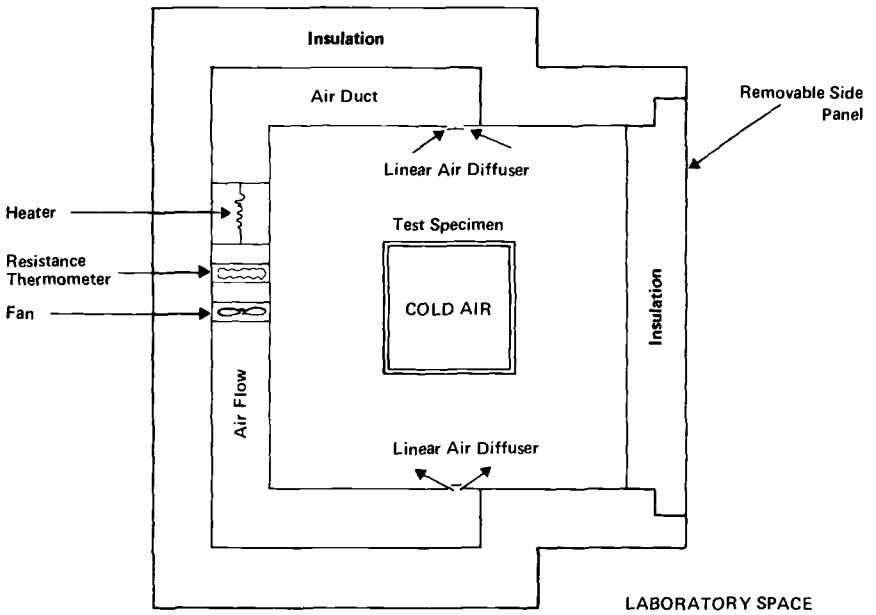

FIG. 2—*Cross section of calibrated hot box.*

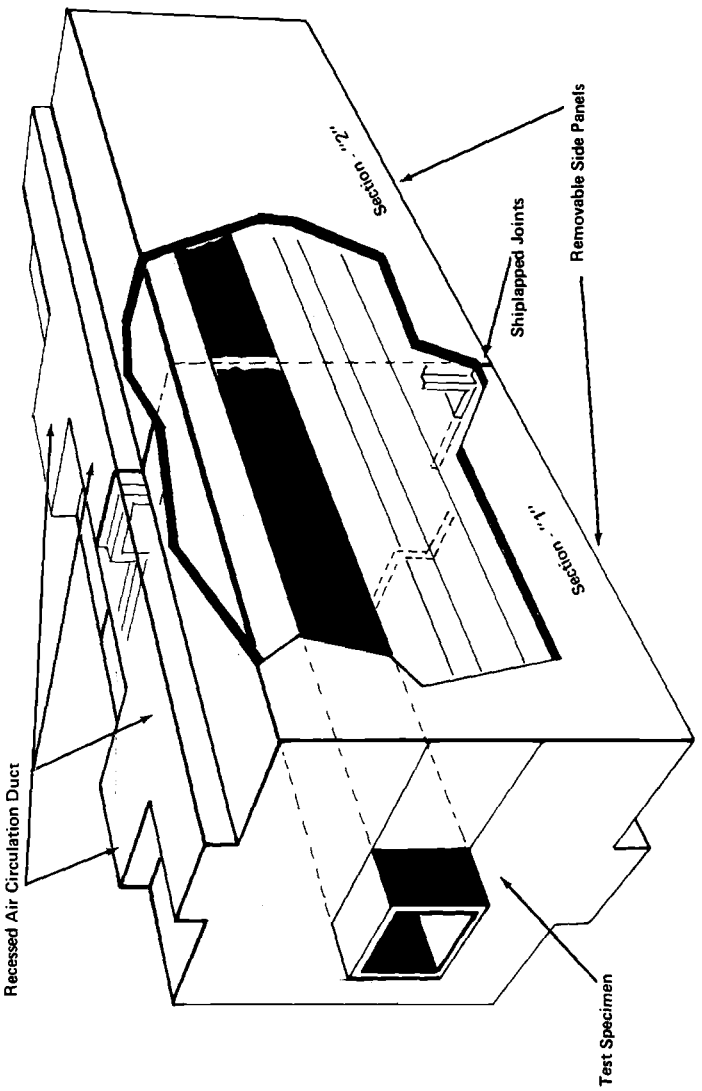

FIG. 3—Calibrated hot box with installed specimen.

and side panel. When a straight section of duct is tested, the sections are joined and the test specimen enters and leaves the ends of the box. When elbows are tested, only one section is used and the test specimen enters the end and leaves the side of the box. The box is 3.0 m (10 ft) long with a 0.91 m (3 ft) square interior. Box sections are supported by carts with adjustable heights.

Each section has its own air circulation system. Small circulation fans are located in recessed air ducts. The fans have a free delivery capacity of 0.026 m^3/s (55 ft^3 min) and a maximum power draw of 6 W. Air is supplied through a linear air diffuser in the bottom of the box and returned through a linear air diffuser in the top of the box. Linear diffusers deliver a constant slot velocity along their lengths. The linear diffusers and their supply ducts are recessed so that the tops of the diffusers are flush with the interior surface of the box. The circulation system is designed to maintain a uniform air velocity below 0.25 m/s (50 ft/min) around the test specimen. Actual measurements indicate the velocity to be approximately 0.13 m/s (25 ft/min).

Electric resistance heaters coupled with a temperature controller maintain a nearly constant box temperature. Using the same control approach described for the loop air temperature, fine nickel wire serves as the temperature sensor. Test data show that the average box temperature is maintained within 0.3 K (0.5° F) over a test period of several hours.

For most tests, the temperature uniformity of the box was within 1.4 K (2.5° F). This value is based on maximum measured temperature differences along the supply and return air diffusers.

Instrumentation

A watt-hour meter measures the total energy input to the calibrated hot box. The manufacturer certifies the meter to be accurate within 0.10 percent for any range with a load from 25 to 150 percent of full scale. The meter accuracy is periodically verified by comparing it with another meter.

Electronic pressure transducers measure upstream and downstream orifice pressures. The transducers are calibrated against water manometers with a sensitivity of 0.249 N/m^2 (0.001 in. of water). The gain of the transducer is adjusted so that 1 mV transducer output equals 249 N/m^2 (1 in. of water) pressure. Internal calibration resistors provide a calibration check at the beginning of each test, and calibration against the water manometer is repeated quarterly.

All temperatures are measured with thermocouples that meet the following requirements:

1. National Bureau of Standards premium grade wire,
2. Type T-copper/constantan wire,
3. No. 30 B&S gage wire,

4. inert gas welded wire, and
5. small bead diameters.

Finished thermocouples are spot-checked with a precision mercury thermometer to see that they are within the standard error limits of ±0.42 K (0.75° F) for the operating range of temperatures.

The calibrated hot box temperature is measured with 12 thermocouples. Six thermocouples are located in each section, three each spaced along supply and return air diffusers. The thermocouples are positioned so that the bead is in the center of the diffuser slot.

Surface temperatures of the test specimen are measured at one position in the center of each hot box section. For round ducts, four thermocouples are placed $\pi/2$ rad apart along vertical and horizontal lines. For rectangular ducts, one thermocouple is placed in the center of each side. The thermocouples are fastened with tape that has a surface emittance approximately matching that of the duct surface.

Test specimen air temperature for the calibrated hot-box technique is measured with a thermocouple placed in the center of the ducted airstream before and after the box. The thermocouples are held in place and shielded with a piece of copper tubing. The temperature measurements needed for the temperature-drop technique are obtained with thermocouple grids located at the beginning and end of the test specimen section of the flow loop. A grid consists of 25 thermocouples located at the center of equal segments of the duct cross-sectional area. The bulk mean fluid temperatures, t_1 and t_2, are obtained by averaging the individual temperatures, each weighed according to the air mass flow through its segment. The precentage mass flow through each segment is determined experimentally with pitot-static tube transverses and is assumed to be constant for all test conditions. The laboratory temperature is measured by six thermocouples spaced around the calibrated hot box.

An automatic data acquisition system permits a test to be run over a period of several hours to assure steady heat flow and to determine reproducibility. A brief description of the system, starting at the sensors and ending at the data output, follows.

Thermocouples are referenced to a uniform, highly conductive temperature block located inside an insulated box within the laboratory space. The block, in turn, is referenced to ice point with an electronic compensation network. Referenced thermocouples and pressure transducer voltage outputs are accessed through data scanners. An integrating digital voltmeter measures the accessed sensor output.

Watt-hour meter output is measured with a photoelectric pickup system. Each revolution of the disk generates four voltage pulses which are totaled by an electronic counter.

Data acquisition functions are controlled by a minicomputer. A timer initiates a data scan at precise 60-min intervals. The computer is pro-

grammed to read the totalized watt-hour counts, and then address the sensors in a predetermined sequence. As the data points are read, they are fed to a terminal and recorded on paper and cassette tape. The cassette tape is later used as input for a large data processing machine.

Specimen Preparation

Test specimens are constructed following manufacturer's recommendations, except for joint closure. The calibrated hot box is not designed for test specimens that leak air. To prevent leakage, special care must be taken to seal joints. This normally involves sealing both longitudinal and transverse joints with duct tape.

The clearance between the test duct and the opening in the ends of the calibrated hot box must be insulated. Blocks of urethane foam insulation are hand cut to fit around the test duct. Cracks are stuffed with fibrous glass. Finally, duct tape is applied over the insulation on both the inside and outside of the box.

Figures 4 and 5 are photographs of a completed installation.

Procedure

Each duct specimen is tested at three airflows, representative of its anticipated service conditions. Normal test velocities are 3.6, 7.61, and 12.7 m/s (700, 1500, and 2500 ft/min). These serve as approximate targets for sample ducts used in typical heating and air-conditioning applications.

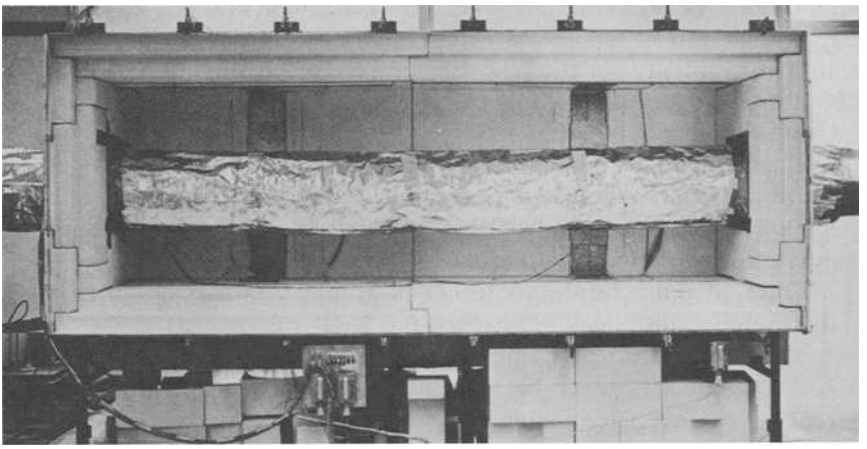

FIG. 4—*Front view of calibrated hot box with side panels removed.*

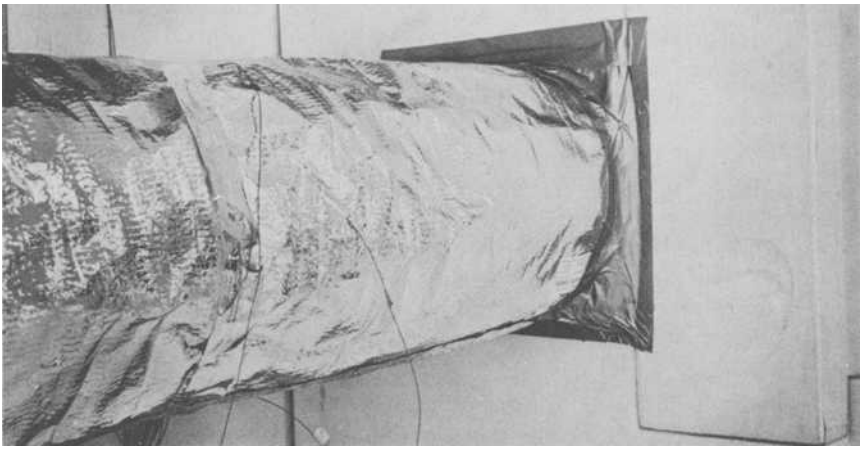

FIG. 5—*Close view of test specimen entering calibrated hot box.*

The desired flow rate is set by adjusting bypass dampers, the variable inlet vanes on the fan, or both.

With the flow rate set, the duct air temperatures and calibrated hot box temperatures are selected and set. The duct air temperature is usually set at the lowest temperature the refrigeration equipment can produce, about 266 K (20°F), unless the test specimen construction indicates that condensation could occur. In this case, chilled fluid bypass and electric reheat are adjusted to provide a higher temperature. The box temperature is set within 0.6 K (1° F) of the ambient laboratory temperature. Recognizing that the laboratory temperature may drift slightly during the test, it is desirable to intially set the box temperature as close as possible to the laboratory temperature.

Using the data acquisition system, the apparatus is monitored hourly until steady heat flow conditions are achieved. Steady heat flow is defined as three consecutive hourly data sets meeting all of the following criteria.

1. Box temperature controller is cycling and maximum average box temperature variation does not exceed 0.3 K (0.5° F).
2. Duct air temperature controller is cycling and maximum variation in duct temperature does not exceed 0.6 K (1° F).
3. Box temperature and ambient temperature are within 1 K (2° F).
4. Maximum difference between watt-hour meter reading is within 5 percent of the average reading.

For sample ducts with very good thermal performance, it may be necessary to tighten Criterion 3 to ensure that heat exchange between box and laboratory does not exceed 5 percent of the heat flow through the duct wall.

After steady heat flow conditions are obtained, a velocity run is started. A run consists of a minimum of three 1-h data sets. Normally several additional data sets are taken. The data acquisition system automatically scans the data hourly. Each data set is treated as an individual observation. Atmsopheric pressure and loop air dew point temperature are recorded at the beginning and end of a velocity run. The average of these readings is used in calculations for each data set.

To complete a test, the procedure is repeated for the other two flow rates.

Box Calibration

Heat exchange between the box and laboratory is designed to be less than 5 percent of the heat flow through the specimen walls. To achieve the desired overall test accuracy of 5 percent, it is necessary to correct the total energy input to the box for the heat exchange between the box and ambient air. Equation 3 is used to do this.

$$q = P - F_b(T_b - T_{am}) \tag{3}$$

The box correction factor, F_b, is experimentally measured by sealing the openings in the end with urethane foam insulation, maintaining the box several degrees above ambient temperature, and metering the energy input to the box. The box correction factor is then computed by dividing the measured energy input by the difference in mean temperature between the box and laboratory. This is done for several 1-h intervals to determine reproducibility. A measured box correction factor follows.

Average Box Correction Factor	No. of Observations	Standard Deviation
2.7 W/K [5.2 Btu/ (h°F)]	12	0.4 W/K [0.7 Btu/ (h°F)]

Test Procedure Verification

To verify the test procedure described in the foregoing, various instruments of the test apparatus were calibrated or their accuracies verified against other instruments. This gave some degree of confidence in the overall accuracy of the procedure. To gain further confidence, a standard duct was built and tested. The construction was such that theoretical heat-transfer calculations were simplified. For this case, a comparison of experimental and theoretical heat transfer for the standard duct provides a means to verify the overall accuracy of the procedure.

Construction of the standard duct was based on the following design

considerations. The duct should approximate the size and thermal transmittance of a typical test specimen. It should be circular to eliminate corner effects, which are difficult to predict. It must be airtight. The insulation material should have a stable thermal conductance with respect to age. It should be flexible enough to install easily, but rigid enough to ensure a uniform thickness. The insulation should be applied in a manner that will minimize joint losses.

To meet these considerations, a one-piece metal pipe was built and insulated with a cellular, elastomeric plastic sheet insulation. The pipe had a 0.25-m (10 in.) diameter and was 3.7 m (12 ft.) long. It was built from rolled sections of 16-gage black iron. Joints were welded and ground smooth. To meet thermal transmittance requirements, two 15.9-mm (5/8 in.) layers of insulation were cemented to the pipe. Two layers of insulation were used so that insulation joints could be staggered.

To compute the thermal transmittance of the calibration duct, interior surface roughness, insulation thermal conductivity, and exterior surface emissivity must be known. The interior surface roughness was assumed to be 0.00015 m (0.0005 ft), the same as galvanized sheet metal ducts. The surface emittance was measured with a disk receiver type of emissometer and found to be 0.79.

Thermal conductance measurements were made on test specimens constructed from two layers of 1.59-mm (5/8 in.) sheet insulation and adhered with contact cement. The construction of the specimens simulated the insulation construction on the duct. Thermal conductance data at three mean temperatures are presented in Table 1. The data are expressed as apparent thermal conductivity to simplify calculations of thermal transmittance.

Calculation of Theoretical Thermal Transmittance for Standard Duct

The following procedure to compute the theoretical thermal transmittance of the standard duct is based on the assumption of steady, one-dimensional heat flow. With this assumption, Eq 4 can be used to compute thermal transmittance.

$$U = \frac{1}{[D_o/(D_i h_i) + (D_o \ln (D_o/D_i)/(2\lambda)] + 1/h_o} \tag{4}$$

The pipe is assumed to have negligible thermal resistance so that the pipe diameter, D_i, is taken to be the outside pipe diameter.

All variables in Eq 4 are known except the film coefficients, h_i and h_o. Assuming a Prandtl number of 1 and using an analogy between heat and momentum transfer, Eq 5 can be derived

$$\nu = Re\, Pr\, f/8 \tag{5}$$

TABLE 1—*Apparent thermal conductivity of insulation on standard duct.*

Apparent Thermal Conductivity W/(m deg. K) (Btu/(hr ft deg. F))	Test Procedure	Mean Test Temperature deg. K (deg. F)	Hot Side Test Temp. deg. K (deg. F)	Cold Side Test Temp. deg. K (deg. F)
0.0395 (0.0228)	ASTM C 177	311 (100)	334 (141)	288 (59.4)
0.0387 (0.0224)	ASTM C 518	297 (75.0)	308 (95.0)	286 (55.0)
0.0379 (0.0219)	ASTM C 177	281 (46.5)	291 (64.3)	271 (28.6)

TABLE 2—*Comparison of theoretical and experimental thermal transmittance for standard duct.*

Number of Observations	Air Velocity m/s (fpm) Avg.	σ [b]	Experimental Transmittance W/ (m^2 deg. K) [BTU/(hr ft^2 deg. F)] Avg.	σ [b]	Theoretical Transmittance W/ (m^2 deg. K) [BTU/(hr ft^2 deg. F)]	Percent Difference[a]
9	6.55 (1200)	0.76 (150)	0.0294 (0.167)	0.0003 (0.002)	0.0296 (0.168)	0.7
13	15.9 (3130)	0.10 (20)	0.0299 (0.170)	0.0007 (0.004)	0.0308 (0.175)	2.9
17	19.9 (3920)	0.27 (53)	0.0301 (0.171)	0.0003 (0.002)	0.0308 (0.175)	2.3

Footnotes: a. Based on theoretical value

b. Standard deviation

Equation 5 can be corrected for nonunity Prandtl numbers by multiplying by the Prantl number to the 2/3 power. Substituting $(h_i D_i/\lambda_f)$ for ν, taking 0.72 as the Prandtl number for air in the range of test temperatures, and applying the correction, Eq 6 results

$$h_i = 0.072\,\lambda_f Re\, f/D_i \tag{6}$$

Equations yielding slightly different values can be found in heat-transfer texts. However, the effect of the interior film coefficient, h_i, on the thermal transmittance of the standard duct is minimal.

The outside surface coefficient, h_o, is a combination of radiant and convective heat transfer. This can be expressed with

$$h_o = h_c + h_r \tag{7}$$

Assuming free convection over a horizontal cylinder, Eq 8 yields the convective coefficient, h_c

$$h_c = 0.53\,\lambda_f\,(GrPr)^{0.25}/D_o \tag{8}$$

The Grashof number is defined by

$$Gr = \rho^2\, g\, \beta\, D_o^3\,(T_b - T_s)/\mu^2 \tag{9}$$

To simplify calculations, the mean temperature between the box air and specimen surface was assumed to be 291 K (65°F) in order to evaluate the parameters $g\,\beta\,\rho^2/\mu^2$.

To compute the radiant coefficient, h_r, the standard duct was assumed to be a small gray body in a black surrounding. For this case, h_r can be computed from Eq 10*a* (SI units) or Eq 10*b* (U.S. customary units)

$$h_r = \frac{0.567 \in \left(\left(\frac{T_a}{100}\right)^4 - \left(\frac{T_s}{100}\right)^4\right)}{(T_a - T_s)} \tag{10a}$$

$$h_r = \frac{0.171 \in \left(\left(\frac{T_a + 459.6}{100}\right)^4 - \left(\frac{T_s + 459.6}{100}\right)^4\right)}{(T_a - T_s)} \tag{10b}$$

For a true theoretical solution, T_s is unknown, so an iterative technique is applied. A value of T_s is assumed. Then, G_r, h_c, h_r, h_o, and U are computed from Eqs 9, 8, 10, 7, and 4, respectively. The heat flux is computed from Eq 1 and a new surface temperature is computed from

$$T_s = T_b - q/(h_o A_o) \tag{11}$$

Finally, the old and new values of surface temperature are compared. If they are within 1 percent, the interation is ended. Otherwise, the new surface temperature is used and the calculation procedure repeated.

Comparison of Theoretical and Experimental Transmittance for Standard Duct

Table 2 lists results of tests on the standard duct. The data show agreement within 3 percent between theoretical transmittance and average experimental transmittance. This agreement is within the 5 percent design accuracy for the procedure. The agreement is quite good, considering that theoretical calculations are probably subject to as many errors as experimental measurements. The agreement is taken as verification of the procedure.

Conclusions

An experimental approach to measure the thermal transmittance of air duct systems under different operating conditions and configurations has been developed. The accuracy of the approach has been verified and three years' experience has shown it to be a practical procedure.

Acknowledgment

The author thanks the Thermal Insulation Manufacturer's Association, Inc., whose desire to learn more about the thermal performance of their products made this project possible.

R. C. Svedberg,[1] *R. J. Steffen,*[1] *A. M. Rupp,*[2] *and J. W. Sadler*[1]

Evaluation of High-Temperature Pipe Insulations Using a 16-In.-Diameter Pipe Test Apparatus*

REFERENCE: Svedberg, R. C., Steffen, R. J., Rupp, A. M., and Sadler, J. W., **"Evaluation of High-Temperature Pipe Insulations Using a 16-In.-Diameter Pipe Test Apparatus,"** *Thermal Transmission Measurements of Insulation, ASTM STP 660*, R. P. Tye, Ed., American Society for Testing and Materials, 1978, pp. 374–405.

ABSTRACT: The thermal performance of candidate pipe insulation systems for the sodium piping at the Fast Flux Test Facility (FFTF) in Richland, Wash., has been tested at pipe temperatures up to 838.7 K (1050°F) using a 40.64-cm (16 in.) pipe test rig. Where applicable, procedures outlined in the ASTM Test for Thermal Conductivity of Pipe Insulation (C 335-69) were followed. These tests have demonstrated the feasibility of measuring thermal performance using large-diameter, guarded pipe test systems. To compare and evaluate the large-diameter pipe test results, the thermal performance of these insulations was also measured by an independent testing laboratory on a 7.62-cm (3 in.) pipe test apparatus.

Mineral wool, calcium-silicate, and aluminum-silica refractory fiber blanket-type insulations were evaluated on both the 40.64-cm (16 in.) and 7.62-cm (3 in.) pipe test apparatus. A contractor-installed calcium silicate and a duplex calcium-silicate-mineral wool system were also tested on the 40.64-cm (16 in.) pipe test apparatus to investigate thermal performance resulting from different installation procedures.

These measurements of the thermal performance of insulations assembled on large-diameter testing apparatus have been shown to be both feasible and informative. In cases where the insulation can be installed in a seam-free manner, that is, few cracks and gaps, the thermal properties are in excellent agreement with those measured on the standard 7.62-cm (3 in.) pipe test system.

In cases where installation is difficult and seam cracks and gaps occur, the additional heat losses can be evaluated on the large-diameter pipe test apparatus.

KEY WORDS: pipe insulation, heat transmission, guarded pipe test apparatus, calcium-silicate, insulation, thermal conductivity, alumina-silica insulation, block-type insulate, blanket-type insulation

*Original experimental data were measured in U. S. customary units.

[1]Fellow engineer, manager, Mechanical Design and Analysis, SURF Project, and project manager, MHD Generator Materials Development Program, respectively, Advanced Energy Systems Division, Westinghouse Electric Corp., Pittsburgh, Pa. 15236.

[2]Senior engineer, Advanced Reactor Division, Westinghouse Electric Corp., Cheswick, Pa. 15024.

The thermal performance of installed piping insulation is usually never measured on large-diameter pipes. Most of the thermal data available to designers are derived from guarded hot plate or pipe tests as per the ASTM C177 Tests for Steady-State Thermal Transmission Properties by Means of the Guarded Hot Plate (C 177-76) or Thermal Conductivity of Pipe Insulation (C 335-69), respectively. This paper presents data measured on a 40.64-cm-diameter (16 in.)[3] pipe test apparatus which describes the thermal performance of three high-temperature pipe insulations in as-installed configurations. The use of large-diameter pipe insulation test facilities is shown to be feasible, and this report describes the apparatus and provides data which substantiates its utility. Installation techniques for these insulations duplicated those used at the Fast Flux Test Facility (FFTF) in Richland, Wash. The following insulation systems were tested:

1. mineral wool (Epitherm-1200; Eagle Picher),
2. alumina-silica refractory fiber blanket (Cerablanket; Johns-Manville),
3. calcium-silicate (Thermo 12; Johns-Manville),
4. fiber glass cloth encapsulated refractory fiber blanket (Encapsulate Cerablanket; Johns-Manville),
5. calcium-silicate-mineral wool (48 Mineral Fiber) composite system (installed on pipe test apparatus by professional installers).
6. calcium-silicate (installed on pipe test apparatus by professional installers).

The mineral wool, alumina-silica, and calcium-silicate were evaluated by an independent testing laboratory[1] on the 7.62-cm (3 in.) pipe test apparatus as specified by ASTM Method C 335. A direct comparison of thermal conductivity is made between the manufacturer's data, the 7.62-cm (3 in.) pipe test data, and the 40.64-cm (16 in.) pipe test data. The considerations outlined in the ASTM Method C 335 were followed as closely as possible during construction of the 40.64-cm (16 in.) pipe test apparatus and the evaluation of the thermal performance. Hopefully, the data presented herein may serve as a basis for expanding the test method to include larger pipe test apparatus.

Experimental Apparatus

The guarded pipe test method, ASTM C 335-69, was used as a guide for building 40.64-cm-diameter (16 in.) test apparatus and for measuring the thermal performance of the selected insulations. In this 40.64-cm-diameter (16 in.) apparatus a portion of the FFTF sodium piping system

[3]16-in. and 3-in. designations are nominal and used to identify specific apparatus.
[4]Dynatech, Inc., Cambridge, Mass.

was simulated by using a stainless steel pipe section and incorporating the insulation support structure designed for the FFTF piping.

The pipe test apparatus was 2.438 m (8 ft) long. The central test section was 1.22 m (4 ft) long, and the guarded heater sections were 0.61 m (2 ft) long. Figure 1 shows an axial cross-sectional schematic of the pipe test apparatus. Slot type gaps 12.7 mm (0.5 in.) wide and 15.87 cm (6.25 in.) long were machined at six locations around the circumference to thermally isolate the center test heater section from the guard heater section. This reduced axial conduction heat loss through the pipe by 76 percent. The pipe wall thickness was 6.4 mm (0.250 in.). Chromalox tubular heating elements of triangular cross section were clamped to the inside diameter of the 40.64-cm (16 in.) pipe. Three independent and controllable heater circuits were used, one on the test section and two in the guarded heater section. The heater installation is shown in Fig. 2. Thermocouples were spot welded to the outside diameter of the test pipe at the axial locations shown in Fig. 1. The axial locations were repeated at 2.09 rad (120 deg) and 4.19 rad (240 deg) as measured from the top of the pipe.

The readings from thermocouples mounted at 2.54 cm (1.0 in.) from each side of the machined slots were used to indicate when a balanced thermal condition existed between the guard and test sections. Baffles of insulation materials were placed inside the pipe at the guard-test section interfaces to prevent conductive heat transfer between the three independently heated sections. Insulation was also placed inside the guard heater ends of the pipe. The thermocouple signals were fed to a reference junction and recorded by a multichannel digital voltmeter system. Voltmeters, ammeters, and a-c wattmeters were used to monitor and measure the power applied to each of the three independent heater sections. Temperature errors are estimated to be about ± 1 K, and power was determined to ± 0.5 W.

The insulation was installed on a 0.381-mm (0.015 in.) stainless steel inner jacket supported by standoffs from the test pipe. These standoffs are shown in Fig. 3. For sodium piping insulation, trace heaters are located in the annulus between the pipe and the inner jacket.

The insulation was installed over the inner jacket using standard procedures for blanket and block-type insulations. A stainless steel outer jacket was wrapped around the insulation and held in place by strap-breather spring assemblies.

Experimental Procedure

At least five steady-state heat loss measurements were made on each insulation system covering the range of pipe temperatures from approximately 366.5 K (200°F) to 838.7 K (1050°F) except as noted. The electrical input to the heaters was controlled so that the ramp rate did not exceed

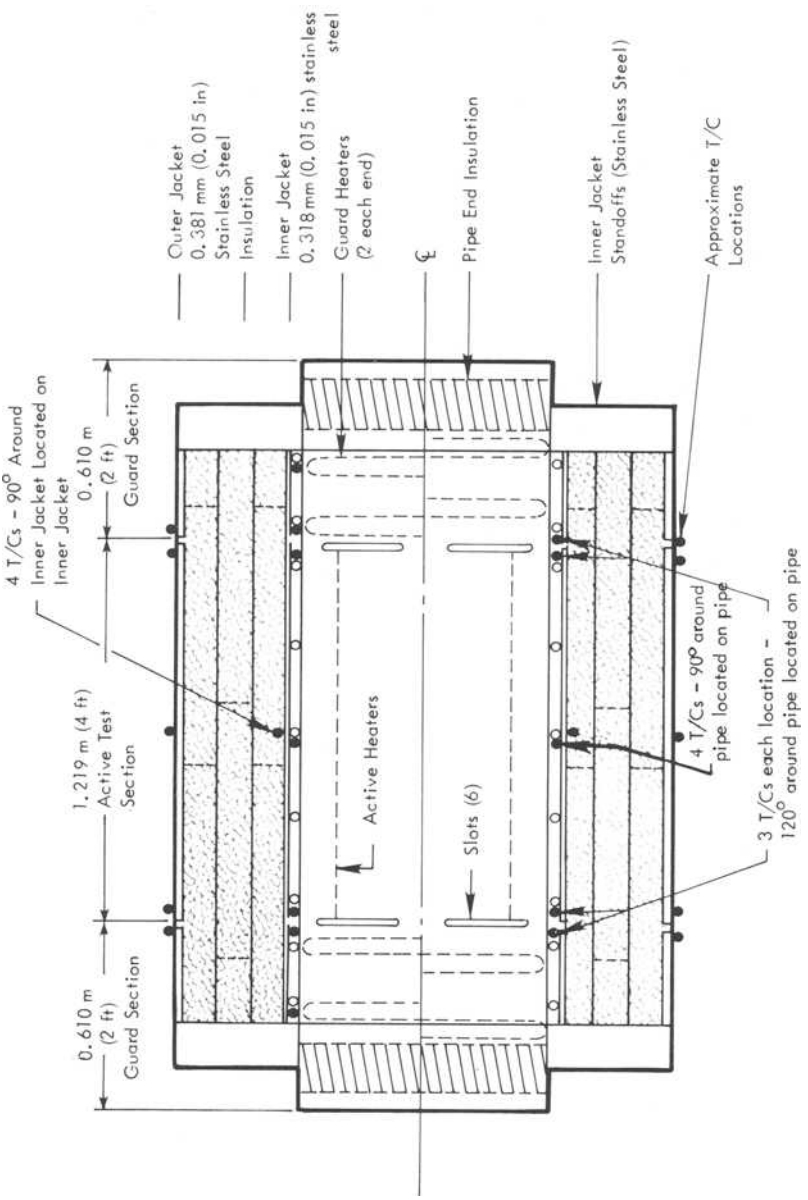

FIG. 1—*Schematic of the 40.64-cm (16 in.) pipe test system.*

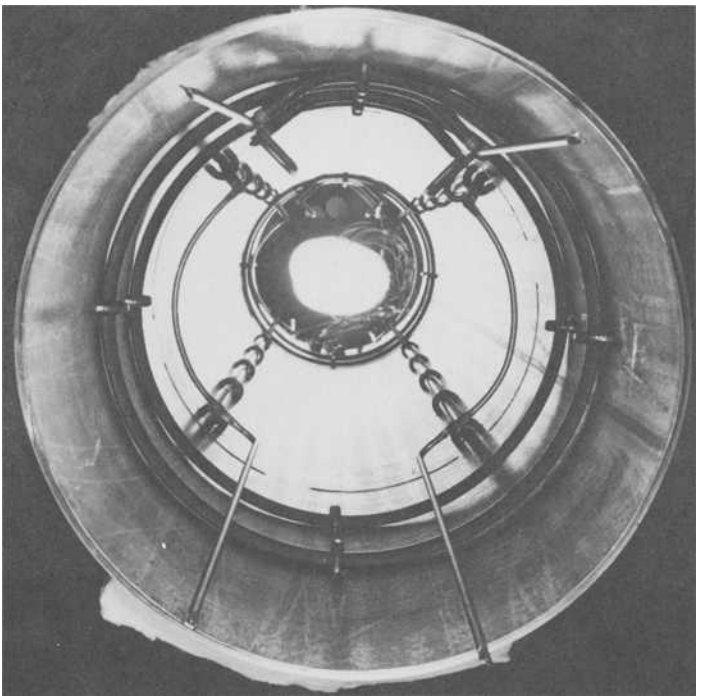

FIG. 2—*Heater placement inside the 40.64-cm (16 in.) test pipe.*

55.6 K (100°F) per hour from room temperature to 699.8 K (800°F) and 27.8 K (50°F) per hour from 699.8 K (800°F) to 838.7 K (1050°F). The power into the guard heaters was adjusted to maintain a temperature difference of less than ±2 K (3.6°F) or 0.5 percent of the pipe test temperature across the slot gaps of the heater pipe and guard ends.

Steady-state conditions were assumed when the guard heater-test heater temperature difference was within ±2 K or 0.5 percent of the test temperature. Three sets of steady-state data were recorded at half-hour intervals. If these readings were within ±1 K (1.8°F) over the time span, then the average value of the three readings for each thermocouple was used in calculating thermal performance data.

Experimental Results

The experimental results are presented for each of six system tests. Relevant observations concerning the characteristics of the particular insulation installation procedures are included as part of the specific experimental system. In a test utilizing an apparatus of this size, the fit-up

of the insulation is most important when discussing the thermal behavior (heat losses of the system). In a system test, one is measuring the heat losses for the system and not the conductivity of a homogeneous insulation.

Mineral Wool

The insulation was received in 914-mm-long by 50.8-mm-thick (3 ft by 2 in.) preformed sections. The 457.2- and 558.8-mm-diameter (18 and 22 in.) pipe size layers were received in two half-sections, and the 660.4-mm (26 in.) pipe size layer was in three sections. The sections were lightweight, and installation was not difficult. The insulation was easily cut to fit with a hand-held hacksaw blade.

The insulation layers were arranged so that butted seams in adjacent layers were not in line. Breather springs were used on the banding straps between all insulation layers and on the outer jacket. Gaps as large as 12.7 mm (0.5 in.) wide on the outer layers were stuffed with insulating material. The completed test setup as pictured from the guarded heater end for the mineral wool insulation is shown in Fig. 4.

The mineral wool was tested over a mean insulation temperature range of 333 K (140°F) to 501 K (442°F). Because of excessive outer skin temperatures, the testing was halted before completion of the planned test

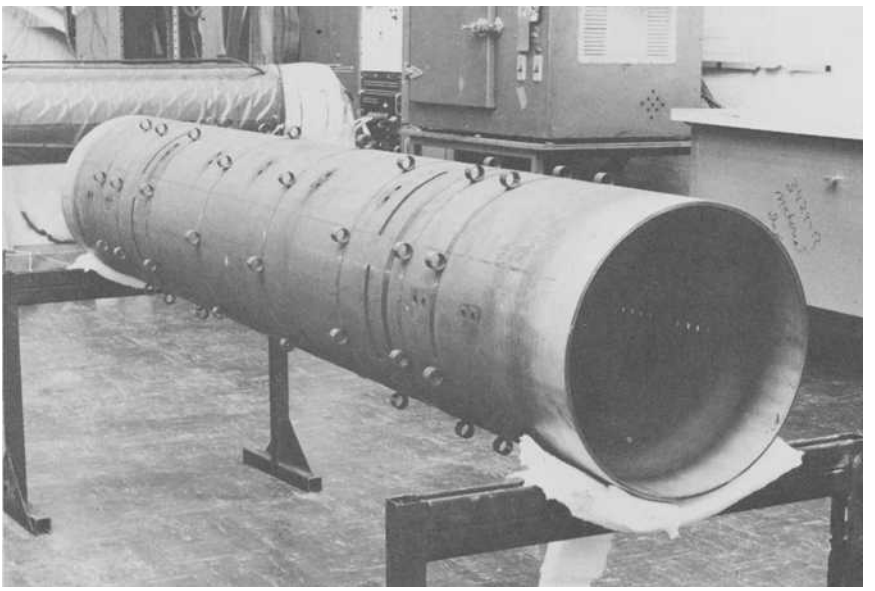

FIG. 3.—*Insulation standoffs installed on 40.64 (16-in.) test pipe.*

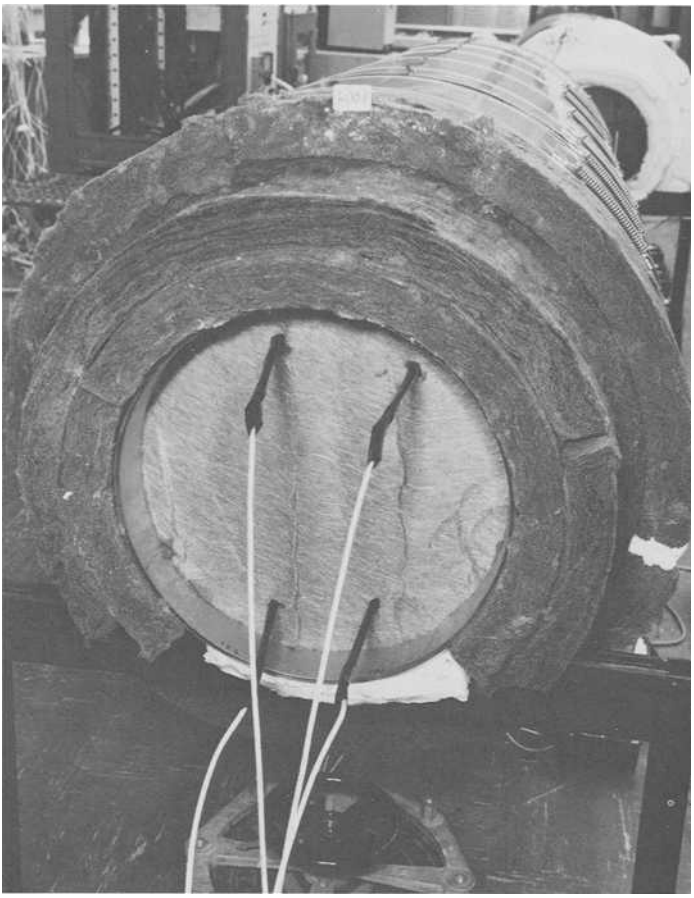

FIG. 4—*Mineral wool during testing at 589 K (600°F) heater temperature.*

program. Axial temperature profiles for each set of equilibrium temperature data points are shown in Fig. 5. The power input to each heater section is shown in parentheses under each temperature profile. The testing order is shown to the right of the graph in Fig. 5 and in all subsequent graphs. The outer jacket temperature distribution was measured, and the readings are summarized in Table 1 with the other systems tested. The standard deviation of the surface temperature measurement is a good indication of the homogeneous behavior of a particular insulation system. The large standard deviation of surface temperature reading signifies more hot spots and heat leaks due to installation irregularities.

The thermal performance data are tabulated in Table 2 along with the average temperatures and test section power inputs.

To evaluate how the 40.64-cm (16 in.) pipe test apparatus results compare with the results obtained using the standard 7.62-cm (3 in.) pipe test and with the data presented by the manfacturer's literature, a common property must be used. As a result, thermal conductivity of the installed insulation was calculated along with thermal conductance, even though the insulations on the 40.64-cm (16 in.) apparatus were built up and not homogeneous as defined in the ASTM Definition of Terms Relating to Thermal Insulating Materials (C 168-67). The 40.64-cm (16 in.) pipe test thermal conductivity is calculated by using the inner jacket and outer jacket temperature and the measured thickness of the installed insulation. These data are plotted in Fig. 6. The installed insulation density was not

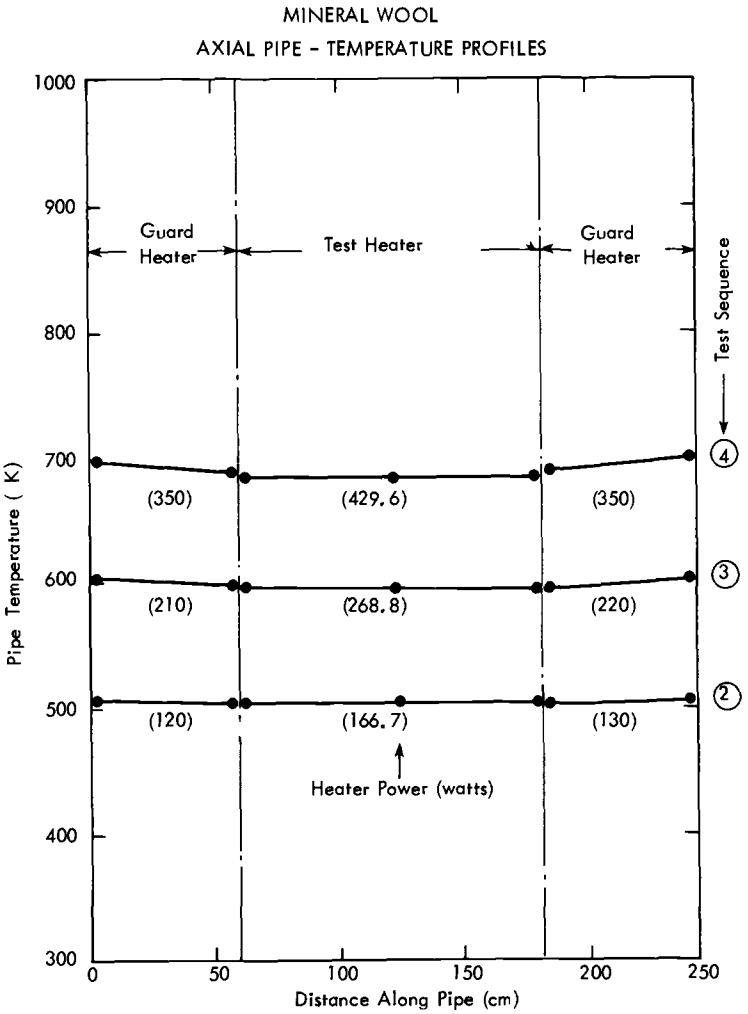

FIG. 5—*Mineral wool axial pipe temperature profiles.*

TABLE 1—*Surface temperatures—stainless steel outer jacket*

Insulation	Pipe Temperature, K	No. of Readings	Average Temperature, K	Standard Deviation	High Temperature, K	Low Temperature, K
Mineral wool	811	42	328	6.05	344	316
Calcium-silicate	710	47	328	17.79	407	308
Alumina-silica refractory fiber blanket	840	44	317	4.19	328	313
Calcium-silicate[a]	843	45	330	22.15	467	313
Calcium-silicate/[a] mineral wool[a]	743	45	327	7.216	346	317

Note: °F = (1.8 K) − 460.
[a]Contractor installed.

TABLE 2—*Mineral wool insulation test data.*

Test Order	System Conductance[a]		Insulation Thermal Conductivity, k		Test Section Power, W	Mean Temperature		Average Pipe Temperature, K	Average Outer Jacket Temperature, K	Average Inner Jacket Temperature, K
	$W/m^2 \cdot K$	$Btu/\cdot ft^2 \cdot deg\ F$	$W/m \cdot K$	$Btu\text{-}in./h \cdot ft^2 \cdot deg\ F$[c]		System, K	Insulation, K			
1	0.42	0.074	0.050	0.35	56.1	338.6	334.0	381.3	295.9	372.0
2	0.53	0.093	0.060	0.42	166.7	404.5	397.4	505.6	303.3	491.5
3	0.60	0.106	0.068	0.47	404.7	452.4	444.3	595.6	309.2	579.4
4	0.75	0.133	0.080	0.58	494.0	501.2	492.9	684.5	317.8	667.9

Notes:
Pipe radius = 20.3 cm (8 in.).
Inner jacket radius = 23.2 cm (9 in.).
Outer jacket radius = 38.44 cm (15.1 in.).
Pipe test section area = 1.557 m^2 (16.76 ft^2).
Inner jacket test section area = 1.751 m^2 (18.85 ft^2).
Insulation thickness = 15.5 cm (6.1 in.).
[a]Conductance area is based on pipe area.
[b]$Btu/h \cdot ft^2 \cdot deg\ F = 5.675\ W/m^2 \cdot K$.
[c]$Btu\text{-}in./h \cdot ft^2 \cdot deg\ F = 6.935\ W/m \cdot K$.

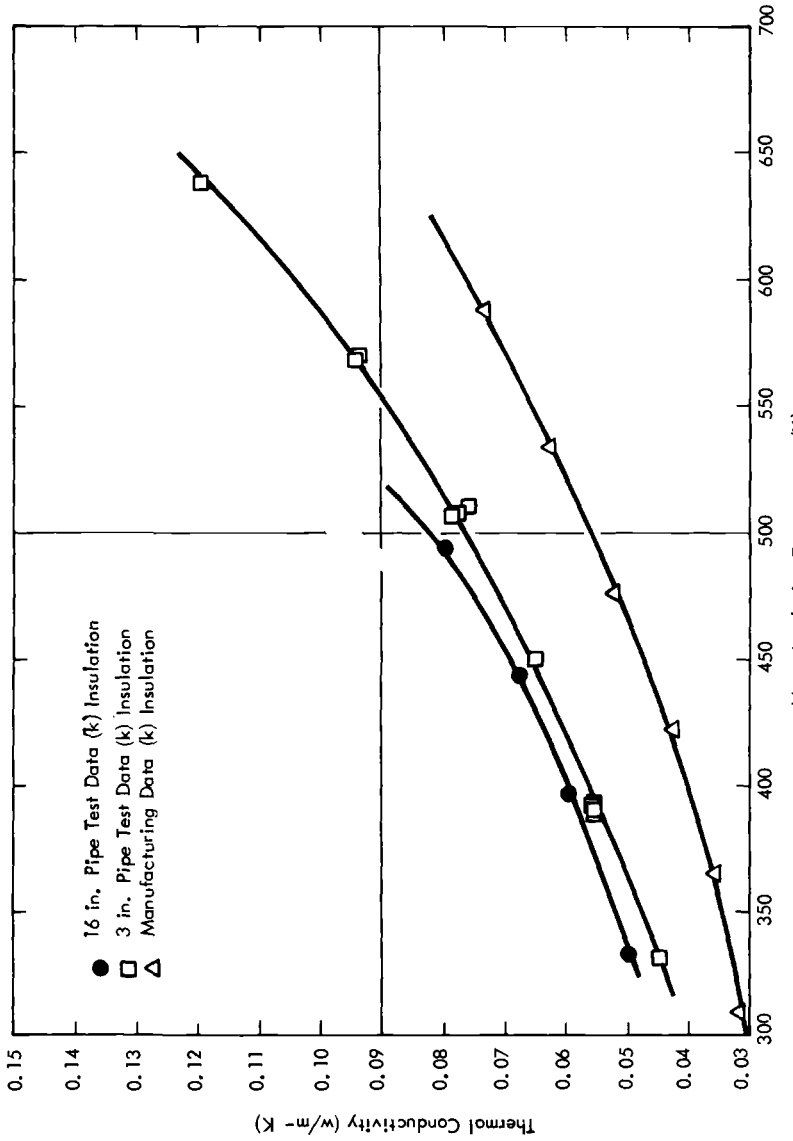

FIG. 6—*Comparision of thermal conductivity for mineral wool.*

as required by ASTM Method C 335, although this could be done by first weighing the amount of insulation and by measuring its installed volume.

Calcium-Silicate

The hydrous calcium-silicate insulation for these experiments was supplied as an inner layer with 0.914-m-long (3 ft) half sections, 101.6 mm (4 in.) thick, and an outer layer consisting of 18 truncated pie-shaped pieces 76.2 mm (3 in.) thick by 0.914 m (3 ft) long.

The insulation was difficult to install because of the many outer layer segments. The excessive amount of handling, required in order to fit the many outer layer sections, caused an undesirable amount of dust. The preformed inner layers fit the irregular shape of the inner stainless steel jacket. The outer layer segments left gaps between the inner and outer insulation layers as well as longitudinal gaps as large as 12.7 mm (0.5 in.) wide between the outer layer segments. These gaps were stuffed with fiber insulation to reduce the loss of heat.

An overall view of the apparatus prior to the installation of the outer jacket is shown in Fig. 7. Breather springs were employed only on the banding straps of the outer jacket.

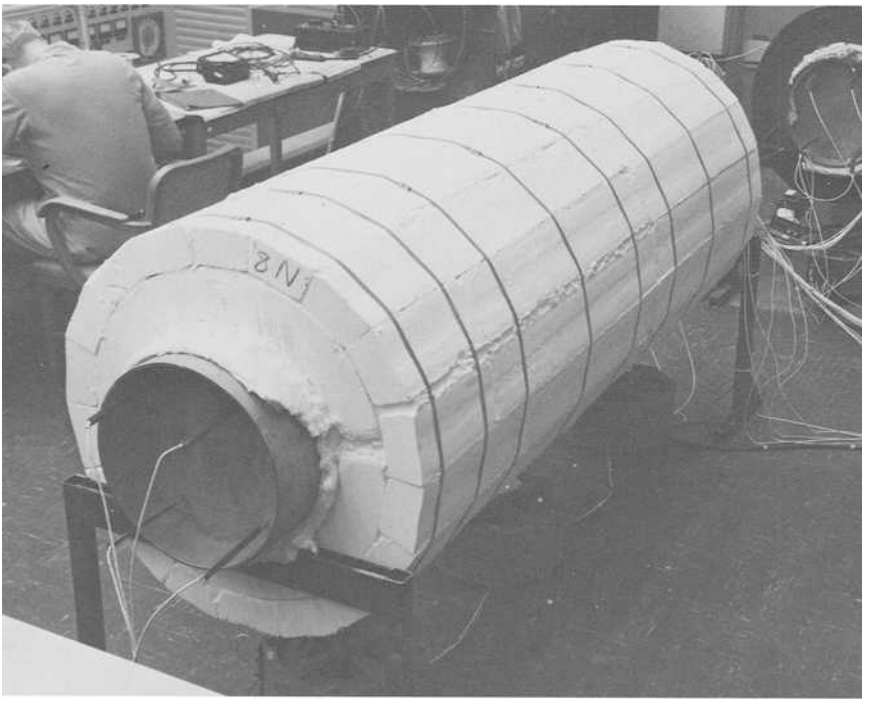

FIG. 7—*Calcium-silicate insulation before outer jacket was installed.*

Thermal conductance measurements were made over a mean temperature range of 330.4 to 597 K (135 to 615°F), which included (1) a four-day degradation test at 852.6 K (1975°F) heater pipe temperature; (2) wrapping the outer skin with 1.814-kg (64 oz) canvas while heater pipe temperature was at 852.6 K (1075°F); and (3) two thermal cycles from 852.6 K (1075°F) to 477.6 K (400°F) and back to 852.6 K (1075°F). The axial temperature profiles for these tests are shown in Fig. 8 along with the respective heater input power and test sequence. The surface temperatures taken when the pipe temperature was at 710 K (818°F) are summarized in Table 1. The maximum hot-spot temperature was 407 K (273°F).

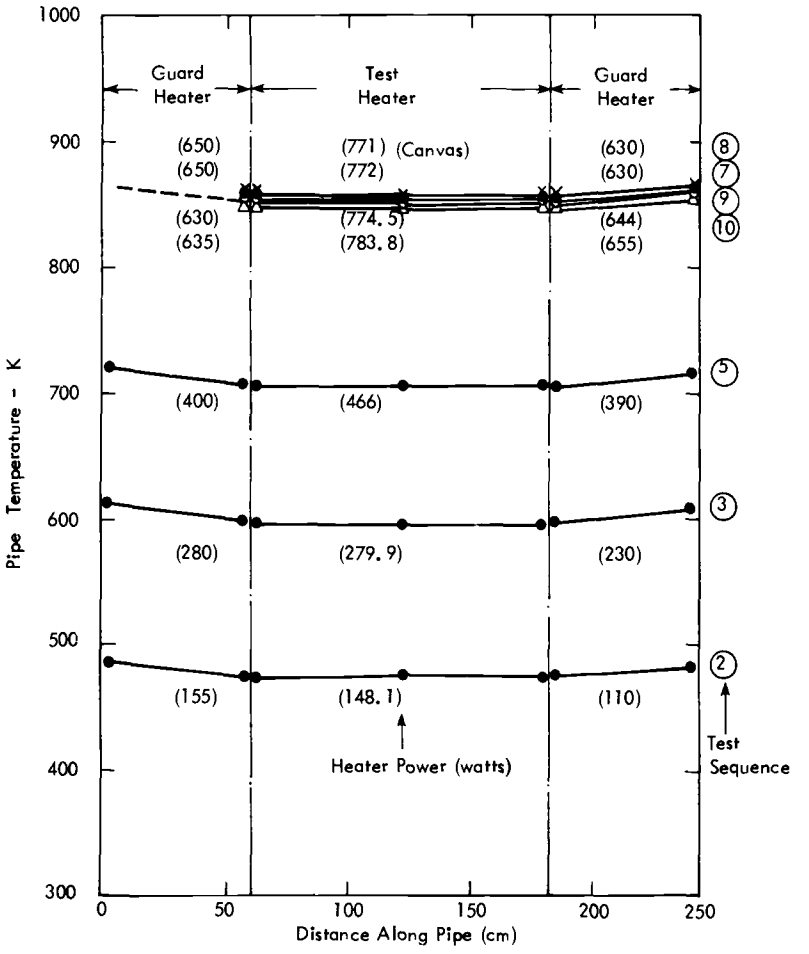

FIG. 8—*Calcium-silicate axial pipe temperature profiles.*

The results of the aforementioned tests are tabulated in Table 3 along with other pertinent information. The data include (1) the thermal conductance of the system and (2) the thermal conductivity of the insulation.

The experimental thermal conductivities are compared in Fig. 9 with the reported manufacturer's conductivities and 7.62-cm (3 in.) pipe test conductivity data. The conductivity determined at a mean temperature of 333.2 K (140°F) is greater than the conductivity determined for the next higher mean temperature. This difference is attributed to the water present in the as-received material which was not completely driven off at this temperature. (As in a plant situation, the insulation was not predried for these tests.) Condensation of water at one of the overlapping seams of the stainless steel outer jacket was noted while the mean temperature of the insulation was being increased from 381.8 to 443.8 K (227.6 to 339.2°F).

The thermal conductivity measured on the 40.64-cm (16 in.) pipe test is only slightly higher than the 7.62-cm (3 in.) pipe test data at the lower temperatures. However, the conductivities diverge rather sharply as temperature increases. This divergence is due to the difference in the insulation installation between the pipe test apparatus. The 40.64-cm (16 in.) insulation system consisted of two layers as described earlier which when installed produced many axial and radial cracks through which heat could escape. The 7.62-cm (3 in.) pipe test insulation was assembled from two half-sections 101.6 mm (4 in.) thick and provided only two axial discontinuities through which heat loss could occur.

Wrapping the entire outer stainless steel jacket with the equivalent of 1.814 kg (64 oz) canvas only raised the average temperature of the system slightly and had no effect on the measured heat losses.

Neither the four-day soak at 852 K (1075°F) pipe temperature nor the two thermal cycles from 852 K (1075°F) pipe temperature to 478 K (400°F) and back to 852 K (1075°F) affected the thermal conductance.

After testing, the outer jacket was removed. It was observed that the circumferential butt joints of the 0.914-m (3 ft) sections had gaps ranging from 3.2 to 9.5 mm (0.125 to 0.375 in.). Radial cracks were also observed in the outer layers of the insulation.

Alumina-Silica Refractory Fiber Blanket

The alumina-silica insulation was received as 7.62-m-long (25 ft) rolls, 1.22 m (4 ft) wide by 25.4 mm (1 in.) thick. The density of the material was reported by the manufacturer to be 128 kg/m^3 (8 lb/ft^3). The 25.4-mm-thick (1 in.) fiber material was the minimum thickness needed to prevent the insulation from pulling apart in handling.

Seven layers of insulation were wrapped around the inner jacket. The odd number layers consisted of two 1.22-m-wide (4 ft) pieces of insulation wrapped and butted at the center of the test section. The even-numbered

TABLE 3—*Calcium-silicate insulation test data.*

Order of Testing	System Conductance[a]		Insulation Thermal Conductivity, k		Test Section Power, W	Mean Temperature		Average Pipe Temperature, K	Average Outer Jacket Temperature, K	Average Inner Jacket Temperature, K
	$W/m^2 \cdot K$	$Btu/h \cdot ft^2 \cdot degF$[f]	$W/m \cdot K$	$Btu\text{-}in/h \cdot ft^2 \cdot degF$[g]		System, K	Insulation, K			
1	0.56	0.099	0.080	0.56	68.5	336.1	330.4	375.2	297.2	363.6
2	0.55	0.098	0.073	0.51	148.2	389.1	381.8	475.1	303.1	460.5
3	0.63	0.110	0.081	0.56	279.9	452.5	443.8	569.0	308.9	518.7
4	0.75	0.132	0.095	0.66	456.7	509.9	502.4	705.5	314.3	690.5
5	0.77	0.135	0.097	0.67	466.6	510.9	503.4	706.7	315.2	691.7
6	0.96	0.169	0.118	0.82	790.9	589.6	585.0	855.2	324.1	845.9
7[b]	0.94	0.166	0.116	0.80	772.0	588.8	584.4	852.6	325.0	843.7
8[c]	0.95	0.167	0.117	0.81	771.0	596.5	592.9	857.5	318.9	850.4
9[d]	0.95	0.167	0.116	0.81	774.5	588.2	584.0	851.5	324.9	843.2
10[e]	0.96	0.170	0.119	0.82	782.5	585.1	581.3	846.3	323.9	838.3

Notes:

[a]Conductance area is based on pipe area.

[b]After four days, soak at pipe temperature of 852 K (1075°F).

[c]Double wrap of 0.907 kg (32 oz) canvas on outer jacket.

[d]After first cycle [852 K (1075°F) to 478 K (400°F) to 852 K (1075°F)].

[e]After second cycle [852 K (1075°F) to 478 K (400°F) to K (1064°F)].

[f]$Btu/h \cdot ft^2 \cdot deg\ F = 5.675\ W/m^2 \cdot K$.

[g]$Btu\text{-}in./h \cdot ft^2 \cdot deg\ F = 6.935\ W/m \cdot K$.

Pipe radius = 20.3 cm (8 in.).

Inner jacket radius = 23.2 cm (9.1 in.).

Outer jacket radius = 42.0 cm (16.55 in.).

Pipe test section area = 1.557 m^2 (16.76 ft^2).

Inner jacket test section area = 1.774 m^2 (19.1 ft^2).

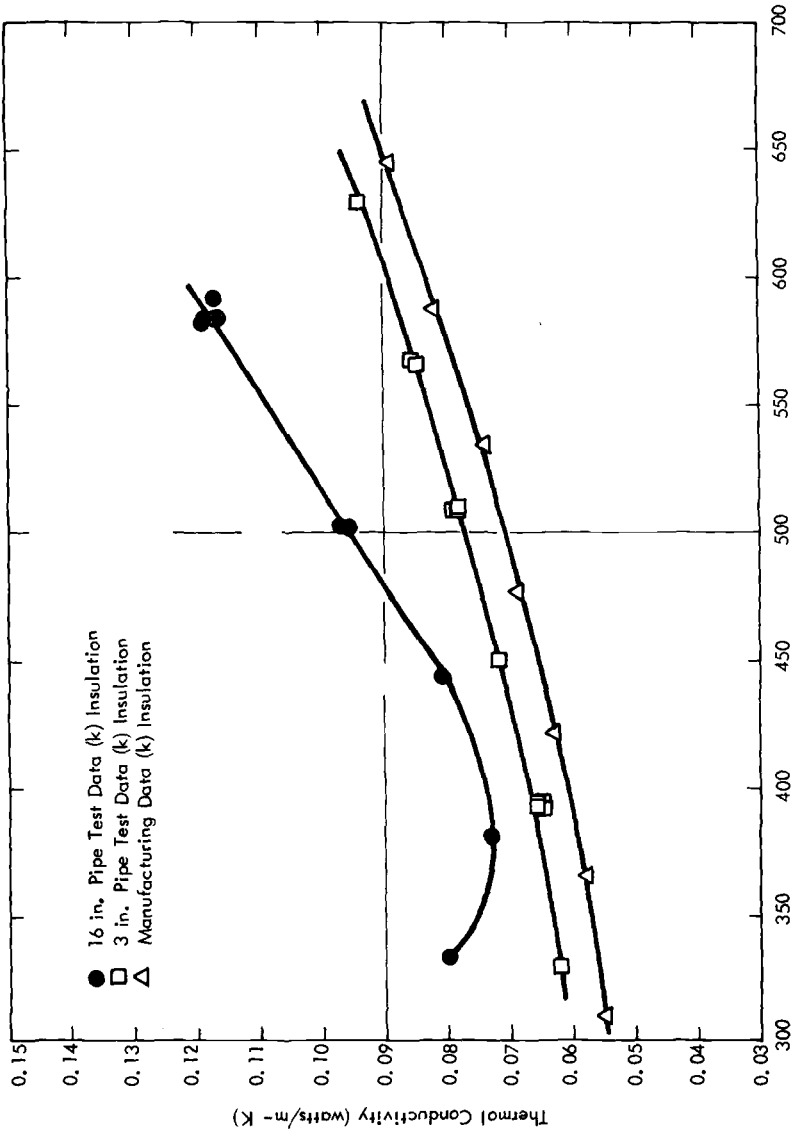

FIG. 9—*Comparison of thermal conductivity for calcium-silicates.*

layers of insulation consisted of one 1.22-m-wide (4 ft) piece and two 0.61-m-wide (2 ft) pieces of insulation wrapped and butted at the guard test section interface. The axial insulation seams were located at the bottom of the test system and were overlapped so that no three consecutive layers of insulation had the same axial seam location. The completed alumina-silica insulation on the 40.64-cm-diameter (16 in.) pipe system is shown in Fig. 10. Breather springs were used only on the outer stainless steel banding straps.

Four steady-state thermal measurements were made covering a mean temperature range of 405 to 583 K (270 to 590°F) for the system.

The axial temperature profiles for the five equilibrium test measurements are shown in Fig. 11 along with the heater power and test sequence. The surface temperatures are listed in Table 1. The surface temperatures were very uniform ranging from 313 to 328 K (103 to 130°F) over the entire test section. The thermal properties for the alumina-silica test system are tabulated in Table 4 and plotted in Fig. 12. The close agreement between the 40.64-cm (16 in.) and 7.62-cm (3 in.) pipe test can be attributed to the ability to apply the insulation uniformly on both test systems. Neither a four-day soak at 839 K (1050°F) nor a thermal cycle between 839 and 478 K (1050 and 400°F) affected the thermal performance.

Post-test observation included no residue deposited on the inner surface of the outer jacket, no gaps in the butt joint seams in either the axial or radial direction, and no evidence of any discoloration in any of the seven layers.

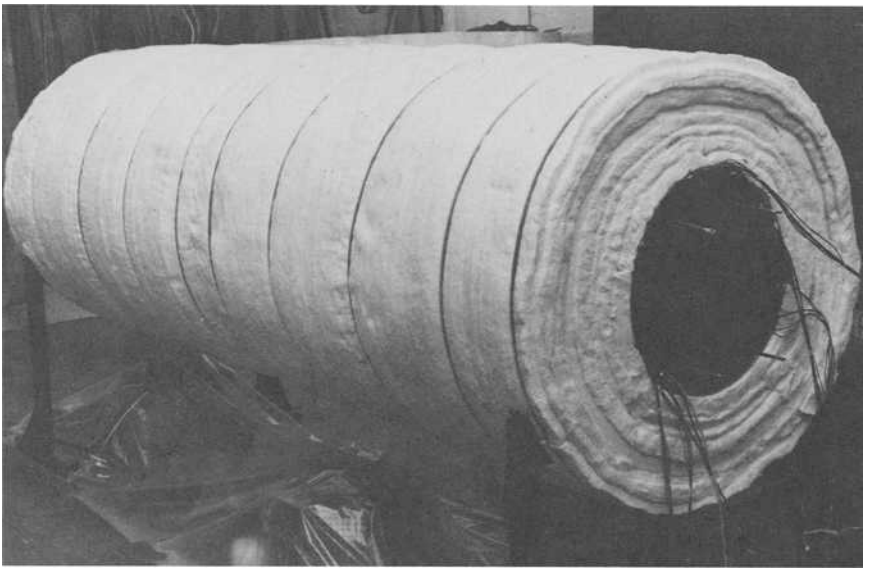

FIG. 10.—*Wrapped alumina-silica insulation assembly before outer jacket installation.*

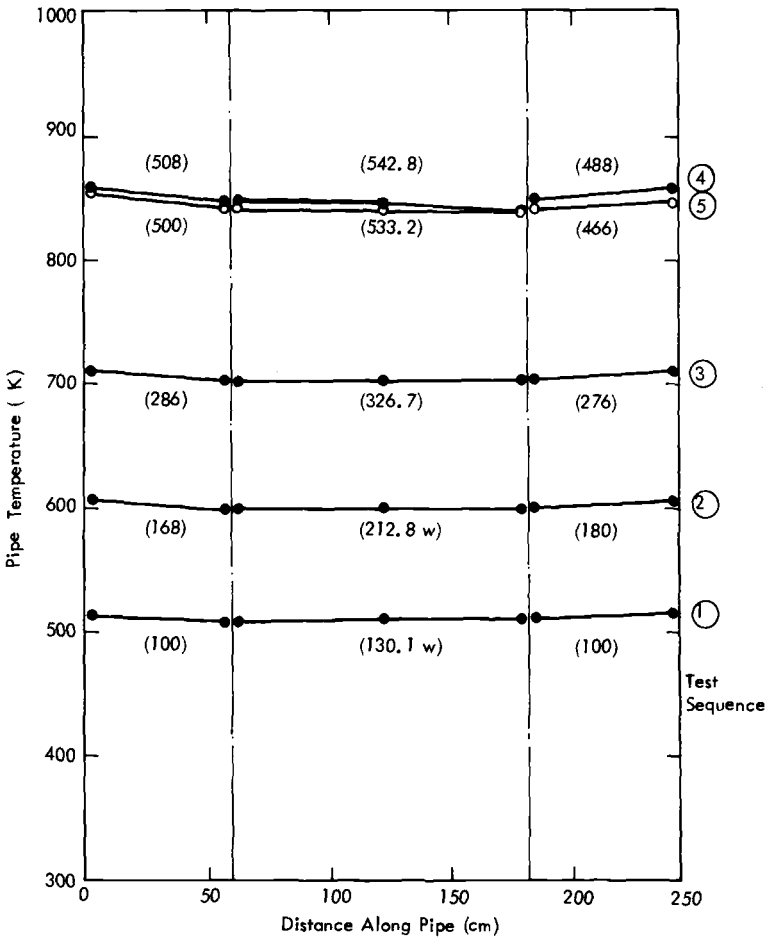

FIG. 11—*Axial pipe temperature profiles for alumina-silica refractory fiber blanket.*

Fiber Glass-Covered Refractory Fiber Insulation

The fiber glass insulation used in this test sequence consisted of precut blankets incorporating clips for field wiring. The inner layer was a 25.4-mm-thick (1 in.) insulation enclosed in a stainless steel wire mesh. The second, third, and fourth layers were 50.8-mm (2 in.) layers of insulation enclosed in a fiber glass cloth cut to proper circumferential dimensions for each particular layer. Each layer was 0.81 m (32 in.) wide.

Each layer of insulation was installed such that the axial seam was located at 0.79, 2.36, or 3.93 rad (45, 135, or 225 deg), thereby ensuring that seams did not coincide with the thermocouples spaced around the test assembly. Circumferential seams were similarly staggered.

TABLE 4—*Alumina-silica refractory fiber test data.*

Order of Testing	System Conductance		Insulation Thermal Conductivity, k		Test Section Power, W	Mean Temperature		Average Pipe Temperature, K	Average Outer Jacket Temperature, K	Average Inner Jacket Temperature, K
	$W/m^2 \cdot K$	Btu/h·ft²·deg F[c]	W/m·K	Btu-in./h·ft²·deg F[d]		System, K	Insulation, K			
1	0.40	0.070	0.051	0.36	130.2	405.7	401.2	510.9	300.5	501.5
2	0.46	0.081	0.059	0.41	212.8	452.5	447.8	600.6	304.5	591.0
3	0.53	0.094	0.067	0.47	326.1	506.3	502.1	727.9	309.8	694.4
4	0.66	0.116	0.083	0.57	542.8	583.0	580.0	847.2	318.9	840.9
5[a]	0.66	0.116	0.082	0.57	533.2	578.8	575.9	840.0	317.5	834.3
6[b]	0.66	0.116	0.083	0.57	534.6	580.2	577.2	840.0	320.3	834.4

Notes:
[a]Data taken after 4 days at pipe temperature of 841.5 K (1055°F).
[b]Data taken after first cycle [841.5 K (1055°F) to 477.6 K (400°F) to 841.5 K (1055°F)].
[c]Btu/h·ft²·deg F = 5.675 $W/m^2 \cdot K$.
[d]Btu-in./h·ft²·deg F = 6.935 W/m·K.
Pipe radius = 20.3 cm (8.0 in.).
Inner jacket radius = 22.9 cm (9.02 in.).
Outer jacket radius = 42.1 cm (16.57 in.).
Pipe test section area = 1.557 m^2 (16.76 ft^2).
Inner jacket test section area = 1.754 m^2 (18.88 ft^2).

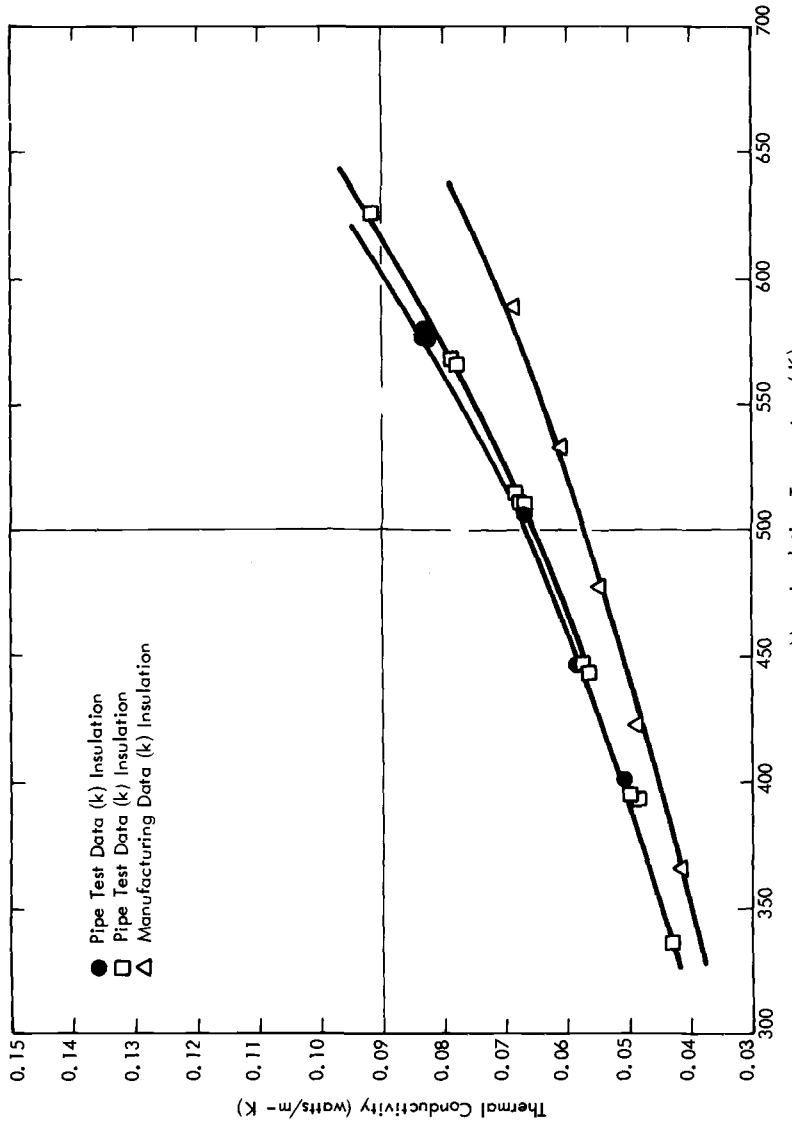

FIG. 12—*Comparison of thermal conductivity data for alumina-silica refractory fiber blanket.*

No difficulty was encountered in installing the insulation layers. While the nominal insulation thickness was to be 0.178 m (7 in.), the actual thickness was 0.203 m (8 in.) based on circumference measurements. This increase in thickness apparently results from bunching of the flat insulation blankets as they are wrapped to conform to the pipe, as well as the effect of the wiring clips. For a given number of layers, this effect should be more pronounced for those cases where the ratio of insulation thickness to pipe diameter is greatest.

The thermal properties were measured for insulation mean temperatures ranging from 367 to 589 K (200 to 600°F). The partially assembled test system is shown in Fig. 13. The axial temperature profiles are shown in Fig. 14 for the equilibrium temperatures measured. The calculated thermal properties are tabulated in Table 5. Surface temperatures as given in Table 1 indicate a very homogeneous insulation with no hot spots, similar to that reported for the nonencapsulated refractory-fiber insulation test. The thermal conductance is plotted in Fig. 15.

Calcium-Silicate Installed by Outside Contractor

The insulation specified for this fixture was received in the following sizes:

Half cylinders: 0.475 m (18 in.) inside diameter by 0.089 m (3.5 in.) thick by 0.914 m (36 in.) long

Quarter cylinders: 0.635 m (25 in.) inside diameter by 0.089 m (3.5 in.) thick by 0.914 m (36 in.) long.

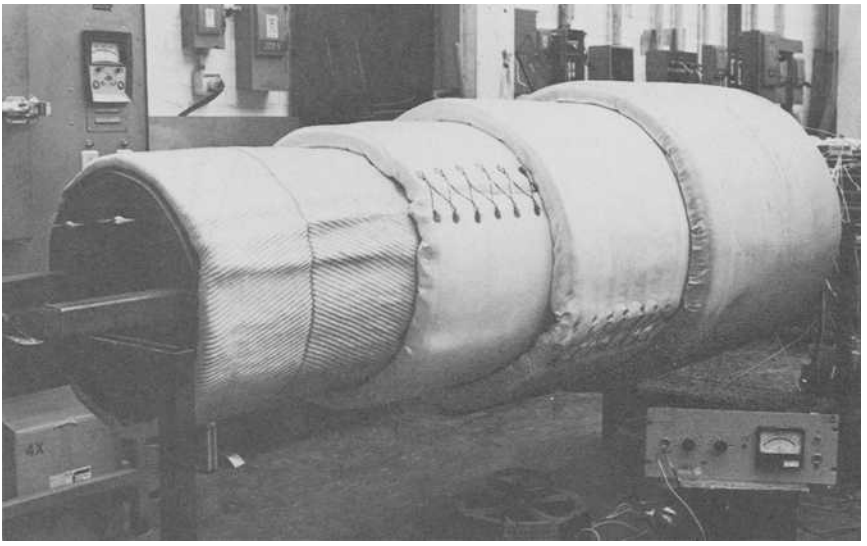

FIG. 13—*Partially assembled encapsulated alumina-silica insulation system.*

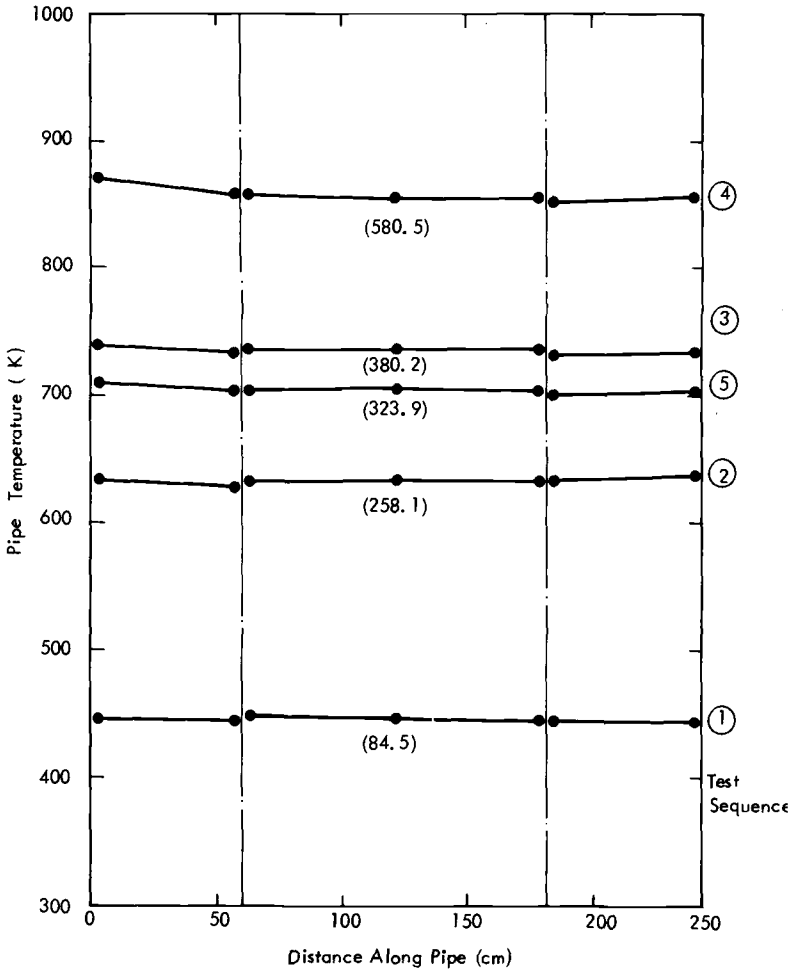

FIG. 14—*Axial temperature profiles for encapsulated alumina-silica refractory fiber blanket.*

The inner jacket and outer layer of the calcium-silicate insulation were held in place with tie wire. The inner layer was held in place with 6.4 mm (0.25 in.) by 0.51 mm (0.020 in.) stainless steel banding straps. The outer jacket was held in place with 6.4 mm (0.25 in.) by 0.51 mm (0.020 in.) stainless steel breather spring assemblies.

Small seams were sealed by local hammering to upset the insulation. Large seams were filled with loose alumina-silica packed and hammered.

Tie wires were locally hammered during the tensioning process to embed the wire in the surface of the insulation. This action minimized the interference on the inside diameter of the next insulation layer.

TABLE 5—*Alumina-silica refractory fiber blanket.*

Order of Testing	System Conductance		Insulation Thermal Conductivity, k		Test Section Power, W	Mean Temperature		Average Pipe Temperature, K	Average Outer Jacket Temperature, K	Average Inner Jacket Temperature, K
	$W/m^2 \cdot K$	$Btu/h \cdot ft^2 \cdot degF$	$W/m \cdot K$	$Btu\text{-}in/h \cdot ft^2 \cdot deg\ F^b$		System, K	Insulation, K			
1	0.38	0.067	0.051	0.36	84.5	376.1	372.8	448.2	304.0	441.5
2	0.52	0.091	0.068	0.47	258.1	472.5	469.3	634.1	310.9	627.6
3	0.58	0.102	0.076	0.53	380.2	525.9	522.9	736.9	314.9	730.9
4	0.70	0.123	0.092	0.64	580.5	590.6	586.9	857.2	324.0	849.8
5	0.53	0.094	0.069	0.48	323.9	506.9	505.3	703.0	310.8	699.8

Notes:
[a]$Btu/h \cdot ft^2 \cdot deg\ F = 5.675\ W/m^2 \cdot K$.
[b]$Btu\text{-}in./h \cdot ft^2 \cdot deg\ F = 6.935\ W/m \cdot K$.
Pipe radius = 20.3 cm (8 in.).
Inner jacket radius = 22.9 cm (9.01 in.).
Outer jacket radius = 43.3 cm (17.05 in.).
Pipe test section area = 1.549 m (16.76 ft^2).
Inner jacket test section area = 1.753 m^2 (18.87 ft^2).

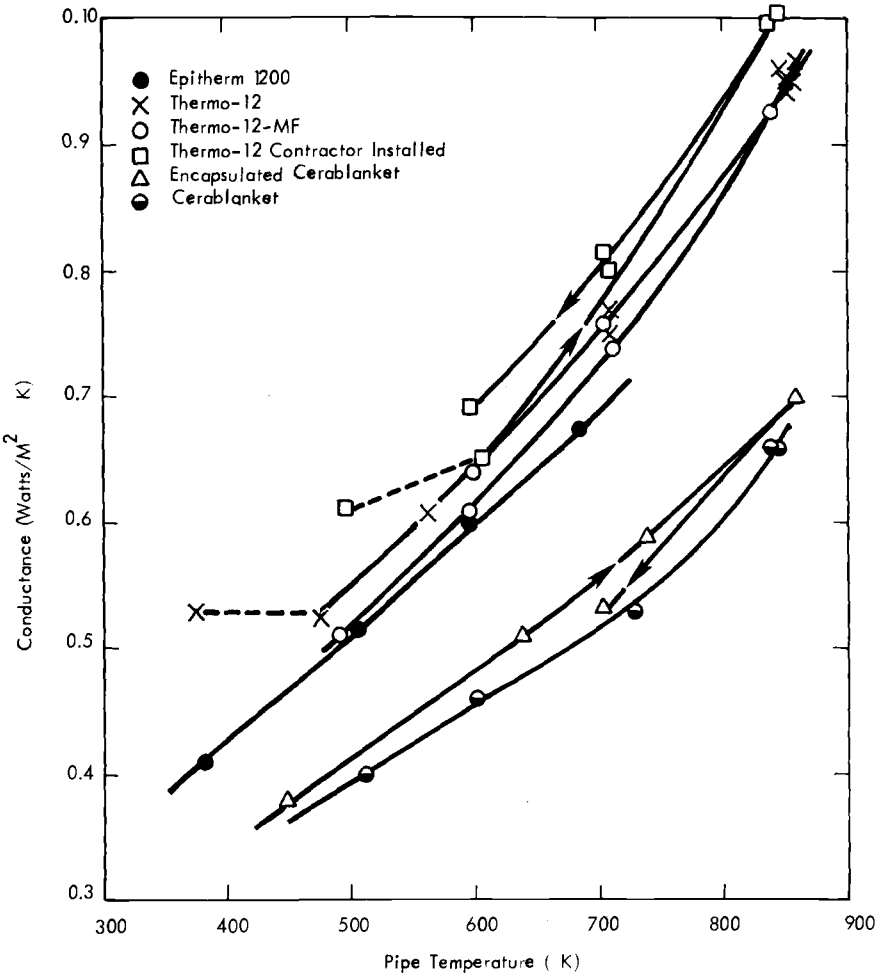

FIG. 15—*Thermal conductance* (C) *as a function of pipe temperature for all systems tested.*

During assembly of the second layer of calcium silicate, it was noted that the radius of curvature appeared to be too large to properly fit the circumference. To improve the fit and reduce the circumferential gaps between layers, the four quarter segments were split axially and wired in place.

Figure 16 shows the completed calcium-silcate insulation assembly prior to installing the outer jacket. Steady-state measurements were made at mean insulation temperatures of 399, 458, 513 and 595 K (258, 364, 463, and 611°F). The axial temperature profiles are shown in Fig. 17 along with heater input power and test sequence. The outer jacket temperatures are

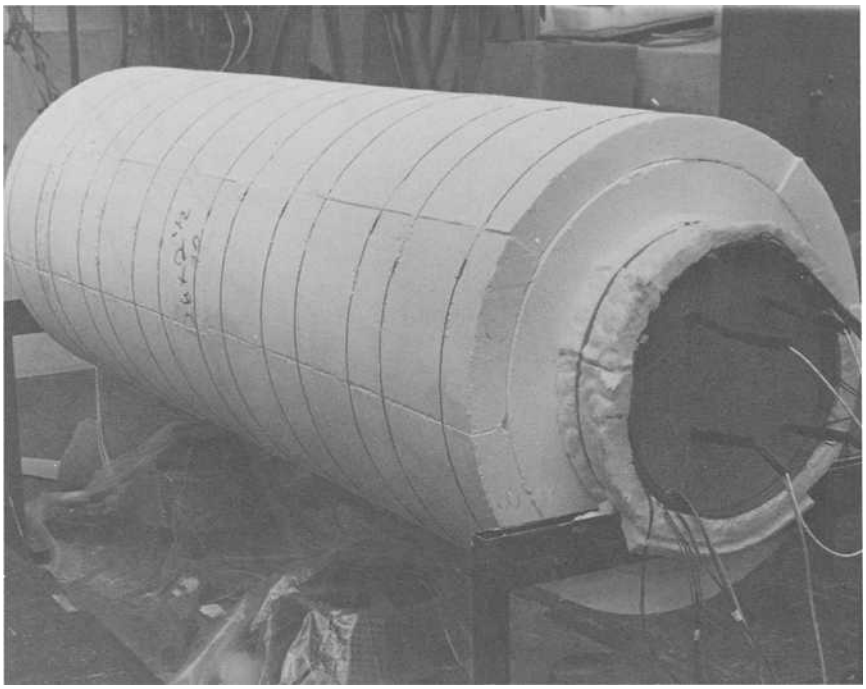

FIG. 16—*Contractor-installed calcium-silicate before outer jacket installation.*

summarized in Table 1 for a pipe temperature of 843 K (1057°F). Several hot spots at 467 K (380°F) were measured on the surface, and these were attributed to a shrinkage gap of about 11.1 mm (0.438 in.). Many gaps opened during the thermal testing. The thermal performance data are tabulated in Table 6, and the system conductance is plotted in Fig. 15. The plot shows the values calculated from measurements during cooldown to be consistently higher than those calculated from measurements during heatup. This difference is due to changes in the insulation system at temperature such as loss of water, cracking, and opening of shrinkage gaps. Cracking of the preformed insulation segments was evident during disassembly. Run 5b (Fig. 17) shows an effect of removing the outer jacket on the pipe temperature. Thermal performance does decrease, although the magnitude of the effect cannot be determined because of insufficient data.

Calcium-Silicate-Mineral Fiber Installed by Outside Contractor

The insulation specified for this fixture was received in the following sizes:

Half cylinders (calcium silicate): 0.475 m (18 in.) inside diameter by 0.089 m (3.5 in.) thick by 0.914 (36 in.) long

Quarter cylinders (calcium silicate): 0.635 m (25 in.) inside diameter by 0.064 m (2.5 in.) thick by 0.914 (36 in.) long

Half sections (mineral wool): 0.762 m (30 in.) inside diameter by 0.025 m (1 in.) thick by 0.61 m (24 in.) long

The inner jacket and both layers of the calcium-silicate were held in place with tie wire. The single outer layer of mineral wool was held in place with 6.3 by 0.51-mm (0.25 by 0.020 in.) stainless steel banding straps. The outer jacket was held in place with 6.3 by 0.51-mm (0.25 by 0.020 in.)

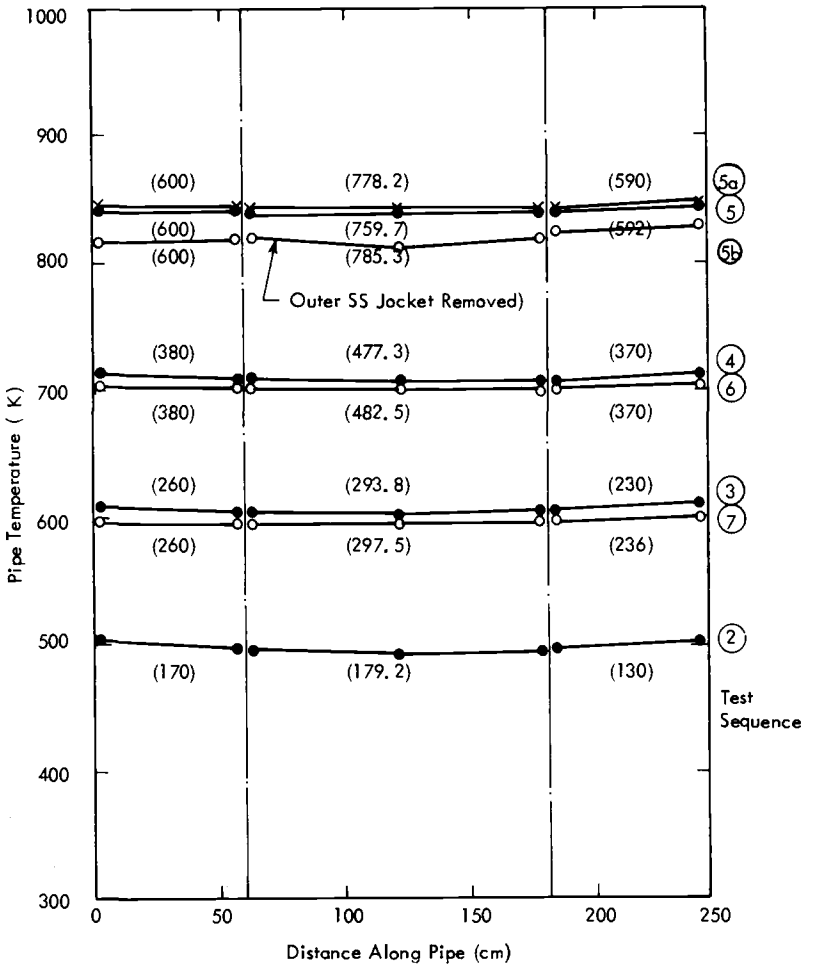

FIG. 17—*Axial temperature profiles of contractor-installed calcium silicate.*

TABLE 6—*Calcium-silicate (installed by outside contractor) thermal test data.*

Order of Testing	System Conductance		Insulation Thermal Conductivity, k		Test Section Power, W	Mean Temperature		Average Pipe Temperature, K	Average Outer Jacket Temperature, K	Average Inner Jacket Temperature, K
	$W/m^2 \cdot K$	$Btu/h \cdot ft^2 \cdot degF^a$	$W/m \cdot K$	$Btu\text{-}in./h \cdot ft^2 \cdot deg\ F^b$		System, K	Insulation, K			
2	0.610	0.107	0.076	0.53	179.2	399.7	392.8	494.5	304.8	480.8
3	0.650	0.114	0.079	0.55	293.8	458.2	451.3	603.9	312.5	590.2
4	0.800	0.141	0.095	0.66	477.3	513.0	509.4	708.0	323.9	695.2
5	0.990	0.174	0.117	0.81	759.7	592.8	587.0	839.4	346.1	827.9
5A	1.010	0.178	0.119	0.83	778.2	595.5	590.3	843.5	347.4	831.9
6	0.83	0.146	0.099	0.69	482.5	515.1	509.4	701.6	328.6	690.7
7	0.69	0.122	0.084	0.58	297.5	457.9	451.7	595.9	319.8	583.6

Notes:
[a]$Btu/h \cdot ft^2 \cdot deg\ F = 5.675\ W/m^2 \cdot K$.
[b]$Btu\text{-}in./h \cdot ft^2 \cdot deg\ F = 6.935\ W/m \cdot K$.
Pipe radius = 20.3 cm (8.0 in.).
Inner jacket radius = 23.2 cm (9.1 in.).
Outer Jacket radius = 41.0 cm (16.2 in.).
Pipe test section area = 1.557 m^2 (16.76 ft^2).
Inner Jacket test section area = 1.778 m^2 (19.14 ft^2).

stainless steel banding strap breather spring assemblies. All radial and circumferential seams were staggered to minimize heat leaks.

The same precautions and general assembly techniques used on the contractor-installed calcium-silicate insulation were employed on this test. A picture of the test assembly is shown in Fig. 18 prior to installing the stainless steel outer jacket. Steady-state heat losses were measured at mean temperatures of 397, 453, 512, and 585 K (254, 355, 461, and 593°F). The equilibrium axial temperature profiles are plotted in Fig. 19, showing the test and guard section power inputs and the test sequence. The surface temperatures are summarized in Table 1. These results show a maximum temperature of 346 K (163°F), a minimum temperature of 316 K (110°F), and an average over temperature of 327 K (127°F). The calculated thermal properties are presented in Table 7, and the system thermal conductance is plotted in Fig. 15. The thermal conductance of the composite calcium-silicate mineral insulation system was about 10 percent lower than the all-calcium-silicate system. Run 5a, Fig. 19 shows the effect on pipe temperature of removing the stainless steel outer jacket. The exact effect on system conductance cannot be determined because of insufficient data. Disassembly showed gaps and cracks formed in the insulation as noted for all calcium-silicates reported by this paper.

Discussion of Results

The test results shown in Figs. 6, 9, and 12 compare the thermal conductivities of the insulations 40.64-cm for the (16 in.) pipe test, the standard

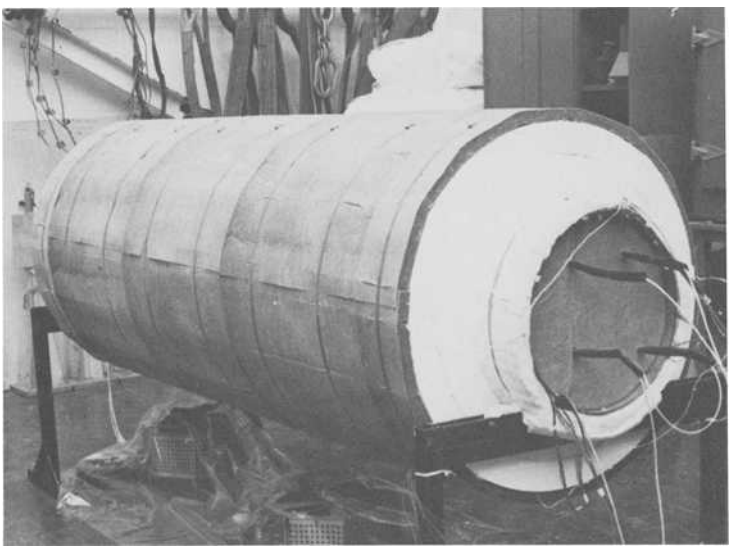

FIG. 18—*Combination calcium-silicate-mineral wool insulation prior to outer jacket installation.*

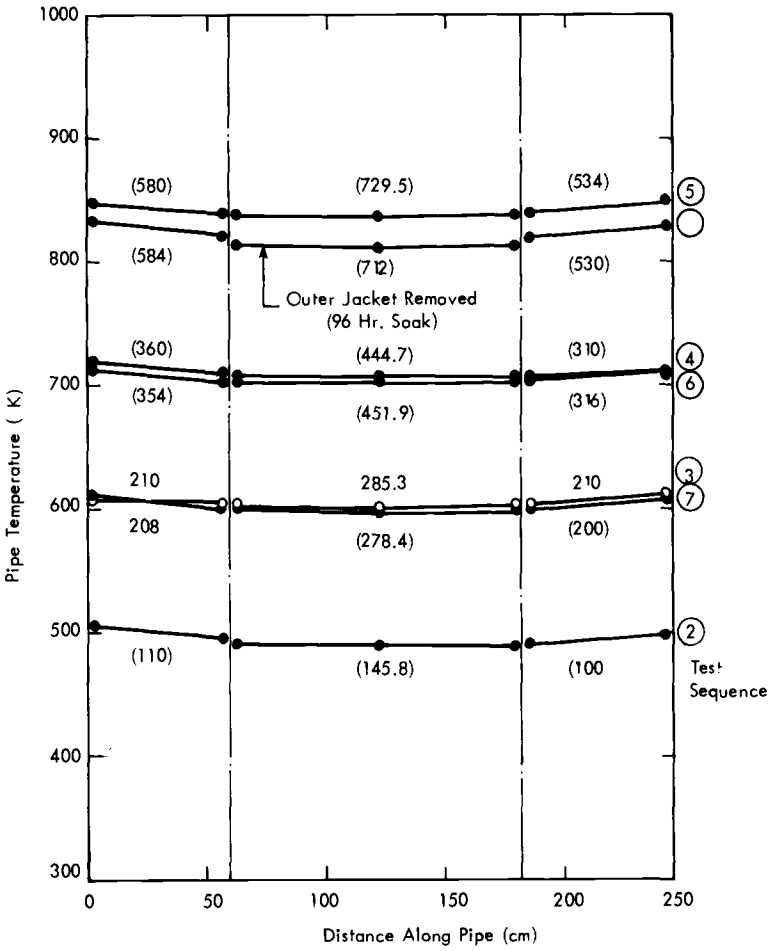

FIG. 19—*Axial temperature profiles for calcium-silicate-mineral wool contractor-installed insulation.*

7.62-cm (3 in.) ASTM Method C 335 pipe test, and the manufacturer's supplied data. In spite of the shortcomings of calculating a conductivity value from the 40.64-cm (16 in.) pipe test results, it is the only means of attempting to compare experimental results to evaluate reliability of the large-diameter pipe test results.

The alumina-silica refractory fiber test results for the 7.62-cm (3 in.) pipe test and the 40.64-cm (16 in.) pipe test are in excellent agreement as shown in Fig. 12. At temperatures below 500 K (441°F), the points fall on the same straight line. At 600 K 40.64-cm (16 in.) pipe test values are about 4 percent higher than the 7.62-cm (3 in.) pipe test data. Considering

TABLE 7—*Calcium-silicate-mineral wool thermal test data.*

Test Order	System Conductance		Insulation Thermal Conductivity, k		Test Section Power, W	Mean Temperature		Average Pipe Temperature, K	Average Outer Jacket Temperature, K	Average Inner Jacket Temperature, K	Thermo-12 48 MF Interface Temperature, K
	$W/m^2 \cdot K$	$Btu/h \cdot ft^2 \cdot degF$	$W/m \cdot K$	$Btu\text{-}in./h \cdot ft^2 \cdot degF$		System, K	Insulation, K				
2	0.51	0.099	0.064	0.45	145.8	396.8	391.1	489.5	304.1	478.1	334.8
3	0.63	0.111	0.077	0.54	278.4	453.3	448.1	596.2	310.3	585.9	360.0
4	0.74	0.130	0.089	0.62	444.7	512.4	508.8	706.5	318.3	699.2	402.0
5	0.93	0.164	0.112	0.78	729.5	584.9	582.0	837.3	332.5	831.5	457.0
6	0.76	0.135	0.092	0.64	451.9	512.1	508.5	702.6	321.5	695.5	406.2
7	0.64	0.113	0.079	0.55	285.3	456.6	452.0	599.7	313.4	590.7	371.4

Notes:
[a]$Btu/h \cdot ft^2 \cdot deg\ F = 5.675\ W/m^2 \cdot K$.
[b]$Btu\text{-}in./h \cdot ft^2 \cdot deg\ F = 6.935\ W/m \cdot K$.
Pipe radius = 20.32 cm (8 in.).
Inner jacket radius = 22.9 cm (9.0 in.).
Outer jacket radius = 41.12 cm (16.19 in.).
MF-Thermo 12 interface radius.
Pipe test section area = 1.557 m^2 (16.76 ft^2).
Inner jacket test section area = 1.753 m^2 (18.87 ft^2).

the differences in insulation thickness and other factors, this is excellent agreement between these test systems.

The data for the mineral wool system in Fig. 6 show good agreement between the 40.64-cm (16 in.) and 7.62-cm (3 in.) pipe tests, the 40.64-cm (16 in.) pipe test data being of about 6 percent higher than the 7.62-cm (3 in.) pipe test. The variation from the manufacturer's sales data is also shown.

The calcium-silicate system exhibited the largest deviation between the 40.64-cm (16 in.) and 7.62-cm (3 in.) pipe test results. The lowest temperature data point on Fig. 9 for the 40.64-cm (16 in.) pipe test is not valid because of moisture initially present in the insulation when testing. As mean insulation temperature increases, the conductivity differences between the system increase. This is the result of radiation-type heat losses through the gaps in the insulation.

The deviations between the 40.64-cm (16 in.) pipe test and 7.62-cm (3 in.) pipe test conductivity values appear to be directly related to the number of joints in the installed insulation system. Many joints and gaps were evident in the calcium-silicate insulation. After one thermal cycle, these gaps widened, and insulation effectiveness was impaired as indicated by the data shown in Fig. 15. The contractor-installed calcium-silicate system conductance was larger after one temperature cycle. The mineral wool insulation was more forgiving during installation but still contained a number of seams. The alumina-silica, on the other hand, was installed without axial seams and the radial seams were overlapped. Another indication of the presence of seams is the variation in the outer jacket insulation temperature. Table 1 shows the largest variation of surface temperature for the calcium-silicate insulation and the lowest for the alumina-silica refractory fiber blanket. The duplex calcium-silicate-mineral wool system showed a more uniform surface temperature, but the thermal conductance of the system was not much different from that measured for the standard calcium-silicate.

A guarded pipe test apparatus can be used to measure the thermal properties of large-sized insulation systems. As shown, the fit-up of the insulation is important. Kimball[5] has demonstrated the utility of large-diameter tests in the cryogenic region using calibrated end caps to account for the heat losses.

The large-diameter pipe test results indicate that the installation of the insulation can have a great effect on the thermal performance of the insulation system. In many cases, thermal performance analyses of an insulation system cannot rely on homogeneous insulation thermal property data, but the designer must know the effects of installation, shrinkage, and fit-up.

[5]Kimball, L. R. in *Heat Transmission Measurements in Thermal Insulations, ASTM STP 544*, American Society for Testing and Materials, 1974, pp. 135–146.

The purpose of the paper is to demonstrate the feasibility of scaling up the standard ASTM Method C 335 to larger pipe sizes. Real-size insulation system heat loss values are required to enable a designer to evaluate a plant insulation system and to adequately size a heating, ventilating, and air-conditioning (HVAC) system to handle heat losses and to be able to predict surface temperatures of the outside of the insulation.

The scale-up of the pipe test from 7.62-cm (3 in.) to 40.64-cm (16. in.) did not pose any difficulty. Equilibrium temperatures and balanced temperatures were readily achieved. An analysis of the possible heat leaks leading to errors in conductivity values indicates that a 2 K (3.6°F) difference between the guard and test section would result in about 13 to 23 W being transferred axially through the pipe and inner jacket into or out of the test heater section, depending on temperature. At the low temperature, a 13-W power uncertainty would mean a 10 percent uncertainty in conductance, while at the highest temperature this would cause a 3 percent error in conductance values.

Conclusions

1. The guarded pipe test procedure can readily be adapted to testing insulations on large-diameter pipe.
2. The largest differences between 7.62-cm (3 in.) and 40.64-cm (16. in) pipe test results were found in the system where the insulation assembly resulted in gaps and discontinuities in the insulation.
3. Where insulation could be installed identically (for example by wrapping a refractory fiber blanket on the test pipe), excellent agreement in pipe test data between 7.62-cm (3 in.) and 40.64-cm (16 in.) pipe test apparatus is found.

Other Parameters and Measurements

C. G. Bankvall[1]

Forced Convection: Practical Thermal Conductivity in an Insulated Structure Under the Influence of Workmanship and Wind

REFERENCE: Bankvall, C. G., **"Forced Convection: Practical Thermal Conductivity in an Insulated Structure Under the Influence of Workmanship and Wind,"** *Thermal Transmission Measurements of Insulations, ASTM STP 660*, R. P. Tye, Ed., American Society for Testing and Materials, 1978, pp. 409–425.

ABSTRACT: This paper describes the practical heat resistance in an insulated wall structure as influenced by workmanship and forced convection. Experimental investigations of crossbar walls are compared with calculations. Examples show the influence of heat resistance of insulation installation, airflow along the insulation, and airflow through the insulation. Full information on theoretical calculations and experimental investigations can be found in footnote 2.

KEY WORDS: thermal insulation, permeability, forced convection, air leakage, workmanship, thermal conductivity

Nomenclature

- A Area, m^2
- B_0 Permeability, m^2
- B Permeance, m
- d Thickness, diameter, m
- L Length, m
- p Pressure, Pa
- R Thermal resistance, m^2K/W
- Q Volume flow, m^3/s
- V Velocity, m/s
- λ Thermal conductance, $W/m \cdot K$
- ρ Density, kg/m^3
- η Viscosity, Ns/m^2

The external wall of a building has as its primary function the preservation of the desired indoor climate. Therefore, certain requirements are put on the different layers of the wall structure.

[1]Doctor of engineering, Docent, Statens Provningsanstalt, Swedish National Testing Institute, Box 857, S-501 15 Borås, Sweden.

In principle, the layers in a crossbar wall have the following function. The outside panel or brick wall protects against rain and direct wind. The airspace behind this enables ventilation of moisture. The wind-protective sheet will secure insulation from external air movements. The insulating material gives the structure its main thermal resistance. The vapor barrier protects from moisture transport from inside and gives the wall its main airtightness. On the inside a board is mounted to facilitate the required surface treatment, for example, with paint or wallpaper. In this way the airtightness of the wall is normally further enhanced (Fig. 1).

The thermal resistance of the structure depends mainly on the insulating properties of the thermal insulation. In an actual structure the cold bridges from crossbars will increase the heat transfer. The thermal resistance observed in practice, however, will also be influenced by workmanship and forced convection. The installation of the insulation will influence the final function. This is obvious, since often the thermal resistance of the insulating material is more than an order of magnitude greater than the resistance in the airspace which it fills. The effect is, however, poorly understood in quantitative terms. The same is true for air movements due to forced convection. By forced convection is meant air movements governed from outside, for example, by wind or mechanical ventilation. It is obvious that such air movements as well as those due to natural convection will influence the heat transfer in a structure or in a permeable insulating material.

Laboratory Experiments

In order to find the effects of workmanship and forced convection, investigations were made on a crossbar wall in the laboratory. The wall structure and the actual test area used were selected from field inventories, made at building yards. These field inventories showed what kind of workmanship could normally be expected when the insulation was in-

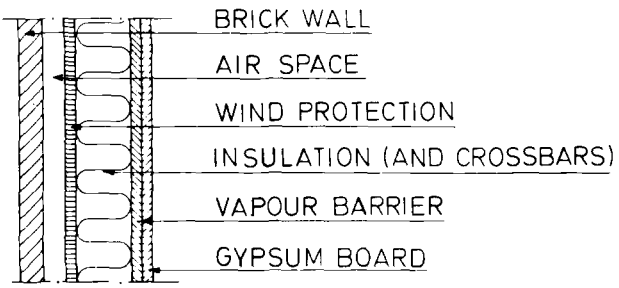

FIG. 1—*External multilayer wall.*

stalled. Field measurements were also made to indicate what pressure differences could be found over, for example, the height or the thickness of a wall. These investigations gave information about how the laboratory experiments should be set up.[2]

The test wall was mounted between two climatic chambers. One regulated to +20°C and the other to −20°C. The pressure difference over the test wall could be controlled up to 20 Pa by evacuating the warm chamber somewhat.

The crossbar wall contained a test area which in its center had a cross of crossbars (Fig. 2). By having this cross in the test area, various forms of insulation installation could be simulated within the area. This was achieved as indicated in the figure, which corresponds to defects recorded in practice.

The depth of the crossbar space was 0.145 m. On the inside of the insulation was a plastic foil and a gypsum board. On the outside, different types of wind protection were mounted. On the outside, different types of wind protection were mounted. Outside this wind protection there was an airspace where the airflow could be regulated. The thermal resistance value for the test area was measured by hot box with an accuracy estimated to be better than 8 percent.[2]

The insulating materials used in the experiments were chosen with

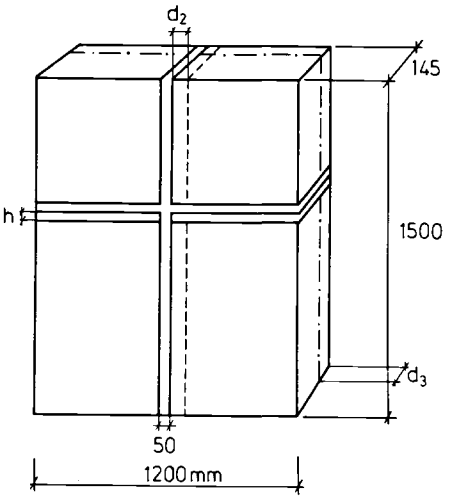

FIG. 2—*Crossbar test wall with example of insulation installation defects:* h = *horizontal "air crack"*; d_2 = *vertical "air crack"*; d_3 = *airspace, warm side.*

[2]Bankvall, C. G., "Påtvingad konvektion. Praktisk vårmeledningsförmåga under inverkan av arbetsutförande och vind", Statens Provningsanstalt, Borås, Sweden, 1977 (in Swedish; summary and figures in English).

regard to their permeability. The thermal conductance values were approximately identical. The aim was to investigate to what extent air movements, either in built-in air spaces around the insulation or due to forced convection from outside, would influence the heat transfer in the insulation itself. The materials under investigation are listed together with measured parameters

	ρ, kg/m^3	B_0, m^2	λ, W/m·K, at 0°C
Glass fiber	16	40×10^{-10}	0.034
Rock wool	40	20×10^{-10}	0.0335
Cellular plastic	20	...	0.033

In one part of the investigations, measurements were performed with different kinds of wind protection. In this case, too, the wind protection materials were chosen with regard to their permeance since this is the most important factor when evaluating the influence from forced convection. The wind protection materials were mainly the following

	d, m	B, m	λ, W/m·K, at 0°C
Asphalt-impregnated porous fiberboard	0.013	3.8×10^{-10}	0.07
Mineral wool board	0.03	150×10^{-10}	0.03

Workmanship

In practice, the thermal resistance of a crossbar wall will depend upon the workmanship during installation of the insulation. Field investigations have shown that deficient workmanship generally leads to insulation that insufficiently fills the space to be insulated; that is, the material is cut or mounted so that air spaces or cracks are formed around the insulation.[2] Generally, two main kinds of air spaces are noted: (1) "The crack" is an air space going through the insulation from the warm to the cold side; and (2) "the space" is an air space on one side of the insulation, either the warm or the cold side (compare Fig. 2). To study the influence of spaces or cracks on the heat transfer, measurements were made on the test wall carrying such defects. These measurements were then compared with theoretical calculations.

The heat-transfer coefficient in air cracks or in air spaces was evaluated theoretically by calculation of the convective and the radiative heat transfer. The result from one such calculation is shown in Fig. 3, giving the heat-transfer coefficient for a vertical crack of varying width as a function of insulation thickness.

Figure 4 shows the results from measurements on the test wall with vertical cracks in the insulated space. The figure indicates fair agreement

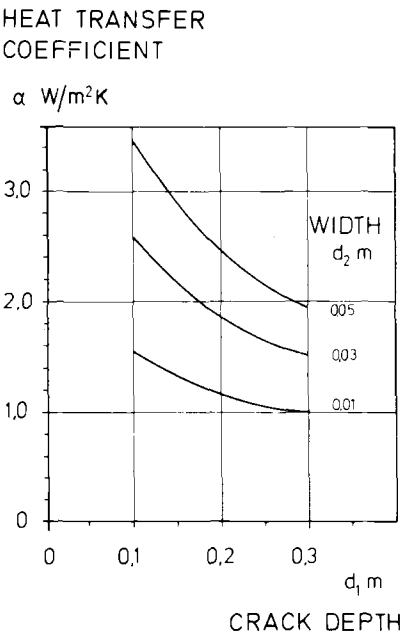

FIG. 3—*Calculated heat-transfer coefficient for vertical air crack (width,* d_2*; depth,* d_1*;* $T_m \simeq 0°C$*;* $\Delta T \simeq 35°C$*).*

between the measured values and the calculated curve. This was also true with the other mineral-wool insulation. In case of the cellular plastic, however, consistently lower values were measured as compared with theoretical predictions. This was attributed to the difficulty in completely filling the insulated space with this insulation, which had a very low compressibility. To make installation possible, the material had to be cut with height and width 5 mm less than the space to be insulated.

Measurements on horizontal cracks and on air spaces in the insulated space showed similar results. All measurements were performed in the absence of any influence of forced convection on the structure.

Comparisons between the theoretical analysis and the laboratory measurements indicate that the theoretical model could be used to illustrate the influential factors. A representative example is given in Fig. 5, which shows the dominant effect on the thermal resistance value of a vertical air crack in an insulated crossbar space. The figure reveals that the higher the thermal resistance, the greater the influence of air cracks. This example also shows that the important factor is the extent to which the insulating material fills the space to be insulated. The measurements also demonstrated that the permeabilities of the different insulation materials used in this study were of no importance to the overall thermal resistance of the wall.[2]

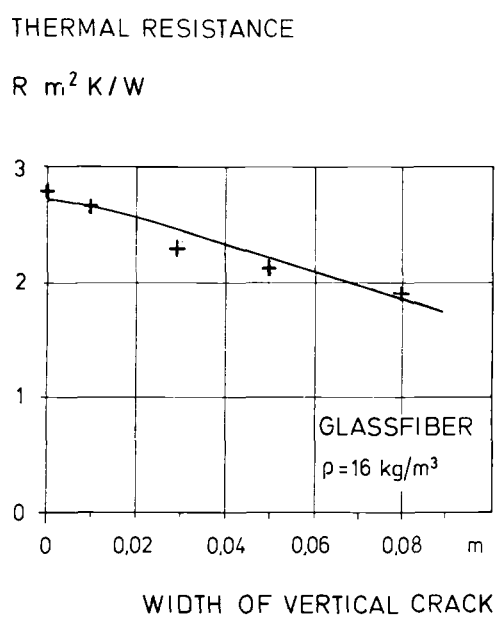

FIG. 4—*Reduction of thermal resistance due to vertical crack in insulated space of test wall (compare Fig. 2). Comparison between measured values and calculated curve.*

Forced Convection

The heat transfer in a structure can be affected by forced convective airflow. Factors governing this flow are the pressures around the structure and the flow resistances in the materials and in the joints between materials.

Two different kinds of forced convection can be considered in principle. One is airflow through an insulated structure and the other is airflow along an insulated structure, Fig. 6. In the first case the airflow is mainly from warm to cold side at right angles to the wall layers. In the second case the airflow is mainly along the layers, eventually passing sections of the insulation without going from warm to cold side. The two types of forced convection are defined separately; in practice, however, intermediate types are common.

To calculate airflow due to forced convection, the following equations were used.

In the case of turbulent airflow the equations for pipeflow were used.

$$\frac{\Delta p}{\Delta x} = \beta \cdot \rho \cdot \frac{V^2}{2 d_R}$$

where

β = friction factor (defined in footnote 2)
Δp = pressure difference,
Δx = flow length,
ρ = density,
V = velocity, and
d_R = pipe diameter.

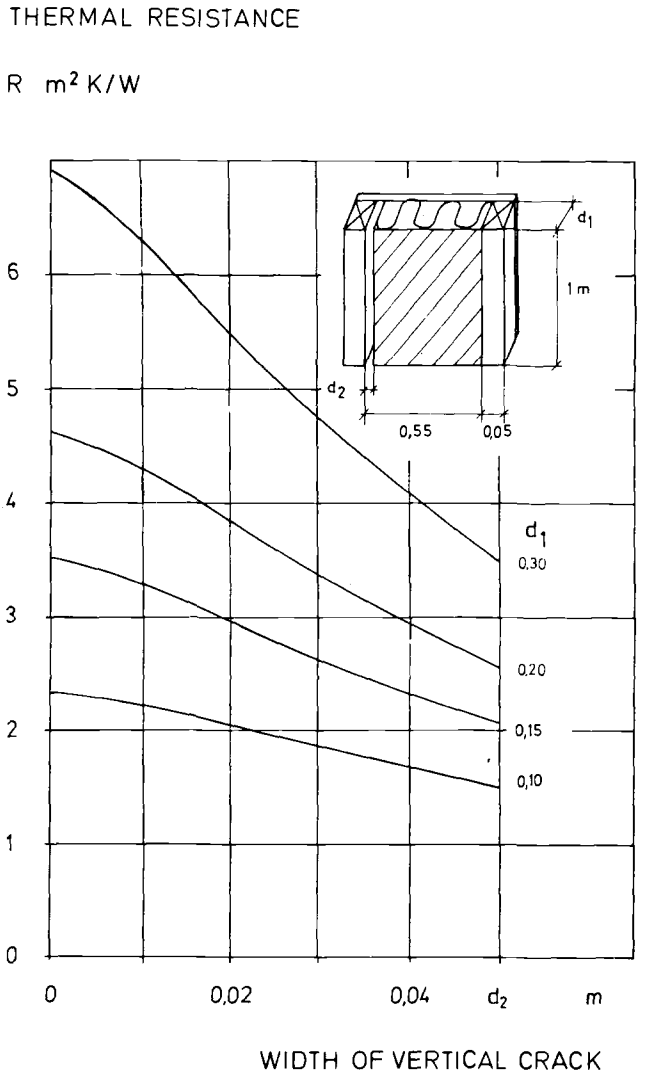

FIG. 5—Reduction of thermal resistance in crossbar wall due to vertical crack in insulated space with varying insulation thickness: λ (insulation) = 0.035 W/m·K.

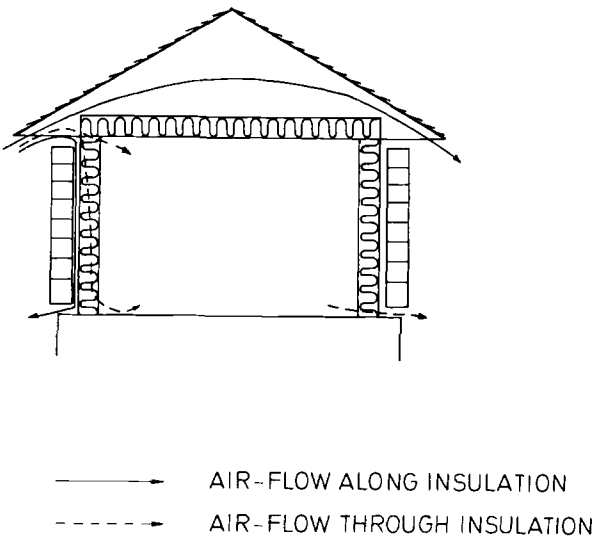

FIG. 6—*Principal types of forced-convective influence on thermal insulation.*

In cases of bends, elbows, and contraction or expansion in the pipeline, the following equation was used

$$\Delta p = \xi \cdot \rho \cdot \frac{V^2}{2}$$

where ξ defines a loss coefficient.[2]

The foregoing equations are true for circular cross sections. For other cross sections, approximate calculations were made by using the hydraulic diameter

$$d_H = \frac{4A}{S}$$

where A is the area and S the perimeter of flow.

For laminary flow in an air space or in a crack, the following equation was used

$$\frac{\Delta p}{\Delta x} = 12\eta \frac{V}{b^2}$$

where b is the crack width and η the viscosity.

Airflow through cracks can be calculated in principle from the foregoing equations. This, however, presupposes a detailed knowledge of the flow path and its dimensions and surface properties. In many cases, therefore, empirical equations of the general type expressed in the following are used

$$Q = V \times A = \alpha \times \Delta p^{\gamma}$$

where α and γ are derived from measurements and vary with different structures. $\gamma = ½$ indicates that the flow is turbulent; $\gamma = 1$ indicates that it is laminar. Q denotes the volume flow (m^3/s).

For calculation of flow through openings in thin layers, the following equation was used[3]

$$Q = 0.827 \times A \times \Delta p^{1/2}$$

Flow through joints, in wind protection sheets, for example, was evaluated by the following equation derived from measurement[4]

$$Q = 0.28 \times 10^{-5} \times L \times \Delta p^{0.75}$$

for a nailing distance of 100 mm. L denotes the length of the joint.

For overlapping and clamped joints in vapor barriers, measurements yielded the following equation[5]

$$Q = 2 \times 10^{-7} \times L \times \Delta p$$

For flow through permeable material, the equation used was

$$Q = \frac{B_o}{\eta} A \frac{\Delta p}{\Delta x}$$

This equation is valid only for laminar flow; that is, at moderate flow velocities, higher velocities require corresponding measurements, giving permeability (B_o) that varies with velocity.

The flow characteristic of a layer can also be described by its permeance B

$$B = B_o/d$$

Airflow Along Insulation

Airflow along an insulation can be illustrated as in Fig. 7. The figure shows an outer wall consisting of a brick wall, and air space, wind protection, and an insulated crossbar space. The ventilation in the air space is facilitated by openings over and at the bottom part of the brick wall. In some cases the permeability of the brick wall may contribute to the ventilation of the air space.

Depending upon the pressure difference in the air space and the wind

[3]*IHVE Guide Book A 1970*. The Institution of Heating and Ventilation Engineers, London, 1971.

[4]Nylund, P. O., "Vindtäthet hos flerskiktsväggar," *Byggmästaren*, No. 11, Stockholm, 1966.

[5]Granum, H., Svendsen, S., and Tveit, A., "Lette treveggers vindtetthet," NBI, Report No. 7, Oslo, 1954.

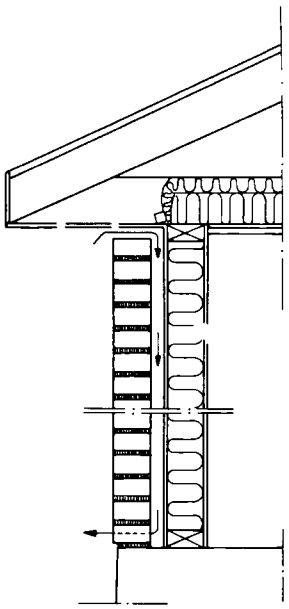

FIG. 7—*Airflow in air space along insulated crossbar structure with outer brick wall.*

protection, there may exist an interchange of air between the air space and the insulation. This interchange varies over the height of the insulated space. The results of calculations for an insulated space with a height and width of 1 m are shown in Fig. 8. The pressure over the height of the space was 5 Pa. The insulating material had a specific permeability of $B_o = 40 \times 10^{-10}$ m^2. The insulation thickness was 10 cm. In Fig. 9, the air interchange between the air space and the insulation has been considerably reduced by a wind protection of asphalt-impregnated porous fiberboard. The calculations were based on the previously presented equations.

To establish the influence of this type of airflow on the thermal resistance of the insulated space, experiments were conducted with the crossbar wall. The forced convection was simulated by regulating an airflow along the wall on the cold side. The airflow velocity was 2.5 m/s, corresponding to a pressure gradient of 0.7 Pa/m. Comparisons were made with fully insulated walls, wind protected in different ways (Fig. 10). The reduction in thermal resistance due to the forced convective flow was less than 10 percent, even for the unprotected insulation. The measured values are also in fair agreement with calculations.

Measurements were carried out also on the crossbar wall with defects in its insulation installation. Figure 11 shows the reduction in thermal resistance for the crossbar wall with vertical cracks under the influence of forced convection. When the wall was unprotected and exposed to full

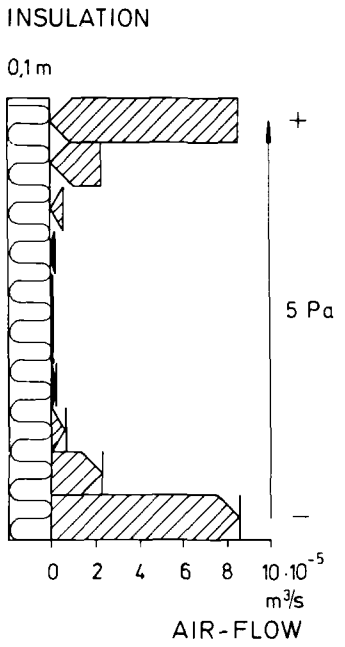

FIG. 8—*Air interchange between insulation and air space with airflow along the insulated space (compare Fig. 7): insulation thickness, 0.1 m; height, 1 m;* $B_0 = 40 \times 10^{-10}$ *m²; pressure difference over height, 5 Pa/m; unprotected insulation.*

forced-convection airflow velocity ≃ 2.5 m/s (2.5), there was a substantial decrease in thermal resistance. Also, with reduced forced-convection airflow velocity ≃ 0.1 m/s (0), the decrease was noticeable. When, on the other hand, the structure was protected by an asphalt-impregnated porous board, the reduction in thermal resistance was substantially reduced. Measurements on other insulations showed approximately the same results.[2]

In conclusion, these measurements indicated that for an insulation well installed and well protected from the wind, there was little influence from the permeability of the insulating material. At high loads of forced convection, the unprotected structure showed a larger reduction in thermal resistance when the permeability of the insulating material increased. This applied especially in the case with defects in the insulation installation. Wind-protective covering with high permeance gave a slightly higher reduction in heat resistance, especially if high permeance was combined with high permeability in the insulating material. The influence of an airflow along the insulation when installation defects are present in the insulated space is illustrated by the experimental investigations.

The heat transfer in the fully insulated wall can be calculated theoret-

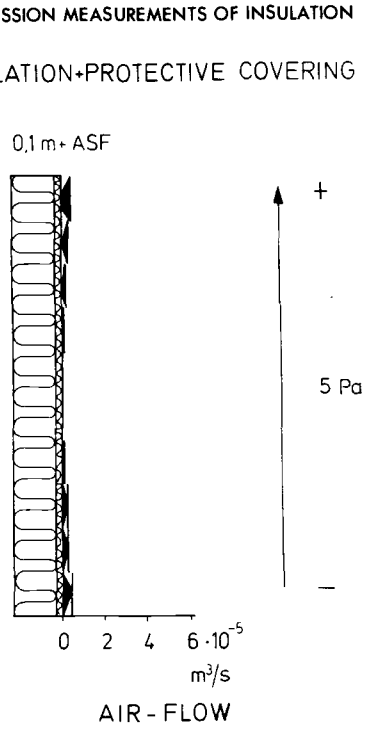

FIG. 9—*Air interchange between insulation and air space with airflow along the insulated space (compare Fig. 7): insulation thickness, 0.1 m; height, 1 m;* $B_0 = 40 \times 10^{-10}$ *m²; pressure difference over height, 5 Pa/m; wind protection by asphalt-impregnated board (ASF,* $B = 3.8 \times 10^{-10}$ *m).*

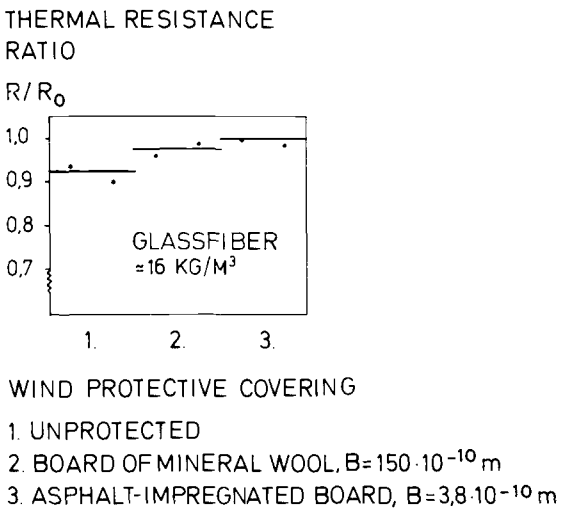

FIG. 10—*Reduction in thermal resistance of crossbar wall. Insulation thickness, 0.15 m. Pressure difference over height of test wall, 0.7 Pa/m. Comparison between measured values and calculated levels.*

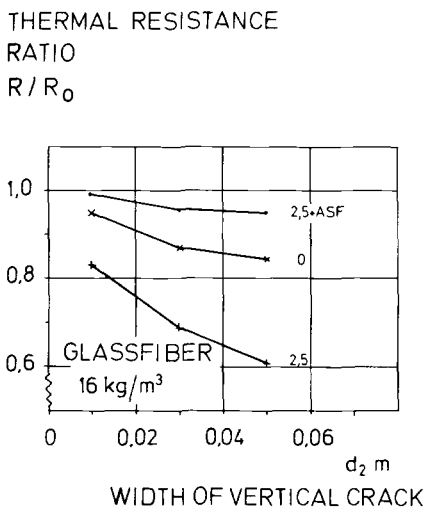

FIG. 11—*Reduction in thermal resistance of crossbar test wall with vertical crack and varying wind-protective covering,* $B = 3.8 \times 10^{-10}$ *m, and airflow along the insulated space. ASF: Protected by asphalt-impregnated board; 2.5: 2.5 m/s (≈ 0.7 Pa/m); 0 : 0.1 m/s.*

ically as well. This is shown in Fig. 12, where the thermal resistance for an insulated structure is given as a function of pressure difference over the height of the insulated space, thermal insulation thickness, and different wind-protective covering with varying thermal resistance and permeance. The insulated structure with high thermal resistance is more sensitive to this kind of forced convection. This structure will also require a wind protection with low permeance. The figure also shows how the mineral-wool board initially increases the thermal resistance of the structure. This increase is gradually lost when the forced convection increases.

Airflow Through Insulation

Airflow through an insulated crossbar wall is exemplified in Fig. 13. The airflow from the outside passes mainly through openings at the top and bottom of the brick wall and only partly through the wall itself. The main crossbar part of the wall has a wind protection on the outside and a vapor barrier and a board on the inside. Through this part of the wall, the air will flow through the materials themselves and through the joints between materials in the different layers. The inside board and its vapor barrier constitute the main protection against airflow through the wall. For these layers, joints between materials and small aircracks around electrical installations, for example, may be of great importance with regard to the airtightness of the wall.[2]

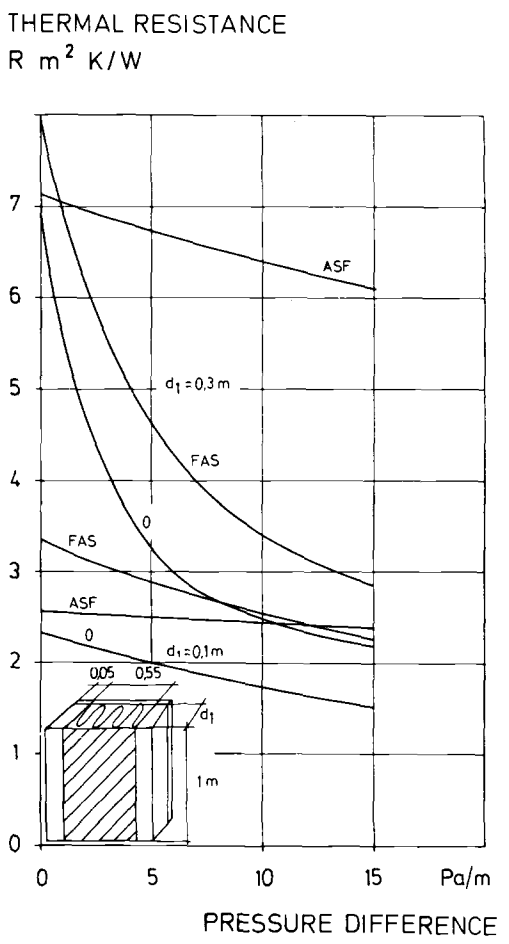

FIG. 12—*Reduction in thermal resistance of crossbar wall due to flow along the insulated space. Insulation,* $B_0 = 40 \times 10^{-10}$ *m² and* $\lambda = 0.035$ *W/m·K. Wind-protective coverings. ASF: asphalt-impregnated board,* $B = 3.8 \times 10^{-10}$ *m. FAS: mineral-wool board, 0.03 m,* $B = 150 \times 10^{-10}$ *m. O : unprotected.*

The airflow through the wall can be calculated from the equations presented previously. In each layer, the flow resistance of the material itself, of joints between materials, and of eventual holes has to be considered.

The effect of airflow on the thermal resistance through the crossbar wall was investigated in the test situation presented previously. To study the influence of airflow through the insulation, holes were made in the inside board and in the vapor barrier (hole area in vapor barrier: $A = 2.36 \times 10^{-4}$ m²; in inside board: $A = 4.55 \times 10^{-4}$ m²). Measurements were made

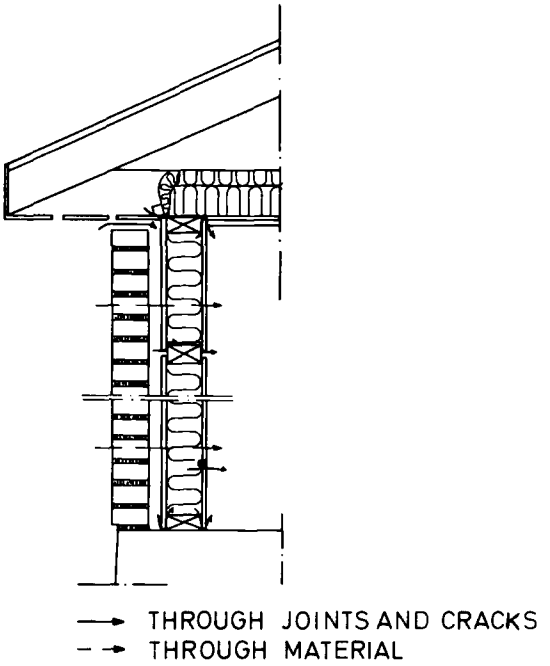

FIG. 13—*Principal ways of airflow through insulated crossbar structure with air space and outer brick wall.*

of various thermal insulations with different wind protections. In some measurements, half the number of holes in the inside gypsum board were covered by tape. Results from the measurements are shown in Fig. 14. The measured values indicate a lesser reduction in the heat resistance value than the theoretically-calculated curve. The difference, however, is well within the accuracy of determining the hole area in reality. Therefore, these observations can be accepted as in sufficient agreement with theory. The results were similar for all the different kinds of insulations.

Using the previous equations, calculations were made of the thermal resistance of a typical insulated crossbar space. Figure 15 shows the decrease in thermal resistance for two insulation thicknesses and two different cases, one with vapor barrier, the other without. The results shown are obtained with different kinds of wind protection. The influence from the wind protection is mainly twofold. One is the enhanced thermal resistance and the other is the increase in total resistance to airflow through the structure.

In summary, to prevent airflow through the insulated structure, the airtightness of the vapor barrier and partly of the inside board is of great

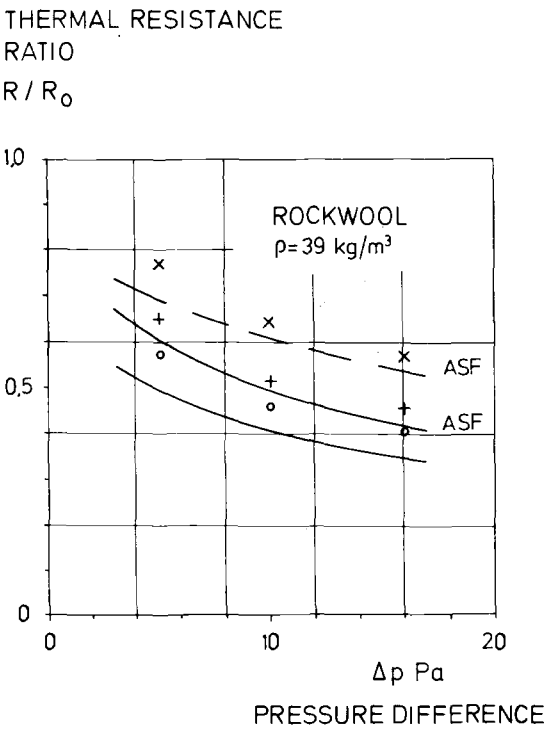

FIG. 14—Reduction in thermal resistance due to airflow through the insulated crossbar test wall, with and without wind protection by asphalt-impregnated board. Holes through the gypsum board and the vapor barrier according to the text (+,o); half the holes in the gypsum board covered by tape (x). *ASF: wind protection by asphalt-impregnated board;* $B = 3.8 \times 10^{-10}$ *m. Otherwise unprotected. Comparison between measured values and calculated curves.*

importance. If there are holes and defects in these layers, the permeance of the wind protection can be of importance to the overall airflow through and the heat resistance of the wall. An insulated wall structure with such defects, however, will normally show a considerable reduction in its thermal resistance due to forced convective airflow.

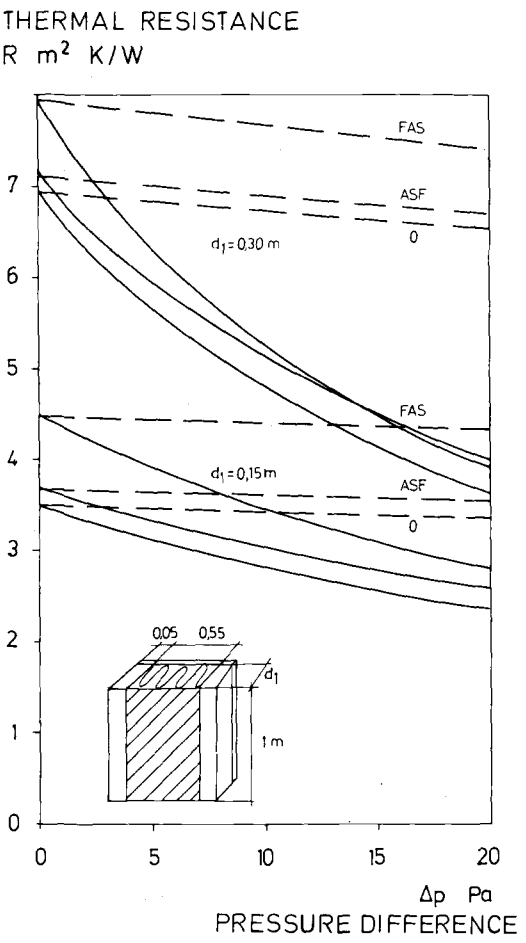

FIG. 15—Reduction in thermal resistance due to airflow through the insulation and with (—) and without (—) vapor barrier: insulation thickness d_i(m). λ *(insulation) = 0.035 W/m·K. Wind-protective covering. ASF: asphalt-impregnated board,* $B = 3.8 \times 10^{-10}$ *m FAS: mineral-wool board, 0.03 m,* $B = 150 \times 10^{-10}$ *m O : unprotected.*

T. Ashworth,[1] *W. G. Lacey,*[1] *and E. Ashworth*[1]

Drift Measurement Technique Applied to Poor Conductors

REFERENCE: Ashworth, T., Lacey, W. G., and Ashworth, E., "**Drift Measurement Technique Applied to Poor Conductors,**" *Thermal Transmission Measurements of Insulation, ASTM STP 660*, R. P. Tye, Ed., American Society for Testing and Materials, 1978, pp. 426–436.

ABSTRACT: Many applications require knowledge of thermal properties, over a wide range of temperature, to within 5 percent. The speedy and economical acquisition of the data is often a prime concern. We are investigating the potential of the very simplest system (an unguarded plate system), used in a drift mode rather than in a steady-state mode, to fulfill this need.

When heat flows across a specimen whose mean temperature is drifting slowly and linearly with time, a term of the form $C_F(dT/dt)$ must be added to the steady-state equation. Data are taken over a given temperature range with the temperature both increasing and decreasing; the value of C_F is then adjusted until the two sets of data produce the same value of conductivity. Since C_F is a function of the density of the specimen and its specific heat at constant pressure, an approximate value of the thermal diffusivity is obtained as a by-product in this drift mode of operation.

The successful application of the technique is illustrated by both drift technique and steady-state measurements on microconcrete over the temperature range −20 to +60°C. Corrections for heat losses and nonlinear heat flow have been appraised by finite-element analysis and by comparisons with data from adiabatic linear heat flow systems. Our objective is to develop the apparatus for use up to 500°C.

KEY WORDS: thermal conductivity, thermal diffusivity, drift measurement technique, microconcrete

Thermal conductivity measurements can be divided into three general classifications corresponding to three classes of applications: measurements with high absolute accuracy, measurements with high consistency, and measurements with moderate absolute accuracy. The first class, typified by the precision measurements of the National Bureau of Standards (NBS) [*1*],[2] is necessary for standards. Many systems are capable of a

[1]Professor of physics, graduate research assistant, and assistant professor of mining engineering, Physics Department, South Dakota School of Mines and Technology, Rapid City, S. Dak. 57701.

[2]The italic numbers in brackets refer to the list of references appended to this paper.

high degree of repeatability, but due to factors such as difficult-to-determine heat losses, they cannot provide high absolute precision; this is often the case when working at high temperatures. Such systems can be very effective in applications requiring absolute precision when they are calibrated with standard specimens. In many applications, particularly those involving specimens of high variability (such as core samples), the requirement is to make measurements of moderate absolute precision, say 5 to 10 percent, in a short period of time. Measurement demands here are of the third type. This type of application is becoming of much greater relative importance, mainly because of energy-related problems of underground nuclear waste disposal, *in situ* retorting of shales and lignites, and general heat-transfer problems. Many of these applications involve vapor migration and often phase transitions as well.

The purpose of the work described is to determine the potential of a non-steady-state measurement technique to provide rapid acquisition of thermal conductivity data of adequate accuracy (10 percent) for types of material and applications mentioned in the foregoing. Its potential for operation in the second classification is being evaluated as the project progresses. Simplicity of design and operation are the fundamental objectives and design criteria. Thus an unguarded plate apparatus is being used; it allows the simplest possible construction, and any specimen which can be fabricated into a cylindrical disk can be mounted in a few minutes. As will be shown, in principle, simultaneous determination of both conductivity and thermal diffusivity is possible. In this respect the system has resemblence to the heat flowmeter apparatus described by Shirtliffe, Stephenson, and Brown [*2*]. The potential for continuous data by the drift measurement technique is of obvious value when phase transitions are involved. Previous experience indicated that this type of apparatus can be used in the conventional steady-state mode with temperature gradients as low as $50°Km^{-1}$ to yield conductivities with random errors of no more than 10 percent, usually much less. Thus the system potentially has many desirable features for investigation of energy-related materials.

The performance of the system will be illustrated by data on microconcrete, whose conductivity is a function of the water content, and in which water vapor does migrate under a thermal gradient.

Rather than cite a large collection of articles and papers, the reader is referred to *Thermal Conductivity* (R. P. Tye, Ed.) [*4*] for all the necessary background on measurement techniques. Chapters by McElroy and Moore ("Radial Flow Methods"), Danielson and Sidles ("Non-Steadystate Methods"), and Laubitz ("Analysis of Heat Losses") are particularly germane. A compilation of the properties of concrete has been given by Neville [*5*].

Theory of Operation

Heat flow in any system is described by the general energy conservation equation

$$\vec{\nabla}\,\lambda\vec{\nabla}T = -\dot{Q}(x,y,z) + \rho c_p \frac{\partial T}{\partial t} \tag{1}$$

where

λ, ρ, and c_p = thermal conductivity, density, and specific heat respectively, of the conducting medium,

T = temperature at point (x,y,z), and

$\dot{Q}\ (x,y,z)$ = internal heat generated within an elementary volume located at that point.

Thus for heat flow across a specimen in the form of a right circular disk from which there are no edge losses (that is, linear or axial heat flow) and which has no internal sources of heat, Eq 1 becomes

$$\vec{\nabla}^2 T = \frac{\partial^2 T}{\partial x^2} = \frac{\rho c_p}{\lambda}\frac{\partial T}{\partial t} = A\frac{\partial T}{\partial t} = \frac{1}{D}\frac{\partial T}{\partial t} \tag{2}$$

provided λ may be considered constant; $D = \lambda/(\rho c_p) = 1/A$ is the thermal diffusivity of the material.

Transient solutions for this equation can be found by the superposition integral method (see, for example, Hildebrand [3]). However, for the boundary conditions appropriate for the apparatus, albeit idealized as shown in Fig. 1, the response is a complicated series of exponential terms. Below, a simpler and more lucid derivation is presented for the special case in which the temperature of the heat sink varies linearly with time.

If we assume that a steady drift condition has been attained so that $\partial T/\partial t$ is constant and has the same value at all points within the specimen, then Eq 2 yields

$$T = A'x^2 + Bx + C$$

where

$$A' = \frac{A}{2}\frac{\partial T}{\partial t}$$

and for the boundary conditions specified in Fig. 1,

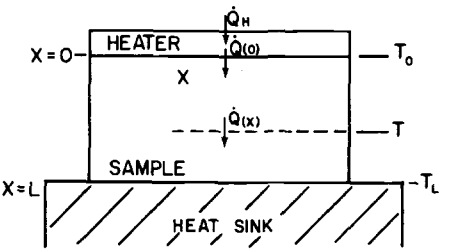

FIG. 1—*Boundary conditions.*

$$T = A'x^2 + \frac{T_L - T_o}{L} x - A' Lx + T_o \tag{3}$$

The amount of heat absorbed per unit time by an elementary disk of thickness dx and area A_o is $dq = A_o dx\, c_p\, \rho\, (\partial T/\partial t)$. Therefore

$$\dot{Q}(x) = \dot{Q}(o) - \int_o^x d\dot{q} = \dot{Q}(o) - A_o c_p \rho\, x \frac{\partial T}{\partial t} = \dot{Q}(o) - 2A_o A'\lambda x \tag{4}$$

For the system considered, Fourier's law gives

$$\dot{Q}(x) = -\lambda A_o \vec{\nabla} T = -\lambda A_o \frac{\partial T}{\partial x} \tag{5}$$

Substituting for $\dot{Q}(x)$ from Eq 4 and $\partial T/\partial x$ from Eq 3 gives

$$\lambda = -\frac{[\dot{Q}(o) - 2A_o A'\lambda x]}{A_o \left[2A'x + \left(\frac{T_L - T_o}{L} - A'L\right)\right]} \tag{6}$$

But since λ is assumed constant, this expression must have the same value at all values of x. Choosing $x = 0$ therefore gives

$$\lambda = \frac{\dot{Q}(o)\, L/A_o}{(T_o - T_L) + A'L^2} = \frac{\dot{Q}(o)\, F}{\Delta T + (C_D/\lambda)\, \partial T/\partial t} \tag{7}$$

where F is the form factor L/A_o and

$$A'L^2 = \frac{L^2 \rho c_p}{2\lambda} \frac{\partial T}{\partial t} = \frac{C_D}{\lambda} \frac{\partial T}{\partial t} \tag{8}$$

$$C_D = \frac{\lambda L^2}{2D} \text{ or } D = \frac{\lambda L^2}{2\, C_D} \tag{9}$$

Equation 7 correctly reduces to the steady-state equation when $\partial T/\partial t$ is zero.

Of the energy supplied to the heater, a portion is used to raise the temperature of the heater and the remainder flows into the upper surface of the specimen. Thus

$$\dot{Q}_H = \dot{Q}(o) + H \frac{\partial T}{\partial t} \tag{10}$$

where $\dot{Q}_H$ is the rate of energy dissipation in the heater, and H is the heat capacity of the heater; heat losses from the heater are neglected. Substituting for $\dot{Q}(o)$ in Eq. 7 yields

$$\lambda = \frac{\left(Q_H - H \frac{\partial T}{\partial t}\right) F}{\Delta T + (C_D/\lambda) \frac{\partial T}{\partial t}} \tag{11}$$

If the portion of Q_H adsorbed by the heater is small, so that

$$\left(\frac{\partial T}{\partial t} H\right) / \dot{Q}_H << 1$$

then a binomial expansion gives

$$\lambda = \frac{\dot{Q}_H F}{T + \left(\dfrac{C_D + HF}{\lambda}\right) + \dfrac{\partial T}{\partial t}} \tag{12}$$

using the relation $\lambda \simeq \dot{Q}_H F/T$ and neglecting the second-order term.

Equation 12 contains three unknowns: λ, C_D, and H. So far we have treated these three unknowns as two unknowns, the conductivity λ and the drift correction factor $C_F = (C_D + HF)$; to determine them, an experimental procedure involving two conditions must be used. Upward drift and downward drift of temperature were chosen; the data reduction technique is described in the following. When the determination of C_F by this method has been thoroughly validated, the additional task of calibrating the heater to find H will be considered. If successful, this will then allow simultaneous determinaton of both the thermal conductivity and thermal diffusivity. In the present apparatus, $C_D \simeq HF$ for the concrete specimen.

Apparatus

Figure 2 shows the configuration of the apparatus; it is entirely conventional. The specimen chamber is contained within a spring-loaded pressure plate assembly, surrounded by removable insulation and enclosed in an outer protective box. The specimen chamber is designed to hold a 1.27-cm-thick by 12.7-cm-diameter circular disk of microconcrete or any other solid. The specimen is sandwiched between a heater plate and a cooling unit. The heater plate consists of 20 m of No. 28 double-nylon-wrapped manganin wire uniformly woven into a window screen pattern, coated with enamel, and ovenbaked between two 16-mm by 12.7-cm copper disks to form an integral unit. The heater leads are brought out through heat-shrink tubing which is secured with epoxy into recesses milled into the heater plate to prevent excessive flexing and eventual failure of the wire leads. Two grooves are milled into the heater plate surface to accommodate copper-constantan thermocouples. The thermocouples are enameled into the grooves and their leads are brought out through tubing as were the heater leads. One thermocouple is referenced to room temperature in a heavy brass block for the purpose of computing the absolute temperature of the specimen. The second thermocouple is a differential thermocouple whose other junction is located in a recess milled into the

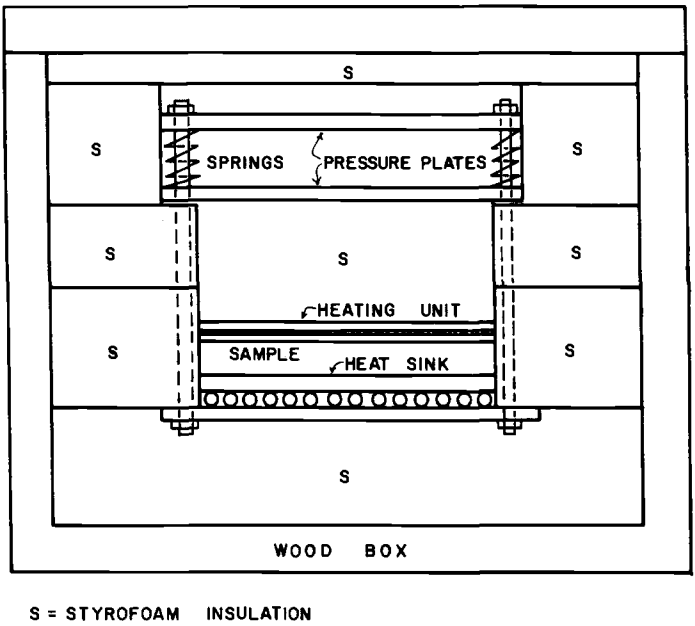

FIG. 2—*Unguarded plate apparatus.*

heat sink on the surface in contact with the cold side of the specimen. This thermocouple provides the temperature gradient across the specimens as well as determining the mean temperature of the specimen in conjunction with the absolute thermocouple. Separate tests with additional thermocouples embedded in the specimen showed no significant (within 1 percent) differences between these thermocouples and the ones embedded in the copper plates. These tests were carried out at and slightly above room temperature.

The heat sink is a 4.8-mm-thick disk of copper, 12.7 cm in diameter, with 4.8-mm-outside-diameter copper tubing sweat-soldered to its bottom in a spiral pattern.

The heater plate, specimen, and cooling unit are held in thermal contact under pressure by a system of steel plates and springs. The entire specimen chamber is surrounded by high-grade styrofoam or fiber glass insulation and closely fitted into the 30-cm-square by 20-cm-high wooden box constructed of 2-cm-thick sides, bottom, and removable top.

The simple measuring system used is shown in Fig. 3.

Heat Loss Corrections

Energy supplied to the heater is dissipated from its edges and the edge of the specimen, and through the styrofoam between the heater and the

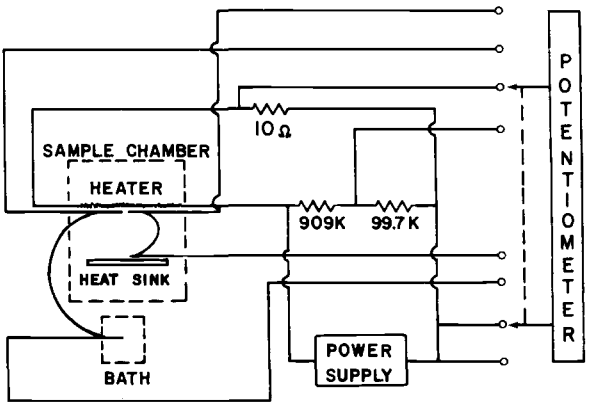

FIG. 3—*Measurement system.*

pressure plate, as well as through the specimen. To account for the conduction through the upper styrofoam, we introduce a factor $F_1(T)$ into Eq 12, while a second factor, $F_2(T)$, is used for all the edge losses. Thus

$$\lambda = \frac{\dot{Q}_H F}{\Delta T + \frac{C_F}{\lambda}\frac{\partial T}{\partial t}} F_1(T)F_2(T) \tag{13}$$

Both factors F_1 and F_2 are evaluated by a finite-element analysis of the system and by calibration using specimens of known conductivity. It is also easy to estimate F_1 from the geometry and properties of the materials. With a specimen of the same conductivity as the styrofoam, F_1 equals 0.80. For concrete specimens, F_1 is approximately 0.99.

Simple calculations do not provide accurate estimates for F_2, but they can be used to give upper and lower bounds [*6*]. We have shown that values between 0.95 and 0.99 can be expected at 300 K. These favorably large values result from the chosen ratio of specimen diameter to thickness of about 10:1. Finite-element analyses and calibration values of F_2 are both about 0.98. At temperatures approaching 400 K, the estimated value of F_2 drops to about 0.70. Thus we believe the certainty of the product $F_1 F_2$ to be about 2 percent up to 310 K. Moreover, the error thereby invoked is systematic and will not detract from investigations involving ratios of conductivity such as the variation of λ with temperature.

Experimental and Interpolation Procedure

Steady-state data are taken by the normal procedure of measuring the temperature difference across the specimen for two or more values of $\dot{Q}_H$

at a given mean temperature. Spurious voltages in the differential thermocouple can then be eradicated from the computed values.

To obtain drift data, a constant rate of supply of energy to the heater is established and then the temperature of the fluid circulating through the heat sink is caused to increase at a slow linear rate, usually between 5 and 20°K h^{-1}. A period of 30 to 60 min is usually needed for a steady drift condition to be established, after which t and ΔT are carefully recorded as functions of time. When the desired upper temperature has been exceeded by a few degrees, the direction of drift is reversed, and data taking resumes when a steady condition is reestablished.

Values of λ for the upward drift (λ_u) and the downward drift (λ_d) are first obtained by setting C_F equal to zero. Typically the two values, plotted against temperature, differ widely. The value of C_F is then varied to bring the two curves as nearly as possible to coincidence. Normally C_F is slightly temperature dependent. The λ_u and λ_d curves cannot then be expected to agree over a wide range of temperature if only a single constant value of C_F is used. It is intended to modify the data reduction code to allow C_F to be determined as a linear function of temperature by a least-squares regression. However, for the present, the value of C_F is adjusted by increments to obtain agreement at various temperatures.

For C_F nonzero, a simple iterative technique is applied to Eq 13 for the calculation of λ. Provided the drift rate is not excessive, the magnitude of the coefficients of this equation ensure rapid convergence of the method.

Results

Before commencing work on the concrete specimen, measurements were taken on a specimen of nylon for which the conductivity was known. These measurements had the primary objective of providing a calibration point. Also, the first set of data taken clearly illustrated the need for a constant drift rate; otherwise the data contains unacceptable scatter.

Figure 4 shows data obtained on a specimen of microconcrete. More careful temperature regulation was effected; the drift rate did decrease significantly during the first half of the experiment, but the changes were slow and steady. Transients were present below 280 K and in the λ_d curve above 300 K. Temperature changes of at least 5 K are required for steady conditions to develop. In the range 280 to 300 K the corrected values show the variation of C_F with temperature. A larger value of C_F is required at 280 K, while the values used (225 $Jm^{-1}K^{-1}$) are appropriate for 300 K. This apparent decrease in C_F with increasing temperature is partially due to some water loss during the progress of the experiment.

Fully corrected data obtained with somewhat longer runs are shown in Fig. 5. In view of the difficulty of maintaining a constant accurately known

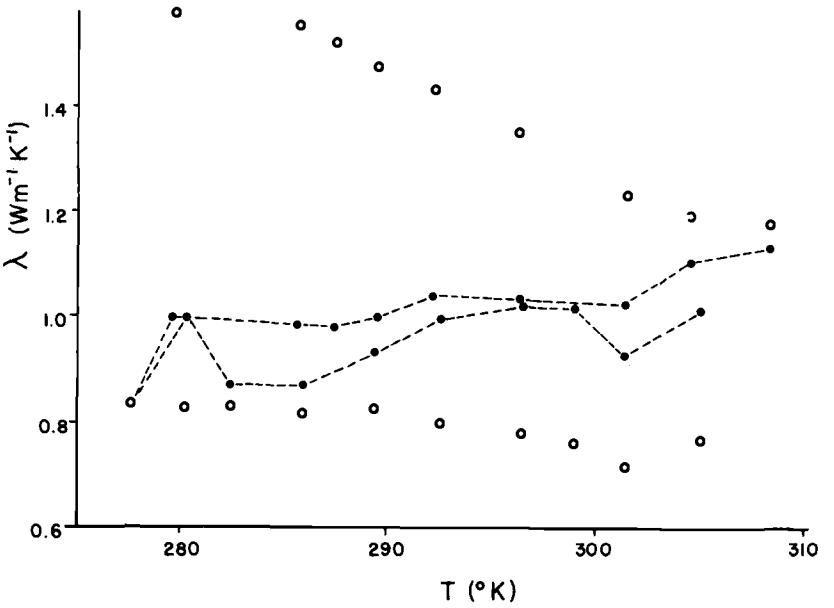

FIG. 4—*Drift correction effects: Specimen—3.9 percent moisture content microconcrete;* 0*—data without drift correction;* •*—data with drift correction* (C_F = 225 $Jm^{-1}K^{-1}$).

water content in the specimen, the repeatability of the data is satisfying, as is the demonstration of systematic dependence upon water content. All the measurements employed a temperature gradient of 2 K cm^{-1}. Although many more tests are required to substantiate the total efficacy of the drift measurement technique, the agreement with values obtained at 290 K by the steady-state method is encouraging.

Also, these data are in good general agreement with previous data given in the references for other types of concrete, both in terms of magnitude and the dependency on water content and temperature.

Using the approximation $C_D \simeq HF$, an approximate value of $D = 6 \times 10^{-7}$ m^2s^{-1} is obtained. Typical values for the properties of concrete taken from Ref. *3* indicate a value of diffusivity of about $5 \times 10^{-7} m^2s^{-1}$. Agreement between these two estimates is encouraging and suggests that further developmental work would be worthwhile.

Discussion

In deriving the simple theory for the continuous method of measurement, the important limitations inherent in the approximations must be clearly recognized. Variations in λ due to the temperature distribution within the specimen must be kept small, as must heat capacity and density

variations. Fortunately all of these conditions are met if the drift rate is kept small. Its constancy is also a requirement.

This investigation was of the nature of a feasibility study; thus presentation of a detailed error analysis of the technique would be inappropriate at this stage of its development. However, the system has been used to take a significant amount of data using steady-state operation. Most of this measurement has been on nylon and styrofoam specimens whose conductivity was known. These measurements verified the heat loss correction factors, and thereby provided some measure of calibration. The agreement between steady-state values for nylon and concrete with those obtained by the drift method is then taken as an indication that the latter technique does produce viable results.

Clearly, this non-steady-state method, by its very nature, cannot compete with steady-state measurements when the limits of accuracy are challenged. However, the continuous nature of the data and the speed of their acquisition are of considerable advantage when a precision of 5 to 10 percent is adequate. Using three different values of Q_H, it requires two days to obtain one value of conductivity by the steady-state method for the concrete specimen. In an equal time period, a complete set of con-

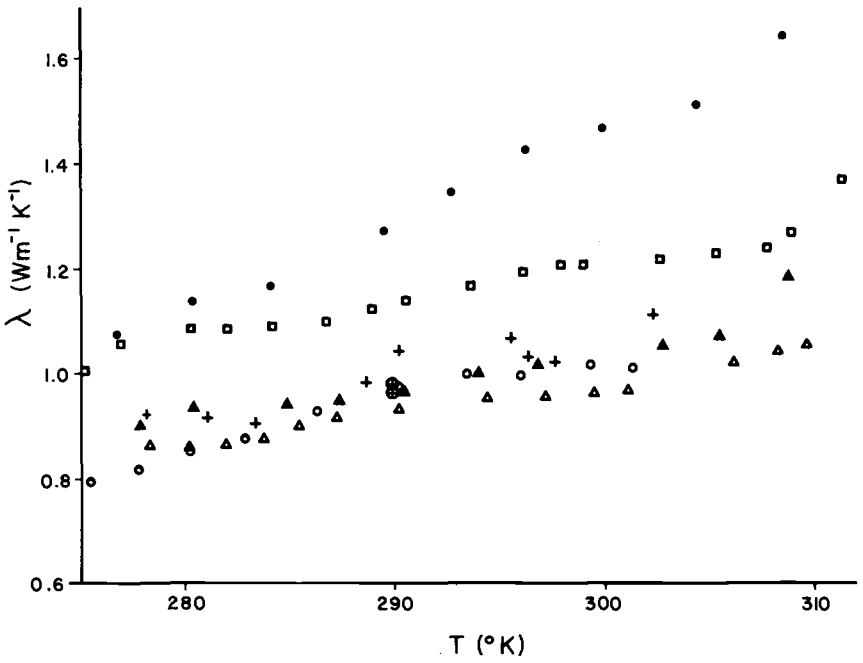

FIG. 5—*Thermal Conductivity of Microconcrete:* •*–8.7 percent moisture content;* □*—5.6 percent moisture content;* △ *and* +*—3.9 percent moisture content;* ○ *and* △*—0 percent moisture concent;* ⊕*—steady-state measurement, 3.4 percent moisture content.*

tinuous data over a temperature range of 35 K was obtained. As our technique is improved and some automation added to the apparatus, a temperature range of 200 to 400 K, depending upon the specimen, could be fully explored in four or five days.

References

[1] Hust, J. G., Powell, R. L., and Weitzel, D. H., *Journal of Research of the National Bureau of Standards*, Vol. 72-A, 1970, pp. 673–690.
[2] Shirtliffe, C. J., Stephenson, D. G., and Brown, W. C., National Research Council of Canada, Research Paper 638, 1974.
[3] Hildebrand, F. B., *Advanced Calculus for Applications*, Prentice Hall, 1962.
[4] Tye, R. P., Ed., *Thermal Conductivity*, Academic Press, New York, 1969.
[5] Neville, A. M., *Properties of Concrete*, Wiley, New York, 1973.
[6] Loomer, J. E. and Ashworth, T., *Proceedings* South Dakota Academy of Science, Vol. 51, 1972, pp. 238–243.

Summary

Summary

In many ways the energy crisis can be considered a blessing in disguise. Certainly it brought upon us the realization that our supply of energy in convenient forms was finite. Furthermore, it could be seen that a concerted international effort would be required to solve what is a global problem. There is no one solution: solar, wind, tidal, nuclear, fusion, and the other proposed newer sources of energy, coupled with measured efficiency in current forms of energy production and conservation, all have their particular position in time and place in the overall scene.

Conservation may be considered a prime subject in the short- and medium-term solution of the problem. Within this overall subject, thermal performance of insulations is a major factor. With only a cursory study, it soon becomes apparent that our knowledge of the thermal performance of thermal insulation materials and systems is inadequate whatever the application. The subject of thermal insulation is no longer simple in terms of consideration only of materials applications and results obtained as a result of laboratory tests. Thermal insulations have to perform in the real world where steady-state conditions are virtually unknown. We have to know more about their performance under realistic conditions in order to design and operate better systems and to be more certain of the energy savings. The economic factors of poor thermal performance are available to all of us when monthly statements of utilities costs are received.

Thermal insulation performance and its measurement has always been prominent in the activities of ASTM C16 Thermal Insulation Committee. For the past 25 to 30 years various symposia have been devoted to the subject. In examining the subject in more detail, it becomes obvious that the scope of the symposia, unless it was restricted to a particular topic, as in 1966, widens at each successive meeting. This reflects the growing complexity of the subject, and the contents of the present publication are ample evidence of this fact.

In the 1973 symposium, the C16.30 Thermal Measurements Subcommittee presented a position paper on "What Property Do We Measure." This outlined the basic philosophy that thermal insulation material or

system is, in fact, a complex entity which could not be considered in simple physical terms. The concept of thermal conductance or thermal resistance was proposed and the term "thermal conductivity" eliminated unless it was truly applicable. Since that time the subcommittee has been involved in the revision of their test specifications to reflect this philosophy. It is to be hoped that other national and international standards will follow this example. In 1973 the C16.30 subcommittee also recommended that much work should be carried out in the area of reference materials production and evaluation since our knowledge of thermal performance will improve only when we are satisfied that our measurement techniques are adequate.

There are several contributions to the present publication which extend these subjects first discussed in 1973. The subcommittee itself provides a further position paper amplifying the need not only for reference materials of known thermal performance, but for a variety of materials of different sizes and forms to provide a range of thermal conductances for a wide range of applications and temperature. This is a logical extension of the first paper since it is realized that problems of measurement of different orders of thermal conductance exist and can be remedied only if measurement apparatus and techniques can be evaluated by use of known reference specimens.

The need for reference materials is now more urgent since it is expected that laboratory accreditation for the evaluation of insulating materials and systems will be in force in the United States by 1979. Furthermore, there are indications that the accreditation of test laboratories and organizations is becoming an international subject. Clearly the whole subject is one where intense activity among members of the insulation community within ASTM C16 and International Standards Organization (ISO) 163 committees is expected in the next two years.

The paper by Bertasi et al indicates that the subject of reference materials is important to the insulation field in Europe. As a result of this work in the United States and Europe, it is clear that the molded high-density fibrous glass board (~250 kg/m^3) has been studied enough to accept that it is truly a reference material. Since the symposium, the National Bureau of Standards has analyzed all of its measurements on this material and has recommended that it be classed as a Standard Reference Material. However, this one material is clearly not sufficient for the total requirements.

Papers by Degenne et al and Pelanne highlight the problems which face us if we talk in terms of an insulating material having a thermal conductivity. Clearly both papers show how radiation heat transfer predominates in low-density materials. They further illustrate the errors in measurements of thermal performance which can be made unless a material or system

is evaluated in its actual thickness or at such a thickness that the thermal resistance is directly proportional to thickness.

The accuracy of the results in these thick specimens is still dependent upon there being available a number of thick reference specimens, both for qualifying guarded hot-plate apparatus and for calibrating heat flow-meter equipment. However, the present uncertainties in the accuracy of measurements of thick specimens of low-density materials, when the measurements are properly carried out, are less than the errors which can arise by evaluating the thermal resistance in terms of the results obtained on a thin specimen. As more reference materials become available and additional apparatus is used, these uncertainties will be reduced still further.

The present ASTM Tests for Steady-State Thermal Transmission Properties by Means of the Guarded Hot Plate (C 177-76) and the Heat Flow Meter (C 518-76) implemented the new concepts in 1976. The methods are currently accepted by a wide section of the thermal insulation industry and are being incorporated in various U.S. and Canadian Government specifications. These standards are recognized internationally as the leading documents in their field as to their direct applicability to the real performance characteristics of thermal insulations as opposed to the limited physical concept of thermal conductivity.

The original philosophy of the 1973 symposium was that better insulation practices would follow when we knew more about the heat-transfer mechanisms in insulation. Recently, more attention has been paid to modeling of heat-transmission materials, especially fibrous insulations, and four papers on this topic are included in the present publication. Three of the authors related their model to experimental results, and the overall picture in this area is encouraging. The paper by Pelanne relating light transmission measurements to thermal performance characteristics in building insulation is of considerable interest and the extension of the principle to other temperatures should be considered.

A completely new topic covered herein is the application of transient measurement techniques for determining thermal performance of insulations. Until recently, steady-state measurement techniques have been the only ones utilized for evaluating thermal performance. One of the objectives of the present symposium was to present to the attendees possible alternatives, particularly since there is always the definite need to reduce the time of measurement whenever practical.

An international selection of analytical and experimental papers on this subject was presented and, as in many other subjects, no definite conclusions were forthcoming. Jeschke outlined the German experience, including the development of a national specification for refractory materials. While these methods appear to be very promising for the thermal

conductivity range of these types of materials, the range is somewhat above that of the basic thermal insulations. Two papers from the United Kingdom presented opposing views. Jackson et al indicated that the line source heat flow method can be used for fibrous insulations at elevated temperatures by means of measurements with heat flow in two perpendicular directions coupled with an analysis. In application, two measurements have to be made on the same specimen, one with the line source lying along the fibers and one with the line source perpendicular to the fibers. However, Davis indicated that there were still problems with the method. The analytical paper by Fine also indicated that the line source method was not truly applicable on materials where radiation was the significant heat-transmission mode. Thus the whole subject is open for further analytical and experimental contributions for fibrous and cellular materials.

Since the 1973 symposium when the first paper on the calibrated hot-box technique for evaluating building systems was presented, a number of such facilities have been built and more experience has been gained. Furthermore, the calibrated-system approach has also been used for non-building applications. The paper by Miller et al outlines a further advance on a system for building components. This hot-box facility can be used in both the calibrated and guarded modes as well as for steady-state or dynamic conditions, and thus is a very reliable tool for research purposes. The approach by Lauvray for studying duct systems is also new and potentially of great use in an industrial field which until now has been somewhat neglected.

These measurement systems are both large and expensive to develop and to operate. However, they are absolutely necessary to enable one to obtain the necessary basic information on the real-life performance of thermal insulation systems and thus to bridge the gap between laboratory measurement and field test studies. Ultimately, field testing is the only sure way of measuring actual performance.

It has been estimated that currently there is more energy lost from industrial systems than from buildings. Thus the subject of high-temperature insulation is most relevant. Much of the current thermal performance information for high-temperature thermal insulations has been obtained from small-scale horizontal flat-plate and horizontal pipe-oriented apparatus. Results for this orientation can be transposed directly for the vertical orientation, particularly for heterogeneous and reflective-type insulation systems. External and internal convective heat transfer can be a very significant factor in the vertical orientation. In addition, applicability of the results from small-scale tests to larger-scale systems has not been verified.

Several contributions to the present publication indicate that some much-needed attention is now being paid to this subject. Hollingsworth

in his paper covers the results of a round-robin series of measurements carried out on one specimen of a pipe insulation material by a large number of organizations. Svedberg et al describe a large high-temperature pipe apparatus while Allmon and Wahle provide details of a new high-temperature hot-box facility specifically designed to investigate reflective-type insulation systems. Collectively the papers just touch the surface of the whole subject and only illustrate how much additional work is required in this area.

The excellent agreement in the results of the round robin indicate clearly that one can have great confidence in the present ASTM Test for Thermal Conductivity of Pipe Insulation (C 335-69) when run in the horizontal orientation. The preliminary results obtained on mass-type insulations in both the hot-box apparatus and on the large pipe are very encouraging. We can only look forward with great anticipation to further papers by these and other authors describing their experiences with the more complex heterogeneous systems.

It is to be hoped that these papers will stimulate others to carry out the necessary analytical and experimental work which will allow us to have the same confidence in results obtained for this orientation as those for the horizontal direction. The development and use of the larger-scale apparatus are necessary to evaluate not only the thermal performance characteristics of heterogeneous materials in systems, but also to study heat-transfer mechanisms in more detail, the effects of joints, and the effects of forced convection. Once reliable, quantitative laboratory studies have been made, the results of field studies, particularly those by thermography, can be better interpreted.

Three papers from Scandinavia relating to factors which affect overall systems performance illustrate the advances made in this geographic region compared with the materials approach still taken by many others. Of particular interest are two papers by Bankvall illustrating the very real effects of both natural and forced convection in building structures. This is an area where more quantitative information is required, and Sweden is to be commended in being among the leaders in this matter. The paper by Thirst and Probert from the United Kingdom described a particular system for insulated roofs. Clearly, systems evaluation is the subject of topical interest. It is where we should see a great deal of impetus in the future.

While system studies of the total thermal insulation system are directly relevant to our present and future requirements, studies on the individual materials should not be neglected since they are complementary. Concern is very often expressed at the lack of knowledge of materials performance after installation in buildings or in an industrial system. The past decade has seen a vast improvement in the individual techniques available for determining thermal properties under "ideal" laboratory conditions. It

must be realized, however, that during and after installation, thermal insulation materials are subjected to real-world conditions, and among these there are a number of critical factors which can influence performance.

Two of these factors are discussed herein. Dechow and Epstein deal with some effects of moisture on cellular plastics, and moisture effects on porous media are also discussed by Bomberg and Shirtliffe. Moisture may affect thermal insulation both in terms of the immediate decrease in thermal resistance as the moisture is picked up and the possible longer-term problems caused by environmental cycling.

Bomberg and Shirtliffe, in another paper, describe their work on the effects of various parameters, but especially density, on the thermal performance of cellulose fiber insulations. This material has become very widely used in North America, particularly for retrofit applications. It is also one where a great deal of controversy does exist both on absolute value of thermal resistance and the variations with "settled" density. The present results help to reduce these areas of controversy.

The topics covered advance our knowledge in two very specific cases devoted to thermal insulation materials used in buildings. However, they only highlight the necessity for more detailed and systematic studies dealing both with the different affecting parameters and with all materials, whether used for buildings or industrial applications.

To summarize, therefore, the papers of the present Symposium have continued to bring about the realization that the thermal insulation field is both complex and multifaceted. Measurement techniques are developing and improving and there is now more confidence in the results of such studies. Materials and systems are better understood and they too are being improved. International cooperation in the field, essentially begun at the 1973 symposium, is continuing to flourish, which augurs well for the results of the future activities of the newly established ISO Committee 163 on Thermal Insulation.

There is much we now know but there is a great deal more that we do not. Given the expertise and enthusiasm of the present group of authors and those whom they stimulate, we should expect to see remedies to this problem in the coming years. We should thus expect to see further symposia in this continuing series.

R. P. Tye

Senior scientist, Dynatech R/D Co., Cambridge, Mass. 02139; symposium chairman and editor.

Index